

DECLARATION

The work contained in this thesis is original, except as acknowledged in the customary manner, and has not been submitted previously for a degree at any university. To the best of my knowledge and belief, this thesis contains no material previously published or written by another person, except where due reference is made.

The author consents to the thesis being made available for photocopying and loan if accepted for the award of the degree.

Jonathan Peter Salo
Adelaide, Australia
30 May 2005



EVALUATING SITES FOR SUBSURFACE CO₂
INJECTION/SEQUESTRATION: TANGGUH,
BINTUNI BASIN, PAPUA, INDONESIA

(VOLUME 1: Text)

Jonathan P. Salo

Supervisors:
Dr. Simon C. Lang
Dr. John G. Kaldi

Australian School of Petroleum
University of Adelaide
South Australia
S.A. 5005

May 2005

ACKNOWLEDGEMENTS

The author expresses his gratitude to BP for their sponsorship and support. Particular thanks are extended to John A. Marcou (BP Tangguh Subsurface Development Manager 2000-2002); Dr. Neil Davis (BP Acting Tangguh Subsurface Development Manager 2002-2003); Achmadi T. Kasim (BP Tangguh Subsurface Development Manager 2003-2004); Dr. Godofredo Perez (Reservoir Engineer); Frans J. P. Silitonga (Reservoir Engineer); and Pranoto (BP Geophysicist).

The author would also like to thank the University of Adelaide, particularly the Australian School of Petroleum (ASP). The author wishes to express sincere gratitude to Dr. Simon C. Lang and Dr. John G. Kaldi for their time and assistance as supervisors and their keen interest in guiding the research, particularly in sedimentology/sequence stratigraphy and seal capacity/potential.

The author also wishes to thank the following ASP staff for time and assistance in their respective geological specialties, particularly Professor Richard Hillis (geomechanics and fault reactivation); Dr. Jochen Kassin (geologic modelling and geostatistics); Dr. Jerry Meyer (fault reactivation); Dr. Tobi Payenberg (sedimentology); Dr. Richard Daniel (seal evaluation); and Andy Mitchell (geophysics). The author also thanks fellow students Dr. Mark Tingay for FMI/FMS processing, and Dr. Takeshi Nakanishi for advice in probabilistic prospecting.

The author would also like to thank the GEODISC Programme of the APCRC (now the CO2CRC) and their key personnel including Dr. Peter Cook, Dr. Andrew Rigg, Dr. John Bradshaw, Dr. Jonathan Ennis-King, and especially Catherine Gibson-Poole for their kind assistance and helpful insights.

In addition, the author would like to thank Steve Tyson, of GeoVisual Systems, for his assistance with 3D geologic modelling, and numerous customizations to the GeoCARD software program.

Thanks also to Ben Royal, and especially Nathan Ceglar, for assistance with drafting and compilation. Finally, I would like to express thanks to my wife, Nurkayati Salo, and my son, Jason Michael Salo, for being patient and forgiving of the long periods of time spent away from home in the course of this study.

Jonathan Peter Salo

October 2004

ABSTRACT

The venting of anthropogenic CO₂ emissions into the atmosphere at increasing rates is probably influencing global warming and climate change. The Tangguh LNG development project in Papua, Indonesia will produce significant volumes of CO₂, which might be vented into the atmosphere. The LNG process will necessitate the separation of CO₂, estimated at 2.4 trillion cubic feet (TCF_{sc}), from the natural gas reserves prior to liquefaction and shipping. This study screens and assesses the possible alternatives to atmospheric venting, and recommends subsurface CO₂ injection and sequestration/storage in saline aquifers. The study identifies specific subsurface locations for several Environmentally-Sustainable Sites for CO₂ Injection (ESSCI) in Bintuni Basin, where the Tangguh production fields are located.

Alternatives to atmospheric venting of the estimated CO₂ volume at Tangguh include both non-geologic and geologic disposal options. Non-geologic options such as biosphere sinks (enhanced forest or agricultural growth), deep-ocean sinks (subsea dispersal), and direct commercial usage (e.g. use in beverage or fertilizer production, fire-retardant manufacturing) are impractical and of questionable impact in remote Papua, Indonesia.

Several subsurface geological disposal options were investigated, but the most viable geologic disposal option for Tangguh CO₂ is injection into the downdip aquifer leg of the Roabiba Sandstone Formation hydrocarbon reservoir. Injected CO₂, at supercritical phase, is expected to migrate updip into the sealed structural traps at Vorwata or Wiriagar Deep, as the natural gas reserves are produced.

A probabilistic ranking of data quality and quantity for five potential ESSCI reservoirs determined that the Middle Jurassic Roabiba Sandstone Formation has the highest likelihood of viable ESSCI sequestration/storage.

A probabilistic ranking of data quality and quantity for eight ESSCI structural traps within the western flank of Bintuni Basin, determined that Vorwata, followed by Wiriagar Deep, are the most viable ESSCI structural traps at the Middle Jurassic reservoir level.

Five potential ESSCI seals were evaluated and it was determined the best seal potential occurs in the Pre-Ayot Shales, directly overlying the Middle Jurassic reservoir at Vorwata. This unit is capable of holding a 3300 to 4660 foot (1006 to

1420 meter) CO₂ column. Seal integrity of the Pre-Ayot is very good because it is a relatively homogeneous deep-water shale that is composed primarily of ductile illite and kaolinite clays with a minor quartz and feldspar content. Sequence stratigraphy analysis suggests that the zone extends over the entire Vorwata three-way dip closure, with thickness between 17 feet (5 m) and 233 (71 m) feet.

The maximum effective storage capacity of the Middle Jurassic reservoirs for each structure was calculated, taking into account irreducible water, trapped water, and trapped residual gas pore volumes. The Vorwata structure is capable of storing 19.3 TCFsc supercritical CO₂ at reservoir temperature and pressure. The Wiriagar Deep structure has potential storage capacity of 3.5 TCFsc, and Ubadari 2.8 TCFsc, at their respective reservoir temperatures and pressures.

A 'Rating Product Ranking' was developed to quantify the results of the quality and quantity of four factors: Reservoir Data, Structure Data, Seal Data, and Storage Ratio. Each structure, and the respective top and lateral seal overlying the Middle Jurassic reservoirs, was evaluated. The net result was that Vorwata rated a 0.88 on a scale of zero to one, where 1.0 represents 100% confidence in ESSCI potential. Ubadari and Wiriagar Deep scored, respectively, 0.52 and a 0.45.

Finally, the structures were evaluated for relative proximity to the proposed CO₂ source (i.e. the LNG plant location). With a weighted distance factor calculated with the Rating product for each potential injection site, Vorwata rated 0.88 on a scale of zero to one, Wiriagar scored 0.24, and Ubadari scored only 0.09.

The Middle Jurassic 'Roabiba Sandstone Formation reservoir' at the Vorwata structure has the greatest potential as an ESSCI storage site. The Middle Jurassic 'Aalenian Sandstone Formation reservoir' at the Wiriagar Deep is the second-best potential ESSCI storage site. The subsurface ESSCI injection location proposed for the 'Roabiba Sandstone Formation' aquifer, 10 km southeast and down-dip from the known gas-water contact (GWC), is on the southeast Vorwata plunging anticlinal nose. An alternate potential ESSCI injection location proposed for the 'Roabiba Sandstone Formation' aquifer is 6 km south of and down-dip from the known gas-water contact (GWC) on Vorwata structure southern flank.

A key issue was to determine the possible risk of fault re-activation from CO₂ injection. NE-SW striking vertical faults have the highest risk of re-activation requiring an increase of over ~1460 psi (103 kg/cc) over hydrostatic at 14,000 ft TVDss (4267 m), for slippage to occur. The closest fault with a high risk of re-

activation is 5 km northwest of the recommended ESSCI site location. Supercritical CO₂ pressure is not expected to exceed the estimated pressure determined to cause fault re-activation.

A 3D geological model of the Mesozoic interval was constructed over a large area of western Bintuni Basin. The model was constructed so as to preserve as much geological heterogeneity as possible yet still have a manageable number of active cells. Faults were incorporated into the model as strike-slip vertical fault surfaces (or indexed fault polygons) as a separate attribute.

The geo-cellular model was built suitable for importation into a reservoir simulator (VIP), and a 25-year simulation run for natural gas production from the Vorwata Middle Jurassic reservoir, with concurrent CO₂ injection downdip into the Vorwata Middle Jurassic aquifer at the primary recommended ESSCI site location. The simulation verified the recommended location with the CO₂ slowly migrating into the Vorwata structural trap within the Middle Jurassic reservoir, and not compromising the hydrocarbon reserves or production.

It is recommended that additional data be acquired such as conventional core, formation water samples, and specific logs such as dipole-sonic, multi-chambered dynamic formation testers (MDT), and mechanical rotary sidewall coring tools (MSCT).

Lastly, several CO₂ monitoring methods and techniques are recommended for Tangguh to monitor CO₂ migration, pressures, and potential leakages. One such method is a vertical monitoring well at the recommended injection site. Other monitoring techniques include smart well completions, detection monitors at production wells with tracers injected prior to CO₂ injection. In addition, crosswell seismic surveys, electromagnetic methods, and electrical-resistance tomography techniques are suggested during the injection phase.

TABLE OF CONTENTS

TITLE PAGE	
ACKNOWLEDGMENTS	i
ABSTRACT	iii
TABLE OF CONTENTS	vi
PART I – INTRODUCTION	1
1. INTRODUCTION.....	2
1.0 Rationale and Aim.....	2
1.1 Background on Global Warming.....	2
1.2 Greenhouse Effect.....	4
1.3 Greenhouse Gases.....	6
1.4 Carbon Dioxide.....	11
1.5 Complete Carbon Cycle.....	13
1.6 Anthropogenic CO ₂	16
1.7 Non-geological CO ₂ Disposal Options.....	16
2. PROJECT AREA BACKGROUND.....	20
2.1 Location	20
2.2 Concession history and current status.....	21
3. EVALUATION OF GEOLOGICAL SEQUESTRATION OPTIONS.....	27
3.1 CUCS (CO ₂ in unmineable coal-bed sequestration).....	28
3.2 CECMP (CO ₂ for enhanced coal-bed methane production).....	29
3.3 CDOGR (CO ₂ in depleted oil/gas reservoirs).....	30
3.4 CCV (CO ₂ in cavity or void).....	31
3.4.1 Salt domes, mines, and tunnels.....	31
3.4.2 New Guinea Limestone Group member (NGLG)....	31
3.4.2.1 Eocene carbonates.....	31
3.4.2.2 Oligocene Limestone Formation.....	32
3.4.2.3 Faumai Formation.....	32
3.4.2.4 Kais Limestone Formation.....	32
3.4.2.5 Nonsuitability of the NGLG for CO ₂	33
3.4.2.6 Nonsuitability of CDOGR for CO ₂	34
3.4.2.6.1 Insufficient Storage Capacity	34
3.4.2.6.2 Supercritical Phase Instability...	35
3.4.2.6.3 Unsuitable Mineralogy.....	36

TABLE OF CONTENTS

3.4.2.6.4 Karstification.....	37
3.4.2.6.5 Salawati Basin Distance.....	37
3.5 CEOR (CO ₂ for enhanced oil recovery).....	38
3.6 CEGR (CO ₂ for enhanced gas recovery).....	38
3.7 CSA (CO ₂ in saline aquifer).....	39
3.7.1 CSA in non-hydrocarbon bearing structural traps....	39
3.7.2 CSA in hydrocarbon bearing structural traps.....	40
4. REGIONAL TECTONIC AND STRUCTURAL HISTORY.....	41
4.1 Paleozoic.....	41
4.2 Mesozoic.....	44
4.3 Cenozoic.....	50
5. LITHOSTRATIGRAPHY AND SEDIMENTOLOGY.....	55
5.1 Lithostratigraphic Overview Of The Bird's Head.....	55
5.2 Database Summary.....	58
5.3 Lithostratigraphy And Sedimentology Summary.....	60
5.3.1 Permian.....	60
5.3.2 Triassic.....	64
5.3.3 Early Jurassic.....	64
5.3.4 Middle Jurassic.....	64
5.3.4.i.1 Aalenian Sandstone.....	65
5.3.4.i.2 Roabiba Sandstone.....	66
5.3.5 Late Jurassic.....	69
5.3.5.i.1 Pre-Ayot Clastics Succession.....	69
5.3.5.i.2 Pre-Ayot Shale.....	69
5.3.5.i.3 Ayot Limestone Formation.....	71
5.3.5.i.4 Upper Late Jurassic Shales.....	72
5.3.5.i.5 Glauconitic Unconformity.....	73
5.3.6 Late Cretaceous.....	74
5.3.7 Late Paleocene Succession.....	76
5.3.7.i.1 Sand-Prone 'Lower Member' Interval....	78
5.3.7.i.2 Sand-Prone 'Middle Member' Interval...	80
5.3.7.i.3 Sand-Prone 'Upper Member' Interval....	83
5.3.7.i.4 Mud-Prone Interval.....	84
5.3.8 Eocene Succession.....	86

TABLE OF CONTENTS

5.3.9	New Guinea Limestone Group (NGLG).....	87
5.3.9.i.1	Oligocene Limestone Formation.....	87
5.3.9.i.2	Faunai Formation.....	88
5.3.9.i.3	Kais Limestone Formation.....	90
5.3.10	Steenkool Formation.....	91
PART II – INJECTIVITY.....		93
6.	STRATIGRAPHY.....	94
6.1	Stratigraphic Methodology.....	94
6.1.1	Seismic Stratigraphy.....	96
6.1.2	Palynological Biozonation.....	100
6.1.3	Wireline Log Motifs and Stratigraphic Correlations..	101
6.2	Paleogeographic Facies Maps for Tangguh Sequence Stratigraphy..	104
6.3	Detailed Sequence Stratigraphy Framework for Tangguh.....	107
6.3.1	Late Permian.....	116
6.3.2	Triassic and Early Jurassic.....	117
6.3.3	Aalenian MJ-4 (Middle Jurassic).....	120
6.3.4	Bajocian/Early Bathonian MJ-3 (Middle Jurassic)...	123
6.3.5	Late Bathonian MJ-2 (Middle Jurassic).....	131
6.3.6	Callovian MJ-1/LJ-11 (Middle-Late Jurassic).....	132
6.3.7	Ayot Limestone Formation LJ-9 (Late Jurassic).....	140
6.3.8	Upper Late Jurassic LJ-8 to LJ-2 (Late Jurassic).....	142
6.3.9	Late Cretaceous.....	143
6.3.10	Cenozoic Succession.....	145
6.4	Limitations and Alternatives.....	146
6.5	Re-interpretation of the Bird’s Head Tectonic/Structural History....	147
7.	RESERVOIR CHARACTERIZATION.....	153
7.1	Whole Cores, Core Plug Analyses, and DST Data.....	153
7.2	Reservoir Quality.....	156
7.2.1	Late Permian Reservoir Quality.....	156
7.2.2	Aalenian Sandstone Formation Reservoir Quality....	163
7.2.3	Callovian and Bathonian/Bajocian Roabiba Sandstone Formation Reservoir Quality.....	165
7.2.4	Ayot Limestone Formation Reservoir Quality.....	170

TABLE OF CONTENTS

7.2.5	Late Cretaceous Reservoir Quality.....	171
7.2.6	Late Paleocene Reservoir Quality.....	172
7.2.7	NGLG Reservoir Quality.....	174
PART III – CONTAINMENT.....		176
8.	ESSCI STRATA EVALUATION.....	177
8.1	Late Permian Reservoir ESSCI Potential.....	179
8.2	Middle Jurassic Reservoir ESSCI Potential.....	182
8.3	Late Cretaceous Reservoir ESSCI Potential.....	185
8.4	Late Paleocene Sand-Prone Interval ESSCI Potential.....	186
8.5	New Guinea Limestone Group Reservoir ESSCI Potential.....	188
8.6	ESSCI Stratum Rating and Ranking.....	190
9.	ESSCI STRUCTURE EVALUATION.....	193
9.1	Vorwata Structure ESSCI Potential.....	194
9.2	Wiriagar Deep Structure ESSCI Potential.....	196
9.3	Ubadari Structure ESSCI Potential.....	198
9.4	Roabiba Structure ESSCI Potential.....	199
9.5	Ofaweri Structure ESSCI Potential.....	200
9.6	Wos Deep Structure ESSCI Potential.....	201
9.7	Kalitami Structure ESSCI Potential.....	201
9.8	Saritu Deep Structure ESSCI Potential.....	202
9.9	Ranking Structural Trap ESSCI Potentials.....	203
10.	ESSCI SEAL EVALUATION.....	205
10.1	Overview of Reservoir/Seal Couplets and Seal Potential.....	205
10.2	Mercury Injection Capillary Pressure Methodology.....	207
10.3	Roabiba Reservoir Top and Lateral Seals.....	216
10.4	Roabiba Reservoir Regional Seals.....	224
10.5	Limitations.....	228
10.6	Discussions Regarding Seal Capacity, Geometry, and Integrity...	231
10.7	Seal Potential Conclusions.....	246
10.8	ESSCI Seal Evaluation.....	249
11.	CO ₂ STORAGE CAPACITY ANALYSIS AND WEIGHTED DISTANCE FACTORING.....	252
11.1	ESSCI CO ₂ Storage Capacity Analysis And Evaluation.....	252

TABLE OF CONTENTS

11.2 Integrating ESSCI CO ₂ Storage Capacity Analysis with Reservoir, Structure, and Seal Potential ESSCI Evaluations.....	253
11.3 Distance/Economics Factor Weighted Rating and Ranking.....	257
12. CO ₂ INJECTION FAULT RE-ACTIVATION RISK EVALUATION.....	260
PART IV – CO₂ INJECTION-SITE RECOMMENDATION AND GEOLOGIC MODEL VERIFICATION.....	266
13. CO ₂ INJECTION SITE LOCATION RECOMMENDATIONS.....	267
14. TANGGUH GEO-CELLULAR MODEL.....	272
14.1 The Geological Test Model.....	273
14.2 The Preliminary Geological Model.....	275
14.3 The Final 3D Geologic Model.....	279
14.4 The Modeling Strategy.....	281
14.4.1 Zones Versus Layers in the Geological Model.....	281
14.4.2 Limitations on Volume of Active Cells in the Geological Model.....	285
i. Incorporation of Faults into the Final Tangguh 3D Geologic Model.....	286
ii. Attributes and Variograms in the Geological Model.....	287
14.5. Results of the Final 3D Geologic Model.....	291
14.6. Preliminary Reservoir Simulation Results.....	292
14.7. Conclusions.....	293
PART V – IMPLICATIONS FOR IMPLEMENTATION.....	294
15. DRILLING AND DATA RECOMMENDATIONS FOR EXPLORATION AND INJECTION WELLS.....	295
15.1. Recommendations on Future Tangguh Well Data Acquisitions.....	295
15.1.1. Steenkool/Sele Formations.....	296
15.1.2. Kais/Faumai Formations (NGLG).....	297
15.1.3. Eocene/Paleocene Formations.....	299
15.1.4. Late Cretaceous Interval.....	301
15.1.5. Jurassic Sequences.....	302
15.1.6. Triassic/Permian Sequences.....	303
15.1.7. Final Remarks on Data Acquisition.....	304

TABLE OF CONTENTS

15.1.8. Conclusions.....	305
16. EVALUATION OF SUBSURFACE CO₂ MONITORING.....	306
16.1. Surface Measurements.....	306
16.2. Smart Well Completions.....	307
16.3. Seismic.....	308
16.4. Time-Lapse 3D ('4D') Seismic Surveys.....	308
16.5. Downhole Seismic.....	309
16.5.1. VSP.....	309
16.5.2. Cross-well Seismic Tomography.....	310
16.5.3. Single-well Sonic Logging.....	310
16.5.4. Microseismic Imaging.....	311
16.6. Electromagnetic Methods.....	312
16.7. Surface Electromagnetic Measurements.....	312
16.8. Cross-well Electromagnetic Methods.....	313
16.9. Downhole to Surface Electromagnetic Methods.....	313
16.10. ERT (Electrical Resistance Tomography).....	313
16.11. Gravity.....	314
16.12. Tracers	314
16.13. Limitations and Advantages.....	315
16.14. Subsurface CO ₂ Monitoring Conclusions and Recommendations.....	315
 PART VI – CONCLUSIONS, POSTSCRIPT, AND REFERENCES.....	 320
17. Conclusions.....	321
18. Postscript.....	335
19. References.....	340
 VOLUME 2 (FIGURES and APPENDICES)	
 PART VII – FIGURES.....	 1
PART VIII – APPENDICES.....	191
Appendix 1 :DST-PTA Summary.....	191
Appendix 2: Petrophysical Summary.....	205
Appendix 3: Porosity and Permeability Summary (V-10).....	229
Appendix 4: Core Plug/Chip Atlas.....	238

LIST OF TABLES

Volume 1

Table 1.1: Current averaged atmospheric gas composition	8
Table 5.1: Bintuni Basin gross intervals and formation/member	59
Table 6.1: Core and cuttings depth shifts at each well	95
Table 6.2a: Sequence stratigraphy zone/boundary depths at Tangguh	97
Table 6.2b: Sequence stratigraphy zone/boundary depths at Tangguh (cont.)	98
Table 6.3: Isopach thickness for zones/members	99
Table 6.4: Palynological zonation scheme used by Core Laboratories	103
Table 6.5: Palynological/Ichnological/Sedimentological/Log Motif charts	108-113
Table 7.1: List of all intervals cored and examined in Tangguh area	157
Table 7.2: Master list of new plug analyses (2002-2003)	158
Table 7.3: Core and cuttings depth shift for all wells	159
Table 7.4: Reservoir depth table	160
Table 7.5: New core plug porosity and permeability results	169
Table 7.6: Paleocene core plug porosity and permeability result summary	173
Table 8.1: Data confidence factor matrix for probabilistic HC exploration	178
Table 8.2: Data confidence factor matrix for ESSCI stratum at Tangguh	183
Table 8.3: Table of data confidence factor rating for ESSCI stratum	192
Table 9.1: Data confidence factor matrix for ESSCI structures at Tangguh	197
Table 9.2: Table of data confidence factor rating for ESSCI structures	204
Table 10.1: Core plug/chip MICP analyses results	208
Table 10.2: Example of GEODISC geochemical calculator	212
Table 10.3: CO ₂ column height calculator	213
Table 10.4: Measured salinities for major reservoirs	214
Table 10.5: Temperatures and pressures at datum for major reservoirs	215
Table 10.6a: Sensitivities to varied threshold pressures	218
Table 10.6b: Sensitivities to varied contact angles	219
Table 10.6c: Sensitivities to varied interfacial tension	220
Table 10.7: Comparison of seal capacities and column heights for various seals	226
Table 10.8: Bulk XRD analyses on core plug/chip seal samples	233
Table 10.9a: Petrographic analysis for V-1 and V-2 core plugs	235
Table 10.9b: Petrographic analysis for V-2 and V-7 core plugs	236
Table 10.9c: Petrographic analysis for V-10 core plugs	237
Table 10.9d: Petrographic analysis for V-10 core plugs (cont.)	238
Table 10.9e: Petrographic analysis for V-10 core plugs in aquifer leg	239
Table 10.10: Summary of seal capacity, geometry, integrity, and potential	248
Table 10.11: Data confidence factor matrix for ESSCI seals at Tangguh	251
Table 11.1: Calculator for CO ₂ storage volume in Tangguh structures	254
Table 11.2: Rating Product for ESSCI rankings	255
Table 11.2: Distance weighted rating	259
Table 12.1: List of Tangguh area leak-off tests/formation integrity tests	261
Table 12.2: Table of Tangguh area wells with FMI/FMS borehole image logs	262
Table 14.1: Zonation and layering scheme for preliminary geological model	278
Table 14.2: Zonation and layering scheme for final Tangguh geologic model	284
Table 14.3: Numerical facies codes used in the attribute 'SimpleFacies_Use'	288
Table 14.4: Variogram models and numerical codes for paleodepositional facies	290
Table 14.5: Variogram models, structures, and parameters for stochastically populating cells in the final geologic model	290
Table 14.6: The search ellipse parameters for paleodepositional facies	291

LIST OF TABLES (Appendices) Volume 2

Appendix 1: DST-PTA Summary Tables	191
Appendix 2: Petrophysical Summary Tables	205
Appendix 3: Core Plug Porosity and Permeability Table 1998 (V-10 well)	229

LIST OF FIGURES Volume 2

Fig. 1.1: Changes in atmospheric CO ₂ composition plotted from ice core	2
Fig. 1.2: Change in CO ₂ concentrations over a millennium	3
Fig. 1.3: Change in CO ₂ concentrations and temperature over a millennium	3
Fig. 1.4: Change in CO ₂ concentrations and temperature over 400,000 yrs	4
Fig. 1.5: Change in GHG over a millennium	5
Fig. 1.6: Projected thermal expansion of sea level	6
Fig. 1.7: Projected sea level from thermal expansion and land-ice melt volume	6
Fig. 1.8: Projected SE coastal USA inundation from sea level rise	7
Fig. 1.9: Projected loss of polar ice caps (N. Pole)	8
Fig. 1.10: Map of global oceanic thermohaline circulation system	9
Fig. 1.11: CO ₂ PVT phase diagram	10
Fig. 1.12: LANDSAT image of Cameroon volcanic fields	11
Fig. 1.13: Aerial photograph of Lake Nyos and crater rim after CO ₂ bubble	11
Fig. 1.14: Temperature change relationship to GHG concentrations	12
Fig. 1.15: Schematic of the Complete Carbon Cycle (CCC)	13
Fig. 1.16: Schematic of the Bio-Geological Carbon Cycle	13
Fig. 2.1: Indonesia location map	14
Fig. 2.2: Map of Bird's Head PSC boundaries and gas/oil fields	15
Fig. 2.3: Map of Tangguh development area with gas fields	16
Fig. 3.1: ESSCI CO ₂ cross-sectional geological options schematic	17
Fig. 3.2: Bintuni Basin lithostratigraphic column	18
Fig. 3.3: Location map of production fields in Bintuni and Salawati Basins	19
Fig. 3.4: Map of shallow oil fields, seeps, and deep exploration wells in 1993	20
Fig. 3.5: Map of 'kitchen area' for source rock hydrocarbon generation	21
Fig. 4.1: Papua, Indonesia and Bird's Head area location map	22
Fig. 4.2: Paleotectonic map Cretaceous/Tertiary (K/T Boundary)	23
Fig. 4.3: Paleotectonic map Middle Oligocene	24
Fig. 4.4: Paleotectonic map Late Oligocene	25
Fig. 4.5: Paleotectonic map Early Miocene	26
Fig. 4.6: Paleotectonic map Middle Miocene	27
Fig. 4.7: Paleotectonic map Late Miocene of Banda Arc collision	28
Fig. 4.8: Paleotectonic map Pliocene	29
Fig. 4.9: Foreland and Piggyback basin formations map	30
Fig. 4.10: Kitchen area map of Bintuni and Berau basins	30
Fig. 4.11: Thermal maturity history plot for Bintuni Basin source rocks	31
Fig. 5.1: Early stratigraphic column for Bintuni Basin	31
Fig. 5.2: Examining the cores	32
Fig. 5.3: Fluvio-lacustrine Late Permian shale in core	33

Fig. 5.4: Late Permian marine sandstone in core (WD-3)	34
Fig. 5.5: Near-top Late Permian sandstone in core (WD-3)	35
Fig. 5.6: Late Permian sandstone in core (V-1)	36
Fig. 5.7: Late Permian/Middle Jurassic unconformity in core (WD-3)	37
Fig. 5.8: Aalenian Sandstone Formation and overlying MJ-4 shale (WD-3)	38
Fig. 5.9: Aalenian Sandstone Formation in core (WD-3)	39
Fig. 5.10: Various depositional facies Aalenian Sandstone Formation (WD-3)	40
Fig. 5.11: Roabiba Sandstone Formation in core (WD-2)	41
Fig. 5.12: Roabiba Sandstone Formation in core (WD-7)	42
Fig. 5.13: Sedimentological features Roabiba Sandstone Formation core (WD-3)	43
Fig. 5.14: Sedimentological features Roabiba Sandstone Formation core (V-2)	44
Fig. 5.15: <i>Helminthopsis</i> or <i>Helminthoida</i> ichnological fabric (V-2)	45
Fig. 5.16: Callovian (LJ-11) marine shale in core (V-10)	46
Fig. 5.17: Ayot Limestone Formation in core (WD-3)	47
Fig. 5.18: Ayot belemnite death assemblage in core (WD-3)	48
Fig. 5.19: Upper Late Jurassic altered volcanic tuff (WD-3)	49
Fig. 5.20: Base Late Cretaceous/Top Late Jurassic unconformity (WD-3)	50
Fig. 5.21: Near-Base Late Cretaceous carbonate (WD-3)	51
Fig. 5.22: Late Paleocene Sand-Prone Interval Middle Member in core (WD-2)	52
Fig. 5.23: Late Paleocene Sand-Prone Interval Middle Member in core (WD-2)	53
Fig. 5.24: Late Paleocene Mud-Prone Interval (WD-3)	54
Fig. 5.25: Oligocene Limestone Formation outcrop photograph (E. Onin-1)	55
Fig. 5.26: Near-top Faumai Formation coherency image 1632 ms TWT	56
Fig. 5.27: Faumai Formation coherency image 1660 ms TWT	57
Fig. 5.28: Faumai Formation coherency image 1892 ms TWT	58
Fig. 5.29: Kais Limestone Formation coherency image 1200 ms TWT	59
Fig. 5.30: Kais Limestone Formation coherency image 1320 ms TWT	60
Fig. 5.31: Kais Limestone Formation coherency image 1340 ms TWT	61
Fig. 5.32: LANDSAT image of Berau bay and Bintuni Bay	62
Fig. 5.33: Aerial photograph of the Wiriagar River and Wiriagar Swamp	63
Fig. 6.1: Stratigraphic geological cross-section A – A'	64
Fig. 6.2: Stratigraphic geological cross-section B – B'	65
Fig. 6.3: Stratigraphic geological cross-section C – C'	66
Fig. 6.4: Stratigraphic geological cross-section D – D'	67
Fig. 6.5: Stratigraphic geological cross-section E – E'	68
Fig. 6.6: Extensional Mesozoic rifting along Australian NW Shelf margin	69
Fig. 6.7: Bintuni Basin Mesozoic stratigraphic column	70
Fig. 6.8: A20 Aalenian isopach map	71
Fig. 6.9: Early A20 paleogeographic facies map	72
Fig. 6.10: Late A20 paleogeographic facies map	73
Fig. 6.11: Bajocian/Bathonian gross isopach map	74
Fig. 6.12: R10 isopach map	75
Fig. 6.13: R10 paleogeographic facies map	76
Fig. 6.14: R20 isopach map	77
Fig. 6.15: R20 paleogeographic facies map	78
Fig. 6.16: R30 isopach map	79
Fig. 6.17: R30 paleogeographic facies map	80
Fig. 6.18: R40 isopach map	81
Fig. 6.19: R40 paleogeographic facies map	82
Fig. 6.20: R50 isopach map	83

Fig. 6.21: Early R50 paleogeographic facies map	84
Fig. 6.22: Late R50 paleogeographic facies map	85
Fig. 6.23: R60 isopach map	86
Fig. 6.24: R60 paleogeographic facies map	87
Fig. 6.25: R70 isopach map	88
Fig. 6.26: R70 paleogeographic facies map	89
Fig. 6.27: R80 isopach map	90
Fig. 6.28: R80 paleogeographic facies map	91
Fig. 6.29: Base Pre-Ayot (MFS) GR correlation	92
Fig. 6.30: Callovian Roabiba gross isopach map	93
Fig. 6.31: CU10 isopach map	94
Fig. 6.32: CU10 paleogeographic facies map	95
Fig. 6.33: CU20 isopach map	96
Fig. 6.34: CU20 paleogeographic facies map	97
Fig. 6.35: CU30 isopach map	98
Fig. 6.36: CU30 paleogeographic facies map	99
Fig. 6.37: CU40 isopach map	100
Fig. 6.38: CU40 paleogeographic facies map	101
Fig. 6.39: CU50 isopach map	102
Fig. 6.40: CU50 paleogeographic facies map	103
Fig. 6.41: Pre-Ayot Formation gross isopach map	104
Fig. 6.42: PA10 isopach map	105
Fig. 6.43: PA10 paleogeographic facies map	106
Fig. 6.44: PA20 isopach map	107
Fig. 6.45: PA20 paleogeographic facies map	108
Fig. 6.46: PA30 isopach map (version 1)	109
Fig. 6.47: PA30 paleogeographic facies map	110
Fig. 6.48: PA30 isopach map (version 2)	111
Fig. 6.49: PA60/Ayot Limestone Formation isopach map	112
Fig. 6.50: PA60/Ayot Limestone Formation paleogeographic facies map	113
Fig. 6.51: BHMC paleotectonic migration map	114
Fig. 7.1: Wiriagar Deep/Ubadari cross-section with core & DST intervals	115
Fig. 7.2: Vorwata cross-section with core & DST intervals	116
Fig. 7.3: Permian well correlation cross-section V area	117
Fig. 7.4: Late Permian porosity vs. permeability cross-plot	118
Fig. 7.5: Aalenian well correlation cross-section WD-V area	119
Fig. 7.6: Aalenian Top Depth Structure Map	120
Fig. 7.7: Aalenian effective porosity map	121
Fig. 7.8: Aalenian porosity vs. permeability cross-plot	122
Fig. 7.9: Aalenian & Roabiba well correlation cross-section WD-V area	123
Fig. 7.10: Tangguh area seismic line W-E, surface to Base Cretaceous	124
Fig. 7.11: Cross-sectional schematic with simultaneous onlap & truncation	125
Fig. 7.12: Roabiba well correlation cross-section V area	126
Fig. 7.13: Bajocian/Bathonian/Callovian Roabiba Top Depth Structure Map	127
Fig. 7.14: Callovian Roabiba effective porosity map	128
Fig. 7.15: Bajocian/Bathonian Roabiba effective porosity map	129
Fig. 7.16: Roabiba porosity vs. permeability cross-plot	130
Fig. 7.17: Tangguh area Jurassic pressure gradients vs. depth graph	131
Fig. 7.18: Roabiba V-10 core porosity vs. permeability cross-plot	132
Fig. 7.19: Roabiba V-10 log and core porosity vs. permeability cross-plot	133

Fig. 7.20: Ayot porosity vs. permeability cross-plot	134
Fig. 7.21: Late Cretaceous Top Depth Structure Map	135
Fig. 7.22: Late Cretaceous porosity vs. permeability cross-plot	136
Fig. 7.23: Late Paleocene Middle Member porosity vs. permeability cross-plot	137
Fig. 7.24: Late Paleocene well correlation cross-section WD-V area	138
Fig. 7.25: Late Paleocene Sand-Prone well correlation cross-section WD area	139
Fig. 7.26: Kais Limestone Formation (NGLG) Top Depth Structure Map	140
Fig. 8.1: Kais-Faumai salinity difference map	141
Fig. 9.1: Distance to structures from LNG plant map	142
Fig. 10.1: Stratigraphic cross-section of regional seals	143
Fig. 10.2: Geological schematic of regional seals	144
Fig. 10.3: CO ₂ Column Height sensitivities due to varied contact angle	145
Fig. 10.4: CO ₂ Column Height sensitivities due to varied interfacial tension	146
Fig. 10.5: Map of areal extent for Roabiba top seals in the Tangguh area	147
Fig. 10.6: Photograph of severely altered core sample due to storage conditions	148
Fig. 10.7: Photograph of regional seals in slabbed cores	149
Fig. 10.8: Calculated seal capacity from wireline log analysis	150
Fig. 11.1: Relative storage capacity diagram	151
Fig. 11.2: Geologic cross-sectional schematic of proposed injection plan	152
Fig. 11.3: Graph of distance to proposed injection sites	153
Fig. 12.1: Leak-Off Test (LOT) gradient contour map	154
Fig. 12.2: Nafe-Drake Plot	155
Fig. 12.3: Vorwata vertical stress profile with depth	156
Fig. 12.4: Wiriagar Deep vertical stress profile with depth	157
Fig. 12.5: Tangguh area vertical stress contour map	158
Fig. 12.6: Formation pore pressure distribution with depth	159
Fig. 12.7: Rose diagram and depth vs. directional orientation graph	160
Fig. 12.8: Mohr diagram and planes-to-poles diagram	161
Fig. 12.9: Map of the in-situ horizontal stress orientations	162
Fig. 12.10: Fault risk of re-activation map for Tangguh area	163
Fig. 12.11: Fault risk of re-activation depth-slice map at ~14,000 ft TVDss	164
Fig. 13.1: Map of recommended surface injection site locations	165
Fig. 13.2: Subsurface location map of recommended Vorwata injection sites	166
Fig. 13.3: Map of subsurface CO ₂ reservoir volume at Vorwata	167
Fig. 13.4: Map of subsurface CO ₂ reservoir total volume at Vorwata	168
Fig. 14.1: Map of test model area	169
Fig. 14.2: Test model populating geo-cells with sonic values	170
Fig. 14.3: Base Late Cretaceous surface	171
Fig. 14.4: Tangguh coarse grid model with wells/base Late Cretaceous	172
Fig. 14.5: 2D mesh draped on base Late Cretaceous surface	173
Fig. 14.6: Fence display through wells and surfaces from model	174
Fig. 14.7: Wireline log display through surfaces at wells	175
Fig. 14.8: Bounding surfaces menu	176
Fig. 14.9: Work flow diagram	177
Fig. 14.10: Scheme and codes for facies polygons within the model	178
Fig. 14.11: Example of digitized paleogeographic map facies polygons	179
Fig. 14.12: Facies polygons displayed in GEOCARD as an attribute	180
Fig. 14.13: Example of paleogeographic map and facies attribute in model	181
Fig. 14.14: Fault compartment polygons	182
Fig. 14.15: Fault compartment polygons as an attribute	183

Fig. 14.16: Fault compartment boundaries for transmissibility multipliers	184
Fig. 14.17: Reservoir simulator screen capture of grids, zones, and attributes	185
Fig. 14.18: Reservoir simulator screen capture at Year 0 from injection	186
Fig. 14.19: Reservoir simulator screen capture at Year 5 from injection	187
Fig. 14.20: Reservoir simulator screen capture at Year 20 from injection	188
Fig. 14.21: Reservoir simulator screen capture at Year 25 from injection	189
Fig. 18.1: Vorwata Mesozoic core palynology/biostratigraphy chart	190

LIST OF FIGURES (Appendix 4)

Volume 2

Fig. 1: Core Plug/Chip Atlas Guide	239
Fig. 2: Core Plug/Chip Atlas: WD-2, 7377' 11"	240-241
Fig. 3: Core Plug/Chip Atlas: WD-2, 7380' 0"	242-243
Fig. 4: Core Plug/Chip Atlas: WD-2, 8681' 3"	244-245
Fig. 5: Core Plug/Chip Atlas: WD-2, 8753' 2"	246
Fig. 6: Core Plug/Chip Atlas: WD-3, 7548' 9"	247-248
Fig. 7: Core Plug/Chip Atlas: WD-3, 7549' 2"	249-250
Fig. 8: Core Plug/Chip Atlas: WD-3, 7552' 7"	251-252
Fig. 9: Core Plug/Chip Atlas: WD-3, 7558' 8"	253-254
Fig. 10: Core Plug/Chip Atlas: WD-3, 7956' 3"	255
Fig. 11: Core Plug/Chip Atlas: WD-3, 9238' 0"	256-257
Fig. 12: Core Plug/Chip Atlas: WD-3, 9272' 1"	258-259
Fig. 13: Core Plug/Chip Atlas: WD-3, 9274' 1"	260-261
Fig. 14: Core Plug/Chip Atlas: WD-3, 9286' 2"	262-263
Fig. 15: Core Plug/Chip Atlas: WD-3, 9309' 8"	264-265
Fig. 16: Core Plug/Chip Atlas: WD-3, 9325' 0"	266-267
Fig. 17: Core Plug/Chip Atlas: WD-3, 9328' 4"	268-269
Fig. 18: Core Plug/Chip Atlas: WD-3, 9344' 1"	270-271
Fig. 19: Core Plug/Chip Atlas: WD-3, 9364' 9"	272-273
Fig. 20: Core Plug/Chip Atlas: WD-5, 9509' 0"	274
Fig. 21: Core Plug/Chip Atlas: WD-5, 9509' 5"	275-276
Fig. 22: Core Plug/Chip Atlas: WD-7, 7962' 6"	277-278
Fig. 23: Core Plug/Chip Atlas: WD-7, 7981' 6"	279-280
Fig. 24: Core Plug/Chip Atlas: WD-7, 8452' 5"	281-282
Fig. 25: Core Plug/Chip Atlas: WD-7, 8471' 1"	283-284
Fig. 26: Core Plug/Chip Atlas: WD-7, 8497' 9"	285-286
Fig. 27: Core Plug/Chip Atlas: WD-7, 8524' 7"	287
Fig. 28: Core Plug/Chip Atlas: V-1, 11765' 9"	288
Fig. 29: Core Plug/Chip Atlas: V-1, 11787' 7"	289
Fig. 30: Core Plug/Chip Atlas: V-1, 11790' 9"	290-291
Fig. 31: Core Plug/Chip Atlas: V-1, 11797' 7"	292
Fig. 32: Core Plug/Chip Atlas: V-1, 11902' 3"	293-294
Fig. 33: Core Plug/Chip Atlas: V-1, 11904' 3"	295-297
Fig. 34: Core Plug/Chip Atlas: V-1, 11909' 7"	298
Fig. 35: Core Plug/Chip Atlas: V-1, 11914' 6"	299
Fig. 36: Core Plug/Chip Atlas: V-2, 12582' 7"	300-301
Fig. 37: Core Plug/Chip Atlas: V-2, 12584' 8"	302-303
Fig. 38: Core Plug/Chip Atlas: V-2, 12585' 8"	304-305
Fig. 39: Core Plug/Chip Atlas: V-2, 12594' 4"	306-307

Fig. 40: Core Plug/Chip Atlas: V-2, 12600' 3"	308-309
Fig. 41: Core Plug/Chip Atlas: V-2, 12757' 6"	310-311
Fig. 42: Core Plug/Chip Atlas: V-2, 12865' 7"	312-313
Fig. 43: Core Plug/Chip Atlas: V-2, 12901' 5"	314-315
Fig. 44: Core Plug/Chip Atlas: V-2, 13020' 6"	316-318
Fig. 45: Core Plug/Chip Atlas: V-2, 13025' 6"	319-321
Fig. 46: Core Plug/Chip Atlas: V-2, 13030' 1"	322-324
Fig. 47: Core Plug/Chip Atlas: V-7, 13118' 3"	325-326
Fig. 48: Core Plug/Chip Atlas: V-7, 13123' 8"	327
Fig. 49: Core Plug/Chip Atlas: V-7, 13136' 10"	328-329
Fig. 50: Core Plug/Chip Atlas: V-7, 13143' 6"	330
Fig. 51: Core Plug/Chip Atlas: V-7, 13152' 5"	331-333
Fig. 52: Core Plug/Chip Atlas: V-10, 3944.43 m	334-336
Fig. 53: Core Plug/Chip Atlas: V-10, 3947.64 m	337-339
Fig. 54: Core Plug/Chip Atlas: V-10, 3954.46 m	340-342
Fig. 55: Core Plug/Chip Atlas: V-10, 3965.57 m	343-345
Fig. 56: Core Plug/Chip Atlas: V-10, 3966.82 m	346-348
Fig. 57: Core Plug/Chip Atlas: V-10, 3967.10 m	349-351
Fig. 58: Core Plug/Chip Atlas: V-10, 4021.25 m	352-353
Fig. 59: Core Plug/Chip Atlas: V-10, 4021.86 m	354
Fig. 60: Core Plug/Chip Atlas: V-10, 4022.20 m	355
Fig. 61: Core Plug/Chip Atlas: V-10, 4025.08 m	356
Fig. 62: Core Plug/Chip Atlas: V-10, 4025.80 m	357
Fig. 63: Core Plug/Chip Atlas: V-10, 4025.98 m	358
Fig. 64: Core Plug/Chip Atlas: V-10, 4026.18 m	359-361
Fig. 65: Core Plug/Chip Atlas: V-10, 4028.15 m	362
Fig. 66: Core Plug/Chip Atlas: V-10, 4029.58 m	363
Fig. 67: Core Plug/Chip Atlas: V-10, 4029.70 m	364
Fig. 68: Core Plug/Chip Atlas: V-10, 4031.55 m	365-366
Fig. 69: Core Plug/Chip Atlas: V-10, 4034.51 m	367-369
Fig. 70: Core Plug/Chip Atlas: V-10, 4035.40 m	370
Fig. 71: Core Plug/Chip Atlas: V-10, 4036.23 m	371
Fig. 72: Core Plug/Chip Atlas: V-10, 4039.62 m	372-373
Fig. 73: Core Plug/Chip Atlas: V-10, 4040.20 m	374-375
Fig. 74: Core Plug/Chip Atlas: V-10, 4042.62 m	376-377
Fig. 75: Core Plug/Chip Atlas: V-10, 4044.81 m	378-379
Fig. 76: Core Plug/Chip Atlas: V-10, 4045.92 m	380-381
Fig. 77: Core Plug/Chip Atlas: V-10, 4049.40 m	382-383
Fig. 78: Core Plug/Chip Atlas: V-10, 4052.13 m	384-385
Fig. 79: Core Plug/Chip Atlas: V-10, 4052.64 m	386-387
Fig. 80: Core Plug/Chip Atlas: V-10, 4056.02 m	388
Fig. 81: Core Plug/Chip Atlas: V-10, 4057.32 m	389
Fig. 82: Core Plug/Chip Atlas: V-10, 4058.58 m	390
Fig. 83: Core Plug/Chip Atlas: V-10, 4059.26 m	391
Fig. 84: Core Plug/Chip Atlas: V-10, 4060.90 m	392
Fig. 85: Core Plug/Chip Atlas: V-10, 4063.45 m	393
Fig. 86: Core Plug/Chip Atlas: V-10, 4067.60 m	394
Fig. 87: Core Plug/Chip Atlas: V-10, 4068.50 m	395
Fig. 88: Core Plug/Chip Atlas: V-10, 4076.30 m	396-397
Fig. 89: Core Plug/Chip Atlas: V-10, 4081.32 m	398-399

Fig. 90: Core Plug/Chip Atlas: V-10, 4082.85 m	400-401
Fig. 91: Core Plug/Chip Atlas: V-10, 4090.85 m	402-403
Fig. 92: Core Plug/Chip Atlas: V-10, 4093.80 m	404-405
Fig. 93: Core Plug/Chip Atlas: V-10, 4095.50 m	406
Fig. 94: Core Plug/Chip Atlas: V-10, 4101.30 m	407-408
Fig. 95: Core Plug/Chip Atlas: V-10, 4117.70 m	409-410
Fig. 96: Core Plug/Chip Atlas: V-10, 4126.30 m	411-412
Fig. 97: Core Plug/Chip Atlas: V-10, 4126.69 m	413-414
Fig. 98: Core Plug/Chip Atlas: V-10, 4128.92 m	415-417
Fig. 99: Core Plug/Chip Atlas: Fractured & Faulted Cores of Seals	418-419
Fig. 100: Core Plug/Chip Atlas Guide	420

PART I
INTRODUCTION

1.0 Rationale And Aim

Concern amongst the world's nations regarding global warming as a consequence, at least in part, of increasing greenhouse gas emissions has galvanized action for not only governments, but also some multinational companies. Notwithstanding the ongoing debate about *exactly* how global warming is/will be manifesting itself, the facts are clear; the rate of increase in global atmospheric carbon dioxide (CO₂) concentration is accelerating; and irrespective of whether anthropogenic atmospheric CO₂ emissions are ultimately responsible, or merely contributory, the impact on world climate, especially for low-lying nations, has the potential to be disastrous. Although the Kyoto Protocol (1997) has so far been ratified by 189 nations, it is still awaiting Russia to sign-on to be enacted (UNFCCC, 2004), and not all nations are actively participating (i.e. United States, Australia, and of course, most of the developing-world). However, large multinationals, notably British Petroleum (BP) and Shell have taken the stance to at least start doing something about reducing emissions (O'Leary, et al., 2001). After a review of these broad issues, the **aim** of this thesis is to develop the concepts, and devise a practical technical plan, for the capture and subsurface disposal of CO₂ emissions from a liquefied natural gas (LNG) project in Papua, Indonesia, currently being developed by BP.

1.1 Background on Global Warming

Climate change due to global warming has been the topic of intense scientific debate and popular interest since 1975 (Broecker, 1975; Mathews, 1976). Many studies regarding climate change, global warming, and the role of greenhouse gases in global warming have been carried out and the number of studies under way currently is growing daily (Forest, et al., 2004; Webster, et al., 2003). This introduction will briefly summarize all latest results of the completed studies and draw attention to some of the significant research still ongoing.

In 1992, the United Nations set up the United Nations Framework Convention on Climate Change (UNFCCC) as a UN body to fund, collate, and synthesize and report coordinated research regarding climate change, global warming, greenhouse gas emissions (including CO₂), forward modelling, to the Intergovernmental Panel on Climate Control (IPCC) for dissemination and publication (UNFCCC, 2004). Extreme climatic shifts and increased frequency of severe weather systems have been predicted

in studies, summarized in the IPCC's 1997 Report (IPCC, 1997) and 2001 Report (IPCC, 2001) as one of the dire consequence of global warming. Carbon dioxide (CO₂), methane (CH₄), and water vapor (H₂O) are atmospheric GHG constituents, and the increasing concentration of atmospheric CO₂ from anthropogenic sources is especially thought to be contributing to increased global warming rates (Broecker, 1975; Watson, 2001; Bradshaw, et al., 2000). Studies conducted over the past three decades, starting with Broecker's original research (1975) though Knutson's recent National Oceanic and Atmospheric Administration global warming and climate change modelling, have concluded that climatic change is indeed occurring and that the changes have been accelerated/alterd by anthropogenic 'greenhouse gas' (GHG) emissions. Furthermore, many of the studies including Edmonds, et al. (1986) and the IPCC reports (1997, 2001), have concluded that the rate of increased global warming, and hence climatic change, is accelerating, and that the increased acceleration is *continuing due to ever increasing anthropogenic emission rates of GHG into the atmosphere.*

The unanimous vote of all 189 sovereign nation members of the United Nations in Kyoto, Japan in 1992 led to the ratification Kyoto Protocol to limit the increase of CO₂ atmospheric emissions from anthropogenic sources, and eventually reduce these emissions over time (UNFCCC, 2004). This historic treaty was then follow up by the Bonn Accord in June of 2001, that set the exact limits of CO₂ atmospheric emissions to be allowed by each individual nation, and then by the Marrakech Accord in November of 2001, which established a carbon-trading scheme, credits for carbon 'sinks', and penalties for exceeding carbon emission quotas (UNFCCC, 2004). The Kyoto Protocol on GHG emissions will come into force when the treaty is approved by the governments of at least 55 of the Protocol signatory countries representing 55% of the 1990 global anthropogenic CO₂ emissions. At the time of publication, 123 nations had signed the Protocol, requiring only the formal acceptance by Russia to take effect (UNFCCC, 2004).

The United States, after organizing and approving the Kyoto Protocol of 1997, was the sole abstention from the Bonn and Marrakech Accords, however U.S. President George W. Bush stated, 'We all believe technology offers great promise significantly to reduce emissions - especially carbon capture, storage and sequestration technologies' (Bush, 2001; BBC and Kirby, 2001; Whitehouse, 2002).

The world's nations are not the only ones concerned and acting on GHG emissions, and atmospheric CO₂ concentration reductions in particular. Many international corporations are also beginning to act on CO₂ emissions. BP Ltd Inc. for example, is a major energy company leading the way for environmental protection for the planet, and has begun a global strategy of reducing CO₂ emissions by sequestering greenhouse gas emissions, rather than venting them to the atmosphere (Lord Browne, 2003). It is with this stated goal that BP is pursuing the geological subsurface sequestration of CO₂ gas from production of liquefied natural gas (LNG) at the Tangguh Project in Papua, Indonesia, the subject of this research.

1.2 Greenhouse Effect

The Earth's atmosphere, primarily composed of nitrogen (N₂), oxygen (O₂), carbon dioxide (CO₂), and water vapor (H₂O) allows a large percentage of solar radiation in the form of visible light to heat the Earth's surface (Levine, 2004). Part of this energy is normally re-radiated by the Earth as long-wave infrared radiation, some of which is absorbed by carbon dioxide and water vapor in the atmosphere and reflected back to the Earth as heat. The capture and reflecting of the infrared radiation causes the Earth's surface (land and ocean) and lower atmosphere to have an increased temperature than would otherwise be the case. Erroneously referred to as the 'greenhouse effect', the Earth's atmosphere is transparent to the transmission of short wavelength radiation in the form of the sun's visible light, but is essentially opaque to the longer wavelengths re-radiated from the surface, trapping the radiated heat in the atmosphere. 'Global warming' is the term applied to an increase in the temperature of the Earth's upper and lower atmospheres caused by an increase in atmospheric 'greenhouse gases', notably carbon dioxide, methane, and water vapor which ultimately tends to increase the average temperature of the Earth's surface, especially its oceans (Trenberth, 2001). In this study the term 'greenhouse gases' refers to the process whereby the upper and lower atmospheric temperatures, but especially the lower atmospheric temperature increases due to an 'enhanced greenhouse effect' caused by increasing concentrations of the gases and vapors identified above.

Several different processes control the net thermal budget of the Earth. The overall thermal budget is determined primarily by the net solar and cosmic radiation influx and capture, and by the dissipation of the Earth's original core heat from its early gravitational agglomeration/formation combined with radioactive element decay

within the mantle and crust, and finally, locally by the distribution of landmass and oceans on the crustal surface (changing over time due to continental drift of tectonic plates).

The first of these, the net solar and cosmic radiation flux, varies over time due to changes in net radiation received from the sun and from the cosmos over geological/astronomical time (Shaviv and Veizer, 2003), and also from changes in the Earth's relative distance and position relative to the sun (Beer, 2000).

Three types of variations in the Earth's orbit result in solar radiation input variations over geologic time, and this results in cyclic variations of climate over time commonly referred to as the 'Milankovitch Cycles', after the Serbian scientist who first noted them (Milankovitch, 1920).

The eccentricity cycle refers to the periodicity of the elongation of the Earth's orbit around the Sun, the obliquity cycle refers to the periodicity of the Earth's rotational axis with respect to its orbital plane, and finally the precession of the Earth's axis (a wobble, so to speak, to the planet's axis over time). The eccentricity of the Earth's orbit ranges from 0 to 0.05 from the current value of 0.016 completing a cycle approximately every 92,000 to 100,000 years (House, 1995). The obliquity of the Earth varies from 24°36' to 21°39' from the current position of 23°30' over a cycle time of approximately 41,000 years (House, 1995). Finally the axial precession results in a wobble of the axis from 21° to 24° over a cycling time of 16,000 to 26,000 years with 21,000 years being the usual stated time period (House, 1995).

At present we are just past the peak of the last 100,000 year 'greenhouse' maximum, following the last ice-age at 18,000 years before the present (YBP). Without the impact of anthropogenic contributions, the next few thousand years are destined to be a cooling cycle, ultimately ending in a glacial maximum ~80,000 years from now, based on ice-age/interglacial warming cyclicality noted in the Vostok ice cores (Petit, et al., 1999).

Currently, approximately 10% of the Sun's net solar radiation reaching the earth is reflected directly back into space by reflection from the atmosphere, a further approximately 6% of solar radiation is scattered by atmospheric molecular refraction, winding up deflected back in space. The remaining 84% makes it to the surface of the planet, equivalent to about 288 watts/sq. m. on average (Houghton, 1997). Much of this radiation, estimated at 240 watts/sq. m. on average, is reflected as 'black body' radiation off the surface, back into the atmosphere. This is the average calculated

reflectance off of the Earth's surface, given the present obliquity, eccentricity, and precession of the Earth relative to the Sun. The absorption and reflectance of 'greenhouse gases' including water vapor in the atmosphere leading to 'enhanced greenhouse effect' results in only 236 watts/sq. m. being re-radiated back into space from the earth's surface (Houghton, 1997). Therefore, for the planet's entire surface, an additional 4 watts/sq. m. on average is being reflected back to the lower atmosphere and surface resulting, in an increase of the planet's net thermal budget (Houghton, 1997).

1.3 Greenhouse Gases

The effect of atmospheric warming by atmospheric greenhouse gases was first deduced, in 1827, by the French scientist Jean-Baptiste Fourier, famed for his contributions in mathematics, particularly in devising Fourier transforms methodology; and archaeology, particularly as scientific advisor to Napoleon Bonaparte during the French invasion and occupation of Egypt where he systematically recorded and catalogued ancient Egyptian monuments along the Nile for the first time (SMSUSt.A, 2004).

The Earth's atmosphere is composed primarily of nitrogen (N₂) and oxygen (O₂), but the trapping of re-radiated heat energy from the earth's surface is effected mainly by the trace gaseous constituents in the Earth's atmospheric composition, primarily carbon dioxide (CO₂), water vapor (H₂O), ozone (O₃), nitrous oxide (N₂O), Freon (F₁₁ and F₁₂), methane (CH₄), and chlorofluorocarbons (CFC's such as CC₁₂F₂ and CC₁₃F) (Levine, 2004). These trace gases are collectively referred to as the 'greenhouse gases' (GHG) (Table 1.1). These GHG act to trap re-radiated heat energy from the planet's surface in the infrared wavelength returning it to the surface, in much the same manner as a greenhouse's windows. These 'greenhouse gases' are responsible for approximately 70% of the Earth's net surface energy input (Houghton, 1997).

The main product of the increased fossil fuel combustion is an increase in atmospheric concentrations of anthropogenic carbon dioxide, although an increase of other trace gases such as chlorofluorocarbons (i.e. Freon gas, a refrigerant/coolant), nitrous oxide (a minor pollutant from combustion), and methane, due again largely to anthropogenic sources, may also be accelerating 'enhanced greenhouse effects' on Earth leading to 'global warming' (IPCC, 2001). The concern in these scientific and

political debates is that the greenhouse effect on Earth may be intensified and that natural long-term climatic changes may be accelerated with short-term climatic extremes adversely impacting the Earth's biosphere.

Studies based on ice core gas inclusion composition analysis from the Siple ice cores, combined with direct atmospheric measurement from the World Meteorological Association at the Mauna Loa Observatory in Hawaii indicate a dramatic rise in mean atmospheric CO₂ concentrations in (Figure 1.1) over the past one hundred-fifty years (IPCC, 2001). This relatively recent rise in atmospheric CO₂ concentrations is even more apparent when ice core gas inclusion composition analysis from the Antarctic and Greenland spanning the past millenium (Figure 1.2) are analysed (Mann, et al., 1999). Oxygen isotope ratios and gas inclusion analysis from these ice cores can also provide temperature data over the past millennium, which when plotted together with change in atmospheric CO₂ concentrations (Figure 1.3), appear to show a strong correlation (IPCC, 2001). Analyses of the Antarctic Vostok ice cores (Shackleton, 2000; IPCC, 2001) indicate that clear correlations between global temperature and atmospheric CO₂ concentrations can be measured from ice core data over the past 400,000 years (Figure 1.4), with the overall carbon cycle apparently being driven by 100,000 year Milankovitch eccentricity orbital forcing.

“At the 100,000-year period, atmospheric carbon dioxide, Vostok air temperature, and deep-water temperature are in phase with orbital eccentricity, whereas ice volume lags these three variables. Hence, the 100,000-year cycle does not arise from ice sheet dynamics; instead, it is probably the response of the global carbon cycle that generates the eccentricity signal by causing changes in atmospheric carbon dioxide concentration” (Shackleton, 2000).

It is the massive increase in mean global atmospheric CO₂ concentrations (red curve) at present on the 400,000 year plot ('0' years before present), however, that is the greatest cause of concern (Figure 1.4), surpassing any previously measured atmospheric CO₂ concentrations in the past 400 millennia. After analyzing the global mean temperature data it appears that a real increase of global mean annual temperature by more than 0.4°C has occurred during the late 19th and early 20th centuries and that the rate of increase has accelerated since the mid 20th century with an overall average increase of almost 1.0°C over the past century (IPCC, 2001).

It has been estimated reliably that an increased concentration of atmospheric carbon dioxide (CO₂) has contributed up to 70% of the ‘enhanced greenhouse effect’ to date, with methane (CH₄) about 24%, and nitrous oxide (N₂O) and the various Freon/chlorofluorocarbons the remaining 6% (Houghton, 1997). This relatively recent increase in atmospheric CO₂ concentrations has been linked in scientific and political debates to the onset of the Industrial Revolution approximately 200 years ago, and the increased combustion of fossil fuels, such as coal, oil, and natural gas (IPCC, 2001).

Molecular Species (*GHG)	Relative Concentration (in ppbv#)	Primary Source	Lifetime/Status
N ₂ O	7.81 x 10 ⁸	Biological	Long Term
O ₂	1.01 x 10 ⁸	Biological	Long Term
H ₂ O *	1 x 10 ⁶ - 10 ⁷	Physical	Long Term
Ar	9.34 x 10 ⁶	Radiogenic	Permanent
CO ₂ *	3.5 x 10 ⁵	Biological, Geological, Industrial	Increasing
Ne	1.8 x 10 ⁴	Geological	Permanent
He	5.2 x 10 ³	Radiogenic	Escaping
CH ₄ *	1.6 x 10 ³	Biological	Increasing
Kr	1.0 x 10 ³	Geological	Permanent
H ₂	5.0 x 10 ²	Biological	Variable
N ₂ O *	3.0 x 10 ²	Biological	Increasing
CO	1.0 x 10 ²	Photochemical, Industrial	Increasing
SO ₂	<10 ²	Industrial, Photochemical	Variable
O ₃ *	<10 ²	Photochemical	Variable
Xe	9 x 10 ¹	Geological	Permanent
NO, NO ₂ , NO _x	variable	Biological	Very Short Term
CH ₃ Cl	6.0 x 10 ⁻¹	Biological	Short Term
CCl ₂ F ₂ *	1.9 x 10 ⁻¹	Industrial	Increasing
CCl ₃ F *	1.7 x 10 ⁻¹	Industrial	Increasing
CCl ₄ *	1.2 x 10 ⁻¹	Industrial	Increasing
CH ₃ CCl ₃ *	9.8 x 10 ⁻¹	Industrial	Increasing
CF ₄ *	7.0 x 10 ⁻¹	Industrial	Increasing
CH ₃ Br *	1.0 x 10 ⁻²	Biological	Increasing

Table 1.1: The Earth’s current averaged atmospheric gas composition with greenhouse gas (GHG) constituents indicated (#ppbv is parts per billion by volume), (adapted from Encyclopaedia Britannica, 2001).

Confirmation regarding the linkage of increased concentrations of CO₂, CH₄, and N₂O to anthropogenic sources is evident in the ice core gas inclusion

compositional analysis for sulphate particle aerosols produced from the combustion of coal, which became widespread as a fossil-fuel source by 1850 (Figure 1.5a). Gas inclusion analysis shows an increase in sulphate aerosols in Greenland ice cores from 1850 (Figure 1.5b) increasing at an exponential rate (IPCC, 2001).

The data clearly shows increased rates of atmospheric GHG emissions during the past and continuing into the present, and forward modelling indicates that the rate of increase for GHG emissions will continue rising until well past 2100 (IPCC, 2001). There is widespread concern about the probability that these greenhouse gas concentrations are causing, or *at least* accelerating and exacerbating, an increased rate of warming for the overall global climate, and that this ‘coaster effect’ will also continue until well past 2100 (IPCC, 2001).

The effects of a global climatic warming, while not completely predictable, are generally understood to potentially have the ability to cause greater variance in severe weather extremes and frequency including: severe draughts and desertification in some regions; increased rainfall and flooding, and particularly super-hurricanes/typhoons in other regions; and the possibility of destabilizing frozen methane and CO₂ hydrate clathrates on the ocean floor and under permafrost in subpolar/temperate regions, due to higher atmospheric temperatures, and eventually higher ocean temperatures (IPCC, 2001).

The US National Oceanic and Atmospheric Administration’s Geophysical Fluid Dynamics Laboratory (GFDL) modelling of *only* thermal ocean volume expansion due to increased ocean surface temperatures projects a 1 meter rise (Figure 1.6) in global sea level by 2200 (NOAA, 2004). However, the current melting of glacial ice from European/Greenland alpine and continental glaciers is probably responsible for the rise in mean sea level during the past decade of 0.2 to 0.8 mm already observed in Europe, by the European Environmental Agency (EEA, 2004). The EEA recently released their 2004 report, which predicts a global sea level rising 0.9 meter by 2100 (Figure 1.7) (EEA, 2004).

Global sea level rise has the potential to produce devastating results, particularly for impoverished low-lying coastal nations (such as those of Micronesia, Bangladesh, Vietnam, and Indonesia, to name just a few examples) but also to the richer, developed nations of the world. Global sea level rise would potentially result in the loss of large low-lying coastal areas containing major cities with large

populations (Figure 1.8), and the loss of critical agricultural production areas (EEA, 2004).

Perhaps of most concern, and possibly most costly (in terms of life and finances), is the potential for sea level rise globally due to the combined thermal expansion of ocean waters and increased water volume in the oceans/seas due to melting of glacial ice in Antarctica and Greenland. The IPCC has calculated that in ‘...the Netherlands, mainly below present sea level...Protection against sea level rise next century will require no new technology. [Existing] dykes and sand dunes will need to be raised; additional pumping will also be necessary to combat incursion of saltwater into freshwater aquifers. It is estimated that an expenditure of about 10 thousand million [US] dollars would be required for protection against a sea level rise of 1 meter’ (IPCC, 1997). This high cost applies to a developed country, which already has an extensive and complex infrastructure for sea level control. The cost in human life, natural ecology and habitats, and economic infrastructure to low-lying underdeveloped countries would qualify as nothing short of catastrophic.

Some islands in the South Pacific such as Fiji, Suva, and Kirabati have already encountered problems with saline water encroachment in island aquifers, higher than normal storm surges, and rises in average coastal sea levels (NTFA, 2003). As June 2003, the National Tidal Facility of Australia recorded a 5.9mm/annum rise for Fiji, during the period 1993 through 2003 (NTFA, 2004).

Finally, the melting of massive ice-shelves in frozen polar seas could potentially release vast volumes of fresh, less-dense water into the oceans (Figure 1.9) and disrupt the global thermohaline system of ocean circulation (Broecker, 2001; EEA, 2004). The thermohaline oceanic current system is a thermal and salinity distribution/transfer system bringing warm, fresh water to the northern latitudes, and colder, saline, denser water to the equatorial ocean regions (Figure 1.10). A disruption of this system could potentially induce abrupt climate flips (ESR, 2004). The continued global warming by GHG emissions is projected to make northern Europe warmer and potentially change the climate from temperate to sub-temperate with more precipitation (EEA, 2004). However, an eventual disruption of the oceanic thermohaline current system could occur due to melting of the polar caps, which potentially can abruptly flip northern Europe’s climate into cool, temperate to sub-polar climes (Broecker, 1975; Stocker and Schmitter, 1997; Broecker, 2001; ESR, 2004).

1.4 Carbon Dioxide

Carbon dioxide (CO₂) was first identified as a unique gas in the 17th century by a Belgian chemist, Jan Baptist van Helmont (b.1580 – d.1644), who noted it as a product of fermentation and combustion (Britannica, 2001). It exists in a gaseous phase at Earth's standard surface pressure 0.1MPa (1Atmosphere or bar) and standard temperature of 21°C (70°F) and is quite unreactive (NIST, 2003). It has a property known as 'supercriticality' under increased pressure and temperature where it behaves with dense, liquid phase properties while technically in a gaseous phase. If gaseous compression is carried out above a 'critical temperature', no phase change occurs but the gas behaves as a fluid due to its super-compressed state. If the same compression is performed at a temperature below the 'critical temperature', then a 'bona fide' liquid phase will form. The point where all three phase boundaries (solid, liquid, and vapor) meet is called the 'triple point' and is at -56.6°C (69.9°F) and 0.51 MPa (5.1 Atmospheres), as shown in Figure 1.11.

The 'supercritical point' is where CO₂ gas has increased density but has fluid-like properties (Bachu, 2000). The supercritical point for carbon dioxide can be seen on Figure 1.11 at 31.1°C (87.4°F) and 7.38 Mpa (73.8 bar/atmospheres or 1,071 psi) (NIST, 2003). If CO₂ liquid is brought to atmospheric pressure it freezes to a crystalline solid called 'dry ice' which sublimates (passes directly into gas vapor phase without melting) at normal atmospheric pressure above temperatures of -78.5°C (-109.3°F), and at temperatures above 1,700°C (3,100°F) it begins to breakdown into carbon monoxide and oxygen molecules (Chemicalogic, 2004).

CO₂ is slightly soluble in water forming 1.79 volumes per volume of water at 0°C or 32°F, and at atmospheric pressure (i.e. 1 bar), forming a weak acid solution, called carbonic acid. Ignited magnesium will burn in a carbon dioxide environment, but carbon dioxide generally does not support the combustion of most materials (Chemicalogic, 2004). At surface atmospheric pressure, CO₂ is a colorless gas with a slightly sharp odor and a sour taste (Britannica, 2001).

Carbon dioxide is a normal constituent of exhaled respiration in animals. Prolonged exposure to concentrations of 5% CO₂ (by volume) causes unconsciousness and, eventually, death due to asphyxiation in humans and animals (Britannica, 2001). Evans, et al. (1993; and 1994) reported that more than 1,500 people and over 5,000 head of cattle died from CO₂ asphyxiation at villages bordering Lake Nyos, Cameroon in 1986 when an enormous bubble of concentrated CO₂

breached the surface of the lake (Figure 1.12). The CO₂ was probably volcanically derived, according to Evans, et al. (1993, and 1994) from the Oku Volcanic Field and had been trapped beneath an algal vegetative mat on the surface of the lake before gas buoyancy pressure ultimately ‘breached the seal’ (Figure 1.13).

Carbon dioxide is a naturally occurring, minor constituent of the Earth's atmosphere (at approximately 3.5 volumes in 10,000), released by a variety of natural processes (Table 1.1). Natural genesis includes volcanic out-gassing from volcanoes, respiratory exhalations and gaseous discharges from animals, the combustion/burning of carbon-containing organic matter such as vegetation, the fermentation/decay of organic matter by bacterial agents, the respiration by plants in the photosynthesis of carbohydrates, and the chemical-mechanical breakdown of soils and rock minerals by weathering (IPCC, 1997; Evans, et al., 1993). The four major anthropogenic sources of atmospheric CO₂ are as follows (IPCC, 2001; IPCC, 1997):

- 1) Power plant emissions from combustion of organic material such as wood, and fossil fuels such as coal, oil, and natural gas in power plants and factories for electricity generation.
- 2) Transportation emissions based on internal combustion engines in various vehicles (cars, trucks, trains, and aircraft) using fossil fuels such as gasoline, diesel (derived from oil or liquefaction of natural gas), and natural gas.
- 3) The separation, and venting into the atmosphere, of naturally occurring CO₂ from subsurface production of oil and natural gas at wellheads.
- 4) Industrial activities that vent CO₂ as an industrial by-product into the atmosphere from numerous diverse applications such as petrochemical processing, manufacturing processes, and the compression of natural gas in LNG plants.

The commercial uses for carbon dioxide (CO₂) are limited to: ‘sweeping’ oil or gas reservoirs for additional hydrocarbon recovery, in enhanced oil/gas recovery projects (Rigg and Bradshaw, 2000; Holtz, et al., 2000; Bachu, 2000); carbonating beverages, such as soft drinks, mineral waters, beer, etc. for human consumption (IPCC, 1997; IPCC, 2001); for cooling or refrigeration purposes (IPCC, 1997; IPCC, 2001); as a combustion retardant in fire extinguishing systems (IPCC, 1997; IPCC,

2001); as an inflation gas for life rafts and life jackets (IPCC, 2001); in the production of ammonia (IPCC, 1997; IPCC, 2001); in transferring coal (IPCC, 1997); in the manufacture of foam-rubber and some plastics (IPCC, 2001); in promoting the growth of plants in greenhouses (IPCC, 1997); and for immobilizing animals before slaughter in abattoirs (IPCC, 1997).

1.5 Complete Carbon Cycle

The 'Complete Carbon Cycle' (CCC) refers to the bio-geochemical CO₂ cycle on Earth that includes the CO₂ interactions between the atmospheric gases, the terrigenous minerals of rocks and soils, the waters of the oceans and seas, and the planet's biota (living organisms both plant and animal).

As described briefly above, carbon in the form of CO₂ exists in trace amounts in the atmosphere. It also exists as CO₂ and in other molecular forms in greater amounts in soil, rocks, and bodies of water.

Plants utilize solar energy, CO₂, and H₂O to synthesize carbohydrates from which organic tissue is formed, in a process called photosynthesis (Britannica, 2001). In hemispheric springs and summers this process becomes more pronounced due to increased solar radiation and warmer temperatures, which accelerate plants uptake of CO₂ from the atmosphere (EO NASA, 2004). In the Northern Hemisphere the cyclicity of the bio-carbon cycle is more pronounced than in the Southern Hemisphere because of greater landmass in the Northern Hemisphere and the larger forestation in the northern latitudes (EO NASA, 2004). The bio-carbon cycle reflects the concentrations of atmospheric CO₂ decreasing by a few percent between spring to autumn periods due to increased plant photosynthesis utilizing CO₂ during the spring and summer seasons followed by a relative decrease in plant photosynthesis during autumn and winter (these couple of percentage points amount to tens of billions of tons of CO₂). This bio-carbon cycle results in about a 3% drop in CO₂ concentrations in the Northern Hemisphere during the growing season (spring and summer) (EO NASA, 2004). Decaying plant detritus in the form of dead leaves and plants during the autumn and winter period actually release previously bio-sequestered CO₂ back into the atmosphere, causing a net increase in atmospheric CO₂ due to CO₂ released by decay versus CO₂ removed from the atmosphere by the reduced level of photosynthesis (EO NASA, 2004).

The CCC (as opposed to merely the bio-carbon cycle) also involves exchanges of CO₂ between the atmosphere and the ocean (EO NASA, 2004). The ocean-carbon cycle exchanges are dynamic (two way) and are determined by complex geo-chemical and physical processes (PMEL NOAA, 2004). Atmospheric carbon dioxide contains much less carbon than the concentration of carbon in the oceans stored through geo-chemical reactions as carbon dioxide (CO₂), bicarbonate ion {HC₃-}, and carbonate ion {(CO₃)₂-} (PMEL NOAA, 2004). Prior to two hundred years ago there was a net average release of carbon dioxide from oceanic sequestering of dissolved CO₂ into the atmosphere. The dynamic cycle has since changed to the ocean acting as a CO₂ 'sink' with the chemical equilibrium reaction running the opposite way, due to increases in overall CO₂ atmospheric concentrations, and it's relative proportion to other GHG in the atmosphere (Figure 1.14). Atmospheric CO₂ is now, overall, dissolving in greater proportions into seawater than being released back into the atmosphere, with the rate of exchange to the ocean even greater for colder waters (PMEL NOAA, 2004).

There is a flux when the atmosphere and surface waters exchange CO₂ to equalize their respective CO₂ partial pressure. The flux from the atmosphere to the oceans is proportional to the atmospheric CO₂ partial pressure, which in turn is proportional to the ratio of the masses of CO₂ and dry air in the atmosphere. The atmosphere-surface ocean flux can therefore be expressed as: $FAS = kAScA$

Where FAS is the flux of carbon from the atmosphere to the surface of the ocean, kAS is a constant interpreted as an average over the global ocean surfaces and time, and cA is the mass of carbon in the atmosphere (Edmonds, 1986).

The IPCC (Houghton, 1997) estimated from modeling that 2 gigatonnes (Gt) of carbon dioxide added to the atmosphere annually are absorbed by the oceans. Previously the release of sequestered CO₂ from the oceans to the atmosphere and eventually to the land resulted in the net production of organic matter and the chemical weathering of minerals in continental rocks (Edmonds, 1986). Currently, any change in the concentration of atmospheric CO₂ results in a far greater change in carbon dioxide (CO₂), bicarbonate ion {HC₃-}, and carbonate ion {(CO₃)₂-} concentrations in the ocean (Edmonds, 1986). Similar 'atmospheric with oceanic' dynamic equilibrium reactions occur with the other main constituents in the atmosphere, namely molecular nitrogen (N₂) and oxygen (O₂, O₃) (PMEL NOAA, 2004).

The geologic carbon cycle also forms a large part of the overall ‘complete carbon cycle’ (EO NASA, 2004). The dynamic geo-carbon cycle both adds and removes carbon from the atmosphere, primarily thorough volcanic activity that vents CO₂ directly from the Earth’s interior to the atmosphere and oceans (EO NASA, 2004; UND, 2004; MacKenzie, et al., 2001).

This is mainly through the formation of carbonates that sequester huge volumes of carbon ‘naturally’ via mineral precipitation (PMEL NOAA, 2004), and though the deposition/formation of sedimentary rocks in the form of coal, peat, and carbonaceous shale, that sequester huge amounts of carbon and various carbon compounds in solid form (MacKenzie, et al., 2001). Lastly, thermogenic and biogenic sourced carbon dioxide gas is sequestered, as a gas, in subsurface reservoir rock strata (clastics and carbonates) (MacKenzie, et al., 2001). Finally, the weathering of carbonate, soil, coal and peat, carbonaceous shale, other minerals, and even the thawing of permafrost cover, releases CO₂ back into the atmosphere (MacKenzie, et al., 2001; EO NASA, 2004).

When CO₂ comes in contact with water, at least a certain portion will dissolve into the water to form a weak acid, called carbonic acid (Britannic, 2001). This weak acid plays an important role in the weathering of rocks and breakdown of minerals that can lead to release of CO₂ back into the atmosphere. The global carbon cycle (A) past and (B) present, of the global CO₂ environment, on a long-term geologic basis, is presented in Figure 1.15.

The bio-carbon cycle occurs during the life-span of an organism or the time period between a repeat of seasons, an order of only one year, but the atmospheric – oceanic carbon cycle occurs over a time-span of thousands of years (Wollast and MacKnezie, 1989). In fact, if all the CO₂ were removed overnight from the atmosphere the oceans would release CO₂ back into the atmosphere in the dynamic equilibrium discussed above and would result in a new concentration of CO₂ at around 280 ppmv in only a couple of thousand years (a period of time referred to by oceanographers as the ‘stirring time’). However, geological time scales on the order of millions of years measure the geo-carbon cycle (Figure 1.16). The bio-carbon cycle, the atmospheric-oceanic carbon cycle, the geo-carbon cycle, and, now, the anthropogenic-carbon cycle all interact with each other in a complex, dynamic process (IPCC, 1997).

1.6 Anthropogenic CO₂ Contributions To Climate Change

The United Nation's Intergovernmental Panel on Climate Change (IPCC, 1997), seventeen national academies of sciences (IPCC, 2001), and the European Union (EEA, 2004) have concluded that as a result of the anthropogenic-carbon cycle addition to the CCC, global temperatures will continue to rise, with average global surface temperature projected to increase by between 1.4°C and 5.8°C above 1990 levels by the year 2100, base on the range of model forecasts (IPCC, 2001). The summary of forecast modelling predictions suggest a doubling of atmospheric CO₂ levels by 2040, estimated to cause a 3°C increase in average global mean temperature, with a 12°C increase at the poles, that will result in at least a half-meter sea level rise due to thermal expansion and glacial melt (Jean-Baptiste and Ducroux, 2001).

“The latest 2001 IPCC report reaffirms in much stronger language that the climate is changing and the major cause is from human effects on changing the composition of the atmosphere through the use of fossil fuels and deforestation” (Trenberth, 2001).

1.7 Non-Geological CO₂ Disposal Options Considered

“Business as usual is no longer a viable option” (BBC, 2001). There are several potential options for minimizing the increase of anthropogenically sourced carbon dioxide into the atmosphere (IPCC, 2001). In general, they can be itemized as follows:

1. Increased fossil fuel efficiency (hence, decreasing the production of, and the combustion of, fossil fuels such as coal, gas, and oil (Kurushima, 2001; Schaap and McMullen, 2001; DOE, 2004;).
2. Changing to ‘non-greenhouse gas emission’ alternative fuels (such as hydroelectric, nuclear, wind, geothermal, tidal, and solar power generation systems that can decrease the production of, and the combustion of, fossil fuels such as coal, gas, and oil) (Copin, et al., 2001; Gifford, et. al., 2001; Jean-Baptiste and Ducroux, 2001).
3. The capture and sequestration of CO₂ where possible to prevent it's entering the ‘atmospheric-oceanic’ carbon cycle. This includes various

potential subsurface CO₂ injection and geological sequestration options (Bachu, 2001; Rigg and Bradshaw; 2001)

A considerable time is required for the research and experimental phase of the first two options (Copin, et al., 2001). There are also environmental impacts associated with several of the ‘alternate energy’ methods contained in the second option. This includes cost per unit of megawatts from alternative sources, radioactive emissions and waste products associated with nuclear energy sources (Dunstan, 2002) and potential noise pollution from wind turbine generators, which are currently blocking development of several major wind turbine projects in Europe, Australia, and even the USA (Milam, 2004). Options such as geothermal and tidal power are limited geographically to local areas where they are technically or physically feasible. Finally, the world-wide implementation of any of the second options (after finally being researched and developed) would require a great deal of lead-time for technical (Copin, et al., 2001), commercial, global-scale implementation, and ‘normal rates of technological development and implementation’ will not be sufficient to meet targeted deadlines set by the Kyoto Protocol and subsequent accords related to Kyoto (Shinn, et al., 2001).

Nevertheless options one and two should not be ignored. Conversely, they should in fact be the end goal for sustainable economic and human growth on the planet. The point is, that the long lead-time needed to research, develop and potentially implement options one and two require an interim solution to mitigate CO₂ emissions immediately. Only the third option already has a proven experimentation background, modeling history and, developed technology to make significant impacts towards limiting increasing rates of CO₂ atmospheric concentrations now (Cook, et al., 2000).

There are several sequestration options and technologies that can be utilized in the capture and long-term storage of carbon dioxide (CO₂) to prevent it’s entering the ‘atmospheric’ carbon cycle. The options can be categorized as follows:

1. Forestation/agricultural ‘sinks’ whereby carbon dioxide is taken out of the atmosphere, after release, by means of ‘enhanced capture’ in the bio-carbon cycle via a forest planting/management program, and an increased ‘plant biota agricultural program’ (IPCC, 1997; IPCC, 2001).

2. Oceanic ‘sinks’ whereby carbon dioxide is captured at a point source, and disposed of in deep ocean sequestration including ‘pluming’ of CO₂ at depth in deep-ocean pipeline schemes, ‘sinking’ of towed ‘dry-icebergs’ into deep-ocean trenches, and the injection of CO₂ below seafloor methane hydrate accumulations to form CO₂ hydrates (IPCC, 1997; IPC, 2001; Herzog, et. al., 2001).
3. Geological sequestration whereby carbon dioxide is captured at a point source and injected into the subsurface rock strata for long term disposal via subsurface reservoir-rock storage, coal-bed adsorption, or precipitation of carbon bearing minerals (Bachu, 2000; Cook, et. al., 2000, Bradshaw, et al., 2000).

Option #1 suffers from several limitations. The main limitation is that it captures, and then sequesters CO₂ after the release into the atmosphere. Other factors limiting effectiveness are the lag time required to take sufficient volumes of CO₂ out of the atmosphere by planting, the limited amount of arable land on the planet’s surface available for such an approach, and the fact that the sequestering time via the bio-carbon cycle may be limited to only decades, or even years, because the plants/trees eventually die, or are burned, and the CO₂ trapped in their tissue is released back into the atmosphere through decay.

The Royal Society, issued a report from a ‘Forest CO₂ Sinks Working Group’ which concluded that the ‘amounts of CO₂ that can be stored are small compared with emissions from ...fossil fuels’ (Royal Society, 2004). Furthermore, it concluded that the magnitude of the potential sinks were modest, and would be used up in a few decades. Stability is also an issue, cutting down the trees or natural decay will release the carbon once again, and conversion of the land to wetland may release methane, another greenhouse gas, back into the atmosphere. Global warming therefore can convert forest ‘sinks’ to ‘sources’ of carbon dioxide (BBC, 2001).

Option #2, ‘oceanic sinks’, is practically limited because it is not proven to be technologically sound, environmentally safe, and socially-politically acceptable. A recent computer study published by the American Geophysical Union (AGU) concluded that for underwater marine pipelines ‘...using computer models, carbon

dioxide particles of four millimeters or less can be released as a plume...' at the minimally safe depth of 600 meters, although 800 meters is still safer, and with the plume release point at 950 meters virtually no 'outgassing' occurs and the CO₂ stays in supercritical state (Drange, et al., 2001). The AGU authors proposed venting CO₂ at depth in the Norwegian North Sea where the acidic CO₂ plume would then be carried by current flows into the Atlantic Ocean at depth. They concluded the technology for such a CO₂ release into the oceans was currently possible, and the cost of engineering implementation might be cheaper than the current Norwegian government tax on CO₂ atmospheric venting from oil/gas production (Drange, 2001).

The AGU study emphasized that their theoretical, computer modeled conclusions must be studied further, including the result of large scale 'undersea plumbing'(Drange, et al., 2001). Drange's fellow researcher, Guttorm Alendal, stated, '...we foresee [at least] a 10 to 15 year time frame before this option can be used operationally' (Vendetti, 2001). Furthermore, continues Alendal, the project may not be environmentally sound as the '...potential dangers to marine life may be the biggest drawback of the whole procedure' (Vendetti, 2001).

The Japanese RITE program has also conducted research into the potential of ocean sequestration, and concluded it was technically and economically feasible (Masuda, 2001), but did not address the potential environmental impact. The Royal Society (2004) concluded that increasing acidity of ocean pH potentially represents an environmental risk and announced the funding of research to assess the impact.

Furthermore, the environmental risks posed by injecting or bubbling a CO₂ stream into deep oceanic waters also applies to other proposed 'oceanic sink' methods such as freezing CO₂ (dry-ice) and disposing of them in deep ocean sea beds, or injecting CO₂ to form hydrates (similar to naturally formed CO₂ and methane hydrates found on the sea bed and under onshore permafrost areas) on or under the immediate seafloor (Uchida, et al., 2001; Hirai, et al., 2001).

Option #3, 'geological sequestration' has been confirmed as economically viable, technologically feasible, and environmentally safe in many areas (Bachu, 2000; Cook, et. al., 2000, Bradshaw and Rigg, 2001). This research study aims to document and demonstrate this concept, and present a practical plan for the potential disposal of CO₂ at the Tangguh LNG development project in Papua, Indonesia.

2.0 PROJECT AREA BACKGROUND

The project area is located in Indonesia, and is associated with the Tangguh Liquefied Natural Gas (LNG) Project. The Tangguh LNG Project is being developed by BP, and comprises six offshore and onshore gas fields with a total reserve potential (proved, probable, and possible) reserve of generally ‘dry gas’ estimated at 24 trillion cubic feet (TCF) (Robertson and Downey, 2000). This large volume amounts to four billion barrels of oil equivalent (4 BBOE), and contains ~10% CO₂ (Kasim, et al., 2000). The subsurface data available from British Petroleum (BP), Atlantic Richfield Inc. (ARCO), British Gas (BG), and Pertamina are in ‘imperial units’ (ie. feet, inches, psi, etc.) although surface distances are given in ‘SI’ units (kilometers). Therefore, imperial units have been preserved in this study and all discussions, results, and conclusions are measured/referenced accordingly, although key outcomes have the equivalent metric (SI) unit listed in brackets after the imperial unit.

2.1 Location

The regency of Papua (formerly known as Irian Jaya), in the Republic of Indonesia, forms the western part of the island of New Guinea, the world’s second largest island after Greenland (Figure 2.1). The eastern half of the island is the independent sovereign state of Papua New Guinea. The island as a whole has an area of 868,000 sq km, and Papua covers 394,000 square km.

The northwest portion of Papua is known as the ‘Kepala Burung’, or Bird’s Head. The ‘mouth’ of the Bird’s Head is Berau/Bintuni Bay. The Tangguh LNG Project is the name of the liquefied natural gas (LNG) development program of several gas fields on three different Production Sharing Contract (PSC) blocks located in the ‘Bird’s Head’ region of Papua (Figure 2.2). The three natural gas production concessions are the Wiriagar PSC, the Berau PSC, and the Muturi PSC. The proposed location for the LNG plant and shipping terminal is on the south coast of Bintuni Bay, south of the Vorwata gas field, on the Babo PSC. The Wiriagar, Berau, and Muturi PSC’s encompass the primary gas fields slated for production, and are all currently operated by BP. Gas production for the Tangguh LNG Project is scheduled to begin in 2007.

BP operates two additional concessions in the area that are not currently involved in the Tangguh LNG Project development. These two blocks, the West Arguni PSC and East Arguni PSC, are exploration blocks located onshore to the

south, and offshore to the east in Bintuni from the Tangguh LNG Project gas fields (Figure 2.2).

2.2 Concession History And Current Status

The sedimentology and lithostratigraphy of Berau and Bintuni Basins is known from both outcrops and well data. Early explorers of the 20th century first documented some of the outcrop lithologies, when Papua was a Dutch colony, known as the Dutch East Indies (Pieters, et al., 1983; Pigram and Panggabean, 1981). The Dutch petroleum exploration company *Nederland Nieuw-Guineese Petroleum Maatschappij* (NNGPM), explored and drilled some of the first wells in the region, starting in the 1935 through 1962, including the earliest Wasian and Mogoi oilfield wells, followed in the 1970's to 1990's by field work and exploration drilling programs of Phillips, Total, Conoco, and Occidental Petroleum, Atlantic Richfield (ARCO), and British Gas (BG) (Visser and Hermes, 1962; Pieters, et al., 1983; Pigram and Panggabean, 1981; DeBoer, 2004; Dolan and Hermany, 1988; Perkins and Livsey, 1993; Fraser, et al., 1993).

The Wiriagar PSC is a relatively small block located onshore of the northern coast of Bintuni Bay and it lies over the culminating crest of a subsurface anticline of the same name. The onshore PSC was originally part of a much larger onshore concession, operated by *Nederland Nieuw-Guineese Petroleum Maatschappij* (NNGPM) in the 1930's through the early 1960's (Visser and Hermes, 1962). The NNGPM drilled the first two Wiriagar wells in 1939 and 1950 (Wiriagar-1 and Wiriagar-2 respectively) but both were dry holes (Dolan and Hermany, 1988). The earliest discoveries in the Bird's Head were made by NNGPM at the Wasian Field on the northern onshore edge of Bintuni Basin, and Jagiro Field in Salawati Basin. These oil discoveries were made in the relatively shallow Upper Miocene Kais Limestone Formation, and were generated from pre-Tertiary source rocks (Dolan and Hermany, 1988). After Irian Jaya was integrated into the Republic of Indonesia, the onshore block was named the Kepala Burung Selatan 'A' (KBSA PSC), which was acquired and explored by Conoco from 1977 to 1990 (Dolan and Hermany, 1988; Robertson and Downey, 2000).

Conoco exploration of the onshore KBSA PSC starting in 1977, resulted in the drilling of over 20 wells on the block. This exploration program led to the 1981 discovery on the Wiriagar-3 of a very shallow 'light oil' accumulation that flowed

3096 BOPD (Dolan and Hermany, 1988). Wiriagar (shallow) oilfield production of 37.3° API gravity ‘light oil’ from the shallow Miocene Kais Limestone Formation, approximately 3 km north of Bintuni Bay, eventually came online (Dolan and Hermany, 1988). Dolan and Hermany (1988) concluded the ‘oil’ was pre-Tertiary sourced, like the earlier Wasian and Jagiro discoveries, and noted the potential for deeper and pre-Tertiary liquid hydrocarbon reservoirs in Bintuni Basin.

The Wiriagar (shallow) oilfield was ultimately relinquished by Conoco and taken over by Pertamina, where production of ‘light oil’ continues on a limited basis with a large produced water cut. In 1993 ARCO acquired the new onshore Wiriagar PSC, consisting of a smaller portion of the KBSA PSC Production from this shallow carbonate ‘oilfield’ continues on a very limited basis to this day with a large water cut produced. The top of the production reservoir is at approximately 1532 ft TVDss (i.e. True Vertical Depth subsea). The volumetrics are very small with the total OOIP (original oil in place) estimated at only 3.5 MMBO (Dolan and Hermany, 1988). Atlantic Richfield Wiriagar Inc. (ARCO) acquired the small ‘Wiriagar PSC’ portion of the former Conoco block in the early 1990’s and spudded the Wiriagar Deep supergiant gas field discovery well in 1994 (Salo, 1994).

The Wiriagar Deep (WD) gas field was initially discovered on the Wiriagar Block in August 1994. Wiriagar Deep #1 was spudded in February 1994 and drilled to a total depth (TD) of 8500 ft, measured depth from the rotary kelly-bushing (RKB), by May 1994. While drilling the well gas and condensate shows were observed in Paleocene turbidites, fractured Cretaceous marl, and Middle Jurassic (Aalenian) sands, which when drill-stem tested (DST) cumulatively flowed at a rate of approximately 30 million standard cubic feet/day (MMscfd) of gas with 45 barrels of condensate per day (BCPD) (Salo, 1994). The Wiriagar Deep gas field was subsequently delineated as extending offshore to the Berau PSC in Bintuni/Berau Bay, based on interpretation of reservoir pressures (Salo, 1994). The areal extent of the gas field was confirmed with the Wiriagar Deep #2 well, drilled in 1995 by ARCO and Occidental Petroleum, plus minor partners (Salo, 1996c). The location of these two WD wells, and all of the subsequent appraisal and delineation wells are illustrated in Figure 2.3.

The offshore Berau PSC was originally licensed and explored in part by Phillips Petroleum Inc., the offshore concession was later acquired by Occidental Petroleum Inc through it’s wholly owned subsidiary Occidental Berau. Occidental

eventually drilled a total of three wells on the offshore Berau PSC, including three gas/condensate discovery wells, Roabiba #1, Ofaweri #1, and the Vos #1. The Roabiba #1 was spudded July 1990 on a small 'pop-up' structure atop the Wiriagar anticline. This well drilled to a TD of 12,007 ft RKB, and successfully tested gas at 23.6 MMscfd, and 37 BCPD from an interval of Middle Jurassic sandstones (perforations over depths 11,055 ft to 11,156 ft RKB). While the gas accumulation penetrated was relatively small, the well was highly significant as it was the first well to successfully test pre-Tertiary gas in Indonesia (Perkins and Livsey, 1993).

Following the Roabiba #1 discovery well test, Occidental shot a 1,706 line-kilometer 2D seismic survey over the Roabiba discovery and calculated this to be a non-commercial gas accumulation in a remote frontier area (Casarta, et al., 2004). Occidental then resumed their exploration program on the concession with a two well drilling campaign in May 1992. Two separate structures, smaller than Roabiba, were drilled with one exploration well each in the hope of making an oil discovery.

The first well of the new drilling campaign was the Ofaweri #1 testing a new structure approximately 11 km to the southwest of Roabiba #2. The well was a gas discovery well, having encountered and logged gas pay. This pay was wireline tested (RFT) with gas samples successfully recovered confirming moveable natural gas in Middle Jurassic sands (Perkins and Livsey, 1993). This structure was interpreted as smaller than the Roabiba structure accumulation (Bulling, et al., 1998).

The final well, Vos #1, explored yet another smaller structure 20 km southwest of Ofaweri, also encountering gas shows in Middle Jurassic sands. However, no tests were conducted although gas pay was recorded (Perkins and Livsey, 1993). The Vos #1 was Occidental's last well drilled on the block as operator. In February 1995, ARCO farmed-in to the Berau PSC, assuming a 60% interest and operatorship, under its subsidiary Atlantic Richfield Berau Inc.

The extension of the Wiriagar Deep gas field into the Berau Block was established by the drilling of the Wiriagar Deep #2, ARCO's first well on the offshore block. The well was spudded in September 1995, 15 km southeast of the Wiriagar Deep #1 location, as a delineation/appraisal well. The well reached TD in October 1995 at a driller's measured depth of 9755 ft (RKB). Approximately 450 ft of commercially significant net pay thickness was encountered and the well, when tested (DST), cumulatively flowed 110 MMscfd of gas from six intervals within Paleocene turbidite/debris flow channels and Middle Jurassic (Aalenian and Bajocian/Bathonian)

shallow marine sandstones (Salo, 1996c). Three additional offshore appraisal/delineation wells were subsequently drilled by ARCO for the Wiriagar Deep gas field on the Berau Block (Wiriagar Deep #3, #4, and #5), and a further three onshore appraisal/delineation wells were drilled on-structure on the Wiriagar PSC Block (Wiriagar Deep #6, #7, and #8) (Bulling, et al., 1998).

The Vorwata gas field was discovered by ARCO in February 1997 with the drilling and testing (DST) of the Vorwata #1 well, located on the eastern-most boundary of the offshore Berau PSC Block. The well cumulatively flowed 31 MMscfd of gas from perforated intervals in Middle Jurassic and Late Permian sands (Bulling, et al., 1998). An appraisal well, the Vorwata #2, was subsequently drilled and tested (DST) in May 1997, 17 km southeast, and downdip, from the Vorwata #1 location. The well flowed almost 34 MMscfd of gas.

After the discovery and testing of the Vorwata #1 well, ARCO sanctioned a 3D seismic survey in early 1997 covering Wiriagar, Berau, and Muturi PSC's. This survey would include all of the major gas fields discovered to date, namely Vorwata, Wiriagar Deep, Roabiba, Ofaweri, and Vos. This 3D survey totalled 1,708 square kilometres, including about 1,400 square kilometres of marine seismic survey with the remainder coming from Wiriagar Deep transition zone seismic survey (shallow marine and adjacent coastal) and land seismic survey (Figure 2.3). In addition, a 2D survey was acquired in early 1997 over the Ubadari prospect located west of the other gas fields.

In addition to containing a major portion of the Wiriagar Deep gas field accumulation, the Berau PSC also contains the major portion of the 'V' or 'Vorwata' supergiant gas accumulation. The gas accumulation is contained almost entirely in the Jurassic reservoir, trapped by a three-way dip closure of the Vorwata ('V') anticlinorium structure, also referred to as the Sebyar anticline/structure by Perkins and Livsey (1993). The name Sebyar refers to the anticline (Vorwata) previously penetrated with the drilling of the Sebyar #1 well onshore, by Total in 1986 (Perkins and Livsey, 1993). This onshore block was previously operated by Total Indonesia Inc. but was later relinquished by Total and incorporated as a partly onshore and partly offshore concession as the Muturi PSC, operated by British Gas Indonesia Inc. Ltd. (BG). Total's Sebyar #1 well drilled onshore on the northern flank of the Vorwata structure, well north of the Jurassic gas-charged sandstone reservoir limit

(Figure 2.3), and as such did not encounter the supergiant gas field accumulation (Perkins and Livsey, 1993).

When ARCO began drilling on the Vorwata structure in the Berau PSC, in 1996, British Gas (BG) began its' own exploration drilling program in the offshore portion of the adjacent Muturi PSC concession. The BG Muturi block lies generally to the east of the Berau PSC, but a small portion lies to the north of the eastern Berau PSC margin (Figure 2.3). BG chose to spud their first well, the Nambumbi #1, 5 km to the northwest of ARCO's Vorwata #1 discovery well, and encountered gas shows from a thin Jurassic sand that was unable to flow gas when tested (DST) due to poor porosity and permeability (Bulling et al., 1998). The second well drilled, the Sakauni #1, was located approximately 25 km east from Nambumbi #1 across a syncline from the Vorwata structure (Figure 2.3). The well was located north of the Middle Jurassic sandstone reservoir truncation line and resulted in a dry hole, eventually reaching TD in the Late Permian (Bulling, et al., 1998).

ARCO meanwhile drilled two further appraisal wells on their Berau PSC's Vorwata structure (Vorwata #3, and #4), which flowed 29 MMscfd and 36 MMscfd of gas, respectively, when tested (Bulling, et al., 1998). The second of these wells drilled in July 1997, Vorwata #4, also confirmed interpretations that the gas-charged closure crossed the Berau-Muturi boundary and was located, in part, on the BG Muturi PSC (Bulling, et al., 1998). An agreement was formed by ARCO and BG and well costs for the Vorwata #4, and some subsequent wells, were split between Berau and Muturi partners, with some data exchanges included.

A total of seven additional Vorwata appraisal/delineation wells were eventually drilled (Vorwata #5, #6, #7, #8, #9, #10, and #11) by ARCO, BG, or Berau/Muturi partners cooperative venture (Figure 2.3). These wells confirm a supergiant gas field within a Middle Jurassic (Bathonian/Bajocian) sandstone reservoir at the Vorwata structure. Many delineated the GWC (gas-water contact), while others encountered 'perched water' in the middle of the field (Bulling, et al., 1998).

In 1998, whilst ARCO was appraising/delineating the Vorwata gas field, the exploration well Ubadari #1 was spudded in August 1997 on the Ubadari prospect, located approximately 37 km southwest of the WD-1 well (Figure 2.3), and reached a TD of 8710 ft (RKB) in October 1997. The well, subsequently tested, flowed

significant gas and condensate rates from Middle Jurassic and Paleocene sandstone reservoirs.

An appraisal well, the Ubadari #2 tested the structure further to the south across a major fault closure, and encountered Paleocene sandstone reservoir, and thick downthrown Jurassic sandstone reservoirs, all devoid of hydrocarbon pay.

As a result of this comprehensive data collection, the proved, probable, and possible reserves in the six Bintuni Basin gas fields amount to 24 TCF (Robertson and Downey, 2000), and form the basis for the planned Tangguh LNG Project. Most of the reserves are contained within the Vorwata supergiant gas field, with production set to start in 2008 (BP, 2004).

3.0 EVALUATION OF GEOLOGICAL SEQUESTRATION OPTIONS

The environmentally safe and sustainable subsurface geological sequestration/storage of CO₂ holds the most promise for the immediate disposal of CO₂ from either wellhead hydrocarbon production or power-plant fossil fuel combustion effluents. There are several possible subsurface CO₂ disposal options that have been demonstrated to be potentially feasible based on either small-scale pilot-projects or large-scale commercial projects. These options are briefly summarized and are then addressed as to their respective applicability in the Tangguh Project located in the Bird's Head area of Papua, Indonesia.

The GEODISC (acronym for **GE**ological **DIS**posal of CO₂) project is a consortium of Australian governmental agencies, Australian academic institutions, and private industry companies. The GEODISC project has identified the various potential geological subsurface CO₂ sequestration options available, as ESSCI's (Bradshaw, et al.; 2000; Cook, et al., 2000; Rigg and Bradshaw, 2001; Rigg, et al, 2001). 'ESSCI' is the GEODISC derived terminology for a viable subsurface CO₂ injection and sequestration formation at a specific location site. The technically feasible subsurface geological sequestration/storage options, are as follows:

1. CUCS (CO₂ in unminable coal-bed sequestration)
2. CECMP (CO₂ for enhanced coal-bed methane production)
3. CDOGR (CO₂ in depleted oil/gas reservoirs)
4. CEOR (CO₂ for enhanced oil recovery)
5. CEGR (CO₂ for enhanced gas recovery)
6. CCV (CO₂ in cavity or void)
7. CSA (CO₂ in saline aquifer)

These seven potential geological subsurface CO₂ sequestration options are graphically illustrated in a cross-sectional schematic (Figure 3.1), modified after Bradshaw, et al. (2000), Cook and Rigg (2000), Rigg and Bradshaw (2001). The applicability and viability of each of these potential CO₂ sequestration options is, of course, dependant on the actual location (in both a regional as well as local context) being considered for potential CO₂ disposal or storage (Bachu, et al., 1994; Bachu, 2000; Bradshaw, et al.; 2000; Cook, et al., 2000; Beecy, et al., 2001; Rigg and Bradshaw, 2001). The Tangguh LNG Project has natural gas production planned,

starting in 2007 (BP, 2004). These natural gas accumulations are certified (proved, probable, and possible) at 24 trillion cubic feet of gas at standard surface conditions (TCFsc) of natural gas. These gas accumulations have a significant CO₂ content, estimated at ~10% of the reservoir reserves. This amounts to approximately 2.4 TCF(sc) of natural CO₂ to be disposed of, plus the emissions from the LNG production facility, which will likely be significant. The above potential geological subsurface CO₂ sequestration options are therefore examined in detail, specifically in regard to their respective applicability and viability in the Tangguh area of the Bird's Head region in Papua, Indonesia.

3.1 CUCS (CO₂ in unminable coal-bed sequestration)

The first option, injection of CO₂ into unmineable coal-beds (CUCS), has been proposed for GHG sequestration by several authors (Holloway, 1996; Byrer and Guthrie, 2001; Erickson and Jensen, 2001). The option is based on the fact that coal will preferentially adsorb CO₂ gas, but for practicality requires that the coalbeds are not likely to be mined. If mined, the excavation and crushing process would release all of the CO₂ intended for sequestration disposal (Holloway, 1996, Byrer and Guthrie, 2001). The option also necessitates, for efficiency and storage capacity that the coal bed/seam be areally extensive, with a minimum thickness of two feet (Byrer and Guthrie, 2001). Additionally, technical viability of this option dictates that the prospective coal bed/seam is in a drillable area, and that the seam itself possess coal characterizations favorable to injectivity and storage (i.e. suitable cleat and fracture character, suitable roof and floor rock, suitable coal rank, etc.) (Erickson and Guthrie, 2001). The feasibility of this option has been demonstrated where favorable conditions for the requirements detailed above exist, such as the San Juan Basin pilot project, conducted by BP Amoco in Colorado USA (Erickson and Jensen, 2001).

This subsurface sequestration option is impractical in the Tangguh Field region due to the lack of unusable coal seams. In the sense of 'unusable' being synonymous with 'unminable'.

The only known, documented coal seams in the Tangguh Project region exist in basal Middle Jurassic and Late Permian sedimentary rocks, and are on the order of 1 inch to 2 feet in thickness. As noted previously, for feasibility the coal bed/seam should be greater than 2 ft in thickness. Furthermore, the shallowest depth of burial for any of these coal seams is 7800 ft true vertical depth subsea (TVDss) at the

culminating crest of the Wiriagar Deep anticlinorium. Generally speaking, coals buried at depths greater than 7000 ft will generally lack sufficient microporosity, and significant geometry of open fractures and cleats (macroporosity), necessary to allow preferential adsorption of CO₂ to the coals (Hetherington and Thambimuthu, 2003; Ogha, et al., 2003; Obdam, et al., 2003). Therefore, the lack of significantly thick coal seams distributed over a large areal extent in the Tangguh Project region, at a reasonable burial depth that permits open fractures and cleats, renders this option technically impractical (Livsey, et al., 1992; Bullings, et al., 1998; Livsey and Charleton, 2000).

3.2 CECMP (CO₂ for enhanced coal-bed methane production)

The CECMP potential option has been documented by numerous authors (Bachu, 2000; Bradshaw, et al., 2000; Cook, et al., 2000; Rigg, et al., 2001; DOE, 2004), and the idea has been successfully implemented in both pilot projects (Hetherington and Thambimuthu, 2003) and small-scale commercial applications (Erickson and Jensen, 2001; Obdam, et al., 2003). The basic concept of CECMP is that a production well is drilled into a desirable coal seam with sufficient coal rank, microporosity, and fracture/cleat characterization to produce coal-bed methane (CBM). Coal rank is a quantitative description of the amount of ‘coal gas’, primarily methane (CH₄), present in any given grade of coal (Hetherington and Thambimuthu, 2003; Ogha, et al., 2003). The San Juan Basin, Colorado has a long established commercial CBM project in operation (Erickson and Jensen, 2001; DOE, 2004). In a variation on CBM production, a second injector well is drilled into the same producing coal seam, and CO₂ for sequestration and disposal is injected into the coal. The coal will preferentially adsorb carbon dioxide (CO₂) and release methane (CH₄), (Hetherington and Thambimuthu, 2003; Ogha, et al., 2003).

Furthermore, the same coal characteristics of the Tangguh region described above rule out the second option, namely that of CO₂ sequestration with enhanced coal-bed methane gas recovery (CECMP). There is no potential for coal-bed methane gas production in the Tangguh Field region because geological evidence to date (Livsey, et al., 1992; Bullings, et al., 1998; Livsey and Charleton, 2000) indicate a lack of coal seams/beds of appreciable thickness greater than 2 ft, in the immediate Bintuni Basin area, at relatively shallow depths. As with the CUCS option, the lack of sedimentologically significant coal seams, at a reasonable burial depth that permits

open fractures and cleats (macroporosity) with sufficient microporosity, makes the CECMP option non-feasible in the Tangguh Project region.

3.3 CDOGR (CO₂ in depleted oil/gas reservoirs)

The third option is the potential for injection of CO₂ into depleted oil/gas field reservoirs for sequestration (CDOGR). This option has been evaluated by Houghton (1997); IPCC (2001); Bradshaw, et al. (2000), Cook, et al., (2000), Rigg, et al., (2001), Rigg and Bradshaw (2001), Bradshaw, et al., (2003), Kuuusraa and Pekot, 2003) as potential one of the lowest risk CO₂ sequestration/storage site options due to a proven seal, reservoir, and trapping mechanism. There is also potential for cost reduction due to the presence of in-situ oil/gas production infrastructure, in terms of roads, pipelines, and possibly even the wellbores for injection (Kuuusraa and Pekot, 2003). There is a somewhat higher risk of seal breach due to pre-existing wellbores with reactive-CO₂ cement, however remedial non-reactive CO₂ cementation could potentially correct that risk (Celia and Bachu, 2003).

The CDOGR option is not a feasible potential option for the Tangguh area due to the lack of depleted oil/gas fields in the area with sufficient storage capacity. Production fields such as Wiriagar (shallow), Wasian-Mogoi, and various Salawati Basin fields currently have some continuing production, and as such are discussed in detail in section 3.5 CEOR (CO₂ for enhanced oil recovery). The Wiriagar shallow oilfield, has some limited production albeit with a large water cut from the Miocene Kais Limestone Formation, with a structural top depth of 1530 ft TVDss (Dolan and Hermany, 1988; Perkins and Livsey, 1993; Bulling, et al., 1998). The Wasian-Mogoi Fields also are shallow Miocene Kais Limestone Formation oilfields with some minor continuing production (Dolan and Hermany, 1988; Perkins and Livsey, 1993; Bulling, et al., 1998). Salawati Basin fields are also shallow Miocene Kais Limestone Formation oilfields with some minor continuing production (Bulling, et al., 1998). Whether considered for CDOGR sequestration or CEOR sequestration, the Wiriagar (shallow), Wasian-Mogoi, and various Salawati Basin fields suffer the same drawbacks that render them as unsuitable for CO₂ sequestration, shallow burial depth insufficient to keep CO₂ sequestered in a supercritical phase, a carbonate reservoir mineralogy reactive with, and prone to dissolution by, the acidic sequestered CO₂, and insufficient storage capacity. These are addressed in greater detail in section 3.5 CEOR.

3.4 CCV (CO₂ in cavity or void)

This option involves the subsurface geological sequestration of CO₂ in underground cavities and voids, and potentially includes abandoned mine shafts and tunnel complexes, salt domes, extensive fracture systems, and caves. These potential ESSCO sequestration/storage sites are discussed in detail regarding possible applicability in the Tangguh area.

3.4.1 Salt domes, mines, and tunnels

There are no known subsurface cavities or voids in the Tangguh area in the categories of unused (or active) mines or tunnels. There are also no known salt domes in the Tangguh area, or in the greater Bird's Head region. There is, however, a massive 'lost circulation' zone that has been encountered repeatedly in the drilling of wells in the Berau/Bintuni Bay area. The 'lost circulation zone' is in the Kais Limestone and Faumai Formations, which comprise a significant part of the New Guinea Limestone Group (NGLG). This lost circulation zone is probably due to a complex, widespread series of interconnected fractures and karstified subsurface sinkholes.

3.4.2 New Guinea Limestone Group (NGLG)

The NGLG that could feasibly be a CO₂ injection and sequestration/storage option for the Tangguh project, due to having vugs and fractures (Dolan and Hermany, 1988; Bullings, et al., 1998). A detailed discussion of the formation is presented in 5. LITHOSTRATIGRAPHY AND SEDIMENTOLOGY. The NGLG members from the base up consist of poorly defined units starting with the basal Eocene carbonates, the Oligocene Limestone, the Faumai Formation, and the Kais Limestone Formation (Figure 3.2). A brief overview of each is presented below.

3.4.2.1 Eocene carbonates

The Eocene carbonates have been identified in outcrops in the Sorong Fault/Shear Zone hills (SFZ), the Lengguru Thrust/Fold Belt mountains (LTFB), and the Kumawa-Onin-Misool (KOM) anticlinal ridge (Dolan and Hermany, 1988; Bullings, et al., 1998). It has rarely been seen at wellsite in the Berau/Bintuni Bay area from subsurface cuttings or cores, mainly due to massive 'lost circulation' whilst

drilling. The ARCO wells drilled in the Berau/Bintuni Bay to Wiriagar to KOM region have generally been drilled 'blind', that is with no drilling fluid returns, nor cuttings, to surface (Salo, 1996c; Salo, 1997a-g; Salo 1998a-b). The Eocene carbonates were seen on the Wiriagar Deep #1, and on some of the earlier Occidental Petroleum wells in the Bintuni Bay area, and is characterized by fractures and vugginess (Salo, 1994).

3.4.2.2 Oligocene Limestone Formation

The Oligocene Limestone Formation is thought to exist only in outcrops in the LTFB, the KOM peninsula, and in synclinal troughs in the Berau/Bintuni Bay subsurface. The fractured and vuggy carbonate character of the Oligocene Limestone Formation is supported by well logging data such as dipole sonic waveform analyses, and FMI/FMS Imaging, indicating vugs and open fractures (Bullings, et al., 1998).

3.4.2.3 Faumai Formation

The Faumai Formation is the Bird's Head regional name utilized by BP/ARCO for the Early Miocene member of the New Guinea Limestone Group (NGLG). Due to massive 'lost circulation' whilst drilling, all ARCO and BG wells drilled in the Berau/Bintuni Bay region have been drilled 'blind'. Limited wireline log data through this interval confirm this formation is very vuggy, with common open fractures, especially in the 'blind drilling' interval that extends from the overlying Kais Limestone Formation through to the underlying Eocene Succession.

3.4.2.4 Kais Limestone Formation

This massive carbonate lies unconformably atop another massive carbonate sequence, the Faumai Formation, and as such is the top-most member of the NGLG. The shallowest portion of the Kais Limestone Formation is an oil (retrograde condensate) producer in numerous small, shallow, local fields in the Tangguh Project area. These fields include the Wiriagar Shallow retrograde condensate field on the Wiriagar PSC, the Wasian-Mogoi oil fields on the Muturi PSC, and various fields in the Salawati basin (Visser and Hermes, 1962; Dolan and Hermany, 1988; Perkins and Livsey, 1993; Bullings, et al., 1998). The top of the Kais Limestone Formation, and the hydrocarbon production is quite shallow ranging from 1530 ft to 2700 ft, with the

seal being the claystones of the overlying Plio-Pleistocene Steenkool Formation (Dolan and Hermany, 1988).

The base of the limestone is commonly fractured and vuggy, and prone to total loss of drilling fluid returns on wells (Dolan and Hermany, 1988; Perkins and Livsey, 1993; Salo, 1994; Salo, 1996c; Salo, 1997a-g; Salo, et al., 1997; Salo 1998; Bullings, et al., 1998)

There is no competent seal or cap intervening between the lower NGLG members briefly described earlier (such as the Eocene carbonates, Oligocene Limestone Formation, and the Faumai Formation), and the NGLG's top-most member, the Kais Limestone Formation. Therefore, the only effective seal for the entire NGLG is the Steenkool Formation.

3.4.2.5 Nonsuitability of the NGLG for CO₂

The lack of data regarding the NGLG, due to lost circulation and 'blind' drilling makes the formation and individual members a very high risk based on the data quantity and quality (or lack thereof, regarding both).

The fractured and vuggy nature of the NGLG, particularly the subsurface karstified nature of the Faumai Formation and the Kais Limestone Formation, might make the NGLG appear to potentially possess good injectivity and large storage capacity for possible CO₂ sequestration/storage, however the direct communication the fractures provide from the underlying members to the overlying Kais Limestone Formation poses a high risk for potential CO₂. The top depth of the NGLG Formation structural crests between 1530 ft and 2700 ft in most areas of Bintuni Basin places the base seal at or above the minimum depth of ~2600 to 2700 ft TVDss to keep sequestered CO₂ in a supercritical phase (Bachu, et al., 1994, Bachu, 2000; Ennis-King and Paterson, 2001).

Carbonate mineralogy is not desirable for sequestration reservoir composition. According to Watson, et al. (2003a and 2003b), calcareous minerals including limestone dissolve in the presence of supercritical CO₂ due to complex geochemical reactions of the carbon dioxide with Ca rich mineral groups. This dissolution of limestone can result in a lack of matrix strength within the reservoir, which is an undesirable reaction to the sequestration/storage of CO₂ in the subsurface.

The lack of sufficient data quality and quantity regarding most of the NGLG interval, the fractured and vuggy nature of the reservoir's primary porosity, the

carbonate reservoir mineralogy that is prone to dissolution by CO₂, and the shallow depth of the base seal above the average depth to maintain a supercritical CO₂ phase, all pose a high risk for sequestration within the NGLG. Each of these factors, on its own, preclude the NGLG from being considered a viable, and environmentally sustainable ESSCI site for CO₂ sequestration.

3.4.2.6 Nonsuitability of CDOGR for CO₂

Wiriagar shallow, Wasian-Mogoi, and the various Salawati Basin fields are all mature production fields that are either still lingering in production, or have been shut-in recently due to high water cut volumes. They are all unsuitable, however, for Tangguh LNG Project CO₂ sequestration.

Three of them are actually situated locally to the Tangguh Project area, and these are the shallow Wiriagar shallow field (retrograde condensate), Mogoi, and Wasian oilfields (Dolan and Hermany, 1988; Bulling, et al., 1998). All three are located in the Tangguh Project development area (Figure 3.3). The Wiriagar shallow condensate field lies over the culminating crest of the Wiriagar Deep gas accumulation on the onshore BP Wiriagar PSC block, and the Wasian and Mogoi oil fields are located on the British Gas (BG) Muturi PSC block. Unfortunately, these fields all have the same drawbacks as potential CO₂ sequestration sites; a lack of sufficient storage capacity; a shallow depth for reservoir top/base seal, preventing storage of CO₂ in a supercritical phase; and unsuitable reservoir host mineralogy. These drawbacks are discussed in detail separately.

3.4.2.6.1 Insufficient Storage Capacity

The shallow Kais Limestone oilfields in Bintuni Basin have estimated reserve volumes that are extremely small (proved plus probable), therefore, the ‘value-added’ additional recoverable reserves are negligible. Wiriagar shallow field is estimated to have had 3.9 MMBO (millions of barrels) of ‘original oil in place’ (OOIP), with 2 MMBO recoverable (~50% recoverable), the Wasian Field had 35.4 MMBO OOIP, with 7 MMBO recoverable (~20% recoverable), and the Mogoi Field had 58.7 MMBO, with only 11.7 MMBO recoverable (~20% recoverable) (G. Perez, personal communication, 2001). The small volumes these shallow fields can potentially sequester is so small that significantly greater CO₂ storage capacity would be needed to dispose of the Jurassic reservoir CO₂ volumes. Even together, these three ‘almost-

depleted' fields in the region are still not viable as CO₂ injection/sequestration sites for the estimated 2.4 TCF_(SC) of CO₂ to be disposed of at the Tangguh LNG Project.

3.4.2.6.2 Supercritical Phase Instability

All of these shallow fields in the Kais Limestone Formation have the handicap of being too shallow for viable CO₂ injection/sequestration. The increased CO₂ density when in a supercritical state, allows a greater CO₂ volume to be sequestered in the containment area, and also reduces the buoyancy pressure exerted on the base of the top-seal. One of these factors greatly lessens the seal risk factor of CO₂ injection/sequestration, and the other factor greatly increases the potential storage volume of the containment lithology. Both factors are dependent upon the CO₂ being in a 'supercritical' state.

In a gaseous non-critical state, CO₂ it is extremely mobile and voluminous. As originally identified by Holloway (1996) and Holloway, et al. (1996), and confirmed also by Ennis-King and Paterson (2001) as part of the GEODISC Project in Australia (See Figure 1.11). The exact temperature and pressure with depth, vary according to specific location, but in generally in most areas, due to overburden the confinement pressure below ~2600 ft. (~800m) is greater than 1,071 psi (7.38 megapascals or MPa), allowing CO₂ to remain in a supercritical state.

The Wiriagar shallow field is located at a mere 1532 ft TVDss (Dolan and Hermany, 1988) and therefore would be above the minimal depth for keeping a CO₂ in a supercritical phase. The top of the Kais Limestone Formation is a mere 502 ft for the Jagiro sub-field of the Mogoi, 1030 ft for the main Mogoi Field, and 2700 ft for the Wasian Field (Perez, G, personal communication of BP in-house data, 2001). In all of these cases, the top reservoir depth is far less than the requisite 2600 ft to keep CO₂ in a 'supercritical' state, except the Wasian Field, where the top depth of 2700 ft is uncomfortably close to the 2600 ft average minimum depth.

Given the lack of intra-NGLG seals, there is every reason to suppose that injection anywhere into the NGLG carbonates would lead to communication with the Faumai Formation and ultimately the top-most Kais Formation. Certainly the oil or condensate 'charge' to the Wasian, Mogoi, and Wiriagar shallow fields occurred through fractures and faults from the base of the NGLG to the top-most member, the Kais Limestone Formation (Dolan and Hermany, 1988; Perkins and Livsey, 1993).

The seal capacity of the overlying Steenkool formation is not known with certainty, however, the widespread presence of leakage from the numerous small hydrocarbon fields in the Kais Limestone Formation (Wiriagar Shallow, Wasian-Mogoi, and the Salawati Group Fields) with small original formation pressures indicates that the seal capacity of the Steenkool is not very good (Figure 3.4). Furthermore, numerous oil seeps at surface in the Bintuni Basin area support the notion that the Steenkool seal has been breached by low in-situ pressure oil accumulations at many locations (Perkins and Livsey, 1993). The injection of a supercritical state CO₂ into a strata at a confining depth of less than 2600 ft, with an estimated pore pressure of less than 8 MPa, could ultimately lead to the CO₂ flashing into a full gaseous phase and result in breaching of the Steenkool seal with relatively small pressures.

3.4.2.6.3 Unsuitable Mineralogy

The third mitigating factor is that the prospective NGLG host reservoirs/aquifers are all carbonate varieties, in the form of limestone, dolomites, ankerites, and iron-calcites. Recent studies indicate that carbonate reservoirs/aquifers, particularly the limestone (Ca-rich) end member are far from ideal as suitable CO₂ sequestration strata due to CO₂-reactivity and dissolution (Watson, et al., 2003a; Watson, et al., 2003b).

The sequestration of CO₂ in carbonate reservoirs is not recommended (Holloway, et al., 1996) due to geochemical reactions of injected CO₂ with carbonate minerals. Research shows that injection of CO₂ into carbonate media leads to dissolution of the carbonate minerals in the vicinity of the injection well, and as the injected CO₂ migrates away from the borehole, carbonate minerals precipitate out as pressure reduces or temperature rises, thereby reducing effective permeability and the ability to inject further amounts of CO₂. The subject of CO₂ equilibrium within carbonate reservoirs still an ongoing research topic (Riding, et al., 2003; Watson, et al., 2003b). However, the results of a technical literature review suggest that carbonate reservoirs lacking in-situ CO₂ will not be in equilibrium with injected CO₂ gas (supercritical or otherwise), and run the risk of reservoir dissolution immediately around the injection borehole (Holloway, 1996; Watson, et al., 2003a and 2003b). New carbonate minerals could subsequently be precipitated away from the borehole that could occlude permeability (Holloway, 1996; Watson, et al., 2003a and 2003b).

A ‘sealing reaction rim’ due to occluded permeability from newly precipitated minerals could stop the migration of injected CO₂ and potentially cause a pressure build-up around the injection borehole. Furthermore, there is the distinct possibility that the initial dissolution of carbonate minerals around the immediate borehole vicinity could cause subsidence in the overlying strata (including the seal). It is possible that subsidence of the ‘cap-rock’ could pose a significant risk to seal integrity, possibly resulting in a catastrophic seal breach with an escape of CO₂ to the surface (Holloway, 1996).

3.4.2.6.4 Karstification

The massive NGLG carbonate sequence is mostly a lost-circulation zone. More than 26 out of 30 wells that have penetrated the entire Tertiary section in the Tangguh Project area have had totals to near-total losses in circulation whilst drilling (Bulling, et al., 1998). This resulted in a dearth of data over of the interval. Little, if any, drill cuttings were successfully lagged to surface. Wireline logging operations became difficult in most of these boreholes, which required constant ‘topping-up’ with drilling fluid to minimize the risk of deadly H₂S gas blowouts. The complete loss of circulation can be traced to the vuggy and fractured nature of the NGLG carbonates. This has been verified by the FMI/FMS images obtained with great difficulty on a handful of wells in the area (Bulling, et al., 1998), and also from seismic survey amplitude slices over the Tangguh area of Bintuni Basin (Davis, N, personal communication, 2002). Geologically, this fractured and vuggy characterization was ascribed to karstification of the carbonate during the Miocene (Dolan and Hermany, 1988). This karstified nature of the NGLG in the Tangguh Project area precludes these formations, and all other members of the NGLG, from being considered a viable, and environmentally sound ESSCI site for CO₂ sequestration.

3.4.2.6.5 Salawati Basin Distance

The drawbacks detailed above for the Wiriagar shallow, Wasian, and Mogoi near-depleted shallow fields, also apply equally to the various Salawati Basin fields. The Salawati Basin is located almost 300 km. (approximately 200 miles) to the NW of the proposed BP LNG plant location, and as such is not in the immediate vicinity of the Tangguh LNG Project (which lies entirely in Bintuni Basin). While economic

costs and environmental issues will not be discussed in detail here, these are certainly drawbacks to be considered in regard to suitability of Salawati CO₂ injection/sequestration. The Salawati Basin fields are all located a considerable distance from the Tangguh project area (almost 300 km from the proposed LNG plant). Salawati Basin is therefore in BP's 'Economic Development Area IV' in Berau/Bintuni Bay, and considered by BP to be 'economically difficult to develop' (BP, 2002).

Ultimately, however, a more detailed consideration of the Salawati Basin is beyond the contracted scope of this study, as it would require access to non-BP, proprietary Salawati Basin data a unique CO₂ geological sequestration study, and detailed basin model.

Therefore, the Salawati Basin fields are unsuitable as potential ESSCI sites for the same technical reasons as the Wiriagar shallow, Wasian, and Mogoi fields, but also suffer the added drawback of being located a considerable distance of almost 300 km away from the anticipated point-source, the proposed LNG plant location.

3.5 CEOR (CO₂ for enhanced oil recovery)

The potential for CO₂ sequestration in a reservoir with enhanced oil recovery (CEOR) has been discussed in detail in the previous section of CO₂ sequestration in a depleted oil or gas reservoir (CDOGR). The only potential fields are the Bintuni Basin near-depleted fields of Wiriagar shallow, Wasian, and Mogoi and they are not suitable as potential ESSCI sites. Likewise, the more distant, Salawati Basin fields suffer from the same nonsuitability and also suffer from greater distance from the anticipated point source of the CO₂ in Bintuni Basin.

3.6 CEGR (CO₂ for enhanced gas recovery)

The potential for CO₂ sequestration in a reservoir with enhanced gas recovery (CEGR) in the Bintuni Basin area is not viable because of a lack of depleted gas fields in the area. The only gas fields in the Bintuni Basin area are the yet to be produced deeper fields such as Vorwata, Wiriagar Deep, Roabiba, Ofaweri, Wos, and Ubadari (Bulling, et al., 1998).

In regards to CEGR it should be noted that U.S. Government DOE (Dept. of Energy) reports conclude that: 'Carbon sequestration offers the oil and gas industry a

major opportunity for a new, economic value-added industry, that simultaneously reduces CO₂ emissions and increases ...oil and gas supplies' (Beecy, 2001).

If the injected CO₂ can be confidently modeled to migrate slowly towards the natural gas accumulation up-dip, the CO₂ can actually be utilized to maintain reservoir pressure during production phase, and provide some contributory increased efficiency to the 'sweep' of the reservoir ahead of the formation water-front drive. However, should be noted that the sweep efficiency of CO₂ at the depths envisioned for injection and sequestration into these deeper gas fields have been shown to be of minor added 'value' or 'efficiency' (Ennis-King and Paterson, 2001). Therefore, the main purpose would be for the sequestration of the CO₂ and not for the enhanced gas recovery aspect.

3.7 CSA (CO₂ in saline aquifer)

The injection and sequestration CO₂ into a saline reservoir/aquifer (CSA) has not only been proposed but has been demonstrated to be technically feasible, and environmentally sustainable in both laboratory studies and commercial projects. This is the subsurface geological sequestration methodology used in the Sleipner Project in offshore Norway (Holloway and van der Straaten, 1995; Chadwick, et al., 2003;). In the Sleipner project, the CO₂ separated and captured from natural gas production is injection and sequestered in the Utsira Sandstone saline aquifer (Holloway, 1996; Czernichowski-Lauriol, et al., 2003).

3.7.1 CSA in non-hydrocarbon bearing structural traps

The option is technologically sound, geologically feasible, and environmentally safe and potentially sustainable over a long geological timeframe (Holloway and van der Straaten, 1995; Holloway, 1996; Chadwick, et al., 2003; Czernichowski-Lauriol, et al., 2003). There are two potential structures in the Tangguh area that contain saline aquifers within dip-closed or dip/fault closed structural traps with no significant hydrocarbon accumulations. One structure is the Kalitami structure, which is part structural dip closure and part stratigraphic trap closure of sandstone units along the N-S trending Sekak Ridge (Figure 2.4). A single well was drilled into the structure, during the 1970's by Phillips Petroleum (the Kalitami-1X), and it encountered sandstone stratum of various ages, and at various

depths, with no hydrocarbon accumulations noted (Perkins and Livsey, 1993; Bulling, et al., 1998).

The second possibility is the ‘S’ structure, sometimes referred to as the ‘Sartu’ structure. This structure might appear promising due to proximity to the proposed LNG plant location, which is directly over the subsurface structural closure of ‘S’ and has been seismically interpreted as having four-way dip closure, but has yet to be drilled (J. Marcou, personal communication, 2002). However, there is a high probability that any reservoirs encountered in exploratory drilling on the ‘S’ structure could have significant hydrocarbon accumulations, since this structure appears to lie directly in a hydrocarbon migration fairway from the Bintuni basin deep kitchen area (Figure 3.5).

3.7.2 CSA in hydrocarbon bearing structural traps

There is also the potential option of injecting CO₂ into the water leg, down-dip of a hydrocarbon accumulation, within a structural trap with proven containment. This would potentially allow consideration of all of the structures with known hydrocarbon accumulations in the Tangguh area, (in addition to the ‘S’ structure should future drilling result in a additional discoveries).

If considered for application in the Tangguh project then this option potentially overlaps with the option mentioned in section 3.6 CEGR (i.e. CO₂ sequestration with enhanced gas recovery), due to the potential for enhanced gas recovery (even if the ‘added production drive’ or ‘added-value’ is relatively small). In the case proposed for Tangguh, CO₂ could be injected into the down-dip water leg of the primary natural gas production reservoir concurrent with the production, at up-dip locations, from the same reservoir.

This novel application of injecting into the down-dip water-leg of the hydrocarbon reservoir opens up the potential for CO₂ injection and storage in the primary gas reservoirs at Tangguh, including the Middle Jurassic sandstone reservoirs in the Vorwata, Wiriagar Deep, Ubadari, Roabiba, Ofaweri, and Wos structural closures.

4.0 REGIONAL TECTONIC AND STRUCTURAL HISTORY

A review of previously published data regarding the Bird's Head tectonic and structural history is presented with a new interpretation, in light of new and original detailed sequence stratigraphy carried out for this thesis.

Papua is the eastern-most reGENCY in Indonesia, located on the island of New Guinea. The northwestern portion of Papua is referred to as the 'Bird's Head' region (Kepala Burung) because of resembling the head of a bird. Bintuni Basin is a foreland basin in the Bird's Head that formed west of the leading thrust fault of the Lengguru Thrust/Fold Belt (LTFB) (Figure 4.1).

The Bird's Head region has a complex, and poorly understood tectonic and structural history and has been given short shrift in the geological literature, with the broader continental tectonic reviews covering Australian-New Guinea often lumping the western Kepala Burung region together with all of the New Guinean terranes (Scotese, 2000). Most of the detailed 'New Guinean' tectonic studies simply terminate maps and cross-sections at the base of the Bird's Head, and ignore the Bird's Head 'tectonic microplate' in most discussion (Ali, et al., 1985). The literature presenting the tectonic and structural history for the Bird's Head often has conflicting models or conclusions (Veevers, et al., 1986). The lithostratigraphy of the northern Australian/New Guinean margin is poorly documented due to the lack of well penetrations and the large area (Livsey and Charlton, 2000).

The complex geological history of the Bird's Head area can be traced back, with some relative certainty to the late Paleozoic as part of the 'Pangean' supercontinent, and the subsequent Mesozoic breakup into 'Gondwanaland', through the Quaternary tectonic collision phase that resulted in the formation of the Bintuni foreland basin to the west, and the LTFB to the east in the Bird's Head microplate or micro-continent (Pigram and Davies, 1987; Fraser, et al., 1993; Hall; 1996).

4.1 Paleozoic

Most of the southern portion of the island of New Guinea shares the same tectonic plate as the Australian continent, often referred to as the Australian-New Guinea plate, or ANGP (Veevers, et al., 2000).

During the Paleozoic, most of the earth's landmasses were joined together in supercontinental tectonic settings named 'Laurasia', 'Pangea', and 'Gondwana'. The geological history of the Australian-New Guinean plate during the Paleozoic is

difficult to unravel, because of deep burial and subsequent deformation (Scotese and McKerrow, 1990; Metcalfe, 1996; Veevers, et al., 2000).

The cratonic blocks of South America, Africa, Antarctica, India, Australia and New Guinea, as well as their associated intracratonic and peri-cratonic basin systems, comprised the Gondwana supercontinent from, at least, the Cambrian through the progressive onset of continental breakup completed during the Mesozoic (Veevers, et al., 2000).

During the Late Carboniferous, Permian, and Early Triassic the South Pole was located within, or very near, the Australian continent (Embleton, 1986; Veevers, et al., 2000).

Gondwana drifted to become virtually centered over the paleo-South Pole during the Carboniferous/Early Permian Period, with massive polar glacial ice sheets covering large portions of the landmass. While there is no direct evidence of glaciation on the New Guinea landmass, there is ample geological evidence of 'continental ice-sheet glaciation' on the Northern Australian Craton (Veevers, et al., 1986; Scotese and McKerrow, 1990; Metcalfe, 1996; Schmidt and Clark, 2000; Veevers, et al., 2000). The Bird's Head region was situated between 45° south during the Late Carboniferous and 60° south by the end of the Permian. While the northern most limit of this Carboniferous/Permian paleo-glaciation is unknown, geological evidence supports the approximate mapping of continental glaciation as far north as the Gulf of Carpentaria area, and highlands glaciation as far north as the Townsville area on the northeast margin (Embleton, 1986; Veevers, et al., 2000).

During this period, the Bird's Head region and the entire north west shelf margin of Australia and the northern New Guinea margin of the plate had a cool temperate climate with peat bogs forming on subaerially exposed fluvial/lacustrine sediments (Bradshaw, et al., 1988; Scotese and McKerrow, 1990; Livsey and Charlton, 2000; Bradshaw, et al., 1994b; Veevers, et al., 2000; Scotese, 2000). These peat bogs would eventually be preserved in the geological record of the Bird's Head region as the Middle to Late Permian coals and carbonaceous shales encountered in the Wiriagar Deep and Vorwata wells. The organic rich coals and carbonaceous shales of the Late Permian, with high total organic content (TOC) and relatively high hydrogen indices (HI), are thought to be some of the primary source rock of the Bintuni/Berau Bay hydrocarbon fields (Chevallier and Bordenave, 1986; Dolan and

Hermany, 1988; Perkins and Livsey, 1993; Salo, 1994; Salo, 1996a-c; Livsey and Charlton, 2000).

It was during the Permian, that a major rifting event, known as the Tethys-oceanic extension, occurred in the 'Pangean Supercontinent'. This concept of a Late Paleozoic and Mesozoic paleo-oceanic basin, originally suggested by Dr. Suess in 1893 (Tollman and Krystan-Tollman, 1985), formed as part of a scissor-like extensional rifting between the Eurasian northern Pangea landmass and the Australian-Antarctic-Indian-African southern landmass of Pangea is still widely accepted. The Tethys is defined by a unique set of fauna, facies, paleogeography and tectonics, and comprises Permian, Triassic, Jurassic, Cretaceous, and finally Paleocene marine and non-marine sedimentary rocks (Tollman and Krystan-Tollman, 1985).

The oldest sedimentary rocks identified in Bintuni Basin wellbore cuttings are Late Permian continental coals and fluvial to lacustrine clastic rocks with occasional latest stage Permian marine rocks as indicated by palynological (Waton et al, 1994, 1996a-e, 1997a-i) and ichnological facies analyses (Pemberton 1997a-e). Paleoenvironmental mapping indicates that cool temperate peat bogs formed during the Late Permian Period over the Bird's Head area (Scotese 2000). Cool temperate fluvial clastics and peats were deposited on the broad Permian plains of the Bird's Head, not unlike the Siberian peat mires of today (Lang, et al, 2000). These Late Permian peat mires and fluvial clastic sediments would eventually become the coal and carbonaceous shale deposits identified in drill cuttings in the Tangguh area (Salo, 1994; Salo, 1996c). This was the initial deposition of terrestrial organic matter in local sediments, which would ultimately source thermogenic natural gas in the Bird's Head region (Harrington, 1997). These coaly/carbonaceous sedimentary rocks share the gas-prone characteristics of many Australian coal basins such as the Bonaparte Basin, Perth Basin, Cooper Basin, Bowen and Sydney Basins (Harrington, et al, 1989).

A large extinction event involving a record number of species coincided with the rapid global warming at the Permo-Triassic boundary. The mass extinction event occurred at 250 Ma (the end of the Tartarian Stage), with paleontological fossil evidence indicating that as many as 96% of all marine species became extinct, almost 80% of all terrestrial vertebrate families were lost, and large proportion of terrestrial plant species disappeared (Hallam, 1998). Various mechanisms have been proposed

for the P/Tr Boundary rapid global warming and mass extinctions, including the Bedout bolide impact on the paleo-NW Shelf margin of the ANGP (Becker, et al., 2004), solar or cosmic radiation fluctuations (Shaviv and Veizer 2003), and unprecedented volcanic activity (Retallack, 1990).

The Berau/Bintuni Bay wellbore cuttings and cores also confirm that the Permian terrestrial non-marine and marine palynomorphs are overlain by oxidized Triassic clastics and evaporites at the East Onin #1 well location (Salo, 1996a and 1996b). The Triassic evaporite and red-bed sedimentological facies are widespread in many parts of the world (Figure 4.12) according to Tollman and Krystan-Tollman (1985). Denison and Koepnick (1995) estimates that the global oceanic coverage of the continents during the Late Permian was less than at any other time. By the earliest Triassic, the climate in the Bird's Head was warm and arid (Scotese 2000).

4.2 Mesozoic

The opening of the Tethys seaway commenced in the very Late Carboniferous, in the eastern most portion of Pangea, with the development of a scissor-like extension rifted from the east to west. Initially, the southern Pangean landmass, composed of the present-day New Guinean micro-continent/Australian plate/Indian plate, rifted from the northern Pangean landmass with the suture running just south of the present-day Indochina/Afghanistan boundary of the Eurasian continent (Yeates, et al., 1987). By the Middle Triassic the rift had reached the Rif area between Spain and Morocco (Ali, et al., 1985).

The development of the Tethys from east to west can be characterized by a similar series of geological facies, and marine flora and fauna, concurrently tracking the event over time. Tollman and Krystan-Tollman (1985) described the Triassic sedimentary sequences and fossils from 'Spain to Timor to Indonesia' as being distinctly unique and typical of the Tethys rift event.

Triassic sedimentary rocks, in the rare instances where they are encountered in the Bird's Head region, are described as red-beds (Visser and Hermes, 1962) indicating a period of prolonged subaerial exposure and oxidation in an arid environment of the Bird's Head. These Triassic red-beds are limited in aerial extent to the Onin/Babo area of the southern Bird's Head, and are absent north of the current southern Berau/Bintuni Bay shoreline, due to an erosional unconformity, and also to the south in the Arafura Sea area (Visser and Hermes, 1962; Bradshaw, et al, 1990;

Salo, 1996a-b). In addition to the extensional rifting of the Tethys which tore the Pangean supercontinent apart, two distinct arms of the Tethys opened up, a northern branch ('Paleo-Tethys') and a more southerly branch ('Tethys Ocean'), as indicated by Scotese (2000). Two additional results occurred from this: 1) there was rapid deepening from the rifting to both arms of the Tethys, with basic igneous rocks, and deep sea sediments deposited, and; 2) flat marginal seas formed along the Tethys borders with evaporates commonly deposited during the Triassic on sabkha coastal plains and on failed marginal shallow rifts (Tollman and Krystan-Tollman, 1985; Yeates, et al., 1987).

Triassic strata of the Bird's Head region indicate an arid, coastal plain possibly with evaporitic pans (a 'sabkha plain' paleo-depositional environment not unlike the present day NW Australian coastal margin) located very proximal to the southern landmass' Tethys marine margin. Occasional marine pulses intercalated with a continental depositional environment have been identified by palynological analyses (Waton, et. al., 1996e). Where the Triassic sediments exist in the southern Bird's Head, they generally consist of continental sedimentary rocks, including evaporites and sub-aerially exposed and oxidized clastics ('red-bed' shales and silts), as described by Visser and Hermes (1962). The Triassic Tipuma Formation (originally spelled in the Dutch variant as Tipoema), is composed of green and red mottled claystone and siltstone with vugs interpreted as evaporite dissolution cavities (McConachie et al, 2001). Wellbore cuttings from the East Onin #1 encountered evaporitic phases (anhydrite and melanterite) from the earliest 'Jurassic to Triassic(?)' interval (Waton et al, 1996e), based on petrographic analysis and XRD (Salo 1996a-b).

This lithostratigraphy of the Bintuni/Berau Bay wells broadly correlate with the Tethys-rift development, the global paleo-environment, and the overall geological history of the continents. From the Permian through Triassic, the regional Tethys extension led to the development of a major intracontinental rift system that lay inboard of an Andean-type arc through eastern Indonesia and northern New Guinea (Charlton, 2000a).

Warm, well-drained environments extended over much of the continental landmasses, and even Polar latitudes experienced warm temperate climates. The Mesozoic Era may have experienced the warmest global environment in the last 550 million years of Earth history (ie. since the beginning of the Paleozoic Era).

On a first order scale, global eustacy swung from a massive low-stand during the cold to cool temperate Permian environment, to a global transgressive event that reached a highstand during the middle Late Triassic. First order, global eustacy fell during the very Late Triassic, continuing into the Early Jurassic. A transgressive system tract then began during the Pliensbachian (middle Early Jurassic), only reaching the same Triassic highstand relative global sealevel during the Toarcian to Aalenian stages (Middle Jurassic). Berggren, et al. (1995) concluded that from the Pliensbachian, relative mean sealevel rose slowly but steadily until the mid-Tithonian of the Late Jurassic, when a slight regressive event occurred, to be followed by the earliest Cretaceous when sea level rose sharply (based on both, Hallam's 1992 Long-Term Eustatic Curve, and Haq's 1987 Long-Term Eustatic Curve recalibrated to Gradstein 1994, and Berggren, et al., 1995).

Whatever the cause of this global warming and the unprecedented rise in mean sea level starting at the end of the Permian, it culminated with the global highstand and maximum flooding surface of the Late Cretaceous. The global transgression and subsequent highstand, combined with a northwesterly current direction associated with the peak of the continental breakup (Ali, et al., 1985), had a major impact on the local depositional geology of the Bird's Head region.

During the ensuing transgressive phase of the Triassic, only limited continental areas were drowned, and the hot and arid climate resulted in the continued continental deposition of fluvial clastic sediments, paleosols, and occasional evaporites, leaving classic Triassic 'red-beds' preserved in only a spotty manner across the Bird's Head region (Retallack, 1990; Retallack, 1995). Increased erosional rates in the Arafura Sea area of the ANGP margin, south of the Bird's Head, during the Late Triassic and earliest Jurassic, resulted in most of the Triassic section being stripped off (Bradshaw, et al., 1988; Bradshaw, et al., 1990).

In the earliest Jurassic, the Bird's Head region was still associated with the southern 'Pangean' landmass consisting of Australian/Antarctic/Indian 'supercontinent' (Veevers, et al., 1986; Yeates, et al., 1987; Bradshaw, et al., 1988; Bradshaw, et al., 1994a; Bradshaw, et al., 1994b; Veevers, et al., 2000). Bordering on the southern margin of the Tethys marine coast, the 'Australian-New Guinean' continental margin was to undergo an important phase of geological history, this prolific extensional basin area of the north western margin of Australia has been dubbed the 'Westralian Superbasin' by some authors (Yeates, et al., 1987; Bradshaw,

et al., 1988; Bradshaw, et al., 1994a; Bradshaw, et al., 1994b; Veevers, et al., 2000). In the Berau/Bintuni Bay area of the Bird's Head, high organic content carbonaceous marine shales of the Early Jurassic were deposited that are also likely source rocks for some of the hydrocarbons of the region (Dolan and Hermany, 1988; Livsey, et al., 1992; Perkins and Livsey, 1993).

Meanwhile, North America and Europe had rifted apart due to a new, approximately north-south oriented, 'proto-Atlantic' marine rift that had commenced during the Jurassic (Scotese, 2000). This report will follow the nomenclature of Hall (1996), and Scotese (2000), in labeling the Mesozoic Period's post-extensional rift landmass composed of Antarctica/Africa/India/Australia/New Guinea as 'Southern Gondwana'. This label does not exactly correspond to the same landmass as the pre-Pangean supercontinent 'Gondwana' of the mid-Paleozoic Era except in a very 'approximate' sense, and therefore the use of it in the post-extensional rifted Mesozoic Period timeframe is unfortunate.

During the early Jurassic virtually all of the globe's landmasses appear to have been 'ice-free' (Embleton, 1986), with warm temperate to hot arid or hot tropical climates pervasive (Scotese, 2000). The Bird's Head was still attached to the ANGP, which had drifted northward during the counter-clockwise rotation of the Australia/New Guinea/India/Antarctic 'supercontinent', from 60° south latitude during the Permian, to 45° south by the Triassic, and finally to 28° south by the Late Jurassic (Embleton 1986; Scotese 2000).

An arid but warm sub-tropical paleo-environment probably resulted in increased erosion from plutonic and volcanic rocks located in highlands in the interior of the Australian-New Guinea northern craton (Yeates, et al., 1987; Bradshaw, et al., 1988; Bradshaw, et al., 1994b). Fluvial run-off would then have transported these clastic rocks far from the orogenic highland sources to the subsiding plate margins of extensional boundary, resulting in the deposition of relatively clean, well-sorted, marine sandstones along the Westralian Superbasin along western and northwestern margins, including the Bird's Head area (Bradshaw, 1993; Bradshaw, et al., 1994a; Bradshaw, et al., 1994b). During the Middle Jurassic, thick fine- to medium-grained sands were deposited in a restricted marine embayment in the Bird's Head region as indicated by palynological analysis of spores and pollen (Waton et al, 1994, 1996a-e,

1997a-i) and ichnological facies/fabric analyses of trace fossil burrows and tracks (Pemberton 1997a-e).

These sandstone reservoirs are preserved as the 'Aalenian Sandstone Formation' and the 'Roabiba Sandstone Formation', and they are the two major Mesozoic hydrocarbon reservoirs in the Bintuni Basin (Bullings, et al., 1998; Casarta, et al., 2004).

The Roabiba Sandstone formed as part of a much broader coastal plain and shoreface succession that fringed the continental margin of Southern Gondwana. This is evidenced by the similarity of the Aalenian Sandstone Formation and Roabiba Sandstone Formation of the Berau/Bintuni Bay area with the Middle Jurassic Plover-Frigate-Sandpiper succession in the NW Shelf region of Australia (Yeates, et al., 1987; Bradshaw, et al., 1994b). Subsequent tectonic and structural events would contribute to the diagenesis of these sands, at least in the Bird's Head region, into 'world-class' hydrocarbon sandstone reservoirs (Bullings, et al., 1998; Robertson and Downey, 2000; Robertson, 2004; Casarta, et al., 2004).

The Earth's 'global warming' phase continued through the Late Jurassic until reaching, perhaps, the warmest global temperatures known in post-Cambrian times during the Middle Jurassic to early Late Jurassic. Most Gondwanan landmasses had warm to hot climates by the earliest Late Jurassic (Scotese, 2000). Continued marine transgression during the Late Callovian, either due to global eustacy or regional subsidence, resulted in more fine-grained clastics, silts and clays, being deposited in the paleo-Tangguh area marine embayment, overlying much of the Aalenian to Bajocian/Bathonian sands (Bullings, et al., 1998). The Roabiba Sandstone Formation of Berau/Bintuni Bay was rapidly buried by fine-grained clastic sediments that would become the Roabiba and Aalenian Sandstone Formations' marine-shale cap-rock. As the transgression progressed, the Middle Jurassic estuarine sands became drowned by the deeper water deposition of Late Jurassic (Oxfordian to Tithonian Stages) silts, clays, and the 'Ayot Limestone' Formation (Bulling, et al., 1998).

This rise in global mean sealevel, during most of the Mesozoic Era, has been attributed to various causes, including polar ice cap melting, tectonic plate drift, and increased sea floor spreading due to volcanic activity. By the end of the Late Jurassic, sedimentation rates (and possibly accommodation space) must have been low, as a condensed section is seen just below the unconformity between the Late Jurassic and the Late Cretaceous (Watson P., personal communication, 2001).

A significant fall in relative sealevel occurred during the very latest Late Jurassic and Early Cretaceous (Haq, et al., 1987; Berggren, et al., 1995), and this coincided with a sharp increase in global average mean temperature (Scotese, 2000), at least suggesting the two events are possibly related. This regressive phase, perhaps concurrent with tectonic uplift in the northern Bird's Head region, may have resulted in the erosion of some Late Jurassic (Tithonian) and any Early Cretaceous sediments that may have existed in the Bird's Head, since a major unconformity exists in the Tangguh area with the entire Early Cretaceous absent (Bulling, et al., 1998). This was most likely a transcontinental margin event, since this unconformity can be mapped from Bonaparte Basin on the Australian NW Shelf (Longley, et al, 2002) across the Arafura Sea to Papua, Indonesia (Charlton, 2000a; Netherwood, 2000). Renewed deposition occurred in the Tangguh area with marine carbonate sediments being blanketed over the entire Bird's Head region beginning with shallow to shelfal carbonates interbedded with argillaceous limestone during the Middle Cretaceous and conformably grading to deep marine calcareous shales and finally relatively 'clean' noncalcareous shales by the end of the Mesozoic (Salo, 1994; Salo, 1996a-c; Salo, 1997a-g; Salo, et al., 1998a; Bulling, et al., 1998). Tectonically controlled subsidence may also have contributed, regionally, to increased water depth and drowning of Late Jurassic clastic sediments, but global eustasy also continued rising during the Cretaceous and must have contributed to the Bird's Head relative sealevel rise.

McConachie, et al. (2001) relate the Bird's Head regional seal, for underlying strata, to the relative sealevel deepening during the Cretaceous accompanied by deposition of shelfal carbonate facies and marine shales. The Late Cretaceous was also proposed as a seal for underlying Jurassic strata, in Bintuni Basin, by Dolan and Hermany (1988) and Perkins and Livsey (1993), although they concluded that the Late Cretaceous in Bintuni Bay was primarily shale, rather than the marl and limestone encountered on Wiriagar Deep and Vorwata wells (Salo, 1994; Salo, 1996a-c; Salo, 1997a-g; Salo, et al., 1998a; Bulling, et al., 1998), as noted by McConache (2001). The global eustatic rise was accompanied regionally in the Bird's Head area, by an increased accommodation space for sedimentary paleodeposition, due to a regional rifting event. During the Late Cretaceous, extensional rifting occurred in the Bird's Head region that probably was related to continental rifting along the northern margin of ANGP. Extension was thought to have commenced during the Turonian, and continued into the Maastrichtian, by which

time the continental margin terrane had finally separated from the Australian continental landmass (Charlton, 2000).

Whatever the cause, the deposition of continuously deeper-water marine sediments progressed until the last stage of the Cretaceous (Maastrichtian). A maximum flooding surface defined by the highest gamma ray GAPI count is visible in Wiriagar Deep well completion logs (Salo, 1994; Salo, 1997a-j). This boundary marking the end of the Maastrichtian (the last stage of the Cretaceous) and the beginning of the Cenozoic also represent a dramatic change in the global environment, global sea level, and the second largest but perhaps most famous, mass extinction event of Earth history.

Therefore, the complete break-up of the Southern Gondwana landmasses were already in motion by the end of the Mesozoic and the onset of the Paleocene (65 Ma). The ANGP margin was recognizable with the current tectonic plate boundary as early as the Paleocene (Figure 4.2). The extensional rifting of Antarctica from the southern Australian-New Guinea continental margin and the divergence of the Indian subplate, along with the detachment of several smaller subplates such as Argo/Lhasa, West Burma, etc., from the ANGP western margin had began (Veevers, et al., 1986; Yeates, et al., 1987; Bradshaw, et al., 1988; Bradshaw, et al., 1994a; Bradshaw, et al., 1994b; Veevers, et al., 2000; Longley, et al., 2002).

4.3 Cenozoic

The Cenozoic Period was a tectonically active time for the Bird's Head region. The Cenozoic tectonic history drastically shaped the geography, geological structure, and the very fabric of the Bird's Head region.

The onset of the Cenozoic Era is marked by the 'K/T Boundary', which is shorthand in the geological sciences for the Cretaceous/Tertiary Boundary. As with the mass extinction event, global climatic shift, and change in global sea level which coincided that marked the Permo-Triassic Boundary (P/Tr Boundary), the causality of the mass extinction event, global climatic shift, and change in global sea level which occurred at the K/T Boundary is the subjected of controversial, and sometimes heated debate, in scientific circles. Most geologists agree that the Earth entered a cooling phase in global climate (Scotese, 2000), with a concurrent loss of almost 20% of marine cartilaginous fish species, and almost 45% of all the continental vertebrate species (Milner, 1998). The reason for this is not understood, nor is the exact

causality. However, of the vertebrate species, the complete demise of all of the remaining 24 families of Mesozoic dinosaurs occurred, including the Theropods, Sauropods, Pterosaurs, and the marine Plesiosaurs (Hallam, 1998). Explanations regarding the causality of these concurrent events (climatic change, onset of global sealevel fall, mass extinctions) range from the massive and prolonged Deccan and Central Siberian basalt/volcanic vent flows, to greenhouse gas or solar radiation fluctuations, to one or more massive extraterrestrial bolide impacts, such as the Chixulub impact shown on Figure 4.2 (Alvarez, et al., 1980; Hallam, 1998; Milne, 1998; Maguire et. al., 1998).

The Paleocene, therefore, opened on a note of dramatic global change, environmentally, as well as geologically. As noted in the previous section of this chapter, the ANGP had rifted from the Antarctic Plate, and the extensional event with the Indian continental subplate, and numerous smaller subplates (Argo/West Burma, Lhasa, etc.) along the western margins was well under way. The next major tectonic event affecting the northern ANGP was the subduction of the Caroline Plate to the north, and concurrent with a sinistral sliding (i.e. oblique slip) in a manner relative to the northern margin of the ANGP during the Paleocene (McCaffery, 1996).

The tectonics of the Papua region, during the earliest Cenozoic, were driven principally by the west-northwest convergence of the Pacific oceanic plate with the northward drift of the ANGP, although the Pacific plate and ANGP were not in direct contact due to the intervening Philippine Sea and Caroline subplates. (Packham, 1996). The oblique slip of the Caroline and Pacific plates relative to the ANGP would continue through the Paleocene and Eocene, into the Oligocene. During the early Cenozoic the Philippine Sea plate began a compressional episode with the Sundaland plate, a Eurasian sub-plate, and the northern ANGP margins (Packham, 1996; Hall, 1996; Veevers, et al., 2000).

By the Tertiary, it is apparent that the Bird's Head microplate and other 'microplates' such as Misool, Sula, Bura, had already become detached from the ANGP. There are numerous proposals regarding the exact timing and orientation of the movement by Ali, et al., (1985), Struckmeyer et al. (1993), Fraser, et al. (1993), Packham (1996), and Hall (1996) all varying in detail. However, in general, the Bird's Head region became a distinct microplate, detached from the ANGP, by the Early Jurassic at earliest (Fraser, et al., 1993), or the Paleocene-Eocene at latest (Hall, 1996). The Bird's Head micro-continent (BHMC) subsequently drifted northward.

By the Late Paleocene and Early Eocene, compressional subsidence in the region between New Guinea and Australia drowned the Aru Basin, resulting in the Sea of Arafura forming (Pigram and Pangganbean, 1984; Pigram and Davies, 1987; Yeates, et al., 1987; Bradshaw, et al., 1988; Bradshaw, et al., 1994a; Bradshaw, et al., 1994b; Veevers, et al., 2000).

The Sorong Fault/Shear Zone (SFZ) is thought to be a reactivated sinistral slip fault running through the northern-most BHMC, delineating the northern margin of the Bintuni Basin. Packham (1996) proposed the westward drift of the Bird's Head, concurrent with decreased paleolatitude and a counter clock-wise rotational component induced by a paleo-SFZ, took place between the Early Jurassic and Middle Eocene, with the BHMC lying of the northwest margin of New Guinea by the Eocene.

During the Late Paleocene to Early Eocene period, an uncertain climate prevailed over the Bird's Head region, with Scotese (2000) indicating an arid subtropical climate in the Early Eocene giving way to a wet, tropical paleoenvironment by the Middle Eocene. The deeper marine shelf and slope Paleocene sediments in Bintuni Basin, composed of turbidite and gravity flows deposited, are preserved particularly well at the Wiriagar Deep #1 (Salo, 1994) and Wiriagar Deep #2 (Salo, 1996c) locations.

These turbidite and debris-flow sandstone channels and fans with shelfal to slope (bathyal) shales in the Bintuni/Berau Bay area, give way to shallow water coastal facies sands intercalated with sabkha plain evaporates and fine-grained clastics (silts and silty sands) during the Eocene, on the northwest Bintuni Basin margin as noted between depth interval 4700 ft to 5000 ft on the Wiriagar Deep #1 Well Completion Log (Salo, 1994).

During the Oligocene, global sealevel continued falling (Haq, et al., 1987; Berggren, 1995). This marine regression, with a shallower marine depositional facies in the Bintuni Basin area, led to the development of a massive carbonate platform (Figure 4.3), the oldest member of the New Guinea Limestone Group (NGLG) named the Faumai Formation (see Section 5.Lithostratigraphy and Sedimentology).

Although this paleo-depositional environment continued through the Oligocene (Scotese, 2000), an erosional unconformity removed much of the Oligocene in the Bird's Head region (Bulling, et al, 1998) by peneplanation that occurred by the Late Oligocene as relative sealevel dropped (Figure 4.4).

During the beginning of the Early Miocene, a relative rise in sealevel (Figure 4.5) as indicated by Hall (2000) led to the renewed onset of platform and reef carbonate deposition in the Bintuni Basin area. As the Miocene progressed (Figure 4.6), the BHMC underwent a massive counter-clockwise rotation from the reactivation of a shear zone along the northwestern margin (the Sorong Fault/Shear Zone) in what Hall (1996) has labeled the 'bacon-slicer'. This resulted in tectonically sheared off margins, including Buru, Sulu, and Misool islands, from the Australian/New Guinea northwest margin as shown in Figure 4.6 (Packham, 1996; Hall, 1996). The BHMC detachment was dated by Hall (1996) as Miocene, but was 'accreted' back to the ANGP during the later Miocene (Hall, 1996; Hall, 2000). This seems unlikely based on the Jurassic data previously discussed, however, the Bird's Head was most likely further rotated counter clock-wise by 10° due to reactivation of the SFZ during the Miocene, and was certainly re-attached to the ANGP by the Middle to Late Miocene (Packham, 1996)

The collision of the Eurasian, Sundaland subplate with the ANGP can be fixed at between 12 and 15 Ma, during the Early to Middle Miocene, based on the 1000 km. length of subducted slab in the vicinity of Timor (McCaffrey, 1988; McCaffrey, 1989; Packham, 1996).

Therefore, during this 25 to 12 Ma time frame the detached BHMC drifted and re-accreted to the original 'parental' ANGP. By the 10 Ma (Figure 4.7), the collision of the Eurasian plate (the Sundaland sub-plate), from the NW, with the northern margin of the ANGP and the BHMC, initiated the development of the Banda fore-arc island chain making up eastern Indonesia, and the tectonic deformation of the BHMC. This tectonically induced orogenic/basinal structuring resulted in the Miocene-Pliocene creation of the present-day Bintuni Foreland Basin and the Berau Piggyback Basin to the west of the LTFB, as shown in Figure 4.9 (McCaffrey, 1988; Dolan and Hermany, 1988; McCaffrey, 1989; Fraser, et al., 1993; Perkins and Livsey, 1993; Packham, 1996).

Deformation associated with re-activation of Mesozoic/Early Cenozoic faults along margins of basement highs (that had formerly been carbonate platform/reef nucleating centers), is primarily responsible for the series of 'en echelon' plunging anticlines, and even provided wrench-fault bounded closure on the Ofaweri, Ubadari and 'P' anticlinal structures (Dolan and Hermany, 1988; Fraser, et al., 1993; Perkins and Livsey, 1993). The major plunging anticlines, with near-parallel axes, would

come to be the three- and four-way dip closure traps, Vorwata and Wiriagar Deep (Dolan and Hermany, 1988; Perkins and Livsey, 1993; Keho and Samsu, 2002; Yoshino, et al., 2003)

The Miocene Kais Formation deposition ceased at the end Miocene/beginning of the Pliocene when a continued fall in global sea level ended the carbonate deposition phase (Dolan and Hermany, 1988; Perkins and Livsey, 1993; Hall, 2000). The Steenkool Formation claystone was deposited, forming the seal for the shallow Kais Limestone Formation reservoirs in the Salawati Basin, and in the Wiriagar (shallow), Wasian, and Mogoi fields of Bintuni Basin (Dolan and Hermany, 1988; Perkins and Livsey, 1993; Yoshino, et al. 2003).

In addition to the Sundaland and Caroline subplate tectonic collisions with the BHMC resulting in the creation of structural traps (compressional folding of the Wiriagar and Vorwata anticlinoriums), this tectonic event also acted as a catalyst for the generation of the hydrocarbons to fill them (Figures 4.8). The foreland basin 'deep', created by the tectonic collisions, resulted in deeper burial of basin centers resulting in 'kitchen areas' for thermal generation and expulsion of hydrocarbons from the kerogen-rich Permian and Early Jurassic stratum (Figure 4.10).

The thermal maturation in the 'kitchen area' of the foreland basin deep, was such that the optimum oil generation window is thought to have been reached during the onset of the Pliocene, approximately 5 Ma (Figure 4.11). The source beds in the Bintuni Basin kitchen area reached the gas generation window, which requires greater thermal maturity, by 3 Ma (Dolan and Hermany, 1988; Livsey and Perkins, 1993; Harrington, 1997). These basins are still likely to be generating hydrocarbons at the optimum oil and gas thermal regimes and burial depths in the basinal margins. Migration of these hydrocarbons has continued from the Pleistocene to present-day, gradually filling the Vorwata, Roabiba, Ofaweri, and Wiriagar anticlinoriums, and eventually spilled into the Ofaweri, Wos, and Ubadari structures far to the west (Bulling, et al, 1998; Robertson, 2004).

5.0 LITHOSTRATIGRAPHY AND SEDIMENTOLOGY

The descriptions and discussions of the lithostratigraphy and sedimentology of the Bird's Head region, with particular focus on Bintuni Basin, are based mainly on data acquired since 1986, from exploration and appraisal/delineation wells drilled by ARCO and BG.

5.1 Lithostratigraphic Overview Of The Bird's Head

Early work on the Bird's Head lithostratigraphy was done on outcrops far away from the Tangguh LNG production area. Field-work was hampered along the coast and the foothills by a mix of crocodile infested mangrove swamp, karstified hills covered in dense tropical cloud forest (with hidden vegetation-covered sinkholes), and fault scarp cliffs on rugged mountain peaks jutting out of the tropical rain forest jungle canopy up to heights reaching up to elevations of 3200 ft (1000 m) above mean sea level (MSL). Many of the early Dutch geologists died of malaria and tropical fever (L. Casarta, personal communication, 1993, 1994, 1995, 1996).

One of the problems stemming from the early field mapping is the identification by numerous local names, of essentially the same lithostratigraphic unit (Fraser, et al., 1993). ARCO decided to use geo-chronological nomenclature - Aalenian Sandstone and Late Cretaceous Marls - for most of the formations and strata, with some notable exceptions - Roabiba Sandstone and Faumai Formation (Bulling, et al., 1998). The well data acquired in the Berau/Bintuni Bay area is mainly limited to the areas of commercial hydrocarbon accumulation (Figure 2.3), and consist of generally, very good quality data consisting of drill cuttings descriptions, conventional core analyses, wireline logs, but only limited seismic survey data (Bulling, et al., 1998).

The discussion of the lithostratigraphy and sedimentology, for this study, will be limited to the strata encountered in the exploration, appraisal, and delineation wells drilled the Berau/Bintuni Bay area. The nomenclature for these lithostratigraphic units will be based on the nomenclature and stratigraphic units pervasive in the BP/ARCO/BG archived data. These lithological descriptions are also discussed from the proposed perspective of evaluating them as potential ESSCI reservoir/seal couplets in a possible Tangguh CO₂ injection and sequestration project.

The Late Paleozoic and Mesozoic formations, preserved in Bintuni Basin wells, are generally identified as consisting of:

- ◆ Late Permian shales and undifferentiated sandstones;
- ◆ Early Jurassic shales and undifferentiated sandstones;
- ◆ Middle Jurassic shales, Aalenian Sandstone, and Roabiba Sandstone
- ◆ Ayot Limestone;
- ◆ Upper Late Jurassic shales;
- ◆ Late Cretaceous marl.

The Paleozoic and Mesozoic strata also have type-locale formation names, and although these names change over relatively short distances, some workers still cling to these names in both external publications (Figure 5.1), and also ‘in-house’ reports (Visser and Hermes, 1962; Dolan and Hermany, 1988; Perkins and Livsey, 1993; Fraser, et al., 1993). The generalized Berau/Bintuni Basin lithostratigraphy is shown in Figure 3.2.

The Cenozoic nomenclature is less straightforward. The naming convention that has arisen in the youngest/shallowest subsurface interval begins with the Cretaceous-Tertiary unconformity (the K/T Boundary). The immediate formation overlying the K/T Boundary, the Late Paleocene, has a mix of geochronologic and lithostratigraphic nomenclature. The Late Paleocene formation overlies the Late Cretaceous unconformably in most locations, with what is designated the ‘Paleocene Sand Prone Lower Member’ as the most basal unit; followed by a stacked turbidite/debris flow channel (only at the Wiriagar Deep #2 and #4 well locations) interbedded with shelf slope and shelf toe shales, collectively labelled the ‘Paleocene Sand Prone Middle Member’; overlying this member is the ‘Paleocene Sand Prone Upper Member’ (Bulling, et al., 1998). These sand prone members are potentially significant, secondary hydrocarbon production reservoirs (after the Middle Jurassic ‘Aalenian’ and ‘Roabiba’ sandstone reservoir accumulations) on the Wiriagar Deep structure (Bulling, et al., 1998). They are also potential ESSCI strata for CO₂ sequestration.

All three of the Late Paleocene Sand Prone Members (Lower, Middle and Upper) are capped by the Late Paleocene ‘Mud Prone’ interval which is areally extensive, quite thick (i.e. several hundred feet), and provides the regional seal for the underlying Paleocene sandstone reservoirs (Salo, 1994; Salo, 1996c; Salo, 1997a-g;

Salo, 1998a-b; Bulling, et al., 1998). The Eocene overlies the Paleocene and consists of undifferentiated claystone and sandstone for the most-part. A thin to moderately thick evaporite layer (<10 ft) has been identified in some wells drilled on the north coast of Bintuni Bay, including Wiriagar Deep #1 (Salo, 1994). This early Eocene evaporite consists of anhydrite or anhydrite intercalated with dolomite. It has not been formally named (Salo, 1994).

Towards the near-top of the Eocene, a massive platform carbonate is occasionally encountered in onshore outcrops and subsurface wellbores (Salo, 1994; Salo, 1996a-c; Salo, 1997a-g; Salo, 1998a-b; Bulling, et al., 1998). The massive carbonate was deposited from the early Eocene, through the Oligocene, and into the Late Miocene, based on nannofossils and microfaunal marker taxa. The Eocene to Miocene carbonate encountered in the Bird's Head region is now acknowledged to be a part of the New Guinea Limestone Group (NGLG) (Perkins and Livsey, 1993; Bulling, et al., 1998). The NGLG is pervasive throughout the island of New Guinea but was not recognized as such in Papua early on (i.e. prior to 1993), especially in the Bird's Head region (Visser and Hermes, 1962; Dolan and Hermany, 1988). Regionally, there are many different names for this carbonate group and individual members. Hence, it has received numerous 'member' names across the Bird's Head area including, but not limited to the "Sirga", "Sago", "Faumai", "Klasafet", "Sekau", and "Kais" (Visser and Hermes, 1962; Dolan and Hermany, 1988; Nurzaman and Pujianto, 1994). Some of these names are clearly limited to specific age and sequential positioning as a NGLG member, such as the top most Middle to Late Miocene Kais Limestone Formation (i.e. Klasafet in places) (Perkins and Livsey, 1993; Bulling, et al., 1998). Other carbonate members, however, have very blurred lines of distinction, having been tagged with a type-locale formation names when mapped in field outcrop (i.e. Sirga, Sekau, Sago).

The Eocene-Oligocene carbonate is in fact, the earliest development of the New Guinea Limestone Group (NGLG) platform/occasional shelfal carbonate (Dolan and Hermany, 1988). The name used by the ARCO team, in the Berau/Bintuni Bay area, for the Oligocene limestone interval, was simply the 'Oligocene Limestone Formation' (Bulling, et al., 1998). Although, conversely the entire Eocene to Early Miocene carbonate sequence, where the Oligocene Limestone is absent, was simply referred to by ARCO as the 'Faumai Formation' from the base of the carbonate growth to the unconformity at the Middle Miocene (Bulling, et al., 1998). The

Middle Miocene unconformity is widespread in areal extent across the Bird's Head, and the NGLG carbonate member above the unconformity is known as the Kais Limestone Formation, which was, and locally still is, an oil or condensate production reservoir (Dolan and Hermany, 1988; Perkins and Livsey, 1993; Bulling, et al., 1998).

Capping the Kais Limestone Formation is a Pliocene to Pleistocene claystone, poorly indurated, with small discontinuous sand lenses, pebble lags, and shell hash storm deposits interbedded locally. This claystone unit has the formation name 'Steenkool' and is commonly used to denote the entire fluvio-deltaic sequence of sedimentation from the earliest Pliocene through the Pleistocene (Dolan and Hermany, 1988; Bulling, et al., 1998). It ranges from 1500 ft thick at the Wiriagar Deep #1 well location (Salo, 1994), to many thousands of feet thick over Bintuni Basin depocenter (Dolan and Hermany, 1988; Bulling, et al., 1998).

5.2 Database Summary

The summary of lithostratigraphic units commonly used by the BP/ARCO teams in the Tangguh project area, from oldest to youngest according to Bulling, et al., (1998) are listed in Table 5.1

The regional Mesozoic lithostratigraphy and sedimentology, using Wiriagar Deep #3 (WD-3), Wiriagar Deep #2 (WD-2), and Vorwata #10 (V-10) as the 'type' wells is presented below, but certain key intervals are also in-filled with core from the Wiriagar Deep #1 (WD-1), Wiriagar Deep #5 (WD-5), Wiriagar Deep #7 (WD-7), Vorwata #1 (V-1), and Vorwata #2 (V-2) wells (Figure 5.2). Most of the ARCO/BG core available is from the Mesozoic and latest Paleozoic intervals, although a few cores were taken by ARCO in the lower Late Paleocene. No ARCO or BG core is available above the lower Late Paleocene (Bulling, et al., 1998). Few ARCO or BG logs were run over the Quaternary and Tertiary intervals, except for portions of the Late Paleocene interval (Bulling, et al., 1998).

Most of the Upper Eocene through Middle Miocene is a massive lost circulation zone for drilling (Bullings, et al., 1998). These intervals are obviously examined and discussed in far less detail.

In addition to the original wellsite core and cuttings descriptions, sedimentological evaluations were also done on cores by Dr. Chris Cook at Core

GROSS INTERVAL	FORMATION/MEMBER NAME	GROSS LITHOLOGY AND REMARKS
1. Late Permian		undifferentiated shales, thin sandstones, rare coals and common carbonaceous shales are likely source rocks where thermally mature
2. Triassic		undifferentiated 'red-bed' oxidized shales, thin sandstones, and evaporites
3. Early Jurassic		undifferentiated shales, thin sandstones, rare coals are probable co-generative source rocks where thermally mature
4. Middle Jurassic		shales and thick sands
	A) Aalenian Sandstone	clean marine sandstones
	B) Roabiba Sandstone	clean marine sandstones
5. Late Jurassic		cap/seal shales, sandy siltstones, thin carbonates
	A) Pre-Ayot Shales	shale
	B) Ayot Limestone	regional marker bed
	C) Upper Late Jurassic Shales	shale
	D) Jurassic/Cretaceous unconformity	glauconitic marker bed
6. Late Cretaceous		predominantly undifferentiated argillaceous limestone/marl
7. Late Paleocene		turbidites, debris flow channel sands, shales
	A) Sand-Prone 'Lower Member'	basal turbidite sands interbedded with shales
	B) Sand-Prone 'Upper Member'	top-most turbidite sands interbedded with shales.
	C) Sand-Prone 'Middle Member'	turbidite channel cutting-out the 'Upper Member' but not the 'Lower Member'.
	D) Mud-Prone Interval	predominantly shales.
8. Eocene		undifferentiated shales/claystones, occasional water bearing sands, occasional carbonates near-top, rare evaporites (anhydrite) on the north coast of Bintuni Bay
9. New Guinea Limestone Group (NGLG)		carbonate succession
	A) Oligocene Limestone Formation	rarely preserved vestiges found only in the synclinal troughs
	B) Faunai Formation	areally widespread and thick platform carbonate, Eocene-Middle Miocene
	C) Kais Limestone Formation	massive platform/reefal carbonate, widespread over Bird's Head, Mid-Late Miocene
10. Steenkool Formation		clastic sediments, Pliocene to Pleistocene massive claystone with discontinuous sand or silt lenses, fossil shell hash, carbonaceous/organic detritus including woody lignite clasts and actual organic tree debris

Table 5.1: Table of Bintuni Basin gross intervals and formation/member names, with a generalized gross lithology description and remarks.

Laboratories Indonesia, and both were incorporated into the final well reports (Salo, 1994; Salo, 1996c; Salo, 1997a-g; Salo, 1998a-b; Perry, 1997; Perry, et al., 1997; Indro, et al, 1997; Forbes, 1998). Biostratigraphy based on integrated palynological and palaeontological analyses, was carried out by Dr. Paul Waton at Core Laboratories Indonesia, on cores as well as drill cuttings (Waton, et al., 1994; Waton, et al., 1996a-e; Waton, et al., 1997a-h; Waton, et al., 1998a-d). In addition, Dr. George Pemberton of the University of Calgary, examined the whole cores in Jakarta for ichnology in 1997 at ARCO offices (Pemberton, 1997a-f). The cores from presumed Paleocene deepwater facies were also examined by Dr. Donald R. Lowe of Stanford University in 1998, at the ARCO offices in Jakarta (Lowe, 1998). Almost all of the Mesozoic cores from all Tangguh area wells were also examined in detail for this study, reviewing and building on existing core logs by Tye and Hickey (1999) and Pemberton (1997a-f). The cores were digitally photographed and are presented in this study.

5.3 Lithostratigraphy And Sedimentology Summary

The lithostratigraphy and reservoir sedimentology of Bintuni Basin, using the type wells mentioned above, is presented from the oldest gross interval up to the youngest gross interval. Reservoir formations or members with gross intervals are discussed in greater detail under subheadings.

5.3.1 Permian

The top Late Permian has been penetrated by Bintuni Basin wells including WD-1, WD-2, Wd-3, WD-6, and the V-1. Cores have rarely been cut through Late Permian intervals on Bintuni Basin wells.

The basal portion of the WD-3 reached total depth in Late Permian and the lithology was alternating interbedded shales and sandstones, with some minor coal stringers. The sandstones appeared to have 'residual' hydrocarbons only, and were unproductive at the WD-3 location due to poor permeability in the sandstone (Salo, 1997b-c).

The shales can be generally characterized as dark to medium gray, to light gray; and varicolored and mottled below 9800' (including gray, brown, lavender, and greenish colored varieties); firm to soft; carbonaceous in part possibly grading to bitumen adjacent to coal seams. The shales are silty in part, grading locally to

siltstones, and even sandstones. The shales are generally silicified in part, particularly where faulted or sheared, as the frictional heat from movement seems to have ‘glazed’ the siliceous clays into a pseudo-porcelanite along the fracture/movement planes. Micro-disseminated carbonaceous material, coaly clasts, coaly plant debris, and even coal-filled rootlets were common to locally abundant (Salo, 1997b-c).

Coals were rare, with only several very thinly bedded coal stringers encountered. All were bituminous; black in color; brittle to firm; with a metallic to vitreous luster in part, and with conchoidal fractures; argillaceous, grading locally to carbonaceous shale. The coals, and the carbonaceous shales, are of interest for their hydrocarbon sourcing potential (Chevallier and Bordenave, 1986; Dolan and Hermany, 1988; Livsey, et al., 1992; Perkins and Livsey, 1993; Salo, 1997b-c; Harrington, 1997).

Several Late Permian sandstones near TD were all conventionally drilled, and as mentioned previously the cuttings sample quality was extremely poor in this Permian section of the hole. A thin-bedded sandstone was encountered at 9595 ft was only 10ft thick, on wireline logs. This sandstone was off-white; very fine to fine grained; subangular to subround; weakly cemented with kaolinite; no fluorescence nor cut fluorescence was observed, and the only gas peak recorded (23 units) was attributable to a thin coal in the middle of the reservoir. This sandstone had no hydrocarbon shows (Salo, 1997b-c).

Additional sandstone members were identified from the drill cuttings (Salo, 1997b-c) and the wireline log with tops at 9623 ft, 9657 ft, 9717 ft, and 9855 ft. In cuttings, the sandstones were generally similar in lithological characteristics, to the one previously described at 9595 ft. All the sandstones were pale white, with individual grains being clear, frosted white, gray, green, black and even rarely red/orange; very fine to fine grained; subangular to subround; mineralogy was predominantly quartz grains; lithic rock fragments, feldspar, and with some glauconite or chlorite; predominantly weakly cemented to unconsolidated with only a trace of calcareous and kaolinitic cement evident; nil to poor visible porosity, but a fair to good porosity was inferred from the drillbit ‘rate of penetration’ (ROP) below 9855 ft (Salo, 1997b-c).

The entire uppermost shale and the top-most Permian sandstone were cored in Core No.15, on WD-3. Taxa assemblage indicative of the Late Permian identified in either cuttings or core, at WD-3, included *Lunulasporites valgaris*, *Protohaploxypinus*

limpidus, *Striatopodocarpidites* spp., *alisporites/Sulcatosporites* spp., *Stratiobietpollenites* spp., *Uncertae sedis*, *Weylandites lucifer*, and *Praecolpatites sinuosus* (Waton, 1996b). The paleodepositional environment is interpreted as non-marine (fluvio-lactistrine) with occasional marine pulses, based on the abundance of terrestrial striate bisaccates, and absence of marine taxa until the upper-most Permian where dinocysts and acritarchs were recorded (Waton, 1996b). The cuttings and core from the WD-2 Late Permian interval also yielded a variety of bisaccate dominated assemblages (Waton, 1996a).

The palynological data from WD-3 agrees well with Pemberton's 'burrow and track' trace fossil ichnological facies evaluation (1997a), and with this author's original evaluation (Salo, 1997b-c), of terrestrial deposition with occasional evidence of marine deposition near the top of the succession. In Core No. 15, on WD-3, Pemberton identified a wholly terrestrial, non-marine ichnofacies present from the base of the core at driller's measured depth 9566 ft up to 9552 ft (RKB). The core contains unburrowed mudstones containing terrestrial roots, thin coals, and is interpreted as freshwater upper delta plain (Figure 5.3). This is followed by a marginal marine 'embayment' environment from 9551 ft to 9525 ft with a trace fossil assemblage including *Arencolites*, *Planolites*, and *Palaeophycus*. This low diversity and sparse suit of trace fossils was indicative of a brackish, low salinity water assemblage interpreted as lower delta plains/embayment headwaters environment (Pemberton, 1997a).

From 9525 ft to 9500 ft there is a tidal channel characterized by cryptic bioturbation (Pemberton, 1997a). Graded bedding with minor cross-bedding was visible to the author in this core interval, substantiating a marginal marine channel depositional environment. This is overlain by a brackish water embayment assemblage, from 9500 ft to 9488 ft, similar to that seen in interval 9551 to 9525 ft (Pemberton, 1997a).

A single Late Permian sandstone is available in core from WD-3, with the reservoir top at driller's measured depth 9483 ft RKB. It can be found between gross wireline log interval 9494 ft to 9590 ft, and is interpreted as a marine sandstone, based on presence of 'in-situ marine glauconite' in the lithological descriptions (Salo, 1997b-c), presence of marine palynomorph assemblage in the palynological study (Waton, 1996a), and a marine ichnological facies determination from trace fossil burrows (Pemberton, 1997a).

This near-top Late Permian sandstone (Figure 5.4) is heavily laminated with shale streaks, and lenses, and occasionally mixed in a sandstone/shale bioturbated pattern, especially near the top. The sandstone in Core No.15, was described by Salo (1997b-c) as, off-white to cream to light gray, occasionally medium gray; with common dark gray patches and clasts of clay, shale, and/or carbonaceous material intercalated with the sands; very fine to very coarse grained in part with some granule to pebble clasts; stacked series of graded bedding with cross bedding occasionally visible (Figure 5.5); predominantly quartz; very common to locally abundant feldspars, kaolinite (possibly a feldspar alteration product), mica books (muscovite) as clasts/grains, and occasional to common lithic granite rock fragments. The mineral assemblage suggests a granitic parental rock source for the clasts (a ‘granite wash’ in part?). The sandstone commonly had both disseminated coaly and/or carbonaceous clasts scattered throughout, and mixed clay/shale laminae with carbonaceous material streaked and shot through the sands in an irregular, nonparallel pattern (filamentary laminae), as discreet patches, and as ‘bedded’, parallel, near-horizontal, thin layers. The sandstone was generally well cemented with a siliceous and kaolinitic cementation/matrix (Figure 5.6). The sandstone was generally noncalcareous, with a trace of scattered green glauconite nodules indicating a marine depositional setting, and visible porosity was generally very poor to tight, due to well developed cementation (Salo, 1997b-c).

The upper-most Late Permian sedimentary rocks in WD-3 core consist of dark gray to grayish black shale, hard to firm, calcareous in part, silty in part, and with trace glauconite nodules (Salo, 1996b-c). This interval is described as having *Asterosoma*, *Anconichnus*, *Helminthopsis*, and *Palaeophycos* present (Pemberton, 1997a).

The top of the Permian in the Wiriagar Deep #3 is identified by palynological analysis at driller’s measured depth 9472 ft (Figure 5.7), and adjusted to the wireline logging depth of 9477 ft (-9428 ft TVDss) by overlying the core gamma-ray log with the open-hole wireline gamma-ray log (Waton, 1996a).

The very top of the Late Permian is a nonconformable contact with the overlying Jurassic (Figure 5.7). Pemberton found this surface to be a ‘*Glossofungites*’ surface. Pemberton (1997a) observed protrusive spreiten in some burrows including fan-shaped *Rhizocorralium* and *Diplocraterion*.

5.3.2 Triassic

The top of the Late Permian is generally truncated by a regionally widespread erosional unconformity, although the Triassic is present in some rare locales, including outcrops to the north in the Sorong Shear/Fault Zone hills, and to the east in the LTFB mountains (Visser and Hermes, 1962). It is also either present 'in-situ' or preserved as reworked lithic clasts and palynomorphs in earliest Jurassic (EJ-1 biozonation category) sedimentary rocks, as identified from drill cuttings of the East Onin #1 well, located on the Kumawa-Onin-Misool anticline (KOM) (Salo, 1996a-b; Waton, et al., 1996e). With the absence of Triassic sedimentary rocks across most of the study area, the Late Permian is most often directly overlain by Jurassic rocks. There is no evidence of Triassic reservoir rock stratum present either as potential hydrocarbon exploration targets, or as potential CO₂ sequestration ESSCI sites, in the Bird's Head region.

5.3.3 Early Jurassic

The Early Jurassic successions are rarely encountered in the Berau/Bintuni Bay area wells. East Onin #1 is an example where EJ-1 (Early Jurassic palynological biozonation number 1) has been penetrated by drilling (Waton, et al., 1996e). Outcrops of Early Jurassic rocks have been identified in the Lengguru Thrust/Fold Belt Mountains and the Sorong Fault/Shear Zone hills. These outcrop areas are quite distal from the immediate Berau/Bintuni Bay area (Bulling, et al., 1998). As the lithostratigraphic interval areal extent is limited, and data on it is lacking, it will not be addressed in detail here.

5.3.4 Middle Jurassic

As mentioned previously, Core No.15, from WD-3, intersected the unconformity between the Late Permian and the Middle Jurassic. The youngest mid-Jurassic sedimentary rocks overlying the unconformity are 'Aalenian' sandstones, which have been labelled as the 'Aalenian Sandstone Formation' by ARCO. The undifferentiated Middle Jurassic successions, at the WD-3 location, consist of only the MJ-3 and the MJ-4 palynological biozonations, (i.e. Middle Jurassic 3 and Middle Jurassic 4). The lithology overall, is composed of a well developed MJ-4 sandstone (the Aalenian), capped by an MJ-4 shale layer, which in turn is overlain by the Roabiba Sandstone Formation (MJ-3/MJ-2/LJ-11) (Bulling, et al., 1998).

The bottom of Core No.13 and the top of Core No.14 (from WD-3) captured, in entirety, the shale ‘break’ present between the overlying Roabiba Sandstone Formation reservoir, and the Aalenian sandstone reservoir (Figure 5.8). The shale break, as originally described at wellsite by the author (Salo, 1997b-c), was very dark gray to black; very hard; silicified in part, grading locally to a porcelaneous shale; very well indurated and compacted; fissile in part with very thin platy cleavage (almost ‘slate-like’ in appearance); generally smooth textured, with a vitreous to matte luster; a trace of scattered mica flakes (muscovite) and fossil relics (pyritized in part) including a single unidentified species of mollusk bivalvia; and was generally noncalcareous/nondolomitic (Salo, 1997b-c).

The underlying Aalenian Sandstone Formation, and the overlying Roabiba Sandstone Formation, are interpreted as shallow restricted marine embayment sheet-like sands, and the intervening shale break is interpreted to be a maximum flooding surface (MFS), which drowned the underlying Aalenian marine sandstone. The underlying and overlying sandstones are described in greater detail below.

5.3.4.i.1 Aalenian Sandstone Formation

The top of the cored Aalenian Sandstone Formation reservoir is at driller’s measured depth 9396 ft RKB on the WD-3 well, but can be found at the equivalent wireline logging depth of 9402 ft. Core No.14 cored the Aalenian Sandstone Formation in entirety. The base of the Aalenian reservoir is very sharply truncated at driller’s depth 9471 ft. This same sharp basal contact can also be seen on the wireline log at 9477 ft, equivalent wireline logging depth.

The Aalenian Sandstone Formation is a tan to light gray to medium and dark gray with depth; friable to hard; generally very fine grained, although occasionally fine to medium grained and rarely very coarse grained in parts; well sorted in the predominantly fine grained intervals, and moderately to poorly sorted in the coarser intervals; with grains predominantly subangular to subrounded (Salo, 1997b-c).

The slightly arkosic sandstone is predominantly composed of quartz grains, with trace scattered feldspars and muscovite grains, and only traces of lithic rock fragments. It is very argillaceous in part with common dark gray laminations and streaks, ranging from a few feet thick (such as cored interval 9407 ft to 9411 ft) to ‘paper-thin’ (such as 9420 ft) irregular microlaminations (Figure 5.9). Scattered plant

debris and coaly/carbonaceous clasts are present, as is siliceous cementation with depth in the form of syntaxial quartz overgrowths (Salo, 1997b-c).

The Aalenian sandstone at WD-3 has numerous cycles of graded bedding, as well as cryptic bioturbation in part, in-filled burrows, rare cross-bedding, and soft-sediment deformation, clearly visible in the core photographs of Figure 5.10 (Salo, 1997b-c).

The Aalenian Sandstone Formation was identified as Aalenian, based on MJ-4 palynomorph taxa assemblage in the core. Some palynoflora including *Callialasporites dampieri* and *Callialasporites turbatus* corroborate this interval in the WD-3 cores as dating from the earliest stage of the Middle Jurassic in the respective WD-3 core (Aalenian/MJ-4) and also the WD-2 core (Waton, et al., 1997b; Waton, et al., 1997a). Waton interpreted the low diversity of other marine palynomorphs within the tax assemblage, including *Dissiliodinium granulatum*, *Dissiliodinium psilate*, and variety of achritarchs, as indicative of a stressful restricted marine environment with a significant freshwater influence (Waton, et al, 1997b).

Pemberton (1997b) likewise found the ichnological assemblage characteristic of a marginal marine to restricted marine brackish water paleo-depositional environment. Pemberton (1997b) described the sandstone reservoir as an incised valley or tidal channel fill complex.

Aalenian Sandstone Formation porosities and permeabilities are discussed further, in detail, in Chapter 7. Reservoir Characterization.

5.3.4.i.2 Roabiba Sandstone Formation

The WD-2 and WD-3 Roabiba Sandstone Formation described originally by the author at wellsite (Salo, 1996c; Salo, 1997b-c) is a slightly argillaceous sandstone with tan to very light gray color (Figure 5.11); very fine grained; very well sorted; subrounded; moderately well cemented with a calcareous cement; and dominantly quartzose with only scattered calcite grains, and traces of lithic rock fragments observed (Figure 5.12), (Salo, 1997b-c).

The sandstone is cryptically bioturbated, with irregular, nonparallel, thin clay streaks, laminae, and discontinuous patches presenting a 'marbled' pattern overall. Cryptic bioturbation and trace fossil burrowing (Figure 5.13) characterize the Roabiba Sandstone Formation at Wiriagar Deep (Salo, 1994; Salo, 1996c; Salo, 1997a-f).

The Roabiba Sandstone Formation is thicker and sedimentologically more complex at Vorwata, than at Wiriagar Deep, since much of the Roabiba has been erosionally removed at Wiriagar Deep (Bulling, et al., 1998). Whole cores were obtained on several Vorwata wells through some, or all, of the Roabiba Sandstone Formation interval (Vorwata #1, Vorwata #2, Vorwata #4, Vorwata #6, Vorwata #7, and Vorwata #10). The most complete core coverage of the Roabiba Sandstone Formation interval at Vorwata is from the Vorwata #2 (V-2) and Vorwata #10 (V-10) wells (Bulling, et al., 1998).

The Roabiba Sandstone Formation at Vorwata was cored almost in entirety on the V-2 well, where ~405 ft of whole core was obtained from a 420 ft gross interval. The Roabiba sandstone at V-2 is generally described in Core No.1 through Core No.6 as a white to off white to light gray, rarely tan, colored sandstone; generally clean with traces of dark gray to black thin, wavy shale microlaminations and inclusions. It is predominately fine to medium grained, and occasionally exhibiting graded bedding successions of fine to medium grain; with grains generally subangular to subrounded and rarely angular in part; and generally well sorted. The sandstone is predominantly 'clean' quartz grains with occasional minor to trace feldspar grains, trace glauconite and pyrite nodules; weakly to well cemented with dominantly siliceous, and rarely calcareous, cementation; resulting in friable to firm, and rarely hard to very hard, rock strengths. There are traces of lithic rock fragments, and argillaceous white clay (kaolinitic) or shaley clasts; and rare black carbonaceous inclusions. There are rare fossil shell fragments, mica flakes, and dolomite cement noted over a 100 ft interval, between 12,900 ft and 13,000 ft driller's measured depths RKB (Perry, 1997).

The sedimentological character of the Roabiba Sandstone Formation at Vorwata can be generalized as clean, massive quartzose sands with common cross-bedding and flaser drapes (Figure 5.14).

Waton, et al., (1996a) identified the Roabiba Sandstone Formation at WD-2 as Bajocian to early Bathonian (MJ-3) based on the relative palynomorph abundances of taxa including *Corollina* spp., *Callialasporites* spp., *Dissiliodinium granulatum*, and marine dinocysts such as *Nannoceratopsis gracillis*. The biostratigraphy of the Roabiba Sandstone Formation at the various Wiriagar Deep and Vorwata well locations is generally suggestive of shallow marine paleo-depositional environment slightly distal but proximal to strong freshwater fluvial influences in a restricted

marine paleoenvironment (Waton, et al., 1994; Waton, et al., 1996a-d; Waton, et al., 1997a-j).

Pemberton (1997b,e,f) recorded a very limited assemblage of ichnogenus present in WD-2 and WD-3 Roabiba Sandstone Formation cores. The WD-2 Roabiba cores are characterized by *Skolithos* and *Dipocraterion* prevalent in the top of the sandstone, and the intra-sandstone interval dominated by *Teichinus*, with occasional *Helminthopsis*, *Schaubcyndrichnus*, and *Zoophycos* observed (Pemberton, 1997e).

Pemberton's (1997e) assessment of the Wiriagar Deep Bajocian/Bathonian paleo-depositional facies from ichnological facies interpretation is one of a lower offshore marine to restricted brackish water environments. The trace fossil suite at Vorwata is slightly more varied, with the V-2 Roabiba Sandstone Formation cores exhibiting abundant *Teichichnus* and *Zoophycos*, but also common to scattered *Planolites*, *Palaeophycus*, *Lockeia*, *Helminthopsis*, *Asterosoma*, *Chondrites*, *Thalassinoides*, *Ophiomorpha*, *Anconichnus*, and *Schaubcylindrichnus* (Pemberton, 1997e-f). He characterized the base Roabiba Sandstone Formation interval at Vorwata as a stressed, brackish marine paleoenvironment, becoming much stronger marine towards the top of the unit, until finally ending in a 'full shallow marine tongue' (Pemberton, 1997e-f).

Photographs of Roabiba Sandstone Formation core in Figure 5.15, from V-2, show numerous vertical burrows in a relatively clean, massively bedded sandstone interval at 12599 ft, overlain by a probable *Helminthoida* or *Helminthopsis* fabric dominating a large interval with few other ichnogenus observed (Dr. K. Bann, personal communication, 2003), supporting Pemberton's (1997e-f) observations, and interpretation of a stressed, restricted marine embayment.

The Roabiba Sandstone Formation core, at Wiriagar Deep and Vorwata, was also logged by Tye and Hickey (1999) for reservoir architecture, but relied on Waton, et al., (Waton, et al., 1994; Waton, et al., 1996a-d; Waton, et al., 1997a-j), and Pemberton (1997a-f) for palynological and ichnological data and interpretations. Tye and Hickey (1999) generally described the Roabiba Sandstone Formation cores at Wiriagar Deep and Vorwata as being deposited in a 'brackish bay' paleoenvironment.

The consensus of workers converge on the common interpretation that the Roabiba Sandstone Formation has a range of sedimentological features that are varied, but generally limited to deposition in a paleogeographical environment consisting of a very large, marine embayment with strong terrestrial freshwater input.

5.3.5 Late Jurassic

Overlying the Roabiba Sandstone Formation are Callovian (MJ-1 and LJ-11) to Oxfordian sedimentary rocks (LJ-10 and LJ-9). There is a widespread erosional unconformity at the Wiriagar Deep structure that results in Oxfordian (LJ-10 and LJ-9) sedimentary rocks directly overlying the Bathonian/Bajocian (MJ-3) Roabiba Sandstone Formation (Waton, et al., 1994; Waton, et al., 1996a-d; Waton, et al., 1997a-j).

At the Vorwata structure, however, there is an erosional unconformity dated palynologically as late Middle Jurassic (MJ-2/MJ-1) that results in Callovian MJ-1 or LJ-11 sandstone or shale being preserved overlying the Bathonian/Bajocian Roabiba Formation (Waton, et al., 1994; Waton, et al., 1996a-d; Waton, et al., 1997a-j).

Where sandstone is present, on various Vorwata wells, it has erroneously been described by ARCO as Bathonian/Bajocian ‘Upper Roabiba Formation’, and where shales are capping the Bathonian/Bajocian ‘Main Roabiba Formation’ they have been labelled as Late Jurassic Shales. In any case, as the Late Jurassic drew to a close a condensed section (CS) was deposited in the Bird’s Head region (Waton, personal communication in 2001). The Late Jurassic interval is discussed in greater detail below as the Pre-Ayot Clastics Succession and the Ayot Limestone Formation.

5.3.5.i.1 Pre-Ayot Clastics Succession

This study concludes that the data supports the Upper Roabiba Formation being assigned to the Pre-Ayot Clastics Succession based on the Upper Roabiba Formation belonging biostratigraphically to the Callovian (MJ-1/LJ-11), (Waton, et al., 1997d-h; Waton, et al., 1998a-d). However, the Upper Roabiba Formation has been described lithostratigraphically and sedimentologically, above, as the ‘Roabiba Sandstone Formation’, since ARCO did not distinguish between Callovian Roabiba Sandstone Formation and Bajocian/Bathonian Roabiba Sandstone Formation. The remainder of Pre-Ayot Clastics Succession is a massively bedded Callovian (LJ-11), Pre-Ayot Shale that is pervasive over the entire Vorwata area, but is not present at Wiriagar Deep (Bulling, et al., 1998).

5.3.5.i.2 Pre-Ayot Shale

The Pre-Ayot Shale interval unit is the top-seal ‘cap-rock’ for the Roabiba Sandstone Formation at the Vorwata structure (Bulling, et al., 1998). This unit was

cored at the Vorwata area in only a single core by BG, Core No.1 on the Vorwata #10 well (Figure 5.16). The shale is massively bedded with few sedimentological features evident. The core was not available to ARCO in the 1990's, and was not evaluated by Pemberton.

The shale core was described by the author, for this study, after three years of storage. The shale is medium dark gray; hard to very firm, splintery in part but generally with blocky cleavage; silty in part; rarely micromicaceous in part; traces of nodular glauconite, and with occasional calcite filled fractures. There are no visible fossils, although a few rare possible in-filled burrows were noted, with no definitive ichnological facies identifiable.

Waton, et al. (1998d), dated the cored interval of the Pre-Ayot Shale to the Callovian (LJ-11) biostratigraphic zonation based on a palynomorph assemblage that includes *Wanaea spectabilis*, *Wanaea digitata*, *Wanaea thysonata*, *Wanaea indotata*, *Scriniodinium ceratophorum*, *Scriniodinium crystallinum*, *Ctenidondinium Tenellum*, and *Rigauadella aemula*.

Overlying a limited portion of the Vorwata area, but not present at the Wiriagar Deep area, is the Callovian LJ-11 shale is the LJ-10 sandstone (Waton, 1997). This sandstone has not been cored, and is known only from drill cuttings.

This Callovian to earliest Oxfordian sandstone (dated as LJ-11) was originally described from cuttings by the author (Salo, 1997g) as a glauconitic lithic and arkosic sandstone, light green to greenish gray mottled with blackish to dark brownish gray irregular clay streaks and laminae. Grains are round to subrounded, with occasional elongated grains; dominantly quartz with common nodular glauconite, common lithic rock fragments, common feldspars, and common to occasional calcite/limestone grains/cement. The sandstone is very well cemented with a calcareous cementation in addition to the calcite/limestone grains, and is fossiliferous with numerous marine species including foraminifera, mollusk bivalves, belemnites and nautiloids (often these fossil test were composed of brown calcite).

Waton (1998d) described the taxa assemblage distribution over the entire Pre-Ayot Clastic Succession, based on both core and cuttings, as indicative of a marine transgression with a proximal shallow marine paleo-depositional environment near the base of the interval progressively becoming more deeper water, and distal to terrestrial miospores and influences. Since only cuttings samples exist through the sandstone interval, it is difficult to assess any sedimentological features that might be

present in the interval. Based on the combination of palynological taxa assemblage, presence of glaucony, and marine macrofauna, the sandstone could represent a deeper water sandstone facies such as a turbidite fan or submarine shelfal channel fill, but might equally represent a shoreface facies.

The interval is overlain by a uniformly thick carbonate unit found over the entire Tangguh area, the Ayot Limestone Formation (Bulling, et al., 1998).

5.3.5.i.3 Ayot Limestone Formation

The Ayot Formation carbonate was originally described from WD-3 core at wellsite by the author (Salo, 1997b-c), generally as: medium to dark gray, but occasionally very dark gray to dark brownish gray; hard to very hard; silicified in part; recrystallized and dolomitic in part; cryptocrystalline to microcrystalline. Glauconite nodules were scattered throughout the entire limestone sequence, with macro and microlaminated appearance evident also throughout the entire sequence. Fossil shell debris (Figure 5.17) is common, although no diagnostic palaeontological index fossils are present in the formation, hence palynological assemblages are used for biozonation. Coral fragments are common. Abundant belemnite tests, locally found as ‘mass death assemblages’, are encountered occasionally near the base of the Ayot Formation, shown in Figure 5.18 (Salo, 1997b-c).

The Ayot Limestone Formation is pervasive over the entire Wiriagar Deep and Vorwata areas with a fairly uniform thickness ranging from 39 ft to 59 ft (Bulling, et al., 1998). The interval is palynologically dated as Oxfordian (Late Jurassic) based on the definitive LJ-9 acmes *Hystrichosphaeridium pachydermum* and *Oligosphaeridium diliculum*, in addition to stereotypical *Dingodinium swanense* and *Cribroperidium perforans* (Waton, et al., 1998c). Other taxa acmes indicative of LJ-9 are *Productodinium cheni*, *Scriniodinium crystalinui*, and *Cribroperidium scottii* (Waton, et al., 1996b). The abundance of palynomorphs is indicative of high marine biological productivity (Waton, et al., 1998c; Waton, et al., 1996b).

A widespread unconformity is found at the base of the unit, irrespective of the underlying strata at any particular Wiriagar Deep or Vorwata well location, identifiable in both core and cuttings palynologically due to the absence of LJ-10 taxa (Waton, et al., 1994; Waton, et al., 1996a-d; Waton, et al., 1997a-h; Waton, et al., 1998a-d).

The combination of palynological data, marine macrofauna including corals, and the presence of a basal unconformity suggest a peneplanation of the Tangguh area, with development of a marine shelfal complex over the entire area. Bioclastic carbonates composed of poorly sorted microcrystalline packstone enveloping large shell tests are commonly formed from restricted embayment shelfal deposits such as the Lower Cretaceous Pearsall Formation of south Texas (Loucks, 1977; Enos, 1983) or low energy epeiric-sea deposits such as the present-day Great Bahamian Bank ((Enos, 1974; Enos; 1983).

5.3.5.i.4 Upper Late Jurassic Shales

The Late Jurassic, Kimmeridgian/Oxfordian shales overlying the Ayot Limestone Formation were described by the author at wellsite as a medium to dark gray porcelanite; hard to very hard; very silicified and well indurated; slightly dolomitic but of a variable calcareous nature ranging from noncalcareous to very calcareous in streaks; and commonly had micro-disseminated black carbonaceous specks scattered throughout. The shale is very ‘glassy-smooth’ textured with a vitreous luster, and prone to conchoidal fracturing. Massive bioturbation is common; as are common to locally abundant micro and macrofossils including foraminifera, mollusk bivalves, ammonites, and belemnites (Salo, 1997b-c).

Due to a coring problem on the WD-3, the cored interval was randomly broken on the rig floor. An admirable attempt was made to piece it together, but there is no certainty that core segments/chips were correctly reassembled, and the absolute depths within this cored interval cannot be known with any degree of confidence (Salo, 1997b-c). Nevertheless, there is a potential geo-chronological marker (which has also been seen in cuttings at WD-1 and WD-4) in the form of a thin, siliceous and possibly smectitic, waxy pale to bright greenish clay streak at approximately 9326 ft to 9329 ft with yet another ‘belemnite mass death-assemblage’ deposit incorporated at 9327 ft to 9328.5 ft. This green shale may possibly represent an altered tuff, as it appears to have a high siliceous content and is grading into a ‘porcelanite’. The silica may have been supplied by devitrification of the glassy tuff during alteration. The shales also has finely scattered green glauconite nodules, imparting the bright green color, and has traces of pyrite present. A calcite filled series of high angle fractures is also evident, and some of the fractures appeared to be slickensided in part (Figure 5.19).

Palynological analysis identified assemblages dominated by *Sentusidinium* spp., *Sentusidinium pilosum*, *Chlamyдохorella* spp., *Omatia montgomeryi*, *Productodinium chenii*, and *Fistulacysta simplex* collectively dating the interval to LJ-8 through LJ-7, or late Oxfordian to early Kimmeridgian (Waton, et al., 1997b). Waton, et al. (1997b) suggested that the paleo-depositional environment was sublittoral open marine, and assemblage distribution suggests a deepening of the marine facies, indicating a transgression.

The overall clutch of palynological data, very well preserved macrofossil tests, glaucony, and ultra fine clastic rocks indicate an marine transgression, which drowned the embayed shelfal Ayot Limestone Formation, progressively deepening the Tangguh area facies until it was a low energy, open marine environment.

5.3.5.i.5 Glauconitic Unconformity

There is a significant number of belemnite fossils concentrated together at the Late Jurassic/Late Cretaceous Unconformity horizon, at driller's measured depth 9288 ft RKB, on WD-3 (Salo, 1997b-c). Pemberton (personal communication, 1998) has explained this 'mass death assemblage' as a "belemnite hash due to bottom current sorting/sweeping and resultant preferential accumulation" (Figure 5.20). The 'belemnite hash' at 9289 ft driller's measure depth, correlates to 9296 ft wireline log depth when shifted by 7 ft to match core GR log with wireline GR log curves. The result is that the glauconite bed response on wireline logs is coincidental with the glauconitic belemnite mass death assemblage, and is confirmed by palynological data as the Late Jurassic/Late Cretaceous unconformity. Typical wireline log response across the unconformity and through the top-most Jurassic erosional surface is high gamma-ray spike (GR), low resistivity (DLL), and high density (FDL) readings, due to abundant glauconite.

The marker bed significance was first identified in the WD-1 cuttings/wireline logs in 1994 (Salo, 1994). This glauconite marker bed has been observed on virtually all wells in the Berau/Bintuni Bay area in cuttings (Salo, 1994; Salo, 1996a-c; Salo, 1997a-g; Perry, 1997; Perry; et al., 1997; Indro, et al., 1997; Salo, 1998a-b). This 'Base Cretaceous glauconite marker' bed is easily discernable from drill cuttings, whole core, and wireline logs in all Wiriagar Deep and Vorwata wells. This is also the case with the WD-3 well, where the dataset includes whole core, wireline logs, and Petcom petrophysical logs over the interval at depth 9294 ft to 9300 ft TVDss

wireline log depth, and whole core interval 9287 ft to 9295 ft driller's measured depth. It is distinct and pronounced due to glauconite nodules making up to 50% of the rock (although preferentially in-filling fossil burrows, fossil casts and moulds, and bioturbation tracks). This is an excellent regional marker bed for identifying the Cretaceous/Jurassic unconformity boundary in the Wiriagar Deep/Vorwata Fields.

There is a distinct lack of Early Cretaceous microfauna, nannoflora, palynoflora, and macrofauna in all Wiriagar Deep and Vorwata wells (Waton, et al., 1994; Waton, et al., 1996a-d; Waton, et al., 1997a-h; Waton, et al., 1998a-d). The Late Jurassic is directly overlain by the Late Cretaceous at all Tangguh well locations. This is clearly due to a regionally induced, areally widespread erosional event tectonic event, which quite possibly is related to the Late Jurassic/Early Cretaceous unconformity noted along the entire northwest shelf of the Australian continental margin (Yeates, et al., 1987; Pigram and Davies, 1987; Bradshaw, et al., 1988; Bradshaw, et al, 1994a; Bradshaw, et al., 1994b; Struckmeyer, et al., 1995; Charlton, 2000a-b; Longley, et al., 2002).

5.3.6 Late Cretaceous Succession

The Late Cretaceous Succession is pervasive over the entire Berau/Bintuni Basins area. The Late Cretaceous Succession ranges from wireline log depth 8963 ft to 9295 ft (-8914 ft to -9246 ft TVss) at the WD-3 location. The lithology of the Late Cretaceous can be generally characterized as very calcareous clays becoming increasingly calcareous with increasing depth, finally being classified as interbedded marls and argillaceous limestone near the base.

There are very few cores through the Late Cretaceous Succession in the Berau/Bintuni Basins area. No cores were taken on Vorwata wells, but the WD-3 did core portions of it (as were portions of the Late Cretaceous in the WD-4, WD-6, and WD-7 wells). The basal portion of the Late Cretaceous was cored from 9233 ft to 9294 ft after depth shifting to match the wireline logging depths, but unfortunately, did not core the argillaceous limestone section above the Base Late Cretaceous. (Salo, 1997b-c).

The core was originally described at wellsite by the author (Salo, 1997b-c) as very dark grayish brown to reddish brown marl; very hard; very silicified, smooth textured, vitreous luster in part, and with a tendency towards conchoidal fracturing (grading to a porcelaneous marl with depth); moderately dolomitic (with a large

ankerite and siderite component); common fossiliferous debris, especially with spherical multichambered foraminifera (Figure 5.21); occasional very finely disseminated black carbonaceous material scattered throughout; and slightly silty in part.

Waton, et al. (1997c) identified the Late Cretaceous based on nannofloral, palynofloral, and microfaunal analyses. The nannofloral marker taxa included *Archangelskiella cymbiformis*, *Micula decussate*, and *quadrum sissinghii*. Palynofloral marker taxa included *Coronifera oceanica*, *Leiospheridia* spp., and *Adnatosphaeridium* spp., consistent with a Late Cretaceous interval. Microfaunal marker taxa included *Abathomphalus mayaroensis*, *Globotruncanita arca*, *Globotruncanita conica*, *Globotruncanita stuarti*, *Globotruncanita elevata*, *Globotruncanitastuartiformis*, *Globotruncanita ventricosa*, *Dicarinella*, and *Marginotruncana*. The combination of microfaunal, nannofloral, and palynofloral marker taxa date the overall Late Cretaceous interval as Cenomanian to Maastrichtian (Waton, et al., 1997c).

Maastrichtian sedimentary rocks were delineated by paleontological analysis from depth 8963 ft to 9166 ft (Waton, et al., 1997c), and this interval was described by Salo (1997b-c) as a brownish gray and medium to dark gray marl, interbedded with some minor argillaceous limestone stringers and calcareous shales. The marls were generally firm to very firm, rarely soft; very fissile with platy cleavage; micro-laminated with layers of differing clay amounts or clay types. The solubility of these micro-laminations varied and were differentially washed-out by the drilling mud giving a “stacked-plate” appearance to the cuttings. The marls appeared to be very well indurated; with the brown variety possibly containing a very high ankerite/siderite content, and appeared to be gradational in part with the interbedded argillaceous limestone lenses and calcareous shales (Salo, 1997b-c).

Waton, et al., interpreted the combined palynoflora, nannoflora, and microfaunal analysis, including benthonic marine fauna such as *Pullenia*, *Uvigerina*, *Bolivinoidea*, and *Gevalinella*, as indicative of a bathyal marine paleo-depositional environment over most of the Tangguh area based on Wiriagar Deep and Vorwata well data (Waton, et al., 1994; Waton, et al., 1996a-d; Waton, et al., 1997a-h; Waton, et al., 1998a-d).

The presence of macrofaunal planktonic foraminifera and deepwater benthic foraminifera, and the bulk sedimentological composition of fine clays and carbonates,

are indicative of a widespread, bathyal marine paleoenvironment in the Tangguh area. That the marine environment deepened with time is supported by the presence of Maastrichtian benthonic marine fauna and bathyal flora, and increasing clay content (relative to carbonate fraction) towards the top of the Late Cretaceous interval.

5.3.7 Late Paleocene Succession

The Paleocene interval was encountered from wireline logging depths 7500 ft to 8963 ft (-7451ft to -8914 ft subsea TVD) in the WD-3. The Late Paleocene Succession overlies the Cretaceous unconformably in most locations, with the Early Paleocene absent or eroded out. The 'Paleocene Unit' is further subdivided into units designated the 'Paleocene Lower Sand-Prone Member' as the most basal unit; followed by a stacked turbidite/debris flow channel (only at WD-2 and WD-4) labelled the 'Paleocene Middle Sand Prone Member'; and overlying both of these member is the 'Paleocene Upper Sand Prone Member' (Bulling, et al., 1998). These sand-prone members are all interpreted by Lowe (1998) as shelfal to deep-water turbidite sandstone fans and lobes or, as in the case of the 'Middle Member', a stacked turbidite channel deposits. These sand prone members were originally described at wellsite by the author as a series of turbidite fans and shelfal channels. In particular, the Middle Member sandstone unit was described as a 'stacked turbidite channel' (Salo, 1996b; Salo, 1997b-c), and the various Upper and Lower Member sandstone units described as turbidite shelfal-toe or sea-floor fan lobe deposits (Salo, 1994; Salo, 1996c; Salo, 1997b-f).

A re-examination of the cores by the author (2001 and 2002) led the author to conclude that the sandstone units cored are indeed classic turbidite channels and floor fans, as originally defined by Bouma. The issue of nomenclature and classification schemes has explored by various authors including, Bouma (1962), Lowe (1998), Lowe and Guy (2000), Shanmugam (1996), Shanmugam (2000), Bouma and Stone (2000), Gani (2003; and 2004). However, the definitions of many terms, and the plethora of new terms including debrites, gravites, densites, in addition to turbidites, and the acknowledgment that individual flows may consist multiple components depending on what portion of the flow is sampled, renders area of classification schemes as extremely problematic. The field of deepwater marine clastic depositional facies is confused with absolutely no consensus on nomenclature, as literature review demonstrates. The confusion of workers in deepwater clastic rocks is concisely

describe in numerous technical articles by Shanmugam (1996), Lowe (1998), Shanmugam (2000), Lowe and Guy (2000), Bouma and Stone (2000), Gani (2003; and 2004) "...A new perspective on the turbidity current and debris flow problem" (Lowe and Guy, 2000). Titles such as: "High-density currents: are they sandy debris flows?" (Shanmugam, 1996); "Crisis for a general term referring to all types of sediment gravity flow deposits" (Gani, 2003); clearly give an accurate sense of the disarray in the field of deepwater sediments. Therefore, the author concludes that the original description by Bouma (1962) and Bouma and Stone (2000) follows the principal of Occum's Razor, and is the best valid working definition of a deepwater clastic gravity flow. The descriptions by the author in 1994-1997 of the Late Paleocene's Lower, Middle, and Upper Members, and by Lowe (1998) describe these sandy members as deep-water turbidite complexes, and this description is still valid.

These Sand-Prone Interval turbidite deposits are not generally found off the Wiriagar Structure and 'P' structure, they are thin and rare on the Ubadari structure where they are not gas charged, and they are almost entirely absent on the Vorwata structure (Bulling, et al., 1998).

The Late Paleocene Lower, Middle, and Upper Members are capped by a flooding event with a pronounced gamma spike that is correlatable (Bulling, et al., 1998). The overlying interval is predominantly shale and has been categorized as the Late Paleocene Mud-Prone Interval.

The entire Late Paleocene interval is easily identifiable as such, at the Wiriagar Deep and Vorwata areas by Frame's (Frame, et al., 1997a-i) microfaunal and nannofloral analyses, but palynofloral is often non-diagnostic due to lack of preservation of potential marker taxa (Frame, et al., 1997a-i; Waton, et al., 1996b). The microfaunal marker taxa include reworked *Planorotalites psuedomenardii*, *Morozovella acuta*, *Morozovella inconstans*, *Morozovella praecursoria*, *Morozovella psuedobuloides*, *Morozovella uncinata*, and *Morozovella trinidadensis*. Late Paleocene nannofloral marker taxa include *Fasciculithus tympaniformis* and *Toweius eminens rap.* (Frame, et al., 1997a-i; Waton, et al., 1994; Waton, et al., 1996a-d; Waton, et al., 1997a-h; Waton, et al., 1998a-d).

The various Paleocene succession members will be discussed in greater detail separately, from the deepest (and oldest) strata, to the shallowest for the Wiriagar and 'P' structures. No cores have been taken in the Cenozoic interval in the Vorwata area by ARCO or BG (Bulling, et al., 1998).

5.3.7.i.1 Sand-Prone ‘Lower Member’ Interval

At the driller’s measured depth of 8938 ft on WD-3, there is a distinct change in lithology. Given the difference of 10 ft to 20 ft between the driller’s measured depths (used for measuring core depths and for determining ‘lagged’ cuttings depths), and the wireline logging depths, this change probably coincides with the unconformable contact between the base of the Paleocene and the top of the Cretaceous. Paleontological analysis (Frame, et al., 1997a-i; Waton, et al., 1997b), and a distinct wireline log change (Salo, 1997b-c), indicate that there is an unconformity at wireline log depth 8963 ft. The interval of the Sand Prone ‘Lower Member’ of the Late Paleocene, extends from wireline log depth 8561 ft, to the unconformity with the underlying Late Cretaceous at 8963 ft (-8512 ft to -8914 ft TVD subsea) on the WD-3.

A thin shale interval lies directly over the K/T Boundary unconformity. The shale can be summarized as medium brown to rust colored in part, and medium to occasionally dark gray in part; firm; very calcareous; micro-laminated with clays of differing water-reactivity, such that the drillbit cuttings took on a “stacked plate” appearance due to differential clay erosion in the drilling fluid (i.e. washing out in the mud) (Salo, 1997b-c).

Overlying this shale at the driller’s measured depth of 8842 ft is a turbidite sandstone, composed of an arkosic litharenite sandstone which was off-white to cream to very light gray with a greenish tint visible under white-light microscopy. The greenish tint is due to the presence of glauconite and chlorite. The sandstone, as described at wellsite from Core No.11, is generally very fine grained; very well sorted; firm to friable; moderately cemented with a siliceous cementation; predominantly quartz with common lithic rock fragments (primarily igneous rock detritus clasts as grains); common to rare feldspars, rare glauconite; scattered calcite and dolomite as grains; and some chlorite staining of the rock overall. Rare ‘paper-thin’ near-horizontal, parallel clay laminations are prominent, especially through the interval 8552 ft to 8856 ft. The visible porosity is overwhelmingly very poor, and the cored interval of the reservoir appeared extremely tight (Salo, 1997b-c).

The shale overlying this sandstone is captured in the base of Core No.8, and in Core No.9 and No.10. It is described at wellsite as reddish brown to rust colored, to chocolate brown, with rare patches of light to dark gray often as burrow-fill, grading locally to porcelaneous shale. The shale is hard to very hard; very calcareous to

slightly dolomitic and probably Fe-oxide stained and may have had a significant siderite component. The shale commonly has inclusions: micro-disseminated black carbonaceous material and woody coal clasts; trace glauconite and trace scattered micromica (muscovite); and a trace silt in part (Salo, 1997b-c).

A major shear/fault zone at 8823 ft to 8828 ft is prominent in the core, characterized by slickensided fracture planes, some calcite filled and some not, hairline to 1 cm. wide, in a series of parallel to subparallel 'en echelon' major fractures with a regular series of antithetic calcite filled fractures intersecting the main fractures at a 35° to 45° angle, giving a trellis, cross-hatched appearance overall. The core is not oriented (Salo, 1997b-c).

Another deep-water sandstone was cored in its entirety by Core No.8. The top of this sandstone is at 8745 ft driller's measured depth, although after adjustment to match wireline logging depths its sharply defined top can be found at wireline log depth 8755 ft on the WD-3 Completion Log. The reservoir is a litharenite sandstone, described by Salo (1997b-c), as cream to very light gray, to off-white with a tan hue. The sandstone is slightly friable to firm, occasionally hard; very fine to medium grained, rarely coarse grained; predominantly quartz, clear to frosted white but often orange hematite stained, yellow limonite stained, and green chlorite stained; very abundant lithic rock fragments, including chert, mottled orange-red-black igneous fragments, and gray to grayish brown shale/siltstone fragments as grains/clasts; common to occasional feldspars, both as feldspar lathes and as relic feldspars altering to kaolinite and other clays; common green glauconite nodules; common finely disseminated coaly/carbonaceous organic debris; scattered 'coin-sized and shaped' dark to medium gray clay lenses intercalated with the sands (especially at depth 8747 ft); and pronounced bioturbation with clay burrow fill (especially at 8748 ft); trace scattered fossils and relic tests, including foraminifera and belemnites; and a trace of disseminated mica flakes (muscovite) and pyrite. There is generally poor calcite cement, with visible porosity ranging from nil to good, with fair generally being the mode (Salo, 1997b-c).

Overlying this reservoir is a minor shale interval of almost 50 ft. The shale is described in the top of Core No.8 as: slightly silty; slightly siliceous in part (grading locally to a porcelaneous shale); chocolate brown to medium brown with some rust tints, and rarely medium gray and brownish gray in color. The shale is hard to very hard; very calcareous to slightly dolomitic and probably Fe-oxide stained and has a

significant siderite component; commonly with micro-disseminated black carbonaceous material and woody coal clasts with some occasional pyrite replacement mixed with carbonaceous material; trace glauconite and trace scattered micromicac (muscovite); and silty in part. It is bioturbated in part, and fossiliferous in part with common foraminifera tests, and with rare scattered dark brown-black 'fish scale-like' debris (Salo, 1997b-c).

Numerous other deep-water sandstones of the Late Paleocene Sand Prone Lower Member are scattered between the top of the 'Lower Member' at 8561 ft wireline log depth, and the top of the massive 50 ft shale previously described. These sandstone intervals, ranging in thickness from 1-12 ft thick, are separated by 1-5 ft shale breaks.

The common but diverse range of foraminiferal and nannofossils taxa noted previously indicate a distal, deep marine, bathyal paleo-depositional environment for the shales and sandstones of the Lower Member (Frame, et al., 1997a-i; Waton, et al., 1997b). The very fine to medium grain-size of the sandstone units ranging from a few feet to the tens of feet in thickness with laminations, combined with biostratigraphic depositional analysis, suggest deepwater turbidite fan lobes on the deep seafloor at the base of a shelf. The ponding of turbidite sands at shelf bases is characterized by distinct depositional lobes of medium-grain sandstone transported by Newtonian fluid turbulent flow, with minor graded bedding, and sharp basal and top bed boundaries (Bouma, 1962; Gani, 2004).

5.3.7.i.2 Sand-Prone 'Middle Member' Interval

The Late Paleocene Sand-Prone 'Middle Member' is not present in all Wiriagar Deep wells, consistent with its interpretation as a turbidite channel. To date, only the WD-2 and WD-4 wells have penetrated it (Salo, 1996c; Salo, 1997a).

This stacked channel member was incised through the Sand-Prone 'Upper Member', and into the top of the 'Lower Member', and filled with a channel flow over several different discharge/sedimentary events. Nearly the entire sequence of channel fill was captured in the WD-2 coring and, therefore, the description originally provided by the author comes from the WD-2 cores (Salo, 1996c).

The top of this 'stacked sequence' is seen at wireline depth 7568 ft (-7519 ft TVDss) on the WD-2 Completion Log. Described by the author (1996c) as a stacked turbidite channel sequence with several cycles of fine sandstone coarsening upwards

to conglomeratic intervals composed very fine to coarse sandstone grain matrix supporting quartz and lithic rock fragment pebbles, cobbles, and abundant shale ‘rip-up’ clasts. As defined by Bouma (1962; Bouma and Stone, 2000), and confirmed by Lowe (D. Lowe, personal communication; 2001) the conglomeratic portions of the channel-fill, composed of granule to pebble to cobble sized quartz grains mixed with shale rip-up clasts, in all likelihood represent the localized turbidity current portion of the flow, ‘floating’ on top of, and at the front of, and on the sides of, the fine-grained sandy slurry flow (Figure 5.22).

The ‘cleaner’ sandstone portions of the cycles are characterized as arkosic to subarkosic litharenites and sublitharenites. The sandstone portions are generally light gray, very fine to fine grained, with common medium sized grains. The sandstones are conglomeratic in part, grading finally to ‘bona-fide’ conglomerates at the top of each individual ‘debris-flow’ sequence. Although light gray overall, individual grains of the reservoir range across the entire spectrum. The varieties of quartz range in color from opaque and frosted white to dark gray, rose, orange, and yellow representing smoky quartz, rose quartz, citrine quartz, and jasper quartz. The conglomerates are composed of locally abundant to common shale and siltstone and sandstone ‘rip-up’ clasts. They are generally medium to dark gray, black, tan, and occasionally red and orange. The common to locally abundant feldspars are off-white to various shades of gray, with a trace scattered glauconite nodules (reworked) that were green (Figure 5.22). Also present, are variable amounts of kaolinite and siliceous cement, with a distinct snowy-white cryptocrystalline to microcrystalline appearance. There are also trace hollow micro-concretions/micro-dissolution vugs lined with medium-sized dolomite rhomb crystals (Salo, 1996c).

The turbidite sandstone members range in hardness from crumbly and friable to very firm, probably related to the degree and composition of the reservoir cementation. The reservoir ranges from very well to very poorly cemented, with some intervals characterized by calcareous or dolomitic cement, and other intervals cemented by siliceous cement. Kaolinite is present as occasional cementation, and as grains (probably the result of feldspar grain alteration). Figure 5.23 illustrates a clean sequence from the WD-2 stacked turbidite channel, just below the rip-up clasts (Salo, 1996c).

The entire field of classification and nomenclature is acknowledged by most workers to be muddled and a major problem for specialists in this field (Bouma, 1962;

Lowe, 1998; Lowe and Guy, 2000; Shanmugam, 1996; Shanmugam, 2000; Bouma and Stone 2000; Gani, 2003; Gani, 2004). However, recognizing that there is a difference in fluid flow physics and resultant deposit appearance between high-density high-turbulence flows (current/fluid driven) and slurry/debris-type flows (gravity/slump driven) as defined by many of the workers above, this author points out that the presence of rip-up clasts, large cobbles, pebbles, and high density inclusions apparently deposited after ‘floating’ on the top of a high-density, high-turbulence flow event, still supports the definition of this channel-fill sequence as a turbidite with the more ‘classic Bouma’ fine-grained to coarse-grained sandstone graded bedding cycles within it (Figure 5.22). The author does not believe the Wiriagar Deep Late Paleocene cores qualify for categorization in recently defined deepwater sediment flows such as debrites, densites, gravites, etc. (Bouma, 1962; Lowe, 1998; Lowe and Guy, 2000; Shanmugam, 1996; Shanmugam, 2000; Bouma and Stone 2000; Gani, 2003; Gani, 2004).

Lowe (1998) interpreted this ‘stacked sequence’ as a large incised channel cutting through ‘Upper Member’ sequences, and noted the absence of red mudstone clasts (indicative of the Lower Member shale coloration). Lowe concluded that the incision may therefore have stopped at the top of the lower member, with the implication that the Middle Member post-dates the Upper Member and has incised it at WD-2 and WD-4. Lowe also postulated that the ‘Middle Member’ well data, the inferred sea-floor topography, and similarities to the ‘Lower Member’ paleo-depositional environment indicate a north-by-slightly northeast to south by southeast channel orientation and flow for the channel, although this is inconclusive due to the lack of paleo-current data (Lowe, 1998). Lowe (D. Lowe, personal communication; 2001) characterized the ‘Middle Member’ as a thick, normally, graded turbidite channel deposit. It should be noted that the WD-2 and WD-4 well locations clearly constrain a submarine canyon or channel orientation as NNE-SSW.

Pemberton (1997c-d) identified the Paleocene ‘Middle Member’ ichnocoenose as characterized by the *Anconichnus*, *Chondrites*, *Cosmoraphe*, *Helminthopsis*, *Ophiomorpha*, *Nereites*, *Palaeophycus*, *Planolites*, *Skolithos*, *Subphyllochorda*, *Teichichinus*, *Thalassinoides*, and *Zoophycos* ichnogenera. His evaluation is that the ichnological facies assemblage represented a fully marine, outer shelf to upper slope paleoenvironment, with the turbidite and debris flow event fauna representing shelf to slope deep-water deposition and not basin-floor turbidite fans or lobes. He speculated

that the presence of the marine fauna in tempestuous turbidity events may have been due to the ‘Doomed Pioneer’ faunal model, and that the mechanism for the generation of these turbidites and debris flows may have been due to a rapid increase in slope angularity caused by tectonic events (Pemberton, 1997c-f).

This study finds the data supports the conclusion that the Middle Member is a submarine canyon or channel fill sequence, or perhaps part of a series of located of submarine canyons or channel fill sequences, on an outer marine shelf slope.

5.3.7.i.3 Sand-Prone ‘Upper Member’ Interval

Overlying the Sand-Prone ‘Lower Member’ Interval at most Wiriagar Deep well locations, but cut out by the Middle Member incised channel and therefore absent at the WD-2 and WD-4 locations, is a very massively bedded, thick shale sequence comprising the Upper Member (Bulling, et al., 1998). This shale, at WD-3, is at the driller’s measured depth 8360 ft to 8590 ft (8370 ft to 8596 ft wireline logging depths). The shale is generally light gray brown to medium brown to dark gray; soft and amorphous to firm and tabular/platy/blocky; calcareous to very calcareous (grading locally to a marl); and below 8560 ft (driller’s measured depth) silty in part. The shale in cuttings, has a differentially eroded microlaminated structure that gives rise to a “stacked plate-like” appearance to individual cuttings fragments (Salo, 1997b-c).

Above this massive shale, at WD-3, is yet another series of deep-water sandstone reservoir sequences, at 8244 ft to 8370 ft wireline log depth. This sandstone of the Sand-Prone Upper Member consists of a series of five sandy carbonate reservoirs separated by relatively thin 8 ft to 25 ft thick shale breaks. The calcareous sandstones grade locally into arenaceous limestone, and are generally white to off-white to cream; soft to firm in cuttings; a cryptocrystalline to microcrystalline mudstone with very abundant quartz sand grains, grading locally to a very calcareous or limy sandstone; argillaceous in part with primarily kaolinite clays; and silty in part. The sand grains are generally quartz, with occasional lithic rock fragments; commonly silt to very fine grained in size, rarely medium grained; round to subrounded; and scattered throughout a limestone cement/matrix (Salo, 1997b-c).

The interbedded shales differ from the previously described shales, most notably in color but also in all other characteristics. These shales up to driller’s measured depth of 8130 ft are medium brown to slightly reddish brown, and brownish

gray (the shales above 8130 ft are generally gray hued). The shales are soft to only slightly firm, often being thin and runny when circulated up as drill cuttings; calcareous; and very slightly silty to rarely finely sandy in part (Salo, 1997b-c). Above 8146 ft wireline log depth (and 8125 ft driller's measured depth) is the Late Paleocene Formation's Mud-Prone Interval (Bulling, et al., 1998).

Similar to the Lower Member, this Upper Member appears to be of a lower slope to sea-floor, deepwater paleo-depositional facies sediment, composed of mainly very fine grained clay sediments with coarser-grained, ponded turbidite fan sandstone lobes interbedded. The turbidite fan quartz sandstone grains are possibly incalated with some shelfal carbonate rip-up clasts and shell debris.

5.3.7.i.4 Mud-Prone Interval

The Mud Prone Interval is primarily claystone or shales but has some sandstone streaks. One such sandstone was cored in entirety on WD-3 by Core No.5.

The sandstone was originally described by the author (Salo, 1997b-c) as very laminated, with almost "varve-like" microlaminations in conjunction with more massive alternating shale and sandstone laminations on the order of 4 inches to 8 inches thick. The sandstone is a subarkosic sublitharenites: off-white to very light gray; very fine to fine grained, rarely medium grained; commonly interbedded with shale lenses, and also interlaminated with "paper-thin" to 1 inch wide shale/claystone streaks, parallel to subparallel to horizontal; dominantly quartz; but with common to locally abundant lithic igneous rock fragments; common to occasional feldspar grains; with rare mica (muscovite); but with common carbonaceous or coaly clasts; and rare pyrite and chert nodules. The sandstone is generally very well cemented with a dolomitic/calcareous cement; moderately well sorted; and angular to occasionally subangular. The mineral assemblage, and angularity are suggestive of a 'granite-wash' in part (Salo, 1997b-c).

A second, massive sandstone/conglomerate was also cored almost in entirety above this shale interval seen only in cuttings. The top of this reservoir is at 7918 ft (driller's measured depth) on the WD-3 cores (7924 ft wireline log depth). The WD-3 Core No.2, No.3, and No.4 cored almost the entire reservoir, a portion of which is shown in Figure 5.24 (Salo, 1997b-c).

The conglomerate/sandstone in the cores are generally off-white to light gray with a slight tan/brownish tint overall; very fine grained to rarely cobble sized,

although medium grained to coarse grained with scattered pebbles being the mode; angular to subround. Although predominantly quartzose, there are very common to locally abundant fossil shells, resembling a 'shell hash' of 10% to 20% shell fragments including belemnites, foraminiferas, and bivalves; abundant to very common feldspars; very common lithic rock fragments (both igneous and shaley); trace glauconite; and traces of pyrite. The quartz grains are in part stained green from chlorite, citrine yellow from limonite, and red/orange from hematite. The lithic fragments are locally abundant as shaley 'rip-up' clasts; and also included common to locally abundant coaly/carbonaceous clasts, rarely with a woody structure. Cementation is predominantly carbonates (calcite and dolomite) with some kaolinite in part. The cores have rare dissolution cavities and channels visible (Salo, 1997b-c).

The shales are generally dark gray, and slightly silty, becoming very calcareous to marly, and light and medium gray above 7770 ft. The shales are generally: firm to slightly hard and well compacted; calcareous to very calcareous grading to marl locally. The shale are siltier and less indurated/compacted at shallower depths. The shales become silty and graded locally to a calcareous siltstone, and dolomitic in part by driller's measured depth 7500 ft (Salo, 1997b-c).

The Late Paleocene Mud Prone Interval carbonates included marls, limestones, and limy dolomites. The marls are generally light to medium gray, to brownish gray; soft to occasionally firm to slightly hard; commonly amorphous and soluble 'lumps' to blocky/platy cuttings; sticky and gummy in part; silty to very silty in part; and commonly grade to and from an very calcareous shale (Salo, 1997b-c).

The crystalline carbonates are generally a gradational rock type with the silty shales and marls. The carbonates are generally thinly bedded having a maximum thickness of less than 6 ft between 7500 ft and 7900 ft, and on average are only 2 ft thick. While the carbonate characteristics range from a marl, to a generally 'clean' dolomitic limestone, the typical crystalline dolomitic limestone can be summed up as off white to cream to buff/tan, mottled; hard to very hard; cryptocrystalline to microcrystalline limestone and recrystallized dolomitic limestone; silty to 'clean' to occasionally argillaceous in part, grading to marl locally, especially with depth (Salo, 1997b-c).

The Late Paleocene shale succession represents a deepwater facies for the paleo-depositional environment of the Tangguh area. The presence of the small-scale stacked channel turbidite sandstones, combined with ichnological facies and

palynological/palaeontological data that indicate a deepwater depositional environment, demonstrate that the Late Paleocene interval represents a deepwater depositional facies at Tangguh, with the Wiriagar Deep area in particular, located at the shelfal edge. The presence of the Sand-Prone Middle Member, which is a stacked turbidite channel-fill sequence that cut out the Upper Member at WD-2 and WD-4 was located on the paleo-geographic shelf slope. The Vorwata area may represent a more distal, bathyal marine environment resulting in the Vorwata area's Paleocene interval being less sand-rich, and predominantly Mud-Prone.

5.3.8 Eocene Succession

At WD-1, the Eocene was originally described by the author as an interbedded sequence of carbonates (limestone and more often dolomites), claystones, occasional sandstones, and evaporites (anhydrite) (Salo, 1994). The top of the Eocene is more and more carbonate-rich (with less clastic sand and evaporitic lenses intercalated) and the shallower interval is the earliest member of the massive carbonate sequence known as the New Guinea Limestone Group (NGLG) (Dolan and Hermany, 1988). This carbonate group is areally extensive, blanketing widespread areas of the island of New Guinea. In much of New Guinea, including Wiriagar Deep, the NGLG is a platform carbonate, with continued deposition through the Oligocene and into the Late Miocene (Dolan and Hermany, 1988; Perkins and Livsey, 1993; Bulling, et al., 1998).

The Eocene Interval is identified from foraminiferal and nannofossils marker taxa, with palynoflora analysis lacking definitive marker taxa to be diagnostic at the Wiriagar Deep and Vorwata areas. Frame, et al. (1997a) and Waton, et al. (1994) identified an assemblage of foraminifera consistent with an Eocene age for the interval, including *Lacazinella wichmanni*, *Nummulites* spp., and *Fasciolites* sp. This foraminiferal assemblage in conjunction with the nannofloral assemblage including *Discoaster lonoensis*, *Discoaster* cf. *saipenensis*, *Discoaster* cf. *barbadiensis*, *Discoaster bisecta*, *Discoaster tani nodifer*, *Cribrocentrum reticulatum*, and *Helicosphaera euphratis* clearly identify the Eocene interval at the WD-1 location (Waton, et al., 1994).

Mixed clastic and carbonate, with minor evaporite lithologies indicate a shallow marine to shelfal marine paleogeographic depositional facies accommodation space where flat coastal plains adjacent to a marginal marine shoreline were

periodically subaerially exposed and dry, arid 'sabkha plain' evaporites (anhydrite) formed ultimately becoming interbedded with marine limestone/dolomites (Salo, 1994).

5.3.9 New Guinea Limestone Group (NGLG)

The New Guinea Limestone Group (NGLG) is locally comprised of the top-most Late Eocene carbonates (as discussed above), Oligocene Limestone Formation, Faumai Formation, and the Kais Limestone Formation, in the Berau/Bintuni Basin area of the Bird's Head, in NW Papua. The basal NGLG interval was identified as Eocene, and has already been described above as a member of the Eocene Succession.

5.3.9.i.1 Oligocene Limestone Formation

The Oligocene Limestone Formation is present in the Bird's Head region only in Lengguru Thrust/Fold Belt (LTFB) and Kumawa-Onin-Misool Ridge (KOM), outcrops, and in the synclinal trough subcrops of Bintuni Basin (Figure 5.30). The Oligocene Limestone Formation has rarely been penetrated by wells in the area, since it exists only in the synclinal troughs (Bulling, et al., 1998). These vestiges of preserved Oligocene Limestone Formation have been seismically mapped between the Wiriagar Deep, Vorwata, Wos and Ubadari structures, but it was eroded on the anticlinal structure tops where most of the exploratory and delineation drilling has been concentrated (Bulling, et al., 1998). Peneplaning of the region at the end of the Oligocene stripped Oligocene Limestone Formation from the anticlinal structure crests and flanks. Unfortunately, the actual rocks of the Oligocene in the subsurface have not been seen, even in drill cuttings, due to massive 'lost circulation' whilst drilling. The fractured and vuggy carbonate character is supported by rare well logs, such as dipole sonic waveform analyses and FMI/FMS borehole imaging, confirming vugs and open fractures (Salo, 1996a-b).

Overall, the entire NGLG carbonate succession is characterized by workers as a shallow marine platform carbonate (Dolan and Hermany, 1988; Perkins and Livsey; 1993; Salo, 1996a-b; Bulling, et al., 1998; Hall, 2000). The author originally interpreted the Oligocene Limestone in outcrop on the KOM ridge, at East Onin #1 well location (Figure 5.25), as a massive platform carbonate sequence, although it was not described in detail or measured (Salo, 1996a-b). The calcareous content and fossiliferous nature of the rock were noted, however, and at the request of the author,

palynological/paleontological analysis at wellsite dated the outcrop as Oligocene (P. Waton, personal communication, 1994).

5.3.9.i.2 Faumai Formation

The Faumai Formation is the Bird's Head regional name used by BP/ARCO for the Eocene to mid-Miocene member of the New Guinea Limestone Group (NGLG), where the Oligocene Limestone Formation is absent. It has been described by some workers as the Eocene member of the NGLG (Pigram and Sukanta, 1989), the Paleocene through Mid-Oligocene member of the NGLG (Perkins and Livsey, 1993), and as the Eocene to Oligocene member of the NGLG (Dolan and Hermany, 1988; Nurzaman and Pujianto, 1994). It is described here based solely on the rare cuttings acquired from near the formation top, at the Middle to Early Miocene level, due to massive 'lost circulation' at depth, mentioned earlier.

Originally described by the author at wellsite (Salo, 1994; 1996c; 1997b-c), the Faumai Formation is generally characterized as interbedded limestone and dolomite. The dolomite is tan to light brown, to cream colored; and hard to very hard, occasionally firm. Overall it is very recrystallized with a cryptocrystalline to occasionally microcrystalline fabric, but fossiliferous (with foraminifera tests and gastropod/mollusk shell debris) in part, calcareous and grading in part to dolomitic limestone, rarely very slightly argillaceous in part, and with only traces of scattered pyrite. The dolomites are generally tight with nil visible matrix porosity, but with locally common vugs, dissolution channels, and fractures (Salo, 1994; Salo, 1997b-c).

The limestone is described as off white to cream to rarely translucent, firm to hard, with a cryptocrystalline to microcrystalline fabric and with a slightly sucrosic texture in part. The limestone is generally not argillaceous, but common slightly to very dolomitic, grading locally to dolomite (Salo, 1994).

Waton, et al. (1996b) identified limited cuttings at the WD-3 well (prior to losing circulation) from the top interval of the Faumai Formation as Early to Middle Miocene based on nannoflora marker taxa, ranging over either Miocene or Miocene to Oligocene, including *Sphenolithus heteromorphus* (Middle to Early Miocene limited) and *Sphenolithus delphix* (Early Miocene to Late Oligocene).

It should be noted that there are no cores through the Faumai Formation on Vorwata and Wiriagar Deep wells, and drill cuttings were only obtained in the top-

most Faumai Formation above the ‘lost circulation’ zone on those wells. Only on Occidental’s R-1 and O-1 wells had cuttings through the entire Faumai Formation.

Only these two Occidental wells (R-1 and O-1) in addition to several the ARCO Vorwata and Wiriagar Deep wells obtained any wireline logs other than gamma ray over the Faumai Formation and the overlying strata (possible sealing units). The quality of the wireline logs from the Occidental wells is poor as a result of abundant lost circulation material (LCM) and cement (from cement plugs to restore circulation) in the hole. ARCO ran basic wireline logs suites, and both cased-hole and open-hole VSP logs (vertical seismic profile tool), through the Faumai Formation in an attempt to solve velocity to depth conversion problems associated with the 3D seismic survey ARCO conducted (Keho and Samsu, 2002).

Based solely on limited top-formation drill cuttings from ARCO’s wells (Salo, 1994; and Salo 1996a through 1997e), Occidental’s descriptions of drill cuttings (R-1 and O-1), wireline log suites from a few ARCO wells (including FDL density, CNL porosity, dipole sonic, FMI/FMS borehole imaging, and VSP), and coherency image slices from the time domain of the 3D seismic survey it has been interpreted that the Faumai Formation is probably a shelfal platform carbonate that is very vuggy due to karstification, resulting from an aerial exposure during the Middle Miocene which resulted in the unconformity which separates the Middle/Late Miocene Kais Limestone from the underlying Faumai Formation (Dolan and Hermany, 1988; Perkins and Livsey, 1993; Bulling, et al., 1998; Waton, et al., 1994; Waton, et al., 1996a-d; Waton, et al., 1997a-h; Waton, et al., 1998a-d).

The carbonate commonly is faulted and has open fractures, especially in the ‘blind drilling’ interval that persists down into the top-most Eocene carbonates. The fractures, faults, and vuggy dissolution, in combination with a subnormal formation pressure, is probably the cause of the lost circulation encountered on wells drilled in Bintuni Basin. A series of horizontal coherency images from the 3D seismic survey set through the Faumai Formation as time-slices is interpreted as imaging fractures, faults, vugs, and enormous dissolution sink-hole cavities in the formation (Figures 5.26 through 5.28) similar to the karst surface landforms seen in surface analogues outcrops such as the dolinas, poljes, speleothems, klufthkarren, rillenkarrren, solution pipes, kamenitza, and relic karst terra-rossa alteration zones (Quinlan, 1972; Folk and Assereto, 1976; Estaban and Klappa, 1998). Analogues with the Faumai Formation’s karstification abound, including visible karst surface landforms in the Garraf

Mountains of NE Spain; Mayan Mountains of Belize and the Yucatan, Mexico; and the Straits of Florida (Estaban and Klappa, 1998).

5.3.9.i.3 Kais Limestone Formation

This Late Miocene massive carbonate lies unconformably, in the Berau/Bintuni Basin, atop another massive carbonate sequence, the Faumai Formation. The Kais Limestone Formation was originally described at wellsite by the author (Salo, 1994; Salo, 1996c; Salo, 1997b-f) as predominantly a dolomitic limestone, milky white to cream, buff to very light gray, and rarely tan to light brown. Generally firm, the limestone is cryptocrystalline to microcrystalline, very dense and massive, with a trace of pyrite near the top, and slightly argillaceous in part. Dolomitization is very pronounced near the top of the carbonate, with a dolomitic (and ankerite) component. Laboratory analyses from the equivalent interval in the WD-1 well shows a high ankerite, and Fe-calcite component in both the massive Kais Limestone and Faumai Formations (Salo, 1994).

The author originally described the Kais Limestone Formation on the WD-3, WD-2, and WD-1 wells as a dolomitic limestone; milky white to cream to tan to buff, and rarely light brown to light gray; firm to very hard; with a cryptocrystalline fabric recrystallized in part to microcrystalline, with a sucrosic texture in part. The formation is locally rich in relic fossils and is only rarely slightly argillaceous in part, with a trace of pyrite. Fossils identified in cuttings included coral branches, foraminifera, and more rarely gastropods and mollusks. The carbonate is generally tight with nil visible matrix porosity but some vuggy and moldic porosity is evident (Salo, 1997b-c; Salo, 1996c; Salo, 1994). It should be noted that petrographic and mass-spectrometer analysis from the Kais Limestone Formation in the WD-1 well shows a high ankerite, and Fe-calcite component in the carbonate samples (Salo, 1994). This is similar to compositional analysis results reported by Conoco in the shallow Wiriagar field wells (Dolan and Hermany, 1988). Conoco obtained 244 ft of cores on their shallow well, the Wiriagar #3, and did sedimentological and petrographic analyses on the core samples. They identified more than one intraformational diagenetic horizon as resulting from either subaerial exposure or very near-surface fresh-water diagenesis that resulted in formation of moldic porosity, dissolution vugs, solution channels, and fracturing, some occasionally floored by vadose silts (Dolan and Hermany, 1988).

Dolan and Hermany (1988) described the mineralogy as calcium carbonate with zones of Fe-rich dolomitization, and characterized the limestone as coral boundstone, dolomitized coral packstone, and fossiliferous grainstone.

Watson, et al. (1996c) identified the Kais Limestone Formation interval with the definitive marker taxa, *Discoaster Quinqueramus* (Late Miocene), from the top-most Kais Limestone Formation interval.

The top of the Kais Formation, and the hydrocarbon production section is quite shallow ranging from 1530 ft to 2700 ft, which effectively precludes the Kais Limestone Formation from being potential CO₂ ESSCI sites. Furthermore, due to dissolution of carbonates, especially limestone, in the presence of CO₂ streams, the Kais Limestone Formation and the Faumai Formation are considered to be unsuitable for ESSCI type containment and sequestration.

Finally, it should be noted that the fractures, dissolution vugs and cavities that are not only abundant in the Faumai Formation, and cause loss of circulation during drilling of wells, but also exists within the lower Kais Limestone Formation in some locations in the Berau/Bintuni Basins. Coherency images derived from the ARCO 3D seismic survey dataset have also been interpreted as showing fractures/faults, and some dissolution cavities/vugs in the middle to basal Kais Formation interval (Figures 5.29 through 5.31).

5.3.10 Steenkool/Sele Formation

The original type area of the Steenkool Formation occurs in outcrops near the base of the Lengguru Thrust/Fold Belt (Visser and Hermes, 1962). It is traditionally described as a Pliocene to Pleistocene, shallow marine to brackish water paleo-depositional facies consisting of swamp and coastal shallow marine clays, silts, sands, and organic detritus from the prolific river discharges (Visser and Hermes, 1962; Dolan and Hermany, 1988). But that definition has been broadened to include the Sele, classified as the Holocene to present-day clastic shallow marine to brackish swamp clays, silts, organic detritus, and occasional sands being deposited from the current river discharges. The division between the Steenkool and the Sele formations is not readily apparent without detailed palynological analysis, which has not been done on rock samples from Occidental, ARCO, or BG wells in the Bintuni Basin area.

Therefore, the Steenkool and Sele formations are combined for the purposes of this study, and the Steenkool, therefore, has a 'working definition' of Pliocene to

Present shallow marine to brackish swamp clastics and organic detritus, in Bintuni Basin.

The subsurface lithology seen in drill cuttings was undifferentiated loose sands, conglomeratic in part, and claystone (Salo, 1994; Salo, 1996c; Salo, 1997b-c). The sands are generally medium to coarse grained quartz, pebble sized in part, and subangular to subround dominantly quartz but with a rare trace of lithic fragments as pebbles. Grains are poorly sorted, and generally loose and unconsolidated, although when rarely cemented, the cementation is vis-à-vis a non-calcareous clay matrix (Salo, 1997b-c; Salo, 1994).

The clay is light to medium gray to greenish gray (possibly chloritic in part), soft and amorphous in cuttings, very sticky and gummy textured, very water soluble and water reactive, non to slightly calcareous in part, slightly sandy to silty in part, slightly fossiliferous in part with occasional shell fragments, and with a trace of pyrite (Salo, 1997b-c; Salo, 1994).

Deposition of this lithostratigraphic unit is continuing today in the Wiriagar Swamp, Berau Bay, and Bintuni Bay areas of the Bird's Head, as can be readily seen in LANDSAT image (Figure 5.32) and aerial photograph (Figure 5.33) of the Bintuni Basin swamp and bay area.

PART II

INJECTIVITY

6.0 SEQUENCE STRATIGRAPHY

The first detailed sequence stratigraphy framework for the Mesozoic interval of the Berau and Bintuni Basins was done for this study. Previous efforts to construct a suitable framework were hampered by lack of interpreted seismic images at the depth of investigation required for the Mesozoic interval. Confusion regarding the depths shifting of drill cuttings data to match wireline logs also contributed to errors in interpreting the stratigraphic relationship between key reservoir and seal units. This study attempts to resolve these conflicts.

6.1 Stratigraphic Methodology

The stratigraphy of the entire Tangguh area was evaluated using all of the data provided by BP, including seismic horizons, paleontology and palynology, regional structural geology, lithostratigraphy, well log motif correlations, and ichnological facies and fabric studies. These data sets were evaluated, collated, and integrated to form a coherent and realistic sequence stratigraphic framework, that was then compared with global eustacy curves for the Mesozoic as established by Haq, et al. (1987), and subsequently updated by Berggren, et al. (1995).

Scattering of seismic energy during the seismic survey acquisition phase was caused by a thick carbonate succession, the NGLG, at relatively shallow depths, which in turn resulted in very poor seismic resolution at the depths of interest. Only two seismic horizons relevant to the Mesozoic interval were available from the interpreted 2D and 3D seismic data volumes, the 'Base Late Cretaceous' and the 'near-Top Late Permian', and even these are poorly imaged over vast areas of the greater Tangguh region. Other horizons of importance such as the 'Top Pre-Ayot Shale sealing unit', 'Base Pre-Ayot Shale sealing unit', 'Top Roabiba Sandstone Formation reservoir', and the 'Top Aalenian Sandstone Formation reservoir' were beyond resolution, seismically, in the study area. These horizons were created as 'phantom' surfaces, however, constrained by a combination of wireline log identifications, and palynological 'biozonation' identifications based on the analyses of conventional cores, sidewall cores, and drill cuttings (in that preferential order).

The original combined biostratigraphic reports, summarizing palaeontological and palynological analyses by Waton, et al. (1994, 1996a-e, 1997a-h, and 1998a-d) were scrutinized to form an overall framework of biozonations based on age of deposition. A careful adjustment of biozonation age intervals, well by well, was

carried with cuttings data depth shifted based on laboratory whole core gamma-ray log correlations to open-hole wireline gamma-ray logs (where cores were available), and extrapolated to shift the biozonation ages for wells/intervals with only drill cuttings. The depth shifts in drill cuttings and core samples are listed below in the 'Depth Shift Table' (Table 6.1).

After the establishment of an overall biozonation age framework, the lithostratigraphy and the open-hole well log motifs were evaluated within each unique biozonation age interval by the author. The initial correlations within each biozonation age interval were then refined using ichnological facies identified by Pemberton (1997a-f) to further refine the stratigraphy on a well by well basis for each interval.

Well Name	Log Shift Based on Core GR Add (ft)	Log Shift Based on Wireline Log Extrapolation Add (ft)
Ubadari-1	5	
Ubadari-2	9	
Vorwata-1	10 - 12	
Vorwata-2	15	
Vorwata-3		18
Vorwata-4	30	
Vorwata-5	25	
Vorwata-6	16	
Vorwata-7st	14	
Vorwata-8		0
Vorwata-9		2
Vorwata-10st	Cores cut on original hole, wireline logs run on sidetrack	
Vorwata-11		0
Wiriagar Deep-1	7	
Wiriagar Deep-2	15 - 18	
Wiriagar Deep-3	7 - 10	
Wiriagar Deep-4	4	
Wiriagar Deep-5st	10	
Wiriagar Deep-6	14 - 18	
Wiriagar Deep-7	10	
Wiriagar Deep-8	7	
Ofaweri-1		?
Roabiba-1		?
Wos-1		?

Table 6.1: Table of core and cuttings depth shifts at each well, based on core gamma-ray (GR) correlated and depth shifted to wireline log gamma-ray GR, or driller's measured depth from RKB corrected by wireline log TD depth.

Finally, the refined and detailed internal stratigraphy of each biozone interval were correlated between wells, and these correlations were then integrated with the core facies identification from a study by Tye and Hickey (1999).

A review of the sedimentological data and the development of a revised stratigraphic framework also produced a coherent and comprehensive model of the Jurassic interval sequence stratigraphy, supported by paleogeographic facies maps over the Tangguh area. The maps represent a series of approximate time slices showing shifting facies belts through the Jurassic indicating an overall progression of fluvial-deltaic, to shoreline, to barrier-lagoon, and finally to offshore fully-marine environments. These maps predict continuous high quality seal coverage over the Vorwata anticline (the shales of the Pre-Ayot interval and the Late Jurassic Shale interval), and also predict a thick Jurassic 'Roabiba' sandstone reservoir (the sandstones of the Bajocian/Bathonian Roabiba interval and the Callovian Roabiba interval) with favorable porosity and permeability characteristics for CO₂ injection. The result is a coherent and detailed model of the sequence stratigraphy (Table 6.2) of the Tangguh region that differs substantially from the previous paleo-depositional conclusions and stratigraphic zonations as summarized by Bulling, et al., (1998). The sequence stratigraphic framework was compared with the most recent 'global eustacy' curves (Berggren, et al., 1995) and a 'most likely' hypothesis for the 1st order controls on the sequence stratigraphy made (i.e. tectonic uplift/subsidence versus global eustacy change). Isopach maps were also constructed for each of the sequence stratigraphic units/zones, with gross thickness of intervals presented as a list in Table 6.3. This sequence stratigraphic framework, with appropriate reservoir character or sealing potential, was eventually incorporated into a 3D geological model (using GeoCARD modelling software) of the Tangguh area in Bintuni Basin.

6.1.1 Seismic Stratigraphy

The dataset for seismic stratigraphy is quite limited in the Tangguh area, due the presence of a thick Tertiary carbonate unit near surface, overlying the Jurassic interval. Several vintage 2D seismic surveys were conducted prior to 1994, and a 3D seismic survey was conducted over the Wiriagar Deep, Vorwata, and Ubadari anticlinal structures in 1997. All of them are limited in resolution at depth by the scatter of the seismic source energy in the thick Tertiary carbonate unit, the New

Formation-Interval	Sequence Boundary	Ofaweri-1	Roabiba-1	Nambumbi-1	Sakauni-1	Vorwata-1	Vorwata-2	Vorwata-3	Vorwata-4	Vorwata-5	Vorwata-6	Vorwata-7ST	Vorwata-8	Vorwata-9	Vorwata-10ST	Vorwata-11
Top Late Cretaceous Marl	K/T Unc	8976	10223	12205	12235	11053	11666	11376	11522	11962	11900	12355	11920	12010	12038	12396
Base Late Cretaceous	K Unc	9530	10598	12809	12828	11550	12202	11884	12075	12521	12464	12848	12451	12579	12611	12920
Top Upper Late Jurassic Shales	K Unc	9530	10598	12809	12829	11053	12205	11884	12076	12518	12463	12848	12450	12577	12611	12920
Base Upper Late Jurassic Shales	Top Ayot (mfs)	9611	10780	13037	12846	11692	12294	11982	12132	12589	12576	13012	12464	12618	12693	12941
Top Ayot Limestone Formation	Top Ayot (mfs)	9611	10780	13037	12846	11692	12294	11982	12132	12589	12576	13012	12464	12618	12693	12941
Base Ayot Limestone Formation	Base Ayot	9647	10830	13103	12884	11737	12340	12031	12177	12632	12622	13059	12498	12662	12740	12982
Top PA60	Base Ayot	9647	10830	13103	12884	11737	12340	12031	12177	12632	12622	13059	12498	12662	12740	12982
Base PA60	LJ10 Unc	9649	10840	13113	12896	11743	12344	12037	12183	12636	12628	13062	12501	12666	12749	12990
Top PA30	LJ10 Unc	9649	10840	13113	12896	11743	12344	12037	12183	12636	12628	13062	12501	12666	12749	12990
Base PA30	PA2	9720	10918				12480		12229	12732	12729	13098		12816	13010	13099
Top PA20	PA2	9720	10918				12480			12732	12729	13098		12816	13010	
Base PA20	PA1	9747	10960				12536			12752	12760	13118		12844	13071	
Top PA10	PA1	9747	10960			11757	12536	12053		12752	12760	13118	12570	12844	13071	13099
Base PA10	CU5	9751	10973			11759	12558	12057		12757	12770	13125	12576	12846	13119	13110
Top CU50	CU5	9751	10973			11759	12558	12057		12757	12770	13125	12576	12846	13119	13110
Base CU50	CU4	9756	10977			11765	12560	12063		12760	12772	13131	12579	12849	13124	13115
Top CU40	CU4	9756	10977			11765	12560	12063		12760	12772	13131	12579	12849	13124	13115
Base CU40	CU3	9777	11002			11785	12585	12085		12785	12800	13154	12590	12879	13156	13147
Top CU30	CU3	9777	11002			11785	12585	12085		12785	12800	13154		12879	13156	13147
Base CU30	CU2	9794	11027			11811	12599	12109		12791	12820	13179		12899	13171	13159
Top CU20	CU2	9794	11027			11811		12109			12820	13179			13171	
Base CU20	CU1	9808	11040			11839		12126			12830	13235			13207	
Top CU10	CU1											13235				
Base CU10	MJ2 Unc											13290				
Top R80	MJ2 Unc		11040				12599				12830				13207	
Base R80	R7		11162				12710				12905				13300	
Top R70	R7	9808	11162				12710		12229	12791	12905		12590	12899	13300	13159
Base R70	R6	9869	11293				12721		12253	12844	12944		12632	12953	13435	13194
Top R60	R6	9869					12721		12253	12844	12944		12632	12953	13435	13194
Base R60	R5 (mfs)	9880					12736		12256	12852	12949		12636	12967	13456	13207
Top R50	R5 (mfs)	9880					12736		12256	12852	12949		12636	12967	13456	13207
Base R50	R4	9941					12915		12332	12924	12984		12655	13042	13474	13245
Top R40	R4	9941	11293				12915			12924	12984			13042	13474	13245
Base R40	R3	9966	11315				12979			12985	13057			13090	13533	13272
Top R30	R3		11315	13130		11839	12979			12985	13057			13090	13533	13272
Base R30	R2 (mfs)		11413	13192		11895	13011			13032	13139			13128	13571	13312
Top R20	R2 (mfs)	10008	11413	13192		11895	13011			13032	13139	13290		13128	13571	
Base R20	R1	10039	11435	13202		11915	13026			13039	13150	13307		13134	13576	
Top R10	R1	10039	11435				13026			13039	13150	13307		13134	13576	
Base R10	A1 (mfs)	10052	11504				13047			13074	13165	13380		13155	13608	
Top A20	A1 (mfs)	10052	11456									13380				
Base A20	Top Permian Unc	11968	11461									13429				
Top PZ	Top Permian Unc		11461	13202	12928	11915	13047	12126	12332	13074	13165	13429	12655	13155		13312
TD (in Permian unless otherwise noted)	Well TD	10201	12007	13445	13206	12675	13368	12800	12985	13251	13517	13562	12875	13566	13619 (Roabiba)	13628

Table 6.2A: Table of stratigraphic zone and boundary depths by well for the Tangguh area. All are wireline log depths from RKB, in feet.

Formation-Interval	Sequence Boundary	WiriagarDeep-1	WiriagarDeep-2	WiriagarDeep-3	WiriagarDeep-4	WiriagarDeep-5ST	WiriagarDeep-6	WiriagarDeep-7	WiriagarDeep-8	Kalitami-1X	Wos-1
Top Late Cretaceous Marl	K/T Unc	7320	8030	8963	8528	8995	7714	7977	7576	4100	8274
Base Late Cretaceous Marl	K Unc	7738	8381	9295	8819	9336	8041	8354	8050	4336	8655
Top Upper Late Jurassic Shales	K Unc	7738	8381	9295	8819	9338	8041	8354	8050	4336	8655
Base Upper Late Jurassic Shales	Top Ayot (mfs)	7800	8514	9327	8876	9460	8190	8439	8141	4256	
Top Ayot Limestone Formation	Top Ayot (mfs)	7800	8514	9327	8876	9460	8190	8439	8141	4256	
Base Ayot Limestone Formation	Base Ayot	7845	8554	9364	8920	9496	8227	8481	8186	4281	
Top PA60	Base Ayot	7845	8554	9364	8920	9496	8227	8481	8186	4300	9105
Base PA60	LJ10 Unc	7857	8559	9366	8922	9499	8232	8494	8196	4332	9110
Top PA30	LJ10 Unc	7857								4332	9110
Base PA30	PA2										9435
Top PA20	PA2										9435
Base PA20	PA1										9495
Top PA10	PA1									4345	9495
Base PA10	CU5									4350	9497
Top CU50	CU5										9497
Base CU50	CU4										9503
Top CU40	CU4										9503
Base CU40	CU3										9528
Top CU30	CU3										
Base CU30	CU2										
Top CU20	CU2									4350	9528
Base CU20	CU1									4376	9557
Top CU10	CU1										
Base CU10	MJ2 Unc										
Top R80	MJ2 Unc										
Base R80	R7										
Top R70	R7										9557
Base R70	R6										9592
Top R60	R6				9036		8240				
Base R60	R5 (mfs)				9044		8305				
Top R50	R5 (mfs)						8311				
Base R50	R4						8321				
Top R40	R4		8600			9572	8305				
Base R40	R3		8610			9591	8311				
Top R30	R3		8610		9044	9601	8321				
Base R30	R2 (mfs)		8700		9138	9696	8346				
Top R20	R2 (mfs)		8700	9379	9138	9696				4376	
Base R20	R1		8717	9402	9160	9720				4384	
TopR10	R1		8717	9402	9160	9720	8346	8517		4384	
Base R10	A1 (mfs)		8736	9417	9166	9754	8347	8521		4397	
TopA20	A1 (mfs)	7857	8736	9417	9166	9754	8347	8521	8196		
Base A20	Top Permian Unc	7887	8776	9477	9275	9874	8377	8567	8230		
Top PZ	Top Permian Unc	7887	8776	9477	9275	9874	8377	8567	8230		
TD (in Permian unless otherwise noted)	Well TD	8505	9764	9972	9627	9976	9164	8903	8607		9700 (Aalenian)

Table 6.2B: Table (continued) of stratigraphic zone and boundary depths by well for the Tangguh area. All are wireline log depths from RKB, in feet.

Unit/Well Name	Vorwata-2	Ofaweri-1	Roabiba-1	Vorwata-1	Vorwata-3	Vorwata-4	Vorwata-5	Vorwata-6	Vorwata-8	Vorwata-9	WiriagarDeep-1	WiriagarDeep-2	WiriagarDeep-3	WiriagarDeep-4	WiriagarDeep-5ST
Ayot+PA60	50.0	38.0	60.0	49.6	55.0	49.6	47.0	52.0	37.0	48.0	58.0	45.0	39.0	46.0	39.0
Ayot	46.0	36.0	50.0	45.0	49.0	45.0	43.0	46.0	34.0	44.0	45.0	40.0	37.0	44.0	36.0
PA60	4.0	2.0	10.0	4.6	6.0	4.6	4.0	6.0	3.0	4.0	13.0	5.0	2.0	2.0	3.0
PA30	105.2	0.0	0.0	0.0	0.0	25.1	64.2	42.0	54.5	95.4	0.0	0.0	0.0	0.0	0.0
PA20	30.4	0.0	90.6	0.0	0.0	0.0	27.9	58.7	8.1	44.8	0.0	0.0	0.0	0.0	0.0
PA10	78.5	0.0	42.4	17.4	20.0	22.3	28.9	41.2	12.3	39.9	0.0	0.0	0.0	0.0	0.0
CU50	2.0	7.4	4.0	5.8	6.3	0.0	2.5	2.0	2.8	3.5	0.0	0.0	0.0	0.0	0.0
CU40	24.9	16.1	25.5	20.0	21.8	0.0	25.5	28.5	10.9	29.9	0.0	0.0	0.0	0.0	0.0
CU30	14.0	24.0	24.9	26.4	23.9	0.0	6.0	19.3	0.0	19.7	0.0	0.0	0.0	0.0	0.0
CU20	0.0	49.6	12.6	27.6	17.0	0.0	0.0	10.2	0.0	0.0	0.0	0.0	0.0	0.0	0.0
CU10	0.0	61.8	0.0	0.0	0.0	0.0	0.0	0.0	0.0	0.0	0.0	0.0	0.0	0.0	0.0
R80	110.8	0.0	122.0	0.0	0.0	0.0	0.0	75.2	0.0	0.0	0.0	0.0	0.0	0.0	0.0
R70	61.2	61.0	105.9	0.0	0.0	24.0	53.2	77.3	42.0	52.5	0.0	0.0	0.0	45.9	71.0
R60	6.7	11.0	4.4	0.0	0.0	3.0	7.7	3.2	4.0	3.4	0.0	0.0	0.0	5.8	4.6
R50	137.1	61.0	62.2	0.0	0.0	76.0	84.1	70.1	19.0	87.1	0.0	53.2	0.0	70.2	51.9
R40	69.4	25.0	31.2	0.0	0.0	0.0	55.3	48.3	0.0	47.7	0.0	24.5	0.0	33.5	27.9
R30	26.9	42.0	47.5	56.3	0.0	0.0	40.5	35.0	0.0	38.3	0.0	63.3	13.5	60.5	41.5
R20	15.0	31.0	21.9	19.7	0.0	0.0	7.2	10.9	0.0	5.8	0.0	17.0	22.5	22.0	24.0
R10	20.8	13.0	19.9	0.0	0.0	0.0	35.0	15.0	0.0	21.2	0.0	19.0	15.0	6.0	34.0
A20	0.0	131.5	48.4	0.0	0.0	0.0	0.0	0.0	0.0	0.0	28.8	40.0	60.0	109.0	120.0

Unit/Well Name	WiriagarDeep-6	WiriagarDeep-7	WiriagarDeep-8	Wos-1	Ubadari-1	Ubadari-2	Kalitami-1X	EastOnin-1ST4	Sakauni-1	Sebyar-1	Vorwata-10ST	Vorwata-7ST	Vorwata-11	Nambumbi-1
Ayot+PA60	42.0	55.0	55.0	5.0	0.0	0.0	28.2	0.0	50.0	59.0	56.0	51.6	49.0	69.0
Ayot	37.0	42.0	45.0	0.0	0.0	0.0	25.0	0.0	38.0	54.0	47.0	47.0	41.0	60.0
PA60	5.0	13.0	10.0	5.0	0.0	0.0	3.2	0.0	12.0	5.0	9.0	4.6	8.0	9.0
PA30	0.0	0.0	0.0	182.3	0.0	0.0	0.0	0.0	28.7	24.4	136.4	0.0	65.4	0.0
PA20	0.0	0.0	0.0	59.8	0.0	0.0	48.3	0.0	0.0	0.0	73.9	29.6	39.1	0.0
PA10	0.0	0.0	0.0	144.9	0.0	0.0	17.6	0.0	3.3	62.6	159.7	31.8	15.4	16.0
CU50	0.0	0.0	0.0	6.0	0.0	0.0	0.0	0.0	0.0	0.0	4.6	6.0	4.5	0.0
CU40	0.0	0.0	0.0	25.0	0.0	0.0	0.0	0.0	0.0	0.0	32.4	22.8	32.0	0.0
CU30	0.0	0.0	0.0	0.0	0.0	0.0	0.0	0.0	0.0	0.0	14.6	25.2	12.4	0.0
CU20	0.0	0.0	0.0	29.0	0.0	0.0	26.0	0.0	0.0	0.0	36.4	56.3	0.0	0.0
CU10	0.0	0.0	0.0	0.0	0.0	0.0	0.0	0.0	0.0	0.0	0.0	54.7	0.0	0.0
R80	0.0	0.0	0.0	0.0	0.0	0.0	0.0	0.0	0.0	0.0	109.2	0	0.0	0.0
R70	0.0	0.0	0.0	35.0	0.0	0.0	0.0	0.0	0.0	0.0	100.7	0	35.0	0.0
R60	0.0	0.0	0.0	0.0	0.0	0.0	0.0	0.0	0.0	0.0	4.3	0	13.0	0.0
R50	0.0	0.0	0.0	0.0	0.0	0.0	0.0	0.0	0.0	0.0	54.4	0	38.0	0.0
R40	35.3	0.0	0.0	0.0	0.0	0.0	0.0	0.0	0.0	0.0	66.4	0	27.0	0.0
R30	53.4	0.0	0.0	0.0	0.0	0.0	0.0	0.0	0.0	0.0	29.1	0	40.0	56.0
R20	19.4	18.2	5.6	0.0	0.0	0.0	8.0	0.0	0.0	0.0	4.9	17	0.0	9.0
R10	6.5	8.8	5.4	0.0	0.0	0.0	13.0	0.0	0.0	0.0	31.6	72.8	0.0	0.0
A20	30.4	46.0	23.0	NP	0.0	0.0	0.0	0.0	0.0	0.0	0.0	48.9	0.0	0.0

Table 6.3: Table of stratigraphic unit thickness at each well in the Tangguh area. This table was the basis for the paleo-depositional facies isopachs created for the Tangguh detailed sequence stratigraphy modeling.

Guinea Limestone Group (NGLG). As a result of this seismic scatter in the datasets, only the Base Late Cretaceous and the Top Permian horizons are resolvable over the Tangguh area.

Numerous interpretation problems were presented by the data initially. All interpreted seismic surfaces, supplied by BP, were cut by irregular polygonal shaped 'holes' in the surfaces, a result of the seismically interpreted faults cutting the surface. These holes were then 'filled' by exporting the surfaces to Schlumberger's GEOFRAME program, using the PETROSYS program to actually fill the holes left from the fault polygons, and then re-importing the surfaces into GeoCARD.

Many surfaces were required for this study, especially in regard to the 3D geologic model construction, and these were created as 'phantomed surfaces' from the two seismic surfaces provided by BP from the 3D seismic survey.

6.1.2 Palynological Biozonation

The key control to identifying intervals of interest in the zonation scheme for detailed sequence stratigraphy was the use of palynological data. The age of a given interval of rock was determined by the identification and interpretation of spore and pollen assemblages (palynology), supplied originally by Waton, et al., of Core Labs Inc. in Jakarta, Indonesia (Waton, et al., 1994 through 1998). The Jurassic palynological results defined the EJ-2 through LJ-1 palynomorph biozonations (where present) for all of the Tangguh area wells used in this study. The interpretation of palynological conclusions, to provide an overall framework to the sequence stratigraphy of the Tangguh area, was a different matter. The original interpretations of the palynological results made by Bulling, et al., (1998), resulted in the Roabiba Sandstone Formation assigned as entirely Bajocian/Bathonian in age.

This incorrect age bracketing was subsequently utilized 'ad hoc' by Tye and Hickey (1999), leading to incorrect 'stratigraphic flow unit' correlations within the Roabiba Formation. However, a re-evaluation of the original palynological datasets for all Tangguh area wells has resulted in a re-interpretation of the Middle Jurassic succession. The result is that a definitive unconformity within the 'Roabiba Sandstone Formation' lithostratigraphic formation has been identified. The new interpretation of the original palynological dataset identifies a portion of the Roabiba Formation as Bajocian and possibly very earliest Bathonian age (MJ-3) and, importantly, the overlying upper member of the Roabiba Formation sandstone reservoir has been identified as being Callovian age (MJ-1/LJ-11). With an MJ-2

unconformable surface bounding the two members, labelled as Bajocian/Bathonian Roabiba Sandstone Formation and Callovian Roabiba Sandstone Formation. This ‘Bathonian unconformity’ (MJ-2) is a well-documented, widespread event along the entire NW Shelf margin of Australia (Yeates, et al., 1987; Bradshaw, et al., 1994a; Bradshaw, et al., 1994b; Longley, et al., 2002), and this Tangguh area ‘Bathonian unconformity’ (MJ-2) is probably co-genetic with it.

6.1.3 Stratigraphic Correlations and Wireline Log Motif Signatures

The wireline log intervals, for each of the wells, were first divided by chronostratigraphic zonations. Using this methodology resulted in gross chronostratigraphic units being delineated, based on the palynological data (Waton, et al., 1994; Waton, et al., 1996a-h; Waton, et al., 1997a-d). This resulted in the identification and zonation of Permian, Jurassic, and Cretaceous intervals, and then the available geological well data zoned according to the appropriate interval. The gross intervals were then subdivided, based on palynological Stages (i.e. Aalenian, Bathonian, Bajocian/Bathonian, and Callovian for the Middle Jurassic Period). For example, Waton states that the Vorwata-5 well rotary sidewall core plugs from depths “...12552’ and 12735’ yielded palynomorph taxa indicative of zone LJ-11 (earliest Oxfordian to late Callovian)...” (Waton, et al., 1998b).

Biozonation based on palynology has a unique classification scheme, with the Aalenian Stage designated as MJ-4 (for Middle Jurassic unit 4); Bajocian/Bathonian and earliest Bathonian designated as MJ-3; middle to late Bathonian designated as MJ-2; earliest Callovian designated as MJ-1 and the middle to late Callovian assigned a Late Jurassic designation of early LJ-11. The Late Jurassic Stages of Oxfordian (oldest) through Tithonian (youngest) have designations ranging from late LJ-11 (oldest) through LJ-1 (youngest). Table 6.4 shows the palynological biozonation of the Jurassic and Cretaceous, as utilized at Core Labs Indonesia by Waton et al. (Waton, et al., 1994; Waton, et al., 1996a-h; Waton, et al., 1997a-d).

Attention to the palynological biozonation (i.e. MJ-3, MJ-2, MJ-1, etc.) of ‘depth shift’ cuttings combined with the previously depth shifted cores resulted in a more detailed zonation of intervals than as merely stages. More importantly, the use of biozonation as a means of chronozonation led to either the identification of, or the confirmation of, intra-stage unconformities. For example the Bathonian Stage of the Middle Jurassic consists of both the MJ-2 and MJ-3 biozonations, with MJ-2 referring

to middle to late Bathonian biozonation of palynomorphs, and the MJ-3 referring to the earliest Bathonian plus the Bajocian biozonation of palynomorphs. Use of this more refined subdivision criteria resulted in the identification of an unconformity dated as MJ-2 (the middle to late Bathonian Stage). According to Waton, et al. (1994; 1996a-h; 1997a-d) no definitive MJ-2 palynomorphs have been identified at any of the Wiriagar Deep and Vorwata well locations in either cuttings or whole rock cores. “The negative evidence of the absence of *Wanaea indotata* or the common *Wanaea acollanis* would argue against zone MJ-2 [being present in the Vorwata #1 well location samples]. Furthermore, zone MJ-2 sediments appear to be absent in other wells drilled in the Berau [Bay area].” (Waton, et al., 1997b).

After the data for all wells located on the Wiriagar Deep and Vorwata structures were delineated by palynomorphs biozonation, the data within each zonation, particularly wire log motifs, palynological assemblages, and ichnological facies identification from whole cores, were characterized and correlated within zonations well-to-well for paleo-depositional facies relationships (Allen, et al., 1979; Allen and Mercier, 1988; Busch and Link, 1985; Lang, 2001). For example, a coarsening-upward gamma-ray profile at the base of a thick, clean, blocky sandstone core that contains shallow marine palynofloral/nannofauna, and has trace fossil burrows indicative of shallow marine facies, in addition to cross-bedding and flaser drapes, could indicate a prograde delta system paleo-depositional facies (Allen, et al., 1979; Allen and Mercier, 1988; Busch and Link, 1985; Lang, 2001). The correlation of this cored well interpretation to an adjacent well with no core can be reasonably justified with cuttings describing similar sandstone lithology, identical palynomorph/nannofossil taxa, and a similar coarsening-upward gamma-ray profile log motif signature. The inference would then be that the well with no core in the sandstone interval *still* represented a prograde delta sequence (Allen, et al., 1979; Busch and Link, 1985; Allen and Mercier, 1988; Lang, 2001). This can be a very useful tool in an area where a limited number of wells are drilled and several lack core through the interval of interest.

		AGE		Ma	PALYNOZONE		
CRETACEOUS	LATE	Turonian	late	88.5	LK4		
			middle-early		LK3		
		Cenomanian	"late"	93.7	LK2	A	
						B	
						C	
			"early"	95	LK1	A	
				B			
				C			
				D			
		EARLY	Albian	late	97	EK1	A
					B		
				C			
			middle	103	EK2		
			early	109	EK3		
	Aptian		late	112	EK4		
			early	118	EK5		
	Barremian		-	124.5	EK6		
	Hauterivian		late	131.8	EK7		
			early	132	EK8		
	Valanginian	late	134	EK8			
early		135	EK9				
		136.5	EK10				
		139.5	EK11				
Berriasian	late	140.7	EK12				
	early	142	EK13				
		143	EK13				
JURASSIC	LATE	Tithonian	"late"	145.6	LJ1		
					LJ2		
			"middle"	147.5	LJ3		
				148.5	LJ4		
		Kimmeridgian	"early"	150	LJ5		
			late	152.1	LJ6		
			middle	153	LJ7		
			early	154	LJ8		
			Oxfordian	late	154.5	LJ9	
				middle	154.7	LJ10	
	MIDDLE	Callovian	early	155	LJ11		
			late	156.5	MJ1		
			middle - early	157.1	MJ2		
				158.5	MJ3		
		Bathonian	-	161.3	MJ4		
		Bajocian	-	166.1	EJ1		
		Aalenian	-	173.5	NOT ZONED		
		Toarcian	-	178.0			
EARLY	Pleins. - Hett.	-	187.0				

Sources: Fraser et al. (1993), Helby et al. (1987), Davey (1987)

Table 6.4: Palynological zonation used, by Waton, et al. at Core Laboratories Indonesia, in all of the biostratigraphic studies of ARCO/BG drill cuttings and cores from Bintuni Basin, Irian Jaya (now known as Papua) (from Waton, et al., 1996b).

6.2 Paleogeographic Facies Maps for Tangguh Sequence Stratigraphy

The Mesozoic reservoirs appear to present the greatest potential storage capacity for possible CO₂ sequestration in the Bintuni Basin region, therefore a sequence stratigraphic framework was constructed for the Bintuni Jurassic interval, particularly in regard to the reservoir and seal couplets. Lowe (1998) had previously constructed a sequence stratigraphic framework for the Bintuni Paleocene reservoirs and seals. The frameworks are then utilized to evaluate and rank potential ESSCI CO₂ injection/storage locations, as discussed in Chapter 8, Chapter 9, and Chapter 10.

The subsequent methodology, following the correlatable zoning within the biozonations, was to construct a series of paleo-depositional environment facies maps for each correlatable zone within all of the biozonations, henceforth referred to as paleogeographic maps. The use of the term ‘zone’ is used since it is the terminology for the chronostratigraphic rock interpretation units used to construct the GeoCARD 3D geological model. Therefore, ‘zone’ can be treated as synonymous with the term ‘chronostratigraphic units’, in this study.

Using well established and proven techniques of sequence stratigraphy, the well data available within each correlatable zone were evaluated (van Wagoner, et al., 1990; Posamentier, et al., 1992; Posamentier and Chamberlain, 1993; Posamentier and James 1993; Posamentier and Allen, 1999; Nummedal, et al., 1993; Haq, 1993).

The standard paleontological/palynological analyses performed on Tangguh area well cores and cuttings, routinely included a chapter on the ‘generic’ paleo-deposition environment of each biozonation. The ‘generic’ paleo-depositional environment ascribed to a given correlatable zone at each well was derived from the macrofaunal, nannofaunal, or palynofloral assemblage environmental niche (Waton, et al., 1994; Waton, et al., 1996a-e; Waton, et al., 1997a-h; Waton, et al., 1998a-d). An example of this is demonstrated in the V-1 well biostratigraphic report for the Middle Jurassic Bajocian/Bathonian (MJ-3) biozone of the Roabiba Sandstone, “The presence...of rare foraminifera at 13008.0’ (core) and nannofossils at 12948.5’ (core) suggests limited marine influence at these [RKB] depths. ...Deposition in a variety of shallow marine and littoral settings is suggested by these microfossil data. The generally low palynomorph species diversity in conjunction with acmes in various taxa, including *Micrhystridium* spp.,....and *Chytreispharidia chytroeides*, suggests phases of environmental restriction” (Waton, et al., 1997b).

The detailed paleo-depositional environment was then expanded upon, for wells with whole rock cores through the zone of interest, by evaluating and then integrating the results from whole rock core ichnological facies and fabric studies by Pemberton (1997a-f) with the overall paleo-depositional environment facies previously established. Pemberton (1997a-f) evaluated the ichnological facies and fabric of the same core interval analyzed by Waton et al., and added far more detail to the generic depositional environment interpreted. Pemberton supplemented the paleo-depositional environment identification for Wiriagar Deep and Vorwata cores, as exemplified by his Vorwata #1 core evaluation, from the same 'zone' as evaluated by Waton et al., above. "Unit...13031.6 ft – 13004.3 ft ...is a fine-grained argillaceous facies that is characterized by *Teichichnus*, *Planolites*, *Palaeophycus*, *Thalassinoides*, *Diplocraterion*, and *Lockeia*. Such a limited, stunted suite is consistent with a brackish bay environment"...and... "Unit 12970 ft – 12943 ft...is a distinctive sand unit ...that is characterized by cryptic bioturbation by meiofauna, *Skolithos*, *Ophiomorpha*, and *Palaeophycus*...the sandstone unit represents a tidal sand ridge..." (Pemberton, 1997f).

Application of a +12 ft depth shift to the core depths (driller's measure depth from RKB) described by Waton and Pemberton above, and also Tye and Hickey's sedimentological core analysis (1999), results in the depths quoted above being shifted 12 ft deeper to match the equivalent interval of wireline log curves.

When the gamma-ray log motif signature is evaluated from a sequence stratigraphic perspective, the depth-shifted interval discussed above by Waton et al., and Pemberton, clearly suggests a classic 'progradational log motif signature' (Table 6.5a - 6.5f). Therefore, when all of these analyses are integrated, a clear chronostratigraphic zonation emerges with the paleo-depositional environment for each zonation and 'zone', at each well with whole cores, clearly identified.

In the case of the 'wireline depth shifted' interval at Vorwata #2 discussed above, (12960 ft to 13020 ft) the interval is key for several reasons.

Firstly, it contains the acme for the basal unit of the MJ-3 (Bajocian/Bathonian), and that acme is commonly found several feet above either the top Aalenian (MJ-4 interval) or the top Permian interval. This acme is present in most of the whole cores obtained in Wiriagar Deep and Vorwata well cores in this interval. "The acme of *Chytreispharidia chytroeides* in core samples 11899.3' and 11904.2'

[from the Vorwata #1 well] is commonly seen in this area near the base of the MJ-3 sediments.” (Waton, et al., 1997b).

Secondly, the gamma-ray wireline log motifs for this correlatable interval in the wells in the Tangguh area exhibit the classic cleaning-upward and a coarsening upward profile of a progradational delta/shoreface. Therefore, this interval is:

- A) Correlatable between almost all of the wells in the Wiriagar Deep and Vorwata area due to the presence in both cores and cuttings of the MJ-3 palynofloral acme *Chytreispharidia chytrooides*;
- B) Also correlatable between Tangguh area wells based on log-motif signature correlations (especially important for correlation to wells with no cores and poor cuttings sample quality);
- C) Establishes a chronostratigraphic datum for paleo-deposition shortly after the onset of the MJ-3 (Bajocian/Bathonian Stage) of the Middle Jurassic;
- D) Represents a sequence stratigraphy boundary where the previous unit underlies this prograde deltaic sedimentation unit;
- E) Combined with the ichnological facies studies of Pemberton (1997a-f), and also the sedimentological core facies study by Tye and Hickey (1999), this paleo-depositional environment within the correlatable framework ‘zone’ can now be used to construct a paleogeographic map representing this particular Jurassic time intervals, corresponding to a correlatable ‘zone’.
- F) Not only can the location, based on correlatable wells be used to map the paleogeographic facies distribution at that given time, but paleo-deposition can be constrained to a specific paleoenvironment, such as a restricted marine or shallow embayment.
- G) Identification of depositional facies within a specific paleo-environment, such as “trough-cross bedding with occasional scours, basal rip-up clasts, and rare trace fossil burrows” can then result in a given well location to be interpreted as being in a tidal-inlet channel within a restricted marine, shallow bay (Tye and Hickey, 1999). Identification of a tidal-inlet channel can then be extrapolated to include adjacent barrier islands with lagoonal or backwater facies landward (Tye and Hickey, 1999).

A cautionary note about the use of the paleogeographic facies maps needs to be mentioned here. The paleogeographic maps presented here are *NOT* meant to represent fixed, absolute maps of sandstone reservoir or overlying shale seal distributions in the Tangguh area. They are meant to represent approximate time slices in which a suite of facies were deposited, eroded, and amalgamated during a finite time interval, based on Walther's Law, whereby vertical superposition of facies for each log motif at each well reflects the lateral distribution of adjacent facies at any given time. The key aspect here is that chronostratigraphic intervals must be conformable successions of genetically related strata.

6.3 Detailed Sequence Stratigraphic Framework for Tangguh

The concepts and applications of applied sequence stratigraphy are regarded as powerful tools in geological subsurface evaluations and modelling (Posamentier and James, 1993). Exxon Corporation originally developed the concepts and techniques in the late 1970's and early 1980's as an extension of seismic stratigraphy for basin stratigraphy (Mitchum, 1977). The general concepts were summarized in the classic SEPM Special Publication by Wilgus et al. (1988). These concepts have been expanded upon since then by numerous other sedimentologists and sequence stratigraphers (Galloway 1989, Miall 1991, Sloss 1991, Posamentier and Allen 1999), with particularly detailed paleo-depositional models being based on present-day analogous depositional sequences and their depositional-environments (Van Wagoner, et al., 1990; Nummendal, et al., 1993; Posamentier, et al., 1992; Schumm, 1993; Posamentier and Allen, 1999).

Sequence stratigraphy is an important application to basin sedimentological modelling and geological event sequencing for several reasons:

- 1) It provides a technique for modelling sediment deposition and erosion within a basinal framework in terms of eustacy (i.e. sealevel changes), tectonism (i.e. uplift and subsidence), and sediment supply;
- 2) It facilitates the understanding and correlation between sediment depositional facies patterns within different portions of the basin as time equivalents; and perhaps most significantly;

Formation	GEOCARD Rock Interpretation Unit ^{4,5}	Nannofossil & Palynomorph Biozonation ¹	Rock Interval Lithology ⁶	Lithofacies Description ^{3,5}	Palynomorphs ¹ and Ichnomorphs ²	Accessory Mineralogical & Paleontological Data ^{1,3,6}	Interpreted Paleo-Depositional Facies ^{3,4,5}	Gamma-ray Wireline Log Motif ^{4,5}	Overall Interpreted System Tracts ⁵	Present in Tangguh Wells
Late Jurassic Shale	LJS10	LJ8-LJ2	Shale, silty shale, porcelaneous shale with possible tuffaceous volcanics.	(From WD-3 core): medium to dark gray shale, very siliceous (grading to porcelaneous shale in part), dolomitic in part, with possible light gray / greenish gray volcanic tuffaceous streak (very porcelaneous).	Belemnites, Bivalves	Trace to locally abundant glauconite. Possible devitrified glass in Tuffaceous streak.	Shelfal(?)		HST(?)	WD-3
Ayot Limestone (& PA60 mfs)	Ayot & PA60	LJ9	Limestone, argillaceous limestone, sandy limestone.	(From WD-3 core): medium gray to dark gray dolomitic limestone, occasionally silty to argillaceous, cryptocrystalline to microcrystalline.	LJ9 Palynological Acme: <i>Cribroperidinium perforans</i> , also <i>Dingodinium swanense</i> , <i>Trichodium sp.2</i> Macrofossils: Belemnites, Bivalves	Trace glauconite in limestone, common glauconite in sandy limestone.	Transgressive Surface (mfs) & then Platform Carbonate		TST	WD-3
Pre-Ayot Shale	PA30	LJ11	Sandstone, silty to argillaceous sandstone.	(From cuttings): very fine to coarse-grained sands with occasional silts, poorly sorted; Primarily quartz with occasional lithic rock fragments / clasts.	Palynological Assemblage: <i>Scrinoidinium ceratophorum</i> , <i>Scrinoidinium galeritum</i> , <i>Vallensiella ovula</i> , <i>Wanaea digitata</i> , <i>Wanaea indotata</i> , <i>Wanaea spectabilis</i> , <i>Cliestosphaeridium</i> Ichnology & Sedimentology Data Not Available (No Core)	Traces glauconite, kaolinite, feldspar, and pyrite.	Progradational & Amalgamated Delta Fan Complex		HST	V-5, V-6, V-8, V-9, V-10st, V-11, Wos-1
Pre-Ayot Shale	PA20	LJ11	Shale, silty shale.	Medium to dark gray, trace to moderate calcareous, occasionally silty shale.	Palynological Assemblage: <i>Scrinoidinium ceratophorum</i> , <i>Scrinoidinium galeritum</i> , <i>Vallensiella ovula</i> , <i>Wanaea digitata</i> , <i>Wanaea indotata</i> , <i>Wanaea spectabilis</i> , <i>Cliestosphaeridium</i> Ichnology & Sedimentology Data Not Available (No Core)	Traces glauconite and pyrite.	Shelfal(?)		TST	V-10st
Pre-Ayot Shale	PA10	LJ11/MJ1	Shale, silty shale.	(From cuttings): medium to dark gray shale; slightly calcareous in part; minor carbonaceous flecks; trace glauconite and pyrite.	Palynological Assemblage: <i>Scrinoidinium ceratophorum</i> , <i>Scrinoidinium galeritum</i> , <i>Vallensiella Ovula</i> , <i>Wanaea digitata</i> , <i>Wanaea indotata</i> , <i>Wanaea spectabilis</i> , <i>Cliestosphaeridium</i> Occasional: <i>Planolites</i> , <i>Chondrites</i>	Traces glauconite and pyrite.	Shelfal(?)		TST	V-10st
Calloviaan Roabiba Sandstone	CU50	LJ11/MJ1	Sandstone, silty to slightly argillaceous sandstone.	Very fine to fine grained sands, poorly to moderately well sorted, occasionally silty & argillaceous, and rarely carbonaceous.	Palynological Assemblage: <i>Scrinoidinium ceratophorum</i> , <i>Scrinoidinium galeritum</i> , <i>Vallensiella Ovula</i> , <i>Wanaea digitata</i> , <i>Wanaea indotata</i> , <i>Wanaea spectabilis</i> , <i>Cliestosphaeridium</i> Ichnology & Sedimentology Data Not Available (No Core)		Upper Shoreface		HST	V-10st
Calloviaan Roabiba Sandstone	CU40	LJ11/MJ1	Sandstone, siltstone.	Coarse to very fine grained sands with some silts, well sorted; with high angle (20-30 deg) tabular and low angle (10-20 deg) tabular/tangential cross-bedding, trough-cross bedding, asymmetric ripple laminae, flaser bedding, scour surfaces.	Palynological Assemblage: <i>Scrinoidinium ceratophorum</i> , <i>Scrinoidinium galeritum</i> , <i>Vallensiella Ovula</i> , <i>Wanaea digitata</i> , <i>Wanaea indotata</i> , <i>Wanaea spectabilis</i> , <i>Cliestosphaeridium</i> Rare to common: <i>Ophiomorpha</i> , <i>Rosselia</i> , <i>Palaeophycus</i> , <i>Asterosoma</i> , <i>Skolithos</i> , <i>Planolites</i> .	Chert granules, shell debris, sandstone/clay/organic clasts.	Tidal Inlet Channel		HST	V-1

Table 6.5a-f: Master Table of Core Lithofacies, Log-Motifs, Palaeontology, and Paleo-depositional Environments for Tangguh Wells.

Formation	GEOCARD Rock Interpretation Unit ^{4,5}	Nannofossil & Palynomorph Biozonation ¹	Rock Interval Lithology ⁶	Lithofacies Description ^{3,5}	Palynomorphs ¹ and Ichnomorphs ²	Accessory Mineralogical & Paleontological Data ^{1,3,6}	Interpreted Paleo-Depositional Facies ^{3,4,5}	Gamma-ray Wireline Log Motif ^{4,5}	Overall Interpreted System Tracts ⁵	Present in Tangguh Wells
Callovian Roabiba Sandstone	CU40	LJ11/MJ1	Sandstone, minor argillaceous sandstone.	Sands, fine to very fine grained; moderately well sorted; with trough-cross bedding and low angle (10-20 deg) tabular cross-bedding; flaser bedding; load casts; scour surfaces.	Palynological Assemblage: <i>Scrinoidinium ceratophorum</i> , <i>Scrinoidinium galeritum</i> , <i>Vallensiella Ovula</i> , <i>Wanaea digitata</i> , <i>Wanaea indotata</i> , <i>Wanaea spectabilis</i> , <i>Cliestosphaeridium</i> Moderate to common: <i>Ophiomorpha</i> , <i>Thalassinoides</i> , <i>Planolites</i> , <i>Glossifungites</i> surfaces.	Rare clay clasts.	Upper Shoreface		HST	V-10st
Callovian Roabiba Sandstone	CU40	LJ11/MJ1	Sandstone, minor shale.	Fine to very fine grained sands, moderately to moderately well sorted; with trough-cross bedding, low angle (10-20 deg) tabular cross-bedding, asymmetric ripple lamination, flaser bedding, mud drapes, convolute laminae, normally graded beds.	Palynological Assemblage: <i>Scrinoidinium ceratophorum</i> , <i>Scrinoidinium galeritum</i> , <i>Vallensiella Ovula</i> , <i>Wanaea digitata</i> , <i>Wanaea indotata</i> , <i>Wanaea spectabilis</i> , <i>Cliestosphaeridium</i> Moderate to common: <i>Ophiomorpha</i> , <i>Thalassinoides</i> , <i>Planolites</i> , <i>Palaeophycus</i> , <i>Teichichnus</i> , <i>Asterosoma</i> , <i>Deplocraterion</i> .	Rare clay clasts, bivalve and gastropod tests.	Middle Shoreface		HST	V-2, V-6
Callovian Roabiba Sandstone	CU30	LJ11/MJ1	Sandstone, minor argillaceous sandstone.	Sands, fine to very fine grained; moderately well sorted; with trough-cross bedding and low angle (10-20 deg) tabular cross-bedding; flaser bedding; load casts; scour surfaces.	Palynological Assemblage: <i>Scrinoidinium ceratophorum</i> , <i>Scrinoidinium galeritum</i> , <i>Vallensiella Ovula</i> , <i>Wanaea digitata</i> , <i>Wanaea indotata</i> , <i>Wanaea spectabilis</i> , <i>Cliestosphaeridium</i> Moderate to common: <i>Ophiomorpha</i> , <i>Thalassinoides</i> , <i>Planolites</i> , <i>Glossifungites</i> surfaces.	Rare clay clasts.	Upper Shoreface		TST	V-1
Callovian Roabiba Sandstone	CU30	LJ11/MJ1	Sandstone, siltstone.	Coarse to very fine grained sands with some silts, well sorted; with high angle (20-30 deg) tabular and low angle (10-20 deg) tabular/tangential cross-bedding, trough-cross bedding, asymmetric ripple lamination, flaser bedding, scour surfaces.	Palynological Assemblage: <i>Scrinoidinium ceratophorum</i> , <i>Scrinoidinium galeritum</i> , <i>Vallensiella Ovula</i> , <i>Wanaea digitata</i> , <i>Wanaea indotata</i> , <i>Wanaea spectabilis</i> , <i>Cliestosphaeridium</i> Rare to common: <i>Ophiomorpha</i> , <i>Rosselia</i> , <i>Palaeophycus</i> , <i>Asterosoma</i> , <i>Skolithos</i> , <i>Planolites</i> .	Chert granules, shell debris, sandstone/clay/organic clasts.	Tidal Inlet Channel		TST	V-2
Callovian Roabiba Sandstone	CU30	LJ11/MJ1	Sandstone, minor shale.	Fine to very fine grained sands, moderately to moderately well sorted; with trough-cross bedding, low angle (10-20 deg) tabular cross-bedding, asymmetric ripple lamination, flaser bedding, mud drapes, convolute laminae, normally graded beds.	Palynological Assemblage: <i>Scrinoidinium ceratophorum</i> , <i>Scrinoidinium galeritum</i> , <i>Vallensiella Ovula</i> , <i>Wanaea digitata</i> , <i>Wanaea indotata</i> , <i>Wanaea spectabilis</i> , <i>Cliestosphaeridium</i> Moderate to common: <i>Ophiomorpha</i> , <i>Thalassinoides</i> , <i>Planolites</i> , <i>Palaeophycus</i> , <i>Teichichnus</i> , <i>Asterosoma</i> , <i>Deplocraterion</i> .	Rare clay clasts, bivalve and gastropod tests.	Middle Shoreface		TST	V-6, V-10st

Table 6.5a-f: Master Table of Core Lithofacies, Log-Motifs, Palaeontology, and Paleo-depositional Environments for Tangguh Wells.

Formation	GEOCARD Rock Interpretation Unit ^{4,5}	Nannofossil & Palynomorph Biozonation ¹	Rock Interval Lithology ⁶	Lithofacies Description ^{3,5}	Palynomorphs ¹ and Ichnomorphs ²	Accessory Mineralogical & Paleontological Data ^{1,3,6}	Interpreted Paleo-Depositional Facies ^{3,4,5}	Gamma-ray Wireline Log Motif ^{4,5}	Overall Interpreted System Tracts ⁵	Present in Tangguh Wells
Callovian Roabiba Sandstone	CU20	LJ11/MJ1	Sandstone, siltstone.	Coarse to very fine grained sands with some silts, well sorted; with high angle (20-30 deg) tabular and low angle (10-20 deg) tabular/tangential cross-bedding, trough-cross bedding, asymmetric ripple laminae, flaser bedding, scour surfaces.	Palynological Assemblage: <i>Scrinoidinium ceratophorum</i> , <i>Scrinoidinium galeritum</i> , <i>Vallensiella Ovula</i> , <i>Wanaea digitata</i> , <i>Wanaea indotata</i> , <i>Wanaea spectabilis</i> , <i>Cliestosphaeridium</i> Rare to common: <i>Ophiomorpha</i> , <i>Rosselia</i> , <i>Palaeophycus</i> , <i>Asterosoma</i> , <i>Skolithos</i> , <i>Planolites</i> .	Chert granules, shell debris, sandstone/clay/organic clasts.	Tidal Inlet Channel		TST	V-10st
Callovian Roabiba Sandstone	CU20	LJ11/MJ1	Sandstone, minor shale.	Fine to very fine grained sands, moderately to moderately well sorted; with trough-cross bedding, low angle (10-20 deg) tabular cross-bedding, asymmetric ripple lamination, flaser bedding, mud drapes, convolute laminae, normally graded beds.	Palynological Assemblage: <i>Scrinoidinium ceratophorum</i> , <i>Scrinoidinium galeritum</i> , <i>Vallensiella Ovula</i> , <i>Wanaea digitata</i> , <i>Wanaea indotata</i> , <i>Wanaea spectabilis</i> , <i>Cliestosphaeridium</i> Moderate to common: <i>Ophiomorpha</i> , <i>Thalassinoides</i> , <i>Planolites</i> , <i>Palaeophycus</i> , <i>Teichichnus</i> , <i>Asterosoma</i> , <i>Diplocraterion</i> .	Rare clay clasts, bivalve and gastropod tests.	Middle Shoreface		TST	V-6
Callovian Roabiba Sandstone	CU10	LJ11/MJ1	Sandstone, silty to argillaceous sandstone.	(From cuttings): Silts and very fine to medium grained sands, poorly to moderately well sorted.	Palynological Assemblage: <i>Scrinoidinium ceratophorum</i> , <i>Scrinoidinium galeritum</i> , <i>Vallensiella Ovula</i> , <i>Wanaea digitata</i> , <i>Wanaea indotata</i> , <i>Wanaea spectabilis</i> , <i>Cliestosphaeridium</i> Ichnology & Sedimentology Data Not Available (No Core)	Occasionally calcareous, occasionally kaolinitic, rarely carbonaceous.	Transgressed In-fill of Incised Valley System		TST	V-7, Ofaweri-1
Bajocian Roabiba Sandstone	R80	MJ3	Sandstone, sandy shale.	Fine to very fine grained sands with minor muds, well to moderately well sorted; with trough-cross bedding, high angle (20-30 deg) tabular and low angle (10-20 deg) tabular cross-bedding; asymmetric ripple lamination, flaser bedding.	Rare to common: <i>Ophiomorpha</i> , <i>Planolites</i> .	Occasional shell fragments.	Beach Foreshore		HST	V-10st
Bajocian Roabiba Sandstone	R80	MJ3	Sandstone, siltstone.	Coarse to very fine grained sands with some silts, well sorted; with high angle (20-30 deg) tabular and low angle (10-20 deg) tabular/tangential cross-bedding, trough-cross bedding, asymmetric ripple laminae, flaser bedding, scour surfaces.	Rare to common: <i>Ophiomorpha</i> , <i>Rosselia</i> , <i>Palaeophycus</i> , <i>Asterosoma</i> , <i>Skolithos</i> , <i>Planolites</i> .	Chert granules, shell debris, sandstone/clay/organic clasts.	Tidal Inlet Channel		HST	V-2
Bajocian Roabiba Sandstone	R80	MJ3	Sandstone, silty to argillaceous sandstone.	Sands with occasional muds, medium to fine grained; moderately to moderately well sorted; with troughcross bedding, asymmetric ripple laminae; flaser bedding; gently inclined laminae; slumped bedding; scour surfaces.	Common to abundant: <i>Ophiomorpha</i> , <i>Thalassinoides</i> , <i>Palaeophycus</i> , <i>Asterosoma</i> , <i>Planolites</i> , <i>Diplocraterion</i> , <i>Glossifungites</i> surfaces.	Organic debris, shell debris, coated grains, chert pebbles, pyrite, root traces, mottled coloring.	Backbarrier (Washover)		HST	V-6

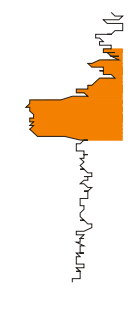
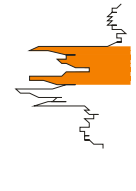
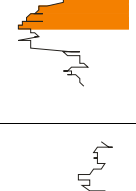
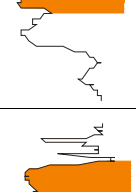
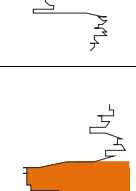
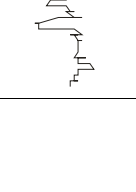
Table 6.5a-f: Master Table of Core Lithofacies, Log-Motifs, Palaeontology, and Paleo-depositional Environments for Tangguh Wells.

Formation	GEOCARD Rock Interpretation Unit ^{4,5}	Nannofossil & Palynomorph Biozonation ¹	Rock Interval Lithology ⁶	Lithofacies Description ^{3,5}	Palynomorphs ¹ and Ichnomorphs ²	Accessory Mineralogical & Paleontological Data ^{1,3,6}	Interpreted Paleo-Depositional Facies ^{3,4,5}	Gamma-ray Wireline Log Motif ^{4,5}	Overall Interpreted System Tracts ⁵	Present in Tangguh Wells
Bajocian Roabiba Sandstone	R70	MJ3	Sandstone, siltstone.	Fine to coarse grained sands, moderately to well sorted; with trough-cross bedding and high angle (20-30 deg) and low angle (10-20 deg) tabular/tangential cross-bedding; symmetric and assymetric ripple laminae; flaser bedding and mud drapes; convolute bedding; reactivation & scour	Common to rare: <i>Ophiomorpha</i> , <i>Thalassinoides</i> , <i>Palaeophycus</i> , <i>Asterosoma</i> , <i>Skolithos</i> , <i>Planolites</i> , <i>Teichichnus</i> , <i>Glossifungites</i> surfaces.	clay clasts	Ebb Tidal Delta		HST	V-5
Bajocian Roabiba Sandstone	R70	MJ3	Sandstone, minor shale.	Fine to very fine grained sands, moderately to moderately well sorted; with trough-cross bedding, low angle (10-20 deg) tabular cross-bedding, asymmetric ripple lamination, flaser bedding, mud drapes, convolute laminae, normally graded beds.	Moderate to common: <i>Ophiomorpha</i> , <i>Thalassinoides</i> , <i>Planolites</i> , <i>Palaeophycus</i> , <i>Teichichnus</i> , <i>Asterosoma</i> , <i>Deplocraterion</i> .	Rare clay clasts, bivalve and gastropod tests.	Middle Shoreface		TST	V-2, V-10st
Bajocian Roabiba Sandstone	R70	MJ3	Sandstone, minor argillaceous sandstone.	Sands, fine to very fine grained; moderately well sorted; with trough-cross bedding and low angle (10-20 deg) tabular cross-bedding; flaser bedding; load casts; scour surfaces.	Moderate to common: <i>Ophiomorpha</i> , <i>Thalassinoides</i> , <i>Planolites</i> , <i>Glossifungites</i> surfaces.	Rare clay clasts.	Upper Shoreface		HST	V-6
Bajocian Roabiba Sandstone	R70	MJ3	Sandstone, silty to argillaceous sandstone.	Sands with occasional muds, medium to fine grained; moderately to moderately well sorted; with troughcross bedding, asymmetric ripple laminae; flaser bedding; gently inclined laminae; slumped bedding; scour surfaces.	Common to abundant: <i>Ophiomorpha</i> , <i>Thalassinoides</i> , <i>Palaeophycus</i> , <i>Asterosoma</i> , <i>Planolites</i> , <i>Diplocraterion</i> , <i>Glossifungites</i> surfaces.	Organic debris, shell debris, coated grains, chert pebbles, pyrite, root traces, mottled coloring.	Backbarrier (Lagoonal)		HST	WD-4, WD-5
Bajocian Roabiba Sandstone	R60	MJ3	Sandstone, minor argillaceous sandstone.	Sands, fine to very fine grained; moderately well sorted; with trough-cross bedding and low angle (10-20 deg) tabular cross-bedding; flaser bedding; load casts; scour surfaces.	Moderate to common: <i>Ophiomorpha</i> , <i>Thalassinoides</i> , <i>Planolites</i> , <i>Glossifungites</i> surfaces.	Rare clay clasts.	Upper Shoreface		TST	V-6
Bajocian Roabiba Sandstone	R60	MJ3	Sandstone, minor shale.	Fine to very fine grained sands, moderately to moderately well sorted; with trough-cross bedding, low angle (10-20 deg) tabular cross-bedding, asymmetric ripple lamination, flaser bedding, mud drapes, convolute laminae, normally graded beds.	Moderate to common: <i>Ophiomorpha</i> , <i>Thalassinoides</i> , <i>Planolites</i> , <i>Palaeophycus</i> , <i>Teichichnus</i> , <i>Asterosoma</i> , <i>Deplocraterion</i> .	Rare clay clasts, bivalve and gastropod tests.	Middle Shoreface		TST	WD-4, WD-5, V-2, V-5, V-10st
Bajocian Roabiba Sandstone	R50	MJ3	Silty shale, sandy shale, sandstone.	Muds and coarse to fine grained sands, with trough-cross-bedding.	<i>Planolites</i> .	Root traces.	Abandoned Channel		TST	V-5
Bajocian Roabiba Sandstone	R50	MJ3	Sandstone, siltstone.	sands with some silts, well sorted; with high angle (20-30 deg) tabular and low angle (10-20 deg) tabular/tangential cross-bedding, trough-cross bedding, asymmetric ripple	Rare to common: <i>Ophiomorpha</i> , <i>Rosselia</i> , <i>Palaeophycus</i> , <i>Asterosoma</i> , <i>Skolithos</i> , <i>Planolites</i> .	Chert granules, shell debris, sandstone/clay/organic clasts.	Tidal Inlet Channel		TST	V-2, V-10st
Bajocian Roabiba Sandstone	R50	MJ3	Sandstone, minor argillaceous sandstone.	Sands, fine to very fine grained; moderately well sorted; with trough-cross bedding and low angle (10-20 deg) tabular cross-bedding; flaser bedding; load casts; scour surfaces.	Moderate to common: <i>Ophiomorpha</i> , <i>Thalassinoides</i> , <i>Planolites</i> , <i>Glossifungites</i> surfaces.	Rare clay clasts.	Upper Shoreface		TST	WD-5
Bajocian Roabiba Sandstone	R50	MJ4	Sandstone, silty to argillaceous sandstone.	Sands with occasional muds, medium to fine grained; moderately to moderately well sorted; with troughcross bedding, asymmetric ripple laminae; flaser bedding; gently inclined laminae; slumped bedding; scour surfaces.	Common to abundant: <i>Ophiomorpha</i> , <i>Thalassinoides</i> , <i>Palaeophycus</i> , <i>Asterosoma</i> , <i>Planolites</i> , <i>Diplocraterion</i> , <i>Glossifungites</i> surfaces.	Organic debris, shell debris, coated grains, chert pebbles, pyrite, root traces, mottled coloring.	Backbarrier (Lagoonal)		TST	WD-4

Table 6.5a-f: Master Table of Core Lithofacies, Log-Motifs, Palaeontology, and Paleo-depositional Environments for Tangguh Wells.

Formation	GEOCARD Rock Interpretation Unit ^{4,5}	Nannofossil & Palynomorph Biozonation ¹	Rock Interval Lithology ⁶	Lithofacies Description ^{3,5}	Palynomorphs ¹ and Ichnomorphs ²	Accessory Mineralogical & Paleontological Data ^{1,3,6}	Interpreted Paleo-Depositional Facies ^{3,4,5}	Gamma-ray Wireline Log Motif ^{4,5}	Overall Interpreted System Tracts ⁵	Present in Tangguh Wells
Bajocian Roabiba Sandstone	R50	MJ3	Sandstone, silty sandstone, carbonaceous shale.	Muds, silts, and medium to very fine grained sandstone; moderately sorted; with trough-cross bedding and low angle (10-20 deg) tabular cross-bedding; parallel and asymmetric ripple laminae.	Continental (freshwater) palynomorphs with no marine taxa.	Organic debris, clay clasts, sulfurous minerals.	Fluvial Channel		TST	WD-2
Bajocian Roabiba Sandstone	R40	MJ3	Sandstone, siltstone.	Fine to coarse grained sands, moderately to well sorted; with trough-cross bedding and high angle (20-30 deg) and low angle (10-20 deg) tabular/tangential cross-bedding; symmetric and asymmetric ripple laminae; flaser bedding and mud drapes; convolute bedding; reactivation & scour surfaces.	Common to rare: <i>Ophiomorpha</i> , <i>Thalassinoides</i> , <i>Palaeophycus</i> , <i>Asterosoma</i> , <i>Skolithos</i> , <i>Planolites</i> , <i>Teichichnus</i> , <i>Glossifungites</i> surfaces.	clay clasts	Ebb Tidal Delta		TST	V-10st
Bajocian Roabiba Sandstone	R40	MJ3	Sandy shale, sandstone, calcareous shale.	Coarse to fine grained sands and muds, with trough-cross-bedding, low-angle (10-20 deg) tabular cross-bedding, wavy bedding.	Rare to common: <i>Ophiomorpha</i> , <i>Thalassinoides</i> , <i>Trypanites</i> , <i>Glossifungites</i> surfaces.	Shale and chert granules, bored lithoclasts, bivalve and gastropod tests, spines.	Transgressed Shoreline		TST	V-2, V-5
Bajocian Roabiba Sandstone	R40	MJ3	Sandstone, minor shale.	Fine to very fine grained sands, moderately to moderately well sorted; with trough-cross bedding, low angle (10-20 deg) tabular cross-bedding, asymmetric ripple lamination, flaser bedding, mud drapes, convolute laminae, normally graded beds.	Moderate to common: <i>Ophiomorpha</i> , <i>Thalassinoides</i> , <i>Planolites</i> , <i>Palaeophycus</i> , <i>Teichichnus</i> , <i>Asterosoma</i> , <i>Deplocraterion</i> .	Rare clay clasts, bivalve and gastropod tests.	Middle Shoreface		TST	WD-4
Bajocian Roabiba Sandstone	R30	MJ3	Massive clean sandstone, argillaceous sandstone, silty shale.	Prograde in-fill of Bay/Estuary by muds, silts, and sands, graded bedding with relic facies preserved in part, including: relic Barrier Island Foreshore, Tidal Inlet, Estuary Channel, Ebb Tidal Delta, Upper and Middle Shoreface.	Palynological Acme: <i>Chytrespharidia chytrooides</i> Common to rare: <i>Ophiomorpha</i> , <i>Thalassinoides</i> , <i>Palaeophycus</i> , <i>Asterosoma</i> , <i>Skolithos</i> , <i>Planolites</i> , <i>Teichichnus</i> , <i>Glossifungites</i> surfaces.	Variable	Strandplain (Progradational in-filled Bay/Estuary)		HST	WD-2, WD-3, WD 4, WD-5, WD-6, V-6, V-10st
Bajocian Roabiba Sandstone	R20	MJ3	Shale, silty shale, carbonaceous shale, sandstone.	Muds, silts, and very fine grained sands with parallel laminae; symmetric and asymmetric ripple laminae; wavy and lenticular bedding; load casts, flame structures.	Rare to moderate: <i>Planolites</i> , <i>Thalassinoides</i> , <i>Asterosoma</i> , <i>Trypanites</i> .	Siderite, pyrite, coated grains, worm tubes, bivalve and gastropod tests, organic debris, clay clasts.	Bay		TST	WD-3, WD-5, V-5, V-6, V-10st
Bajocian Roabiba Sandstone	R10	MJ3	Sandstone, argillaceous sandstone.	Medium to ultra very fine grained sands, moderately to moderately well sorted; with asymmetric ripple laminae; trough-cross bedding, gently inclined laminae, flaser bedding, mud drapes, indistinct bedding, scour surfaces.	Common to abundant: <i>Ophiomorpha</i> , <i>Teichichnus</i> , <i>Cylindricnus</i> , <i>Psilonichnus</i> , <i>Planolites</i> , <i>Glossifungites</i> surfaces.	Organic debris, chert pebbles, clay clasts, root traces, mottled coloring.	Backshore		TST	V-10st
Bajocian Roabiba Sandstone	R10	MJ3	Shale, silty shale, carbonaceous shale, sandstone.	Muds, silts, and very fine grained sands with parallel laminae; symmetric and asymmetric ripple laminae; wavy and lenticular bedding; load casts, flame structures.	Rare to moderate: <i>Planolites</i> , <i>Thalassinoides</i> , <i>Asterosoma</i> , <i>Trypanites</i> .	Siderite, pyrite, coated grains, worm tubes, bivalve and gastropod tests, organic debris, clay clasts.	Bay		TST	WD-2, WD-5
Bajocian Roabiba Sandstone	R10	MJ3	Sandstone, silty sandstone, carbonaceous shale.	Muds, silts, and medium to very fine grained sandstone; moderately sorted; with trough-cross bedding and low angle (10-20 deg) tabular cross-bedding; parallel and asymmetric ripple laminae.	Continental (freshwater) palynomorphs with no marine taxa.	Organic debris, clay clasts, sulfurous minerals.	Fluvial Channel		TST	V-5, V-6 V-7, V-9
Bajocian Roabiba Sandstone	R10	MJ3	Sandy shale, sandstone, calcareous shale.	Coarse to fine grained sands and muds, with trough-cross-bedding, low-angle (10-20 deg) tabular cross-bedding, wavy bedding.	Rare to common: <i>Ophiomorpha</i> , <i>Thalassinoides</i> , <i>Trypanites</i> , <i>Glossifungites</i> surfaces.	Shale and chert granules, bored lithoclasts, bivalve and gastropod tests, spines.	Transgressed Shoreline		TST	WD-3
Formation	GEOCARD Rock Interpretation Unit ^{4,5}	Nannofossil & Palynomorph Biozonation ¹	Rock Interval Lithology ⁶	Lithofacies Description ^{3,5}	Palynomorphs ¹ and Ichnomorphs ²	Accessory Mineralogical & Paleontological Data ^{1,3,6}	Interpreted Paleo-Depositional Facies ^{3,4,5}	Gamma-ray Wireline Log Motif ^{4,5}	Overall Interpreted System Tracts ⁵	Present in Tangguh Wells

Table 6.5a-f: Master Table of Core Lithofacies, Log-Motifs, Palaeontology, and Paleo-depositional Environments for Tangguh Wells.

Aalenian Sandstone & Shale	A20	MJ4	Sandstone.	Fine to coarse grained sands, moderately to well sorted; with trough-cross bedding and high angle (20-30 deg) and low angle (10-20 deg) tabular/tangential cross-bedding; symmetric and asymmetric ripple laminae; flaser bedding and mud drapes; convolute bedding; reactivation & scour surfaces.	Common to rare: <i>Ophiomorpha</i> , <i>Thalassinoides</i> , <i>Palaeophycus</i> , <i>Asterosoma</i> , <i>Skolithos</i> , <i>Planolites</i> , <i>Teichichnus</i> , <i>Glossifungites</i> surfaces.	clay clasts	Ebb Tidal Delta		TST	WD-2, WD-3, WD-4, WD-7, WD-8
Aalenian Sandstone & Shale	A20	MJ4	Sandstone, silty sandstone, carbonaceous shale.	Muds, silts, and medium to very fine grained sandstone; moderately sorted; with trough-cross bedding and low angle (10-20 deg) tabular cross-bedding; parallel and asymmetric ripple laminae.	Continental (freshwater) palynomorphs with no marine taxa.	Organic debris, clay clasts, sulfurous minerals.	Fluvial Channel		TST	WD-6
Aalenian Sandstone & Shale	A20	MJ4	Shale, silty to sandy shale, coal.	Muds, silts, and very fine grained sands with parallel laminae, symmetric and asymmetric ripple laminae, convolute laminae; load casts.	<i>Plantolites</i> , <i>Palaeophycus</i> .	Siderite, organic debris, root traces, and pedogenesis.	Coastal Plain Lacustrine or Poorly Drained Swamp		TST	WD-1, WD-8
Aalenian Sandstone & Shale	A20	MJ4	Sandstone, silty to argillaceous sandstone.	Muds, silts, and medium to very fine grained sandstone; moderately sorted; with trough-cross bedding and low angle (10-20 deg) tabular cross-bedding; parallel and asymmetric ripple laminae.	Rare to occasional: <i>Ophiomorpha</i> , <i>Palaeophycus</i> , <i>Skolithos</i> .	Organic debris, clay clasts, sulfurous minerals, and root traces.	Bayhead Delta		TST	WD-2
Aalenian Sandstone & Shale	A20	MJ4	Sandstone, minor argillaceous sandstone.	Sands, fine to very fine grained; moderately well sorted; with trough-cross bedding and low angle (10-20 deg) tabular cross-bedding; flaser bedding; load casts; scour surfaces.	Moderate to common: <i>Ophiomorpha</i> , <i>Thalassinoides</i> , <i>Planolites</i> , <i>Glossifungites</i> surfaces.	Rare clay clasts.	Upper Shoreface		TST	WD-3, WD-4
Aalenian Sandstone & Shale	A20	MJ4	Sandstone, silty to argillaceous sandstone.	Sands with occasional muds, medium to fine grained; moderately to moderately well sorted; with troughcross bedding, asymmetric ripple laminae; flaser bedding; gently inclined laminae; slumped bedding; scour surfaces.	Common to abundant: <i>Ophiomorpha</i> , <i>Thalassinoides</i> , <i>Palaeophycus</i> , <i>Asterosoma</i> , <i>Planolites</i> , <i>Diplocraterion</i> , <i>Glossifungites</i> surfaces.	Organic debris, shell debris, coated grains, chert pebbles, pyrite, root traces, mottled coloring.	Backbarrier (Washover)		TST	WD-7

¹ from Waton P.V., et. al., 1994 through 1998

² from Pemberton, S.G., 1997a, 1997b, 1997c, 1997d, 1997e

³ from Tye R.S. and Hickey J.J., 1999

⁴ For this study by Dr. Simon Lang 2003

⁵ For this study by Jonathan P. Salo 2003

⁶ from Salo J.P., Final Well Reports 1994 through 1998

Table 6.5a-f: Master Table of Core Lithofacies, Log-Motifs, Palaeontology, and Paleo-depositional Environments for Tangguh Wells.

- 3) It can be used to predict paleo-facies depositional distributions over a geographical area, including the location of reservoir units of a specific facies, and seal-prone paleo-depositional intervals and their respective locations within a paleo-basin (Lang, 2001).

The sequence stratigraphy concepts and techniques developed over the past 25 years are especially useful in regarding to understanding and modelling the depositional sequences of the Bintuni/Berau basins in the Tangguh Project development area. As a result, this study presents a series of original paleogeographic facies maps created for the Mesozoic sequence stratigraphy of the Tangguh area.

The stratigraphic approach utilized for Bintuni Basin in the early to mid 1990's was a combination of seismic stratigraphic, biostratigraphic, and lithostratigraphic methodologies (Dolan and Hermany, 1998; Perkins and Livsey, 1993; Fraser, et al., 1993; Bulling, et al., 1998). Within this approach, the gross overall stratigraphy of the present-day Bintuni/Berau basins through to the ancestral paleo- Bintuni/Berau basins were identified and defined by interpreted seismic reflectors. However, the poor resolution of seismic surveys at depth in Bintuni Basin has limited seismic stratigraphy to identification of a Triassic Rift reflector (ie. near-top Late Permian), a Base Cretaceous reflector, and a Late Miocene reflector (Dolan and Hermany, 1988; Perkins and Livsey, 1993; Fraser, et al., 1993). Gross intervals between these reflectors were named the 'Post-rift Sequence' (Late Triassic to Late Cretaceous), 'Late Post-rift Sequence' (Late Cretaceous to Late Miocene), and 'Recent Syn-Orogenic Sequence' (Late Miocene to Recent) according to Perkins and Livsey (1993).

After biostratigraphic age-dating of cuttings and cores (i.e. Eocene, Paleocene, Cretaceous, Jurassic, and Permian intervals) from wells, the stratigraphic units at well locations were then subdivided, and 'forced-fit' into formations typed at outcrop locations, such as the 'Lower Kembelangan', defined as Triassic through Early Cretaceous, and 'Upper Kembelangan', defined as Late Cretaceous through the Eocene clastic succession (Perkins and Livsey, 1993). While, Fraser et al., (1993) chose to create new 'polysequence' classification schemes with the 'Roabiba Polysequence', defined as Early Callovian to Early Kimmeridgian, and the 'Sebyar Polysequence', defined as Tithonian to early Valanginian'.

Within these previous stratigraphic frameworks, large lithostratigraphic units were treated as a single interval based on shared or similar lithological characteristics

(i.e. 'Roabiba Sandstone Formation'). The lithostratigraphy of the Mesozoic interval in the Tangguh area is summarized in the Berau/Bintuni Basins Stratigraphic Column (Figure 3.2).

A systematic review of all the data from the Mesozoic interval in the Tangguh area revealed that these previous stratigraphic frameworks by Perkins and Livsey (1993), and Fraser et al., (1993) were ill-suited for defining sequence boundaries identifiable from ARCO/BG well data, and for constructing Mesozoic interval 'zones' in a Tangguh area 3D geological model (GeoCARD). Extensive ARCO/BG whole core coverage through many key Mesozoic intervals at Wiriagar Deep and Vorwata well locations resulted in abundant detailed ichnological fabric and facies, sedimentological, and paleontological/palynological studies. These datasets include ichnological fabric and facies analyses by Pemberton (1997a-f), sedimentological facies analyses by Tye and Hickey (1999), paleontological analysis by Frame et al., (1997a-i); and palynological analyses by Waton et al. (1994; 1996a-e; 1997a-h; 1998a-d). In addition, all of the key cores through the Mesozoic interval (from ARCO and BG wells) were examined again and the existing logs reviewed in Jakarta during 2001 and 2002 for this study. The core plug/chip samples were taken and analyzed to in-fill gaps in the ARCO/BG whole core plug datasets.

The detailed interpretations by these various workers were occasionally contradictory; therefore, the original 'raw' data sets from the various studies were re-interpreted and integrated, from a sequence stratigraphic perspective, to arrive at a coherent stratigraphic model. The revised sequence stratigraphic framework model has attempted to honor all of the original data. The sequence stratigraphic framework was then used for the subsurface evaluation and interpretation of all of the other datasets including the limited seismic stratigraphy, and the extensive rock properties datasets (wireline logs; whole core, rotary sidewall core, and cuttings rock characteristics including, but not limited to, porosity, permeability, pyrolysis, etc.).

The data, within this sequence stratigraphy framework was then evaluated using subjective probabilistic matrices and factoring to rate, and then rank, the various reservoirs, structures, and seals, as potential ESSCI CO₂ injection and sequestration sites. The data was incorporated into the integrated 3D geological model (GeoCARD), which was imported into a reservoir simulator (VIP) to verify that the simulated CO₂ migration rate, direction, and pressure matched the predicted ESSCI CO₂ migration rate, direction, and pressure at the proposed, highest-ranked injection sites.

The revised Mesozoic sequence stratigraphy of the Tangguh area is presented in a series of five stratigraphic geological cross-sections. The five cross-sections are all flattened on the base Ayot Limestone Formation since it is pervasive across the entire Tangguh area, and is ‘near to’ or ‘coincident’ with the Pre-Ayot MFS.

Cross-sectional line A-A’ runs NW to SE (Figure 6.1) parallel to the Wiriagar Deep structure’s Mesozoic paleo-depositional strike. Cross-sectional line B-B’ runs SW to NE (Figure 6.2) and is parallel to the Wiriagar Deep structure’s Mesozoic paleo-depositional dip.

Cross-sectional line C-C’ runs W to E (Figure 6.3) along the Vorwata structure’s Mesozoic paleo-depositional strike. Cross-sectional line D-D’ runs NW to SE (Figure 6.4) oblique to the Vorwata structure Mesozoic paleo-depositional strike, and cross-sectional line E-E’ runs SW to NE (Figure 6.5) parallel to the Vorwata structure’s Mesozoic paleo-depositional dip.

A summary table of the sequence stratigraphic/model zones is presented in Table 6.2a-b, and a brief description of this sequence stratigraphy, is presented below.

6.3.1 Late Permian

For ESSCI CO₂ injection and sequestration modelling purposes, the top of the Late Permian is the deepest, and oldest, important bounding surface. The Late Permian surface is identifiable from seismic stratigraphy, as a near-top Late Permian reflector (Bulling, et al., 1998; Keho and Samsu, 2002).

Below the Late Permian seismic surface (approximately 248 ma) are Late Permian sedimentary rocks of the Tatarian to Ufimian Stage (Waton, et al., 1994; Waton, et al., 1996a-e; Waton, et al., 1997a-h; Waton, et al., 1998a-d).

Stratigraphically, the top Late Permian represents both an erosional unconformity sequence boundary (SB), and a flooding surface (FS), and as such is a key bounding surface to constrain the overlying Jurassic interval. The top-most Late Permian shale is a maximum flooding surface (MFS), or a near-maximum FS, since erosion may have removed the actual MFS on WD-3, and is readily identifiable on wireline logs due to a high gamma-ray (GR) spike at the top or near-top (Salo, 1994; Salo, 1996c; Salo 1997a-c). The top Late Permian surface is also characterized by trace fossil burrowing on an exposed, dewatered substrate including vertical, cylindrical, ‘U’ or tear shaped pseudo-borings, sparse to densely branching dwelling

burrows, or mixtures of burrows and dwellings. This represents a ‘*Glossifungites*’ surface (Pemberton, 1997a).

The oldest sedimentary rocks overlying the Late Permian surface boundary (SB), encountered in the immediate Tangguh area and dated palynologically, are Aalenian (MJ-4) in age (Waton, et al., 1994; Waton, et al., 1996a-e; Waton, et al., 1997a-h; Waton, et al., 1998a-d). The unconformity, in the Tangguh area, has resulted in the entire Triassic interval being eroded (Perkins and Livsey, 1993; Bulling, et al., 1998), therefore the Late Permian SB represents approximately 73 million years of missing rocks (Waton, et al., 1994; Waton, et al., 1997b-c).

As discussed in Chapter 5. LITHOSTRATIGRAPHY AND SEDIMENTOLOGY, the Late Permian is described from palynological and ichnological studies as deposited primarily in a continental/fluvial paleo-environment with minor marine pulses near the top of the unit (Pemberton, 1997a; Waton, et al., 1994; Waton, et al., 1996a-e; Waton, et al., 1997a-h; Waton, et al., 1998a-d). The base of the Late Permian unit has never been penetrated by drilling in the Tangguh area.

This study concludes that during the Late Permian, the Tangguh area was continental with a series of cool-climate fluvial and lacustrine sediments deposited including temperate, cool-climate, raised peat-mires analogous to the Siberian peat bogs of the Ob River basin of Russia (Lang, et al.; 2000). Occasional marine pulses into the Wiriagar Deep and Vorwata areas then occurred during the latest Late Permian, depositing interbedded marine clastic sedimentary rocks (shales, silstones, and occasional delatic sandstones) with the continental clastic sedimentary rocks and peats. The entire ancestral proto-Bintuni Basin area was uplifted (and perhaps major portions of Papua including the Arafura Sea area), subaerially exposed and eroded during the Triassic and earliest Jurassic, with all of the Triassic and perhaps some of the upper Late Permian rocks subsequently removed.

6.3.2 Triassic and Early Jurassic

A major uplift in the northern Australian-New Guinea Plate (ANGP) margin during Triassic times removed up to three kilometers of sediments through erosion in the Arafura Sea area, immediately south of the Bird’s Head, Papua (Yeates, et al., 1987; Bradshaw, et. al, 1990; Veevers, et al., 2000). This unconformity accounts for the lack of definitive Triassic sedimentary rocks in the Tangguh area between

Permian and Jurassic Periods, and is most-probably related to the Triassic unconformity identified at wells in the Dampier, Offshore Canning, Browse, Bonaparte, and Arafura Trough basins of Australia's NW Shelf (Longley, et al. 2002).

The onshore East Onin #1 well (EO-1) is located more than 75 km SW of the Wiriagar Deep Field on the Onin Peninsula, although the EO-1 is outside the study area it is significant for the preservation of Early Jurassic sedimentary rocks. The EO-1 encountered Early Jurassic sediments containing "undifferentiated earliest Jurassic" palynomorphs and occasional reworked Triassic palynomorphs at TD (Waton, et al., 1996a). These sedimentary rocks, encompassing the Pliensbachian to Hettangian stages of the Early Jurassic (EJ-2), were characterized by paleontological/palynological analyses as ranging from continental paleo-depositional environments to intertidal to marine (Waton et al. 1996a). These were, in turn, overlain with sediments that were characterized as deposited in a transitional littoral to marine sublittoral paleo-environment, definitively dated by palynology from the Toarcian stage (EJ-1) of the Early Jurassic (Waton, et al., 1996a). Early Jurassic cores (EJ-2/EJ-1) from the EO-1 were also interpreted by Pemberton (1997f) as deposited in a full marine to shelfal facies.

Early Jurassic sediments from the Toarcian Stage (EJ-1) were also identified palynologically, by Waton, et al. (1998e) from rotary sidewall cores and drill cuttings on the Ubadari #2 (U-2) well, located approximately 50 km to the SW from the Wiriagar Deep Field. The Toarcian palynomorph assemblages at U-2 were interpreted by Waton et al., (1998e) as continental to shallow marine or littoral facies, overlain by the Middle Jurassic Aalenian (MJ-4) rocks. The Aalenian palynomorph assemblages are concluded to be transgressive marine to restricted shallow marine facies that were proximal to freshwater input, based on 5% acritarchs and the limited diversity of marine dinocysts (Waton, et al., 1998e).

The Ubadari #1 (U-1) well location is approximately 4 km N of the Ubadari-2 well location, and is also approximately 50 km to the SW from the Wiriagar Deep Field. It also contains sedimentary rocks with probable in-situ Toarcian Stage (EJ-1) palynofloral marker taxa, with palynomorph assemblages and depositional facies similar to the U-2 (Waton, et al., 1997i).

Although the EO-1, U-1, and U-2 wells are not within the subsurface geological study area, nor contained in the 3D model area, they are, nevertheless, crucial data linchpins from a sequence stratigraphy perspective. These important well

controls clearly indicate that a marine environment existed 100 km to the SW of Wiriagar Deep (at EO-1) during the Early Jurassic, with marine transgression reaching the area of the Ubadari wells (U-1 and U-2) by the Toarcian stage of the Early Jurassic, 50 km to the SW from the Wiriagar Deep.

Palynomorph assemblages have dated the oldest sedimentary rocks overlying the Late Permian SB unconformity, at Wiriagar Deep and Vorwata well locations, as Aalenian Stage, MJ-4 (Waton, et al., 1994; Waton, et al., 1996a-e; Waton, et al., 1997a-h; Waton, et al., 1998a-d). Relatively thick Early Jurassic (EJ-2/EJ-1) sedimentary rock units at the EO-1, U-1, and U-2 locations indicate that sediment supply was probably not interrupted during the Early Jurassic. It follows, that the Wiriagar Deep and Vorwata areas of Bintuni Basin was subaerially exposed during the Triassic and/or Early resulting in erosion.

In summary, an EJ-2 marine setting is indicated at the East Onin-1 location, and this was followed chronostratigraphically by EJ-1 marine sediments at both Ubadari well locations, with a deeper marine paleo-depositional facies identified at EO-1 than at U-1 and U-2 locations. The Early Jurassic Period was then followed by a variety of early Middle Jurassic, Aalenian Stage (MJ-4), marine paleo-depositional facies sedimentation preserved across the entire region ranging from the EO-1 location in the SW, to the Wiriagar Deep well locations to the NE. Therefore, the distribution of sediments dated from palynological marker taxa and assemblages suggest that the period of Triassic/Early Jurassic erosion in the Wiriagar Deep and Vorwata area ceased when a marine transgression occurred across the Bird's Head region of Papua from the SW towards the NE, during the latest Early Jurassic. Palynological analyses (Waton, et al., 1994; Waton, et al., 1996a-e; Waton, et al., 1997a-h; Waton, et al., 1998a-d) revealed Aalenian palynofloral marker taxa overlying Late Permian marker taxa at all Wiriagar Deep well locations, and Bajocian palynofloral marker taxa overlying Late Permian marker taxa at all Vorwata well locations. These analyses suggest uplift and erosion in the Bird's Head during the Triassic, with a marine transgression proceeding from the southwestern EO-1 location during the Pliensbachian to Hettangian (EJ-2), to the U-1 and U-2 locations by the Toarcian (EJ-1), and finally the Wiriagar Deep area by the Bajocian (MJ-3) (Waton, et al., 1994; Waton, et al., 1996a-e; Waton, et al., 1997a-i; Waton, et al., 1998a-e).

This overall marine transgression possibly occurred as a series of eustatic rises and falls in global sealevel during the Early Jurassic with progressively higher

sealevels reached on each of the intervening highstands. The global eustacy curve, of Haq et al., (1987), modified and updated by Berggren et al., (1995) is provided in the Bintuni basin stratigraphic column in Figure 3.2. From a sequence stratigraphic perspective, two events can possibly be considered responsible for the Early Jurassic and Middle Jurassic SW to NE marine transgression across the Bird's Head region:

- 1) An extensional rifting event, possibly failed and incomplete, resulted in detachment or semi-detachment the Bird's Head area from the northwest margin of the Australian-New Guinea plate during the Jurassic, possibly related to West Burma, Lhasa, and Argoland block rift and detachment events (Figure 6.6). Thermal sag, whether associated with an extensional rifting event or a failed rift, would have allowed some marine transgression into previously continental areas (Vail, et al., 1984; Yeates, et al., 1987; Bradshaw, et al., 1994a; Bradshaw, et al., 1994b; Charlton, 2000; Veevers, 2000; Longley, et. al. 2002).
- 2) A series of global eustatic rises in sealevel, totaling approximately 50m (Vail, et al, 1984; Haq, et al., 1987; Berggren, et al., 1995), which occurred from the Hettangian Stage lowstand (EJ-2) until the Aalenian Stage (MJ-4) highstand (Figure 6.7).

Quite likely, both events played a contributing part in the marine transgression during the Early Jurassic in the Bird's Head region. The proto-Tethys rift allowed oceanic proximity to the paleogeographic location of the Bird's Head on the newly formed northern Australian-New Guinea plate (ANGP) margin by the Early Jurassic (Veevers, 2000), and the penecontemporaneous eustatic global sealevel rise drowned low relief coastal topography, particularly in extensional rift and thermal sag regions adjacent to the paleo-coastline.

6.3.3 Aalenian MJ-4 (Middle Jurassic)

As alluded to previously, sedimentary rocks dated palynologically to the earliest Middle Jurassic Stage, the Aalenian (MJ-4), have been identified in well cuttings and/or cores from the Wiriagar Deep well locations. With the exception of the Vorwata #7 well, and possibly the Vorwata #3 well, no Aalenian palynofloral

marker taxa have been conclusively identified in the Vorwata area (Waton, et al., 1997b-h; Waton, et al., 1998a-d).

This has been interpreted as a Middle Jurassic marine transgression during the Aalenian Stage that reached a highstand during the following Bajocian/Bathonian Stage, with the maximum limit of marine transgression encompassing most of the Wiriagar Deep area, but not reaching the Vorwata area with the notable exception of the Vorwata-7 well location (Waton et al. 1998e). The Aalenian sedimentation has been interpreted as occurring in an embayment, or a restricted marine paleo-depositional environment (Waton, et al., 1994 through 1998; Pemberton 1997b, 1997d, 1997e).

The Aalenian succession in the Wiriagar Deep area is typically composed of silty marine shales and stacked, fine to medium-grained, cross-bedded sandstones with occasional thinly bedded intercalated coal seams. These sandstones and shales typically contain marine palynomorph taxa and marine ichnological trace fossil assemblages deposited on the Top Permian sequence boundary, and are indicative of a marine transgression. The nature of the Top Late Permian Unconformity SB suggests rather, that widespread peneplanation took place during the Triassic/Early Jurassic prior to the deposition of the Aalenian succession.

Benthonic foraminifera (*Lenticulina* spp.) identified in the deepest Aalenian Stage (MJ-4) samples from the East Onin #1 well (Waton, et al., 1996a), indicates a deeper marine facies present to the SW than seen in the equivalent Aalenian interval at the Ubadari and Wiriagar Deep well locations, and also deeper than identified in the underlying Early Jurassic sedimentary rocks (EJ-2 and EJ-1) at East Onin. These are consistent with the interpreted SW to NE, Early Jurassic marine transgression across the western Tangguh area.

The Wiriagar Deep area contains Aalenian sedimentary rocks (MJ-4) that are bounded by the underlying Late Permian SB unconformity and the overlying Bajocian/Bathonian (MJ-3) sedimentary rocks. On most Wiriagar Deep wells there is an intervening Bajocian/Bathonian MJ-3 shale (labelled by ARCO as the 'Pre-Roabiba Shale Formation') overlying the Aalenian MJ-4 sandstone reservoir. The highest gamma-ray value in this shale is found within the top few feet overlying the Aalenian sandstone. This quite probably represents a maximum flooding surface. Therefore, for modelling purposes the biostratigraphic stratigraphic MJ-4/MJ-3

boundary and the Pre-Roabiba Shale maximum flooding surface are considered coincident.

Extensive whole core coverage through the Aalenian sedimentary rocks at most of the Wiriagar Deep well locations has resulted in abundant detailed ichnological fabric and facies, sedimentological, and palynological studies. These include ichnological fabric and facies analyses by Pemberton (1997b and 1997e-f), sedimentological facies analyses by Tye and Hickey (1999), and palynological analyses and palynological facies interpretations by Waton et al. (1994; 1996a-e; 1997a-h), and sedimentological facies examination of the core.

There is some evidence of an incised valley system, in the Tangguh area, as a depo-center for this transgressive marine sedimentation. However, no definitive, elongate, paleo-topographic low has been identified, with more than a single channel sedimentary fill in the area, which is the definitive hallmark of incised valley complexes (Zaitlin, et al., 1994). The Aalenian sedimentary rocks are zoned as a sequence stratigraphic unit labelled the A20 zone. The geometry of the A20 zone could indicate a transgressive shoreface merely contained within a broad, but shallow, embayment. An isopach map of the entire A20 zone interval in the Tangguh area, is presented in Figure 6.8.

Using the integrated 'raw' dataset from these various researchers, the Aalenian rocks have been identified in their correct stratigraphic position at Wiriagar Deep well locations and the V-3 and V-7 wells. The paleo-depositional facies interpretation in this paper was integrated with log motif signatures for wells containing the Aalenian interval (see Table 6.5a through 6.5f), to generate Aalenian Stage (MJ-4) paleogeographic facies maps of the Tangguh area encompassing the area from Wos-1 well in the SE to Wiriagar Deep-1 in the NE, to Sakauni-1 in the NW to the proposed LNG plant location in the SW. These represent two 'time-slice snapshot' of the area containing the Wiriagar Deep, Vorwata, Roabiba, Ofaweri, and Wos structural traps.

A20 Aalenian (MJ-4)

The first 'time-slice snapshot', is labelled as the 'Early A20', and is the interpreted paleogeographic facies of the Tangguh area shortly after the onset of Aalenian deposition in the area (Figure 6.9). The second time-slice snapshot is labelled as the 'Late A20', and is the Late Aalenian paleogeographic facies of the

Tangguh area (Figure 6.10), just prior to the onset of the Bajocian/Bathonian (MJ-3) deposition.

These two Aalenian paleogeographic facies maps portray a very broad marine transgression over the Ubadari to Wiriagar Deep area, while the Vorwata area remained subaerially exposed and continental during the Aalenian. This interpretation was dictated by the large area encompassing the eight Wiriagar Deep wells (15 km x 25 km) and the two Ubadari wells (50 km southwest from the nearest Wiriagar Deep well), in conjunction with the interpretation of a restricted marine environment proximal to freshwater input which resulted in stressed paleo-depositional environments for marine palynomorphs and trace fossil taxa at all of the Wiriagar Deep and Ubadari well locations (Waton, et al., 1994; Waton, et al., 1996a-e; Waton, et al., 1997a-h; Pemberton, 1997b; Pemberton, 1997d-e).

Overall, the two Aalenian Stage paleogeographic facies maps depict the paleo-depositional environment of the Aalenian marine transgression proceeding from the present-day SW to NE relying on evidence in the East Onin and Ubadari well data.

6.3.4 Bajocian/Early Bathonian MJ-3 (Middle Jurassic)

Palynological marker taxa (discussed in detail in Chapter 5. LITHOSTRATIGRAPHY AND SEDIMENTOLOGY) and assemblages identify the Bajocian/Early Bathonian (MJ-3) as present at all Wiriagar Deep and Vorwata wells (Waton, et al., 1994; Waton, et al., 1996a-e; Waton, et al., 1997a-i; Waton, et al., 1998a-e). The Bajocian/Bathonian Stage is palynologically zoned as MJ-3, based on marine palynomorphs and trace fossil taxa at all of the Wiriagar Deep and Ubadari well locations (Waton, et al., 1994; Waton, et al., 1996a-e; Waton, et al., 1997a-h; Pemberton, 1997b; Pemberton, 1997d-e). Palynomorphs including dinocysts and marine palynoflora are also commonly present in the Bajocian/Bathonian sediments of the Tangguh area (Waton, et al., 1994; Waton, et al., 1996a-e; Waton, et al., 1997a-h; Pemberton, 1997b; Pemberton, 1997d-e).

The Bajocian/Bathonian (MJ-3) succession in the Tangguh area is characterized a stacked, on-lapping series of very-fine to medium-grained, marine sandstones with some trough-cross bedding, low angle tabular bedding, and flaser bedding, containing moderate to common *Ophiomorpha*, *Thalassinoides*, *Planolites*, and *Asterosoma* ichnological trace fossil fabrics (Pemberton 1997b and 1997d-e).

This Bajocian/Bathonian interval (MJ-3) contains most of the 'Roabiba Sandstone Formation' reservoir. Previously, ARCO nomenclature assigned the overlying Callovian sandstone (MJ-1/LJ-11) member of the 'Roabiba Sandstone Formation' present in the Vorwata area only, to the Bajocian/Bathonian (Bulling, et al., 1998).

Therefore, for the purposes of this study, the entire Roabiba Formation is now subdivided stratigraphically into the underlying Bajocian/Bathonian (MJ-3) Roabiba Sandstone Formation and, the overlying Callovian (MJ-1/LJ-11) Roabiba Sandstone Formation. However, reinterpretation of the original 'raw' data shows the upper 'Roabiba Formation', previously assigned to Late Bathonian (MJ-3), has been re-assigned to the Callovian (MJ-1/LJ-11), with an intra-formational unconformity present (Vail, et al., 1984; Waton, et al., 1994; Waton, et al., 1996a-e; Waton, et al., 1997a-i; Waton, et al., 1998a-e).

The Bajocian/Bathonian (MJ-3) sequence is defined by the underlying Top Aalenian (MJ-4), which is near-concurrent with a MFS, as previously noted. The top of the Bajocian/Bathonian (MJ-3) sequence is bounded by the Bathonian Unconformity (MJ-2), a sequence boundary, with Callovian (MJ-1 and LJ-11) sedimentary rocks overlying it (Waton, et al., 1994; Waton, et al., 1996a-e; Waton, et al., 1997a).

The palynofloral taxa in conjunction with the identification of acritarchs and marine dinocysts indicate a restricted marine paleo-depositional environment with varied degrees of freshwater influence (Waton, et al., 1994; Waton, et al., 1996a-e; Waton, et al., 1997a-i; Waton, et al., 1998a-e). This clearly shows that the marine transgression, which began in the Early Jurassic, continued through the Aalenian and into the Bajocian, since the areal extent of the Aalenian marine taxa was limited to the Wiriagar Deep area, and the Vorwata Bajocian sedimentary rocks and taxa directly overlie the top Late Permian unconformity. A comparison of the gross Aalenian interval isopach (Figure 6.8) with the gross Bajocian/Bathonian interval isopach (Figure 6.11) shows the overall direction of the Middle Jurassic transgression in Bintuni Basin.

Furthermore, a shallow marine to littoral paleo-depositional environment was indicated in the two Ubadari wells by Waton, et al. (1997i and 1998e), which is consistent with a continued marine transgression that made the Ubadari area, 50 km SW of Wiriagar Deep, more distal to the Bajocian/Bathonian paleo-coastline but still

within a broad embayment. The embayment is estimated to have been more than 50 km wide x 100 km long, with the present-day Berau Bay/Bintuni Bay having similar dimensions but being a more mud-rich analogue (Figure 5.38).

The Bajocian/Bathonian (MJ-3), bounded at the base by the top Aalenian MFS sequence boundary, and on the top by the MJ-2 (Late Bathonian) unconformity sequence boundary, is divided into eight separate chronostratigraphic zones within the gross interval, each consecutively shallower in depth, labelled R10, R20, ... through R80 ('R' standing for Roabiba). The complete suite of Bajocian/Bathonian zones are shown at the Roabiba #1 well location on a stratigraphic cross-section E - E' (Figure 6.5). These picks are based on shale breaks, interpreted as flooding surfaces, log motif signature correlations, and in some cases, such as the R30 zone, a definitive palynological acme present only in that zone.

A representative paleogeographic facies map has been interpreted for each zone. Note, that present-day orientations are discussed, and isopachs and paleogeographic maps oriented according to the present-day cardinal points, for clarity. However, paleogeographic orientations are likely to have been different at their respective time of deposition with respect to true north.

R10 Bajocian/Early Bathonian (MJ-3)

The oldest and lower-most zone, the R10, is a sandy to silty mud lithology (Salo, 1994; Salo, 1996c; Salo, 1997a-f), and is interpreted as a continuation of the marine transgression that began sedimentation in the paleo-Bintuni Basin during the Aalenian (Figure 6.12). The shoreface, at the time of the R10, had drowned most the Wiriagar Deep area and the western half of the Vorwata area, with the paleo-coastline trending roughly NW to SE, and the transgression mainly progressing from the SW to SSW (Figure 6.13). Bayhead deltas were poorly developed, and the present-day Burdekin Delta (Australia) is an appropriate analogue to the R10 paleo-Bintuni Basin as a huge coastal delta-plain (Lang, et al, 1990).

R20 Bajocian/Early Bathonian (MJ-3)

The R20 unit is also a sandy to muddy siltstone lithology (Salo, 1994; Salo, 1996c; Salo, 1997a-f), and is interpreted as a late stage of the marine transgression, because the marine encroachment finally encompassing all of the Wiriagar Deep and the Vorwata area, with the exception of the Vorwata #3 (V-3), Vorwata #4 (V-4),

Vorwata #8 (V-8), and Vorwata #11 (V-11) well locations, as shown in the isopach of the R20 interval (Figure 6.14). The R10 and R20 units are absent in these four locations and are therefore interpreted as being in non-depositional continental paleo-environments. Nambumbi #1 (N-1) and Vorwata #1 (V-1) are interpreted as fluvial and deltaic facies respectively, based on palynological (Waton, et al., 1998f; Waton, et al., 1997b) and ichnological data (Pemberton, 1997b; Pemberton, 1997e-f). These two wells provide a control on the location and orientation of the paleo-coastline during the early Bajocian/Bathonian, as interpreted in the paleogeographic map of zone R20 in the paleo-Bintuni Basin area (Figure 6.15).

R30 Bajocian/Early Bathonian (MJ-3)

The R30 is an extremely important stratigraphic zone within the entire Bajocian/Bathonian Interval zonation scheme, as the interval contains the index palynomorph taxa, *Chytroeisphaeridia chytrooides* (Waton, et al., 1994; Waton, et al., 1996a-e; Waton, et al., 1997a-i; 1998a-e), in both cores and the cuttings at almost all Tangguh area well locations. As Waton, et al., (1997b, p.23) states in the Vorwata #1 well biostratigraphic report, “The acme of *Chytroeisphaeridia chytrooides* in core samples 11899.3’ and 11904.2’ (43%) is commonly seen in this area near the base of the MJ-3 sediments”.

The R30 zone consists of cleaning-upward, progradational series of shelfal mudstones and shoreline sandstones (Salo, 1994; Salo, 1996c; Salo, 1997a-f), and is interpreted as a basinward progradational in-filling highstand systems tract from gamma-ray log motif interpretation (Figure 6.5a-f), on virtually all wells in the area (Allen, et al., 1979; Allen and Mercier, 1988; Busch and Link, 1985; Lang, 2001). The isopach for the R30 zone is presented in Figure 6.16.

The MJ-3 acme allowed a further degree of correlation confidence in regards to the correlation of the areas progradational log motif discussed above, and also as a basis for the building of stratigraphic sequences overlying this zone. The interpreted paleo-geographic map for the R30 zone is shown in Figure 6.17.

This high-stand systems tract (HST) represented by the R30 zone, consists of in-filling of the accommodation space resulting in the offshore extension of the paleo-coastline and associated deltaic complexes, with relict barrier island foreshores, relict tidal channels, relict lagoonal deposits preserved as a broad strandplain complex, perhaps analogous to the present-day sand-rich Gilbert and Mitchell River strandplain

complexes on the eastern shore of the Gulf of Carpentaria in Australia (S.C. Lang, personal communication, 2003).

The progradational in-filling of the embayment with sediments could have been the result of a huge sediment supply disgorging from several bayhead deltas along the embayed coastline, which outpaced the relative sealevel rise of the Bajocian/Bathonian, or alternatively, the rate of the marine transgression may have slowed or halted temporarily. In either case, sediment supply outpaced the accommodation. This was to change during the subsequent R40 sequence stratigraphic zone.

R40 Bajocian/Early Bathonian (MJ-3)

The R40 zone, overlying the acme R30 zone, is a massive, fine to medium-grained, relatively well-sorted quartzose sandstone bedding (Salo, 1994; Salo, 1996c; Salo, 1997a-f), occasionally preserving trough-cross bedding, low angle tabular bedding, and minor flaser (Tye and Hickey, 1999). The R40 unit represents a renewal of marine transgression, resulting in the entire Wiriagar Deep and Vorwata area inundated except in the V-4, V-8, and Sakauni-1 (S-1) well location area, as shown by the R40 isopach (Figure 6.18). The R40 transgressive systems tract (TST) was areally widespread across the Wiriagar Deep and Vorwata area, although it is absent at the V-7 and V-3 well locations due to subsequent erosive incision (Figure 6.18). Increasing subsidence to the SE (seen repeatedly throughout the Middle Jurassic and Late Jurassic intervals) created increased accommodation space over the Vorwata area, particularly towards the southeast, but still within a restricted marine (very large embayment) environment, as shown on the paleo-geographic facies map for the R40 zone (Figure 6.19).

R50 Bajocian/Early Bathonian (MJ-3)

The R50, which is a very thick, massively bedded, fine to medium-grained, quartzose stacked sandstone succession (Salo, 1994; Salo, 1996c; Salo, 1997a-f). An isopach map of the entire R50 zone is presented in Figure 6.20.

The R50 zone, in most of the Vorwata well cores, has been identified as a mix of tidal channel, backshore, and foreshore depositional facies, however the basal R50 Wiriagar Deep #2 (WD-2) core contain sedimentary features such as trace fossil burrowing through thin parallel and planar laminations of clay interbedded with

moderately sorted fine to medium grain sandstones beds, indicative of a sandy tidal flat facies (Tye and Hickey, 1999). The adjacent Wiriagar Deep #5 (WD-5) basal R50 core contains tidal channel sedimentary features, such as well-sorted, clean sandstones with occasional scour surfaces, trough-cross beds, and some rare basal channel rip-up clasts (Tye and Hickey, 1999). The Early R50 paleo-geographic facies map (Figure 6.21) reflects this distribution of sedimentary features preserved in cores.

However the upper R50 zone seen in cores shows a marked paleo-facies change at the WD-2 and WD-5 well locations. Core in the upper R50 zone at WD-2 shows fluvial features such as tabular cross-bedding, asymmetric ripple laminae, and parallel laminae (Tye and Hickey, 1999). Core from the upper R50 zone at WD-4, originally described by the author at wellsite, is a medium to fine grained argillaceous sandstone with occasional mica (muscovite), poorly sorted, with microlaminations to 0.5 mm laminations of subparallel mudstone/claystone, claystone clasts (Salo, 1997a). The slabbed core from WD-4 exhibited lagoonal sedimentological features such as with abundant clay content, showing planar-tangential cross bedding, asymmetric current-ripple laminae, and load casts, with clay drapes and clay clasts (Tye and Hickey, 1999). These features were confirmed by the author upon re-examination of the core in 2001 and 2002.

The fluvial nature of the upper R50 sediments at WD-2 and WD-4 locations are supported by palynological analyses. Palynological (Waton, et al., 1996a; Waton, et al., 1996c) analyses found terrestrial miospores in the cores from the upper R50 zone at WD-2 and WD-4, indicating a freshwater depositional environment or at least one that was 'subject to strong freshwater fluvial inputs'.

To briefly summarize the sequence stratigraphy of the R30 through R50 zones at the Tangguh area, the R30 represented a high stand systems tract (HST) with progradation of the entire shoreface, resulting in the preservation at numerous well locations of relict barrier islands, tidal channels, and washover/backwater depositional facies.

The R40 zone is interpreted as a renewed transgressive system tract (TST), with deeper marine paleo-depositional facies identified overlying the R30 HST sedimentation in cores. The Early R50 is interpreted to once again represent a phase of shallower marine deposition overall, with backshore tidal flats developing in the western embayment at WD-5.

The Late R50 shows a continuation of a HST with progradation of the interior bay, especially the development of fluvial to lagoonal/lacustrine depositional facies in the western margin at WD-2 and WD-2 (Figure 6.22).

R60 Bajocian/Early Bathonian (MJ-3)

The R60 zone is a relatively thinly bedded arenaceous shale (Salo, 1994; Salo, 1996c; Salo, 1997a-f), and is interpreted as a maximum flooding surface (MFS) present over all of the Vorwata area (it has probably been eroded out at the V-1, V-3, and V-7 well locations by the Late Bathonian/MJ-2 unconformity). It has been eroded out over most of the Wiriagar Deep area by the Oxfordian/LJ-10 erosional unconformity. An isopach map of the thinly bedded R60 unit/zone is presented in Figure 6.23.

This unit is interpreted as coinciding with the end of the transgressive systems tract (TST), and is indicative of the maximum marine transgression in the Tangguh area during the Bajocian/Bathonian Roabiba period (Figure 6.24).

R70 Bajocian/Early Bathonian (MJ-3)

The R70 zone is a massive, fine to medium-grained, quartzose sandstone that is generally very clean at many well locations where core exists (Salo, 1994; Salo, 1996c; Salo, 1997a-f). The isopach of the R70 zone is shown in Figure 6.25.

Core through this interval at WD-4 and WD-5 is described as typical of foreshore facies with occasional low-angle tabular cross-bedding and rare flaser bedding (Tye and Hickey, 1999). The R70 interval in core from V-2, V-5, V-6, and V-10 are interpreted to represent middle shoreface depositional facies with rare cross-bedding, convolute laminae, asymmetric ripple laminae, and flaser bedding (Tye and Hickey, 1999). Tye and Hickey (1999), however, identified core in the V-4 as ebb-tidal channel inlet (which is rarely preserved, T. Payneberg, personal communication, 2004) with tabular and low angle tangential cross bedding, convolute bedding, flaser bedding, mud drapes, and numerous scour surfaces.

This study interprets the R70 zone as a Bajocian/Bathonian (MJ-3) highstand systems tract (HST), with infilling of the shallow embayment occurring from the shallowest paleo-bathymetry in the north towards the bay depo-center in the south. The paleo-coastline is interpreted as oriented approximately W to E in the Tangguh

area during this time period, with possible sand-rich strandplains present to the north (Figure 6.26).

R80 Bajocian/Early Bathonian (MJ-3)

The R80 zone represents the youngest and shallowest, zone of the Bajocian/Bathonian (MJ-3) Roabiba Formation sedimentation preserved in the Tangguh area wells. The R80 unit is a massively bedded, fine to medium-grained, quartzose sandstone (Salo, 1994; Salo, 1996c; Salo, 1997a-f), with occasional trough-cross bedding, low angle tabular bedding, and flaser bedding preserved (Tye and Hickey, 1999). An isopach map of this massively bedded R80 unit/zone is presented in Figure 6.27.

The R80 unit/zone, where it is preserved at wells, is truncated at the top by a regionally widespread Late Bathonian/MJ-2 unconformity at the Vorwata area, and by a regionally widespread Oxfordian/LJ-10 unconformity at the Wiriagar Deep area. The unconformable sequence boundary at the top of the Bajocian/Bathonian (MJ-3) Roabiba Sandstone is overlain at much of the Vorwata area by the Callovian (MJ-1/LJ-11) sediments labelled as the CU10 unit.

As indicated on the paleogeographic facies map for the R80, large areas of the Tangguh region were subsequently uplifted and eroded out (Figure 6.28). The prominent red line on the paleogeographic facies maps delineates the northern and western areas (with hatchmarks) uplifted and eroded, with R80 sandstone sedimentary rocks preserved only at the Vorwata-2, Vorwata-6, Vorwata-10st, and the Roabiba-1 well locations.

The zone was interpreted in core as barrier island beach sands (V-10), tidal channel sands (V-2), washover sands (V-6) by Tye and Hickey (1999). The R80 at the Roabiba-1 well location (with no core available) has been re-interpereted based on gamma-ray log motif signature as consistent as a foreshore depositional environment, following the paleo-depositional facies for the R80 at V-2, V-6, and V-10 and Walther's law.

The Bajocian/Bathonian eustatic sealevel rise was a global event of supreme significance (Figure 6.7), as sealevel rose by more than 60 m (200 ft) from the lowstand at the end of the Aalenian to the maximum sea level at the very end of the Bajocian/Bathonian (Haq, et al, 1987; Berggren, et al. 1995). The marine transgression, rarely preserved in the eight total zones of the Bajocian/Bathonian (MJ-

3) Roabiba Formation, was probably due to the long-term eustatic rise in global mean sealevel, in conjunction with subsidence in the SE area of Vorwata and probable uplift of a horst block along the V-3 and V-4 strike. This accounts for the thin Bajocian/Bathonian (MJ-3) Roabiba Sandstone Formation interval at the V-4 location, with unconformities at the top and the base (Waton, et al., 1997e).

6.3.5 Late Bathonian MJ-2 (Middle Jurassic)

There are no Late Bathonian rocks preserved in the Tangguh area, based on the lack of any identifiable palynofloral, nannoflora, microfauna taxa indicative of the MJ-2 biozonation. A global eustatic fall during the Bathonian resulted in a mean sea level drop of approximately 45m, or 150 ft (after Haq, et al., 1987; modified from Berggren, et al., 1995). This drop in mean sea level (see eustacy curve in Figure 6.7) accounts for:

- 1) the absence of Late Bathonian (MJ-2) sedimentary rocks in the Tangguh area (Waton, et al., 1994; Waton, et al., 1996a-e; Waton, et al., 1997a), and;
- 2) an areally widespread unconformity across the Vorwata area that incised into, and removed some of the underlying Bajocian/Bathonian (MJ-3) sedimentary rocks, particularly at the V-1, V-3, V-4 and V-7 well locations. Waton, et al., finds that the palynological "... evidence suggests that this interval [Bajocian/Bathonian MJ-3 Roabiba Formation] is truncated by an unconformity... with MJ-2...Bathonian strata missing" (Waton, pp. 5-6, 1998e).

The isopach maps of the R30 through R80 units/zones clearly show an elongate incision through the underlying Bajocian/Bathonian Roabiba units (Figures 6.16 through 6.27) at the V-1, V-3, V-7 area.

A second, slightly less deep incision into MJ-3 rocks at the Vorwata-10 location suggests the possible presence of a second incised valley system 20 km SE of the incised valley at the V-1, V-3, and V-7 location.

The geometry of the MJ-3 and the MJ-1/LJ-11 intervals, especially when flattened on the Base Ayot, clearly indicates an unconformable incision between the Bajocian/Bathonian MJ-2 Roabiba Formation and the Callovian MJ-1/LJ-11 Roabiba

Formation at the Vorwata area (apparent in the stratigraphic cross-sections Figure 6.4 and 6.5). The especially deep incision geometry at the Vorwata well locations mentioned above, support the interpretation of an incised valley system at this location (V-1, V-3, and V-7). The possibility of a second incised valley to the E-SE of the V-10 location, also suggests the interpretation that an incised valley complex may have formed during the Late Bathonian regression (RST) and lowstand (LST), which produced the Late Bathonian unconformity (MJ-2).

6.3.6 Callovian MJ-1/LJ-11 (Middle - Late Jurassic)

This gross stratigraphic unit, the Callovian (MJ-1/LJ-11) is found only at the Roabiba and Vorwata areas, and is not present on Wiriagar Deep wells. The stratigraphic sequence is defined at the base by the Late Bathonian (MJ-2) unconformity sequence boundary (SB), and at the top by an Oxfordian (LJ-10) unconformity, defined by palynological analyses as widespread across the entire Tangguh area (Waton, 1996a-e; Waton, et al., 1997a-h; Waton, et al., 1998a-d).

Palynological biozonation of the entire Callovian (MJ-1/LJ-11) deposition is definitive in the Tangguh area, based on an assemblage containing *Scriniodinium ceratophorum*, *Scriniodinium galeritum*, *Vallensiella ovula*, *Wanaea digitata*, *Wanaea indotata*, *Wanaea spectabilis*, and *Cliestosphaeridium* (Waton, et al., 1997c). Waton, et al., (1997c) find a nonconformable interruption of palynomorph taxa characterizing the MJ-2 at the V-2 well. This unconformity is regionally widespread with the absence of MJ-2 marker taxa or assemblages at all Tangguh area wells (Waton, 1996a-e; Waton, et al., 1997a-h; Waton, et al., 1998a-d).

Regarding the upper sequence boundary, Waton, et al., (1998c, p.7) concluded that at V-2 "...there is no palynological data for the presence of Oxfordian, LJ-10, sediments, suggesting...a minor stratigraphic hiatus".

Therefore, Callovian is bounded at the base by the Late Bathonian (MJ-2) sequence boundary (discussed above), and the top by the Oxfordian (LJ-10) sequence boundary. The Callovian is divided into two gross intervals for this study. The older, and deeper interval is designated the Callovian Roabiba Sandstone (undifferentiated MJ-1/LJ-11), and the overlying younger interval is designated the Pre-Ayot (LJ-11). These two gross intervals are delineated by an intervening maximum flooding surface based on wireline log motif interpretations. The boundary defining the top of

Callovian Roabiba Sandstone and the base of the Pre-Ayot maximum flood surface (MFS).

The MFS is characterized as a maximum high gamma-ray peak on top of Callovian Sandstone Formation (Figure 6.29), with massively bedded marine shales overlying the Callovian Roabiba Sandstone (Perry, et al., 1997; Salo, 1997g; Salo, 1998a-b). Both gross intervals of the Callovian are further subdivided into zones based on correlatable flooding surfaces. An isopach of the entire Callovian Sandstone sequence is shown in Figure 6.30.

The Callovian (MJ-1/LJ-11) Roabiba Sandstone, is subdivided into a series of five stratigraphic zones labelled the CU10, CU20, CU30, CU40, and CU50 (with CU10 being the oldest and CU50 being the youngest).

CU10 Callovian (MJ-1/LJ-11)

The CU10 sandstone as described from cuttings at the V-7 well, is generally very fine to fine, with only rare medium-grained quartz present; with poor to moderate sorting; dominantly quartzose but with some scattered feldspars and altered feldspar/kaolinite grains (Fuller and Dahlini, 1998).

Palynological analyses of cuttings has shown the interval to be either MJ-1 or LJ-11 at both well locations, based on the palynofloral marker taxa, *Wanaea digitata*, and the presence of marine microplankton as indicative of a marine paleo-depositional environment (Wall, et al., 1990; Waton, et al., 1997h).

The interval has only been encountered on the Roabiba #1 (R-1) and V-1 wells and has never been cored. Therefore, no ichnological nor sedimentological data is available for the zone. It has been identified solely from cuttings and wireline log interpretations as a transgressive sandstone deposit.

An isopach for the CU10 zone is shown in Figure 6.31. The isopach distribution is related to the paleo-geographical facies map for the CU10 presented in Figure 6.32. The isopach and map are both based on the fact the MJ-2 Late Bathonian unconformity SB underlies the CU10 zone, and that surface, defined is described as erosional (at the CU20/R80 contact, to be discussed in the immediate next section, *CU20 Callovian (MJ-1/LJ-11)*). Therefore the areally widespread MJ-2 Late Bathonian erosional unconformity SB *probably* was due to a relative sea level fall. Hence, the renewed deposition of the overlying marine Callovian Roabiba Sandstone zones CU10 and CU20 probably was due to renewed marine transgression.

When relative sealevel began to rise once again during the Callovian Stage (MJ-1/LJ-11), sedimentation in the Tangguh area resumed, with incised valley topographic lows at the Roabiba-1 and Vorwata-7st well locations receiving the first marine transgressive sediments of the Callovian Unit (MJ-1/LJ-11) Roabiba Formation. The stratigraphic cross-section C-C' (Figure 6.3) clearly shows the geometry of the incised valley filled with Callovian Roabiba sedimentary rocks. The stratigraphic cross-section E-E' (Figure 6.5) follows the axial incision through R-1 and V-7, with V-3 on the flank of the incision. The isopach map of the gross Callovian (MJ-1/LJ-11) Roabiba Sandstone Formation (Figure 6.30) illustrates the very elongate geometry of the Callovian (MJ-1/LJ-11) Roabiba Sandstone succession.

There is an intra-Callovian Roabiba Sandstone flooding surface, between the CU10 and CU20 zones, identified on wireline logs for the R-1 and V-1 wells (Figure 6.3 through 6.4), which defines the boundary between the CU10 and CU20 zones.

CU20 Callovian (MJ-1/LJ-11)

The MJ-2 (Late Bathonian) unconformity SB is directly overlain by the lowest portion of the cored sandstone in the V-2 well, and interpreted as CU20 zone (the CU10 zone is absent at the V-2 well location). The basal contact with the underlying Bajocian/Early Bathonian Roabiba Sandstone zone (R50 through R80) is described by Tye and Hickey (1999) as scour surface topped with a firmground. Pemberton (1997f) describes the contact as a '*Glossifungites*' surface.

The sandstone itself is described at wellsite originally (Perry, et al., 1997) as mottled dark brown and light tan, medium grained; predominantly a clean, well sorted, quartzose sandstone with rare 'fresh' feldspar grains; rarely with a patchy argillaceous matrix. An isopach of the CU20 zone is shown in figure 6.33.

The sandstone was described by Tye and Hickey (1999) as containing numerous clay laminae and low angle tabular and tangential bedding; fluid escape structures and dishes, cross-bedding and flaser drapes. Both Tye and Hickey (1999) and Pemberton (1997f) describe the core as containing rare *Planolites*, *Skolithos*, and *Diplocraterion* trace fossil burrows. This assemblage of features is interpreted as characterizing a tidal inlet paleo-depositional facies.

The paleogeographic facies map for CU20 (Figure 6.34) depicts the early phase of the marine transgression, where the incised valley complexes were flooded,

with sediment deposition initially progressing up the paleo-topographic lows of the incised valleys.

CU30 Callovian (MJ-1/LJ-11)

The core in the CU30 zone, described at the V-2 wellsite, is a sandstone generally very fine to fine, with moderate sorting; common white kaolinite clay matrix, dominantly quartzose but with some scattered feldspars and altered feldspar/kaolinite grains, and common clay microlaminations and clay clasts as inclusions (Perry, et al., 1997). An isopach of the CU30 zone is shown in Figure 6.36.

The sandstone was described by Tye and Hickey (1999) as containing numerous clay laminae and low angle tabular and tangential bedding; occasional fluid escape structures and dishes, cross-bedding and flaser drapes, and rare scour surfaces (Tye and Hickey 1999), and *Planolites*, *Skolithos*, and *Diplocraterion* trace fossil burrows (Pemberton, 1997f). This is interpreted as characterizing a tidal inlet paleogeographical depositional facies.

By the CU30 time period, the entire paleo-coastline was drowned in a transgressive systems tract (TST) and Callovian marine sediments were deposited over the entire Wiriagar Deep and Vorwata area, although they are currently preserved only at the Vorwata area.

CU40 Callovian (MJ-1/LJ-11)

The core was originally described at the V-2 wellsite by Perry (Perry, et al., 1997) as an argillaceous sandstone generally very fine to fine, with only rare medium-grained quartz present; with poor to moderate sorting; common white kaolinite clay matrix, dominantly quartzose with common feldspars and altered feldspar/kaolinite grains, and common clay microlaminations and clay clasts. The isopach for the CU40 zone shows a widespread and thick deposition of sandstones along the paleo-embayment coastline (Figure 6.37).

The core was described as an argillaceous sandstone with clay as laminations and as inclusions, and abundant ichnofossil burrows, limited to the *Skolithos*, *Teichichnus*, and *Palaeophycus* varieties (Tye and Hickey, 1999; Pemberton, 1997f). No other primary sedimentary features were noted in this upper 20 ft of core and this interval was characterized as a middle shoreface paleo-depositional facies (Tye and Hickey, 1999).

The paleogeographic facies map for the CU40 zone shows the interpretation of a TST with widespread deposition of shoreface sandstones in the Wiriagar Deep and Vorwata areas, although erosion (LJ-10 erosional unconformity) subsequently removed these sediments from the Wiriagar Deep area (Figures 6.38).

CU50 Callovian (MJ-1/LJ-11)

The CU50 zone is a relatively thin (6 - 7 ft) sandstone cap at the very top of the Callovian Roabiba Sandstone sequence. The interval has never been cored, and has been identified only through wireline log correlations. It is defined as the low gamma-ray (GR) interval prevalent at the top of the more massive Callovian Roabiba Sandstone, an example of which can be seen on the GR for the V-1 well in Figure 6.29.

It has been described fairly consistently from cuttings at wellsite as a loose to rarely calcareous cemented sandstone, medium grained, with common pyrite (Perry, et al., 1997). The distribution and thickness of the zone is shown in Figure 6.39.

There are no sedimentological nor ichnological data available due to the lack of cores through the zone. Although the low GR count, and the calcareous nature of the sandstone may be a diagenetic feature, the CU50 is nonetheless identifiable on logs, and mappable. It has been interpreted, based on wireline log motif signature and areal distribution, as a minor HST (Figure 6.40) where sediment supply outpaced accommodation space and minor progradational in-filling occurred locally around delta fronts.

PA10 Callovian (LJ-11)

Overlying the Callovian Roabiba Formation is the younger, upper Callovian gross interval designated the Pre-Ayot (LJ-11), which is subdivided into three stratigraphic zones labelled PA10, PA20, and PA30 (Figure 6.3 and 6.5). The Pre-Ayot Formation base is bounded by the Callovian MFS (sequence boundary) at the Vorwata area, and the top of the interval is bounded by the Oxfordian LJ-10 unconformity, as discussed in the Callovian Roabiba Sandstone sections. An isopach of the entire Pre-Ayot sequence succession, at the Tangguh area, is shown in Figure 6.41.

The interval is mainly known from cuttings and wireline logs. There are no cores through the zone, therefore no sedimentological and ichnological analyses are

available. The PA10 zone as described from cuttings at the V-9 wellsite by the author, is shale; dark gray to occasionally medium gray; firm to hard; moderately indurated; fissile with platy to blocky cleavage; and non-calcareous (Salo, 1998a).

Watson, et al., (1998b) identified the zone as firmly LJ-11 based on diagnostic palynofloral marker taxon such as *Wanaea digitata*, and also from the overall taxa assemblage including *Scriniodinium ceratophorum*, *Scriniodinium galeritum*, *Wanaea spectabilis*, and *Vallensiella ovula*. Watson, et al., (1998b) interpreted the entire assemblage of terrestrial miospores and marine floras as suggesting a proximal marine setting with strong freshwater influence at the base of the zone and becoming more decidedly deeper, distal marine towards the top of the zone, indicative of a possibly transgressive systems tract.

An isopach of the zone is shown in Figure 6.42. This study concludes the PA 10 zone represents a TST, with an MFS present within the zone. This transgressive event drowned the entire Tangguh area. This transgression, coincided with a major global sea level rise (Figure 6.7) following a Late Bathonian maximum lowstand. Although tectonic subsidence can not be ruled as contributory, the role of eustasy is clearly a driving factor in this TST event at Tangguh. The interpreted paleogeographic facies map of the TST is presented in Figure 6.43.

PA20 Callovian (LJ-11)

The lithology PA20 zone consists of silty marine shales, calcareous to non-calcareous in part, with at least one possible tuffaceous ash zone of possible volcanic origin.

Cuttings were described at wellsite, by the author at V-9, as shale; dark gray to black; very hard; very well indurated; composed of silty clays; fissile with a platy to blocky cleavage; non to slightly calcareous; possibly carbonaceous.

Only a single core has been obtained to date in the Pre-Ayot interval, at the V-10 location, and that core was a mistaken attempt at coring the deeper Roabiba sandstone. The sedimentological and ichnological data available for this interval are therefore almost non-existent. The core was not described in detail at wellsite by BG geologists. Difficulty in placing the V-10 core in the appropriate zone is due to the core having been taken on the original V-10 borehole by BG, which was not wireline logged. The well was subsequently plugged back and sidetracked with wireline logs run on the V-10ST (sidetrack). The core was subsequently matched at Core

Laboratories to the most reasonable *equivalent* interval in the sidetracked hole wireline logs. The core was re-examined, and described by the author in 2001 and 2002, however, and is most likely from the PA20 zone. Waton et al., (1998b) firmly dates the core to a definitive LJ-11 biostratigraphic unit based on *Wanaea digitata*, as well as a distal marine environment based on the small proportion of terrestrial miospores.

The author described the core in 2002, as a very dark gray to black shale; hard; very well indurated; with blocky cleavage; cryptic bioturbation from trace fossil burrows at the top three feet of the core and rare possible concretions. No bedding features or other distinctive sedimentological features were noted.

Bo Tye logged the core (Tye and Hickey, 1999) but apart from the core log itself, the core is not discussed at all in the report. Pemberton, contracted by ARCO, did not have the BG core available in 1997, and therefore did not conduct an ichnological analysis of the core. Tye's core log (Tye and Hickey, 1999) indicates four feet of bioturbation at the top of the core, consisting of *Planolites*, *Palaeophycus*, *Chondrites*, and *Helminthopsis*. The remainder of the core was barren of trace fossil burrows and casts, although general concretions, pyrite concretions, and calcareous concretions were noted throughout the 80 ft core. Tye also noted two Crinoids, two Pelecypods, and several fossil ghosts in the lower 20 ft of the core.

An isopach of the zone is shown in Figure 6.44. The cuttings descriptions, and wireline log curves, particularly the GR indicate that the shale is interbedded with silty shale lenses, perhaps indicating a cyclicity of distal followed by slightly more proximal depositional environments during the PA20 interval. A comparison of the paleogeographic facies maps for the PA10 and the PA20 zones (Figure 6.45) shows the authors interpretation of slightly more proximal paleogeographic environment for PA20 sediments at Vorwata wells.

PA30 Late Callovian (LJ-11)

The top of the zone at Vorwata is defined by an erosional unconformity SB (Waton, et al., 1997b-h; Waton, et al., 1998a-d). Palynological analysis shows the PA30 zone to be definitively Late Callovian (LJ-11), based on *Wanaea digitata*, *Wanaea spectabilis*, *Vallensiella ovula*, *Scriniodinium ceratophorum*, *Scriniodinium galeritum*, and *Cliestosphaeridium* sp.1 (Waton, et al., 1998b). The base of the zone is

defined by an interpreted MFS boundary between the PA20 and PA30 zones, characterized by a very high GR spike (Figure 6.3, 6.4, and 6.5).

Palynological analyses of cuttings at all Vorwata and Wiriagar Deep wells yield results similar to those at V-9, where the Early to Middle Oxfordian (LJ-10) biostratigraphic interval is absent, indicating a nonconformable succession in the Late Jurassic (Waton, et al., 1998b). Palynofloral marker taxa indicative of the Late Oxfordian (LJ-9), including *Dongodinium swanense* and *Cribroperidinium perforans*, were abundant from the interval overlying the PA30 zone in V-9 cuttings (Waton, et al., 1998b), and also all Vorwata and Wiriagar Deep wells (Waton, et al., 1994; Waton, et al., 1996a-d; Waton, et al., 1997a-h; Waton, et al., 1998a-d). The unconformity is therefore areally widespread over all of the Wiriagar Deep and Vorwata areas, and perhaps over much of the Bintuni Basin (Bulling, et al., 1998).

The PA30 is composed of primarily sandstone, with a silty shale toe at the base of the sandstone interval, at the Vorwata area (Salo, 1998a-b). The PA30 zone is recognizable as a low GR and fast sonic transit time (DT) on Vorwata wireline logs displayed on cross-sections in Figure 6.3, 6.4, and 6.5. No cores are available for the sandstone section of the PA30, although the top, bioturbated interval, of the core previously described in zone PA20, might possibly be basal PA30 'silty shale', if Core Laboratories' placement of the V-10 core from the original borehole to its' equivalent stratigraphic wireline log depth in the sidetracked hole is correct (Figure 6.3). That core interval has already been described above in the PA20 zone discussion.

The sandstone section of the PA30 zone was described by the author, originally, from cuttings at wellsite (Salo, 1998a-b) as a kaolinitic sandstone, off-white to very light gray; composed of quartz sands grains with common to locally abundant kaolinite as both matrix and as grains/clasts; common calcareous and slightly dolomitic; with traces of chert, feldspar, lithic rock fragments; and glauconite; and was microlaminated with kaolinite streaks.

The presence of glauconite indicates a marine paleo-depositional environment for the sandstone, the abundant clays, especially kaolinite, with traces of feldspar are suggestive of weathering products. Given that the zone is defined at the top by an unconformity SB, the PA30 zone may represent an alteration zone that was exhumed and exposed during an erosional event. Because the LJ-10 unconformity has eroded away LJ-11 sedimentary rocks at the Wiriagar Deep area, the interpretation of the

original paleogeographic facies is problematic. An isopach of the PA30 zone is shown in Figure 6.46. This isopach is suggestive of a Mahakam River delta analogue building from a sediment point source to the north of Sakauni #1/Vorwata #4 (Allen and Mercier, 1988; Allen and Chambers, 1998). The thick PA30 interval at Wos #1 location could be the result of either a second prograde delta margins with a point source north of the Wiraigar Deep #6 location (subsequently eroded off) as depicted in Figure 6.47, or simply the result of longshore-drift and paleocurrent transport of PA30 sediments from the paleo-delta at Vorwata along the coast, analogous to the modern day current transport of massive amounts of sand at Fraser Island from a point source well to the south along the coastline of Australia (Boyd, et al., 2004). A second isopach (Figure 6.48) is shown that presents the alternative ‘longshore drift and paleo-current’ sand transport interpretation for the PA30 zone.

The Pre-Ayot (LJ-11) PA30 unit is therefore interpreted to be sand-rich progradational delta complex, as depicted in the PA30 paleogeographic facies map (Figure 6.47), and the progradational delta at the Vorwata area location was aerially extensive.

In summary, all of the paleogeographic facies maps of both Callovian gross intervals (the Callovian Roabiba Formation interval and the Pre-Ayot interval) depict a major marine transgression due to relative sea level rise, which was coincident with a 100m (>320 ft) global eustatic rise in mean sea level (Haq, et. al., 1987; Berggren, et al., 1995) during the Late Jurassic (Figure 3.2).

6.3.7 Ayot Limestone Formation LJ-9 (Late Jurassic)

The base Ayot Limestone is defined by an unconformity SB, and the top is bounded by a MFS, representing a deepwater marine shale characterized by a high GR spike (Figures 6.1 through 6.5). Waton stated that “the absence of...LJ-10 palynofloras suggests the presence of a minor stratigraphic hiatus” at the Vorwata-11 well location, which is consistent with findings for the other Tangguh area wells (pp.8, 1998j). At Wiriagar Deep area, the unconformity is present, but includes the absence of the Callovian (MJ-1/LJ-11) sedimentary rocks as well. With Bajocian/Bathonian palynofloral taxa and sedimentary rocks directly overlain by Late Oxfordian (LJ-9) palynomorphs and sedimentary rocks (Waton, et al., 1994; Waton, et al., 1996a-d; Waton, et al., 1997a). Furthermore, the LJ-9 interval, called the Ayot zone, is the equivalent of the lithostratigraphic formation known as the Ayot

Limestone Formation. It is fairly uniformly thick at 39 to 59 ft, and is pervasive over the entire Tangguh area of Bintuni Basin (Bulling, et al., 1998).

The PA/60 shale is a gray to greenish-gray, calcareous, glauconitic, and sandy shale, and is also characterized by a high GR spike (Figures 6.1 through 6.5). This has been interpreted as a maximum flooding surface (MFS) that is near coincidental with the Oxfordian LJ-10 unconformity.

The glauconitic clastic rocks are designated the PA60 zone, but is conformable to, and probably co-genetic with, the overlying Ayot Limestone (Salo, 1997b-c). The PA60 and the Ayot Limestone Formation have both been palynologically dated as LJ-9 (Late Jurassic, Late Oxfordian Stage). “The LJ-9 marker *Cribroperidinium perforans*, the LJ-9 and older ranging *Dingodinium swanense*, together with common *Trichodium sp.2*, are indicative of the presence of LJ-9, Late Oxfordian sediments”, (Waton, pp.4, 1998f).

The Ayot Limestone was originally described by the author at the WD-3 wellsite from a single core available through the interval. The Ayot Limestone is cryptocrystalline to microcrystalline, gray to greenish gray, fossiliferous limestone, dolomitic and/or very siliceous, and commonly very glauconitic. Coral and mullock fragments are rare but unidentifiable ghost fossils and fossil relicts are common (Salo, 1997b-c).

An isopach of the combined PA60 and Ayot Limestone zones is presented in Figure 6.49 showing a fairly uniform thickness (the PA60 is very thinly bedded at 2 ft to 7 ft). The sequence stratigraphy of this Jurassic gross interval is straightforward. The entire Tangguh area was uplifted along the N-S Sekak Ridge and the E-W Kemum High. This resulted in erosion from the NW intersection of the Sekak and Kemum towards the SE, based on the geometry of the underlying angular unconformity with underlying beds dipping SE (Bulling, et al., 1998).

The entire Tangguh area was possibly subaerially exposed and eroded during the LJ-10 interval, and the extreme mineral alteration and diagenesis of the PA30 sandstone (LJ-11) is possibly due to exposure as a weathering surface.

A marine transgression then drowned the Tangguh area and the angular unconformity, resulting in the widespread deposition of the near-uniformly thick PA60 MFS, followed by the growth of the Ayot Limestone platform carbonate. The Ayot Limestone Formation and the underlying maximum flooding surface PA60 zone are presented as one interval and are captured in paleogeographic facies map

PA60/Ayot (Figure 6.50). As relative sea level continued rising, the platform carbonate was submerged into a bathyal marine environment and blanketed in a deeper water marine shale, the Upper Late Jurassic Shales.

6.3.8 Upper Late Jurassic Shales LJ-8 to LJ-2 (Late Jurassic)

The Upper Late Jurassic Shales sequence is bounded by a MFS at the base, defined by a high GR spike in the shales directly atop the Ayot Limestone zone. The top of the Upper Late Jurassic Shales sequence is defined by a widespread, pervasive, unconformity SB. The top SB is named the Cretaceous unconformity, or K unconformity, and is based on the complete absence of Early Cretaceous sedimentary rocks in the Tangguh area (Bullings, et al., 1998).

The only whole core from this interval is from the WD-3 well. Therefore, there is a paucity of sedimentological and ichnological data pertaining to this unit. As a result, no subdivision of this interval has been made during this study, and no paleogeographical facies map has been constructed.

The Upper Late Jurassic Shales, based on the one WD-3 core and on cuttings from other wells, are described by the author, (originally at wellsite) as composed primarily of marine shales and silts with minor, thin-bedded sandy lenses, and possibly a thinly bedded volcanic tuffaceous member (Salo, 1994, Salo, 1996a-c, Salo, 1997a-g; Salo, 1998a-b).

Waton, et al., (1996c) did not find nannoflora or microfauna as diagnostic in the WD-3 core through the Upper Late Jurassic Shales, however, palynofloral marker taxa including *Sentusidinium* spp., *Sentusidinium pilosum*, *Chlamydothorella* spp., and *Omatia montgomeryi* confirm Early Kimmeridgian (LJ-8) sedimentary rocks in the MFS directly above Ayot Limestone zone. The LJ-8 palynomorphs were then overlain by sedimentary rocks containing *Productodinium chenii* and *Fistulacysta simplex* identifying the shales as Middle Kimmeridgian (LJ-7). At WD-3 well location, the LJ-7 shales are directly overlain by Late Cretaceous carbonate rocks (Waton, et al., 1996c).

Waton et al. (1996c) described the paleo-depositional environment as an open marine, based on a 'markedly lower' variety and number of terrestrial miospores, with marine palynomorphs 'overwhelmingly dominant', and the abundance of marine dinocysts comprising 80% of the organic debris in the core samples

This has been interpreted as a continued marine transgression depositing Upper Late Jurassic Shales from the global eustatic sealevel rise that continued until the middle Tithonian Stage, the final, and youngest, stage of the Late Jurassic (Bulling, et al., 1998; Waton, et al., 1996c). The global rise in sea levels around the world came to an end during the mid-Tithonian Stage, when sea levels first reached a global highstand and then began falling (Haq, et al., 1987; Berggren, et al., 1995).

The eustatic fall in sealevel ultimately led to an approximately 100 m (320 ft) drop in global mean sea level during the Early Cretaceous (Berggren, et al., 1995), which in the Tangguh region resulted in approximately 50 million years non-deposition and/or erosion of the top-most Late Jurassic sedimentary rocks and all Early Cretaceous sedimentary rocks (Figure 3.2).

6.3.9 Late Cretaceous

The base of the Late Cretaceous is bounded by the unconformable SB between the Upper Late Jurassic Shales and the base of the Late Cretaceous Succession. This surface is readily identifiable in the Tangguh area from drill cuttings and cores due to the presence of a pronounced glauconitic marker bed at the Late Jurassic/Late Cretaceous unconformity (Salo, 1994, Salo, 1996a-c, Salo, 1997a-g; Salo, 1998a-b).

This surface is also readily identifiable from wireline logs (GR and DT) due the 'signature' of the glauconitic marker bed at the base of the Late Cretaceous carbonate unit (Figure 6.1 through 6.5). Lastly, this is one only two Mesozoic-related surfaces that is identifiable on seismic survey data in the Tangguh area (the only other one being the Late Permian/Jurassic unconformity SB).

The top of the Late Cretaceous is bounded by a areally widespread unconformity SB in the Tangguh area (Bulling et al., 1998). The earliest Paleocene is absent over the entire Tangguh area, with either latest early Paleocene or Late Paleocene clastic sedimentary rocks directly overlying Late Cretaceous carbonates (Salo, 1994, Salo, 1996a-c, Salo, 1997a-g; Salo, 1998a-b).

The dating of this predominantly carbonate succession as Late Cretaceous is based on marker taxa of microfauna and nannofossils, and paleo-depositional environments are based primarily on foraminiferal assemblages. Waton et al., (1996c) dated the marls and limestones of the Late Cretaceous as Santonian to Maastrichtian based on nannofossils assemblages of *Archangelskiella cymbiformis*, *Micula decussate*, and *Quadrum sissinghii*, along with *Eiffelithus eximius*. Microfaunal

marker taxa included *Abalathomphalus mayaroensis*, *Globotruncata arca*, *Globotruncata aegyptiaca*, *Globotruncata conica*, *Globotruncata stuarti*, *Globotruncata elevate*, *Globotruncata stuartiformis*, *Globotruncata ventricosa*, as well as *Dicarinella* and *Marginotruncata*. Analyses of cuttings from this interval on other Wiriagar Deep and Vorwata wells, suggests that some Cenomanian sediments containing Cenomanian nannofossils and microfauna may be present in the Tangguh area (Waton, 1996a-e; Waton, et al., 1997a-h; Waton, et al., 1998a-d).

The prevalence of keeled planktonic foraminifera together with benthic fauna including *Pullenia*, *Uvigerina*, *Bolivinoidea*, and *Gavelinella* indicate a deepwater, bathyal marine environment (Waton et al., 1996c).

The sedimentary rocks were described originally by the author at wellsite from core at the WD-3. The Late Cretaceous is generally composed of very dark grayish brown to reddish brown marl; very hard; very silicified, smooth textured, vitreous luster in part, and with a tendency towards conchoidal fracturing (grading to a porcelaneous marl with depth); moderately dolomitic (with a large ankerite and siderite component); commonly to occasionally fossiliferous (especially with spherical multichambered foraminifera); scattered very finely disseminated black carbonaceous material scattered throughout; and slightly silty in part (Salo, 1997b-c).

Cuttings, from the Late Cretaceous, were originally described by the author, at various wellsites, as primarily a limestone unit overlying a basal marl. The limestone was white to cream to very light gray colored; firm to slightly hard; cryptocrystalline to microcrystalline in part, a lime mudstone in part; mudstone grading to a wackestone in part; argillaceous (kaolinite) in part to very argillaceous and chalky textured in part; and with the 'stacked plate or book' appearance due to differentially soluble micro-laminations. The marl intervals were particularly micro-laminated with micro-laminations of clay with differential solubility (Salo, 1994; Salo, 1996c; Salo, 1997a-h; Salo, 1998a-b).

A globally pervasive marine lowstand was reached during the Early Cretaceous. This occurred during the Valanginian Stage of the Early Cretaceous (Berggren, et al., 1995). This massive drop in sealevel perhaps accounts for the areally widespread unconformity of Late Jurassic to Early Cretaceous age, which can be traced from the NW Shelf of Australia across the northern margin of the ANGP margin and into the Bird's Head region of NW Papua, Indonesia (Longley, et al., 2002).

The Cenomanian to Maastrichtian sedimentary rocks in the Tangguh area coincide with an all-time highstand for global sea level (Haq, et al., 1987; Berggren, et al., 1995). This global HST can be seen on Figure 3.2, and the paleo-depositional interpretation of the Late Cretaceous sedimentary rocks at Tangguh being from a deepwater, bathyal environment would indicate this assessment is correct.

6.3.10 Cenozoic Succession

The sequence stratigraphy of the Cenozoic is not defined in this study for several reasons:

- 1) The stratigraphy and the architecture of the Late Paleocene Succession, including the turbidite channel and fan deposits, as described by Lowe (1998) is accepted by the author for this study.
- 2) Based on Lowe's assessment, and the inherent nature of the maximum geometry of turbidite channel and fan complexes, it is believed by the author to be unlikely that the Late Paleocene could accommodate (ie. sufficient storage capacity) the 2.4 TCF of CO₂ needed to potentially be disposed of at Tangguh.
- 3) A lack of data regarding the areal extent of the reservoirs and the seal potential (ie. thickness, areal extent, mineralogy/petrology based on core samples) render this interval as high-risk for potential CO₂ disposal.
- 4) The reservoirs will not be available for potential CO₂ sequestration/storage. The Tangguh LNG Project scheduled development plans for the Middle Jurassic reservoirs (with the estimated 10% CO₂ content) to be produced first. The development plans schedule the Late Paleocene turbidite reservoirs to be produced last, and these reservoirs have little, if any, CO₂ associated with them (J. Marcou, BP Subsurface Development Manager, personal communication, 2002).

As for the Eocene to Miocene carbonate succession, the NGLG, there are severe limitations in data associated with blind drilling of the interval with no cuttings or core of rock from the interval. This presents any potential CO₂ sequestration/storage in the NGLG as an extremely high risk.

The Cenozoic interval will be discussed further in Chapter 8, 9, and 10 regarding applicability and potential risks associated with possible CO₂ sequestration/storage in Cenozoic interval reservoirs or aquifers.

6.4 Limitations and Alternatives

Despite the use of accepted stratigraphic techniques, there are none-the-less fundamental or practical limitations when using these ideas with subsurface geological modelling of the Bintuni/Berau basin for potential CO₂ injection and sequestration/storage. The seismic stratigraphic approach is severely limited in a practical way by the thick near-surface carbonate interval of the New Guinea Limestone Group (i.e. Kais Formation and Faumai Formation). This Miocene to Late Eocene carbonate unit ranges from approximately 3500 ft to over 6000 ft in the Bird's Head region and overlies the reservoirs of interest. Seismic energy during surveys are dispersed at this carbonate interval, resulting in poor seismic resolution at the depth intervals of interest. A 1997-1998 3D seismic survey carried out under ARCO improved the resolution of seismic imaging at some intervals compared to the previous vintage 2D seismic surveys, particularly at the Tertiary interval, however, the Paleozoic and Mesozoic intervals are still limited in resolution to only two fair-quality interpreted reflectors, the Top Late Permian and the Near-Base Late Cretaceous. Sequence boundaries and intervals from the Permian to the Late Cretaceous are for the most-part beyond the resolution of even the newest reprocessed 3D images.

Extensive whole core coverage through many key Mesozoic intervals at Wiriagar Deep and Vorwata well locations has resulted in detailed ichnological fabric and facies, sedimentological, and palynological studies. These include ichnological fabric and facies analyses by Pemberton (1997a-e), sedimentological facies analyses by Tye and Hickey (1999), and palynological analyses and palynomorph environment interpretations by Waton et. al. (1994 through 1998). A systematic review of all the data from the Mesozoic interval in the Tangguh area incorporated these datasets into a rigorous sequence stratigraphic framework. This forms the foundation for ESSCI (Environmentally-Sustainable Site for CO₂ Injection) risk factoring and site location ranking, in addition to providing the basis for the 3D geo-cellular model to be constructed in GeoCARD.

All of the key cores through the Mesozoic interval (from ARCO and BG wells) were examined by the author in 2001 and 2002, and compared with Tye and Hickey's (1999) core log and report. These new findings, were integrated with a systematic review of the previous datasets resulted in a new interpreted sequences stratigraphy framework, and the first detailed geo-cellular 3D model of the Mesozoic interval in Bintuni Basin. The new interpretation and model honors, to the best of the author's knowledge, all of the available data.

It was recommended to conduct a high-resolution palynological and biostratigraphic of Mesozoic whole cores in the Vorwata wells, particularly the Vorwata #7 which had not been analysed previously by Waton or Pemberton. However, the results of the analyses were not available for inclusion in this study.

Some minor possible alternative facets to the conclusions presented here are discussed in Chapter 18. Postscripts.

6.5 Re-interpretation of the Bird's Head Tectonic/Structural History

A new sequence stratigraphy data set has been produced by this study. However, there are clearly implications for the interpreted tectonic and structural history of the region based on the new stratigraphy of the Berau/Bintuni Basins area, and these need to be addressed in the overall tectonic history overview.

The new and original stratigraphy data included integrating all of the data provided by BP, (including seismic survey data with and wellsite and post-drilling lithostratigraphic and sedimentological analyses). Existing paleontological and palynological analyses were integrated with ichnological facies and fabric studies and newly re-interpreted with significantly different results and implications. As a result of this re-evaluation of existing data, the original cores were closely re-examined (amounting to over three thousand feet of Mesozoic whole cores being re-evaluated and digitally photographed for the first time), the existing core logs reviewed in detail.

This study has generated a new and original set of paleogeographic facies maps for the Tangguh region, covering stratigraphic intervals from the end of the Late Permian (242 Ma) through to the beginning Late Cretaceous (99 Ma). This new Mesozoic series of paleogeographic maps for the Berau/Bintuni Basins area offers a new perspective on what has been demonstrated to be a rather ambiguous published tectonic history for the Bird's Head region of Papua, Indonesia.

A brief summary of the implications involving new and original set of paleogeographic facies maps for the Tangguh region is:

1. The Triassic unconformity (Permian/Jurassic SB) represents a regionally widespread erosional surface, from the Bird's Head micro-continent (BHMC) in NW Papua, Indonesia to the Arafura Sea, Australia (Bradshaw, et al., 1990).
2. In the BHMC, marine transgressions appear to proceed from the present-day SW towards the NW, from the late Early Jurassic through the Middle Jurassic.
3. In the Tangguh area, clastic sediment sourcing during the Middle Jurassic was clearly in an arc from the present-day N and E, with vectors suggesting an overall sediment influx from the NE.
4. Very rapid, major marine transgression from the present-day S towards the N drowned the entire Tangguh area during the early Late Jurassic.
5. The Late Jurassic/Cretaceous unconformity found in the BHMC probably represents the most-northerly aspect of a transcontinental Late Jurassic/Cretaceous unconformity found along the entire NW shelf margin of the ANGP boundary.
6. Resumption of sedimentation in the Tangguh area during the Late Cretaceous appears to be primarily marine platform carbonate deposition with minor clastic sedimentary input from the present-day E, limited to the present-day eastern edge of the Bintuni Basin area.

Previously published and fairly well documented tectonic events include:

1. Extensional rifting along the NW Shelf margin due to the opening of the Tethys Ocean during the Triassic to Jurassic Periods.
2. Renewed extensional rifting along the NW Australia subsequently led to the migration of the Indian subcontinent, Lhasa, and Argo/West Burma sub-plates from the ANGP during the Late Jurassic and Early Cretaceous Periods (Longley, et al, 2002).
3. Re-accretion of the Bird's Head microplate to the New Guinea portion of the ANGP by beginning of the Neogene Period, since Miocene

deformation of the Berau/Bintuni Basins area is known to have resulted in the formation of the Wiriagar Deep and Vorwata anticlines, and was caused by the collision of the Banda sub-plate arc from the west, and the Caroline Pacific sub-plate from the north, with the more southerly ANGP .

A possible failed intracontinental extensional rift had begun to separate the Bird's Head area from the main Australian-New Guinea plate according to Charlton (2000). However, this research into Tangguh area data suggests that the Bird's Head block may have undergone complete extensional rifting and thermal sag, detaching from the NW Shelf of the Australian-New Guinea plate at the end of the Late Jurassic/beginning Early Cretaceous. Geological evidence from the Tangguh area also suggests that this 'rift and drift' may have been completed by the Late Paleocene. The Early Cretaceous is absent in the Tangguh area, and this unconformity is correlatable with the Late Jurassic/Early Cretaceous unconformity along the NW Shelf that marks the extensional rifting, thermal sag, and tectonic drift of the Argo/Lhasa, and West Burma blocks from the (ANGP). It is clear that 'rift, sag, and drift' may also account for the Tangguh areas Jurassic/Cretaceous unconformity. The renewed deposition in the Tangguh area during the Late Cretaceous consists of primarily platform carbonates, indicating a widespread change in overall paleo-depositional environments from a bay/estuarine environment proximal to continental landmasses, to a more open marine environment distal from any terrigenous clastic source.

This could have been due to a regional thermal sag of the Bird's Head plate after detachment, since global sea level was clearly at a HST (highstand systems tract) by the mid-Campanian. The BHMC would have extensionally rifted from the NW Shelf margin of Australia during the Cretaceous, sometime between the end of the Late Jurassic around 150 Ma (Tithonian) and the Early Paleocene at 65 Ma.

The Tangguh area wells all have a non-conformable contact between the Late Cretaceous and the upper Early Paleocene in common (Figure 3.2). The thinly-bedded Early Paleocene and extensive Late Paleocene sedimentary rocks are all shelfal to deepwater shales, with turbidite channels and turbidite floor-fan deposits (Salo, 1994; to 1996a-c; 1997a-f; Lowe, 1998).

Therefore, the new sequence stratigraphy of the Bird's Head region's Tanguh area, when reconciled with the broader tectonic history as outlined above, leads to the possibility that the Bird's Head microplate began extensional rifting during the end Late Jurassic/Early Cretaceous, as depicted in Figure 6.51, similar to the Greater India subcontinent, Argo/Lhasa, and West Burma microplates (Longley, et al., 2002). This would account for the correlatable transcontinental Late Jurassic/Cretaceous unconformity found along the entire NW shelf margin of the Australian-New Guinea plate boundary, *which correlates up into the Bird's Head microplate*. Extension was thought to have commenced during the Turonian, and continued into the Maastrichtian, when the BHMC was completely separated from the Australian-New Guinea plate margin (Charlton, 2000).

Since the most northerly rifted sub-plates identified to date (ie. Argo/Lhasa, West Burma) have proximal, Jurassic clastic depocenters associated with them, the Bird's Head microplate could not have rifted from them, since the Berau and Bintuni basins represent an additional significant, major, proximal Jurassic clastic depocenter (Longley, et al., 2002). This leads to the intriguing possibility that the Bird's Head was originally located north of these other rifted blocks, possibly in an area previously thought to be 'sediment starved' during Jurassic times, known as the 'Arafura Delta' according to Longley, et al (2002). This proposed ancestral home for the BHMC might be the present-day SW corner of the Arafura Sea, roughly north of the Darwin coastline. This would imply the Bird's Head has not migrated very far from its' initial breakup. Furthermore, if a counterclockwise rotation of $<90^\circ$ was associated with the microplate rift and migration event, then the Mesozoic parental sourcing would have come from the Australian interior, just as the Jurassic depocenters of the Lhasa and Argo/West Burma blocks did. Ali and Hall (1995) documented paleomagnetic evidence that the Sula microplate detachment from the Australian-New Guinea plate (ANGP) margin occurred by the Late Cretaceous with a counterclockwise rotation of 40° , and the comparison by Giddings' et al., (1993) of Kemum High terrane palaeomagnetic data with Australian APWP suggested that the BHMC may have been rotated 55° counterclockwise between the Early Jurassic and mid-Eocene.

Did the Paleogene migrations of the Sundaland plate and the associated Banda sub-plate from the west toward the east contribute to the Bird's Head counterclockwise rotation and northward migration? The geometry of the various microplate boundaries would suggest this. Packham (1996) found palaeomagnetic

evidence of an additional 10° counterclockwise rotation during the Banda Arc tectonic collision in the Miocene. This evidence of Packham (1996), together in totum with Giddings, et al. (1993), suggests that at least a 65° counterclockwise rotation of the BHMC may have occurred between the early Jurassic and mid-Miocene, with the greatest degree of rotation associated with the Late Jurassic/Early Cretaceous extensional rifting from the NW Shelf.

However, the preservation of the Oligocene carbonate member only in the synclinal troughs between Wiriagar Deep, Vorwata, Roabiba, and Saritu clearly indicates that the peneplaning of the Bintuni Basin rocks at the end of the Oligocene post-dated compressional folding. In addition, the peneplanation of the area following sub-aerial exposure and erosion of the region was due to uplift, rather than relative sealevel fall due to eustasy alone. This major unconformity found at the base of the Miocene is a prominent feature on the seismic survey data, and is responsible for the erosion of significant amounts of Eocene and all Oligocene sedimentary rocks from the tops of the anticlinal structures in the Tangguh area of Bintuni Basin (Bulling, et al., 1998).

Therefore, it can be inferred that this BHMC deformation and erosion is probably due to an Oligocene tectonic collision of the BHMC, the ANGP, and a proto-island arc system related to the subduction of the Sundaland and Caroline sub-plates (Bulling, et al., 1998). This tectonic event would have preceded the later Miocene collision between the BHMC, ANGP, Caroline, and Sundaland plates. However, the Oligocene transpressional folds would probably have been nucleating centers for additional inversion during the Miocene tectonic event.

In summary, the BHMC had detached sometime between the Late Jurassic and the Late Cretaceous from the main ANGP, and undergone a counterclockwise rotation of at least 55°. The breakup unconformity is seen in the Early Cretaceous SB in the Tangguh area. Thermal sag, possibly combined with the Late Cretaceous global HST led to the Tangguh area being blanketed with a Late Cretaceous marine platform carbonate, and Paleocene deepwater shales. Oligocene subduction of the Caroline plate below the Sundaland plate and ANGP resulted in compression along the northern ANGP margins and the detached BHMC, producing uplift of the Kemum High terrane in the BHMC and compressional subsidence in the ANGP's Arafura Sea area (Packham, 1996). The transpressional folds caused during this Oligocene event across the central Bird's Head were the nucleating centers for the later reactivation of

Miocene transpressional folds. The base Miocene unconformity resulted in a peneplaned ravinement surface for the renewed deposition of the Miocene platform carbonate members of the western portion of the New Guinea Limestone Group, namely the Faunai and Kais Formations.. These compressional folds may also be the ancestral structural fabric that influenced the location of the later foreland Bintuni Basin during the Miocene. Furthermore, the sinistral sliding along the Sorong Fault/Shear Zone (SFZ), may have contributed to the possible >10° counterclockwise rotation of the Bird's Head microplate during the Late Paleogene and Early Neogene. The cumulative rotation of the BHMC during the Mesozoic through the Neogene changed the Mesozoic Period (particularly in regard to Jurassic sedimentation) terrigenous clastic paleo-source direction from an *actual* paleo-SSE direction to today's *apparent* NNE orientation. The Miocene Caroline plate tectonic collision from the N, and the slightly later Banda arc tectonic collision from the NW-SW, resulted in the Tangguh area currently receiving sediments from uplifted highlands north (Kemum High), east (LTFB), and south (KOM Ridge) of the Bintuni foreland basin and Berau piggyback basin. This possible tectonic history thereby resolves questions regarding the parental source of Jurassic clastic sediments in the Tangguh area from a present-day NE vector. The source vector of Jurassic clastic sediments in the Tangguh area would have originally (at the time of paleo-deposition) been from the S-SE, directly from interior Australian craton.

7.0 RESERVOIR CHARACTERIZATION

Any analysis and rating of a potential ESSCI CO₂ injection and sequestration/storage site must include an evaluation of the potential reservoir/aquifer reservoir character. This study will evaluate specific reservoirs for potential CO₂ injection and sequestration/storage character, including porosity, permeability, and their implications for possible CO₂ injectivity, migration, and storage capacity.

7.1 Whole Cores, Core Plug Analyses, and DST Data

ARCO and BG recovered over 8,000 ft of whole core from various Tangguh area wells between 1994 and 1998 (Bulling, et al., 1998). Cores from Wiriagar Deep wells recovered lithologies from the Paleocene to the Late Permian, including Late Cretaceous Marls, Upper Late Jurassic Shales, Ayot Limestone, the Middle Jurassic Bajocian/Bathonian Roabiba Sandstone Formation and the Aalenian Sandstone Formation. Cores from Vorwata wells generally included the Middle Jurassic Bajocian/Bathonian Roabiba Reservoir and the occasionally the Callovian Roabiba Reservoir. Only rarely were overlying 'Pre-Ayot Shales' or underlying Late Permian sedimentary rocks cored in Vorwata wells. Table 7.1 lists the sample distribution of whole cores in the Tangguh area, by well, for each of the gross stratigraphic units. Core intervals examined, with core logs reviewed, are noted in red. More than 45 drill-stem tests (DST's) were carried out on 15 wells in the Wiriagar Deep, Vorwata, and Ubadari structures. The results of the ARCO DST tests are presented by well in Appendix 1.

Although coring and DST testing were carried out in the Late Paleocene, Late Cretaceous, and Jurassic gross stratigraphic intervals, the majority of the coring and testing was focused on the Middle Jurassic Aalenian Sandstone Formation and the Roabiba Sandstone Formation reservoirs. The intervals of whole core coverage and DST testing are presented in Figure 7.1 (Wiriagar Deep and Ubadari structures) and Figure 7.2 (Vorwata structure) as cross-sectional schematics identifying the gross stratigraphic intervals for cores and tests by individual wells in the Tangguh area. Although more than 2,000 whole core plugs had been analyzed previously by ARCO and BG (the results of which were available for this study), key gaps in the data set were identified by the author. For example, Vorwata plug sampling and analyses had previously been limited to Roabiba Sandstone Formation intervals that were hydrocarbon bearing, to the exclusion of the water-wet 'aquifer' intervals. Analyses

of whole core plugs from stratigraphically important wells such as V-7 and V-10 were either limited or nonexistent. The V-10 well location, on the plunging anticlinal southern Vorwata flank, made the V-10 cores especially critical. Furthermore, the V-10 location at the GWC (the GWC actually being cored in this well), and the well proximity to potential down-dip water leg ESSCI CO₂ injection sites in the area, made core plug analyses from the V-10 cores all the more crucial.

Approximately 3,000 ft of whole cores from both Wiriagar Deep and Vorwata wells were examined in 2001 and 2002 by the author. Previous laboratory results from both ARCO and BG whole core sample plugs were matched to the slabbed whole core, and a new set of fresh representative core plugs were selected for various laboratory analyses at the University of Adelaide's Australian School of Petroleum (ASP) facilities or associated laboratories.

More than 100 additional core plug samples were selected from existing cores for this study, sampling representative lithology and facies to perform additional laboratory analyses necessary for the purpose of this study. These plug samples were then analyzed to in-fill gaps in the pre-existing ARCO/BG whole core plug datasets.

A list of the new core sample plugs/chips from Wiriagar Deep and Vorwata wells is presented in Table 7.2. The original driller's measured depth for the core plug is given, as is the core GR (gamma-ray) to wireline GR correlation shifted depth. The depth shift for whole cores in each well at the Jurassic interval is shown in Table 7.3. The various analyses carried out on the various plugs/chips is also indicated for each sample. As per convention, the suite of analyses carried out on potential seal lithologies differs from that carried out on potential reservoir lithologies, furthermore, the project's budgetary and time constraints also demanded that only absolutely essential data gaps be filled by the new core plug/chip analyses.

The three plugs had insufficient material for analyses and do not appear on the Table 7.2, nor were any analyses performed on them. The remaining 98 plugs were then inventoried and analyzed.

Ninety-eight plugs of sufficient quantity were eventually received by the author, and subjected to various analyses that included (but were not limited to) the following:

- 1) Digital plug photography for archiving and inventory purposes;
- 2) Porosity and permeability measurements in thinly interbedded facies for reservoir analysis;

- 3) Petrographic analysis for reservoir quality and sedimentology;
- 4) Scanning Electron Microscopy (SEM) for sedimentological, reservoir, and seal analyses;
- 5) X-Ray Diffraction (XRD) for whole rock and clay mineralogy;
- 6) Mercury Injection Capillary Pressure (MICP) for seal analysis;
- 7) Rock-Eval Pyrolysis for “waste-zone” seal analysis (to test whether the seal has leaked)

Table 7.1 also presents an inventory of the various analyses performed on the samples by original driller’s measured depth from RKB, the ‘corrected/shifted’ equivalent wireline log depth for the sample plug, the lithology of the sample plug, the sequence stratigraphic unit of the plug, the paleo-depositional facies of the plug, and the results from certain analyses such as He-porosity (%) with ‘Net Over-Burden’ of 800 psi (NOB 800 psi), Kair (air-permeability mD) with NOB 800 psi, MICP Entry Pressure (psia), and MICP Threshold Pressure (psia).

A series of figures was also constructed comprising an Atlas of Whole Core Plug and Whole Core Chip Sample Analyses. The Atlas is presented in Appendix D, Figure 1 through Appendix D Figure 99. The order of the Atlas follows the same order of presentation, alphabetically/numerically by well name, as presented in Table 7.1. Appendix D Figure 1, is the format guide for the Atlas Figure 2 through 99. Each sample’s Core Plug/Chip Atlas figure number is also listed in the right hand column of Table 7.1, for easy referencing.

The Atlas of Whole Core Sample Plug Analyses summarizes the various analyses performed at the ASP on each of the sample plugs. Selected digital images of whole core were examined in detail for several feet above and below the depths from which samples were taken. These are presented in the Atlas with annotations regarding sedimentological, sequence stratigraphic, or ichnological trace fossil features in addition to the sample plug depth location on the slabbed whole core.

Close up digital photographs of the selected sample core plug depth benefited from the digital camera flash, and generally have truer color. Both ‘dry’ and ‘wet’ photographs were taken of the slabbed whole core. Only the photos that illustrate the lithology/sedimentology/ichnology of the cored interval best are presented (ie. in some cases only dry, in some cases only wet, and in some cases both dry and wet photographs).

These are then followed by digital pictures of the core sample plug or core chip sample for ASP analyses. In all cases (whole core photography and core sample plug/chip photography), a colorscale and/or grayscale with centimeter scale bar is generally present in the photo, except where whole core photographs have been zoomed in and cropped.

The core sample plug/chip Atlas figures present any analytical results available for a given sample, including: petrographic photomicrographs, bulk mineral-XRD plots, MICP pressure graphs, SEM photomicrographs with accompanying SEM elemental analysis, and porosity and permeability results.

7.2 Reservoir Quality

There are many potential reservoirs in the Tangguh area subsurface for consideration as potential CO₂ injection and sequestration/storage strata. These are listed in order of increasing depth as:

1. Late Permian Fluvio-Deltaic Channel Sandstones
2. Aalenian (Marine) Sandstone Formation
3. Callovian and Bathonian/Bajocian Roabiba (Marine) Sandstone Formation
4. Ayot Limestone Formation
5. Late Cretaceous Marl Succession
6. Late Paleocene Succession
7. NGLG (Faumai Limestone Formation and Kais Limestone Formation)

The top and base wireline log depths (with datum as RKB) for gross intervals of potential ESSCI injection reservoirs is presented in Table 7.4a and 7.4b for all wells in the Tangguh area, including all Wiriagar Deep and Vorwata structures.

7.2.1 Late Permian Reservoir Quality

The Late Permian Succession, in the Tangguh area, is predominantly a interbedded succession of fluvial and interfluvial sandstones, siltstones, and shales overlain by relatively minor tidal marine and fluvio-deltaic sandstone and shale sequences. These sandstone reservoirs are generally characterized as tight, with poor to rarely, at best, fair porosity and permeability. By nature of their paleo-depositional facies, these fluvial and rarely tidal marine fluvio-deltaic reservoirs lack

	WD-1	WD2	WD-3	WD-4	WD-5	WD-6	WD-7	WD-8	V-1	V-2	V-3	V-4	V-5	V-6	V-7	V-8	V-9	V-10*	V-11	E.ONIN-1
PALEOCENE MUD-PRONE INTERVAL SH.			1,5		1,2		1													
PALEOCENE MUD-PRONE INTERVAL SS.			1,2,3,4,5		1		1													
PALEOCENE SAND-PRONE UPPER MEMBER SH.	1,2	1			3															
PALEOCENE SAND-PRONE UPPER MEMBER SS.	2	1,2			3			1,2												
PALEOCENE SAND-PRONE MIDDLE MEMBER SH.		4,5																		
PALEOCENE SAND-PRONE MIDDLE MEMBER SS.		3,4,5																		
PALEOCENE SAND-PRONE LOWER MEMBER SH.	3	5	7,8,9,10,11		3,4,5,6,7,8,9,10,12,13	2,3,5,6	3,4,5,6	3,4,5												
PALEOCENE SAND-PRONE LOWER MEMBER SS.	3		7,8,11		3,4,5,6,7,8,9,11,12,13	1,2,3,4,5	2,4,5,6	3,4,5												
LATE CRETACEOUS MARL			12,13	1		6,7,8	6,7													
EARLY CRETACEOUS																				C
LATE JURASSIC VOLCANIC LAYER			13																	
LATE JURASSIC TOP SHALES			13																	C
LATE JURASSIC AYOT LS.			13				8	6												C
LATE JURASSIC LJ11 UPPER SANDSTONE																				
LATE JURASSIC LJ-11 UPPER SHALE							8	6												C
LATE JURASSIC LJ-11 LOWER SANDSTONE																				
LATE JURASSIC LJ-11 LOWER SHALE																		1		C
MIDDLE JURASSIC MJ-3 UPPER ROABIBA					15 (?)					1		1	1	1	1,2			2		
MIDDLE JURASSIC MJ-3 MAIN ROABIBA		6,7	13	2,3,4	15,16,17,18,19,20	9			1,2	1,2,3,4,5		1,2	1,2,3	1,2	2,			2,3,4,5,6,7,8		
AALLENIAN MJ-4 SHALE (PRE-ROABIBA SH.)		7,8	13,14	4,5		9	8	6	3	5,6			3 (?)							C
AALLENIAN MJ-4 SANDSTONE		8,9	14,15	5,6			8,9	6	3											C
AALLENIAN MJ-4 SHALE (PRE-AALLENIAN SANDSTONE)		9		6 (Intra-Reservoir)																C
PERMIAN SH.		9	15			10	9	7	3	6		2,3								
PERMIAN SS.		9	15			10	9	7	3	6		2,3								
*Some whole cores cut by British Gas (BG) may not be available for analyses.																				

Table 7.1: Table of whole core coverage in the Tangguh area of Bintuni Basin by well, and by formation interval, and listed by the Core Number for that respective well. Cores in red were photographed, examined, and the core logs reviewed, by the author for this study.

Well Name	Core Plug Depth (ft/m)	Plug Depth Shifted (ft)	Lithology	H/V	Petrogr	SEM	XRD	MICP	He φ + Ka	Geochem Pyrolysis	Unit	Facies	Entry P. MICP (psia)	Threshold P. MICP (psia)	Porosity (%)	Permeability (mD)	REMARKS	APPENDIX 4 Figure No.	
Core Plug/Chip Atlas Format Guide																			1
WD2	7368'4"	7386'4"	SS	H					1		PUM	Turb			10.6	0.88	NOB 800psi	n/a	
WD2	7377'11"	7395'11"	SH	V				1		1	PUM	Turb	752	9983				2	
WD2	7380'0"	7398'0"	SH	V				1		1	PMM	Turb	239	5014				3	
WD2	8681'3"	8699'3"	SH	V				1		1	R30	Prograde	889	3520				4	
WD2	8753'2"	8771'2"	SS	H					1		A20	Delta			14.8	529	NOB 800psi	5	
WD3	7548'9"	7556'9"	SH	V				1		1	PMP	Turb	701	4994				6	
WD3	7549'2"	7557'2"	SH	V				1		1	PMP	Turb	342	5983				7	
WD3	7552'7"	7560'7"	SH	V				1		1	PMP	Turb	170	1726				8	
WD3	7558'8"	7566'8"	SH	V				1		1	PMP	Turb	99	2480				9	
WD3	7956'3"	7964'3"	SS	H					1		PMP	Turb			12.27	19.74	NOB 800psi	10	
WD3	9238'0"	9248'0"	LS/MRL	V				1		1	K	Marine	8	8540				11	
WD3	9272'1"	9282'1"	LS/MRL	H				1		1	K	Marine	414	24894				12	
WD3	9274'1"	9284'1"	LS/MRL	H				1		1	K	Marine	601	5000				13	
WD3	9286'2"	9296'2"	LS/MRL	V				1		1	K	Marine	no penetration	no penetration				14	
WD3	9309'8"	9319'8"	SH	V				1		1	K/LJSh	Marine	28	11949				15	
WD3	9325'0"	9335'0"	SH	V				1		1	LJSh	Marine	339	9953				16	
WD3	9328'4"	9338'4"	V. TUFF	V				1		1	LJSh	V.Ash?	9970	14448				17	
WD3	9344'1"	9354'1"	LS/MRL	V				1		1	Ayot	ShallowM	11950	14470				18	
WD3	9364'9"	9374'9"	SS	H					1		R30	Prograde			13.2	0.739	NOB 800psi	19	
WD5	9509'0"	9519'0"	SS	H					1		R70	Foreshore			4.4	0.008	NOB 800psi	20	
WD5	9509'5"	9519'5"	SS	H					1		R70	Foreshore			2.2	0.016	NOB 800psi	21	
WD5	9511'4"	9521'4"	SS	H					1	1	R70	Foreshore			7.3	0.069	NOB 800psi	n/a	
WD7	7962'6"	7972'6"	SH	V				1		1	P/TopK	Marine	730	8471				22	
WD7	7981'6"	7991'6"	LS/MRL	V				1		1	TopK	Marine	6968	11945				23	
WD7	8452'5"	8462'5"	LS/MRL	V				1		1	Ayot	ShallowM	no penetration	no penetration				24	
WD7	8471'1"	8481'1"	LS/MRL	V				1		1	Ayot	ShallowM	8507	14474				25	
WD7	8497'9"	8507'9"	SH	V				1		1	R20	M.Sh	1029	5010				26	
WD7	8524'7"	8534'7"	SS	H					1		A20	W.O.			19	2264.38	sc	27	
V1	11765'9"	11775'9"	SS	H	1				1		CU40	T.Ch			11.2	150	NOB 800psi	28	
V1	11787'7"	11797'7"	SS	H	1				1		CU30	U. Sh			10.3	3.55	NOB 800psi	29	
V1	11790'9"	11800'9"	SS	H	1	1	1	1	1		CU30	U. Sh	294	339	2.5	0.05	NOB 800psi	30	
V1	11797'7"	11807'7"	SS	H	1				1		CU30	U. Sh			13.5	137	NOB 800psi	31	
V1	11902'3"	11912'3"	SH	V			1	1	1	1	R20	Fluv/Delt	339	20700				32	
V1	11904'3"	11914'3"	SH	V			1	1	1	1	R20	Fluv/Delt	1000	5970				33	
V1	11909'7"	11919'7"	SS	H	1				1		R20	Fluv/Delt			3.5	0.052	NOB 800psi	34	
V1	11914'6"	11924'6"	SS	H	1				1		Perm	Fluvial			6.9	1	NOB 800psi	35	
V2	12582'7"	12595'7"	SS	H	1				1		CU30	M. Sh			14.8	19.8	NOB 800psi	36	
V2	12584'8"	12597'8"	SS	H	1				1		CU30	M. Sh			12.4	28.3	NOB 800psi	37	
V2	12585'8"	12598'8"	SS	H	1				1		CU30	M. Sh			15.2	126	NOB 800psi	38	
V2	12594'4"	12607'4"	SS	H	1				1		R80	T. Ch			13.5	477	NOB 800psi	39	
V2	12600'3"	12613'3"	SS	H	1				1		R80	T. Ch			13.1	134	NOB 800psi	40	
V2	12757'6"	12770'6"	SS	H	1				1		R70	M. Sh			15.9	130	NOB 800psi	41	
V2	12865'7"	12878'7"	SS	H	1				1		R50	B. Sh			16.9	1090	NOB 800psi	42	
V2	12901'5"	12914'5"	SS	H	1				1		R40	T. Ch			12.2	0.316	NOB 800psi	43	
V2	13020'6"	13033'6"	SH	V			1	1	1	1	R20	U. Sh	1452	2936				44	
V2	13025'6"	13038'6"	V. TUFF	V			1	1	1	1	R10	Fluv/Delt	706	1262				45	
V2	13030'1"	13043'1"	SH	V			1	1	1	1	R10	Fluv/Delt	702	1439				46	
V7	13118'3"	13132'3"	SS	H	1				1		CU40	U. Sh			9.9	0.233	NOB 800psi	47	
V7	13123'8"	13137'8"	SS	H	1				1		CU40	U. Sh			6.5	0.868	NOB 800psi	48	
V7	13136'10"	13150'10"	SS	H	1				1		CU40	U. Sh			8.5	7.14	NOB 800psi	49	
V7	13143'6"	13157'6"	SS	H	1				1		CU30	M. Sh			9.0	18.8	NOB 800psi	50	
V7	13152'5"	13166'5"	SS	H	1	1	1	1	1		CU30	M. Sh	3	5	10.7	131	NOB 800psi	51	
V10st	3944.43	12941.7	SH	V			1	1	1	1	PA30	Delta	598	4268				52	
V10st	3947.64	12952.2	SH	V			1	1	1	1	PA30	Delta	8507	11951				53	
V10st	3954.46	12974.6	SH	V			1	1	1	1	PA30	Delta	727	8496				54	
V10st	3965.57	13011.0	SH	V			1	1	1	1	PA20	Shelf	4279	5971				55	
V10st	3966.82	13015.1	SH	V			1	1	1	1	PA20	Shelf	1053	5975				56	
V10st	3967.10	13016.1	SH	V			1	1	1	1	PA20	Shelf	705	8497				57	
V10st	4021.25	13193.7	SS	H	1				1		CU20	T. Ch.			8.2	0.318	NOB 800psi	58	
V10st	4021.86	13195.7	SS	H	1				1		CU20	T. Ch.			5.72	271.28	sc	59	
V10st	4022.20	13196.8	SS	H	1				1		CU20	T. Ch.			7.66	96.24	sc	60	
V10st	4025.08	13206.3	SS	H	1				1		CU20	T. Ch.			7.6	40.7	NOB 800psi	61	
V10st	4025.80	13208.6	SS	H	1				1		R80	Foreshore			11.24	290.95	sc	62	
V10st	4025.98	13209.2	SS	H	1				1		R80	Foreshore	insuff/broken					63	
V10st	4026.18	13209.9	SS	H	1	1	1	1	1		R80	Foreshore	3	4	14.5	1080	NOB 800psi	64	
V10st	4028.15	13216.4	SS	H	1				1		R80	Foreshore			14.8	979	NOB 800psi	65	
V10st	4029.58	13221.1	SS	H	1				1		R80	Foreshore			14.4	576	NOB 800psi	66	
V10st	4029.70	13221.4	SS	H	1				1		R80	Foreshore			14.8	1339.39	sc	67	
V10st	4031.55	13227.5	SS	H	1				1		R80	Foreshore			11.9	226	NOB 800psi	68	
V10st	4034.51	13237.2	SS	H	1	1	1	1	1		R80	Foreshore	2	5	12.9	954	sc	69	
V10st	4035.40	13240.1	SS	H	1				1		R80	Foreshore			12.67	506.22	sc	70	
V10st	4036.23	13242.9	SS	H	1				1		R80	Foreshore			12.9	298	NOB 800psi	71	
V10st	4039.62	13254.0	SS	H	1				1		R80	Foreshore			13.47	339.64	sc	72	
V10st	4040.20	13255.9	SS	H	1				1		R80	Foreshore			14.06	239.74	sc	73	
V10st	4042.62	13263.8	SS	H	1				1		R80	Foreshore			12.42	73.41	sc	74	
V10st	4044.81	13271.0	SS	H	1				1		R80	Foreshore			14.5	545	NOB 800psi	75	
V10st	4045.92	13274.7	SS	H	1				1		R80	Foreshore			14.4	165	NOB 800psi	76	
V10st	4049.40	13286.1	SS	H	1				1		R80	Foreshore			10.33	26.75	sc	77	
V10st	4052.13	13295.0	SS	H	1				1		R80	Foreshore			12.07	673.94	sc	78	
V10st	4052.64	13295.0	SS	H	1				1		R80	Foreshore			11.3	298	NOB 800psi	79	

Well Name	Log Shift Based on Core GR Add (ft)	Log Shift Based on Wireline Log Extrapolation Add (ft)
Ubadari-1	5	
Ubadari-2	9	
Vorwata-1	10 - 12	
Vorwata-2	15	
Vorwata-3		18
Vorwata-4	30	
Vorwata-5	25	
Vorwata-6	16	
Vorwata-7st	14	
Vorwata-8		0
Vorwata-9		2
Vorwata-10st	Cores cut on original hole, wireline logs run on sidetrack	
Vorwata-11		0
Wiriagar Deep-1	7	
Wiriagar Deep-2	15 - 18	
Wiriagar Deep-3	7 - 10	
Wiriagar Deep-4	4	
Wiriagar Deep-5st	10	
Wiriagar Deep-6	14 - 18	
Wiriagar Deep-7	10	
Wiriagar Deep-8	7	
Ofaweri-1		?
Roabiba-1		?
Wos-1		?

Jonathan P. Salo 2002

Table 7.3: Depth shift for whole cores and drill cuttings in the Late Permian to Late Cretaceous interval for all Tangguh area wells.

Reservoir Name	WiriagarDeep-1	WiriagarDeep-2	WiriagarDeep-3	WiriagarDeep-4	WiriagarDeep-5ST	WiriagarDeep-6	WiriagarDeep-7	WiriagarDeep-8	Kalitami-1X	Wos-1	Ubadari-1	Ubadari-2
Top Kais (NGLG)	1606	2810	2204	3204	3294	2533	2411	2184	1016	1555	Not Present	Not Present
Base Kais (NGLG)	2548	3710	2843	4054	3991	3506	3164	3078	1700	2600	Not Present	Not Present
Top Faumai (NGLG)	2548	3710	2843	4054	3991	3506	3164	3078	1700	2600	Not Present	Not Present
Base Faumai (NGLG)	4089	4632	5798	4771	4971	4720	4705	4355	2290	7308	Not Present	Not Present
Top Paleocene Sand-prone Intvl.	6455	7333	8146	7932	8414	6940	7144	6731	3506	7860	5097	5390
Base Paleocene Sand-prone Intvl.	7184	7966	8915	8518	8840	7630	7906	7538	4088	8200	5300	5600
Top Late Cretaceous Marl	7320	8030	8963	8528	8995	7714	7977	7576	4100	8274	5351	5643
Base Late Cretaceous Marl	7738	8381	9295	8819	9336	8041	8354	8050	4336	8655	5640	5986
Top Ayot Limestone Formation	7800	8514	9327	8876	9460	8190	8439	8141	4256	9070	6157	6923
Base Ayot Limestone Formation	7845	8554	9364	8920	9496	8227	8481	8186	4281	9114	6203	6980
Top Callovian Roabiba	Not Present	Not Present	Not Present	Not Present	Not Present	Not Present	Not Present	Not Present	4350	9497	Not Present	Not Present
Base Callovian Roabiba	Not Present	Not Present	Not Present	Not Present	Not Present	Not Present	Not Present	Not Present	4376	9557	Not Present	Not Present
Top Bathonian/Bajocian Roabiba	Not Present	8600	Not Present	9036	9572	8240	Not Present	Not Present		9557	Not Present	Not Present
Base Bathonian/Bajocian Roabiba	Not Present	8700	Not Present	9138	9696	8346	Not Present	Not Present		9592	Not Present	Not Present
Top Aalenian	7860	8740	9417	9166	9754	8345	8521	8196			7140	8637
Base Aalenian	7886	8775	9477	9210	9874	8377	8567	8230			7671	8970
Top Permian Reservoir	7925	9455	9510	9319		8400	8620	8260			8000	
Base Permian Reservoir	7945	9487	9532	9330		8414	8624	8283			8080	

Table 7.4a: Measured depths (wireline log depths from RKB in feet) for gross reservoir intervals. Depths not listed at each well are considered non-reservoir rock intervals.

Reservoir Name	Ofaweri-1	Roabiba-1	Nambumbi-1	Sakauni-1	Vorwata-1	Vorwata-2	Vorwata-3	Vorwata-4	Vorwata-5	Vorwata-6	Vorwata-7ST	Vorwata-8	Vorwata-9	Vorwata-10ST	Vorwata-11
Top Kais (NGLG)	3440	4462	4383	7434	4591	6233	5551	5945	6382	6040	5047	7098	7150	?	7709
Base Kais (NGLG)	4170	5202	5465	7966	5458	7234	6348	6830	7372	6890	5887	8057	8036	?	8519
Top Faumai (NGLG)	4170	5202	5465	7966	5458	7234	6348	6830	7372	6890	5887	8057	8036	?	8519
Base Faumai (NGLG)	6302	7952	9352	10030	8644	9998	9056	8978	9642	9376	9301	11418	9734	7893	12050
Top Paleocene Sand-prone Intvl.	6674	9689	11308	11788	10419	11370	10900	10989	11574	11483	11753	11569	11701	11811	12105
Base Paleocene Sand-prone Intvl.	8900	10100	12100	12250	11053	11666	11376	11522	11962	11900	12355	11920	12010	12038	12396
Top Late Cretaceous Marl	8976	10223	12205	12235	11053	11666	11376	11522	11962	11900	12355	11920	12010	12038	12396
Base Late Cretaceous	9530	10598	12809	12828	11550	12202	11884	12075	12521	12464	12848	12451	12579	12611	12920
Top Ayot Limestone Formation	9611	10780	13037	12846	11692	12294	11982	12132	12589	12576	13012	12464	12618	12693	12941
Base Ayot Limestone Formation	9647	10830	13103	12884	11737	12340	12031	12177	12632	12622	13059	12498	12662	12740	12982
Top Callovian Roabiba	9751	10973	Not Present	Not Present	11759	12558	12057	Not Present	12757	12770	13125	12576	12846	13119	13110
Base Callovian Roabiba	9808	11040	Not Present	Not Present	11839	12599	?	Not Present	12791	12830	?	12590	12899	13207	13159
Top Bathonian/Bajocian Roabiba	9808	11040	13130		11839	12599	?	12229	12791	12830	?	12590	12899	13207	13159
Base Bathonian/Bajocian Roabiba	9966	11413	13192		11895	13011	12126	12332	13032	13139	13290	12655	13128	13571	13312
Top Aalenian	10052	11456			Not Present		Not Present	Not Present			13380	Not Present	Not Present		
Base Aalenian	11968	11461			Not Present		Not Present	Not Present			13429	Not Present	Not Present		
Top Permian Reservoir					11990		12190	12357				12769	13175		
Base Permian Reservoir					12025		12221	12403				12778	13255		

Table 7.4b: Measured depths (wireline log depths from RKB in feet) for gross reservoir intervals. Depths not listed at each well are considered non-reservoir rock intervals.

communication and connectivity, both at Wiriagar Deep and Vorwata. Furthermore, the areal extent of the fluvial channels belts and deltaic complexes appears limited.

The thinly bedded, non-correlatable nature of these fluvio-deltaic sandstone reservoirs is evident in the correlation cross-section in Figure 7.3. The datum is the top Late Permian, which identified by palynological analyses (Waton, et al., 1994 through 1998d). The spikey and generally high gamma ray through the thin-bedded reservoir intervals is indicative of the high clay content of the sandstones.

The interval has not been cored extensively in the Tangguh area. Many Tangguh wells either did not penetrate the Late Permian succession, or reached TD as soon as drill cuttings on surface were identified as Permian. As a result, the basal interval of the succession has never been penetrated in the Tangguh area wells, and wireline logging at TD commonly used the Late Permian hole section as ‘rathole’ for the logging toolstring, with the subsequent result of limited wireline log coverage, occasionally of poor quality where available. The formation was only occasionally cored, often by chance when Late Permian Succession sedimentary rocks were captured in the lower part of Jurassic interval coring (Figures 7.1 and 7.2). The Late Permian sandstone core plug analyses by the author, from Permian reservoir in the V-1 well, indicated very poor porosity and permeability characteristics for the reservoir (Figure 5.8), with porosity (He- ϕ) at 6.9% and the permeability (Kair) of only 1 mD.

DST testing was carried out on the WD-1, WD-2, and the V-1 wells. Hole problems resulted in the WD-1 testing intervals that were of poor quality (Salo, 1994). The WD-2 testing produced only water (Appendix 1), but the test indicated an excellent local porosity of 20%, and a permeability of only 0.2 mD (Appendix 1), but flowed only water. The V-1 testing produced 1 MMscfgd from the best Permian sandstone zone with average effective porosity ranging from 8.1% to 9.6% and very low permeabilities of less than 0.1 mD (Appendix 2). A cross-plot of porosity and permeability from whole core calibrated petrophysical data for the best zone (WD-2) is presented in Figure 7.4. The data indicates that the flow came from thin streaks with permeabilities of greater than 1 mD and the maximum calculated permeability for the tested interval being 139 mD.

The poor quality drill-cuttings, occasionally supplemented by limited whole core, have been analyzed for geochronological dating, paleo-depositional environment, and hydrocarbon source and reservoir identification. Ichnological facies

analysis (Pemberton, 1997a-e) and palynological environmental evaluation (Waton, et al., 1994 through 1998f) conclude most of these sandstone reservoirs were deposited in a predominantly continental paleo-geographical environment, with only rare marine pulses contributing some restricted marine flora and fauna. This suggests perhaps a mud-prone estuarine coastal setting. The relatively high clay content of the sandstones, the high degree of compaction, and the abundant cementation result in relatively tight reservoirs with low porosity and occluded pore throat permeability.

Potentially, injectivity into the Late Permian Succession for hypothetical CO₂ sequestration based on the very limited quantity of very poor to fair quality data is possible, but given the generally low quality and variable nature of the reservoir, the risk of limited potential reservoir volume (ie. storage capacity), and the probable lack of connectivity for the various fluvial channel reservoirs, the formation is a very poor potential ESSCI site. The tight nature of sandstone reservoirs with low permeability would probably result in massive fracturing, and formation damage, in the immediate borehole vicinity (J. Marcou, BP Tangguh Subsurface Development Manager, personal communication, 2002).

7.2.2 Aalenian Sandstone Formation Reservoir Quality

The Aalenian Sandstone Formation is composed of shallow marine sandstones, which are primarily present at Wiriagar Deep only. The onlapping, transgressive nature of the sandstone paleo-deposition resulted in thick sedimentation over much of the Wiriagar Deep and the area to the southeast of Wiriagar Deep, but did not reach the Vorwata area.

Correlation cross-sections through representative Wiriagar Deep wells show a relatively thick shale break representing a maximum flood surface intervening between the Roabiba Sandstone Formation and the Aalenian Sandstone Formation at the WD area (Figure 7.5). All wells that encountered the Aalenian Sandstone Formation had extensive wireline logging, and often the reservoir interval was conventionally cored in part or in entirety (Figure 7.1). Drill cuttings were collected on all wells through the interval, and the reservoir was occasionally DST tested (Figure 7.1).

The top depth structure map for the Aalenian Sandstone Formation presented in Figure 7.6 is a phantom surface representation provided by BP, which does not reflect the pinch-out limit of the strata to the east over Vorwata. The formation

interval is beyond the resolution of seismic surveys in the Tangguh area. The Aalenian Sandstone Formation is limited in areal extent to the Wiriagar Deep area (Bulling, et al., 1998). The reservoir properties of the formation were established by petrophysical evaluation of wireline logging suites in all of the Wiriagar Deep wells, calibrated to whole core plug analyses (Appendix 2). Whole core coverage was deemed exceptionally good for this reservoir on the Wiriagar Deep wells. The core plug analyses included Helium porosity (He-Ø) and air permeability (Kair) analysis for reservoir plugs taken at 1 ft intervals through existing whole cores. After initial analyses was completed the core plugs were re-measured at 800 psi confinement pressure according to procedures recommended by J. Marcou and F. Paskavan (ARCO), mainly specifying optimum cleaning and drying methodology for core plugs (Bulling, et al., 1998). Those plug values that were not re-measured were re-calculated based on a formula to correct for overburden depth and reservoir confinement pressure (Bulling, et al., 1998).

The Aalenian reservoir average temperature is 228° F with average reservoir pressure of 4074 psia at the 8735 ft TVDss datum (datum is defined as the ‘Centroid Reservoir’). The average Aalenian reservoir He-Ø is calculated at 13.0%, in the hydrocarbon accumulation at Wiriagar Deep structure, with an average water saturation (Sw) of 26.0%, covering an area of 35,979 acres with an averaged thickness of 25.3 ft (Bulling, et al., 1998).

At the ‘P’ structure (including WD-3), the average Aalenian reservoir He-Ø is calculated at 13.9%, in the hydrocarbon accumulation, with an average Sw of 34%, with an areal extent of only 101 acres at an averaged thickness of 48 ft (Bulling, et al., 1998).

In the WD-2 Aalenian Sandstone Formation porosity (He-Ø) of 14.8% and permeability of 529 mD was measured. In the WD-7 core, the Aalenian Sandstone Formation’s porosity (He-Ø) was 19.0% and permeability was measured at more than 2264 mD!

Digital photographs from WD-3 cores of the Aalenian sandstone reservoir at ‘P’ structure, with their respective sedimentological features and reservoir character noted in annotations, are presented in Figure 5.13. In the WD-3 Aalenian Sandstone Formation, porosities (He-Ø) of 11.6% to 18.5% were measured, and permeabilities ranging from 0.5 mD to 925 mD were recorded. Digital photographs and analyses of

whole core plug samples at the Wiriagar Deep Structure, from WD-2 (Figure 5.14) and WD-7 (Figure 5.15), are also presented.

Average net effective porosity in the reservoir ranges from 17% at WD-7 to 8.5% at Ofaweri #1 (O-1) based on petrophysical analysis calibrated to whole core plug data (Figure 7.7). The average effective porosity map for the reservoir in the Tangguh area more accurately reflects the areal extent of the unit compared to the top depth structure map presented in Figure 7.6. Measured whole core plug permeabilities (Figure 7.8) range from 0.001 mD to several D'arcy (Bulling, et al., 1998).

Wells with DST testing flowed hydrocarbon at significant rates (Appendix 1). The reservoir quality overall is quite good, especially from a hydrocarbon reservoir production perspective. The possibility of sequestering/storing CO₂ in the Aalenian Sandstone Formation is limited to the Wiriagar Deep structure, due to the limited areal extent of the formation. The potential ESSCI reservoir character at Wiriagar Deep for CO₂ sequestration appears very good when evaluated strictly on a reservoir quality basis. Additional ESSCI features such as seal evaluation, fracture and fault re-activation assessment, and potential site locations on the flanks over reservoir aquifer intervals are considered in following chapters.

The Aalenian Sandstone Formation generally has very good injectivity reservoir quality, and good to very good potential for CO₂ injection and sequestration/storage. The formation has a good to very good data set considered very sufficient to judge the ESSCI potential of the reservoir as very good.

7.2.3 Callovian and Bathonian/Bajocian Roabiba Sandstone Formation Reservoir Quality

The Callovian Roabiba Sandstone Formation and Bathonian/Bajocian Roabiba Sandstone Formation are shallow marine sandstones in the Tangguh area. These two strata are in communication with each other at Vorwata, being separated and distinguished by a permeable unconformity with no intervening sealing lithology present. Furthermore, the areal extent of the Callovian Roabiba Sandstone Formation is limited to the Vorwata area and is not present due to a combination of the onlapping trend from the SE towards the NW and erosional truncation over Wiriagar Deep area from uplift combined along the Sekak Ridge to the west, and Kemum High to the north.

Although the recognition of the two units from a sequence stratigraphy perspective is very important, and crucial to any geo-cellular modelling study for stratigraphic unit areal extent and Gaussian simulations of character away from the area of known hydrocarbon containment, it is not necessary to evaluate them as separate entities from an ESSCI rating perspective. The two units are in direct communication, and on a regional scale they are a single potential ESSCI reservoir.

The top of the combined Callovian and Bathonian/Bajocian Roabiba Sandstone Formation reservoir is identified as the 'Top Upper Roabiba' on the geological correlation cross-section presented in Figure 7.9. The cross-section is flattened on the Base Late Cretaceous/Top Late Jurassic boundary (unconformity), which together with the Top Late Permian/Base Late Jurassic (unconformity) are the only horizons resolvable and correlatable on seismic survey lines (Figure 1.10). The cross-section (Figure 7.9) shows the top of the Roabiba Sandstone Formation reservoir through selected example wells across the Wiriagar Deep and Vorwata structures (W-E), based on wireline log correlations. The top and base reservoir horizons are beyond the resolution of seismic surveys due the scattering of seismic energy at the near surface, massively bedded NGLG carbonate sequence (Figure 7.10).

Drill cuttings and extensive suites of wireline logs are available for all Tangguh area wells. Numerous whole cores were taken on a variety of Wiriagar Deep, Vorwata, and Ubadari wells in the Tangguh area (Table 7.1; also Figure 7.1 and 7.2).

Geological cross-sections presented in Figures 6.1, 6.2, 6.3, 6.4, and 6.5 (with the Base Ayot Limestone Formation as the datum), show the internal reservoir sequence stratigraphy of the Callovian Roabiba Formation (if present) and Bathonian/Bajocian Roabiba Formation in the Tangguh area. The reservoir is massively bedded at most locations with local thinning of the Roabiba Sandstone Formation at the V-1, V-3, V-7 area due to deep incision during the MJ-2 erosional event. There is also regional thinning at the northern most edge due to the onlapping from the south, and erosional truncation in the west due to uplift along the Sekak Ridge. The geological schematic in Figure 7.11 illustrates the relationship between the Roabiba Sandstone Formation reservoir and the various truncations and onlap pinchouts. The onlap of the Bathonian/Bajocian Roabiba Sandstone Formation resulted from marine transgressions from the SW to SSW, whereas the onlap of the

Callovian Roabiba Sandstone Formation resulted from marine transgressions from the S to SE. This produced a resulted from marine transgressions from the SW to SSW, which thickens overall from the N - NW towards the S - SE. The overall thickening of the reservoir, with improving reservoir character, towards the SE is evident from the cleaner gamma ray over greater footage between the V-3 and V-10 wells (Figure 7.12).

The reservoir has closure on two major structures, the Wiriagar Deep and Vorwata (Figure 7.13). The two structures have proven top and lateral seals since the WD structure contains an 1800 ft natural gas column, and the V structure contains a natural gas column height of almost 2200 ft.

The reservoir quality is very good in terms of porosity and permeability. The petrophysical results are presented for all Wiriagar Deep and Vorwata wells in Appendix A. The map for the Callovian Roabiba Sandstone Formation in the Tangguh area shows 7% to almost 17% average effective porosity across the Vorwata structure (Figure 7.14), and a map for the Bathonian/Bajocian Roabiba Sandstone Formation shows average effective porosities ranging from 9% to almost 16% across the V structure (Figure 7.15). The porosity versus permeability cross-plot of whole core plugs from all Wiriagar Deep and Vorwata wells with Roabiba Sandstone Formation reservoir core show most plugs have greater than 11% porosity and 60 mD permeability (Figure 7.16). The gas-water contact (GWC) is at ~13,404 ft wireline log measured depth (-13,313 ft TVDss), as shown in Figure 7.17. Tables of DST results from Tangguh area wells are presented in Appendix B. The Roabiba Sandstone Formation reservoir average temperature is 228° F with average reservoir pressure of 4074 psia at the 8735 ft TVDss datum (datum is defined as the 'Centroid Reservoir'). At the Wiriagar Deep structure (including WD-2), the average Roabiba Sandstone Formation reservoir He-Ø was calculated at 12.4%, in the hydrocarbon accumulation, with an average Sw of 17.4%, covering an area of 24,209 acres with an averaged thickness of 82.8 ft (Bulling, et al., 1998).

At the 'P' structure (including WD-3), the average Roabiba Sandstone Formation reservoir He-Ø is calculated at 13.6%, in the hydrocarbon accumulation, with an average Sw of 41%, with an areal extent of only 128 acres at an average thickness of 6 ft (Bulling, et al., 1998).

The Roabiba Sandstone Formation reservoir, at the Vorwata structure, has an average temperature is 256° F with average reservoir pressure of 5841 psia at the

12,845 ft TVDss datum. At Vorwata (including V-2 and V-10), the average Roabiba Sandstone Formation reservoir He-Ø was calculated at 13.6%, in the hydrocarbon accumulation, with an average Sw of 20%, covering an area of 78,520 acres with an averaged thickness of 138 ft (Bulling, et al., 1998). However, the lithostratigraphic unit thickens considerably towards the SE, with the thickness at V-2 being over 400 ft and at V-10 being well over 600 ft.

Reservoir quality was examined in detail for the Roabiba Sandstone Formation, particularly by re-sampling and testing of whole core plugs based on sedimentological facies variation in the Vorwata-10 well, and in-filling data gaps for whole core from V-10 acquired in the water-leg of the reservoir. The list of all V-10 Roabiba Sandstone Formation whole core plug porosities and permeabilities can be found in Appendix 3. New whole core plugs were obtained from four Wiriagar Deep and four Vorwata wells, mainly in the Roabiba Sandstone Formation. These porosity and permeability results are presented in Table 7.5, with the majority (56%) of new plug analyses from the V-10 well. A cross-plot of porosity versus permeability for the new V-10 core plug results (Figure 7.18) clearly shows that the Callovian Roabiba Sandstone Formation has poorer porosity and permeability than the Bathonian/Bajocian Roabiba Sandstone Formation. This evaluation appears compatible with the overall wireline petrophysical results for the Vorwata structure as a whole, where whole core is not always available (Figure 7.19).

Surprisingly, there is little difference between the porosity and permeability of the V-10 Bathonian/Bajocian gas charged interval (13,209 ft to 13,404 ft) and the water-wet aquifer interval of the reservoir (13,405 ft to 13,547 ft - base of last core). The primary difference is the poorer reservoir quality of the Callovian Roabiba compared to the Bathonian/Bajocian Roabiba. This is very good for possible CO₂ sequestration if potential injection sites are located on the southern, or broadly dipping eastern, flanks of the Vorwata structure. Very good porosity and permeability in the aquifer portion of the reservoir are favorable for injection and potential CO₂ accommodation space, and relatively tighter reservoir quality at the top of the reservoir unit (in the top-most Callovian Roabiba stratigraphic units) would add tortuosity to the migratory path of a CO₂ plume. Occluded pore throats and lower permeabilities in the Callovian Roabiba would lengthen the migration time for the CO₂. Furthermore, the vertically migrating plume from the basal injection into the

Well Name	Core Plug Depth (ft/m)	Plug Depth Shifted (ft)	Porosity (%)	Permeability (mD)	REMARKS	Entry P. MICP (psia)	Threshold P. MICP (psia)	Unit	Facies	Lithology	H/V
WD2	7368'4"	7386'4"	10.6	0.88	NOB 800psi			PUM	Turb	SS	H
WD2	8753'2"	8771'2"	14.8	529	NOB 800psi			A20	Delta	SS	H
WD3	7956'3"	7964'3"	12.27	19.74	NOB 800psi			PMP	Turb	SS	H
WD3	9364'9"	9374'9"	13.2	0.739	NOB 800psi			R30	Prograde	SS	H
WD5	9509'0"	9519'0"	4.4	0.008	NOB 800psi			R70	Foreshore	SS	H
WD5	9509'5"	9519'5"	2.2	0.016	NOB 800psi			R70	Foreshore	SS	H
WD5	9511'4"	9521'4"	7.3	0.069	NOB 800psi			R70	Foreshore	SS	H
WD7	8524'7"	8534'7"	19	2264.38	sc			A20	W.O.	SS	H
V1	11765'9"	11775'9"	11.2	150	NOB 800psi			CU40	T Ch	SS	H
V1	11787'7"	11797'7"	10.3	3.55	NOB 800psi			CU30	U. Sh	SS	H
V1	11790'9"	11800'9"	2.5	0.05	NOB 800psi	294	339	CU30	U. Sh	SS	H
V1	11797'7"	11807'7"	13.5	137	NOB 800psi			CU30	U. Sh	SS	H
V1	11909'7"	11919'7"	3.5	0.052	NOB 800psi			R20	Fluv/Delt	SS	H
V1	11914'6"	11924'6"	6.9	1	NOB 800psi			Perm	Fluvial	SS	H
V2	12582'7"	12595'7"	14.8	19.8	NOB 800psi			CU30	M. Sh	SS	H
V2	12584'8"	12597'8"	12.4	28.3	NOB 800psi			CU30	M. Sh	SS	H
V2	12585'8"	12598'8"	15.2	126	NOB 800psi			CU30	M. Sh	SS	H
V2	12594'4"	12607'4"	13.5	477	NOB 800psi			R80	T. Ch	SS	H
V2	12600'3"	12613'3"	13.1	134	NOB 800psi			R80	T. Ch	SS	H
V2	12757'6"	12770'6"	15.9	130	NOB 800psi			R70	M. Sh	SS	H
V2	12865'7"	12878'7"	16.9	1090	NOB 800psi			R50	B. Sh	SS	H
V2	12901'5"	12914'5"	12.2	0.316	NOB 800psi			R40	T. Ch	SS	H
V7	13118'3"	13132'3"	9.9	0.233	NOB 800psi			CU40	U. Sh	SS	H
V7	13123'8"	13137'8"	6.5	0.868	NOB 800psi			CU40	U. Sh	SS	H
V7	13136'10"	13150'10"	8.5	7.14	NOB 800psi			CU40	U. Sh	SS	H
V7	13143'6"	13157'6"	9.0	18.8	NOB 800psi			CU30	M. Sh	SS	H
V7	13152'5"	13166'5"	10.7	131	NOB 800psi	3	5	CU30	M. Sh	SS	H
V10st	4021.25	13193.7	8.2	0.318	NOB 800psi			CU20	T. Ch.	SS	H
V10st	4021.86	13195.7	5.72	271.28	sc			CU20	T. Ch.	SS	H
V10st	4022.20	13196.8	7.66	96.24	sc			CU20	T. Ch.	SS	H
V10st	4025.08	13206.3	7.6	40.7	NOB 800psi			CU20	T. Ch.	SS	H
V10st	4025.80	13208.6	11.24	290.95	sc			R80	Foreshore	SS	H
V10st	4025.98	13209.2			insuff/broken			R80	Foreshore	SS	H
V10st	4026.18	13209.9	14.5	1080	NOB 800psi	3	4	R80	Foreshore	SS	H
V10st	4028.15	13216.4	14.8	979	NOB 800psi			R80	Foreshore	SS	H
V10st	4029.58	13221.1	14.4	576	NOB 800psi			R80	Foreshore	SS	H
V10st	4029.70	13221.4	14.8	1339.39	sc			R80	Foreshore	SS	H
V10st	4031.55	13227.5	11.9	226	NOB 800psi			R80	Foreshore	SS	H
V10st	4034.51	13237.2	12.9	954	sc	2	5	R80	Foreshore	SS	H
V10st	4035.40	13240.1	12.67	506.22	sc			R80	Foreshore	SS	H
V10st	4036.23	13242.9	12.9	298	NOB 800psi			R80	Foreshore	SS	H
V10st	4039.62	13254.0	13.47	339.64	sc			R80	Foreshore	SS	H
V10st	4040.20	13255.9	14.06	239.74	sc			R80	Foreshore	SS	H
V10st	4042.62	13263.8	12.42	73.41	sc			R80	Foreshore	SS	H
V10st	4044.81	13271.0	14.5	545	NOB 800psi			R80	Foreshore	SS	H
V10st	4045.92	13274.7	14.4	165	NOB 800psi			R80	Foreshore	SS	H
V10st	4049.40	13286.1	10.33	26.75	sc			R80	Foreshore	SS	H
V10st	4052.13	13295.0	12.07	673.94	sc			R80	Foreshore	SS	H
V10st	4052.64	13295.0	11.3	298	NOB 800psi			R80	Foreshore	SS	H
V10st	4056.02	13307.8	17.06	18.36	sc			R70	M. Sh	SS	H
V10st	4057.32	13312.1	12.66	14.06	sc			R70	M. Sh	SS	H
V10st	4058.58	13316.2	6.7	0.183	NOB 800psi			R50	W.O.	SS	H
V10st	4059.26	13318.4	9.4	4.59	NOB 800psi			R50	W.O.	SS	H
V10st	4060.90	13323.8	12.04	10.6	sc			R50	W.O.	SS	H
V10st	4063.45	13332.2			insuff/broken			R50	W.O.	SS	H
V10st	4067.60	13345.8	9.97	11.46	sc			R50	W.O.	SS	H
V10st	4068.50	13348.7	13.77	521.03	sc			R50	W.O.	SS	H
V10st	4076.30	13374.3	14.24	6.43	sc			R50	T. Ch.	SS	H
V10st	4081.32	13390.8	10.5	80.1	NOB 800psi			R50	T. Ch.	SS	H
V10st	4082.85	13395.8			insuff/broken			R50	T. Ch.	SS	H
V10st	4090.85	13422.1	11.3	5.89	NOB 800psi	2	8.5	R50	T. Ch.	SS	H
V10st	4093.80	13431.8	11.1	37.1	NOB 800psi			R50	T. Ch.	SS	H
V10st	4095.50	13437.3			insuff/broken			R50	T. Ch.	SS	H
V10st	4101.30	13456.4	11.36	18.17	sc			R40	W. O.	SS	H
V10st	4117.70	13510.2	15.53	840.77	sc			R40	W. O.	SS	H
V10st	4126.30	13538.4	14.86	42.3	sc			R30	Prograde	SS	H
V10st	4126.69	13539.7	13.69	463.77	sc			R30	Prograde	SS	H
V10st	4128.92	13547.0	15.7	475	NOB 800psi	3	5	R30	Prograde	SS	H

insuff/broken: Sample was of either insufficient size or was broken upon arrival in Australia, testing unavailable.

NOB 800 psi: Tested at 800 psia confinement pressure

sc: Tested at standard conditions

Table 7.5: Results of Helium Porosity and Air Permeability Testing on Whole Core Plugs from Reservoir Intervals

Bathonian/Bajocian Roabiba units would spread out laterally when the rate of migration through the overlying Callovian Roabiba units is slowed, dispersing the CO₂ plume laterally before it makes contact with the top-seal cap rock of the Pre-Ayot Shale interval. The reservoir was deposited during the Middle Jurassic and earliest Late Jurassic MJ-3 and MJ-1/LJ-11 biostratigraphic intervals as primarily shallow marine sand-rich restricted marine bay and foreshore transgressive and highstand tracts. Apart from poor seismic survey resolution over the interval, the dataset is very good. The Roabiba Sandstone Formation has very good reservoir quality in general, and particularly, very good injectivity characteristics for potential CO₂ injection and sequestration/storage. The formation has a very good data set considered very ample to sufficient to judge the ESSCI potential of the reservoir as very good.

7.2.4 Ayot Limestone Formation Reservoir Quality

The Ayot Limestone Formation is a potential ESSCI carbonate reservoir, with gas shows commonly recorded whilst drilling through it at Wiriagar Deep (Salo 1994; Salo 1996c; Salo 1997a-e). It appears to be predominantly dense and tight with very poor matrix porosity and permeability, but is locally fractured and probably hydrocarbon charged at Wiriagar Deep (Salo, 1994; Salo 1996c; Salo 1997a-e). It is therefore not a likely candidate for CO₂ sequestration in the Tangguh area.

The potential reservoir stratum is areally pervasive over the entire Tangguh area and is of relatively uniform thickness, ranging from 39 ft to 59 ft in thickness. Geological cross-sections 6.1, 6.2, 6.3, 6.4, and 6.5 are all flattened on the Base Ayot Limestone Formation, and collectively show the Ayot Formation at every well in the Tangguh area.

There are extensive wireline logs and drill cuttings available from the formation at both Wiriagar Deep and Vorwata, with whole core sampling part or all of the formation on the WD-3, WD-7, and WD-8 wells. The formation was also DST tested on the WD-5 well and flowed natural gas at 0.02 MMscfgd (ie. 200,000 cubic feet a day). The hydrocarbons appear to have flowed from fractures (Salo, 1997d and 1997e), since the porosity versus permeability cross-plot of the perforated interval clearly indicates that it is excessively tight (Figure 7.20). The average porosity is less than 1% and the average permeability is less than 0.02 mD over the DST perforated interval.

The data set through the Ayot Limestone Formation is moderate. Based on sufficient enough data, it can be determined that this reservoir most likely has poor ESSCI potential, and as such is a bad choice for potential CO₂ injection and sequestration.

7.2.5 Late Cretaceous Reservoir Quality

From an ESSCI CO₂ sequestration perspective the Late Cretaceous Marls has limited data, inappropriate host reservoir mineralogy (carbonates are not the preferred lithology for CO₂ injection and sequestration/storage), and inappropriate type of porosity (ie. intercrystalline or intergranular matrix porosity is preferred for CO₂ injection and sequestration/storage since fractured reservoir porosity presents greater uncertainty).

Figure 7.21 shows the depth structure map of the Top Late Cretaceous for the Tangguh area. The possibility of potential ESSCI CO₂ sequestration in Late Cretaceous Marl Succession is basically limited to two structural traps, Wiriagar Deep and Vorwata. The distribution of whole cores and DSTs through the Late Cretaceous Marl Succession interval is limited only to several Wiriagar Deep wells (Figure 7.1 and 7.2). Available wireline logs and drill cuttings over this potential reservoir indicate that the formation porosity is generally tight. Evaluation of the interval suggests that the matrix porosity is generally very poor (Bulling, et al., 1998), and the limited whole core plug analysis suggests that the lithology is dense and very tight, but brittle and prone to fracturing (see MICP results in Table 7.2).

While the Late Cretaceous Marl is a possible ‘fractured reservoir’ potentially able to produce commercial quantities of hydrocarbons at other Wiriagar PSC and Berau PSC well locations, it is not fractured, nor hydrocarbon bearing at the WD-3 location. The possible reserves in the Late Cretaceous have not been calculated, although The Late Cretaceous has been drill-stem tested (DST) successfully. The DST on WD-4 flowed at a rate of 5.2 MMscfgd, and 7 BCPD. Significant rates of natural gas flowed from the DST on WD-4. Primarily dry gas (methane) flowed at 5.2 MMscfgd from this formation, however, CO₂ injectivity into fractured marls would likely be problematic, aside from the issue of storage capacity in fractured reservoirs (Salo, 1997a). Figure 7.22 shows the matrix porosity versus permeability cross-plot for the Late Cretaceous perforated intervals WD-4’s DST. The average wireline log primary porosity (excluding calculated fractured porosity from dipole

sonic waveform analysis) is a mere 5%, and the average matrix permeability is only 0.01 mD.

The data set through the Late Cretaceous Marl Succession is good enough to determine that this reservoir most likely has poor ESSCI potential, and as such is a bad choice for potential CO₂ injection and sequestration.

7.2.6 Late Paleocene Reservoir Quality

The Late Paleocene Sand-prone Interval, with proven hydrocarbon reservoirs and therefore proven seal, is limited to the Wiriagar Deep structure only. The Late Paleocene is comprised of an overlying Mud-prone Interval and an underlying Sand-prone Interval. The pick for the top of the Late Paleocene in the Tangguh area is based on palynological analyses of whole cores and cuttings (Frame, et al., 1997a-i). The base of the Mud-prone Interval and top of the Sand-prone Interval is based on a wireline pick for the highest gamma ray spike between the top and the base of the Paleocene, probably representing a maximum flood surface.

The Mud-prone Interval is somewhat of a misnomer as commercially significant quantities of hydrocarbons are reservoirized in thinly bedded turbidite and debris flow sandstone reservoirs, as exemplified by the DST on WD-3, which flowed natural gas at 20.8 MMscfgd (millions of cubic feet per day) and condensate at 50 barrels of condensate per day (BCPD) (Salo, 1997c).

The Sand-prone Interval at Wiriagar Deep is composed of various members, the 'Upper Member' (UP), 'Middle Member' (MM), and 'Lower Member' (LM), as defined by Bulling, et al., (1998). The clastic reservoirs of the Sand-prone Interval are composed primarily of classic turbidite channels and fans, (Dr. R. Lowe, personal communication, 2001; and Lowe, 1998). Within in these members are individual sandstone turbidite and gravity/debris flow channels and fans, probably with varied degrees of interconnectivity between them. There is fair to good core coverage through hydrocarbon bearing Late Paleocene reservoirs on the Wiriagar Deep structure. The summary of the whole core plug analyses from all existing Late Paleocene whole cores is presented in Table 7.6. These whole core plugs were then used to calibrate the petrophysical analyses of the wireline logs for effective porosity and calculated permeability. The laboratory measured permeabilities and porosities from whole core plugs were depth shifted by matching core gamma ray log to wireline gamma ray logs for each well and core. These core plug values were then

Late Paleocene Reservoir Characterization Summary	Mud-prone Interval		Sand-prone Upper Member		Sand-prone Middle Member		Sand-prone Lower Member	
	He Ø (%)	k _{air} mD	He Ø (%)	k _{air} mD	He Ø (%)	k _{air} mD	He Ø (%)	k _{air} mD
WELL								
WD-1								
Average	-	-	11.7*	23.0*	-	-	11.4*	1.1*
Range	-	-	2.9 - 19.5	0.001 - 133	-	-	6.1 - 14.3	0.03 - 2.44
WD-2								
Average	-	-	12.2	9	13.8	17.6	-	-
Range	-	-	1.0 - 17.0	0.001 - 120	4.5 - 20.4	0.002 - 98	-	-
WD-3								
Average	10.8	23.7	-	-	-	-	8.4	0.8
Range	1.7 - 21.0	0.004 - 212	-	-	-	-	1.4 - 15.5	0.001 - 15.9
WD-4								
Average	-	-	-	-	-	-	-	-
Range	-	-	-	-	-	-	-	-
WD-5								
Average					5.74	0.5	3.7	0.15
Range					1.3 - 8.5	0.002 - 1.6	1.2 - 8.5	0.001 - 3
WD-6								
Average	-	-	-	-	-	-	11.5	3.5
Range	-	-	-	-	-	-	2.5 - 17.8	0.001 - 103
WD-7								
Average	7.1	0.6	-	-	-	-	12.1	0.69
Range	2.5 - 14.4	0.01 - 9.2	-	-	-	-	4 - 18.6	0.005 - 12.8
WD-8								
Average	-	-	14.7	55.2	-	-	10.8	1.2
Range	-	-	4.3 - 20.9	0.04 - 265	-	-	3.3 - 16.8	0.01 - 8.7
Wiriagar Deep Average (All Wells)	9.93	18.2	12.87	29.07	9.77	9.05	9.65	1.24
Wiriagar Deep Range (All Wells)	1.7 - 21	0.004 - 212	1 - 19.5	0.001 - 133	1.3 - 20.4	0.002 - 98	1.2 - 18.6	0.001 - 103

* (with 400 psi NOB - Net Overburden Pressure confining stress)

Table 7.6 Late Paleocene Whole Core Plug Helium Porosity and Air Permeability Summary. Various reservoir members of the Late Paleocene are absent on some Wiriagar Deep wells, and most Paleocene reservoir are absent at Vorwata.

plotted as symbols on the petrophysical log track for each wells calculated porosity and permeability curve.

An algorithm was the used to shift the measured porosity and calculated permeability values to ‘best fit’ match the whole core plug laboratory data points. The petrophysical program (Petcom) was then re-run using the calibrated data (Petrophysical results by well, for each of the Paleocene reservoir intervals, are presented in Appendix 2).

Figure 7.23 shows a permeability and porosity cross-plot of the Sand-prone Interval MM on the discovery well, WD-2, which shows the best reservoir quality of any Late Paleocene reservoir with average 13.6% porosity and 52.89 mD over 135 ft of gross reservoir interval.

These turbidites are well developed on the Wiriagar Deep structure, but at Vorwata the gross stratigraphic unit is very thin, and the sandstone reservoirs are either absent or are not well developed. The correlations for these gross reservoir picks can be found in a series of wireline correlations. Figure 7.24 shows an example of the Late Paleocene correlation for selected Wiriagar Deep and Vorwata wells, flattened on the palynological datum for the Top Late Paleocene. The Late Paleocene Mud-prone Interval can be seen thinning dramatically towards the east (over Vorwata), providing very little top seal coverage at Vorwata.

Figure 7.25 shows the correlation cross-section of the same select Wiriagar Deep and Vorwata area wells, but flattened on the high gamma ray peak (MFS) marking the top of the Sand-prone Interval. The Sand-prone Interval is thick and very sand-rich in the Wiriagar Deep area, but similar to the Mud-prone Interval it also is thinning to the east over the Vorwata area, and is less sand-rich. There are no distinct UP, MM, and LM units discernable at the Vorwata area. The Vorwata area was most likely a deep marine paleo-depositional environment, outboard of the shelf edge, during the Late Paleocene Mud-prone and Sand-prone phases (Bulling, et al., 1998).

The data set through the Late Paleocene reservoirs is sufficient enough to determine that this reservoir most likely has a poor ESSCI potential, and as such is a bad choice for potential CO₂ injection and sequestration.

7.2.7 NGLG Reservoir Quality

The Kais Limestone Formation and Faumai Formation are both members of the New Guinea Limestone Group (NGLG), prevalent over much of Papua, Indonesia

and Papua New Guinea. Both NGLG members are discussed in detail previously in Chapter 5. LITHOSTRATIGRAPHY AND SEDIMENTOLOGY regarding their inapplicability as potential ESSCI sites. Much of the Top Kais Limestone Formation subcrops the surface at a depth <2600 ft, commonly considered as the minimum depth required for supercritical phase CO₂, especially at the culminating crest at the NW portion of Wiriagar Deep structure where CO₂ would be expected to migrate (Isworu, et al., 2002). Figure 7.26 shows the Top Kais Limestone Formation Depth Structure Map of the Tangguh area.

There is much more data available for the Kais Limestone Formation, than the Faumai Formation. The Kais Limestone Formation has drill cuttings through the almost the entire formation on most Tangguh area wells, including the shallow Wiriagar Field production wells (Dolan and Hermany, 1988). There is also DST and extensive 10-year production data available. The Faumai Formation has severe limitations to data due to lost circulation through most of the interval resulting in no rock samples. Wireline logs through the Faumai Formation are also extremely limited (Bulling, et al., 1998).

Therefore, the Kais Limestone Formation has ample, sufficient datasets to determine that this reservoir has very poor ESSCI potential due to unfavorable mineralogy and low confinement pressures, and as such is a very bad choice for potential CO₂ injection and sequestration. The Faumai Formation has poor data quantity and quality available, however, based on the very limited data this reservoir has very poor ESSCI potential due to unfavorable mineralogy and low confinement pressures, and as such is a very bad choice for potential CO₂ injection and sequestration.

PART III
CONTAINMENT

8.0 ESSCI STRATA EVALUATION

This study integrated the review and evaluation of the existing geological data from the Tangguh region that had *been collected from a hydrocarbon exploration and appraisal perspective*, with new data and interpretations. These data were then ranked quantitatively and qualitatively by a ‘degree of confidence factor’, from *a CO₂ capture, injection, and sequestration/storage (disposal) perspective*. The quantitative and qualitative ranking of data to establish a ‘degree of confidence factor’ is a well-documented hydrocarbon prospecting and appraisal technique, comprehensively discussed by Rose (2001), and expanded upon by Nakanishi and Lang (2001).

Table 8.1 illustrates the ‘degree of confidence factor for geological expression’ matrix technique visualization. The ‘y-axis’ is the ranking of data quantity labeled very poor, poor, moderate, enough, and plentiful, and a subjective decision of the data quality is necessarily included in this ranking. Obviously, a data set may exist for a particular attribute, such as ‘seismic survey’ for example, but the data set may be so poor in quality as to negate the impact on geological evaluations. The ‘x-axis’ is the ‘expression factor’ ranking based on the data set that allowed the researcher to establish a ranked or rated geological attribute or characterization.

Each cross-chart box in Table 8.1 shows the value assigned to that box based on the end member scaling. Scales run from 0.00 to 1.00 across the top line of boxes such that when ‘Plentiful Data’ is deemed to be available, and the data indicates a negative geological appraisal (for either hydrocarbon reservoir discovery potential, or in this case, environmentally sustainable subsurface CO₂ sequestration and storage) then it is subjectively rated as ‘very bad’, this fields box contains the value 0.00 (the lowest ranking) as an end member.

If, on the other hand, when ‘Plentiful Data’ is deemed to be available, and the data indicates a positive geological assessment then it is rated as ‘very good’ and the cross-chart field box for this has a value set to 1.00 (the highest ranking). It then follows that where ‘Plentiful Data’ is deemed to be available, and the data indicates a only a relatively bad or good geological appraisal, their respective field box values are proportional along the end members scaling (at 0.25, and 0.75, respectively). The ‘even’ chance of geological appraisal is left blank, because logically, if ‘Plentiful

Expression of existence for geologic chance factor

	very bad	bad	even	good	very good
plentiful	0.00	0.25	X	0.75	1.00
enough	0.13	0.31	X	0.69	0.88
moderate	0.25	0.38	0.50	0.63	0.75
poor	0.38	0.44	0.50	0.56	0.63
very poor	X	X	0.50	X	X

Index for confidence levels of existence of data for geological chance factoring.
(Nakanishi and Lang, 2001; modified from Rose, 2001)

Table 8.1: Data confidence factor matrix scaling, by Nakanishi and Lang (2001), after Rose (2001). Plentiful data/very bad confidence level box has the scaling end member rating of 0.00. Plentiful data/very good confidence level has the highest degree of confidence scaling at 1.00. Very poor data/even confidence level for geological chance box is rated as 0.50 as a ternary chart end member. The remaining boxes are then filled scaled to the end-members for various combinations of data quality/quantity and the geological chance factor indicated.

Data' (ie. all the data required to make a judgment in this matrix system) is available, then by definition, one should be able to make a judgment of very bad, bad, good, or very good and not merely even chances of geological success. Likewise, with 'Very Poor' data available (ie. almost none) then surely the value can only be 0.50 or 'even' (ie. anything is possible), and the good and bad judgments can't be made with any degree of great confidence.

Numerous water-bearing strata are present in the Tangguh area subsurface, for potential CO₂ containment, and these need to be screened systematically. Preliminary screening has identified several 'wet' subsurface strata as potential ESSCI strata, including:

- A. Late Permian fluvio-deltaic sandstone reservoirs
- B. Middle Jurassic estuarine 'Aalenian Sandstone Formation' reservoir
- C. Middle Jurassic shallow marine/bay 'Roabiba Sandstone Formation' reservoir
- D. Late Cretaceous Succession
- E. Late Paleocene Sand-Prone Member turbidite clastic reservoirs
- F. NGLG carbonates (Faumai Formation and Kais Limestone Formation)

For the first time, this hydrocarbon exploration technique will be applied to the capture, injection, and sequestration/storage of CO₂ in the Bird's Head area of Papua, Indonesia to numerically quantify the ESSCI rating and ranking process. The quality and quantity of the datasets for each potential ESSCI strata (eg. environmentally-sustainable strata for CO₂ injection and sequestration/storage) is evaluated and discussed below, prior to applying the 'degree of confidence factor for geological expression' matrix technique to numerically rate them.

The GEODISC project, a consortium of academic, government, and industry researchers concentrating on CO₂ injection and disposal in Australia, devised a screening process to systematically risk and rank prospective CO₂ injection and disposal sites by examining containment structure suitability, seal potential, and storage capacity (Bradshaw, et al., 2000; Cook, et al., 2000; Bradshaw and Rigg; 2001; Rigg and Bradshaw; 2001). The GEODISC group also investigated and evaluated geochemical interaction of CO₂ with various fresh and brine waters, CO₂ mineralogical trapping, and other critical aspects of CO₂ disposal (Rigg, et al., 2001).

However, the results of the GEODISC screening process were never quantified mathematically vis-à-vis probabilistic confidence matrices.

This study develops a mathematical approach, whereby, the ‘degree of confidence factor for geological expression’ matrix technique (borrowed from hydrocarbon exploration techniques) is used to evaluate the degree of confidence for a successful geological outcome for CO₂ injection and sequestration/storage by applying the matrix to the following criterion; in the following order:

1. Ranking of reservoir strata for the degree of confidence of a successful geologic outcome of CO₂ injection and sequestration/storage.
2. Ranking of structural traps for the degree of confidence of a successful geologic outcome of CO₂ injection and sequestration/storage.
3. Ranking of seal potential for the degree of confidence for a successful geologic outcome of CO₂ injection and sequestration/storage.
4. Ranking of storage capacity for the degree of confidence of a successful geologic outcome of CO₂ injection and sequestration/storage.
5. Ranking of distance for the degree of confidence of a successful economic outcome of CO₂ injection and sequestration/storage.

The numerical rankings of this criterion from the unique, individual matrices are then factored to yield a final numerical rating value for each individual subsurface injection site, which corresponds to the overall degree of confidence for the successful geologic outcome of CO₂ injection and sequestration/storage at each potential ESSCI site.

8.1 Late Permian ESSCI Potential

The Late Permian succession comprises primarily fluvio-deltaic, fine-grained clastics, namely shales, siltstones, and occasional thin-bedded very-fine to fine grained sandstones.

The Late Permian datasets are from several Wiriagar Deep wells and a few Vorwata wells, and include interpreted seismic surveys, whole cores, sidewall cores, drill cuttings, wireline logs, and rarely formation pressure/fluid sampling tools (eg.

MDT, RCI, RFT) or drill-stem testing (DST) formation pressure and fluid sampling. All of the Tangguh area wells did not penetrate the Late Permian, some wells penetrated the top of the Late Permian sedimentary succession but reached a TD after a very short distance, and none of the wells actually drilled through the entire succession to the base Late Permian.

Seismic resolution is generally poor due to seismic energy scattering at shallower depths caused by the New Guinea Limestone Group (NGLG), and therefore offers little other useable geological data. Although of very poor resolution the seismic surveys have successfully interpreted a near-top Late Permian seismic reflector over major portions of the Tangguh area on the 2D and 3D surveys. This near-top Late Permian horizon has been used as a proxy for the Base Jurassic horizon in the Tangguh area in the 3D geo-cellular modeling. The interpreted seismic data also identified some high-angle, trans-Permian/Jurassic faults.

Some wells such as the V-10 did not penetrate the Late Permian at all (having TD in the Roabiba Formation), other wells such the WD-5 and V-5 drilled between 100 and 200 ft of Late Permian rocks only, while still others such as the WD-2 drilled almost 1000 ft of Late Permian without encountering the base (Figure 7.1 and 7.2). Cuttings samples are, therefore, mainly limited to the top-most interval of the Late Permian in the Tangguh area, and are of use mainly for wellsite lithology and hydrocarbon show descriptions and palynological dating.

Whole cores are very limited in the Late Permian succession with short intervals of Late Permian cored on the WD-2, WD-3, WD-6, WD-7, WD-8, V-1, V-2, and V-4 wells (Table 7.1). Of these eight wells with core, most cored the Permian accidentally when coring of the overlying Aalenian Sandstone Formation or Roabiba Sandstone Formation continued past the base of the Jurassic reservoirs (Figures 7.1 and 7.2). As a result most of the cores are concentrated in the top-most Late Permian and only a few wells obtained purpose drilled whole cores from Permian reservoirs.

Basic wireline logs were routinely run on wells that penetrated the Late Permian interval, however, since the interval was always encountered at TD there was always a large portion of 'rathole' where no log readings were obtained. Finally, wireline logging conveyed formation pressure/fluid sampling tools (eg. MDT, RCI, RFT) and full DSTs were rarely performed on Permian interval sandstone reservoirs. A single DST was carried out in a Late Permian sandstone reservoir on the WD-2

well, which was tight (Salo, 1996c), and two DSTs were carried out on the V-1 well in the Late Permian that were generally tight but eventually flowed 1.0 MMscfgd plus traces of condensate from several co-mingled thin-bedded sandstone reservoirs (Perry, 1997).

The sedimentology indicates that the Late Permian fluvio-deltaic channel sandstones encountered to date are of limited thickness and areal extent, and as a result, likely to have very small potential storage capacity for CO₂. The tight nature of the reservoirs, as evaluated in Chapter 7. RESERVOIR CHARACTERIZATION, suggest that injection into these tight, low permeability units would be difficult and, if successful, would yield very low injection volume rates, and also fracture the reservoir near the borehole, inducing formation damage.

With this limited dataset, the Late Permian fluvio-deltaic sandstone reservoirs are rated as having a 'moderate' quantity of data of moderate quality, indicating 'very bad' geologic chance for successful ESSCI CO₂ injection and sequestration. By applying the 'degree of confidence factor of geological expression for the success of CO₂ injection and sequestration' matrix technique to numerically rate it, the Late Permian reservoirs rates a 0.25 (Table 8.2) out on a zero to one scale (with 1.00 being the highest degree of confidence for sufficient data of good quality indicating a successful geological outcome for ESSCI CO₂ injection and sequestration).

8.2 Middle Jurassic Reservoir ESSCI Potential

The Middle Jurassic reservoirs consist primarily of the Aalenian Sandstone Formation and the Roabiba Sandstone Formation, both of which have an enormous dataset available for evaluation. The Middle Jurassic reservoir datasets include all Wiriagar Deep wells and Vorwata wells, plus two Ubadari area wells, and include extensive whole cores, rotary and percussion sidewall cores, drill cuttings, wireline logs including dipole sonic and formation pressure/fluid sampling tools. Reservoir formation pressure and fluid sampling from DSTs were carried out on almost all Tangguh area wells. Numerous palynological, ichnological, geo-chemical, reservoir character, petrographic, and mineralogical analyses have been carried out on Aalenian Sandstone Formation and the Roabiba Sandstone Formation samples. Additionally, this study carried out numerous new analyses on 3,000 ft of whole core and more than

Geologic data factor for suitable ESSCI reservoir characteristics

	very bad	bad	even	good	very good
plentiful	0.00	Cretaceous 0.25		0.75	1.00
enough	Kais 0.13	Paleocene Members 0.31		0.69	Roabiba 0.88
moderate	Permian 0.25	Ayot 0.38	0.50	0.63	Aalenian 0.75
poor	Faunai 0.38	0.44	0.50	0.56	0.63
very poor			0.50		

Index factors for confidence levels of suitable ESSCI geological data existence.
(After Nakanishi and Lang 2001)

Table 8.2: Data confidence factor matrix for ESSCI stratum in the Tangguh area. The quality and quantity of data for all potential ESSCI stratum are evaluated and then the suitability of each strata rated for ESSCI reservoir characteristics (after Nakanishi and Lang, 2001).

100 new whole core plugs, included the first digital photography of whole core sedimentological features, the first MICP analysis, SEM, bulk XRD, petrographic analysis, and poro-perm analysis. Generally more data is available for the Roabiba Sandstone Formation reservoir (at Wiriagar Deep and Vorwata wells), than is available for the Aalenian Sandstone Formation reservoir.

The greatest lack of data is the generally very poor seismic resolution, at the Mesozoic interval in the Tangguh area, on both the 2D and 3D seismic surveys. The interpreted high-resolution 3D seismic data has identified some high-angle faults in the Jurassic but interpreted horizon reflectors are limited to the base Late Cretaceous and near-Top Late Permian. The near-top Late Permian has been used as a proxy for the Base Jurassic horizon in the Tangguh area for 3D geo-cellular modeling purposes. Seismic resolution is generally poor due to seismic energy scattering at shallower depths caused by the New Guinea Limestone Group (NGLG), and therefore offers little other useable geological data.

In addition to the basic wireline logging tool suite being run, numerous specialty logging tools were run, including dipole sonic, FMI/FMS borehole imaging, magnetic resonance imaging, and formation pressure/fluid sampling tools (ie. MDT, RCI, RFT, etc.).

Drill-stem testing (DST) was also routinely carried out on Middle Jurassic reservoir intervals, which almost invariably flowed natural gas, except for WD-5 flowed minor gas with primarily water due to being on the GWC (Salo, 1997d-e).

The measurements of formation pressures by MDT and DST sampling/testing indicated two huge vertical natural gas columns of approximately 2000 ft each, in the Aalenian Sandstone Formation and the Roabiba Sandstone Formation reservoirs. Flow rates during DST testing commonly yielded gas flows of 30 to 40 MMscfgd from the Jurassic reservoirs for many of the wells (Salo, 1996c; Bulling, et al., 1998).

The lack of good seismic resolution introduces a certain amount of risk for potential ESSCI sequestration in either of the Middle Jurassic sandstone reservoirs. Although a detailed and comprehensive seals evaluation and a fault reactivation risk assessment were carried out, and are discussed in detail later in Part III, there is still some uncertainty regarding faults as conduits.

The sedimentological, ichnological, and palynological data indicates that the Tangguh area Middle Jurassic interval has two very thick, areally extensive shallow

sandstone reservoirs, the Aalenian Sandstone Formation (MJ-4) and the Roabiba Sandstone Formation (MJ-3 capped with an MJ-1/LJ-11 contiguous member) deposited during a series marine transgressions and progradations in a broad embayment during the Jurassic Period. Reservoir evaluation indicates fair to excellent porosity and permeability ranges, with the average character tending to good to very good, as discussed in Chapter 7. RESERVOIR CHARACTERIZATION. The reservoir quality of the Tangguh area Aalenian Sandstone Formation (MJ-4) and the Roabiba Sandstone Formation make them world-class reservoirs, not only for hydrocarbon production, but also as potential ESSCI sequestration strata.

The result is that the data quantity and quality for the Aalenian Sandstone Formation and Roabiba Sandstone Formation can't be rated as 'plentiful' (ie. all the data one could ever want to make a geologically-based decision). As a result, the Roabiba Sandstone Formation is rated as having 'enough' very good quality data that indicates that the geologic chance for successful ESSCI CO₂ injection and sequestration is 'very good'. Therefore, since the Roabiba has far better whole core coverage than the Aalenian, the Aalenian Sandstone Formation is rated as having a 'moderate' quantity of moderately good quality data that still, overall, indicates that the geologic chance for successful ESSCI CO₂ injection and sequestration is 'very good'.

On this basis, applying the 'degree of confidence factor of geological expression for the success of CO₂ injection and sequestration' matrix technique to numerically rate the Aalenian Sandstone Formation reservoir gives a 0.75 factor (Table 8.2) out on a zero to one scale. By applying the 'degree of confidence factor of geological expression for the success of CO₂ injection and sequestration' matrix technique to numerically rate the Roabiba Sandstone Formation reservoir gives a very high degree of confidence 0.88 factor (Table 8.2) on a zero to one scale (with 1.00 being the highest degree of confidence for sufficient data of good quality indicating a successful geological outcome for ESSCI CO₂ injection and sequestration).

8.3 Late Cretaceous Reservoir ESSCI Potential

The Late Cretaceous succession comprises primarily marine marls and carbonates in the Wiriagar Deep area, and carbonates interbedded with several, very-fine grained arkosic and kaolinitic sandstones/siltstones in some Vorwata areas

(particularly V-1, V-2, V-6, and V-9). The Late Cretaceous marls and carbonates are argillaceous to very argillaceous carbonates grading into marl, and have occasionally been misinterpreted at wellsite as ‘very calcareous shales’. The Late Cretaceous marls and carbonates are both a potential reservoir unit and a potential sealing unit.

The Late Cretaceous datasets include interpreted seismic surveys, whole cores, sidewall cores, drill cuttings, wireline logs, and rarely formation pressure/fluid sampling tools (eg. MDT, RCI, RFT) or drill-stem testing (DST) formation pressure and fluid sampling.

The Late Cretaceous seismic survey data in the Tangguh area is generally of poor resolution on both the 2D, and 3D, seismic surveys although it is significantly better than the very poor resolution of the Jurassic and Permian intervals. The base Late Cretaceous is an interpreted horizon with fair to good resolution in most of the Tangguh area. Seismic resolution is relatively poor in the Late Cretaceous succession due to seismic energy scattering at shallower depths, mainly in the vuggy and fractured NGLG carbonates.

All of the available Late Cretaceous whole cores are from several Wiriagar Deep wells (WD-3, WD-4, WD-6, and WD-7), and no whole cores were obtained on Vorwata wells. Drill cuttings were available from all wells in the Tangguh area since no lost circulation problems were present in the Late Cretaceous hole sections.

Palynological analysis was routinely performed on cores and cuttings, and several geo-chemical, petrographic, and mineralogical analyses were carried out on Late Cretaceous samples (whole cores, sidewall cores, and cuttings) by ARCO.

The Late Cretaceous succession is rated as having ‘plentiful’ quantity of good quality data that indicates that the geologic chance for successful ESSCI CO₂ injection and sequestration is ‘bad’. By applying the ‘degree of confidence factor of geological expression for the success of CO₂ injection and sequestration’ matrix technique to numerically rate the Late Cretaceous Succession reservoir gives a 0.25 factor (Table 8.2) on a zero to one scale (with 1.00 being the highest degree of confidence for sufficient data of good quality indicating a successful geological outcome for ESSCI CO₂ injection and sequestration).

8.4 Late Paleocene Sand-Prone Interval ESSCI Potential

The Late Paleocene succession, in the Wiriagar Deep area, is comprised of

predominantly deep-water shales, labeled the Mud-prone Member, and a lower sand-rich succession, labelled the Sand-Prone Interval. The Sand-Prone interval is in turn divided into a LM, MM, and UM (based on stratigraphic position). The sandstone reservoirs of the Sand-Prone interval are charged with over-pressured natural gas in Wiriagar Deep, but are not hydrocarbon charged at the Vorwata area. Therefore, because the Wiriagar Deep reservoirs are commercially significant, a relatively large dataset has been gathered on it, whereas at Vorwata, where there is no commercial accumulation discovered to date, the data set is extremely sparse. The Late Paleocene LM, MM, and UM at Wiriagar Deep, are all shelfal turbidite fans or channels (R. Lowe, personal communication, 2001; Lowe, 1998). Although they are often discontinuous, and lacking connectivity, the LM, MM, and UM are ESSCI evaluated collectively.

The 3D seismic survey over the Tangguh area, has been depth converted and interpreted in the Late Paleocene at Wiriagar Deep area, with very good results. Seismic resolution is fair to good, although still impacted by the scattering of seismic energy due to the relatively thick, overlying Eocene-Miocene carbonate sequence (NGLG). Very little interpretation has been done on the seismic data at the Vorwata area due to the non-commerciality of the interval at that location. Similarly, extensive whole cores have been taken in the reservoir, and occasionally some sealing unit, lithologies at Wiriagar Deep, but no whole cores have been taken at Vorwata area. Drill cuttings are available at Vorwata, but apart from palynological analysis no other empirical analysis or study has been carried out.

Extensive wireline logging suites have been run over the hydrocarbon reservoir intervals at Wiriagar Deep, but only the basic logging suite has generally been run at Vorwata area wells. Extensive wireline logging suites include dipole sonic, FMI/FMS borehole imaging, rotary sidewall core, magnetic resonance imaging, and formation pressure/fluid sampling tools (ie. MDT, RCI, RFT, etc.), in addition to the basic wireline log data acquisition.

Finally, the Late Paleocene gas-charged reservoirs at Wiriagar Deep, were routinely drill-stem tested (DST) and combined with the MDT/RCI data provided an excellent dataset on reservoir temperatures, pressures, and fluid compositions.

Therefore, the Late Paleocene datasets are inclusive of both the 'plentiful' Wiriagar Deep area set and the 'moderate' Vorwata area set. Collectively, these

datasets were judged to be ‘enough’ on the basis of quantity and quality to evaluate the reservoirs for potential ESSCI CO₂ injection and sequestration/storage in the Vorwata area. Evaluation of the data indicates limited potential storage capacity, uncertainty over faults acting as conduits for migration to the overlying Kais Formation at Wiriagar Deep, and uncertainty regarding the connectivity between the LM, MM, and UM turbidite sandstone reservoirs, the geological suitability of the interval clastic reservoirs for successful CO₂ was deemed to be ‘bad’. By applying the ‘degree of confidence factor of geological expression for the success of CO₂ injection and sequestration’ matrix technique to numerically rate the Late Paleocene Sand-Prone Interval reservoirs gives a 0.31 factor (Table 8.2) on a zero to one scale (with 1.00 being the highest degree of confidence for sufficient data of good quality indicating a successful geological outcome for ESSCI CO₂ injection and sequestration).

8.5 New Guinea Limestone Group ESSCI Potential

The New Guinea Limestone Group (NGLG), is pervasive throughout the island of New Guinea, but the character and nature of the NGLG members at the Tangguh area is poorly understood due to a significant lack of data.

8.5.1 NGLG Lack of Data

The thick NGLG carbonate sequence, in the Berau/Bintuni Basins, is a massive lost-circulation zone. More than 26 out of 30 wells that have penetrated the entire Tertiary section in Bintuni Basin have had totals to near-total losses in circulation whilst drilling. This presents a dearth of data over of the interval. Little, if any, drill cuttings were successfully lagged to surface. Wireline logging operations became difficult in most of these boreholes, which required constant ‘topping-up’ with drilling fluid to minimize the risk of deadly H₂S gas blowouts.

The complete loss of circulation can be traced to the vuggy and fractured nature of the NGLG carbonates. This has been verified by the FMI/FMS images obtained with great difficulty on a handful of wells in the area and by coherency images from the 3D seismic survey dataset, at various levels within the Kais and Faumai formations of the NGLG (see Figures 5.30 through 5.36) clearly showing massive fracturing, dissolution cavities, and vugs. This loss of circulation during

drilling has resulted in little physical rock sampling of the NGLG, obtained either through drill cuttings or whole core. The lack of fluids in the borehole due to lost-circulation also resulted in very limited wireline logging on wells penetrating the NGLG formations. This lack of data presents a high degree of risk, and relatively low confidence, for the use of the NGLG members as potential ESSCI CO₂ sequestration/storage sites, especially the Kais and the Faumai Formations.

8.5.2 NGLG Non-suitability as ESSCI Sequestration Sites for CO₂ Due to Insufficient Depleted Field Storage Capacity

The shallow Wiriagar Field (retrograde condensate), and the Mogoi-Wasian Fields are all mature production fields that are either still lingering in production, or have been shut-in recently due to high water cut volumes. They are all unsuitable, however, for Tangguh Project CO₂ sequestration, as discussed previously.

Firstly, they are both extremely small in ‘original oil in place’ volume, therefore, the ‘value-added’ additional recoverable reserves are negligible. Furthermore, the proven containment area of the potential storage volume being extremely small renders the potential volume of injected and sequestered CO₂ as extremely small, unless the ESSCI is filled beyond the OOIP oil/water contact, which then renders the site as extremely high risk. These small volumes these shallow fields could each potentially sequester, with minimal containment risk, is so limited that further CO₂ injection and sequestration sites would still need to be identified and then developed. Even together, or added to the third ‘almost-depleted’ field in the region, they are still not viable as CO₂ injection/sequestration sites, based on the data available.

8.5.3 NGLG Nonsuitability as ESSCI Strata Due to Supercritical Phase Instability at Shallow Depths

The top-most Kais Formation is probably the best documented NGLG interval, in terms of rock samples, wireline logs, and seismic survey datasets, since the lost-circulation zone is generally in the mid to lower Kais Formation at Tangguh. Furthermore, very little data has been obtained from the overlying seal cap-rock (Steenkool Formation) in terms of cores (none) or wireline logs (basic logging suites

circa 1970 to 1990 only). The data that is available, however, is unfavorable for CO₂ containment confidence.

As previously discussed, the top Kais Limestone Formation is quite shallow ranging in subsurface depth from 1530 ft (Wiriagar Retrograde Condensate Shallow) to 2700 ft (Salawati Basin oil and gas fields), which effectively precludes them from being potential CO₂ ESSCI strata because in-situ reservoir pressures above 2600 ft are insufficient to keep an injected CO₂ column in a ‘supercritical phase’.

The increased CO₂ density when in a supercritical state, allows a greater CO₂ volume to be sequestered in the containment area, and also reduces the buoyancy pressure exerted on the base seal. Formation water salinity studies (Isworu, H., 2002) support the conclusion that there is widespread communication between the massively thick Faumai Formation and the Kais Limestone Formation (Figure 8.1). Therefore, the only effective seal for the entire NGLG is the Steenkool Formation, the formation overlying the NGLG’s top-most member, the Kais Limestone Formation.

Therefore, the dataset for the NGLG/Steenkool reservoir/seal couplet is subjectively rated as ‘poor’ at the Oligocene Carbonate and Faumai Formation intervals, and ‘enough’ at the Kais Formation. And, both the ‘poor’ and the ‘enough’ datasets indicate that geological data factor for suitable ESSCI characteristics is ‘very bad’ (ie. unsuitable). By applying the ‘degree of confidence factor of geological expression for the success of CO₂ injection and sequestration’ matrix technique to numerically rate the Faumai Formation reservoir gives a 0.38 factor (Table 8.2) on a zero to one scale, and by applying the matrix technique to numerically rate the Kais Formation reservoir gives a 0.13 factor (Table 8.2), due to the extremely high risk for CO₂ breaching of the Steenkool seal, and the very shallow depth of potential containment.

8.6 ESSCI Stratum Rating and Ranking

The ‘confidence factor rating for geological expression of success’ matrix technique was first expounded on by Rose in AAPG Explorer (2001), and has since been widely applied by oil and gas exploration companies, such as Peter Carragher, Manager of BP’s Portfolio Management Design and Implementation Team, and Glen McMaster, BP’s Risk Assessment Prospect Quality Petroleum Geologist, utilizing this technique to rank the quantity/quality factor level of geological data sets within BP-Amoco from

a hydrocarbon prospecting perspective (personal communication Nakanishi, 2002). However, this technique, already widely used in hydrocarbon prospecting and appraisal, is equally applicable to CO₂ injection and sequestration/storage studies. This study applies this technique, for the first time, to the probabilistic evaluation and data confidence ranking of the Tangguh area gas field dataset for CO₂ injection and sequestration/storage.

The strata tabulated above have been evaluated and placed within the ‘level of confidence’ matrix in Table 8.2. This result has then been tabulated by relative ranking in list format, and can be seen in Table 8.3. Only the Middle Jurassic ‘Roabiba’ and ‘Aalenian’ estuarine sandstone reservoirs rank >70 percentile for ESSCI reservoir suitability (Table 8.2 and Table 8.3). Both actually rank quite high on the *level of confidence for dataset quantity and quality* factoring to geologically characterize the Tangguh area strata for long-term, environmentally safe CO₂ sequestration/storage suitability. The Aalenian reservoir rank was 0.75, and the Roabiba reservoir was 0.88 on a scale “0.00” to “1.00”, where the “1.00” represents the highest degree of confidence of success for the potential sequestration of CO₂, and “0.00” represents the highest degree of confidence in an unsuccessful outcome for CO₂ sequestration. Matrix factor values less than 0.50 indicate either a high degree of confidence for an unsuccessful geological outcome, or a lack of sufficient data quantity or quality to confidently evaluate the outcome from a probabilistic perspective.

In summary, the Roabiba Sandstone Formation ESSCI reservoir rating of 0.88 is very good, and Aalenian Sandstone Formation ESSCI reservoir rating of 0.75 is the second highest degree of confidence factor rating for CO₂ injection and sequestration/storage in the Tangguh area. These are the two ESSCI reservoirs that will be evaluated in further detail for structural trap confidence, top and lateral seal potential, and finally overall stratum/trap/seal set maximum storage capacity.

Intervals Rated	Data Index Confidence Rating
Middle Jurassic Roabiba	0.88
Middle Jurassic Aalenian	0.75
Faunai	0.38
Paleocene Sand-Prone Upper Member	0.31
Paleocene Sand-Prone Middle/Lower Members	0.31
Cretaceous	0.25
Permian	0.25
Kais	0.13

Table 8.3: Table showing results of data confidence factor matrix for ESSCI stratum in Tangguh area. Only the Middle Jurassic reservoirs rate above the 0.50 percentile.

9.0 ESSCI STRUCTURE EVALUATION

Three subsurface trapping mechanisms have been considered for potential containment of CO₂, structural traps, stratigraphic traps, and hydrodynamic traps. Known stratigraphic traps, are unproven, as are hydrodynamic traps, in the Tangguh area. However, structural traps are proven through hydrocarbon accumulations at Tangguh. Furthermore, the hydrodynamics in Bintuni Basin, although poorly understood, suggest that the Jurassic hydrodynamic gradient drives water from the deep basin center towards the gentle dipping western margin of the basin. This produces water migration in Jurassic aquifers as predominantly east to west on the gently dipping western basinal margin. Although this would a high-risk mechanism on its own for subsurface trapping of CO₂, it can perhaps influence potential subsurface CO₂ migration paths.

Therefore, structural traps are the best trapping mechanism, particularly for proposed injection locations on the eastern flank of structures on the western basinal margin. Hydrodynamic gradients could influence injected CO₂ (along with possible reservoir pressure depletion from production of natural gas) to migrate westward and updip into a known, proven, deleted structural trap. Therefore, potential structural traps in the Tangguh area were evaluated for the highest level of confidence, and lowest risk, as long-term subsurface geological trapping mechanisms for CO₂ sequestration. The traps are either dip-closed or combination dip-closure and fault bounded traps. The structural traps evaluated included:

1. Vorwata
2. Wiriagar Deep
3. Ubadari
4. Roabiba
5. Ofaweri
6. Kalitami
7. Wos
8. Saritu

The major structural traps in the Tangguh area have been evaluated for data quality and quantity level of confidence expression in geological characterization.

Having ranked the level of confidence for evaluation of the various datasets first by *strata*, while using a 0.70 cut off for suitability of strata, the major structural trap datasets are evaluated for CO₂ sequestration/storage suitability in the best ranked of the ESSCI strata. Structural traps in the Tangguh area were evaluated using essentially the same methodology as in the preceding chapter for ESSCI strata evaluation. The location of the various structural traps considered in map view is shown in Figure 9.1.

Table 8.1, from the previous section, illustrates the ‘degree of confidence factor for geological expression’ matrix technique for a given attributes geological suitability for CO₂ injection and sequestration. A brief description of the various structural data quality and quantity is presented below prior to applying the matrix factor technique.

9.1 Vorwata Structure

The Vorwata structure is a NW-SE trending three-way dip anticlinal structure plunging to the SE (Bulling, et al., 1998). There is a E-W trending truncation of the Middle Jurassic sandstone reservoirs to the north of the structural closure that is probably due to a combination of depositional onlap and subsequent northly uplift and erosion (Livsey and Perkins, 1993). There is a E-W trending truncation of the Middle Jurassic sandstone reservoirs to the north of the structural closure that is probably due to a combination of depositional onlap and subsequent northly uplift and erosion (Livsey and Perkins, 1993). Vorwata, at the Jurassic level, is approximately 28 km long and more than 20 km wide. The structure encloses 150,000 acres, of which 78,00 acres contain gas (Bulling, et al., 1998).

The structure is apparently filled to the spill-point to the SE at approximately - 13,200 ft TVDss, as tested by the Vorwata #10 well. The gas accumulation is determined as any reservoir rock above the gas-water contact (GWC), which was defined as reservoir rock with adequate porosity above the free-water level (FWL). The porosity cut-off used was >5% effective porosity, based on petrophysical analysis and mapping (Bulling, et al., 1998).

Vorwata structure has abundant quantity of data of generally very good quality at the Mesozoic level. The data consisting of extensive whole cores, rotary and percussion sidewall cores, drill cuttings, wireline logs including dipole sonic and

formation pressure/fluid sampling tools through the primary reservoir interval, the Roabiba Sandstone Formation (the Aalenian Sandstone Formation is not present at the Vorwata area). Reservoir formation pressure and fluid sampling from DSTs were carried out on almost all Vorwata wells. Numerous palynological, ichnological, geochemical, reservoir character, petrographic, and mineralogical analyses have been carried out on the Roabiba Sandstone Formation whole core and cuttings samples. Additionally, this study carried out numerous new analyses on the aquifer leg of the Vorwata #10 well, including the first digital photography of whole core sedimentological features, the sampling of new whole core plugs, the first MICP analysis of the Pre-Ayot Shale cap-rock seal, SEM, bulk XRD, petrographic analysis, and poro-perm analysis. Generally more data is available for the Roabiba Sandstone Formation reservoir (on both the Wiriagar Deep and Vorwata wells), than is available for the Aalenian Sandstone Formation reservoir.

Specialty logging tools were run, in addition to the basic wireline logging tool suite, including dipole sonic, FMI/FMS borehole imaging, magnetic resonance imaging, rotary sidewall coring, and the MDT formation pressure/fluid sampling tools.

Drill-stem testing (DST) was also routinely carried out on many Vorwata wells, all of which almost invariably flowed natural gas from the Roabiba Sandstone Formation. Those wells that had no DST carried out were pressure/fluid sampled by wireline MDT, such as the V-9 well (Salo,1998). DSTs commonly flowed at their tubing restricted maximum flow rate of 36 to 39 MMscfd, such as the Vorwata #4 with almost 37 MMscfd from the Roabiba Sandstone Reservoir (Salo, 1997g).

The reservoir and seal data available, particularly in the aquifer leg on the down dip eastern flank of the structure (V-10) where CO₂ injection might potentially take place for sequestration in the Vorwata structure, is considered to be 'plentiful' quantity and quality for the Middle Jurassic Roabiba Sandstone Formation. Furthermore, the 'plentiful' very good quality data indicates that the geologic chance for successful ESSCI CO₂ injection and sequestration is 'very good'. Therefore, the Vorwata structure is rated "1.00" (Table 9.1) on a zero to one scale, when applying the 'degree of confidence factor of geological expression for the success of CO₂ injection and sequestration' in the Tangguh area.

9.2 Wiriagar Deep Structure

Wiriagar deep structure is a NW-SE trending four-way dip anticlinal structure plunging to the SE (Bulling, et al., 1998). Wiriagar Deep, at the Jurassic level, is approximately 105 km long, although the structural trap for the gas accumulation is 25 km long and more than 10 km wide, with 2000 ft of vertical subsurface relief at the SW limb, and 4000 ft of subsurface relief at the NE limb (Bulling, et al., 1998).

The main Wiriagar Deep structural closure is filled to spill-point with gas on the SW limb, and is in communication with a related adjacent structure called the “P-structure”. The P-structure is WNW to ESE fault bounded (to the north) and dip closed structure plunging to the ESE. The structure is 15 km long and 4 km wide with approximately 800 ft of subsurface relief (Bulling, et al., 1998).

The main Wiriagar Deep and subsidiary P-structure are treated as one structural trap in this study. Together the two structures enclose 38,000 acres gas. filled to the spill-point, although it should be noted that the gas accumulation is determined as any reservoir rock above the GWC, which was defined as reservoir rock with adequate porosity above the FWL (Bulling, et al., 1998). The porosity cut-off used was >5% effective porosity, based on petrophysical analysis and mapping (Bulling, et al., 1998).

The Wiriagar Deep structure has abundant quantity of data rated as generally good quality at the Mesozoic level. The Mesozoic interval at Wiriagar Deep has two potential ESSCI reservoirs that made the ESSCI strata matrix factoring cut-off, the Aalenian Sandstone Formation and the Roabiba Sandstone Formation. The available data consists of extensive whole cores, rotary and percussion sidewall cores, drill cuttings, wireline logs including dipole sonic and formation pressure/fluid sampling. Reservoir formation pressure and fluid sampling from DSTs were carried out on almost all Wiriagar Deep wells. Numerous palynological, ichnological, geo-chemical, reservoir character, petrographic, and mineralogical analyses have been carried out on both the Aalenian Sandstone Formation and Roabiba Sandstone Formation whole core and cuttings samples. Generally more data is available for the Vorwata wells than the Wiriagar Deep wells. Specialty logging tools were run, in addition to the basic wireline logging tool suite, including dipole sonic, FMI/FMS borehole

Geologic data expression for structures suitable for CO₂ storage

	very bad	bad	even	good	very good
plentiful	0.00	0.25	X	0.75	Vorwata 1.00
enough	0.13	0.31	X	Roabiba Ubadari 0.69	Wiriagar Deep 0.88
moderate	0.25	0.38	0.50	0.63	0.75
poor	Kalitami 0.38	0.44	Wos 0.50	Ofaweri 0.56	0.63
very poor	X	X	Saritu 0.50	X	X

Index factors for confidence levels of suitable ESSCI geological data existence.

(After Nakanishi and Lang 2001)

Table 9.1: Data confidence factor matrix for potential ESSCI structures in Tangguh area, only Vorwata, Wiriagar Deep, Roabiba, and Ubadari structures rate approximately 0.70 or better for suitability as ESSCI CO₂ storage sites (modified after Nakanishi and Lang, 2001)

imaging, magnetic resonance imaging, rotary sidewall coring, and the MDT formation pressure/fluid sampling tools. Drill-stem testing (DST) was also carried out on all Wiriagar Deep wells, most of them flowing natural gas from the Aalenian Sandstone Formation and Roabiba Sandstone Formation, except for the WD-5 which was wet (Salo, 1997d and 1997e).

The Wiriagar Deep structure dataset is considered to be of ‘enough’ quantity and quality for the Middle Jurassic reservoir appraisals for successful ESSCI CO₂ injection and sequestration. Furthermore, the data indicates that the geologic chance for successful ESSCI CO₂ injection and sequestration is ‘very good’. Therefore, the Wiriagar Deep structure is rated “0.88” (Table 9.1), on a zero to one scale where one is the highest degree of confidence, and zero is the lowest degree of confidence, when applying the ‘degree of confidence factor matrix’.

9.3 Ubadari Structure

The Ubadari structure is a NW-SE trending three-way dip and fault bounded (to the SSW) anticlinal structure gently plunging to the SE (Bulling, et al., 1998). The gas field Ubadari structure, at the Jurassic level, is approximately 12 km long and almost 4 km wide, with 600-800 ft of vertical subsurface relief. The area of the closure is approximately 8000 acres (Bulling, et al., 1998).

The Ubadari structure has limited quantity of data of generally good quality at the Mesozoic level. Ubadari structure has had only two wells drilled on it, and each of them were located on different fault blocks, greatly offset from each other. The U-1 tested abundant gas from multiple Aalenian and Roabiba sandstone sequences, and the U-2 was wet, with no hydrocarbons encountered (Bulling, et al., 1998).

The available data for the U-1 consists of some whole cores, although the entire reservoir interval was not cored. No cores were taken on the U-2 well. Both wells have rotary and percussion sidewall cores, drill cuttings, wireline log (including dipole sonic and formation pressure/fluid sampling) datasets available. Some palynological and ichnological, analyses was carried out on both Ubadari wells. Generally the data available for each side of the fault block at Ubadari structure is limited to the single well penetrating it, however it is considered ‘enough’ data of good quality to make a judgment regarding the suitability of the structure as a ‘good’

potential ESSCI CO₂ injection and sequestration site at the natural gas charged compartment, to the north of the bisecting structural fault.

Therefore, the natural gas charged compartment of the Ubadari structure is rated “0.69” (Table 9.1), on a zero to one scale where one is the highest degree of confidence, and zero is the lowest degree of confidence, when applying the ‘degree of confidence factor matrix’ technique.

9.4 Roabiba Structure

The Roabiba structure is a small fault bounded pop-up structure located on SE trending flank of the Wiriagar Deep anticlinal structure (Bulling, et al., 1998). The Roabiba structure is approximately 6 km long and 2 km wide, with 900 ft of vertical subsurface relief (Bulling, et al., 1998). The gas accumulation extent and volume is based on the single well drilled to date on the structure due to the lack of seismic resolution of the structure (Bulling, et al., 1998). Petrophysical analysis suggests there is 271 ft of net vertical pay at Roabiba structure (Bulling, et al., 1998).

The Roabiba structure has limited quantity of data of generally fair to good quality at the Mesozoic level. The Roabiba structure has had only a single well drilled on it, the Roabiba #1 (R-1).

The available data for the R-1 consists of drill cuttings, since the Mesozoic reservoir interval was not cored. The well has no rotary sidewall cores (only percussion sidewall cores), and fairly basic wireline log data (no dipole sonic or formation pressure/fluid sampling) available. Palynological analyses were carried out on the well by Robertson Research (Wall, et al., 1990).

The Mesozoic reservoirs, the Aalenian Sandstone Formation and the Roabiba Sandstone Formation, are contiguous and in connection with each other at the R-1 well location, with no intervening shale break between them, to act as a barrier or baffle. This reservoir was DST tested, and flowed natural gas at almost 24 MMscfd (Perkins and Livsey, 1993).

Generally the data available for the Roabiba structure is limited, however it is considered ‘enough’ data of fair to good quality to make a judgment regarding the suitability of the structure as a ‘good’ potential ESSCI CO₂ injection and sequestration site at the natural gas charged compartment, to the north of the bisecting structural fault.

Therefore, the natural gas charged compartment of the Roabiba structure is rated, when applying the ‘degree of confidence factor of geological expression for the success of CO₂ injection and sequestration’ matrix technique to numerically rate the trapping structures in the Tangguh area at a factor of “0.69” (Table 9.1), on a zero to one scale where one is the highest degree of confidence, and zero is the lowest degree of confidence.

9.5 Ofaweri Structure

The Ofaweri structure is a small three-way dip closure structure, with fault assist, located on SW flank of the Wiriagar Deep anticlinal structure (Bulling, et al., 1998). The Ofaweri structure trends NW-SE and is approximately 11 km long and 5 km wide, with approximately 1600 ft of vertical subsurface relief (Bulling, et al., 1998). The gas accumulation volume is based on well data from the sole well drilled to date on structure due to poor seismic resolution over the structure. Petrophysical analysis suggests 260 ft of net vertical pay (Bulling, et al., 1998).

The Ofaweri structure has limited quantity of data of generally fair quality at the Mesozoic level. The Ofaweri structure has a single well drilled to date, the Ofaweri #1 (O-1). The available data for the O-1 consists of drill cuttings, since the Mesozoic reservoir interval was not cored. The well has no rotary sidewall cores (only percussion sidewall cores), and fairly basic wireline log data. The Middle Jurassic reservoir was not DST tested, although there is pressure and fluid sampling data available from a wireline RFT.

Generally the data available for the Ofaweri structure is extremely limited, and as such, is considered a poor quantity dataset of fair quality, yielding overall a ‘poor’ data quantity/quality to make a judgment regarding the suitability of the structure as potentially a ‘good’ ESSCI CO₂ injection and sequestration site.

Therefore, the Ofaweri structure is rated, when applying the ‘degree of confidence factor of geological expression for the success of CO₂ injection and sequestration’ matrix technique to numerically rate the trapping structures in the Tangguh area at a factor of “0.56” (Table 9.1), on a zero to one scale where one is the highest degree of confidence, and zero is the lowest degree of confidence.

9.6 Wos Structure

The Wos structure is a small pop-up, fault-bounded ‘flower’ structure, which is approximately 5 km long and 2 km wide trending WNW to ESE. The structural closure is estimated only from fair quality, vintage, well data. The structure is thought to be a gas accumulation based on gas samples recovered from RFT (repeat formation tester wireline tool) only (Bulling, et al., 1998). Petrophysical analysis suggests that there is 267 ft of net vertical pay in Wos (Appendix 2).

The Wos structure has limited quantity of data of generally fair quality at the Mesozoic level. The Wos structure has had a single well drilled to date, the Wos #1 (W-1).

The available data for the W-1 consists of drill cuttings, since the Mesozoic reservoir interval was not cored. The well has fairly basic wireline log data and no rotary sidewall cores (only percussion sidewall cores). Palynological analyses was carried out on the well (Waton, et al., 1998g), as was MICP on drill cuttings of the overlying seal cap-rock (Salo, 1998; unpublished data). The reservoir was not DST tested, nor is any Mesozoic reservoir formation pressure/fluid sampling data available from wireline logging tools, however mudlog gas detector readings and petrophysical analysis of wireline logs indicate that the structure is hydrocarbon charged with natural gas. This provides some indirect evidence to support the supposition of adequate seal and trap at the W-1 location.

Generally the data available for the Wos structure is extremely limited, and as such, is considered a poor quantity dataset of fair quality, yielding overall a ‘poor’ data quantity/quality to make a judgment regarding the suitability of the structure as only potentially ‘even’ for successful ESSCI CO₂ injection and sequestration at this site. Therefore, the Wos structure is rated “0.50” (Table 9.1), on a zero to one scale where one is the highest degree of confidence and zero is the lowest degree of confidence, when applying the ‘degree of confidence factor matrix’.

9.7 Kalitami Structure

The Kalitami structure is an elongate NNW to SSE trending anticlinal feature that amalgamates with the Ubadari structure to form the Sekak Ridge. The Kalitami structure is approximately 45 km long and 20 km wide, the long axis of which is 22 km from and parallel to the Ubadari axial crest. The depth and area of closure at the

Jurassic interval has not been mapped (Bulling, et al., 1998).

The Kalitami structure has limited quantity of data of generally fair quality at the Mesozoic level. The Kalitami structure has a single well drilled to date, the Kalitami #1X.

The available data for the K-1X consists of drill cuttings and fairly basic wireline log data. There were no conventional cores, rotary sidewall cores (only percussion sidewall cores), or DST. Palynological analyses was carried out on the well. Both the wellsite lithology logs and the wireline logs, combined with palynological analysis, indicate that there is Middle Jurassic sandstone reservoir present at K-1X location (Bulling, et al., 1998). Since all other structures in the area are gas charged (Figure 9.1) and the K-1X was wet, this suggests that there is potentially a problem with either trap or seal (or both) in the Kalitami structure.

Generally the data available for the Kalitami structure is extremely limited, and of very poor quantity, yielding overall a 'poor' data quantity/quality rating to make a judgment regarding the suitability of the structure as only potentially 'very bad' for successful ESSCI CO₂ injection and sequestration at this site. Therefore, the Kalitami structure is rated, at a factor of "0.38" (Table 9.1), on a zero to one scale where one is the highest degree of confidence, and zero is the lowest degree of confidence.

9.8 Saritu Structure

There is virtually no data regarding the Saritu, or 'S' structure since the structure has never been drilled. The only data available is seismic survey data of generally poor resolution at the Mesozoic level, due to the scattering effect of the shallow, massively bedded NGLG carbonate.

Therefore, the Saritu structure is really a flip of the coin. Seismic does yield reflectors, correlatable to surface horizons interpreted as Base Late Cretaceous and near-Top Late Permian. Therefore, it is rated, as simply "0.50" (Table 9.1), on a zero to one scale where one is the highest degree of confidence, and zero is the lowest degree of confidence. There is an equal probability that further data (from future well penetrations) could either prove or disprove the potential for this structure as an ESSCI storage site.

9.9 Ranking structural trap ESSCI potentials

The screening selection process has identified the Middle Jurassic Aalenian Sandstone Formation and the Roabiba Sandstone Formation as the ESSCI strata in Chapter 8. ESSCI STRATA EVALUATION with the highest success confidence for potential CO₂ injection and sequestration.. This assessment included the degree of confidence regarding the injectivity into the potential reservoirs based on available data quantity and quality.

Following that, the screening selection process continued with consideration of the potential structural traps containing Middle Jurassic reservoirs (since the Middle Jurassic reservoirs were the highest ranked potential ESSCI strata). The various structural traps in the Tangguh area, identified from seismic interpretation and well data, were subjectively analyzed for data quality and quantity regarding the degree of confidence for geologically evaluating success of potential long-term sequestration and containment of CO₂ from a ‘containment trap’ perspective. The structural traps, listed above with their relative ranking, appear within the appropriate matrix box in Table 9.1. These results have then been tabulated according to relative ranking in Table 9.2 in a descending list of confidence. Wos, Saritu and Kalitami structures do not make a >50 percentile cut-off, because Wos and Saritu ranked 0.50, and Kalitami a mere 0.38 out of a maximum 1.00 scale for highest degree of confidence. Furthermore, Ofaweri, Roabiba, and Ubadari fail a >70 percentile cut-off. Only the Wiriagar Deep and Vorwata structures have relatively high factors of geologic success for potential ESSCI CO₂ injection and sequestration, based on the subjective appraisal of data quality and quantity available at this time. Vorwata had the best factor at 1.00 (the maximum factor rating), and Wiriagar Deep was rated as 0.88.

Therefore, when considering the two Middle Jurassic reservoirs (the Aalenian Sandstone Formation and the Roabiba Sandstone Formation) as the best potential EESSCI reservoirs from a porosity, permeability and mineralogical standpoint, only the Vorwata (at 1.00) and Wiriagar Deep (0.88) structural traps possess a high degree of confidence, although the Ubadari and Roabiba structures only just fail the >0.70 cut-off with 0.69 factors. These high-graded structural traps, at the Middle Jurassic reservoir, will be evaluated further, for seal potential and storage capacity, in the following chapters.

Jurassic Interval By Structure	Data Index Confidence Rating
Vorwata	1.00
Wiriagar Deep	0.88
Ubadari	0.69
Roabiba	0.69
Ofaweri	0.56
Wos	0.50
Saritu	0.50
Kalitami	0.38

Table 9.2: Table summarizing the potential ESSCI structure data confidence factors matrix for Tangguh area.

10.0 ESSCI SEAL EVALUATION

This section will evaluate the seal potential in the Tangguh area, and rate the reservoir/seal couplets as potential CO₂ ESSCI sequestration sites. The results will then be intergrated with the results from the ESSCI strata matrix factoring and the ESSCI structure matrix factoring to produce a ranking product for degree of confidence for successful potential ESSCI CO₂ injection and sequestration.

10.1 Overview of Reservoir/Seal Couplets and Seal Potential

Reservoirs are defined as any porous and permeable lithology capable of containing fluids and/or gases (this definition includes aquifers). Seals are defined as any lithology capable of retaining a buoyant fluid or gas column. Seal potential is:

- 1) Seal capacity (the calculated CO₂ column height a given lithology can retain)
- 2) Seal geometry (the structural/stratigraphic position, thickness, and areal extent of a given seal lithology)
- 3) Seal integrity (the mechanical and physical properties of a given seal lithology including the rock ductility, compressibility, and propensity for fracturing)

The seal potential of any given lithology needs be evaluated not just by the sealing lithology itself, but as part of a reservoir and seal couplet. This is mainly because the determination of seal capacity is dependent on the capillary threshold pressure of both the reservoir and the seal being evaluated.

Both hydrocarbons and CO₂ exert an upward potential known as buoyancy (the density difference between water and hydrocarbons or water and CO₂). Buoyancy pressure is opposed by the capillary pressure of a lithology, based on the displacement pressure of the largest interconnected pore throats. That is, any given lithology can potentially be a sealing unit if the minimum displacement pressure of the largest interconnected pore throats is greater than the maximum buoyancy pressure exerted by hydrocarbons, CO₂, or any other fluid/gas with a density lower than that of the formation water (Schowalter, 1979; Sneider, 1987; Vavra, et al., 1992; Kaldi and Atkinson, 1993). The CO₂ seal capacity was measured in this study by performing mercury injection capillary pressure (MICP) analysis on both reservoir and seal samples.

In this study, the reservoir evaluated in the Tangguh area is the Middle Jurassic ‘Roabiba’ Reservoir. This includes both the Bajocian-early Bathonian Roabiba (sequence stratigraphic units R10 through R80) and the immediately overlying Callovian Roabiba (sequence stratigraphic units CU10 through CU50), which is present over the Vorwata anticlinorium but is absent at the Wiriagar Deep anticlinorium.

Several potential sealing units are present in the Tangguh area, as identified on the stratigraphic cross-sections of Figure 10.1A and 10.1B. An overlying marine shale deposited during a paleo-flooding event is present at the Vorwata structure as both a ‘top’ and ‘lateral’ seal to the Roabiba Reservoir. This is referred to as the ‘Pre-Ayot Shales’ (sequence stratigraphic units PA10, PA20, and basal shales of the PA30). However, these ‘Pre-Ayot Shale’ potential sealing units are absent over the Roabiba Reservoir at the adjacent Wiriagar Deep structure due to an erosional unconformity. The immediate ‘top’ and ‘lateral’ seals for the Roabiba Reservoir at the Wiriagar Deep anticlinorium are the overlying Ayot Limestone and the Upper Late Jurassic Shales. These two formations have relatively uniform thicknesses over a wide areal extent in the Tangguh region, and extend across both the Wiriagar Deep and Vorwata structures. The Ayot Limestone and Upper Late Jurassic Shales are the ‘top seal’ for the Roabiba Reservoir at Wiriagar Deep and a ‘regional seal’ at the Vorwata structure. Additional ‘regional seals’ for the Roabiba Reservoir, on both structures, are the Late Cretaceous marls and the Paleocene Mud-Prone Member. The seal potential for each of these sealing units, in relation to the Roabiba Reservoir, is analyzed and evaluated for this study. The complex relationship between these various potential seals and underlying reservoir due to the presence of an angular unconformity at the base of the Ayot Limestone Formation is illustrated in geological cross-sectional schematic Figure 10.2

Seal geometry is also analyzed and evaluated for each of the seals. An evaluation of the geometries includes analyses of the thicknesses and areal extent of the seal over the reservoir, and the homogeneity of the seal. Seal geometry analyses include wireline log data, data from core or drill cuttings, and the Mesozoic sequence stratigraphy framework of the Tangguh area constructed for this study.

An analysis of seal integrity includes determining the mechanical and physical properties of a given lithology including the rock ductility, compressibility, propensity for fracturing, and the risk of fault reactivation. The seal integrity for the various

sealing units is evaluated by incorporating the fault and fracture reactivation risks, based on geomechanical modeling by Hillis and Meyer (2003), with wireline log data (FMI/FMS), various analyses of representative sample plugs from whole core (XRD and SEM), descriptions of drill cuttings, and the detailed Mesozoic sequence stratigraphy of the Tangguh area including paleogeographic facies maps constructed for this study.

The integration of seal capacity, seal geometry, and seal integrity for the various potential seals for the Roabiba Reservoir in the Tangguh area are presented in the conclusions of this section.

10.2 Mercury Injection Capillary Pressure Methodology

A list of the core plugs/chips that were analyzed for mercury injection capillary pressure analysis is presented in Table 10.1, as are the interpreted Hg/air system entry and threshold pressures for each sample. All MICP samples were cut into cubes approximately 1 cm x 1 cm x 1cm, thoroughly cleaned, epoxy resinated on 5 of the 6 cube faces (with an original in-situ vertically oriented face left exposed), and then oven dried at 60° C for 72+ hours, prior to testing by the porosimeter.

A total of 37 core sample chips/plugs were prepared and analysed to investigate the sealing capacity and pore-throat aperture size distribution for seals and reservoir lithologies. Tests were performed using a Micromeritics Autopore-III mercury porosimeter. Other laboratory analyses included Helium porosity (He-Ø) and air permeability (Kair) for the 1” core plug samples. The 1.5” core plug samples were analysed for He-Ø and Kair with an 800 psia NOB (Net Over-Burden pressure), by Core Laboratories, Perth. Six representative reservoir samples had MICP analysis performed (in Table 10.1 reservoir samples with MICP analysis are shaded light blue). The remaining 31 MICP samples were considered seal lithologies representing the various ‘top’ and ‘regional’ seals discussed previously. All of the seal samples were derived from either whole core fragments of ~2” thickness, or from vertically drilled core plug (see Table 10.1, column header H/V with “H” = Horizontal to bedding and “V” = Vertical to bedding). Each MICP sample was tested up to a maximum of 60,000 psia. The definition of ‘Threshold Pressure’, in regard to MICP testing, is the pressure at which a continuous filament of mercury (Hg) intrudes the sample. The individual core plug/chip MICP results are graphed and presented as a

Well	Core Plug	Plug Depth	Core Plug	Lithology	H/V	Petrogr	SEM	XRD	MICP	He ϕ	Geochem	Unit	Facies	Entry P.	Threshold P.	Porosity	Permeability	REMARKS
Name	Depth (ft/m)	Shifted (ft)	TVD ss (ft)							+ Ka	Pyrolysis			MICP (psia)	MICP (psia)	(%)	(mD)	
WD2	7377'11"	7395'11"	7346.9	SH	V				1		1	PUM	Turb	752	9983			
WD2	7380'0"	7398'0"	7349.0	SH	V				1		1	PMM	Turb	239	5014			
WD2	8681'3"	699'3"	8650.3	SH	V				1		1	R30	Prograde	889	3520			
WD3	7548'9"	7556'9"	7507.8	SH	V				1		1	PMP	Turb	701	4994			
WD3	7549'2"	7557'2"	7508.1	SH	V				1		1	PMP	Turb	342	5983			
WD3	7552'7"	7560'7"	7511.6	SH	V				1		1	PMP	Turb	170	1726			
WD3	7558'8"	7566'8"	7517.8	SH	V				1		1	PMP	Turb	99	2480			
WD3	9238'0"	9248'0"	9199.0	LS/MRL	V				1		1	K	Marine	8	8540			
WD3	9272'1"	9282'1"	9223.0	LS/MRL	H				1		1	K	Marine	414	24894			
WD3	9274'1"	9284'1"	9225.0	LS/MRL	H				1		1	K	Marine	601	5000			
WD3	9286'2"	9296'2"	9247.1	LS/MRL	V				1		1	K	Marine	no penetration	no penetration			
WD3	9309'8"	9319'8"	9270.8	SH	V				1		1	K/LJSh	Marine	28	11949			
WD3	9325'0"	9335'0"	9286.0	SH	V				1		1	LJSh	Marine	339	9953			
WD3	9328'4"	9338'4"	9289.3	V. TUFF	V				1		1	LJSh	V.Ash?	9970	14448			
WD3	9344'1"	9354'1"	9305.0	LS/MRL	V				1		1	Ayot	ShallowM	11950	14470			
WD7	7962'6"	7972'6"	7922.5	SH	V				1		1	P/TopK	Marine	730	8471			
WD7	7981'6"	7991'6"	7941.5	LS/MRL	V				1		1	TopK	Marine	6968	11945			
WD7	8452'5"	8462'5"	8413.6	LS/MRL	V				1		1	Ayot	ShallowM	no penetration	no penetration			
WD7	8471'1"	8481'1"	8432.0	LS/MRL	V				1		1	Ayot	ShallowM	8507	14474			
WD7	8497'9"	8507'9"	8457.8	SH	V				1		1	R20	M.Sh	1029	5010			
V1	11790'9"	11800'9"	11751.8	SS	H	1	1		1	1		CU30	U. Sh	294	339	2.5	0.05	NOB 800psi
V1	11902'3"	11912'3"	11863.3	SH	V		1	1	1		1	R20	Fluv/Delt	339	20700			
V1	11904'3"	11914'3"	11865.3	SH	V		1	1	1		1	R20	Fluv/Delt	1000	5970			
V2	13020'6"	13033'6"	12984.5	SH	V		1	1	1		1	R20	U. Sh	1452	2936			
V2	13025'6"	13038'6"	12989.5	V. TUFF	V		1	1	1		1	R10	Fluv/Delt	706	1262			
V2	13030'1"	13043'1"	12994.0	SH	V		1	1	1		1	R10	Fluv/Delt	702	1439			
V7	13152'5"	13166'5"	13117.5	SS	H	1	1		1	1		CU30	M. Sh	3	5	10.7	131	NOB 800psi
V10st	3944.43	12941.7	12853.7	SH	V		1	1	1		1	PA30	Delta	598	4268			
V10st	3947.64	12952.2	12864.2	SH	V		1	1	1		1	PA30	Delta	8507	11951			
V10st	3954.46	12974.6	12886.6	SH	V		1	1	1		1	PA30	Delta	727	8496			
V10st	3965.57	13011.0	12923.0	SH	V		1	1	1		1	PA20	Shelf	4279	5971			
V10st	3966.82	13015.1	12927.1	SH	V		1	1	1		1	PA20	Shelf	1053	5975			
V10st	3967.10	13016.1	12928.1	SH	V		1	1	1		1	PA20	Shelf	705	8497			
V10st	4026.18	13209.9	13121.9	SS	H	1	1		1	1		R80	Foreshore	3	4	14.5	1080	NOB 800psi
V10st	4034.51	13237.2	13149.2	SS	H	1	1		1	1		R80	Foreshore	2	5	12.9	954	sc
V10st	4090.85	13422.1	13334.1	SS	H	1	1		1	1		R50	T. Ch.	2	8.5	11.3	5.89	NOB 800psi
V10st	4128.92	13547.0	13459.0	SS	H	1	1		1	1		R30	Prograde	3	5	15.7	475	NOB 800psi

Samples in red indicate analyses performed. Samples in black indicate analyses was proposed but not performed due to budgetary and/or time constraints.
NOTE: Blue-filled cell highlights reservoir core plug samples with MICP performed.

Table 10.1: Table of whole core plugs and chips that had MICP testing performed on them in a detailed Seals Potential evaluation for the Tangguh area.

part of Appendix 4: Core Plug/Chip Atlas (Figures 3 to 5; 7 to 10; 12 to 19; 23 to 27; 31; 33; 34; 45 to 47; 52 to 58; 65; 70; 92; and 99), with an arrow indicating the interpreted Hg/air system threshold pressure on the MICP graphs. This point on the curve (colored green) was picked using the least tangential method for the curve, in conjunction with the ‘incremental Hg pore intrusion volume’ (colored red on the graphs) as an aid in determining when a ‘continuous filament of Hg had intruded’. The ‘Threshold Pressure’ is labelled as “P(th)” on the graphs with the pressure value in psia noted next to it.

The initial increase in pressure during MICP analysis, and the usually small incremental volume of mercury associated with this increase in pressure, is often described as ‘conformance’. Conformance is the process whereby the initial increase in pressure causes the mercury (Hg) to fill surface irregularities on the rock sample, such as nicks, gouges, vugs, or small fractures. The pressure at which mercury first enters the actual pore system of the sample (after conformance) is called the ‘entry pressure’ or the ‘displacement pressure’. The pressure at which sufficient Hg to form a continuous filament enters the rock sample is termed the ‘threshold pressure’. It is the threshold pressure that is used to calculate the seal capacity of a rock.

An interactive Geochemical Website calculator, accessed through the CO₂CRC’s GEODISC website was utilized to convert the MICP results for an Hg/brine system to a supercritical CO₂/brine system (Ennis-King, 2003). This website calculator designed by Dr. Jonathan Ennis-King also calculates the density, viscosity, and viscosibility of the fluids and gases (in this case, brine and CO₂), as well as the theoretical interfacial tension. The program calculates conditions necessary for the CO₂ to remain in a supercritical state.

The capillary pressure conversion equations originally derive from Purcell’s equation (1949), which is:

$$P_{c_{b/hc}} = P_{c_{a/m}} \times \frac{\sigma_{b/hc} \cos \theta_{b/hc}}{\sigma_{a/m} \cos \theta_{a/m}}$$

Where:

- P_c_{b/hc}** = capillary pressure in the brine/hydrocarbon system in psi
P_c_{a/m} = capillary pressure in the air/mercury system in psi
σ_{b/hc} = interfacial tension angle of the brine/hydrocarbon system in dynes/cm
COS θ_{b/hc} = cosine of the contact angle in the brine/hydrocarbon system in degrees
σ_{a/m} = interfacial tension in the air/mercury system in dynes/cm
COS θ_{a/m} = contact angle in the air/mercury system in degrees

Note that the hydrocarbons in Purcell (1949) constitute the non-wetting phase. In converting MICP results from the air/mercury system to the brine/ CO₂ system, the CO₂ is similarly the non-wetting phase. Therefore, Purcell's equation must be rewritten for the brine/CO₂ system as follows:

$$P_{c_{b/co_2}} = P_{c_{a/m}} \times \frac{\sigma_{b/co_2} \cos \theta_{b/co_2}}{\sigma_{a/m} \cos \theta_{a/m}}$$

Where:

- P_c_{b/co2}** = capillary pressure in the brine/ CO₂ system in psi
P_c_{a/m} = capillary pressure in the air/mercury system in psi
σ_{b/co2} = interfacial tension angle of the brine/ CO₂ system in dynes/cm
COS θ_{b/co2} = cosine of the contact angle in the brine/ CO₂ system in degrees
σ_{a/m} = interfacial tension in the air/mercury system in dynes/cm
COS θ_{a/m} = contact angle in the air/mercury system in degrees

Example of the website calculator from screen captures are presented in Table 10.2, with the examples shown taken from the entrees for the Ayot Limestone and Upper Jurassic Shale regional seals.

An interactive Excel calculator spreadsheet (Table 10.3) created by the author (C. Gibson-Poole, personal communication, 2001) then calculates a maximum CO₂ column height through the following transform equation after Smith (1966): (Note that the degrees must be written in radians in MS-Excel, through formula: **PI()/180**).

$$H_{\max} = \frac{(P_{DS} - P_{DR})}{(\rho_b - \rho_{CO_2}) \times 0.433}$$

Where:

H_{max} = the maximum height of the non-wetting phase (CO₂) column before a continuous filament of CO₂ intrudes the largest pore throats (in feet)

P_{DS} = brine/CO₂ displacement pressure of the seal (in psi)

P_{DR} = brine/CO₂ displacement pressure of the reservoir (in psi)

ρ_b = density of the brine (in g/cm³)

ρ_{CO2} = density of the CO₂ (in g/cm³)

0.433 = gravity constant (also the gradient of fresh water in psi per foot)

The reservoir and seal in-situ pressures, temperatures, and salinity are based on data supplied by BP. Density of the brine in the saline reservoirs and overlying seals was based on salinity data acquired during DST tests which flowed formation water after a reasonable ‘clean-up period’ (Table 10.4). Reservoir temperatures and pressures were based on a ‘reservoir look-up table’ designed by the author and G. Perez, which used a mid-reservoir datum (‘Reservoir Centroid’) for each reservoir (Aalenian, Roabiba, and Paleocene reservoirs) on each of the various structural traps (Vorwata, Wiriagar Deep, P-structure, Ofaweri, Roabiba, and Ubadari structural closures) (Table 10.5). Testing the sensitivities to minor variance in temperatures and pressures showed little impact in the calculator spreadsheet. Thus, appropriate reservoir datum pressures and temperatures were simply extrapolated to the adjacent seal for respective seal temperatures and pressures (i.e. Roabiba Reservoir pressures and temperatures at the Vorwata datum were extrapolated to the Pre-Ayot, Ayot Limestone, and Upper Late Jurassic Shale units; Paleocene Reservoir pressures and temperatures at the Wiriagar datum were extrapolated to the Paleocene Mud-Prone Member).

The results of the MICP-derived seal capacities, for respective maximum CO₂ sequestration/storage column heights at each of the Roabiba Reservoir’s potential sealing units, are discussed in detail in the following sections.

Input Parameters		Properties to be calculated	
Pressure (MPa):	<input type="text" value="28"/>	Density, viscosity, solubility and interfacial tension of carbon dioxide and brine	<input type="checkbox"/>
Temperature (C):	<input type="text" value="117"/>	Enthalpy, Fugacity and Speed of Sound for Carbon Dioxide	<input type="checkbox"/>
Salinity (ppm):	<input type="text" value="24810"/>	Formation Volume Factors and Gas-Water Ratio	<input type="checkbox"/>
<input type="button" value="Calculate"/>			

Results

Carbon dioxide density	0.5672 g cm ⁻³
Carbon dioxide phase region	Supercritical
Viscosity	45.13 μ Pa s
Brine density (unsaturated)	0.9752 g cm ⁻³
Brine Compressibility (unsaturated)	4.422e-10 Pa ⁻¹
Brine viscosity	259.6 μ Pa s
Brine viscosibility	1.01e-09 Pa ⁻¹
Solubility of CO2 in brine	51.52 kg per 1000 kg of brine
Brine density (saturated)	0.9851 g cm ⁻³
Interfacial tension	24.21 mN m ⁻¹

TABLE 10.2: Example of the GEODISC geochemical calculator website for CO₂ (designed by J. Ennis-King). Example shown has the variable inputs for, plus the calculated results from, the Upper Late Jurassic Shales regional seal at Tangguh (Ennis-King, 2003).

Well Name	Depth of Sample (in decimal feet, unless noted as m for meters)	Estimated Pressure at Reservoir Datum (Mpa)	Calculated Temp. at Reservoir Datum (deg C)	Total Salinity Measured in Reservoir from DST Flow (mg/L)	CO2 Density (kg/m3)	CO2 Density (g/cm3)	Brine Density (g/cm3)	Interfacial tension (mN/m or dynes/cm)	Contact angle (deg)	Seal Threshold Pressure (air/Hg system) (psia)	Reservoir Threshold Pressure (air/Hg system) (psia)	Seal Threshold Pressure (brine/CO2 system) (psia)	Reservoir Threshold Pressure (brine/CO2 system) (psia)	Height of CO2 Column (ft)	Zone/Unit	Lithology
Vorwata-10st	3944.43m	40	124	21855.0	679.8	0.7	1.025	21.57	0	4268	61	250	3.58	1651	PA30	SH
Vorwata-10st	3947.64m	40	124	21855.0	679.8	0.7	1.025	21.57	0	11951	61	701	3.58	4666	PA30	SH
Vorwata-10st	3954.46m	40	124	21855.0	679.8	0.7	1.025	21.57	0	8496	61	498	3.58	3310	PA30	SH
Vorwata-10st	3965.57m	40	124	21855.0	679.8	0.7	1.025	21.57	0	5971	61	350	3.58	2319	PA20	SH
Vorwata-10st	3966.82m	40	124	21855.0	679.8	0.7	1.025	21.57	0	5975	61	351	3.58	2321	PA20	SH
Vorwata-10st	3967.10m	40	124	21855.0	679.8	0.7	1.025	21.57	0	8497	61	498	3.58	3310	PA20	SH
Vorwata-10st	4026.18m	40	124	21855.0	679.8	0.7	1.025	21.57	0		4	0	0.23	0	R80	SS
Vorwata-10st	4034.51m	40	124	21855.0	679.8	0.7	1.025	21.57	0		5	0	0.29	0	R80	SS
Vorwata-10st	4090.85m	40	124	21855.0	679.8	0.7	1.025	21.57	0		8.5	0	0.50	0	R50	SS
Vorwata-10st	4128.92m	40	124	21855.0	679.8	0.7	1.025	21.57	0		5	0	0.29	0	R30	SS
Vorwata-2	12984.5	40	124	21855.0	679.8	0.7	1.025	21.57	0	2936	61	172	3.58	1128	R20	SH
Vorwata-2	12989.5	40	124	21855.0	679.8	0.7	1.025	21.57	0	1262	61	74	3.58	471	R10	V. TUFF
Vorwata-2	12994.0	40	124	21855.0	679.8	0.7	1.025	21.57	0	1439	61	84	3.58	541	R10	SH
Vorwata-1	11751.8	40	124	21855.0	679.8	0.7	1.025	21.57	0		339	0	19.89	0	CU30	SS
Vorwata-1	11863.3	40	124	21855.0	679.8	0.7	1.025	21.57	0	20700	61	1214	3.58	8099	R20	SH
Vorwata-1	11865.3	40	124	21855.0	679.8	0.7	1.025	21.57	0	5970	61	350	3.58	2319	R20	SH
Vorwata-7	13117.5	40	124	21855.0	679.8	0.7	1.025	21.57	0		5	0	0.29	0	CU30	SS
Wiriagar Deep-7	7922.5	27	100	40951.0	547.5	0.5	1.048	25.47	0	8471	61	587	4.23	2688	P/TopK	SH
Wiriagar Deep-7	7941.5	27	100	40951.0	547.5	0.5	1.048	25.47	0	11945	61	827	4.23	3798	TopK	LS/MRL
Wiriagar Deep-7	8413.6	28	117	24810.0	565.3	0.6	1.031	24.21	0	no penetration		0	0.00	0	Ayot	LS/MRL
Wiriagar Deep-7	8432.0	28	117	24810.0	565.3	0.6	1.031	24.21	0	14474	61	953	4.02	4706	Ayot	LS/MRL
Wiriagar Deep-7	8457.8	28	117	24810.0	565.3	0.6	1.031	24.21	0	5010	61	330	4.02	1616	R20	SH
Wiriagar Deep-3	7507.8	25	88	40951.0	547.5	0.5	1.048	26.11	0	4994	61	355	4.33	1616	PMP	SH
Wiriagar Deep-3	7508.1	25	88	40951.0	547.5	0.5	1.048	26.11	0	5983	61	425	4.33	1940	PMP	SH
Wiriagar Deep-3	7511.6	25	88	40951.0	547.5	0.5	1.048	26.11	0	1726	61	123	4.33	546	PMP	SH
Wiriagar Deep-3	7517.8	25	88	40951.0	547.5	0.5	1.048	26.11	0	2480	61	176	4.33	793	PMP	SH
Wiriagar Deep-3	9199.0	28	117	24810.0	565.3	0.6	1.031	24.21	0	8540	61	562	4.02	2768	K	LS/MRL
Wiriagar Deep-3	9223.0	28	117	24810.0	565.3	0.6	1.031	24.21	0	24894	61	1639	4.02	8108	K	LS/MRL
Wiriagar Deep-3	9225.0	28	117	24810.0	565.3	0.6	1.031	24.21	0	5000	61	329	4.02	1613	K	LS/MRL
Wiriagar Deep-3	9247.1	28	117	24810.0	565.3	0.6	1.031	24.21	0	no penetration		0	0.00	0	K	LS/MRL
Wiriagar Deep-3	9270.8	28	117	24810.0	565.3	0.6	1.031	24.21	0	11949	61	787	4.02	3881	K/LJSh	SH
Wiriagar Deep-3	9286.0	28	117	24810.0	565.3	0.6	1.031	24.21	0	9953	61	655	4.02	3230	LJSh	SH
Wiriagar Deep-3	9289.3	28	117	24810.0	565.3	0.6	1.031	24.21	0	14448	61	951	4.02	4697	LJSh	V. TUFF
Wiriagar Deep-3	9305.0	28	117	24810.0	565.3	0.6	1.031	24.21	0	14470	61	953	4.02	4704	Ayot	LS/MRL
Wiriagar Deep-2	7346.9	27	100	40951.0	547.5	0.5	1.048	25.47	0	9983	61	692	4.23	3171	PUM	SH
Wiriagar Deep-2	7349.0	27	100	40951.0	547.5	0.5	1.048	25.47	0	5014	61	347	4.23	1583	PMM	SH
Wiriagar Deep-2	8650.3	28	117	24810.0	565.3	0.6	1.031	24.21	0	3520	61	232	4.02	1129	R30	SH

TABLE 10.3: CO2 CALCULATOR SPREADSHEET

Property	Vorwata		Wiriagar Deep	
	Jurassic		Jurassic	Paleocene
	Perch	Aquifer	Aquifer	Aquifer
Samples	V-5(MDT-1,DST-1)	WD-5(DST-1)	WD-4(DST-3,-3A)	
Total dissolved solids, mg/L (Calc)	36,911	44,784	72,044	
Specific Gravity at 76 F	1.025	1.031	1.048	
Resistivity, ohm-meters (measured)	0.23	0.21	0.13	
Resistivity, ohm-meters (calc)	0.23	0.21	0.14	
Hydrogen Sulfide	Absent	Absent	Absent	
pH	8.3	8.0	8.0	
Bromide (Br), mg/L	12.7	-	-	
Constituents: mg/L				
Cations:				
Sodium, Na	13,555.3	14,877.1	23,957.2	
Calcium, Ca	190.8	187.9	539.1	
Magnesium, Mg	36.0	34.8	118.5	
Barium, Ba	2.8	1.6	<0.5	
Total Iron, Fe	18.1	0.2	5.1	
Strontium, Sr	56.7	74.6	64.3	
Potassium, K	833.4	2,915.6	4,438.7	
Anions:				
Chloride, Cl	21,855.0	24,810.1	40,951.4	

Table 10.4: Salinity table of gross intervals from formation water produced on DST testing after flowing for 'clean-up' (Courtesy of BP, 2003).

Reservoir Pressure and Temperature at Datum*

Age / Zone	Structure	Datum, ft.SS	Reservoir Pressure @ Datum, psia	Reservoir Temperature @ Datum, °F	Bgi, scf/rcf	Z @ Datum
Paleocene MP	Wiriagar P	-6,650	3,674	191	213	0.9344
		-7,960	3,755	187	218	0.9411
Paleocene SP	Wiriagar P	-7,650	3,979	212	218	0.9616
		-8,240	3,931	194	224	0.9492
	Ubadari	-5,190	2,402	165	154	0.8827
Jurassic	Wiriagar P	-8,735	4,074	228	218	0.9620
		-9,400	4,122	222	220	0.9722
	Ofaweri	-9,780	4,483	N/A		
	Roabiba	-11,170	5,024	258	242	1.0233
	Vorwata	-12,845	5,841	256	268	1.0772
	Ubadari	-7,345	3,291	205	189	0.9238

*Datum used is the respective Reservoir Centroid for each reservoir at each structural closure.

Table 10.5: Table of in-situ pressures and temperatures for various Tangguh area reservoirs normalized to respective mid-reservoir datum conditions, for each major structural closure.

10.3 Roabiba Reservoir's Top and Lateral Seals

The Roabiba Reservoir, at the Vorwata structural closure, is comprised of both the Bajocian to early Bathonian Roabiba sandstone reservoir and the Callovian Roabiba sandstone reservoir, as identified in this work. Six Roabiba Reservoir core plug/chip samples from whole core were tested by MICP analysis. The test results (Table 10.1) include reservoir rock analysis (highlighted in blue under the “MICP Test” column). These results are also presented graphically, by well name, and then by core sample depth in Appendix 4: Core Plug/Chip Atlas.

Of the six samples, four were from the Bajocian Roabiba Reservoir (sequence stratigraphic units R80, R50, and R30) at V-10. This well, located on the southeast margin of the field, is the closest well to potential CO₂ injection sites for Vorwata *having core*. Additional samples, one from V-1 cores and one from the V-7 cores, were tested as representative samples of the Callovian Roabiba Reservoir (sequence stratigraphic unit CU30, which is the sequence stratigraphic unit most widespread over the Vorwata area – see Figure 10.1).

The immediate top and lateral seal for the Roabiba Reservoir at Vorwata is the Pre-Ayot shales (sequence stratigraphic units PA10, PA20, and the lower-most PA30). Six representative samples from this sealing unit were tested by MICP analysis. This ‘top’ seal is also the ‘lateral’ seal for the overall Vorwata structure given the geometry of the 4-way dip closure of the SE plunging anticlinorium.

The MICP results were converted to CO₂ Injection Capillary Pressure equivalents (CO₂-ICP) and then the sensitivities for the variable inputs were examined before calculating the Most Likely Values (MLV's) for the seal core plug maximum CO₂ column heights. Sensitivities of the reservoir threshold pressure were examined, as were sensitivities with varied brine/CO₂ system contact angle, and sensitivities with varied brine/CO₂ system interfacial tension.

If only the four Bajocian Roabiba Reservoir core plug samples are included, the ‘air/Hg system average reservoir threshold pressure’ value is 5 psia (the four MICP sample threshold pressures range from 4 psia to 8.5 psia), whereas, if the additional two Callovian Roabiba Reservoir are include, then the ‘air/Hg system average reservoir threshold pressure’ is 61 psia. Sensitivity evaluations were run using both values in combination with varied contact angles. The results of the sensitivity evaluation for combinations of the various contact angles and average reservoir threshold pressures are presented in Table 10.6a. Table 10.6a presents the results of

seal capacities and maximum CO₂ column heights for each of the sealing MICP samples from the Vorwata #10 well. It should be noted that the column labelled as “Height of CO₂ Column (ft)” shows results that are *the maximum CO₂ column heights that each of the seal samples could theoretically hold barring open fractures*. The appraisal of the suite of MICP seal plugs is evaluated on the far right margin with “Min. CO₂ Column (ft)” referring to the lowest maximum height value of the sample suite, and “Max. CO₂ Column (ft)” referring to the highest maximum height value of the sample suite. “Mean CO₂ Column (ft)” refers to the arithmetic average of the maximum CO₂ column height of the entire suite, and “Mode CO₂ Column (ft)” refers to the most common recurring value of maximum CO₂ column height in the entire suite of seal samples.

The ‘wettability’ of a system is measured by the contact angle through the denser phase in the system (Vavra, et al., 1992). The contact angle in air/Hg systems is commonly accepted to be 140 degrees (Sneider, 1987; Vavra, et al., 1992; Kaldi and Atkinson, 1993). Strongly water-wet hydrocarbon/brine systems generally have a contact angle of 0 degrees (Vavra, et al., 1992), however contact angles of up to 10 degrees have been obtained for Java Sea brine/oil systems (Kaldi and Atkinson, 1993; p377). The brine/CO₂ system contact angle is generally taken to be 0 degrees (C. Gibson-Poole, personal communication, 2001), however, Dewhurst et al., (2001) have suggested that the actual contact angle of the brine/CO₂ system may be greater than 0 degrees. Therefore, sensitivities of values ranging from 0 degrees up to 45 degrees were explored (Table 10.6b). The reservoir threshold pressure used is 61 psia, based on the entire suite of four Bajocian/Bathonian Roabiba and two Callovian Roabiba reservoir MICP samples. The interfacial tension is kept constant at 21.57 dynes/cm, while varying the contact angle first. The maximum CO₂ column height sensitivities to varied contact angle, listed in Table 10.6b are presented as a graph in Figure 10.3.

In a similar fashion, the interfacial tension in the brine/CO₂ system were examined for sensitivities to the maximum CO₂ column height, with values ranging from 5 to 45 dynes/cm evaluated at 5 dynes/cm increments along with the value of 21.57 dynes/cm (calculated by the Geochemical Website calculator as the predicted interfacial tension for the Pre-Ayot Shale seal and the Roabiba Reservoir at the Vorwata structures datum) (Table 10.6c). The reservoir threshold pressure used is 61 psia, as is a contact angle of 0°. The results of this are presented in Figure 10.4.

Well Name	Core Plug Sample Depth (driller's unshifted measured depth referenced from RKB)	Estimated Pressure at Reservoir Datum (Mpa)	Calculated Temp. at Reservoir Datum (deg C)	Total Salinity Measured in Reservoir from DST Flow (mg/L)	CO2 Density (g/cm3)	Brine Density (g/cm3)	Interfacial tension (mN/m or dynes/cm)	Contact angle (deg)	Seal Threshold Pressure (air/Hg system) (psia)	Reservoir Threshold Pressure (air/Hg system) (psia)	Seal Threshold Pressure (brine/CO2 system) (psia)	Reservoir Threshold Pressure (brine/CO2 system) (psia)	Max. Height of CO2 Column (ft)	Zone/Unit	Lithology		
Maximum, Minimum, Mean, and Mode for CO2 Column Height using 0.0 deg contact angle and 61 psia Average Reservoir Threshold Pressure																	
Vorwata-10st	3944.43m	40	124	21855	0.680	1.025	21.57	0	4268	61	250.4	3.58	1651	PA30	SH		
Vorwata-10st	3947.64m	40	124	21855	0.680	1.025	21.57	0	11951	61	701.1	3.58	4666	PA30	SH		
Vorwata-10st	3954.46m	40	124	21855	0.680	1.025	21.57	0	8496	61	498.4	3.58	3310	PA30	SH		
Vorwata-10st	3965.57m	40	124	21855	0.680	1.025	21.57	0	5971	61	350.3	3.58	2319	PA20	SH		
Vorwata-10st	3966.82m	40	124	21855	0.680	1.025	21.57	0	5975	61	350.5	3.58	2321	PA20	SH		
Vorwata-10st	3967.10m	40	124	21855	0.680	1.025	21.57	0	8497	61	498.5	3.58	3310	PA20	SH		
Vorwata-1	11902' 3"	40	124	21855	0.680	1.025	21.57	0		339	0.0	19.89	0	CU30	SS		
Vorwata-7	13152' 5"	40	124	21855	0.680	1.025	21.57	0		5	0.0	0.29	0	CU30	SS		
Vorwata-10st	4026.18m	40	124	21855	0.680	1.025	21.57	0		4	0.0	0.23	0.0	R80	SS	Min. CO2 Column (ft.):	1651
Vorwata-10st	4034.51m	40	124	21855	0.680	1.025	21.57	0		5	0.0	0.29	0.0	R80	SS	Max. CO2 Column (ft.):	4666
Vorwata-10st	4090.85m	40	124	21855	0.680	1.025	21.57	0		8.5	0.0	0.50	0.0	R50	SS	Mean CO2 Column (ft.):	2930
Vorwata-10st	4128.92m	40	124	21855	0.680	1.025	21.57	0		5	0.0	0.29	0.0	R30	SS	Mode CO2 Column (ft.):	3310
Maximum, Minimum, Mean, and Mode for CO2 Column Height using 0.0 deg contact angle and 5 psia Average Reservoir Threshold Pressure																	
Vorwata-10st	3944.43m	40	124	21855	0.680	1.025	21.57	0	4268	5	250.4	0.3	1673	PA30	SH		
Vorwata-10st	3947.64m	40	124	21855	0.680	1.025	21.57	0	11951	5	701.1	0.3	4688	PA30	SH		
Vorwata-10st	3954.46m	40	124	21855	0.680	1.025	21.57	0	8496	5	498.4	0.3	3332	PA30	SH		
Vorwata-10st	3965.57m	40	124	21855	0.680	1.025	21.57	0	5971	5	350.3	0.3	2341	PA20	SH		
Vorwata-10st	3966.82m	40	124	21855	0.680	1.025	21.57	0	5975	5	350.5	0.3	2343	PA20	SH		
Vorwata-10st	3967.10m	40	124	21855	0.680	1.025	21.57	0	8497	5	498.5	0.3	3332	PA20	SH		
Vorwata-10st	4026.18m	40	124	21855	0.680	1.025	21.57	0		4	0.0	0.2	0	R80	SS	Min. CO2 Column (ft.):	1673
Vorwata-10st	4034.51m	40	124	21855	0.680	1.025	21.57	0		5	0.0	0.3	0	R80	SS	Max. CO2 Column (ft.):	4688
Vorwata-10st	4090.85m	40	124	21855	0.680	1.025	21.57	0		8.5	0.0	0.5	0	R50	SS	Mean CO2 Column (ft.):	2951
Vorwata-10st	4128.92m	40	124	21855	0.680	1.025	21.57	0		5	0.0	0.3	0	R30	SS	Mode CO2 Column (ft.):	3332
Maximum, Minimum, Mean, and Mode for CO2 Column Height using 5 deg contact angle and 61 psia Average Reservoir Threshold Pressure																	
Vorwata-10st	3944.43m	40	124	21855	0.680	1.025	21.57	5	4268	61	249.4	3.56	1645	PA30	SH		
Vorwata-10st	3947.64m	40	124	21855	0.680	1.025	21.57	5	11951	61	698.4	3.56	4648	PA30	SH		
Vorwata-10st	3954.46m	40	124	21855	0.680	1.025	21.57	5	8496	61	496.5	3.56	3298	PA30	SH		
Vorwata-10st	3965.57m	40	124	21855	0.680	1.025	21.57	5	5971	61	348.9	3.56	2310	PA20	SH		
Vorwata-10st	3966.82m	40	124	21855	0.680	1.025	21.57	5	5975	61	349.2	3.56	2312	PA20	SH		
Vorwata-10st	3967.10m	40	124	21855	0.680	1.025	21.57	5	8497	61	496.6	3.56	3298	PA20	SH		
Vorwata-1	11902' 3"	40	124	21855	0.680	1.025	21.57	5		339	0.0	19.89	0	CU30	SS		
Vorwata-7	13152' 5"	40	124	21855	0.680	1.025	21.57	5		5	0.0	0.29	0	CU30	SS		
Vorwata-10st	4026.18m	40	124	21855	0.680	1.025	21.57	5		4	0	0.23	0	R80	SS	Min. CO2 Column (ft.):	1645
Vorwata-10st	4034.51m	40	124	21855	0.680	1.025	21.57	5		5	0	0.29	0	R80	SS	Max. CO2 Column (ft.):	4648
Vorwata-10st	4090.85m	40	124	21855	0.680	1.025	21.57	5		8.5	0	0.50	0	R50	SS	Mean CO2 Column (ft.):	2919
Vorwata-10st	4128.92m	40	124	21855	0.680	1.025	21.57	5		5	0	0.29	0	R30	SS	Mode CO2 Column (ft.):	3298
Maximum, Minimum, Mean, and Mode for CO2 Column Height using 20 deg contact angle and 61 psia Average Reservoir Threshold Pressure																	
Vorwata-10st	3944.43m	40	124	21855	0.680	1.025	21.57	20	4268	61	235.3	3.36	1551	PA30	SH		
Vorwata-10st	3947.64m	40	124	21855	0.680	1.025	21.57	20	11951	61	658.8	3.36	4384	PA30	SH		
Vorwata-10st	3954.46m	40	124	21855	0.680	1.025	21.57	20	8496	61	468.3	3.36	3111	PA30	SH		
Vorwata-10st	3965.57m	40	124	21855	0.680	1.025	21.57	20	5971	61	329.1	3.36	2179	PA20	SH		
Vorwata-10st	3966.82m	40	124	21855	0.680	1.025	21.57	20	5975	61	329.4	3.36	2181	PA20	SH		
Vorwata-10st	3967.10m	40	124	21855	0.680	1.025	21.57	20	8497	61	468.4	3.36	3111	PA20	SH		
Vorwata-1	11902' 3"	40	124	21855	0.680	1.025	21.57	20		339	0.0	19.89	0	CU30	SS		
Vorwata-7	13152' 5"	40	124	21855	0.680	1.025	21.57	20		5	0.0	0.29	0	CU30	SS		
Vorwata-10st	4026.18m	40	124	21855	0.680	1.025	21.57	20		4	0	0.22	0	R80	SS	Min. CO2 Column (ft.):	1551
Vorwata-10st	4034.51m	40	124	21855	0.680	1.025	21.57	20		5	0	0.28	0	R80	SS	Max. CO2 Column (ft.):	4384
Vorwata-10st	4090.85m	40	124	21855	0.680	1.025	21.57	20		8.5	0	0.47	0	R50	SS	Mean CO2 Column (ft.):	2753
Vorwata-10st	4128.92m	40	124	21855	0.680	1.025	21.57	20		5	0	0.28	0	R30	SS	Mode CO2 Column (ft.):	3111
Maximum, Minimum, Mean, and Mode for CO2 Column Height using 30 deg contact angle and 61 psia Average Reservoir Threshold Pressure																	
Vorwata-10st	3944.43m	40	124	21855	0.680	1.025	21.57	30	4268	61	216.8	3.10	1430	PA30	SH		
Vorwata-10st	3947.64m	40	124	21855	0.680	1.025	21.57	30	11951	61	607.1	3.10	4041	PA30	SH		
Vorwata-10st	3954.46m	40	124	21855	0.680	1.025	21.57	30	8496	61	431.6	3.10	2867	PA30	SH		
Vorwata-10st	3965.57m	40	124	21855	0.680	1.025	21.57	30	5971	61	303.3	3.10	2008	PA20	SH		
Vorwata-10st	3966.82m	40	124	21855	0.680	1.025	21.57	30	5975	61	303.5	3.10	2010	PA20	SH		
Vorwata-10st	3967.10m	40	124	21855	0.680	1.025	21.57	30	8497	61	431.7	3.10	2867	PA20	SH		
Vorwata-1	11902' 3"	40	124	21855	0.680	1.025	21.57	30		339	0.0	19.89	0	CU30	SS		
Vorwata-7	13152' 5"	40	124	21855	0.680	1.025	21.57	30		5	0.0	0.29	0	CU30	SS		
Vorwata-10st	4026.18m	40	124	21855	0.680	1.025	21.57	30		4	0	0.20	0	R80	SS	Min. CO2 Column (ft.):	1430
Vorwata-10st	4034.51m	40	124	21855	0.680	1.025	21.57	30		5	0	0.25	0	R80	SS	Max. CO2 Column (ft.):	4041
Vorwata-10st	4090.85m	40	124	21855	0.680	1.025	21.57	30		8.5	0	0.43	0	R50	SS	Mean CO2 Column (ft.):	2537
Vorwata-10st	4128.92m	40	124	21855	0.680	1.025	21.57	30		5	0	0.25	0	R30	SS	Mode CO2 Column (ft.):	2867
Maximum, Minimum, Mean, and Mode for CO2 Column Height using 45 deg contact angle and 5 psia Average Reservoir Threshold Pressure																	
Vorwata-10st	3944.43m	40	124	21855	0.680	1.025	21.57	45	4268	5	177.0	0.21	1183	PA30	SH		
Vorwata-10st	3947.64m	40	124	21855	0.680	1.025	21.57	45	11951	5	495.7	0.21	3315	PA30	SH		
Vorwata-10st	3954.46m	40	124	21855	0.680	1.025	21.57	45	8496	5	352.4	0.21	2356	PA30	SH		
Vorwata-10st	3965.57m	40	124	21855	0.680	1.025	21.57	45	5971	5	247.7	0.21	1655	PA20	SH		
Vorwata-10st	3966.82m	40	124	21855	0.680	1.025	21.57	45	5975	5	247.8	0.21	1657	PA20	SH		
Vorwata-10st	3967.10m	40	124	21855	0.680	1.025	21.57	45	8497	5	352.5	0.21	2356	PA20	SH		
Vorwata-10st	4026.18m	40	124	21855	0.680	1.025	21.57	45		4	0.0	0.17	0	R80	SS	Min. CO2 Column (ft.):	1183
Vorwata-10st	4034.51m	40	124	21855	0.680	1.025	21.57	45		5	0.0	0.21	0	R80	SS	Max. CO2 Column (ft.):	3315
Vorwata-10st	4090.85m	40	124	21855	0.680	1.025	21.57	45		8.5	0.0	0.35	0	R50	SS	Mean CO2 Column (ft.):	2087
Vorwata-10st	4128.92m	40	124	21855	0.680	1.025	21.57	45		5	0.0	0.21	0	R30	SS	Mode CO2 Column (ft.):	2356
Maximum, Minimum, Mean, and Mode for CO2 Column Height using 45 deg contact angle and 61 psia Average Reservoir Threshold Pressure																	
Vorwata-10st	3944.43m	40	124	21855	0.67975	1.025	21.57	45	4268	61	177.0	2.53	1167	PA30	SH		
Vorwata-10st	3947.64m	40	124	21855	0.67975	1.025	21.57	45	11951	61	495.7	2.53	3299	PA30	SH		
Vorwata-10st	3954.46m	40	124	21855	0.67975	1.025	21.57	45	8496	61	352.4	2.53	2341	PA30	SH		
Vorwata-10st	3965.57m	40	124	21855	0.67975	1.025	21.57	45	5971	61	247.7	2.53	1640	PA20	SH		
Vorwata-10st	3966.82m	40	124	21855	0.67975	1.025	21.57	45	5975	61	247.8	2.53	1641	PA20	SH		
Vorwata-10st	3967.10m	40	124	21855	0.67975	1.025	21.57	45	8497	61	352.5	2.53	2341	PA20	SH		
Vorwata-1	11902' 3"	40	124	21855	0.67975	1.025	21.57	45		339	0.0	19.89</					

Well Name	Core Plug Sample Depth (driller's unshifted measured depth referenced from RKB)	Estimated Pressure at Reservoir Datum (Mpa)	Calculated Temp. at Reservoir Datum (deg C)	Total Salinity Measured in Reservoir from DST Flow (mg/L)	CO2 Density (kg/m3)	CO2 Density (g/cm3)	Brine Density (g/cm3)	Interfacial tension* (mN/m or dynes/cm)	Contact angle (deg)	Seal Threshold Pressure (air/Hg system) (psia)	Reservoir Threshold Pressure (air/Hg system) (psia)	Seal Threshold Pressure (brine/CO2 system) (psia)	Reservoir Threshold Pressure (brine/CO2 system) (psia)	Height of CO2 Column (ft)	Zone/Unit	Lithology	Average Height of CO2 Column Held by PA Units over Vorwata at Roabiba Level (ft)
Vorwata-10st	3944.43m	40	124	21855	680	0.7	1.025	21.57	0	4268	61	250	3.58	1651	PA30	SH	
Vorwata-10st	3947.64m	40	124	21855	680	0.7	1.025	21.57	0	11951	61	701	3.58	4666	PA30	SH	
Vorwata-10st	3954.46m	40	124	21855	680	0.7	1.025	21.57	0	8496	61	498	3.58	3310	PA30	SH	
Vorwata-10st	3965.57m	40	124	21855	680	0.7	1.025	21.57	0	5971	61	350	3.58	2319	PA20	SH	
Vorwata-10st	3966.82m	40	124	21855	680	0.7	1.025	21.57	0	5975	61	351	3.58	2321	PA20	SH	
Vorwata-10st	3967.10m	40	124	21855	680	0.7	1.025	21.57	0	8497	61	498	3.58	3310	PA20	SH	2929.44
Vorwata-10st	3944.43m	40	124	21855	680	0.7	1.025	21.57	5	4268	61	249	3.56	1645	PA30	SH	
Vorwata-10st	3947.64m	40	124	21855	680	0.7	1.025	21.57	5	11951	61	698	3.56	4648	PA30	SH	
Vorwata-10st	3954.46m	40	124	21855	680	0.7	1.025	21.57	5	8496	61	496	3.56	3297	PA30	SH	
Vorwata-10st	3965.57m	40	124	21855	680	0.7	1.025	21.57	5	5971	61	349	3.56	2310	PA20	SH	
Vorwata-10st	3966.82m	40	124	21855	680	0.7	1.025	21.57	5	5975	61	349	3.56	2312	PA20	SH	
Vorwata-10st	3967.10m	40	124	21855	680	0.7	1.025	21.57	5	8497	61	497	3.56	3298	PA20	SH	2918.29
Vorwata-10st	3944.43m	40	124	21855	680	0.7	1.025	21.57	10	4268	61	247	3.52	1626	PA30	SH	
Vorwata-10st	3947.64m	40	124	21855	680	0.7	1.025	21.57	10	11951	61	690	3.52	4595	PA30	SH	
Vorwata-10st	3954.46m	40	124	21855	680	0.7	1.025	21.57	10	8496	61	491	3.52	3260	PA30	SH	
Vorwata-10st	3965.57m	40	124	21855	680	0.7	1.025	21.57	10	5971	61	345	3.52	2284	PA20	SH	
Vorwata-10st	3966.82m	40	124	21855	680	0.7	1.025	21.57	10	5975	61	345	3.52	2285	PA20	SH	
Vorwata-10st	3967.10m	40	124	21855	680	0.7	1.025	21.57	10	8497	61	491	3.52	3260	PA20	SH	2884.93
Vorwata-10st	3944.43m	40	124	21855	680	0.7	1.025	21.57	15	4268	61	242	3.46	1595	PA30	SH	
Vorwata-10st	3947.64m	40	124	21855	680	0.7	1.025	21.57	15	11951	61	677	3.46	4507	PA30	SH	
Vorwata-10st	3954.46m	40	124	21855	680	0.7	1.025	21.57	15	8496	61	481	3.46	3197	PA30	SH	
Vorwata-10st	3965.57m	40	124	21855	680	0.7	1.025	21.57	15	5971	61	338	3.46	2240	PA20	SH	
Vorwata-10st	3966.82m	40	124	21855	680	0.7	1.025	21.57	15	5975	61	339	3.46	2242	PA20	SH	
Vorwata-10st	3967.10m	40	124	21855	680	0.7	1.025	21.57	15	8497	61	481	3.46	3198	PA20	SH	2829.62
Vorwata-10st	3944.43m	40	124	21855	680	0.7	1.025	21.57	20	4268	61	235	3.36	1551	PA30	SH	
Vorwata-10st	3947.64m	40	124	21855	680	0.7	1.025	21.57	20	11951	61	659	3.36	4384	PA30	SH	
Vorwata-10st	3954.46m	40	124	21855	680	0.7	1.025	21.57	20	8496	61	468	3.36	3110	PA30	SH	
Vorwata-10st	3965.57m	40	124	21855	680	0.7	1.025	21.57	20	5971	61	329	3.36	2179	PA20	SH	
Vorwata-10st	3966.82m	40	124	21855	680	0.7	1.025	21.57	20	5975	61	329	3.36	2181	PA20	SH	
Vorwata-10st	3967.10m	40	124	21855	680	0.7	1.025	21.57	20	8497	61	468	3.36	3111	PA20	SH	2752.77
Vorwata-10st	3944.43m	40	124	21855	680	0.7	1.025	21.57	25	4268	61	227	3.24	1496	PA30	SH	
Vorwata-10st	3947.64m	40	124	21855	680	0.7	1.025	21.57	25	11951	61	635	3.24	4229	PA30	SH	
Vorwata-10st	3954.46m	40	124	21855	680	0.7	1.025	21.57	25	8496	61	452	3.24	3000	PA30	SH	
Vorwata-10st	3965.57m	40	124	21855	680	0.7	1.025	21.57	25	5971	61	317	3.24	2102	PA20	SH	
Vorwata-10st	3966.82m	40	124	21855	680	0.7	1.025	21.57	25	5975	61	318	3.24	2103	PA20	SH	
Vorwata-10st	3967.10m	40	124	21855	680	0.7	1.025	21.57	25	8497	61	452	3.24	3000	PA20	SH	2654.97
Vorwata-10st	3944.43m	40	124	21855	680	0.7	1.025	21.57	30	4268	61	217	3.10	1430	PA30	SH	
Vorwata-10st	3947.64m	40	124	21855	680	0.7	1.025	21.57	30	11951	61	607	3.10	4041	PA30	SH	
Vorwata-10st	3954.46m	40	124	21855	680	0.7	1.025	21.57	30	8496	61	432	3.10	2866	PA30	SH	
Vorwata-10st	3965.57m	40	124	21855	680	0.7	1.025	21.57	30	5971	61	303	3.10	2008	PA20	SH	
Vorwata-10st	3966.82m	40	124	21855	680	0.7	1.025	21.57	30	5975	61	304	3.10	2010	PA20	SH	
Vorwata-10st	3967.10m	40	124	21855	680	0.7	1.025	21.57	30	8497	61	432	3.10	2867	PA20	SH	2536.97
Vorwata-10st	3944.43m	40	124	21855	680	0.7	1.025	21.57	35	4268	61	205	2.93	1352	PA30	SH	
Vorwata-10st	3947.64m	40	124	21855	680	0.7	1.025	21.57	35	11951	61	574	2.93	3822	PA30	SH	
Vorwata-10st	3954.46m	40	124	21855	680	0.7	1.025	21.57	35	8496	61	408	2.93	2711	PA30	SH	
Vorwata-10st	3965.57m	40	124	21855	680	0.7	1.025	21.57	35	5971	61	287	2.93	1900	PA20	SH	
Vorwata-10st	3966.82m	40	124	21855	680	0.7	1.025	21.57	35	5975	61	287	2.93	1901	PA20	SH	
Vorwata-10st	3967.10m	40	124	21855	680	0.7	1.025	21.57	35	8497	61	408	2.93	2712	PA20	SH	2399.65
Vorwata-10st	3944.43m	40	124	21855	680	0.7	1.025	21.57	40	4268	61	192	2.74	1265	PA30	SH	
Vorwata-10st	3947.64m	40	124	21855	680	0.7	1.025	21.57	40	11951	61	537	2.74	3574	PA30	SH	
Vorwata-10st	3954.46m	40	124	21855	680	0.7	1.025	21.57	40	8496	61	382	2.74	2536	PA30	SH	
Vorwata-10st	3965.57m	40	124	21855	680	0.7	1.025	21.57	40	5971	61	268	2.74	1777	PA20	SH	
Vorwata-10st	3966.82m	40	124	21855	680	0.7	1.025	21.57	40	5975	61	269	2.74	1778	PA20	SH	
Vorwata-10st	3967.10m	40	124	21855	680	0.7	1.025	21.57	40	8497	61	382	2.74	2536	PA20	SH	2244.08
Vorwata-10st	3944.43m	40	124	21855	680	0.7	1.025	21.57	45	4268	61	177	2.53	1167	PA30	SH	
Vorwata-10st	3947.64m	40	124	21855	680	0.7	1.025	21.57	45	11951	61	496	2.53	3299	PA30	SH	
Vorwata-10st	3954.46m	40	124	21855	680	0.7	1.025	21.57	45	8496	61	352	2.53	2340	PA30	SH	
Vorwata-10st	3965.57m	40	124	21855	680	0.7	1.025	21.57	45	5971	61	248	2.53	1640	PA20	SH	
Vorwata-10st	3966.82m	40	124	21855	680	0.7	1.025	21.57	45	5975	61	248	2.53	1641	PA20	SH	
Vorwata-10st	3967.10m	40	124	21855	680	0.7	1.025	21.57	45	8497	61	352	2.53	2341	PA20	SH	2071.42

* Interfacial Tension is measured in dynes per centimeter or milliNewtons per meter. Dynes are the unit of force in the cgs system of physical measurements such that a body under it's influence with a free mass of one gram would accelerate at one centimeter per second per second. Newtons are the unit of force in the mks system of physical measurements such that a body under it's influence with a mass of one kilogram would experience an acceleration of one meter per second per second.

TABLE 10.6b: CO2 Column Height Sensitivity, with 21.57 as the interfacial tension and the contact angle varied from 0 to 45 degrees.

Well Name	Core Plug Sample Depth (driller's unshifted measured depth referenced from RKB)	Estimated Pressure at Reservoir Datum (Mpa)	Calculated Temp. at Reservoir Datum (deg C)	Total Salinity Measured in Reservoir from DST Flow (mg/L)	CO2 Density (kg/m3)	CO2 Density (g/cm3)	Brine Density (g/cm3)	Interfacial tension (mN/m or dynes/cm)	Contact angle (deg)	Seal Threshold Pressure (air/Hg system) (psia)	Reservoir Threshold Pressure (air/Hg system) (psia)	Seal Threshold Pressure (brine/CO2 system) (psia)	Reservoir Threshold Pressure (brine/CO2 system) (psia)	Height of CO2 Column (ft)	Zone/Unit	Lithology	Average Height of CO2 Column Held by PA Units over Vorwata at Roabiba Level (ft)
Vorwata-10st	3944.43m	40	124	21855.0	679.8	0.7	1.025	5	0	4268	61	58	0.83	383	PA30	SH	679
Vorwata-10st	3947.64m	40	124	21855.0	679.8	0.7	1.025	5	0	11951	61	163	0.83	1082	PA30	SH	
Vorwata-10st	3954.46m	40	124	21855.0	679.8	0.7	1.025	5	0	8496	61	116	0.83	767	PA30	SH	
Vorwata-10st	3965.57m	40	124	21855.0	679.8	0.7	1.025	5	0	5971	61	81	0.83	538	PA20	SH	
Vorwata-10st	3966.82m	40	124	21855.0	679.8	0.7	1.025	5	0	5975	61	81	0.83	538	PA20	SH	
Vorwata-10st	3967.10m	40	124	21855.0	679.8	0.7	1.025	5	0	8497	61	116	0.83	767	PA20	SH	
Vorwata-10st	3944.43m	40	124	21855.0	679.8	0.7	1.025	10	0	4268	61	116	1.66	765	PA30	SH	1358
Vorwata-10st	3947.64m	40	124	21855.0	679.8	0.7	1.025	10	0	11951	61	325	1.66	2163	PA30	SH	
Vorwata-10st	3954.46m	40	124	21855.0	679.8	0.7	1.025	10	0	8496	61	231	1.66	1535	PA30	SH	
Vorwata-10st	3965.57m	40	124	21855.0	679.8	0.7	1.025	10	0	5971	61	162	1.66	1075	PA20	SH	
Vorwata-10st	3966.82m	40	124	21855.0	679.8	0.7	1.025	10	0	5975	61	162	1.66	1076	PA20	SH	
Vorwata-10st	3967.10m	40	124	21855.0	679.8	0.7	1.025	10	0	8497	61	231	1.66	1535	PA20	SH	
Vorwata-10st	3944.43m	40	124	21855.0	679.8	0.7	1.025	15	0	4268	61	174	2.49	1148	PA30	SH	2037
Vorwata-10st	3947.64m	40	124	21855.0	679.8	0.7	1.025	15	0	11951	61	488	2.49	3245	PA30	SH	
Vorwata-10st	3954.46m	40	124	21855.0	679.8	0.7	1.025	15	0	8496	61	347	2.49	2302	PA30	SH	
Vorwata-10st	3965.57m	40	124	21855.0	679.8	0.7	1.025	15	0	5971	61	244	2.49	1613	PA20	SH	
Vorwata-10st	3966.82m	40	124	21855.0	679.8	0.7	1.025	15	0	5975	61	244	2.49	1614	PA20	SH	
Vorwata-10st	3967.10m	40	124	21855.0	679.8	0.7	1.025	15	0	8497	61	347	2.49	2302	PA20	SH	
Vorwata-10st	3944.43m	40	124	21855.0	679.8	0.7	1.025	20	0	4268	61	232	3.32	1531	PA30	SH	2716
Vorwata-10st	3947.64m	40	124	21855.0	679.8	0.7	1.025	20	0	11951	61	650	3.32	4326	PA30	SH	
Vorwata-10st	3954.46m	40	124	21855.0	679.8	0.7	1.025	20	0	8496	61	462	3.32	3069	PA30	SH	
Vorwata-10st	3965.57m	40	124	21855.0	679.8	0.7	1.025	20	0	5971	61	325	3.32	2150	PA20	SH	
Vorwata-10st	3966.82m	40	124	21855.0	679.8	0.7	1.025	20	0	5975	61	325	3.32	2152	PA20	SH	
Vorwata-10st	3967.10m	40	124	21855.0	679.8	0.7	1.025	20	0	8497	61	462	3.32	3069	PA20	SH	
Vorwata-10st	3944.43m	40	124	21855.0	679.8	0.7	1.025	21.57	0	4268	61	250	3.58	1651	PA30	SH	2929
Vorwata-10st	3947.64m	40	124	21855.0	679.8	0.7	1.025	21.57	0	11951	61	701	3.58	4666	PA30	SH	
Vorwata-10st	3954.46m	40	124	21855.0	679.8	0.7	1.025	21.57	0	8496	61	498	3.58	3310	PA30	SH	
Vorwata-10st	3965.57m	40	124	21855.0	679.8	0.7	1.025	21.57	0	5971	61	350	3.58	2319	PA20	SH	
Vorwata-10st	3966.82m	40	124	21855.0	679.8	0.7	1.025	21.57	0	5975	61	351	3.58	2321	PA20	SH	
Vorwata-10st	3967.10m	40	124	21855.0	679.8	0.7	1.025	21.57	0	8497	61	498	3.58	3310	PA20	SH	
Vorwata-10st	3944.43m	40	124	21855.0	679.8	0.7	1.025	25	0	4268	61	290	4.15	1913	PA30	SH	3395
Vorwata-10st	3947.64m	40	124	21855.0	679.8	0.7	1.025	25	0	11951	61	813	4.15	5408	PA30	SH	
Vorwata-10st	3954.46m	40	124	21855.0	679.8	0.7	1.025	25	0	8496	61	578	4.15	3836	PA30	SH	
Vorwata-10st	3965.57m	40	124	21855.0	679.8	0.7	1.025	25	0	5971	61	406	4.15	2688	PA20	SH	
Vorwata-10st	3966.82m	40	124	21855.0	679.8	0.7	1.025	25	0	5975	61	406	4.15	2690	PA20	SH	
Vorwata-10st	3967.10m	40	124	21855.0	679.8	0.7	1.025	25	0	8497	61	578	4.15	3837	PA20	SH	
Vorwata-10st	3944.43m	40	124	21855.0	679.8	0.7	1.025	30	0	4268	61	348	4.98	2296	PA30	SH	4074
Vorwata-10st	3947.64m	40	124	21855.0	679.8	0.7	1.025	30	0	11951	61	975	4.98	6489	PA30	SH	
Vorwata-10st	3954.46m	40	124	21855.0	679.8	0.7	1.025	30	0	8496	61	693	4.98	4604	PA30	SH	
Vorwata-10st	3965.57m	40	124	21855.0	679.8	0.7	1.025	30	0	5971	61	487	4.98	3225	PA20	SH	
Vorwata-10st	3966.82m	40	124	21855.0	679.8	0.7	1.025	30	0	5975	61	487	4.98	3228	PA20	SH	
Vorwata-10st	3967.10m	40	124	21855.0	679.8	0.7	1.025	30	0	8497	61	693	4.98	4604	PA20	SH	
Vorwata-10st	3944.43m	40	124	21855.0	679.8	0.7	1.025	35	0	4268	61	406	5.81	2679	PA30	SH	4753
Vorwata-10st	3947.64m	40	124	21855.0	679.8	0.7	1.025	35	0	11951	61	1138	5.81	7571	PA30	SH	
Vorwata-10st	3954.46m	40	124	21855.0	679.8	0.7	1.025	35	0	8496	61	809	5.81	5371	PA30	SH	
Vorwata-10st	3965.57m	40	124	21855.0	679.8	0.7	1.025	35	0	5971	61	568	5.81	3763	PA20	SH	
Vorwata-10st	3966.82m	40	124	21855.0	679.8	0.7	1.025	35	0	5975	61	569	5.81	3766	PA20	SH	
Vorwata-10st	3967.10m	40	124	21855.0	679.8	0.7	1.025	35	0	8497	61	809	5.81	5371	PA20	SH	
Vorwata-10st	3944.43m	40	124	21855.0	679.8	0.7	1.025	40	0	4268	61	464	6.64	3061	PA30	SH	5432
Vorwata-10st	3947.64m	40	124	21855.0	679.8	0.7	1.025	40	0	11951	61	1300	6.64	8652	PA30	SH	
Vorwata-10st	3954.46m	40	124	21855.0	679.8	0.7	1.025	40	0	8496	61	924	6.64	6138	PA30	SH	
Vorwata-10st	3965.57m	40	124	21855.0	679.8	0.7	1.025	40	0	5971	61	650	6.64	4301	PA20	SH	
Vorwata-10st	3966.82m	40	124	21855.0	679.8	0.7	1.025	40	0	5975	61	650	6.64	4304	PA20	SH	
Vorwata-10st	3967.10m	40	124	21855.0	679.8	0.7	1.025	40	0	8497	61	924	6.64	6139	PA20	SH	
Vorwata-10st	3944.43m	40	124	21855.0	679.8	0.7	1.025	45	0	4268	61	522	7.47	3444	PA30	SH	6111
Vorwata-10st	3947.64m	40	124	21855.0	679.8	0.7	1.025	45	0	11951	61	1463	7.47	9734	PA30	SH	
Vorwata-10st	3954.46m	40	124	21855.0	679.8	0.7	1.025	45	0	8496	61	1040	7.47	6905	PA30	SH	
Vorwata-10st	3965.57m	40	124	21855.0	679.8	0.7	1.025	45	0	5971	61	731	7.47	4838	PA20	SH	
Vorwata-10st	3966.82m	40	124	21855.0	679.8	0.7	1.025	45	0	5975	61	731	7.47	4841	PA20	SH	
Vorwata-10st	3967.10m	40	124	21855.0	679.8	0.7	1.025	45	0	8497	61	1040	7.47	6906	PA20	SH	

* Interfacial Tension is measured in dynes per centimeter or milliNewtons per meter. Dynes are the unit of force in the cgs system of physical measurements such that a body under it's influence with a free mass of one gram would accelerate at one centimeter per second per second. Newtons are the unit of force in the mks system of physical measurements such that a body under it's influence with a mass of one kilogram would experience an acceleration of one meter per second per second.
J. Salo, October 2003

TABLE 10.6c: CO2 Column Height Sensitivity: Varied Interfacial Tension between 5 and 45, with strongly water-wet brine/CO2 system (contact angle = 0, Reservoir Threshold Pressure = 61).

The evaluation of the sensitivities regarding the air/Hg system average reservoir threshold pressures, varied contact angles, and varied interfacial tensions produced some very clear results. Foremost, the varying of the air/Hg system average reservoir threshold pressure values input as 5 psia vs. 61 psia made very little difference in the CO₂ column heights. The first and second cases presented in Table 10.6a, both with 0 degree contact angle, show very little difference with the spread of ‘Mean CO₂ Column Height’ varying by only 21 ft from a range of 2930 ft vs. 2951 ft., and the highest ‘Max. CO₂ Column Height’ also varying by only 22 ft from a range of 4666 ft vs. 4688 ft. The 21 ft or 22 ft variations are statistically insignificant.

Secondly, the differences in varied contact angles are also minor for values ranging from 0° to 20°. With 61 psia for the air/Hg system average reservoir threshold pressure value as a constant, the ‘Mean CO₂ Column Height’ for 0° is 2930 ft, the ‘Mean CO₂ Column Height’ for 5° is 2919 ft, and the ‘Mean CO₂ Column Height’ for 20° is 2753 ft. That is a variance of less than 180 ft with a column height of almost 3000 ft (Table 10.6c).

The greatest difference is seen only with extremely high contact angles, as seen in the sensitivity cases using 30° to 45° (Table 10.6b). At a 30° contact angle the ‘Mean CO₂ Column Height’ drops to 2537 ft, and at 45 the ‘Mean CO₂ Column Height’ is only 2071 ft.

The greatest variation in calculated CO₂ column heights is found when using different interfacial tensions (Table 10.6c). Interfacial tension of 5 dynes/cm resulted in a calculated CO₂ column height of only 679 ft., and an interfacial tension of 20 dynes/cm resulted in a calculated CO₂ column height of 2037 ft. Since the seal samples are from a sealing lithology known to currently hold a methane column of almost 2200 ft, these are clearly unrealistic interfacial tension values to use. The values of 20 to 30 dynes/cm gave average (mean) CO₂ column height results of 2716 ft and 4074 ft, respectively, and these calculations are more in agreement with other data, such as the current hydrocarbon column height contained at Vorwata in the Roabiba Reservoir. Therefore, the CO₂CRC’s Geochemical Website calculator’s predicted value of 21.57 dynes/cm is the MLV for the Pre-Ayot Shale seals over the Callovian/Bajocian Roabiba Reservoir at Vorwata.

Therefore, several conclusions can be reached about the sensitivities run with varied MICP averaged reservoir threshold pressure and varied contact angle. Varying the averaged MICP reservoir threshold pressures between 5 psia and 61 psia makes

little difference to calculated CO₂ column height. The 61 psia averaged MICP reservoir threshold pressure for the Roabiba Reservoir at Vorwata is the Most Likely Value (MLV) to use. This is consistent with the reservoir characterization and the sequence stratigraphy carried out by the author for the Tangguh area. This sequence stratigraphy framework models the Callovian Roabiba, with its average porosities and permeabilities lower when compared to the Bajocian Roabiba, as areally widespread over the Vorwata structure, including structurally downdip at the proposed CO₂ injection well locations. Other analyses, including effective porosity (PHIEC – derived from Petcom Petrophysics program) and calculated permeability (PERMCALC – also derived from Petcom Petrophysics program) for Vorwata area wells, generally agree with petrographic analysis of visible intergranular porosity and dissolution porosity estimates from the reservoir core plugs used in the MICP analysis. These studies confirm that there is a ‘tighter’ sandstone reservoir with generally poorer porosity and permeability at the top of the Roabiba Reservoir, irrespective of whether it is modelled as Bajocian to earliest Bathonian, or as Callovian in age. *This sensitivity study not only supports the use of all six Roabiba Reservoir samples as ‘representative’ of the Vorwata area Roabiba Reservoir but also, more importantly, clearly shows that even if the Vorwata area Roabiba Reservoir is more heterogeneous than anticipated with ‘tighter’ reservoir intervals, the differences in ‘averaged MICP reservoir threshold pressures’ will have only a minor impact on the maximum CO₂ column height that the top and lateral Pre-Ayot Shale seal can hold.*

In the absence of experimental laboratory research reproducing the actual ‘wettability’ of the brine/CO₂ system of Vorwata’s Roabiba Reservoir and top seal, the most likely value (MLV) for the contact angle is either 0 degrees or a value between 0 degrees and 5 degrees. The first line of reasoning towards an MLV of zero is that in the brine/hydrocarbon system, the brine is the denser phase and the contact angle is measured through the brine with empirical laboratory results usually showing $\theta_{b/hc} = 0^\circ$ (Schowalter, 1979; Vavra, et al., 1992). In the brine/CO₂ system, the brine is also the denser phase and the contact angle is measured through the brine, with the density of ‘supercritical CO₂’ varying only slightly from certain gravities of hydrocarbon (i.e. oil). Therefore, the contact angle between hydrocarbons migrating through a denser phase brine in relation to the solid rock grain surfaces, as measured through the water phase has a $\theta_{b/hc} = 0^\circ$. The ‘wettability’ of the hydrocarbon/water system is defined

as $\text{COS } \theta_{b/hc}$ and is equal to 1° (Schowalter, 1979). The adhesive and cohesive properties of oils and ‘supercritical CO₂’ are likely to be similar. The Roabiba Reservoir aquifer downdip from the GWC is the wetting phase. When ‘supercritical CO₂’ enters the largest of the interconnected pore throats it does not totally displace the pore water, which coats the surfaces of the grains (Kaldi, 2003). Therefore, the assumed value of the contact angle is zero or a value very close to zero and is expressed as, $\theta_{b/co_2} = 0^\circ$, with the ‘wettability’ of the brine and CO₂ system equal to one, and expressed as $\text{COS } \theta_{b/co_2} = 1$ (Schowalter, 1979; Vavra et al., 1992; and Dewhurst et al., 2001). A hydrostatic reservoir condition is assumed for the Roabiba Reservoir at Vorwata, in lieu of any contradictory evidence.

Finally, the Roabiba Reservoir at Vorwata currently contains a known hydrocarbon gas column of almost 2200 ft. This 2200 ft column, is a very ‘dry gas’, composed of 88% methane, 2% ethane and propane, and 10% CO₂ (Bulling, et al., 1998) and is capped by the Pre-Ayot Shale as the top and lateral seals. Since the gas column is primarily methane, it is far less dense than a ‘supercritical CO₂’ column. The less dense the fluid, the greater upward buoyancy it exerts. Just as any given seal can hold a larger (i.e. higher) equivalent oil column than dry gas column, any given seal can hold a larger (greater height) equivalent supercritical CO₂ column than dry gas column. Since the Pre-Ayot demonstrably holds a 2200 ft dry gas column at Vorwata, the Pre-Ayot must be able to hold a column of significantly greater height for supercritical CO₂. The summary of results from ‘sensitivities’ analysis is as follows:

- **Average reservoir threshold pressure**
 - There is little variance in calculated maximum CO₂ column heights when values between 5 psia and 61 psia are used.
 - A 61 psia average reservoir threshold pressure was selected because it includes CO₂-ICP results from ‘tighter’ Callovian reservoir samples.
- **Contact angle in a brine/CO₂ system**
 - There is moderate variance in calculated maximum CO₂ column heights when values between 0° and 45° were used.
 - A 0° contact angle was selected based on extrapolation of empirical HC/brine data.

- **Interfacial tension in a brine/CO₂ system**
 - There is large variance in calculated maximum CO₂ column heights when values between 5 dynes/cm and 45 dynes/cm are used.
 - Values between 20-25 dynes/cm were selected based on extrapolation of empirical data.
 - The exact value for each potential sealing unit examined varied slightly based on differing salinity/density of formation waters and differing depths/pore pressures for each of the seal units. Exact values for each potential sealing unit were derived from the Website Geochemical Calculator.

10.4 Roabiba Reservoir Regional Seals

A map illustrating the areal extent of the Roabiba Reservoir Top Seal across the Tangguh area is presented in Figure 10.5. The Roabiba Reservoir top and lateral seal is the Pre-Ayot Shales only at Vorwata. The Roabiba Reservoir top and lateral seal, at the adjacent Wiriagar Deep anticlinorium, is the Ayot Limestone and the Upper Late Jurassic Shales.

As seen in the cross-sections (Figure 10.1), the Ayot Limestone is a uniformly thick 40 ft to 60 ft carbonate that is present across the entire Tangguh study area. Although it is only the top and lateral seal for the Roabiba Reservoir at the Wiriagar Deep anticlinorium, it is also present over the Vorwata anticline as a regional seal for the Roabiba Reservoir. In addition, there are several other regional seals present across the entire Tangguh area, including the Upper Late Jurassic Shales, the Late Cretaceous, and also the Paleocene Mud-Prone Member.

Seal capacity for each of these sealing lithologies is calculated from MICP testing on representative samples obtained from whole cores through these intervals, and the results are presented in Table 10.7 with the same format as the Table 10.6 Pre-Ayot Top Seal sensitivities table. Based on the results of the Pre-Ayot Top Seal sensitivities (Tables 10.6a, 10.6b, and 10.6c), the MICP averaged reservoir threshold pressure input in the CO₂ column height calculator spreadsheet was normalized to 61 psia, the contact angle used for the brine/CO₂ system was 0°, and the interfacial tension used for the Pre-Ayot Shales at Vorwata was 21.57 dynes/cm. The interfacial tension used for each of the regional seals varied. This is because each regional seal

is at a different burial depth and as such has different confining pressures, and each stratum has different salinities. Therefore, the density of the brine at each potential seal stratum is different. The CO₂CRC Geochemical Website calculator has supplied different MLV's ranging from 21.57 dynes/cm to 26.11 dynes/cm for each of these seal lithologies, based on the different brine densities and pore pressures. The interfacial tensions MLV (Most Likely Value) for each of the potential regional seals are identified in Table 10.7.

The first case presented at the top of the table is the Pre-Ayot Shale top and lateral seal at Vorwata, with the results as discussed above. Results of converting the 6 Vorwata #10 well MICP seal samples (Hg/air system) to a brine/CO₂ system, show one sample from core depth 3944m with the minimum (i.e. smallest maximum) CO₂ column height of 1651 ft, a mean (or average) maximum CO₂ column height for all six samples of 2930 ft, and one sample from core depth 3947m with the highest maximum CO₂ column height of 4666 ft, with the mode (from core depth samples 3954m and 3967m) being 3310 ft.

The second seal capacity evaluation is for the Ayot Limestone and Upper Late Jurassic Shale intervals. These sample results are presented together. One Ayot Limestone sample from the WD-7 and one Ayot Limestone sample from the WD-3 were MICP tested. Interestingly, both resulted in an identical calculated maximum CO₂ column height of 4705 ft. These results represent the greatest maximum CO₂ column height retained and also the mode for the combined Ayot Limestone and Upper Late Jurassic Shale sample group. The remaining four samples tested were from different depths in the Upper Late Jurassic Shale interval in Wiriagar Deep #3. The highest maximum CO₂ column height from the Upper Late Jurassic Shale group samples calculated to a 4697 ft. column (at plug sample depth 9329'), with the minimum CO₂ column height of 3230 ft (core plug 9325'). The mean maximum CO₂ column height for the entire group was 4244 ft. The third seal capacity evaluation presented is the Late Cretaceous Marl interval. Three core plug/chip samples from the WD-3 well and two core plug/chip samples from the WD-7 well were analysed. The highest maximum CO₂ column height calculated to 8108 ft. column (plug sample depth 9272' at WD-3), with the minimum CO₂ column height of 1613 ft. The minimum value was derived from a core plug/chip samples at 9274 ft (ie. only 2 feet

Well Name	Core Plug Sample Depth (Driller's measured depth from RKB)	Estimated Pressure at Reservoir Datum (Mpa)	Calculated Temp. at Reservoir Datum (deg C)	Total Salinity Measured in Reservoir from DST Flow (mg/L)	CO2 Density (g/cm3)	Brine Density (g/cm3)	Interfacial tension (mN/m or dynes/cm)	Contact angle (deg)	Seal Threshold Pressure (air/Hg system) (psia)	Reservoir Threshold Pressure (air/Hg system) (psia)	Seal Threshold Pressure (brine/CO2 system) (psia)	Reservoir Threshold Pressure (brine/CO2 system) (psia)	Height of CO2 Column (ft)	Zone/Unit	Lithology
Pre-Ayot Shale Units as Top and Lateral Seal for Vorwata Roabiba CO2 with contact angle = 0 and Average Reservoir Threshold Pressure = 61 psia															
Vorwata-10st	3944.43m	40	124	21855	0.680	1.025	21.57	0	4268	61	250.37	3.58	1651	PA30	SH
Vorwata-10st	3947.64m	40	124	21855	0.680	1.025	21.57	0	11951	61	701.07	3.58	4666	PA30	SH
Vorwata-10st	3954.46m	40	124	21855	0.680	1.025	21.57	0	8496	61	498.39	3.58	3310	PA30	SH
Vorwata-10st	3965.57m	40	124	21855	0.680	1.025	21.57	0	5971	61	350.27	3.58	2319	PA20	SH
Vorwata-10st	3966.82m	40	124	21855	0.680	1.025	21.57	0	5975	61	350.51	3.58	2321	PA20	SH
Vorwata-10st	3967.10m	40	124	21855	0.680	1.025	21.57	0	8497	61	498.45	3.58	3310	PA20	SH
Vorwata-1	11902' 3"	40	124	21855	0.680	1.025	21.57	0		339	0	19.89	0	CU30	SS
Vorwata-7	13152' 5"	40	124	21855	0.680	1.025	21.57	0		5	0	0.29	0	CU30	SS
Vorwata-10st	4026.18m	40	124	21855	0.680	1.025	21.57	0		4	0	0.23	0	R80	SS Min. CO2 Column (ft.): 1651
Vorwata-10st	4034.51m	40	124	21855	0.680	1.025	21.57	0		5	0	0.29	0	R80	SS Max. CO2 Column (ft.): 4666
Vorwata-10st	4090.85m	40	124	21855	0.680	1.025	21.57	0		8.5	0	0.50	0	R50	SS Mean CO2 Column (ft.): 2930
Vorwata-10st	4128.92m	40	124	21855	0.680	1.025	21.57	0		5	0	0.29	0	R30	SS Mode CO2 Column (ft.): 3310

Well Name	Core Plug Sample Depth (Driller's measured depth from RKB)	Estimated Pressure at Reservoir Datum (Mpa)	Calculated Temp. at Reservoir Datum (deg C)	Salinity Measured in Reservoir from DST Flow (mg/L)	CO2 Density (g/cm3)	Brine Density (g/cm3)	Interfacial tension (mN/m or dynes/cm)	Contact angle (deg)	Seal Threshold Pressure (air/Hg system) (psia)	Reservoir Threshold Pressure (air/Hg system) (psia)	Seal Threshold Pressure (brine/CO2 system) (psia)	Reservoir Threshold Pressure (brine/CO2 system) (psia)	Height of CO2 Column (ft)	Zone/Unit	Lithology
Ayot Limestone & Upper Late Jurassic Shale Units as Regional Seal for Vorwata Roabiba CO2 with contact angle = 0 deg and Average Reservoir Threshold Pressure = 61 psia															
Wirriagar Deep-7	8471' 1"	28	117	24810	0.565	1.031	24.21	0	14474	61	952.99	4.02	4705	Ayot	LS/MRL
Wirriagar Deep-3	9309' 8"	28	117	24810	0.565	1.031	24.21	0	11949	61	786.74	4.02	3881	K/LJSh	SH
Wirriagar Deep-3	9325' 0"	28	117	24810	0.565	1.031	24.21	0	9953	61	655.32	4.02	3230	LJSh	SH
Wirriagar Deep-3	9328' 4"	28	117	24810	0.565	1.031	24.21	0	14448	61	951.28	4.02	4697	LJSh	V. TUFF
Wirriagar Deep-3	9344' 1"	28	117	24810	0.565	1.031	24.21	0	14470	61	952.73	4.02	4705	Ayot	LS/MRL
Vorwata-1	11790' 9"	40	124	21855	0.680	1.025	21.57	0		339	0	19.89	0	CU30	SS
Vorwata-7	13152' 5"	40	124	21855	0.680	1.025	21.57	0		5	0	0.29	0	CU30	SS
Vorwata-10st	4026.18m	40	124	21855	0.680	1.025	21.57	0		4	0	0.23	0	R80	SS Min. CO2 Column (ft.): 3230
Vorwata-10st	4034.51m	40	124	21855	0.680	1.025	21.57	0		5	0	0.29	0	R80	SS Max. CO2 Column (ft.): 4705
Vorwata-10st	4090.85m	40	124	21855	0.680	1.025	21.57	0		8.5	0	0.50	0	R50	SS Mean CO2 Column (ft.): 4244
Vorwata-10st	4128.92m	40	124	21855	0.680	1.025	21.57	0		5	0	0.29	0	R30	SS Mode CO2 Column (ft.): 4705

Well Name	Core Plug Sample Depth (Driller's measured depth from RKB)	Estimated Pressure at Reservoir Datum (Mpa)	Calculated Temp. at Reservoir Datum (deg C)	Total Salinity Measured in Reservoir from DST Flow (mg/L)	CO2 Density (g/cm3)	Brine Density (g/cm3)	Interfacial tension (mN/m or dynes/cm)	Contact angle (deg)	Seal Threshold Pressure (air/Hg system) (psia)	Reservoir Threshold Pressure (air/Hg system) (psia)	Seal Threshold Pressure (brine/CO2 system) (psia)	Reservoir Threshold Pressure (brine/CO2 system) (psia)	Height of CO2 Column (ft)	Zone/Unit	Lithology
Late Cretaceous Marl as Regional Seal for Vorwata Roabiba CO2 with contact angle = 0 and Reservoir Threshold Pressure = 61 psia															
Wirriagar Deep-7	7962' 6"	27	100	40951	0.547	1.048	25.47	0	8471	61	586.77	4.23	2688	P/TopK	SH
Wirriagar Deep-7	7981' 6"	27	100	40951	0.547	1.048	25.47	0	11945	61	827.41	4.23	3798	TopK	LS/MRL
Wirriagar Deep-3	9238' 0"	28	117	24810	0.565	1.031	24.21	0	8540	61	562.29	4.02	2768	K	LS/MRL
Wirriagar Deep-3	9272' 1"	28	117	24810	0.565	1.031	24.21	0	24894	61	1639.06	4.02	8108	K	LS/MRL
Wirriagar Deep-3	9274' 1"	28	117	24810	0.565	1.031	24.21	0	5000	61	329.21	4.02	1613	K	LS/MRL
Vorwata-1	11790' 9"	40	124	21855	0.680	1.025	21.57	0		339	0	19.89	0	CU30	SS
Vorwata-7	13152' 5"	40	124	21855	0.680	1.025	21.57	0		5	0	0.29	0	CU30	SS
Vorwata-10st	4026.18m	40	124	21855	0.680	1.025	21.57	0		4	0	0.23	0	R80	SS Min. CO2 Column (ft.): 1613
Vorwata-10st	4034.51m	40	124	21855	0.680	1.025	21.57	0		5	0	0.29	0	R80	SS Max. CO2 Column (ft.): 8108
Vorwata-10st	4090.85m	40	124	21855	0.680	1.025	21.57	0		8.5	0	0.50	0	R50	SS Mean CO2 Column (ft.): 3794
Vorwata-10st	4128.92m	40	124	21855	0.680	1.025	21.57	0		5	0	0.29	0	R30	SS Mode CO2 Column (ft.): N/A

Well Name	Core Plug Sample Depth (Driller's measured depth from RKB)	Estimated Pressure at Reservoir Datum (Mpa)	Calculated Temp. at Reservoir Datum (deg C)	Total Salinity Measured in Reservoir from DST Flow (mg/L)	CO2 Density (g/cm3)	Brine Density (g/cm3)	Interfacial tension (mN/m or dynes/cm)	Contact angle (deg)	Seal Threshold Pressure (air/Hg system) (psia)	Reservoir Threshold Pressure (air/Hg system) (psia)	Seal Threshold Pressure (brine/CO2 system) (psia)	Reservoir Threshold Pressure (brine/CO2 system) (psia)	Height of CO2 Column (ft)	Zone/Unit	Lithology
Paleocene Mud Prone & Sand Prone Member Regional Seals for Vorwata Roabiba CO2 with contact angle = 0 and Reservoir Threshold Pressure = 61 psia															
Wirriagar Deep-3	7548' 9"	25	88	40951	0.547	1.048	26.11	0	4994	61	355	4.33	1616	PMP	SH
Wirriagar Deep-3	7549' 2"	25	88	40951	0.547	1.048	26.11	0	5983	61	425	4.33	1940	PMP	SH
Wirriagar Deep-3	7552' 7"	25	88	40951	0.547	1.048	26.11	0	1726	61	123	4.33	546	PMP	SH
Wirriagar Deep-3	7596' 9"	25	88	40951	0.547	1.048	26.11	0	2480	61	176	4.33	793	PMP	SH
Wirriagar Deep-2	7377' 11"	27	100	40951	0.547	1.048	25.47	0	9983	61	692	4.23	3171	PUM	SH
Wirriagar Deep-2	7380' 0"	27	100	40951	0.547	1.048	25.47	0	5014	61	347	4.23	1583	PMM	SH
Vorwata-1	11790' 9"	40	124	21855	0.680	1.025	21.57	0		339	0	19.89	0	CU30	SS
Vorwata-7	13152' 5"	40	124	21855	0.680	1.025	21.57	0		5	0	0.29	0	CU30	SS
Vorwata-10st	4026.18m	40	124	21855	0.680	1.025	21.57	0		4	0	0.23	0	R80	SS Min. CO2 Column (ft.): 546
Vorwata-10st	4034.51m	40	124	21855	0.680	1.025	21.57	0		5	0	0.29	0	R80	SS Max. CO2 Column (ft.): 3171
Vorwata-10st	4090.85m	40	124	21855	0.680	1.025	21.57	0		8.5	0	0.50	0	R50	SS Mean CO2 Column (ft.): 1608
Vorwata-10st	4128.92m	40	124	21855	0.680	1.025	21.57	0		5	0	0.29	0	R30	SS Mode CO2 Column (ft.): N/A

NOTE: No cores of regional seals (i.e. Paleocene Shales, Late Cretaceous Marl, Upper Late Jurassic Shales) were obtained on Vorwata wells. Cores obtained on Wirriagar Deep wells were used as a proxy for Vorwata area regional seal evaluations

TABLE 10.7: Comparison of Seal Capacity and CO2 Column Heights Regarding Top and Lateral Seals vs. Overlying Regional Seals for Vorwata Structure Roabiba Reservoir.

deeper than the greatest maximum in the WD-3 well). The mean maximum CO₂ column height for the entire group was 3794 ft, and no mode was present due to the wide scatter of calculated CO₂ column heights. The tremendous range in calculated CO₂ column heights in the Late Cretaceous interval is due to the great lateral and vertical heterogeneity in the rock. The Late Cretaceous succession is very carbonate-rich (i.e. argillaceous limestone/dolomite with locally abundant siderite) at the base that grades into a marl towards the top of the succession, especially in the Wiriagar Deep area. The interval, however, has shaley streaks though it (i.e. calcareous shale), and rare sandstone lenses at some Vorwata wells (Salo, 1997g; Perry, 1997; Perry, et al., 1997).

The final seal capacity evaluation is the Paleocene interval shale, with two samples from the WD-2 well representing the Paleocene Sand-Prone Member (one from the Middle Member {PMM} and one from the Upper Member {PUM}), and four samples from the WD-3 Paleocene Mud-Prone Member {PMP}, which caps the entire Paleocene stratigraphic unit. The maximum CO₂ column height was 3171 ft (WD-2, PUM core plug/chip sample 7377'), the minimum CO₂ column height was 546 ft (WD-3, PMP core plug/chip depth 7552'), and the mean maximum CO₂ column height was 1608 ft, with no mode present for the data set.

The MLV salinity, temperature, brine density, and interfacial tension angles were derived from the calculator spreadsheet in all of the above cases. The (greatest or highest) maximum CO₂ column heights for the Pre-Ayot Shale sample set, and the combined Ayot Limestone and Upper Late Jurassic Shale sample sets, are relatively close with 4666 ft for the former and 4706 for the latter. However, the mean maximum CO₂ column heights vary considerably, with 2930 ft for the Pre-Ayot Shale, and 4244 ft for the combined Ayot Limestone and Upper Late Jurassic Shale sample sets.

The Late Cretaceous Marl values are the most skewed. The most extreme highs and lows are from samples only 2 feet apart in the same well. This also reflects in the lack of a 'mode for maximum CO₂ column height' in the Late Cretaceous group, although a 'mode' is present in both the Pre-Ayot Shale samples and the combined Ayot Limestone and Upper Late Jurassic Shale samples. The implications of this will be discussed later in Section 2.6 "Conclusions Regarding Seal Integrity and Seal Potential".

Finally the Paleocene clearly showed the overall poorest seal capacity to CO₂. It has the lowest calculated column heights of all sealing units in the smallest, highest, and mean (average), maximum CO₂ column heights. The highest overpressures were encountered at the top-most Paleocene reservoirs located near the culminating crest of the Wiriagar Deep anticlinorium. This indicates that the seal at the Paleocene Mud-Prone Member, or the shales capping the upper Sand-Prone Member, apparently are excellent seals capable of retaining these overpressures. However, no whole core through the key potential sealing interval from Wiriagar Deep is available, so seal capacities could not be quantified by MICP testing.

In any case, the potential use of the Paleocene reservoirs for CO₂ injection and sequestration/storage is likely to be eliminated because of a low geological confidence factor for ESSCI success (relative to the Middle Jurassic reservoirs). This is because of uncertainty due to the lack of whole cores through the most-likely potential seal interval, and because the uncertainty over LM, MM, and UM turbidite sandstone reservoir connectivity. Additionally, it probably has insufficient potential storage capacity to sequester the estimated total volume of CO₂ to be disposed. In summary, the Paleocene reservoirs have low degree of confidence factors for the probability of successful ESSCI CO₂ sequestration because of insufficient data of the right quality, and existing data indicates unfavourable geological character for successful sequestration/storage volumes and sweep efficiency due to isolation of reservoir bodies.

10.5 Limitations

The limitations of sampling, testing, and maximum CO₂ column height determination need to be addressed prior to discussions regarding seal capacity, seal geometry, seal integrity and, the conclusions regarding seal potential for the Pre-Ayot Shales, Ayot Limestone, Upper Late Jurassic Shales, Late Cretaceous Marls, and Paleocene shales of the Sand-Prone Member and the Mud-Prone Member. Digital photographs of the various potential shale sealing lithologies are presented in Figure 10.7.

There are some obvious limitations with the physical samples used in MICP testing and results derived thereof. Although cuttings can be used in MICP testing for seal capacity (Purcell, 1949), whole cores are preferred for MICP analysis. Schowalter (1979) ascribed the less accurate 'capillary plateau' results and measured

mercury displacement pressures in cuttings to the scale of lithological heterogeneity being greater than the scale of the drill cuttings.

Cores, obviously, capture more of a given lithology's heterogeneity than diamond bit drill cuttings (approximately <3mm). Furthermore, Dewhurst et al., (2001) stated that "the widespread use of cuttings for capillary pressure determination introduces analytical uncertainty in that most drill cuttings ... are oven dried [at high temperatures] before testing" (Dewhurst, et al., 2001, p5). The drying of cuttings or core plugs frequently causes changes in the clay type (due to dewatering), clay lattice structure, and hence the pore size, shape, and distribution (Dewhurst, et al., 2001).

On more than half of the Tangguh area wells, diamond drill bits were frequently used for drilling the Mesozoic intervals and produced drill cuttings <3mm in size. These drill cuttings were frequently contaminated by 'cavings' (i.e. rock fragments and particles falling in uphole from the drilling bit depth). Also, drill cuttings were routinely oven dried by the 'mud-loggers' at high temperatures (>90° c). Therefore, samples for this study's MICP testing were conducted on core plugs and core chips samples taken from whole core on Wiriagar Deep and Vorwata wells. These cores are deemed far more representative than drill cuttings and less altered by high temperature drying.

A further limitation of samples for all of the rock samples from Wiriagar Deep and Vorwata wells, both whole core and cuttings, is the extended time that the samples were stored under very poor preservation conditions. Wiriagar Deep and Vorwata cores were between 9 ½ years old (WD-1 was cored in 1994) and 5 ½ years old (V-10 was cored in 1998) by the time samples were analysed by MICP testing. The conditions in which cores are stored in Jakarta Indonesia are less than optimum, as the rocks are exposed to high humidity and high ambient air temperatures in a warehouse located on Jakarta Bay that is flooded occasionally by seasonal rains and ocean storm surges. It was evident to the authors during viewing of the cores in 2001 and 2002 that a major amount of *post-coring* diagenesis and mineral alteration had occurred during storage of the cores (Figure 10.6). However, no other samples are available. No new wells have been drilled since the appraisal and delineation phase of the Tangguh Project ended in 1998. Sample selection was such that core plug and core chip samples were picked with extreme care to avoid sampling portions of core that were visibly altered.

It is important that analysed core plugs and chips are unaltered. Of particular concern is the cation exchange capacity (CEC) and alteration of clay minerals, particularly illites, smectites, and sulfides. Also the desiccation and high shrinkage stresses resulting from poor storage and preservation conditions, along with the development of micro-fracturing resulting from in-situ stress relief at surface after coring, would undoubtedly affect the MICP-porosimetry results.

The effects of clay alteration, mineral hydration, core desiccation, and micro-fracturing due to stress-relief at surface would lower the displacement pressures of potential seal samples. This is most evident when one considers the effects of micro-fracturing on seal lithologies in regard to MICP testing. The purposes of the MICP analyses on potential seal samples for CO₂ sequestration/storage were two-fold.

Firstly, explorationists and researchers in the petroleum industry often are faced with the dilemma of having a less than ideal data suite on which to base analyses and decisions. It was possible only to test the seal samples that were available. It would have been remiss for the author to ignore the potential data set available from almost 8,000 ft of core in the area, in regard to maximum CO₂ sequestration/storage column heights. The *overall* effects of clay alterations, mineral hydrations, and post-coring micro-fracturing would be to lower the entry/displacement pressures of potential seal samples, the MICP data results provide at least a minimum CO₂ sequestration/storage column height that a given seal lithology can hold.

Secondly, a series of potential seals were identified, selected, and tested to provide a 'relative' ranking of magnitude for CO₂ sequestration/storage column heights. The results already presented in the previous sections provide evidence that the Pre-Ayot shales interval is a very good seal capable of holding a CO₂ column of almost 3000 ft in the Roabiba Reservoir at the Vorwata area. In contrast, the Paleocene shales of the Sand-Prone Member and the Mud-Prone Member are clearly less effective seals, with their minimum calculated CO₂ column heights being only ~1600 ft and ~800 ft respectively, (although the Paleocene sampling may be unrepresentative due to the lack of cores through the key sealing intervals).

Representativeness of the MICP samples: Firstly, are the whole cores representative of the sealing unit lithologies and their respective heterogeneities over an area as large area as the Tangguh fields? The answer is, probably not very. The cores obtained from most of the Wiriagar Deep and Vorwata wells were driven by petroleum exploration and appraisal objectives. Most of the cores were taken in the

reservoir intervals, and more importantly, the hydrocarbon-bearing reservoir intervals, with seals cored rarely and accidentally, by mistaken coring depth picks (eg. the extremely important Pre-Ayot Shale interval core taken on the V-10 well). Only on WD-1 and WD-3 was the coring of seals pre-planned. These cores were driven with a hydrocarbon exploration focus, as the WD-1 well was ultimately the discovery well for the Wiriagar Deep field, and the WD-3 well was an early delineation well. Appraisal wells on delineated fields generally do not include costly and time-consuming core coverage in non-productive seals. Therefore, there is generally little core coverage planned in sealing units for fields especially prior to the development phase, and Tangguh was no exception. In this regard, this study was fortunate to actually have whole core across all of the various sealing lithologies in the Tangguh area. Whether wisely pre-planned or by fluke, data were obtained from 22 wells covering an area 1625 sq. km. (65 km x 25 km was the minimum area modelled in this study to capture the Vorwata, Wiriagar Deep, Roabiba, and Ofaweri Fields)

Secondly, are the core plugs and core chips that were used representative of the entire sealing unit lithologies? Once again the conclusion is, probably not very. Only 31 core plugs and core chips from five potential sealing lithology intervals were tested. There are possibly up to a million potential core plugs that could be taken through all of the existing seal cores from the Tangguh area if all of the whole cores were divided into 2" long vertically oriented core plugs and then tested in order to obtain a truly representative sample set. This is unfeasible and unreasonable. Obviously, with budgetary and time constraints, and the reduced amount of cores available (due to alteration and fracturing of some cored intervals) the 31 core plugs and core chips selected, although possibly not truly representative of the entire spectrum of seals over the Tangguh area, are thought to be a valid sample base for calculating potential CO₂ column heights.

10.6 Discussions Regarding Seal Capacity, Geometry, and Integrity

The sealing potential of any seal is evaluated based on seal capacity, seal geometry, and seal integrity. The results of the seal capacity, calculated as the maximum CO₂ column height for each sample, were previously discussed and presented in the above sections of this chapter.

Downey (1984, p.53) stated, "...large extrapolations of data are commonly necessary in geologic work, but it is important in assessing seal properties to

remember that *averages* are nearly meaningless in determining the probability of seal ...we are basically concerned with the properties of the “weakest” point of the sealing surface”. Downey stated that the weakest point (i.e. MICP seal threshold pressure) is the important attribute, especially when comparing cores from various wells through the same seal interval. However, it is shown in Table 10.1 that the MICP samples for the Roabiba’s Top/Lateral Seal at Vorwata all come from a single core at a single well, V-10. This cored interval and the representative samples selected from it span more than 75 ft (23 m) of PA20 and basal PA30 sequence stratigraphic units. In this case the maximum CO₂ column height is 4666 ft. The minimum value for maximum CO₂ column height is only 1651 ft. The minimum or smallest calculated value for maximum CO₂ column height could not possibly be right. If it was, there would not be 2200 ft dry gas column at Vorwata in the Roabiba reservoir, or there would be evidence of gas leakage (waste zone) at the crest of the gas accumulation where V-1 well was drilled. There might even be hydrocarbon accumulations in shallower reservoir units at Vorwata above the Roabiba, as there are at Wiriagar Deep (where the Pre-Ayot unit is absent due to an erosional unconformity). In this case, the fact that out of a relatively small sample set there is a mode (i.e. two samples out of six total) with a value for maximum CO₂ column height of 3310 ft is significant. Even more significant is that the deepest MICP shale core plug from 3967.10 m is the closest shale seal sample to the underlying reservoir, and is one of the two samples that have the mode value maximum CO₂ column height of 3310 ft.

Given that the Pre-Ayot Shale seal is *known* to support a 2200 ft dry gas column, then a calculated CO₂ column height of 1651 ft CO₂ column is obviously erroneous. The minimum CO₂ column height that the Pre-Ayot Shales can support at Vorwata in the Roabiba Reservoir is believed to be between 2900 ft and 3310 ft., which encompass both the mean and the mode CO₂ column heights. The highest maximum CO₂ column height that the Pre-Ayot Shales can support at Vorwata in the Roabiba Reservoir is likely to be 4666 ft (based on the sample from 3947.64 m).

The geometry of this sealing unit, as correlated within a sequence stratigraphic framework, is that the Pre-Ayot Shales (PA10, and PA20, and basal PA30) are present in varied thicknesses over the entire Vorwata anticline and the R-1 well location (Figure 10.1B, cross-section E-E’). This is based on the interpretation of the Pre-Ayot Shales interval as a deep-marine, relatively rapid-flooding event that was pervasive

Sample	Mineralogy
11902'3"	Quartz (dominant), Kaolinite (minor), Illite (minor), Chlorite (trace/minor), Feldspar (trace/minor), Pyrite (trace), Siderite (trace), other traces?
11904'3"	Quartz (dominant), Kaolinite (minor), Illite (minor), Chlorite (trace/minor), Pyrite (trace), Feldspar (trace), Siderite (trace), other traces?
13020'6"	Quartz (dominant), Kaolinite (minor), Illite (minor), Chlorite (trace/minor), Siderite (trace), Pyrite (trace), Felspar? (trace), other traces?
13025'6"	Quartz (dominant), Kaolinite (trace/minor), Illite/Muscovite (trace), Siderite (trace), Feldspar (trace)
13030'1"	Quartz (dominant), Kaolinite (minor), Illite (minor), Chlorite (trace/minor), Pyrite (trace), Feldspar (trace), Siderite (trace), other traces?
3944.43m	Quartz (dominant), Plag feldspar [Albite/Anorthite] (minor), Kaolinite (minor), Illite (minor), Chlorite (trace/minor), Calcite (trace), Siderite (trace), Pyrite (trace), other traces?
3947.64m	Quartz (dominant), Kaolinite (minor), Illite (minor), Plag Feldspar (minor), Chlorite (trace/minor), Calcite (trace), Pyrite (trace), Siderite (trace), other traces?
3954.46m	Quartz (dominant), Kaolinite (minor), Plag Feldspar (minor), Illite (minor), Chlorite (trace/minor), Calcite (trace/minor), Siderite (trace), Pyrite (trace), other traces?
3965.57m	Quartz (dominant), Kaolinite (minor), Illite (minor), Chlorite (minor), Calcite (minor), Plag Feldspar (minor), Siderite (trace), Pyrite (trace), other traces?
3966.82m	Quartz (dominant), Kaolinite (minor), Illite (minor), Calcite (minor), Plag Feldspar (minor), Chlorite (minor), Pyrite (trace), Siderite (trace), other traces?
3967.10m	Quartz (dominant), Kaolinite (minor), Illite (minor), Calcite (minor), Plag Feldspar (trace/minor), Chlorite (trace/minor), Pyrite (trace), Siderite (trace), other traces?

Table 10.8: Results of the bulk XRD analyses performed on core plug/chip samples at the ASP, University of Adelaide.

over the entire Wiriagar Deep and Vorwata, but was subsequently removed at Wiriagar Deep by erosion. The LJ-10 erosional unconformity that removed the Pre-Ayot marine shales over the NW portion of the Wiriagar Deep anticlinorium did not incise as deeply into sedimentary rocks at Vorwata. This is because of the uplift activation along the N-S Sekak Ridge and the E-W Kemum High being focussed where they intersect to the NW of the WD-1 well location. The tectonic compressional event that formed the Wiriagar Deep and Vorwata anticlinal structures began in the Oligocene. The result is a Pre-Ayot Shales stratigraphic top seal that has been folded along with the Roabiba Reservoir, resulting in a 3-way dip structural trap with the Pre-Ayot Shales as both the top and lateral seals for the Roabiba Reservoir at Vorwata.

The areal extent of the Pre-Ayot Shales seal lithology has been calculated as covering a minimum area of 39,283 acres over the Vorwata area. This is based on planimetry of the Pre-Ayot Shales over the Vorwata area down to the known GWC at -13,313 ft TVDss (Bulling, et al., 1998). A comparison of gamma-ray (GR) and sonic values (DT) between the Vorwata wells shows very good correlation, with the sonic correlation (stretched or compressed occasionally) of particular significance for seal properties and poro-perm characteristics (Figure 7.3 and 7.12). The sequence stratigraphy framework, by the author, predicts the Pre-Ayot to be present and thickening towards the SE past the V-10 and V-11 well locations, however without well data this is unverifiable. The risk associated with the sequence stratigraphy interpretation is: 1) the lack of well control beyond the known GWC bounding contour (intersected by the V-10 and V-11 wells) and, 2) insufficient seismic resolution to identify the Pre-Ayot interval on seismic lines and hence confirm lateral extent and geometry of the Pre-Ayot in the Tangguh area.

It is likely, however, that the geometry of the sealing unit is extensive: it is a pervasive deep-marine flooding shale deposited as a stratigraphic drape over the Roabiba Reservoir at the Vorwata anticlinal structure, that was subsequently deformed by compressional folding into a stratigraphic trap. Thus, the Pre-Ayot 'cap' is both a top and lateral seal, with a minimum combined PA10 and PA20 shale gross thickness of 17 ft at V-1 to the NW, 19 ft at V-8 to the NE, 133 ft at R-1 to the SW, and a maximum 233 ft at V-10.

Budgetary and time constraints precluded a full suite of analyses (i.e. Petrographic, Bulk XRD, SEM, EDAX, and MICP) on every seal sample, however,

TABLE 10.9a-e: Results of the petrographic analyses performed on whole core plug/chip samples by Dr. S. E. Phillips.**VORWATA-1 & -2**

Well	V-1	V-1	V-1	V-1	V-2	V-2	V-2
Depth (ft)	11,765'9"	11,787'7"	11,790'9"	11,797'7"	12,585'8"	12,594'4"	12,757'6"
Framework grains							
Quartz	46	60	46	41	64	64	65
Feldspar	1	2	2	5	-	Tr	2
Lithics - igneous	2	2	Tr	3	-	-	Tr
- metamorphic	2	Tr	1	2	1	2	1
- sedimentary	Tr	Tr	2	1	1	1	2
Fossils	2	Tr	Tr	-	-	-	-
Mica	-	-	-	1	Tr	-	-
Accessory	-	Tr	Tr	1	1	Tr	Tr
Matrix							
Clay	Tr	-	Tr	8	-	-	2
Organic matter	-	-	-	-	-	-	-
Authigenic							
Hematite	-	-	-	-	4	5	-
Fe micrite	-	-	-	-	-	-	-
Quartz	8	8	Tr	4	8	6	6
Kaolin	5	4	Tr	12	Tr	3	1
Illite	-	Tr	Tr	1	-	Tr	Tr
Fe calcite	9	2	40	-	-	-	-
Dolomite	3	1	-	Tr	-	-	-
?Siderite	5	3	4	5	-	-	-
Pyrite	Tr	Tr	2	4	1	Tr	1
Chlorite	-	-	-	-	-	-	-
Glaucony	-	-	-	-	-	-	-
Barite	-	-	-	-	-	-	-
Porosity							
Intergranular	12	12	-	3	18	17	15
Dissolution	2	3	-	-	1	Tr	1
Intragranular	1	1	2	1	Tr	1	2
Honeycomb	1	1	-	2	-	Tr	1
Micropores	Tr	Tr	-	1	Tr	Tr	Tr
Fractures	-	-	-	4	-	-	-

Tr = trace (less than 1%)

Table 10.9a: Petrographic Analyses Results for Vorwata #1 and Vorwata #2 core plugs.

VISUAL ESTIMATES OF COMPOSITION (Volume %) FOR SAMPLES FROM VORWATA-2 & -7

Well	V-2	V-7	V-7	V-7	V-7	V-7
Depth (ft)	12,901'5"	13,118'3"	13,123'8"	13,136'10"	13,143'6"	13,152'5"
Framework grains						
Quartz	63	58	65	67	67	69
Feldspar	3	3	3	3	3	3
Lithics - igneous	Tr	-	Tr	Tr	-	Tr
- metamorphic	Tr	3	1	-	Tr	Tr
- sedimentary	Tr	Tr	1	1	2	1
Fossils	-	-	-	-	-	1
Mica	2	1	Tr	Tr	Tr	-
Accessory	1	Tr	Tr	Tr	-	Tr
Matrix						
Clay	13	7	-	-	Tr	1
Organic matter	Tr	Tr	-	-	-	-
Authigenic						
Hematite	-	-	-	-	-	-
Fe micrite	-	6	1	1	Tr	Tr
Quartz	2	9	14	10	8	6
Kaolin	Tr	2	3	3	4	2
Illite	1	Tr	Tr	Tr	Tr	-
Fe calcite	-	-	-	-	-	2
Dolomite	Tr	-	-	-	-	Tr
?Siderite	8	-	-	-	-	Tr
Pyrite	3	2	1	2	-	1
Chlorite	-	Tr	-	-	-	-
Glaucony	Tr	-	-	Tr	Tr	Tr
Barite	-	-	Tr	Tr	Tr	-
Porosity						
Intergranular	4	5	7	8	10	12
Dissolution	-	1	1	1	1	Tr
Intragranular	Tr	Tr	Tr	Tr	Tr	Tr
Honeycomb	Tr	2	2	3	3	1
Micropores	-	Tr	Tr	Tr	1	Tr
Fractures	-	-	-	Tr	Tr	-

Tr = trace (less than 1%)

Table 10.9b: Petrographic Analyses Results for Vorwata #2 and Vorwata #7 core plugs.

VISUAL ESTIMATES OF COMPOSITION (Volume %) FOR SAMPLES FROM VORWATA-10

Well	V-10	V-10	V-10	V-10	V-10	V-10	V-10
Depth (m)	4021.25	4021.86	4025.98	4026.18	4034.51	4042.62	4045.92
Framework grains							
Quartz	68	63	68	69	73	67	71
Feldspar	2	2	-	Tr	Tr	-	-
Lithics - igneous	-	-	-	-	-	-	-
- metamorphic	1	1	1	Tr	Tr	Tr	Tr
- sedimentary	2	2	1	1	Tr	Tr	1
Fossils	-	-	-	-	-	-	-
Mica	2	2	Tr	-	-	-	-
Accessory	1	1	-	-	Tr	Tr	Tr
Matrix							
Clay	20	23	-	-	-	5	Tr
Organic matter	Tr	2	-	-	-	Tr	-
Authigenic							
Hematite/jarosite	-	-	8	1	2	7	-
Fe micrite	-	-	Tr	-	-	-	-
Quartz	-	-	7	7	8	5	7
Kaolin	Tr	Tr	2	2	Tr	5	3
Illite	Tr	Tr	-	-	-	Tr	Tr
Fe calcite	-	-	-	-	-	-	-
Dolomite/ankerite	Tr	1	-	-	-	-	-
?Siderite	1	-	-	-	-	-	-
Pyrite	2	2	Tr	Tr	-	Tr	1
Chlorite	-	-	-	-	-	-	-
Glaucony	Tr	Tr	-	-	Tr	-	-
Barite	-	-	-	-	-	-	-
Porosity							
Intergranular	-	-	12	17	16	8	15
Dissolution	Tr	Tr	-	-	Tr	1	1
Intragranular	-	Tr	Tr	Tr	Tr	Tr	Tr
Honeycomb	Tr	Tr	-	-	Tr	-	-
Micropores	-	-	Tr	Tr	Tr	1	Tr
Fractures	-	-	-	2	-	Tr	-

Tr = trace (less than 1%)

Table 10.9c: Petrographic Analyses Results for Vorwata-10 core plugs.

VISUAL ESTIMATES OF COMPOSITION (Volume %) FOR SAMPLES FROM VORWATA-10

Well	V-10	V-10	V-10	V-10	V-10	V-10	V-10
Depth (m)	4049.40	4052.13	4063.45	4076.30	4081.32	4082.85	4090.85
Framework grains							
Quartz	75	68	72	68	68	71	68
Feldspar	-	-	Tr	2	2	1	2
Lithics - igneous	-	-	Tr	-	-	-	Tr
- metamorphic	Tr	Tr	Tr	Tr	Tr	Tr	1
- sedimentary	Tr	Tr	Tr	Tr	Tr	Tr	1
Fossils	-	-	-	-	-	-	-
Mica	Tr	Tr	-	-	Tr	Tr	Tr
Accessory	Tr	-	Tr	Tr	-	-	Tr
Matrix							
Clay	3	-	2	-	2	1	4
Organic matter	-	-	Tr	-	-	Tr	Tr
Authigenic							
Hematite	-	-	-	-	-	-	-
Fe micrite	-	-	-	-	-	-	1
Quartz	8	10	7	8	8	8	6
Kaolin	2	2	2	3	2	2	3
Illite	Tr	Tr	-	Tr	Tr	Tr	Tr
Fe calcite	-	-	-	-	-	-	-
Dolomite	-	-	-	-	-	-	-
?Siderite	-	-	-	-	-	-	-
Pyrite	Tr	Tr	Tr	Tr	Tr	Tr	1
Chlorite	-	-	-	-	-	-	-
Glauccony	-	-	-	-	-	-	-
Barite	-	-	-	-	-	-	-
Porosity							
Intergranular	10	18	15	16	16	15	10
Dissolution	1	Tr	1	2	1	1	1
Intragranular	Tr	Tr	Tr	Tr	Tr	Tr	Tr
Honeycomb	-	-	Tr	Tr	Tr	Tr	Tr
Micropores	Tr	Tr	Tr	Tr	Tr	Tr	Tr
Fractures	-	1	-	-	Tr	Tr	1

Tr = trace (less than 1%)

Table 10.9d: Petrographic Analyses Results for Vorwata-10 core plugs.

VISUAL ESTIMATES OF COMPOSITION (Volume %) FOR SAMPLES FROM VORWATA-10

Well	V-10	V-10	V-10	V-10	V-10	V-10
Depth (m)	4095.50	4101.30	4117.70	4126.30	4126.69	4128.92
Framework grains						
Quartz	68	61	67	68	69	68
Feldspar	3	2	3	3	3	3
Lithics - igneous	Tr	Tr	-	Tr	Tr	Tr
- metamorphic	1	Tr	Tr	Tr	Tr	Tr
- sedimentary	1	Tr	Tr	1	2	Tr
Fossils	-	-	-	-	-	-
Mica	Tr	Tr	Tr	Tr	Tr	Tr
Accessory	Tr	1	Tr	-	-	Tr
Matrix						
Clay	Tr	-	Tr	-	-	Tr
Organic matter	-	-	-	-	Tr	Tr
Authigenic						
Hematite	-	-	-	-	-	-
Fe micrite	-	-	-	-	Tr	-
Quartz	8	7	8	8	9	8
Kaolin	3	1	2	Tr	1	2
Illite	Tr	Tr	Tr	2	2	Tr
Fe calcite	-	-	-	-	-	-
Dolomite	-	10	3	1	Tr	1
?Siderite	-	Tr	4	Tr	Tr	-
Pyrite	Tr	6	Tr	Tr	Tr	-
Chlorite	-	-	-	-	-	-
Glaucony	Tr	Tr	Tr	-	-	-
Barite	-	-	-	-	-	-
Porosity						
Intergranular	12	9	10	12	9	15
Dissolution	3	2	2	2	1	2
Intragranular	Tr	Tr	Tr	1	1	Tr
Honeycomb	Tr	Tr	Tr	Tr	Tr	Tr
Micropores	Tr	Tr	Tr	Tr	Tr	Tr
Fractures	-	-	-	1	2	-

Tr = trace (less than 1%)

Table 10.9e: Petrographic Analyses Results for Vorwata-10 core plugs.

all seal samples were evaluated and appropriate analyses performed as deemed necessary to yield meaningful seal potential conclusions.

The most critical seal samples were the V-10 Pre-Ayot Shale samples discussed above. These were subjected to extensive Bulk XRD, SEM and EDAX analyses, in addition to MICP testing. The qualitative results of the Bulk XRD analyses are summarized and presented in Table 10.8. These indicate that all of the V-10 Pre-Ayot Shale samples 3967m, 3966m, 3965m, 3954m, 3967m and 3944m have essentially the same mineralogy, being composed of primarily ultra-fine silica, kaolinite, illite, and chlorite. These four minerals range in compositional percentage from 5% to 40% each with the four minerals comprising a total of 60% - 90% of the total bulk mineralogy. In addition, trace to minor amounts (less than 5% to a maximum of 20%) of plagioclase feldspar is present in all samples. Calcite is present in bulk volumes between 5% and 20% in the deepest samples 3967m, 3966m, 3965m, and 3954m, but found in concentrations of less than 5% in the upper-most seal samples from 3947m and 3944m. Both siderite and pyrite are present as traces in all samples (less than 5%).

The results of laboratory testing for He- ϕ and Kair on reservoir samples from the Roabiba Sandstone Formation reservoir are presented in Table 7.6. Petrographic point-counts and visual porosity estimates for the Vorwata area Roabiba Sandstone Formation reservoir core plug samples are presented in Table 10.9. SEM and EDAX analyses indicate that primarily illite and kaolinite make up the V-10 samples described above. The SEM images show the Bulk XRD quartz composition as ultra-fine free-floating quartz silt grains set in a clay matrix. These grains are draped by the clay particles and contain virtually no pore spaces resolvable on the SEM. The visual examination of the core plug/chip from 3965.57m shows up to 50% of the surface area covered by euhedral to subeuhedral mica flakes. This was also confirmed by SEM analysis (Appendix 4: Figure 56c), where the mica was identified as muscovite (with locally abundant traces of smectites). Where quartz silt grains are contiguous, the pore throats appear to be occluded by stacked 'kaolinite books', illite, and smectite (Appendix 4: Figure 55c - SEM and EDAX). Furthermore, the MICP results indicate a very small volume of connected pore throats that are less than 2 microns in size (Appendix 4: Figure 56c).

These results indicate a fairly uniform mineralogical composition for the 23m of core analyzed (almost 75 vertical feet of seal from the PA20 and basal PA30

sequences stratigraphic units). These Bulk XRD analyses also confirm the wireline log interpretation and Wellsite Geologist's Progress Log cuttings descriptions that the shales of the PA20 and basal PA30 are very finely silty in part. The wireline log interpretation and Wellsite Geologist's Progress Log cuttings descriptions indicate a cleaner shale interval through the PA10 sequence stratigraphic unit, which directly caps the Roabiba Reservoir at Vorwata. The inference can, hence, be drawn that the PA10 interval is less silty, with less quartz content and with a higher kaolinite and illite content.

Unfortunately, no whole core was obtained in the PA10 unit in any of the Vorwata wells. This must be noted in any evaluation of the Pre-Ayot Shale seal integrity. The 'cleanest shale, providing perhaps the best seal (with most likely the highest maximum CO₂ column height support capability), has not had whole core taken! However, some conclusions regarding Pre-Ayot shale seal integrity can be made. In spite of the relatively high ultra-fine quartz content, very high MICP threshold pressures were measured in testing (4268 psia to 11951 psia), with very high maximum CO₂ column heights calculated (2930 ft average CO₂ column height, and 4666 greatest CO₂ column height). The relatively high clay content of the PA20 and PA30 silty shale units makes for greater ductility, resulting in less brittle rock strengths. The unsampled PA10 unit probably has higher clay content, greater ductility, and less brittleness (based on V_{clay} and V_{shale} from petrophysical evaluation). Based on the existing evidence, the Pre-Ayot Shales are interpreted to possess enough ductility and rock strength to reduce likelihood of mechanical fracturing and faulting due to in-situ stress vectors. This is an important factor when considering the seal potential of the Pre-Ayot versus the regional seals to be discussed below. Grunau (1981) found that of the world's 176 giant and super-giant gas fields known at the time, almost all had evaporite or shale seals.

Finally, no hydrocarbon 'waste zone' has been encountered in the Pre-Ayot Shale seal interval at Vorwata on any of the wells drilled to date. 'Waste zone', is the term applied to detectable hydrocarbons leaking through an overlying cap-rock seal. Furthermore, no significant hydrocarbon accumulations have been found above the Pre-Ayot interval at Vorwata to date. Indeed, only the V-3 well logged rare gas shows in the Cretaceous and these all appear to have been due to swabbing of tight hole during the drilling phase of the well, with very high mud weights recorded in the drilling fluid records (V-3 Completion Log). This gas was likely swabbed gas from

shale intervals and argillaceous limestone, indicating they were not actual ‘gas shows’. Later wireline logging and testing confirmed this. The implication of this is that the Pre-Ayot Shales are a very good seal for the ~2200 ft dry gas pay column at the Vorwata structure. Gas is not leaking at present, and there has not been fault breach to any significant extent, otherwise hydrocarbon indicators would be present at shallower depths above the reservoir.

An appraisal of the various regional seal capacities, seal geometries, and seal integrities is more complex. The results of the seal capacity, calculated as the maximum CO₂ column height for each sample were previously presented for Roabiba Reservoir regional seals, and summarized on Table 10.7. The four major regional seals for the Roabiba Reservoir at Vorwata are, briefly, as follows:

- 1) Ayot Limestone: Top and Lateral Seal for Roabiba Reservoir at Wiriagar Deep, but Regional Seal for the Roabiba Reservoir at Vorwata.
- 2) Upper Late Jurassic Shales: Regional Seal for Roabiba Reservoir at Vorwata and Wiriagar Deep.
- 3) Late Cretaceous Marls: Regional Seal for Roabiba Reservoir at Vorwata and Wiriagar Deep.
- 4) Paleocene Shales of the Sand-Prone and Mud-Prone Members: Regional Seal for Roabiba Reservoir at Vorwata and Wiriagar Deep.

At first glance, the Ayot Limestone and Upper Late Jurassic Shales appear to be very good top or regional seals based on MICP analyses of seal capacity (as discussed previously). The minimum (smallest) CO₂ column height was established at 3230 ft from the Upper Late Jurassic Shales. The two Ayot Limestone samples yielded exactly the same seal capacity (one sample from Wiriagar Deep #7 and one sample from Wiriagar Deep #3) that was also the maximum (greatest) CO₂ column height at 4705 ft. for this grouping (Table 10.7). One sample from the Ayot repeatedly tested by MICP proved to have extremely high threshold pressure that exceeds 60,000 psia (Appendix 4: Figure 24B - MICP graph). The significance of this is that the Ayot Limestone appears to be a relatively homogeneous shallow marine shelfal carbonate, with extremely low porosity and permeability. Additionally, it appears to be pervasive over the Tangguh area with very uniform thickness (Bulling, et al., 1998). This unit is actually the top seal over the Roabiba

Reservoir at the Wiriagar Deep anticlinorium, but it also has potential as an overlying regional seal to the Roabiba Reservoir and the Pre-Ayot Shales top seal at the Vorwata structure.

In regard to seal geometry, it has a uniform thickness over the Tangguh area, ranging from approximately 37 ft (WD-3, WD-6, O-1) to 69 ft (N-1). This unit has significant areal extent, since it is encountered in all Tangguh area wells drilled in the Bird's Head to date, with the exception of the K-1X. The Ayot Limestone is absent at K-1X due to the erosional 'K Unconformity' at the base of the Late Cretaceous. The K-1X lies on the axial flank of the Sekak Ridge, which was actively uplifting during Jurassic and Cretaceous times.

The seal integrity of the Ayot Limestone is not very good. Being a shelfal carbonate, it has lower ductility (resulting in it being very brittle) than all other seal rocks except chert (Downey, 1979, p54). Evidence of this is found at Tangguh. Unlike the Vorwata structure, where no hydrocarbon indicators such as gas accumulations or even gas shows are present in or above the Pre-Ayot Shale top seal, the Ayot Limestone has numerous gas shows recorded on Wiriagar Deep wells, where it is the top seal to the Roabiba Reservoir (see WD-1, WD-2, WD-5, and WD-8 Completion Logs). Both FMI and FMS imaging of several Wiriagar Deep wells indicate open fractures present (Hillis and Meyer, 2003). Therefore, although the tight carbonate fabric of the formation yields high MICP capacity results, the brittle nature of this homogeneous and areally extensive shelfal carbonate results in it easily fracturing. The overlying gas and condensate bearing strata are probably charged by hydrocarbons migrating through fractures in this rock. Examples of these gas charged reservoirs are the Paleocene turbidite sandstones and the fractured and vuggy Kais Limestone Formation (top-most NGLG member), at the Wiriagar Deep structure.

The Upper Late Jurassic Shales are similar to the Ayot Limestone in that the samples analyzed by MICP yielded relatively 'good' seal characteristics (Table 10.7). However, the Upper Late Jurassic Shales exhibit more heterogeneity, mainly due to variable silica content, increased siltiness, and sandy streaks (Figure 10.7). Seal capacity results showed calculated maximum CO₂ column heights ranging from 3230 ft to 4697 ft. but the formation is lacking good ductility and is most-likely very brittle in siliceous intervals. The geometry of this interval is complex. Although it is found in virtually all Tangguh area wells, it's thickness ranges from only tens of feet (at V-8, V-9, V-11 and Saukani #1) to a over 100 feet (at N-1, V-7, and WD-2).

FMI/FMS imaging also showed numerous open fractures, with gas shows, in some Wiriagar Deep wells (but not on any Vorwata wells). Just as with the Ayot Limestone, the fractures cause leakage and most likely charge the overlying gas and condensate bearing strata at the Wiriagar Deep anticlinorium.

This may be due to the presence of an altered volcanic tuff visible in the core from the WD-3 well. Sample 9328' 4" from the WD-3 whole core sampled this interval, and yielded a high MICP seal capacity of 4697 ft. This might be explained by the fact that many volcanic tuffs are rich in volcanic glass, and upon alteration the tuff devitrifies, freeing SiO₂. This can permeate clays in the strata, resulting in a silicified 'porcelaneous shale' which has excellent rock strength, and is very impermeable, but is extremely brittle. An example of this is the Monterey Formation in Central California, which is not a seal but is a fractured shale reservoir that has produced more than one billion barrels of oil since the 1940's (Dunkel, 2001).

At Tangguh, the Late Cretaceous seal interval has the highest seal capacity of all rocks sampled, able to sustain a maximum CO₂ column height of 8108 ft (results from a single sample at 9272' 1" on the WD-3 well). The MICP seal capacity tests also showed a maximum CO₂ column height of only 1613 ft from a sample only 2 ft deeper at 9274' 1". These two values give the range for seal capacity in the Late Cretaceous marls and limestone.

The geometry of this potential sealing lithology is vast. It is found over the entire Tangguh area, having been encountered in every well in the area. It is also areally widespread over most of the Bird's Head, as seen in cores on the East Onin #1 (EO-1) well, located on the KOM Ridge several hundred kilometers to the SW (i.e. KOM = Kumawa-Onin-Misool anticlinal ridge). The base of the Late Cretaceous is one of the few pre-NGLG seismic horizons that can be identified over the entire Bintuni Basin area. It is generally a few hundred to several hundred feet thick in the Tangguh area.

The seal integrity of the Late Cretaceous is compromised by the extreme brittleness of the rock lithology in most areas. It ranges from marl to an argillaceous carbonate to a relatively clean carbonate, with a very high siderite content. Just as with the Ayot Limestone, one sample from 9286' 2" on a WD-3 core had extremely high threshold pressure exceeding an estimated 60,000 psia. Three samples from the core plug were tested and repeated each time, indicating extremely low porosity and permeability, although an entry pressure of 100 psia was established, the threshold

pressure was not reached by 60,000 psia (the pressure testing limit of the porosimeter) (Appendix 4: Figure 14B – MICP graph). The Wiriagar Deep core exhibits slickensided faults and open fractures near the base of the Late Cretaceous at WD-3, with gas shows recorded during drilling and coring. FMI/FMS imaging confirmed numerous open fractures in the Late Cretaceous Marl and similar to the Monterey Shales mentioned previously, this potential sealing lithology is so brittle and fractured at the Wiriagar Deep anticlinorium that it is actually a gas-bearing fractured reservoir.

The Paleocene is divided into a sand-prone lower member (which is further subdivided into the Lower Sand-Prone Member, the Middle Sand-Prone Member, and the Upper Sand-Prone Member). Relatively thick Paleocene Mud-Prone Member shales then cap the sand-prone unit.

The various shale seals that were cored in the Paleocene were analyzed by MICP. The seal capacity of samples from primarily the Mud-Prone Member ranged from a maximum CO₂ column height of only 546 ft to 1940 ft. One sample each from shale ‘caps’ in the Middle Sand-Prone Member and the Upper Sand-Prone Member had maximum CO₂ column heights of only 1583 ft and 3171 ft respectively.

It is the ‘Sand-Prone Member’ shales that serve as top seals or internal baffles, for the hydrocarbon accumulations in the Paleocene. This gas is geochemically related to the dry gas accumulations of the Roabiba Reservoir (Bulling, et al., 1998). These Paleocene reservoirs also have leaking seals, since the Kais ‘condensate’ produced from the shallow Wiriagar field has been typed as genetically linked to the Jurassic Roabiba Reservoir gas accumulations (Dolan and Hermany, 1988; Perkins and Livsey, 1993; Bulling, et al., 1998). All of the reservoirs with significant dry gas or condensate accumulations above the Jurassic Roabiba interval are located on the Wiriagar Deep structure, and all share the same geochemical signature and affiliation (Huizinga, 2000).

The Paleocene seal lithologies are complex, being very heterogeneous with great lateral variability in clay and quartz contents (Lowe, 1998). The paleo-depositional facies and the resultant geometries of the Late Paleocene turbidite reservoirs implies limited connectivity between reservoirs, particularly between the LM, MM, and UM members (Lowe, 1998). This suggests that these reservoirs will have insufficient storage capacity for the potential ESSCI sequestration/storage of CO₂.

Lastly, the characterization of the Paleocene reservoir/seal couplets over the Vorwata structure have a great deal of uncertainty attached to them as *there are no cores through the Paleocene in the Vorwata area*. This is because ARCO and British Gas wells at Vorwata were drilled for hydrocarbon exploration and appraisal purposes, and since no hydrocarbons were encountered in the Paleocene interval at Vorwata, data acquisition received low priority. Therefore, not only are the areal extents of the shale sealing units over the Vorwata area unknown, but the actual characterization and properties associated with any potential seals are also unknown (i.e. paleogeographic facies distribution as interpreted from cores, potential MICP seal capacity from whole core plugs, etc.). This is in contrast to the Ayot Limestone, Upper Late Jurassic Shales, and even to a degree the lower Late Cretaceous regional seal, where sedimentological evaluation combined with palynological/palaeontological/ichnological analyses resulted in the construction of paleo-geographic facies maps showing some reservoir or seal facies deposited over a widespread areal extent.

In conclusion, the various potential Paleocene sealing lithologies over the Vorwata area contain a great deal of uncertainty and as such are ranked with low confidence for seal potential.

10.7 Seal Potential Conclusions

The Pre-Ayot top and lateral seal is currently holding a 2200 ft dry gas hydrocarbon column. This seal is calculated capable of holding a supercritical CO₂ column of at least 3310 ft, and possibly as much as 4666 ft. The Pre-Ayot Shales are interpreted as being an adequate top and lateral seal for CO₂ sequestration/storage in the Vorwata Roabiba Reservoir. The greatest uncertainty associated with this seal potential is the lack of seismic resolution to confidently image and map its lateral extent and properties on the existing 3D seismic survey. There is some risk regarding the Pre-Ayot Shales extent and properties between the Vorwata wells (mainly from the risk of fault seal integrity) but the known ~2200 ft dry gas accumulation column clearly supports the conclusion that the seal potential over the gas accumulation area is excellent.

There is slightly more risk regarding the extent and properties of the sealing unit away from the known gas accumulation area towards the S and SE where the author considers potential CO₂ injection sites to be located. However, the detailed

sequence stratigraphy study in this study, lead to the conclusion that the Pre-Ayot zones PA10, PA20, and basal shales of the PA30 should extend away from the known hydrocarbon accumulation and encompass potential CO₂ injection locations being considered by the author tens of kilometers away. Reconstructions of paleo-geographic facies, predict that those units should be thickening towards these potential CO₂ injection locations, and that the shale sealing properties of the zones should actually be enhanced, as they were more distal from the sedimentary point source and hence can be expected to be less silty and more clay-rich.

The Ayot Limestone, Upper Late Jurassic Shales, Late Cretaceous Marls, and Paleocene shale units are all potential regional seals for the Vorwata structure. Mineralogically, the most-suitable seals are those that are geochemically non-reactive with CO₂ (Watson, et al., 2003a; Watson, et al. 2003b). It has been determined that reservoir CO₂ mixing with formation water will produce carboxylic acid (Krauskopf, 1967; Surdam, et al, 1984; Watson, et al., 2003a; Watson, et al. 2003b). Injected CO₂ will, during migration, eventually come into contact with a potential seal. The more CO₂ stable the composition of the seal, the lower the risk of seal breach. Carbonates, especially calcite, are the most reactive minerals in the presence of CO₂. Chlorite and potassium feldspars are also moderately reactive in slightly acidic waters. Quartz and clays, such as illite and kaolinite, are the least reactive common minerals. Small amounts of calcite, chlorite, and potassic-feldspar present in a reservoir rock composition can enhance mineral trapping of CO₂. This process involves the precipitation of new minerals from minerals previously dissolved by reactions with CO₂ (Surdam, et al, 1984; Watson, et al., 2003a; Watson, et al. 2003b). However, only trace to minor amounts of these CO₂-reactive minerals should be present in a potential seal mineral composition to minimize the risk of sufficient dissolution to cause CO₂ breaching of the seal.

The Ayot Limestone and the Late Cretaceous Marls are at greater risk as potential Roabiba Reservoir CO₂ seals, due to their basic mineralogical composition, than are the Pre-Ayot Shales, Upper Late Jurassic Shales, and the Paleocene Shales. When ductility (related to mineralogical composition) of potential seals are included as a further criterion for determining risk of breaching, then the greater ductility of the Pre-Ayot Shales and Paleocene Shales compared with the brittleness of the Upper Late Jurassic Shales (from interbedded volcanic tuffs) further narrows the selection for the best Vorwata area seal. Finally, the lack of sufficient CO₂ storage capacity, the

	PRE-AYOT SHALES	AYOT LIMESTONE	UPPER LATE JURASSIC SHALES	L. CRETACEOUS MARLS	PALEOCENE SHALES
SEAL CAPACITY (MAXIMUM CO2 COLUMN HEIGHT):	3300 - 4660 ft	4705 ft	3230 ft	1630 ft	546 - ??? ft
SEAL THICKNESS (GEOMETRY):	17 - 233 ft	37 - 69 ft	15 - 190 ft	291 - 660 ft	VARIABLE
SEAL LATERAL EXTENT (GEOMETRY):	OVER ENTIRE VORWATA STRUCTURE	OVER ENTIRE TANGGUH AREA	OVER ENTIRE TANGGUH AREA	OVER ENTIRE TANGGUH AREA	UNKNOWN
SEAL INTEGRITY:	DUCTILE DEEP-WATER MARINE SHALES	BRITTLE SHELFAL CARBONATE	BRITTLE MARINE SHALES WITH VOLCANIC TUFF	VERY HARD & BRITTLE MARL (SIDERITE)	HETEROGENEOUS SHELFAL MARINE SHALES WITH NUMEROUS, DISCONTINUOUS SILT AND SAND STRINGERS, TURBIDITE CHANNELS, DEBRIS/GRAVITY FLOWS
SEAL POTENTIAL:	VERY GOOD SEAL FOR ROABIBA CO2	BRITTLE AND SUBJECT TO FRACTURING	MARINE SHALES & BRITTLE VOLCANIC TUFF	BRITTLE AND SUBJECT TO FRACTURING	DIFFICULT TO ASSESS BASED ON AVAILABLE DATA

TABLE 10.10: CO2 Seal Capacity, Geometry, Integrity, and Potential for various potential sealing units overlying the Roabiba Reservoir .

lack of reservoir connectivity, and the lack of sufficient data regarding the Paleocene Shales, leads the author to conclude that the Pre-Ayot Shales rate as the best top and lateral seal for CO₂ storage. Seal potentials for the Roabiba Reservoir are summarized as a table (Table 10.10).

In conclusion, the Vorwata Roabiba Reservoir represents the best potential CO₂ injection and sequestration/storage reservoir for the Tangguh Project CO₂ volume (estimated at 2.4 TCF_{sc}). The Pre-Ayot Shale Top/Lateral Seal has the best seal potential in the Tangguh area for CO₂ retention/containment (Figure 10.7). This is supported by seal evaluation from sonic wireline log analysis carried out by BP, which calculated an 8000 to 8800 psia seal capacity for the Pre-Ayot Shales and Upper Late Jurassic Shales (Figure 10.8). This dovetails with the expected maximum CO₂ column height pressures derived in this study. The seal potential for the Ayot Limestone, the Upper Late Jurassic Shales, the Late Cretaceous Marl, and the Paleocene shale units is lower due to poorer seal integrity.

Some rock lithologies pose an additional risk due to lack of data, as there are limited cores available, and poor seismic data to assess geometries and faults. However, the laboratory analyses and data evaluation suggest that although the Ayot Limestone, the Upper Late Jurassic Shales, the Late Cretaceous Marl, and the Paleocene shale units are not suitable as primary top and lateral seals, they none-the-less could act as baffles or barriers in the migration of any CO₂ plume which might breach the primary Pre-Ayot top seal. In this circumstance these additional seals would perhaps ensure that any breached primary seal would not result in a CO₂ plume escaping to surface.

10.8 ESSCI Seal Evaluation

A probabilistic factor matrix of the geologic data quality and quantity for successful geological evaluation of ESSCI seal potential in the Middle Jurassic reservoirs at Tangguh has been constructed (Table 10.11), based on the data assessment and seal evaluation presented.

The Pre-Ayot Shale rates a very high degree of confidence, at “1.00”, regarding data quantity and quality. This suggests a very good seal potential for retaining a significantly large CO₂ column height. The Ayot Limestone Formation was rated at 0.63, with relatively moderate amount of generally good quality data at the Wiriagar Deep structure, and fair to poor amount of good quality data at the

Vorwata structure. This suggests that it is a ‘good’ secondary seal to containment at Vorwata within the Roabiba Sandstone Formation reservoir, but that it is too brittle to be an effective top-seal. It is fractured and most-probably was breached by the hydrocarbon column in the Roabiba Sandstone Formation reservoir at the Wiriagar Deep area. The Paleocene Shales lack sufficient data, however, empirically, they hold the largest hydrocarbon column (~2200 ft) of any sealing unit in the Tangguh area. With more data this seal might be rated higher than the current 0.50 factor (ie. 50/50). The Upper Late Jurassic Shales and Cretaceous Marls are not considered very good seals based on the moderate to plentiful, fair to good quality data available. However, they might be significant secondary seals or baffles to CO₂ migration following a potential breach of the primary top-seal. However, as seals for ESSCI CO₂ sequestration in the Middle Jurassic reservoirs, they are rated low, with only 0.38 and 0.25, respectively.

Geologic data factor for suitable ESSCI seal potential

	very bad	bad	even	good	very good
plentiful	0.00	Cretaceous Marl 0.25	X	0.75	Pre-Ayot Sh 1.00
enough	0.25	0.31	X	0.69	0.88
moderate	0.25	Upper LJ Shales 0.38	Paleocene Sh 0.50	Ayot Ls 0.63	0.75
poor	0.38	0.44	0.50	0.56	0.63
very poor	X	X	0.50	X	X

Index factors for confidence levels of suitable ESSCI geological data existence.
(After Nakanishi and Lang 2001)

Table 10.11: Geologic data quality and quantity for success factor probabilistic matrix for effective seal potential in the Tangguh area.

11.0 CO₂ STORAGE CAPACITY AND WEIGHTED DISTANCE FACTORING

The final ESSCI consideration for potential site evaluation of subsurface CO₂ sequestration/storage in the Tangguh area is the storage capacity/sweep efficiency of any reservoir and structure couplet. In addition, the distance from the point source of the CO₂, in this case the proposed LNG plant location, to a proposed injection site must be considered. Obviously, the further the distance the ESSCI injector site is from the point source, the longer the pipeline and the greater the number of compressor stations required along the pipeline route. Although the economics of CO₂ sequestration (\$\$/carbon-credit tonne) and the costs for pipelines and compressor turbines vary with time (and location for hardware costs), a generic formula for distance ratios can be applied. These two components for ESSCI evaluations in the Tangguh area are evaluated in detail below.

11.1 ESSCI CO₂ STORAGE CAPACITY ANALYSIS AND EVALUATION

The CO₂ storage capacity analysis is the determination of the maximum potential CO₂ storage volume for a given structure at respective reservoir conditions. This assumes that all the Middle Jurassic reservoir hydrocarbons are produced and the reservoir depleted, and the structure filled with injected CO₂ to the former hydrocarbon GWC. The maximum CO₂ storage volumes were calculated on the following basis. The volumes of natural gas currently certified in place (for each structure) include the certified proven, probable, and possible reserves, or 3P reserves as certified by DeGolyer and MacNaughton in 1998 (Bulling, et al., 1998). These 3P reserves were assumed depleted by production, with 5% gas remaining as trapped, residual gas (S_{sgr}) in-situ (G. Perez and J. Marcou, personal communication, 2002). An irreducible water saturation (S_{wir}) of 20% was assumed based on the averages from Petcom Petrophysical program (T. Lawrence, personal communication, 1998) over the Middle Jurassic reservoir intervals. It should be noted that the petrophysical evaluation incorporated laboratory S_{wir} results from whole core plugs and rotary sidewall cores where available. The depleted structure was then assumed to be filled to the former GWC with injected CO₂ in the 'supercritical' state. The compression and expansion factor of carbon dioxide was calculated for each reservoir's pressure and temperature.

These calculations (with the assistance of Dr. G. Perez, BP Reservoir Engineer), are considered to be as accurate as possible a calculation of the maximum CO₂ storage volume each structure can hold. A summary of these calculations is shown in Table 11.1. The storage capacities are presented graphically in Figure 11.1.

11.2 Integrating ESSCI CO₂ Storage Capacity Analysis with Reservoir, Structure, and Seal Potential ESSCI Evaluations

A matrix was constructed to rate and rank the suitability for ESSCI injection following the lines of exploration matrix evaluations. This method assesses the combined ESSCI Reservoir Quality, ESSCI Structure Trapping, ESSCI Sealing Potential, and ESSCI Storage Capacity for CO₂ sequestration in Middle Jurassic reservoirs (see Table 11.2).

The equation and principal are similar to probabilistic methodologies used in oil and gas exploration, where source, migration, reservoir, trap, seal, and timing are subjectively estimated to high-grade potential drilling prospects. For the purpose of CO₂ injection and sequestration/storage however, source and timing are irrelevant. The algorithm for the calculated CO₂ injection and sequestration/storage 'Rating Product' is:

Reservoir Factor x Trap Factor x Seal Factor x Storage Factor = Rating Product

Migration is assessed in the geo-cellular/reservoir simulation model, whereby proposed sites for potential CO₂ injection are verified by running a simulated injection at the site using a reservoir simulation program that has a grid and layer foundation (input), and a geo-cellular model that accurately captures the geological heterogeneity. This is addressed in a later chapter.

The 'Rating Product' matrix is comprised of Reservoir Data Q/Q Factor (i.e. the Reservoir Data Quantity and Quality of Expression Factor for Strata) from Chapter 8. ESSCI STRATA EVALUATION; a Structural Trap Data Q/Q Factor from Chapter 9. ESSCI STRUCTURE EVALUATION; and Seal Potential Data Q/Q Factor from Chapter 10. ESSCI SEAL EVALUATION; and finally a Storage Factor for each structure.

Structure	Vorwata	Wirigar Deep	Ofaweri	Roabiba	Ubadari	WOS
Formation	Jurassic	Jurassic	Jurassic	Jurassic	Jurassic	Jurassic
OGIP, TCF	15.51	2.66	0.97	0.95	1.86	0.23
E gas, scf/cf	265	207	228	234	187	208
Datum Pressure, psia	5,847	4,086	4,494	5,032	3,242	4,389
Datum Pressure, bar	399	279	307	343	221	300
Datum Temperature, F	256	243	233	266	192	267
Datum Temperature, C	124	117	112	130	89	131
CO2 Density, kg/m ³	679.75	565.26	623.45	604.99	587.90	547.46
CO2 Compressibility	0.78232	0.66964	0.67674	0.74437	0.54943	0.71769
CO2 Expansion Factor	366	304	336	326	317	295
Equivalent CO2 Storage Volume, TCF	21.42	3.90	1.43	1.33	3.16	0.32
Irreducible Sw	0.20	0.20	0.20	0.20	0.20	0.20
Trapped Sw to CO2	0.23	0.23	0.23	0.23	0.23	0.23
Corrected CO2 Storage Volume Trapped Water, TCF	20.61	3.76	1.38	1.28	3.04	0.31
Trapped Gas Saturation	0.05	0.05	0.05	0.05	0.05	0.05
Corrected CO2 Storage Volume for Trapped Water and Gas, TCF	19.28	3.51	1.29	1.19	2.84	0.29

Table 11.1: Table of calculated volumetrics for the various structure reservoir conditions. Corrected CO₂ Storage Volume with trapped water and gas takes into account a fully depleted reservoir with 5% pore volume of residual trapped gas; plus 23% pore volume of irreducible water saturation; plus trapped formation water leaving a potential supercritical CO₂ storage pore volume listed in TCF CO₂ at standard conditions. Vorwata (vertical purple column) has the largest potential CO₂ storage capacity at almost 19.3 TCF, maximum storage capacity for other structures in the Tangguh area of Bintuni Basin (horizontal purple row) are all less than 4 TCF.

	Q / Q Reservoir Data	Q / Q Structure Data	Q / Q Seal Potential Data	Storage Capacity Ratio	Rating Product
Vorwata	0.88	1.00	1.00	1.00	0.88
Wiragar Deep	0.81	0.88	0.63	1.00	0.45
Ubadari	0.75	0.69	0.63	1.00	0.52
Roabiba	0.81	0.69	0.63	0.55	0.33
Ofaweri	0.75	0.56	0.38	0.59	0.09
Wos	0.75	0.50	0.38	0.13	0.02

Table 11.2: Data Quantity and Quality (Q/Q) matrix ratings by structure for: CO₂ ESSCI Reservoir evaluation (for highest factored reservoir[s] at a given structure), CO₂ ESSCI Structure evaluation (in Middle Jurassic ESSCI reservoirs only), CO₂ ESSCI Seal Potential evaluation (for Middle Jurassic reservoir ESSCI containment by top-seal unit), and CO₂ ESSCI Storage Capacity Ratios (by structure).

These factors (reservoir data, structure data, seal potential, and carbon dioxide storage capacity) were then multiplied to yield a 'Rating Product'. This Rating Product used was to rank the various structures ESSCI potential and high-grade suitable sites for potential injection well locations.

The matrix values assigned for the first column, Q/Q Reservoir Data Factor, derive directly from the geological expression factor for reservoir suitability as successful potential ESSCI site for the estimated 2.4 TCF of CO₂ needed to be sequestered (Chapter 8). At Vorwata structure, only the Roabiba Sandstone Formation reservoir is present, and there is no Aalenian Sandstone Formation reservoir, hence the factor is "0.88". In cases such as Wiriagar Deep and Roabiba structures, where both the Roabiba Sandstone Formation and Aalenian Sandstone Formation reservoirs are present, the Roabiba "0.88" and the Aalenian "0.75", have been averaged to produce "0.81".

The second column, Q/Q Structure Data Factor, is derived directly from the geological expression factor for various structures as successful potential ESSCI traps (Chapter 9) in the Middle Jurassic reservoirs. This is because the Roabiba and Aalenian reservoirs had the highest degree of confidence factor in the Q/Q Reservoir Data Factoring).

The third column, Q/Q Seal Data Factor, which is the 'confidence level' assigned to each ESSCI Seal Potential Factor, at the Middle Jurassic reservoir top-seal lithology (Chapter 10). The known aerial extent of the various Middle Jurassic seals across the Tangguh area structures is shown on the seal coverage map in Figure 10.3. Since the Middle Jurassic reservoirs are topped by an angular unconformity, the sealing units have been eroded and removed towards the northwestern portion of the area. The Kalitami structure is capped only by the Late Cretaceous Marls, whereas Ofaweri and Wiriagar Deep structures have the Ayot Limestone as the top-seal. Only Vorwata and Roabiba structures have the Pre-Ayot Shales present as a top-seal lithology. This unit was empirically the best seal potential (Chapter 10), and the highest degree of confidence for seal potential. In addition, Vorwata and Roabiba alone have the Ayot Limestone, Upper Late Jurassic Shales, and Late Cretaceous Marls present as secondary seals in case of primary seal breach by injected CO₂.

Finally, the Storage Capacity Ratio is the maximum CO₂ storage factor in a given structure. This assumes that all the reservoir hydrocarbons are produced (ie. the

Middle Jurassic reservoir is depleted), and the structure filled with injected CO₂ to the former hydrocarbon GWC. If a structure was calculated to be able to contain *at least* an estimated 2.4 TCF CO₂ it received the maximum factor of 1.00. If it were calculated to contain *less than* 2.4 TCF CO₂ then the ratio was derived by dividing the calculated maximum volume by the 2.4 TCF required to sequester (ie. $Y / 2.4 = R$ where Y is the maximum calculated storage volume from Table 11.1, and R is the ratio derived; if R is greater than or equal to 1 it is expressed as 1).

These matrix factors and the respective storage ratios are multiplied to produce a rating product. The rating product for each structure at the Middle Jurassic reservoir/top-seal couplet is the expression of degree of confidence for the chance of success for CO₂ injection and sequestration/storage.

Based on this rating product, it can be seen that the Vorwata structure has the highest degree of confidence for potential success based on geological evaluation, receiving an “0.88” on a 0.00 to 1.00 scale, (1.00 being the highest degree of confidence for success). As a result of this matrix analysis, empirical observations, geological analyses and evaluations presented in this study, the recommendation is made to potentially inject and sequester/store CO₂ from the Tangguh LNG Project, in the Roabiba Sandstone Formation reservoir in the Vorwata structure. Since the structure contains proved and probable natural gas reserves at the proposed sequestration strata/structure, it recommended that the injection be in the down-dip aquifer leg of the Roabiba Sandstone Formation. The injection should be at a location that allows sufficient migration time to reach the current GWC such that the natural gas accumulation can be produced and depleted prior to the arrival of the CO₂. However, the proposed injection location needs to be as close as possible to the current GWC to minimize seal and fault containment risk.

11.3 Distance/Economics Factor Weighted Rating and Ranking

The structures that rank greater than 0.50 were evaluated by the ‘relative distance’ between the CO₂ source and the location of the potential injection sites (ie. the eastern flank of each structure, down-dip from the known GWC). There is a technical and cost advantage to proposed injection sites on the flanks of structural closures that are closest to the proposed LNG plant (ie. the CO₂ source location).

These technical and economic considerations (greater distance = greater cost) are as necessary to consider in the ranking of ESSCI locations. However, these costs are much more difficult to assign with fixed, valid economic values. Pipeline costs are generally proportional to the distance considered, however, other costs associated with gas compression and injection are much harder to quantify, and may not be linearly proportional. Nonetheless, logic would dictate that when subsurface geological factors are 'normalized', a favorable site proximity to the proposed CO₂ point source should be taken into account when considering the practicality of one proposed site over another.

The distance between the injection location and the proposed LNG plant/ CO₂ source location has been incorporated into the linear distance-weighted formula $1/x * 10$, where 'x' is the distance in kilometers. This distance factor is then multiplied by the Ranking Product previously established for each of the three structures with >0.50 confidence factor of success regarding geological expression of data quality and quantity. This simplistic mathematical approach is linear, and not absolutely accurate in regards to economic costs, but is rather designed as a further relativistic weighted criteria in evaluating potential injection sites. A generic distance and economics matrix has been constructed as an additional weighted factoring element (Table 11.3).

The CO₂ is to be injected in the down-dip aquifer leg of a structural trap with known proven containment, as illustrated in Figure 11.2. Potential injection well locations, in the downdip water-legs on the flanks of the structures, are proposed for all of the Jurassic interval structural closures. The locations of the structural closures, relative to the proposed LNG plant location, are illustrated in map view on Figure 9.1.

The distance of structures from the proposed location of the LNG plant shows Ubadari as the furthest from the plant and CO₂ source, and hence the technically most complex and, economically most costly ESSCI injection well location of the three proposed. If Saritu is excluded due to high degree of uncertainty, then Vorwata is clearly the most favorable of the three, based on both excess storage capacity (Figure 11.1) and proximity to the LNG plant/CO₂ source (Figure 11.3). Therefore, this is the most economically viable and technically feasible of the sites. Furthermore, Vorwata ranks the highest in the data quality and quantity expression factoring. Finally, the geological characteristics such as injectivity permeability ranking, and seal 'cap-rock' confidence ratings make Vorwata rank the highest (Table 11.3).

	R a t i n g P r o d u c t R a n k i n g	D i s t a n c e F r o m P l a n t (1/x km * 10)	D i s t a n c e W e i g h t e d R a t i n g w i t h L i n e a r D i s t a n c e / E c o n o m i c s F a c t o r e d - i n
V o r w a t a	0.88	1.00	0.88
W i r i a g a r D e e p	0.53	0.45	0.24
U b a d a r i	0.52	0.17	0.09

Table 11.3: Table multiplying the ‘Rating Product’ of the ESSCI evaluations times an algorithm for LNG Plant/CO₂ source distance to potential injection site factored as a distance/economics weighted rating, albeit with simple linear distance factoring. Vorwata structure is the ‘relatively’ best, and Ubadari is the ‘relatively’, worst potential ESSCI site location if distance is considered as additional criteria for selecting the best potential ESSCI CO₂ injection location.

12.0 FAULT RE-ACTIVATION FROM CO₂ INJECTION RISK EVALUATION

This research project took into account the risk of fault re-activation due to the subsurface injection and migration of CO₂, and the proximity of potential sites of injection to faults with a high risk of re-activation. A study specific to the Tangguh area was carried out by Hillis and Meyer (2002) for this purpose.

Injection of any fluid, including CO₂, into the subsurface can potentially re-activate pre-existing faults. Any increase in reservoir pressure reduces effective stress and may cause fault slip (Hubbert and Willis, 1957; Hubbert and Rubey, 1959; Hillis, 1998). Fault re-activation and the associated brittle deformation of rock can result in seismicity and increase fault/fracture permeability causing undesired fluid migration through a top seal. Estimates of the risk of re-activation can be made for any fault surface, if the fault geometries and in-situ stress regime are known. Geo-mechanical modelling can then assess the fault slip tendency for a given fault plane surface and determine the maximum sustainable pressures within any given interval.

The fault reactivation risk study includes the interpretation and evaluation of the following: borehole image logs, pressure data from well testing, leak-off tests, wireline logs, well data such as mud weights used while drilling, and geomechanical modelling.

Twenty-four leak-off tests (LOT), and thirty-two formation integrity tests (FIT) from 20 Wiriagar Deep and Vorwata area wells (Table 12.1) were utilized to generate an LOT contour map of the Bintuni Basin (Figure 12.1). The LOT results provided an estimate of the minimum horizontal stress in the area (Hillis and Meyer, 2002). Sonic and density wireline log analysis (Figure 12.2) were then used in determining in-situ vertical stress regimes (Sv) as shown in Figure 12.3 and 12.4. This resulted in the creation of a Tangguh area vertical stress contour map (Figure 12.5). Formation pressure data from DST, MDT/RFT test results (Figure 12.6A), and drilling mud weights were analysed by Hillis and Meyer (2002) to determine pore pressures at various depths in various strata (Figure 12.6B).

Borehole image logs from ten Wiriagar Deep, Vorwata, and Ubadari wells (all in the Tangguh area) were processed by Mark Tingay, and made available for interpretation, representing 24,740 ft of well log images. Only one well's dataset (Ubadari #2) contained unprocessable FMI logs. These borehole images were

Depth ft TVD RT	Test		LOT	FIT	Well	Formation
	ppgMW	psi	ppgEMW	ppgEMW		
1840			9.2		WD#1	
2020	8.6	650	14.7		WD#2	
2135	8.7	490		13.1	WD#3	
2525	8.6	450	11.3		WD#7	
2322	8.6	168	10		WD#8	
2350	8.5	530	12.8		WD#6	
3000	8.6	700		13.0	WD#4	
3335	8.7	610	12.2		WD#5	
4500	8.4	510		10.6	WD#1	
4972	8.9	195	9.6		WD#2	
5632	10.8	840	13.70		WD#8	
6131	10.8	890		13.6	WD#7	
6285	11.3	600		13	WD#6	
6464			14.3		WD#1	
6685	10.0	1500		14.3	WD#2	
7182	10.0	1850	15.0		WD#5	
7210	10.0	1315		13.5	WD#4	
7435	10.2	1160		13.2	WD#3	
2073	8.7	495	13.2		V#1	
4617	8.7	1850	16.4		V#1	
8967	10.0	2330		15	V#1	
11280	14.5	2060		18	V#1	
2057	8.9	310		11.78	NAMBUMBI-1	
8743	8.7	1550	12.1		NAMBUMBI-1	
9938	12.5	2500		17.34	NAMBUMBI-1	
2050	8.7	542	13.8		V#2	
6380	8.7	1120	12		V#2	
10390	9.0	2270	14.20		V#2	Unreliable
5975	9.1	600		11	V#3	
10477	10.6	2890	15.9		V#3	
1670	8.7	375	13.1		V#3	
1567	8.5	235	11.38		V#4	
6060	9.4	1462	14		V#4	
10550	8.6	3500		15	V#4	
1618	8.5	487	14.3		V#5	
6675	9.35	700	11.4		V#5	
11228	10.5	2250	14.4		V#5	
1806	8.5	75	9.3		V#6	
6124	9.2	890		12	V#6	
11137	9.6	2550		14	V#6	
2136	8.7	260		11	V#8	
7251	9.3	650		11	V#8	
11522	11	2500		15	V#8	
1828			11.8		V#7	
5335	8.9	1437	14		V#7	
11264	10.6	3620		16.75	V#7	
1761			12.8		V#9	
7356	9.2	1260	12.49401		V#9	Unreliable
11280	9.8	3050		15	V#9	
11806	10.3	2885		15	V#9	
2364	9.1			11	V#10	
7136	8.5	840		10.76	V#10	
11810	10.5			15	V#10	
2211	8.6			11	V#11	
7970	9.2			11	V#11	
12041	10.5			15	V#11	

Table 12.1: List of Tangguh area leak-off tests/formation integrity tests.

Image Log Data

Well	Image?	Type	Run	Top (m)	Base (m)	File	Comments
Ubadari-1	Y	FMI	1	1330	2440	FBSTB .032 FMI .DYNA	Good image, breakouts galore!
Ubadari-2	N/Y	FMI	-	-	-	-	Unprocessable – no inclinometry
Vorwata-1	Y	FMI	1	2740	3445	FMI .DYNA	Some bad image, BOs & DITFs
Vorwata-2	Y	FMI	1	3166	4070	FMI .DYNA (c20191952)	Breakouts galore!
Vorwata-3	Y	FMI	1	3183	3398	FMI .DYNA (c20192705)	Lots of breakout, some DITF
			2	3383	3581	FMI .DYNA (c20192763)	Lots of breakout, some DITF
			3	3555	3760	FMI .DYNA (c20192647)	Lots of breakout, some DITF
Vorwata-4	Y	FMI	1	3210	3961	FMI .DYNA	Some bad image, lots of BO
Vorwata-5	N	-	-	-	-	-	-
Vorwata-6	N	-	-	-	-	-	-
Vorwata-7st	Y	FMI	1	3415	4136	FBSTB .134 FMI .DYNA (c20193911)	poor image, BOs & DITFs
Vorwata-8	N	-	-	-	-	-	-
Vorwata-9	Y	FMI	1	3602	4130	FBSTB .068 FMI .DYNA (c20194341)	Fairly poor image, some BO
Vorwata-10st	Y	FMI	1	3555	4155	FBSTB .056 FMI .DYNA (c20194886)	Some bad image, BOs & DITFs
Vorwata-11	N	-	-	-	-	-	-
Wiriagar Deep-1	Y	FMS	1	1981	2255	TDIP .009 FMS4 DYNA	Okay image, BO present
Wiriagar Deep-2	N	-	-	-	-	-	-
Wiriagar Deep-3	N	-	-	-	-	-	-
Wiriagar Deep-4	N	-	-	-	-	-	-
Wiriagar Deep-5st	N	-	-	-	-	-	-
Wiriagar Deep-6st	N	-	-	-	-	-	-
Wiriagar Deep-7	Y	FMI	1	1193	1789	FMI .DYNA (c20197370)	Some bad image, some BO
			2	1670	1790	FMI .DYNA (c20197660)	Okay image, BOs & DITFs
			3	1778	1877	FMI .DYNA (c20197486)	Very poor image, a few BOs
			4	2589	2712	FMI .DYNA (c20197094)	Poor image, some BO
Wiriagar Deep-8	N	-	-	-	-	-	-
East Orin-1	N	-	-	-	-	-	-
Kalitami-1X	N	-	-	-	-	-	-
Mogoi Deep-1	N	-	-	-	-	-	-
Nambumbi-1	N	-	-	-	-	-	-
Ofaweri-1	N	-	-	-	-	-	-
Roabiba-1	N	-	-	-	-	-	-
Sakauni-1	N	-	-	-	-	-	-
Sebvar-1	N	-	-	-	-	-	-
Wos-1	N	-	-	-	-	-	-

Table 12.2: Table of Tangguh area wells with FMI/FMS borehole image logs over some or all of the Top Late Paleocene to Late Permian interval over the Tangguh area (courtesy of Mark Tingay).

interpreted and evaluated from the Top Late Paleocene to the Late Permian interval for borehole breakouts and drilling induced tensile fractures (DITF) by Hillis and Meyer (2002).

Breakouts and/or DITFs were visible in all image logs. All wells had a general log suite (DT, RHOB, GR, etc.) over the same Top Late Paleocene and Base Mesozoic borehole interval and were also evaluated in conjunction with the image logs (FMI/FMS). Furthermore, most wells also had specialized (or calculated) logs available, such as petrophysical logs (e.g. bad hole, calcite concentration, coals, etc.).

The orientation of the borehole breakouts and DITF were then used to establish the in-situ horizontal stress regime for the area. From this FMI/FMS dataset 118 drilling induced tensile fractures and 897 borehole breakouts were identified as an aid in determining the in-situ horizontal stress minimum and maximum (SH_{min} and SH_{max}). An example from the Vorwata #3 well is provided to show how the breakouts and DITF analysis was carried out and evaluated (Figure 12.7).

The maximum horizontal stress tensor is the most difficult component in fault re-activation studies to determine (Bell, 1996). Borehole breakouts are intervals within wellbores of poorly resolved, high-conductivity on opposing pads of an FMI/FMS tool. These intervals of poorly resolved high-conductivity zones are thought to be the result of caving of a borehole wall with a preferential orientation due to differences between maximum and minimum horizontal stresses. This produces an elongated borehole in cross-section, where compressive stress at the borehole wall exceeds the compressive strength of the rock. The maximum horizontal stress tensor (SH_{max}) and minimum stress tensor (SH_{min}) can be determined from FMI/FMS image log analysis of the borehole breakout orientations, since the breakout always occurs perpendicular to the SH_{max} orientation (Bradley, 1979; Plumb and Hickman, 1985). Elongation, therefore, occurs in the direction of minimum horizontal stress.

Vertical stress is determined by analysis of the density log since the vertical or overburden stress is the product of the density of the overlying rock column at any particular depth z , and the acceleration due to gravity ($\sim 9.81\text{ms}^{-2}$), according to Bell (1996).

The in-situ stress data combining a Mohr circle of stress diagram with an assumed failure envelope for the fault permits the risk of fault reactivation to be assessed (Figure 12.8).

The analysis, by Hillis and Meyer (2002), concluded that the in-situ stress regime in the Tangguh area is strike-slip ($SH_{max} > S_v > SH_{min}$), with a maximum stress orientation of $\sim 020^\circ N$ at the depths of interest (ie. the Mesozoic interval) from approximately 7,000 ft to approximately 15,000 ft (Figure 12.9) across the Wiriagar Deep and Vorwata areas (Hillis and Meyer, 2002).

Approximately 20 major faults, interpreted from the 3D seismic survey over the Tangguh area, were provided by BP for fault risk assessment and evaluation. The faults were selected based on the following criteria: interpreted fault surfaces had to be relatively robust (ie. high degree of confidence regarding the interpretation); faults had to represent major fault planes, that is faults of either considerable length > 5 km, or having significant throw (in the hundreds of feet); a 'suite' of faults representing an assortment of dip angles and strike directions was required for the analyses. Finally and most importantly, the major faults near the southern and eastern flanks of the Vorwata structure were studied, since this was the area most likely to be high graded for potential CO₂ injection site locations. As a result, 20 faults were selected although, although several separate fault plane surfaces were merged into a single fault plane on two occasions resulting in 14 fault plane surfaces analyzed by fault re-activation assessment programs, such as the Fault Analysis Projection System (FAPS) and Fault Analysis Seal Technology (FAST).

The results of the fault re-activation risk study are that vertical faults striking $\sim 110^\circ N$ have the lowest risk of reactivation, requiring an increase in pore pressure of $\sim 10,000$ psi at the proposed injection depth of -14,000 ft TVDss before failure. Vertical faults striking $\sim 45^\circ N$ and $\sim 175^\circ N$ are at the highest risk of reactivation, requiring a pore pressure increase of $\sim 1,460$ psi over hydrostatic pressure gradient at the proposed injection depth of -14,000 ft TVDss to fail (Figure 12.10). The dominant orientation for faults in the Tangguh area, are steeply deeping faults, striking roughly north-south or east-west. The east-west striking faults are at a low risk of reactivation, requiring a pore pressure increase of $\sim 6,220$ psi over hydrostatic at -14,000 ft TVDss for failure. The N-S striking faults are at a relatively high risk of reactivation if CO₂ injection results in a pore pressure increase of $\sim 1,770$ psi over hydrostatic at -14,000 ft TVDss.

Two faults that have the lowest threshold pressures over the hydrostatic gradient for risk of re-activation are located between the V-5 and V-9 wells in the center of the Vorwata structure. This is due to their north to northwest strike, placing

them at a relatively higher risk of re-activation. These two faults require more than a 1450 psia increase over the existing hydrostatic pressure in the Roabiba aquifer leg to fail, and cause increased structural permeability. However, both faults are located more than 10 km from the most-likely injector site locations (Figure 12.11) and it is considered unlikely that injection pressure buildups immediately around the injector wellheads would translate across such distances. It is also unlikely that pressures induced by the migration of the injected CO₂ plume updip would result in pressure increases of 1450 psi or more over hydrostatic. Furthermore, the conclusions and results of this study identifying the risk associated with varying pressures can actually be used as an aid in the injection and sequestration process, with reservoir modelling identifying the optimal injection rates and pressures so as to not exceed fault re-activation risk limits.

Injector locations and modelling will be examined in greater detail in the following chapters.

PART IV

**CO₂ INJECTION-SITE RECOMMENDATION AND
GEOLOGIC MODEL VERIFICATION**

13.0 RECOMMENDED CO₂ INJECTION SITE LOCATIONS

Four proposed CO₂ injection site locations have been identified in the immediate Tangguh area and ranked by distance from the proposed LNG plant location as shown in Figure 13.1. These four locations have been subjected to a detailed geological evaluation, risk rating, and probabilistic ranking for CO₂ injection and sequestration purposes (Chapters 8 through 12) with the two highest ranked locations shown in Figure 13.2. Based on the data quality/quantity assessment and factoring, and the geological evaluation of the reservoir, trap, and seal datasets, the recommendation for the best potential ESSCI injection sites are in the water-leg from the Vorwata 3P hydrocarbon accumulation, within the Vorwata anticlinorium structural closure, but downdip from the known GWC. Recommended injection sites are located in the Middle Jurassic interval Bathonian/Bajocian Roabiba Sandstone Formation reservoir: 10 km east of the Vorwata #10 well location; and a second alternate site 6 km south of the Vorwata #10 well location. The injection site bottom-hole locations are modelled where the location of the Pre-Ayot Shale seal base/Roabiba Sandstone reservoir structural top depth is at -14,000 ft TVDss (true vertical depth subsea). A geologic cross-sectional schematic of the highest-ranked proposed ESSCI site location is shown in Figure 11.2. The proposed plan is to inject CO₂ into the down-dip aquifer leg of the Bathonian/Bajocian Roabiba Sandstone Reservoir, on the broad, gently dipping eastern flank of the Vorwata structure.

The original vertical pilot hole would serve as the data acquisition borehole for wireline logging and obtaining whole core. The vertical hole could then be used as a monitoring well during the early phases of production from the Vorwata Middle Jurassic natural gas reservoir, prior to sidetracking the potential horizontal leg for CO₂ injection.

If the proposed vertical well incorporates a ‘smart completion’, then monitoring of the aquifer pressure, temperature and fluid movement during production of the natural gas accumulation updip would verify intra-reservoir communication, and enhance confidence in potential CO₂ migration into the containment field. The exact thickness and porosity/permeability characteristics of the Roabiba sandstone reservoir (evaluated from wireline logging obtained on the vertical hole) can be utilized in the construction of a LWD gamma-ray (GR) and resistivity ‘geo-steering model’ for the horizontal injection leg. The vertical pilot hole could then be plugged back with cement and a horizontal injector leg drilled along

depositional strike, with an LWD steering tool following the geo-steering model' (ie. 'resistivity and GR horns').

Ideally, the injector well should be highly deviated or horizontal in order to ensure that the CO₂ migration within the Roabiba reservoir, being buoyancy driven, does not migrate up the injector-well borehole behind casing, and also minimize the plume contact with the 'CO₂ non-reactive cement' used in cementing the casing string. The recommended horizontal injector leg would ideally be picked based on wireline identification, acquired during logging of the pilot hole, of intervals with optimum effective porosity and permeability for injection. If effective porosity and permeability are favorable throughout most of the reservoir interval, as predicted from empirical Roabiba reservoir water-leg core plug data and predicted paleo-geographic facies, then bottom-hole locations approximately 10 to 20 ft above the base of the Roabiba reservoir are recommended. This would maximize the vertical migration time for the CO₂ to travel through most of the Roabiba reservoir maximum thickness prior to reaching the top of the reservoir/base of the seal. By drilling the horizontal injector leg along the strike of the depth contour for the base of the Roabiba, the horizontal migration time from the 'top of the reservoir/base of the seal' updip toward the known GWC can be confidently modeled.

In regard to the best ranked Injector Site (IS #1), on the eastern flank of Vorwata, the depth structure top Roabiba reservoir for the -14,000 ft TVDss contour is well within the closure of the SE Vorwata anticlinal structure, yet is approximately 10 km east of the known gas-water contact (GWC). The injected CO₂ plume would therefore be expected, with high level of confidence, to migrate vertically from the horizontal injector perforations, to the top of the Roabiba reservoir or base of the shale seal. This migration distance and time can only be known with absolute certainty when the vertical pilot hole is drilled and wireline logged, however, it is in excess of 600 ft thick at the V-10 location, which is the nearest well ~10 km to the west (Figure 13.3). The CO₂ plume would then migrate from the top Roabiba reservoir or base seal at -14,000 ft. TVDss updip following the topography of the base seal. The distance to the known GWC depth at -13,300 ft TVDSS is a further 700 ft updip and 10 km laterally.

Details regarding smart well completions, drilling and data acquisition recommendations, and reservoir simulation modeling are addressed in Chapters 14 through 16.

A second potential ESSCI injection location is found on the southern flank of the SE Vorwata anticlinal compartment, also at the -14,000 ft TVDSS contour (Figure 13.2). It is located approximately 6 km south of the V-10 well location and is ranked as the second best ESSCI injector well location, due to closer proximity to high reactivation risk faults running N-S than Injector Site #1 (IS #1) to the east of V-10. Injector Site #2 (IS #2) is also ranked as second-best based on a potentially faster predicted rate of CO₂ migration toward the known GWC.

The migration of CO₂ is controlled by several variables with CO₂ buoyancy/specific gravity and the topography and degree of dip for the base of the sealing unit/ top reservoir unit couplet being the primary factors. Factors such as pressure depletion due to hydrocarbon production and aquifer movement within the injection strata are considered as secondary controls. Since the base of the shale seal is more steeply dipping at the southern flank site than at the eastern flank site, the rate of migration is deduced to be slower at the proposed eastern site. The reservoir modeling will, hopefully, confirm this conclusion. The top reservoir/base seal bedding dip can be seen on the top Roabiba reservoir structural depth map, in Figure 13.2, where the contours clearly are more closely spaced at proposed IS #2 than proposed IS #1.

The aerial extent of 0.5 TCFsc CO₂ supercritical volume at reservoir pressure and temperature is estimated at 1.7 km diameter (Figure 13.3) for the IS #1 location, approximately 10 km east of the Vorwata-10st well, located in the Roabiba reservoir downdip water-leg on Vorwata structure eastern flank. This area with a diameter of 1.7 km is based on a Roabiba reservoir thickness of 400 ft with an effective porosity of 10%, and average permeability of 100 mD or better. Five injector wells are proposed for injecting the total CO₂ volume of 2.4 TCFsc as a supercritical phase. The aerial extent of the estimated 2.4 TCFsc CO₂ volume at reservoir pressure and temperature is shown in Figure 13.4 as circles with a 1.7 km diameter, scaled to CO₂ volume at reservoir conditions for five proposed horizontal injector wells located at IS #1. Five wells have been proposed, per injection site location, to handle the CO₂ volume to be sequestered.

The Tangguh area fault re-activation risk evaluation (Hillis and Meyer 2002) indicated that no high risk re-activation faults are in the immediate area of the proposed injection wells for IS #1 and IS #2. Figure 12.11 shows a depth-slice from the FAPS/FAST program at -14,000 ft TVDss of Wiriagar Deep and Vorwata

structure's fault traces in the Tangguh area, showing the assessment of estimated fault re-activation pressure over hydrostatic in psia. While the NE-SW and N-S trending faults are estimated as being at high risk of activation, they are not adjacent to the immediate area of proposed injection at IS #1 and #2, nor in the immediate anticipated migration path. The nearest fault with a high-risk of reactivation is 5 km to the NW of the V-10 well location, or 15 km from the IS #1 location (Figure 12.11). Pressure build up from injection is not likely to translate across 15 km, and the reservoir pressure at the high-risk fault would be dependent on the supercritical CO₂ buoyancy and total column height previously discussed in Chapter 10 (G. Perez, personal communication, 2002).

Although only 20 representative interpreted faults from the Wiriagar Deep and Vorwata areas were selected for analysis, all of the major faults in the south and southwestern part of Vorwata's structural flanks were analyzed, including the two 'high risk' faults trending NE and N between the V-5 and V-9 wells. Numerous faults at Wiriagar Deep structure striking NE-SW and N-S were not analyzed since their respective strikes and dips were already present in the Vorwata area faults selected. Faults, as indicated by black lines on the Figure 13.3 and 13.4 base maps, in the area around IS #1, IS #2, and V-10 are primarily E-W striking vertical strike-slip faults at very low risk of reactivation (Hillis and Meyer, 2002).

13.1 COORDINATES FOR RECOMMENDED CO₂ INJECTION SITE LOCATIONS

The coordinates for the best 2 proposed injection sites are:

Projection	: UTM
Spheroid	: WGS-84
Unit code	: meters
Ref. Lat.	: 0.0
Ref. Long.	: 132.0 East
Scale factor	: 0.9996
False Northing	: 10,000,000
False Easting	: 500,000

Injection Site Surface Location	Latitude	Latitude	X	Y
IS #1	-2.358405	133.3605	651,280	9,739,250
IS #2	-2.389640	133.2716	641,390	9,735,806

The vertical boreholes are proposed to reach a minimum total depth (TD) of -14,400 ft TVDss, where the base of the Roabiba Sandstone Formation reservoir is

estimated to be. However, the drilling should continue until the actual base of the Roabiba Sandstone Formation reservoir is encountered (and not TD at the proposed or estimated base of the reservoir). Also an additional 150 ft, minimum of 'rathole' is recommended for the wireline logging tool lengths in order to completely log the basal contact of the reservoir and log the reservoir in entirety. Therefore, given that reservoir thickness could exceed 400 ft, and that +150 ft of rathole is required for logging purposes, then drilling contingencies would likely be recommended to -15,000 ft TVDss for the prognosed TD.

14.0 DETAILED GEO-CELLULAR MODEL OF THE TANGGUH AREA

A key goal of the Tangguh CO₂ Capture and Sequestration/Storage Study was to create a static 3D geo-cellular model suitable for upscaling into a simulation model to test the proposed location of CO₂ injector wells as environmentally-sustainable subsurface sequestration/storage sites. The software used to construct the static model was GeoCARD, from GeoVisual Pty Ltd. Dynamic modelling was to be conducted by BP, development operator of the Tangguh LNG Project, using the VIP reservoir simulation software from Landmark.

The grid design in the static model was chosen to reflect the high-resolution sequence stratigraphic framework of the Tangguh area and to capture the expected heterogeneity within the stratigraphic units. No specific considerations were given at this stage to the requirements of the simulation software (VIP), instead static model design focused from the onset on capturing all necessary geological heterogeneity.

Grid design comprises the horizontal resolution of grid cells (x, y or i, j), and the vertical resolution and layering of grid cells (z or k direction). In GeoCARD the grid design in the vertical direction comprises a hierarchical scheme of zones and layers. Zones are defined by bounding surfaces imported from seismic or derived from seismic surfaces. Zones correspond to the major stratigraphic subdivisions in the static model and often represent major flow units for the dynamic model. Within zones vertical heterogeneity is captured by defining layering, which may be constructed three different ways:

1. proportional (four layers everywhere), to reflect successions conformable with overlying and underlying zones,
2. parallel to base (all layers same thickness), to reflect truncation at the top, and
3. parallel to top (all layers same thickness), to reflect onlap of strata onto an underlying discontinuity surface.

Deterministic facies maps were constructed and then imported as a facies attribute into the grid, to be later used as classifiers in the stochastic modelling of porosity and permeability attributes. Porosity was modelled using sequential Gaussian Simulation (SGS), classified by facies. Classified SGS using facies generates a separate and independent SGS for each value of the facies attribute (i.e. for each facies), using as its input distribution only those input data (say, porosity values) that occur within cells of the same facies. For example: all porosity values at wells that occur in cells of facies value 1 (channel) would represent the input

distribution for the first classified SGS, which proceeds to model porosity only in those cells that have facies value = 1 (channel). The program then moves on to facies value = 2, and so on. During simulation this means that any data point for porosity from a cell with a different facies value is ignored. If facies value = 1 is the active classifier, all porosity values from cells of facies 2, 3, 4, etc. are ignored. This is desirable, because values for porosity in adjacent cells, but of different facies should be independent (i.e. porosity in a channel is not influenced by porosity in an overbank).

Several versions of the geo-cellular model were created resulting in a continuously refined model, with the final version being presented to BP in early October 2003. The geo-cellular grid and attributes were then exported from GeoCARD to the VIP reservoir simulation program used by BP for Tangguh production modelling.

This report briefly describes the creation and refinement of the overall geo-cellular model for testing potential Tangguh CO₂ injection and sequestration/storage, and summarizes the methodology and variable inputs used to populate the cells.

14.1 The Geological Test Model

The first GeoCARD model for the Tangguh area was created in May 2002 to test the data exchange between GeoCARD and VIP. There was no attempt at this early stage to produce a model of reservoir geology at Tangguh, instead the model was designed to produce a VIP data exchange file of a realistic data set, representative of the final static model. The area had to be large enough to be representative of the GeoCARD mesh and gridding system to be used ultimately on the final model. The test area had to incorporate some actual wells penetrating the phantom Middle Jurassic surfaces, with valid wireline log data with which to populate the gridded cells with attributes. Finally, the test area was selected from an area that did not have the 'holes' in the surfaces (see discussion below), and encompassed four Vorwata wells.

This area covered a region approximately 32 km long by 10 km wide, draped over the top of the Vorwata anticlinal structure axial crest, and oriented approximately northwest to southeast. The test grid area also captured the following wells: V-2; V-3; V-5; V-6; V-9; and V-10 (Figure 14.1).

The grid design of this test grid was deliberately simple. Vertical resolution comprised two zones. The lower zone encompassed the interval between the Top

Roabiba and Top Aalenian surfaces and consisted of a single layer. The upper zone encompassed the interval between the seismically interpreted Base Late Cretaceous surface and the Top Roabiba surface, and it was divided into 20 proportionally spaced layers. Horizontal cell dimensions were chosen as 750m x 750m.

The cells intersected by the six wells in the test area were populated with numbers, in this case we used the sonic DT curve value ($\mu\text{s}/\text{ft}$) derived from the sonic wireline logging tool. The remaining cells in the test area were then stochastically populated with sonic wireline log attribute DT using Sequential Gaussian Simulation (SGS) (Figure 14.2).

For the construction of the test model surfaces supplied by BP Indonesia were imported into GeoCARD. The following surfaces were used based on well data and interpreted seismic:

1. Mid-Point Datum for Late Paleocene Mud Prone Interval
2. Top Upper Member (Sand Prone Paleocene)
3. Top Middle Member (Sand Prone Paleocene)
4. Top Lower Member (Sand Prone Paleocene)
5. Base Late Cretaceous
6. Top Upper Roabiba (Middle Jurassic)
7. Top Main Roabiba (Middle Jurassic)
8. Top Aalenian Roabiba (Middle Jurassic)

Only some of these surfaces were derived from interpreted seismic surfaces, namely the Paleocene surfaces and the Base Late Cretaceous surface. The remainder of the surfaces supplied by BP were phantom surfaces, each associated with significant uncertainty.

The BP methodology employed for the phantoming below the Base Late Cretaceous was as follows. The interval from the Base Late Cretaceous to the desired phantom surface (for example the Top Upper Roabiba) was created by an isopach method with the thickness calculated from interpreted wireline well logs. This isopached interval was then added to the Base Late Cretaceous surface depth.

All of the Paleocene surfaces supplied by BP were limited in aerial extent to the gas charged reservoir area of the Wiriagar Deep structure. The remainder of the

surfaces below the Paleocene (Base Late Cretaceous and the Middle Jurassic surfaces) were interpreted or phantomed over the entire Berau/Bintuni Bay area.

All surfaces were cut by irregular polygonal shaped ‘holes’ in the surfaces, a result of the seismic interpreted geological faults cutting the surfaces. Phantomed surfaces inherited the ‘holes’ based on the projection of assumed vertical faults.

In June 2002, the test file was exported using the “VIP Export” function of the GeoCARD program. After several attempts and reiterations of exporting the model, data exchange successfully established between GeoCARD and VIP in August 2002.

14.2 The Preliminary Geological Model

In September 2002, a preliminary model was created. This model encompassed the three best-ranked injection sites locations identified previously in the Mesozoic interval, although only the two highest ranked injector sites were actively pursued. The three best potential CO₂ injection site locations, ranked in decreasing order were:

Injector Site #1 (IS #1) – Surface location situated approximately 10 km to the east of the Vorwata-10 well surface location, with proposed injection into the base of the Bajocian Roabiba Sandstone Reservoir. Structurally, this location is on the broad, gently dipping east flank of the Vorwata anticlinal and below the established gas-water contact (GWC).

Injector Site #2 (IS #2) – Situated approximately 6 km to the south of the Vorwata-10 well surface location, with injection into the base of the Bajocian Roabiba Sandstone Reservoir proposed. This structural location is towards the downdip SE end of the Vorwata anticlinal structure and below the established GWC.

Injector Site #3 (IS #3) – Surface location situated approximately 3 km to the NE of the Ofaweri-1 surface location, with proposed injection into the base of the Aalenian Sandstone Reservoir. Structurally, this surface location is approximately at the mid-point of the Wiriagar Deep plunging anticline, approximately 10 km S to SE from the Aalenian Reservoir gas accumulation in the Wiriagar Deep anticline, and downdip from the established Aalenian reservoir GWC. The proposed site places the potential injection point updip from the gas accumulations in the Ofaweri and

Roabiba “pop-up” structures. This location any avoids potential contamination of the Wiriagar Deep, Ofaweri, and Roabiba reservoir hydrocarbon resources.

The CO₂ IS #1 location is favored over the IS #2 location because the base of the sealing unit is less steeply dipping at IS #1 location. This results in the desired longer migration time for the proposed CO₂ plume to reach the GWC from IS #1. The Injection Site Location 3 (IS #3), targets the Wiriagar Deep anticlinal structure Roabiba and Aalenian Sandstone Reservoirs as potential ESSCI’s, and is a distant third (and last) choice for potential CO₂ injection due to higher risk associated with the Wiriagar Deep structure. This study concluded that only the Middle Jurassic Roabiba and Aalenian Sandstone Reservoirs at Wiriagar Deep and Vorwata have sufficient excess CO₂ storage capacity, with a proven seal potential (based on their respective existing natural gas accumulation columns). However, detailed seals evaluation also concluded that the ‘Ayot Limestone’ and ‘Upper Late Jurassic Shale’ cap-rock seals at Wiriagar Deep were leaking. Faulting and fracturing of the ‘Ayot Limestone’ and ‘Upper Late Jurassic Shale’ seal is the probable cause of the seal breach at Wiriagar Deep, making the third injection site location higher risk than the two proposed Vorwata Structure injection site locations.

The area of the coarse gridded model contains all of the Vorwata and Wiriagar Deep structures, and also the Saritu, Ofaweri, and Roabiba small-scale structures also. Furthermore, all of the Wiriagar Deep and Vorwata wells, in addition to the R-1, O-1, N-1, and S-1 wells are captured in the model area. The proposed LNG plant location and the three recommended injection site locations are also all within the gridded model area.

Numerous data-related problems presented themselves initially. One problem were the ‘holes’ in the surfaces supplied by BP (Figure 14.3). These holes were filled by exporting the surfaces to Schlumberger’s GEOFRAME program, using the PETROSYS program to actually fill the holes left from the fault polygons, and then re-importing the surfaces into GeoCARD.

These surfaces were created in PETROSYS, and essentially used the same methodology as BP for creating ‘phantomed’ surfaces. The interval from the Base Late Cretaceous was isopached based on well logs and then the isopached interval was added to the overlying surface resulting in a new surface which honors the well log picks for the horizon.

These newly created surfaces that were imported into GeoCARD, in addition to the three BP-supplied interpreted and phantom surfaces that required modification (and hole-filling), included:

1. Base Late Cretaceous
2. Base Ayot limestone
3. Base 'Upper' LJ-11 shale seal
4. Base LJ-11 incised valley sandstone
5. Top Upper Roabiba sandstone reservoir
6. Top Main Roabiba sandstone reservoir
7. Base Main Roabiba sandstone reservoir
8. Top Aalenian sandstone reservoir
9. Base Aalenian sandstone reservoir

The surfaces were then trimmed to extend over the primary area of interest in the Tangguh region, namely the Wiriagar Deep and Vorwata structures plus the south coast where the LNG plant location has been proposed (Figure 14.4).

A grid-construction mesh of 500 m x 500 m was then created to define the horizontal resolution and spatial orientation of the 3D grid to be constructed (Figure 14.5). All surfaces were then registered so that all share the same origin, gridding size and gridding orientation with the grid-construction mesh.

Each surface was then fitted to all corresponding well picks (Figure 14.6). In wells where the strata are not present, due to either erosion or pinch out, a 'dummy' surface intersection with the well logs was created at some depth below the immediate overlying surface intersection. This is necessary for the next step in the modelling, the clipping of surfaces procedure, which reflects the absence of the strata at any particular well location. All surfaces within the model were fitted at the well log intersections for all wells in the model area (Figure 14.7).

Following this the 500 m by 500 m trimmed surfaces were clipped, whereby if a strata is absent in the subsurface, it is truncated at a given location within the model, by either depth or by another surface. GeoCARD allows both of these options for the clipping process. The method used in this model was as follows: The "500mMesh_BaseAalenian-F" was clipped by the overlying surface

“500mMesh_BaseMainRoabiba-F” and the newly trimmed surface created was named “BaseAalenian-FC” whereby ‘F’ stands for fitted, and ‘C’ for clipped.

This method was used to fit and clip all surfaces in the model area, and the next step was then to create zones with layers. Fitted and clipped surfaces were used to define upper and lower bounding surfaces of zones in the model. The zonation and layering used in the ‘preliminary 3D geologic model’ are presented in Table 14.1.

Zone Name	LayeringStyle	No. of blks or Blk thickness
Ayot	Parallel to top	4
LowerLJ	Parallel to base	4
LJ_Incision	Parallel to top	20.0 ft
UpperRoabiba	proportional	20.0 ft
MainRoabiba	Parallel to top	20.0 ft
PreRoabShale	proportional	4
Aalenian	Parallel to top	20.0 ft

Table 14.1: Zonation and Layering Scheme for Preliminary Geological Model

The variogram parameters and variable inputs used in the ‘preliminary 3D geologic model’ were as follows:

- Single structure variogram, no rotations
 - Exponential structure
 - Nugget value = 0.001
 - Range = 1000m
 - Sill = 1
 - Anisotropy radius ratios for variogram:
 - x=1
 - y=1
 - z=0.011
- Search parameters for random walk during simulation:
 - Search ellipse radii
 - x = 1000m
 - y = 1000m
 - z = 10m
 - minimum number of conditioning data points = 1
 - minimum number of octants with data = 1
 - maximum number of data points per octant = 5

Unfortunately, when producing the VIP Export file, it was noted that cells at the Wiriagar Deep structure location were intersecting. As more than one cell can not intersect and occupy the same space either in the 3D geological model, or in nature, this produced invalid results for cell attributes. Upon investigating this effect further it was noted that this phenomena appeared to be related to the pinching out and truncation of surfaces at the Wiriagar area. This error occurs specifically in areas where a stratigraphic unit is absent, but one or both of its bounding surfaces exist (because they represent copies, phantomed of the base Cretaceous seismic surface, eg. the Top Main Roabiba surface north of the Roabiba erosional limit near the north coast of Berau Bay). This unexpected finding resulted in two decisions. The first action was to trim the model along the eastern flank of the Wiriagar Deep anticlinorium and retain only the Vorwata structure portion of the model, which was unaffected by this modelling problem. The second action was to arrange for GeoVisual Pty. Ltd. to correct this software problem in GeoCARD, and it was promptly rectified by February 2003.

The result was a preliminary 3D geologic model 500 m x 500 m over the Vorwata area, for the Mesozoic interval between the Base Late Cretaceous and Top Permian, representing the Aalenian reservoir where present, the Main Roabiba reservoir, the Upper Roabiba reservoir, and the suspected Callovian incised valley complex at V-3 and V-7 wells. A VIP Export file was subsequently produced and exported for a test run by BP in their reservoir simulator program.

The file covered the entire area of the Vorwata anticline, the Roabiba pop-up structure, the proposed LNG plant location, and the two highest ranked surface sites for CO₂ injection. The best-ranked proposed site is located approximately 10 km east of the surface location for the Vorwata-10st well, and the next best proposed site is approximately 6 km to the south of the Vorwata-10st well surface location.

The workflow of the study and the relationship of the various modules with the construction of the various 3D geo-cellular model versions is presented in Figure 14.9.

14.3 The Final Tangguh 3D Geologic Model

Previous experimental models created in the GeoCARD brought to light several challenges inherent to the Tangguh area model because of the huge areal extent of the region to be incorporated into the 3D model. The new geological and

reservoir model that were produced by the conclusion of this study, tested that the proposed CO₂ injection sites for the Tangguh Project were valid, in terms of:

- A) Proposed CO₂ migration (i.e. modelling tests that the CO₂ plume migrates where intended to, and does not compromise natural gas reserves);
- B) Proposed CO₂ sequestration/storage (i.e. modelling confirms that the necessary volume of CO₂ will be trapped in the intended structure for decades, at least);
- C) Proposed CO₂ safety (i.e. modelling validates that CO₂ remains in a saline aquifer in an environmentally-safe manner, with no leakage).

Although the above modelling and simulations tested are valid only in terms of testing that no breach of seal occurs due to capillary properties. The modelling and simulation does not test the geomechanical properties such as geomechanical fault reactivation, which was evaluated in detail by Hillis and Meyer (2003). At the request of BP (G. Perez, personal communication; January 2003) the final geo-cellular model was to include the Wiriagar Deep and Vorwata anticlinoriums, the Roabiba and Ofaweri structural closures, the proposed LNG site location on the south coast of Berau/Bintuni Bay, and the proposed CO₂ injection site locations. This was due to BP's concern that production drawdown of the natural gas accumulation in Wiriagar Deep, Roabiba, and/or Ofaweri concurrent with CO₂ injection would cause pressure depletion in the Roabiba Sandstone reservoir that might impact the injected supercritical CO₂ plume's migratory path.

The coordinates for the best 2 proposed injection sites are:

Projection	: UTM
Spheroid	: WGS-84
Unit code	: meters
Ref. Lat.	: 0.0
Ref. Long.	: 132.0 East
Scale factor	: 0.9996
False Northing	: 10,000,000
False Easting	: 500,000

Surface Location	Latitude	Latitude	X	Y
IS #1	-2.358405	133.3605	651,280	9,739,250
IS #2	-2.389640	133.2716	641,390	9,735,806

The final geo-cellular model captures the Mesozoic sequence stratigraphy framework created by the author for this study. The resultant sequence stratigraphic model incorporates and, to the best of the author's knowledge, honors all of the data available for the study. The importance of this stratigraphic methodology led to the recommendation for a high-resolution palynological study of existing Vorwata well cores to BP in 2002, although the details of this new high-resolution palynological study are not available for inclusion into this study.

After the detailed sequence stratigraphic model was imported into the final GeoCARD 3D geologic model, the geological model's 3D cell volumes were stochastically populated with key rock properties and attributes, which were then exported to a reservoir simulator (Landmark's VIP) for reservoir simulations. These reservoir simulations appear to verify that the proposed potential CO₂ injection site locations are feasible and environmentally-sustainable, with the potential injected CO₂ plume migrating over decades into the proven structure trap (Vorwata) without compromising the hydrocarbon reserves currently in-situ in the Middle Jurassic reservoir targets.

BP requested two further criteria for inclusion into the geo-cellular model, namely the inclusion of some major faults as potential permeability barriers, and a small number of active cells for migration to the VIP reservoir simulator (Frans Silitonga, personal communications; August 2003 and May 2003, respectively). The final model honors both requests given the limitations regarding both of these issues.

14.4 The Modelling Strategy

The aim was to create a static geological model suitable for subsequent upscaling into a simulation model. Grid design was chosen to capture expected heterogeneity and then be populated by deterministic facies maps. Facies domains were populated stochastically using SGS (porosity) and collocated co-simulation (permeability). Variogram design was initially based on empirical data for similar strata and then iteratively refined to yield results considered realistic given the scarcity of input data.

14.4.1 Zones Versus Layers in the Geological Model

The initial test model (Figures 14.1 and 14.2) was constructed using depth-structure seismic surfaces supplied by BP. As previously mentioned, the Base Late

Cretaceous surface is a significant distance above the top of the Jurassic reservoirs, and forms one of the few reasonably reliable seismic horizons provided by BP.

The sequence stratigraphy of the Mesozoic interval at Tangguh defined stratigraphic units that could not be resolved on seismic survey images at the time of the study (Pranoto, personal communication, June 2002). The detailed sequence stratigraphy, however, was one of the key components for modelling the migration of any potential injected CO₂ plume. All wireline logs were re-correlated within the model using wireline log character signatures, whole core and biostratigraphic data. The resultant new chronostratigraphic stratigraphic framework defines the basic architecture of the static model.

Therefore, in the geo-cellular model, additional surfaces were required that were unavailable from standard seismic interpretation. These additional surfaces were created by calculating an average isopach thickness of the gross stratigraphic unit below the Base Late Cretaceous surface, depth-offsetting it below the Base Late Cretaceous surface, and then fitting the 'phantomed' seismic surface to wireline log/whole core picks at all appropriate wells. This procedure was then repeated numerous times with the next deeper stratigraphic unit being isopach-thickness averaged, depth-offset, and then fitted at each well. One surface was created for the top and one for the base of each gross stratigraphic unit. These surfaces were usually sequence or parasequence boundaries such as unconformities (UNC) and maximum flooding surfaces (MFS), correlatable over large areas of the Tangguh model. These surfaces were then used as bounding surfaces for the identification of only the major stratigraphic zones within the model as follows:

1. Upper Late Jurassic Shales
2. Ayot Limestone
3. Pre-Ayot Shales
4. Callovian Roabiba Sandstone
5. Bathonian-Bajocian Roabiba Sandstone
6. Aalenian Shales and Sandstone

A re-evaluation of previous whole core studies by Waton et al, for palynology (1994 through 1997j), Pemberton for ichnology (1997a-e), and Tye & Hickey (1999)

for sedimentology, was undertaken and integrated into a re-examination of whole core from Wiriagar Deep and Vorwata wells.

These re-evaluations were incorporated into the sequence stratigraphy framework of this study, resulting in a series of highly detailed paleogeographical facies maps. Facies Polygons derived from the paleogeographic maps for each sequence stratigraphic unit were created in drafting packages (CorelDRAW and AutoCAD) using log-motif maps for each chronostratigraphic unit and exported from GeoCARD. The facies maps were then imported back into GeoCARD as facies outlines, resulting in one or more maps for each chronostratigraphic unit. A total of 20 maps were imported, each with numerous polygons showing the outlines of paleo-shorefaces, paleo-deltas, paleo-lagoons, paleo-tidal channels, etc.

The model was stochastically populated using classified (by facies) sequential Gaussian simulation (SGS) for porosity and collocated co-simulation (CCS) for permeability. Multiple realizations were produced. The outcomes appeared to be, in large part, random. It was deduced that irregardless of the layering system used for the “Bathonian-Bajocian Roabiba Sandstone Zone” (proportional, parallel to top, parallel to base), The zone’s ‘layers’ in most cases did not correspond to the chronostratigraphic units identified in the sequence stratigraphic module.

Therefore, each stratigraphic unit in the critical Roabiba Reservoir (eg. R10, R20, R80) was created as a unique zone. New bounding surfaces were created for the top and base of each stratigraphic unit, except where a unit was so thin (such as ~7 ft thickness of the R60) that it was grouped together with the overlying one (R70).

The zonation and layering used in the final 3D geo-cellular model are presented in Table 14.2.

This table of zones and their unique layering schemes representing ‘z’, combined with the regular spacing of 500 m X 500 m for the ‘x’ and ‘y’ cell dimensions, define the grid geometry of the final model.

ZoneNo	Unit	First Layer	Last Layer	Layer style	Layer thickness
1	Upper Late Jurassic Shale	1	2	proportional	n/a
2	Ayot Limestone	3	4	proportional	n/a
3	Pre-Ayot Shales	5	17	parallel to base	50ft
4	Callovian Roabiba Sandstone	18	37	parallel to top	15ft
5	R80 (Bathonian/Bajocian Roabiba Sandstone)	38	84	parallel to base	15ft
6	R70-60 (Bathonian/Bajocian Roabiba Sandstone)	85	108	parallel to base	15ft
7	R50 (Bathonian/Bajocian Roabiba Sandstone)	109	128	parallel to base	15ft
8	R40 (Bathonian/Bajocian Roabiba Sandstone)	129	142	parallel to top	15ft
9	R30 (Bathonian/Bajocian Roabiba Sandstone)	143	166	parallel to base	15ft
10	R20 (Bathonian/Bajocian Roabiba Sandstone)	167	179	parallel to top	15ft
11	R10 (Bathonian/Bajocian Roabiba Sandstone)	180	196	parallel to top	15ft
12	Aalenian Shales and Sandstones (A20)	197	200	proportional	n/a

Table14.2: Zonation and layering scheme for the final Tangguh 3D geologic model.

The grid was stochastically populated with multiple realizations using sequential Gaussian simulation (SGS) for porosity and collocated co-simulation (CCS) for permeability. Considerable effort went into the variogram design to minimize unrealistic clustering of extreme values away from areas of well control.

There are a number of sources of uncertainty in a static geological model over an area as large as Tangguh, which are significant but difficult to quantify. Uncertainties arising out of poor seismic control (and presumably also relatively poor control on time to depth conversion) at the time of this study, are further compounded by subsequent generation of yet more phantomed and manipulated surfaces to build the reservoir model grid, as described above.

Similarly the large geographic area covered by the model, and computational requirements of the simulation software (VIP) requires a certain limit on the number of active grid cells in the simulation grid. Whether this is achieved through upscaling of the data or upscaling of the static model grid, it will result in comparatively large grid cells. This can significantly simplify (distort) structural complexity and may

affect reservoir volume, as well as other factors (eg. apparent migration pathways and migration times).

14.4.2 Limitations on Number of Active Cells in the Geological Model

The request for the smallest number of active cells to be imported into the VIP simulator led to several versions of the geo-cellular model being tested experimentally. Three sizes of ‘framework mesh’ were tested in the course of this study. The 500 m X 500 m mesh, the 750 m X 750 m mesh, and the 250 m X 250 m mesh. This mesh size controls 2 of the 3 inputs on the size, and hence volume, of a given 3D geo-cell. The third dimension of cell volume, depth, is controlled by the zonation and layering scheme previously addressed. It is the construction of the mesh and the zonation/layering scheme that results in the total number of cells in the area to be modelled, with cells either set as ‘active’ or as ‘inactive’.

A model with a grid cell 750 m X 750 m mesh had cell volumes too big to capture heterogeneity. The 750 m X 750 m mesh/grid size severely restricted the importation and use of Tangguh area paleo-depositional facies maps into the GeoCARD model. Many of the paleo-depositional geographic facies, such as fluvial channels, lagoons, foreshore beach complex, etc., commonly had an areal extent of less than one km. The large mesh/grid size of 750 m X 750 m failed to capture the small areal extent of many of the paleo-facies, and as a result this size mesh was not pursued.

A model with grid cell 250m X 250 m mesh was created and tested but resulted in too many active cells in the model making upscaling and upgridding overly complex. The distance between many of the wells in the Tangguh area is approximately five km or greater. Rarely are any of the Tangguh wells significantly closer than ~5 km. This 250 m X 250 m mesh led to the model’s active cells numbering in the millions.

The 500m x 500m grid was chosen, resulting in 132 x 69 (totaling 9108) cells for each layer of the grid. The 500 m X 500 m mesh in conjunction with the final zonation and layering scheme of the final 3D model resulted in approximately 1.8 million total cells in the model volume. Many layers are truncated in the model (due to onlap, faulting, or erosional unconformity, etc.), which results in many cells pinching out. As a result, the final model contained only 313,967 active cells. This was considered a reasonable balance between the total number of active cells in the

model, and preservation of the geological heterogeneity through the majority of the Mesozoic interval across the ca. 65 km X 35 km model area.

14.4.2.i Incorporation of Faults into the Final Tangguh 3D Geologic Model

The construction of a 3D geo-cellular model including faults requires the importation of valid fault surfaces, or indexed fault polygons. As noted previously, during the time of this study there was a lack of interpreted seismic stratigraphic surfaces due to the poor quality of seismic imaging at the depth of interest, and this included a lack of interpreted fault surfaces with any high degree of confidence (Pranoto, personal communication, June 2002).

It was suggested early-on in the modelling process to simply extrapolate major faults from a 1998-vintage ARCO Top Structure Main Roabiba Depth Map, and incorporate them into the model as vertical, strike-slip faults (G. Perez, personal communication, January 2003 and June 2002). Several interpreted 3D fault surfaces were eventually supplied for a fault re-activation risk assessment module. These fault surfaces were found to be so rugose and unrealistic as actual dipping fault plane surfaces that they required extensive smoothing by Hillis and Meyer (2003). The actual 3D seismic survey volume was not available to this study, but clearly future fault maps could be incorporated into the model.

As a result, faults and offsets were not incorporated directly into the grid design. Instead the locations of the main fault blocks were incorporated into the model as a separate attribute (named the “FaultCompartment” attribute).

Major fault traces were digitized and imported as vector graphics into GeoCARD. The “FaultCompartment” attribute was created from polygons in the same way that the paleo-facies attribute, described above, was created from facies values. Note that this method required all fault compartments to be closed at all four sides (i.e. fault-bounded on four sides).

This limitation was overcome by hand-editing “Transmissibility” multiplier attributes. Transmissibility multipliers were then created between faultblocks and hand-edited in GeoCARD’s bitmap attribute editing feature. Transmissibility is discussed in more detail in the later chapter on ‘attributes’. These ‘major’ faults, assumed to be strike-slip and vertical-dipping, can then be controlled in the reservoir simulator as to whether or not they act as barriers to flow.

14.4.2.ii Attributes and Variograms in the Geological Model

The primary attributes used in the populating of the 3D Tangguh static model were attributes generated by sampling from wireline log data or petrophysical analyses results from wireline data at wells. The wireline data used came from wells in the model area previously drilled by ARCO, BG, or Occidental Petroleum. Prior to delivery, wireline log data had been environmentally corrected for borehole size and washouts, drilling fluid salinity and density, and presence of heavy minerals in some lithologies (i.e. pyrite, siderite, etc.) by both various Schlumberger software and by a commonly used petrophysical program (Petcom). Effective porosity had been calculated from environmentally corrected wireline logs (NPHI, FDC, and Sonic) and calibrated to whole core plug data. The calibration of the wireline log data to the laboratory analyses of whole core plugs had been selectively restricted to Helium porosity (He \emptyset) and air permeability (Kair) measurements with an 800 psi confining pressure to normalize all plug testing to 800 psi NOB (net over-burden pressure).

Effective porosity (PHIEC) and permeability (PERMCALC) had been calculated with Petcom, and were loaded into the GeoCARD final model for each of the wells in the Tangguh model area. Attributes generated from either wireline well log data or petrophysical well analysis were loaded into cells intersected by well paths, which is referred to as “blocking” of wells in some software. The outline below lists the key attributes for data blocking of wells.

A. Attributes

- 1.) **Porosity (\emptyset)** as arithmetic mean of all effective porosity values in each cell using PHIEC petrophysical log parameter.
- 2.) **Permeability (k)** as the harmonic mean of all effective porosity values in each cell using PERMCALC petrophysical log parameter.
- 3.) **FaciesAtWell** as mode of facies attribute from cores.
 - a. **FaciesAttribute** from polygons. This populates the model with integer values for facies based on the facies polygons imported earlier. This attribute exists in the entire model, (i.e. not limited to cells intersected by well paths). Facies codes not only reflect the

depositional facies (say, shoreline vs. fluvial), but also major trends in anisotropy (e.g. different orientation of shorelines in the Aalenian and Bajocian). (see Figure 14.10, Figure 14.11, Figure 14.12, and Figure 14.13 for examples).

- b. **SimpleFacies_Use**. This is the facies attribute used in subsequent modelling steps. Constructed by adjusting, where necessary, facies from polygons to more closely match facies from cores (FaciesAtWell attribute). This attribute also summarizes a number of facies, which will be modelled using the same variogram or are otherwise similar lithologically. It also combines occasional rare facies with more common similar ones to simplify the facies model. For example tidal flats, which occur in one small area of only one of the paleo-depositional geographical facies maps was combined with lagoonal facies to simplify the modelling process. Table 14.3 summarizes the numerical facies codes used in the attribute SimpleFacies_Use, which was used during the simulation of the porosity and permeability values.

Facies Code	Reservoir Facies	Facies Code	Reservoir Facies
0	No facies defined	7	“Tidal Inlet R40” – open embayment
1	Fluvial (channel/ overbank/ bayhead delta/ lake)	8	Tidal deltas/tidal inlets
2	-- NOT USED --	9	Barrier bars
3	-- NOT USED --	10	Foreshore/coastal plain
4	Delta/Mouthbars	11	Upper Shoreface
5	Bay/Lagoon/TidalFlats	12	Middle Shoreface
6	-- NOT USED --	13	Lower Shoreface

Table 14.3: Numerical facies codes used in the attribute ‘SimpleFacies_Use’.

- c. **Fault polygons**. Major fault traces were digitized and imported as vector graphics into GEOCARD. **FaultCompartment** attribute was created from polygons in the way that the facies attribute was created from facies values. Note that this method required all fault compartments to be closed on all four sides (i.e. fault-bounded on four

sides). This limitation was overcome by hand-editing Transmissibility multiplier attributes (see Figure 14.14 and Figure 14.15).

- d. **Transmissibility multiplier** attribute. Created using fault polygons. Attribute is 1 where adjacent cells have the same **FaultCompartment** attribute value (i.e. cells are in same fault block). Attribute value is 0 (zero) if adjacent cells are in different fault blocks. One transmissibility multiplier attribute created each for i, j, and k direction. The assumption was made that if faults were sealing (Tmultiplier = 0, no flow), then flow along the fault was also not possible. Consequently all cells in the model along the fault traces have transmissibility multipliers in both i and j-directions set to zero (Figure 14.16).

B) Variograms

- 1.) Different variogram models were designed for various facies to reflect the anisotropy in each facies and also the chronostratigraphic units
- 2.) Variogram design comprises two components: variogram structure(s) and search ellipse(s).

Variogram 'structure' is defined by range, sill and nugget value as well as the type of structure (spherical, Gaussian, exponential, or power curves). Additionally the anisotropy ellipsoid for the variogram and the rotation(s) have to be specified. All of these parameters relate to the spatial variance of attribute values expected. The initial input values were chosen to reflect expected theoretical limits of sediment body geometries, based on sedimentology consulting reports on Tangguh and references therein. The variogram models used for the various facies in modelling both porosity and permeability are presented in Table 14.4.

Facies Code	Reservoir Facies	Variogram
0	No facies defined	Generic Circular
1	Fluvial (channel/ overbank/ bayhead delta/ lake)	Fluvials
2	-- NOT USED --	(Fluvials)
3	-- NOT USED --	(Fluvials)
4	Delta/Mouthbars	Generic Circular
5	Bay/Lagoon/TidalFlats	Shores_1deg
6	-- NOT USED --	Shores_1deg
7	“Tidal Inlet R40” – open embayment	Shores_1deg
8	Tidal deltas/tidal inlets	(Fluvials)
9	Barrier bars	Shores_151deg
10	Foreshore/coastal plain	Shores_151deg
11	Upper Shoreface	Shores_151deg
12	Middle Shoreface	Shores_151deg
13	Lower Shoreface	Shores_151deg

Table 14.4: The variogram models and numerical codes used for the various paleo-depositional facies in the final geologic model.

The variogram structure type; structure values for sill, range, nugget; the search ellipse anisotropy, and the rotations(s) used in the final model are presented in Tables 14.5. The ‘search ellipse’ of the variogram model is a construct used for data sampling during the Monte Carlo simulation random walk in Sequential Gaussian Simulation. Table 14.6 summarizes the search ellipse for the variograms used in the final 3D geologic model.

Variogram model name	Variogram Structure							
	Type	Nugget	Range	Sill	Anisotropy radii ratio			Axis Rotation
					x	y	z	
GenericCircular	spherical	0.06	3000	1	1000	1000	1	none
Shores_1deg	spherical	0.06	3000	1	1000	750	1	z: 1deg
Fluvials	spherical	0.06	3000	1	1000	750	1	z:35deg
Shores_151deg	spherical	0.06	3000	1	1000	750	1	z:151deg

Table 14.5: The variogram models, structures, and parameters used for stochastically populating cells in the final geologic model.

Variogram model name	Search Ellipse			
	l	j	k	rotation
GenericCircular	2000	2000	2.5	none
Shores_1deg	2000	1500	2.5	z: 1deg
Fluvials	2000	1500	2.5	z:35 deg
Shores_151deg	2000	1500	2.5	z: 151deg

Table 14.6: The search ellipse parameters for different paleo-depositional facies in the final geologic model

14.5 Results of the Final 3D Geologic Model

Systematic experimentation was conducted on the designs of variograms to achieve optimal attribute modelling outcomes and minimize unrealistic clustering of high or low values in areas away from well control. It was found during this study that the design of the search ellipse exerted a major influence on attribute modelling results. This is counter-intuitive as the primary purpose of the search ellipse is to economize computing effort. Anecdotal evidence exists from other areas that SGS can be sensitive to ‘search ellipse’ design (Jeffrey Yarus, personal communication, 2003). It is unclear whether this is intrinsic in the method of SGS or an artifact created apparently at random by certain combination of other parameters (such as grid cell size?).

The modelled attributes Porosity-SGS is found in the GeoCARD final model as attribute **Phi_0910_09**. Modelled from **PhiAtWell** using SGS, variogram models (see tables above), and facies attribute to classify SGS. Normal scores transform of input values and back-transformation of results was performed automatically.

Five realization of porosity were then computed. Comparing realizations occasionally highlighted the uncertainty in porosity modelling in the Tangguh dataset, particularly facies with relatively few well intersections (such as barrier island) that show large variations between realizations.

Permeability Collocated Cosimulation (CCS) was modelled from the normal scores transform of **kAtWell_har** using facies attribute as a classifier, with the same variograms that were used for the porosity simulation. Back-transformation of the final result was performed explicitly.

Five realizations of permeability were also computed. A comparison of the realization outcomes occasionally indicated large variation in permeability values between realizations, particularly for facies with limited input data (such as barrier island), and reflect the uncertainty present for that facies.

Overall, the five realizations performed for populating effective porosity and permeability within the Tangguh area model appeared realistic, and showed a pattern of consistency in areas where input datasets were large and of good quality, and showed areas with large variations between realizations, reflecting uncertainty with the actual attribute value range, due to limited input data.

14.6 Preliminary Reservoir Simulation Results

In October 2003, the final geo-cellular model was delivered to BP, and the grid system/attributes from Realization 1 were imported by BP into VIP (Landmark's reservoir simulator program). Pre-processing and upscaling of the grid and attribute files from the final geologic model were carried out by the BP Tangguh Subsurface Development Team (Figure 14.17). When a preliminary visualization was carried out, the simulation for only the Vorwata segment of the model took slightly over 12 hours, however, details of this will not be addressed in this study (Frans Silitonga, personal communication, 2004).

The reservoir simulator preliminary modelling confirms the high level of confidence assigned to one of the two best ranked proposed subsurface injection and sequestration/storage locations for CO₂ from the Tangguh LNG Project (labelled in GEOCARD as 'IS-1' and 'IS-2'). The highest ranked of these two sites, the IS-1, was loaded with three imaginary injector boreholes (labelled 'CO₂ -1', 'CO₂ -2', and 'CO₂ -3'), along with several updip gas production wells over the Vorwata natural gas accumulation.

These three visualized injection sites are readily identifiable in the VIP reservoir simulator screen capture for Year 0 ('year zero') (Figure 14.18). This screen capture represents the period of time when all production and injection development has been completed but initial natural gas production and CO₂ injection has not yet commenced. The layer imaged is the R50 layer of the Bathonian/Bajocian Roabiba Sandstone Reservoir.

The VIP reservoir simulator screen capture for Year 5 (Figure 14.19), shows the visualization of the same layer (R50) after 5 years of natural gas production and

CO₂ injection. The cells with the Vorwata structure Roabiba Reservoir natural gas accumulation are colored bright red, the cells with the Vorwata structure Roabiba Reservoir injected CO₂ plume are colored green, and the water-wet cells in the saline aquifer leg of the Roabiba Reservoir are colored blue. The 3 injector well site locations are labelled as CO2-1, CO2-2, and CO2-3 in the VIP reservoir simulator screen capture and are clustered around the best ranked injection site location recommended in this study (labelled 'InjectionSite_1' in the GEOCARD 3D geological model).

The screen capture for Year 20 (Figure 14.20) shows reddish-purple colored cells representing containment pore volumes that are gas-depleted due to natural gas production. It is clear from the preliminary visualization that only after 20 years of CO₂ injection and migration does the injected CO₂ reach the original GWC.

After 25 years of natural gas production and CO₂ injection (Figure 14.21), the CO₂ plume has only migrated into the cells gas-depleted from production (previously purple in Figure 20) and has still not come into contact with the remaining hydrocarbon reserves. The slight migration noted to the east of the "CO₂ -3" injector well site location after 20 years probably represents the filling of the reservoir injector strata laterally from the bottom-hole location, after migration has filled the entire height of the reservoir from the bottom-hole location to the top seal, and does not indicate down-dip migration of the plume. The plume's migratory vector is clearly updip, and towards the NW, along the topographic base of the top seal.

14.7 Conclusions

The reservoir simulation 'preliminary results' are encouraging and appear to validate the study conclusions that the subsurface injection and sequestration of CO₂ at Tangguh is a technically feasible and valid option. It is a potential solution for the disposal of the estimated 2.4 TCF CO₂ at Tangguh, which can be considered environmentally-sustainable with a high degree of confidence, without risking any proven, probable, or possible hydrocarbon reserves of the area. However, implementation must pass economic hurdles that are not within the scope of this study. The estimated 'CO₂ project' development costs, including CO₂ storage amongst other commercial and possibly political factors, will ultimately determine whether the proposed CO₂ subsurface injection/storage model becomes a reality.

PART V
IMPLICATIONS FOR IMPLEMENTATION

15.0 Drilling and Data Recommendations for Exploration and Injection Wells

Some brief recommendations in regard to data acquisition for both hydrocarbon exploration and potential CO₂ injection wells are presented. Two points need to be noted. Firstly, the type of data sought for exploration wells versus CO₂ injection wells is inherently different in many regards. Therefore, the data acquisition recommendations presented are suggestions for a complete set of data to be used to address a variety of issues on both exploratory and injection wells.

Secondly, any data acquisition program, for either exploratory or injection wells, needs to be tailored to the actual site-specific well location and TD. Furthermore, any final decision on actual implementation of any facet of the recommended data acquisition program would have to include and incorporate financial budgets, time constraints, rig safety, and drilling/acquisition feasibility. An example of this might be a recommendation to obtain conventional core samples. Time constraints on rig availability or rig costs might rule out the acquisition of a core. Likewise, the planned attempt to acquire a conventional core through a given interval might meet with repeated ‘jam-offs’ of the coring assembly down-hole, rendering the cutting of a core impractical (in terms of time and cost). These economic and engineering considerations are not included in this data acquisition recommendations report.

However, the list of recommended data acquisitions for future Tangguh/Babo-Arguni area exploration and injection disposal wells has not been made so broadly as to constitute a ‘Christmas wish-list’. The recommended data acquisitions have been made to address specific ‘data gaps and needs’ from a CO₂ injection and sequestration standpoint, or from a ‘zero emissions program’ viewpoint, and also to address the specific requirements for a hydrocarbon exploration program.

15.1 Recommendations on Future Tangguh Well Data Acquisitions

Geological data acquisition for both exploratory and injection wells can be broadly categorized into several types. They are:

- 1) pre-drill seismic survey data (which may require a VSP or check shots to be carried out at rigsite during the drilling of a well);
- 2) physical rock samples (obtained from drill cuttings, whole rock conventional coring, or wireline sidewall cores);

- 3) petrophysical measurements (obtained from electric, magnetic, acoustic and nuclear instrument readings of the borehole rock properties);
- 4) fluid and geomechanical measurements of the borehole or strata pore-fluids (including leak-off tests for rock strength and integrity at the casing shoe strata, pore pressure and pore fluid analyses from wireline MDT/RFT sampling tools or DST testing).

The recommended data acquisition suggestions have been organized by data type or method (i.e. extended Leak-off tests – eLOT), with the specifics of a formation/unit/member in mind. Reasons or justifications for the acquisition have been included in the discussion after the data item. In some cases, alternative methods or data acquisition systems have been offered or suggested, and occasionally qualified by time and cost considerations.

Schlumberger names and nomenclature have been used to identify wireline logging tools/logs, however, similar tools of comparable quality with similar results are available in most cases from other wireline service companies such as Western Atlas, Halliburton, and GeoPeko. Schlumberger names have been used because of common familiarity by geoscientists and drilling personnel, and to avoid excessive clutter in the text that multiple brand names per tool would introduce.

15.1.1 Steenkool/Sele Formations

The Steenkool and Sele Formations are potential sealing units to the underlying Kais and Faumai carbonates (members of the New Guinea Limestone Group – NGLG). The Kais Formation is a potential hydrocarbon reservoir in the Babo and Arguni PSC's based on production from the Salawati Basin oil and gas fields, the Wasian-Mogoi oilfields, and the shallow Wiriagar field. The Faumai Formation has been proposed variously as a potential CO₂ injection and sequestration site, or as a site for drill cuttings and production formation waters injection and disposal. Given the paucity of data over the potential Steenkool/Sele Formation sealing units, and the Kais/Faumai Formations disposal potential as suggested above, the following recommendations include acquiring datasets on the reservoir/seal couplets. As whole rock is needed for MICP analysis that would yield meaningful 'seal capacity' measurements for the 'cap rock', cuttings have been deemed insufficient. However, as conventional core is generally expensive and time consuming to acquire, this researcher suggests that wireline rotary sidewall cores

(MSCT) would suffice in place of sample plugs from a conventional core. MSCT from the lower-most Steenkool is adequate for MICP ‘seal capacity’ and XRD work rather than conventional core acquisition.

The following data acquisition program is suggested in regard to seal potential for the Steenkool/Sele Formation interval, only if considering sequestration/storage of gas or fluids in the NGLG:

- A) Gas measurements and drill-cuttings collected during drilling.
- B) Conventional core or wireline rotary sidewall core (MSCT cheaper).
- C) Wireline Log Suite
 - 1) GR
 - 2) SP
 - 3) MSFL
 - 4) DLL
 - 5) CNL
 - 6) FDC
 - 7) BHCS
 - 8) MSCT* (if conventional core is not cut and retrieved)
 - 9) FMI/FMS
 - 10) CSAT (Check-shots)

15.1.2 Kais/Faumai Formations (NGLG)

The Kais Limestone Formation and Faumai Formations are both members of the NGLG. The Kais Formation is a potential hydrocarbon reservoir and there is no known, proven seal between the overlying Kais and the underlying Faumai Formations. Both NGLG members are carbonates and are, in some locations, conformable, although at the Berau/Bintuni Bay area there is generally an unconformable sequence boundary dividing them. The Faumai Formation has been proposed variously as a potential CO₂ injection and sequestration site, or as a potential site for produced formation waters and/or drill-cuttings slurry injection and disposal. Given the paucity of data over the Faumai Formation NGLG unit, and its disposal potential as suggested above, it is recommended that conventional cores be obtained.

Whole rock is needed for sedimentary and reservoir analysis, cuttings are very useful but given the Faumai Formation history of ‘total lost circulation’ and the ‘blind drilling’ approach used to drill through it, cuttings have generally not been available and would most likely be costly and time consuming to acquire (i.e. as lost circulation

occurs, cementing the bottom open-hole and then resuming drilling with returns, and cementing again as lost circulation occurs). However, unlike the Steenkool Formation, wireline rotary sidewall cores (MSCT) would not be sufficient to understand and evaluate the nature of the suspected vugs and fractures causing the lost circulation in the Faumai Formation. Therefore, although conventional core is generally more expensive and time consuming to acquire than MSCT rotary sidewall cores, it is the only viable method to recover large-scale whole rock samples for analyses. The best case scenario for MSCT recovery is that dense, nonporous carbonate matrix is recovered, however, the problems associated with the Faumai Formation lie with large scale voids causing the lost circulation, and potentially providing storage capacity for injected material.

A conventional core taken in the lost circulation zone could potentially provide the best opportunity to capture in-situ vugs and fractures. An oriented core would be more informative than a non-oriented core. Gel coring is recommended for improving the successful coring of the formation in order to minimize jamming. The chances of success in recovering a conventional core in a lost circulation zone is actually better than most would think, if the loss zone does not contain collapsed 'rubble' in it.

Based on the author's wellsite experience, and those of drilling superintendents (M. Foster and J. Lloyd, personal communications; 1995, 1996, 1997, 2002), there is no evidence to suggest that the Faumai Formation is characterized by 'rubble zones'. Euhedral calcite crystal lined fractures and dissolution vugs ranging in scale from millimeters to meters can be expected. This is based on the 'football' sized chunk wedged into the bowspring of a logging tool on one of the Wiriagar Deep wells. Therefore conventional core acquisition rather than MSCT rotary cores is recommended for sampling the Faumai Formation.

The lateral log (DLL) is not recommended because the primary rock lithology in this interval is likely to be carbonate, and an induction tool (ILD/AIT) would yield superior resistivity readings. It is unlikely that SP would yield any meaningful readings as there is likely to be little fluid in the annulus.

As the interest in this formation is in the fractures and vugs rather than the rock matrix, running of Dipole Sonic tool (DSI) and the acquisition of full waveforms and Stoneley wavelets rather than the more basic sonic (BHCS) is recommended for shear/fracture analysis. Furthermore, FMI/FMS images can also be used to evaluate

fractures and open vugs in the borehole wall. Continuous borehole temperature logs have been found to be very useful in delineating the actual circulation ‘thief zones’ within the carbonates.

Although the Faumai Formation is subnormally pressured (estimated by BG to be ~8.0 ppg EMW) the formation is likely to be water bearing, and this aquifer fluid content/composition (water analysis) and fluid migration data would be immensely useful to any disposal operation. An open-hole DST, reverse circulated out, would eventually flow the subnormally pressured formation water. A PLT tool data from the test may also prove useful for delineating porous (fractured and vuggy zones) intervals and formation flow directions. The use of an MDT tool on wireline, even in tandem with the dual packer module, is unlikely to be successful in a vuggy and fractured carbonate like the Faumai Formation due to lack of seal for the probe or packers. Furthermore, an MDT, even with a good seal and pumping out the ‘formation filtrate’, is unlikely to recovery anything but drilling fluid (surface water) pumped continuously downhole due to the lost circulation.

Therefore, the following data acquisition program is suggested for the Faumai Formation interval:

- A) Drill gas and cuttings at 10’ interval (if circulation allows this)
- B) Conventional core (run 60’ barrel, but greater than 30’ and less than 60’ recovery would be acceptable)
- C) Wireline Log Suite (assuming WBM or seawater used as drilling fluid)
 - 1) GR
 - 2) ILD/AIT
 - 3) CNL
 - 4) FDC
 - 5) DSI
 - 6) FMI/FMS
 - 7) CSAT (VSP or checkshots up to geophysicist)

15.1.3 Eocene and Paleocene Formations

The Eocene Formation has not been found to be hydrocarbon bearing anywhere in the Bird’s Head region, however, the Late Paleocene Formation is hydrocarbon bearing and commercially significant at the Wiriagar Deep structure. The basal Paleocene, or top-most Cretaceous interval, is also known to have an over-pressured water zone at the Vorwata structure, which has flowed into several of the

Vorwata structure wellbores (i.e. N-1, V-1, and V-9), causing drilling related problems.

The data acquisition program for this chronostratigraphic interval would probably be driven, for the most part, by hydrocarbon exploration perspectives, especially if hydrocarbons are discovered in the Paleocene succession interval. However, from a 'disposal' perspective, water-bearing 'aquifers' in the Eocene or Paleocene also have potential for the injection and sequestration of various material ranging from CO₂, or produced formation waters, to drill cuttings. Water sampling from aquifers is recommended, and can be obtained at minimal cost via wireline MDT tool pressure sampling and fluid pump-out followed by multi-sampling in 450 cc chambers. A DST program is possibly recommended for any hydrocarbon discoveries if petrophysical analysis indicates sufficient moveable volumes, but DST testing is not recommended for 'water disposal' purposes. Likewise, conventional core is not necessary for 'disposal options' alone, but could be considered for hydrocarbon exploration purposes if oil/gas shows are encountered. Wireline MSCT rotary sidewall cores in sealing lithologies (i.e. shale) would be adequate for MICP 'seal capacity', and XRD analyses.

The use of MSFL and DLL and SP are recommended in this hole section if water based mud (WBM) is used. If OBM (oil based mud) is used as the drilling fluid then the ILD/AIT tool can be retained on the wireline logging suite. Therefore the following data acquisition program recommendations are:

- A) Record drill gas and sample 10' intervals for drill cuttings
- B) Conventional core or wireline rotary sidewall cores (wireline MSCT's are suitable for MICP or petrographic analyses)
- C) Wireline Log Suite (if WBM used)
 - 1) SGR (spectral gamma ray)
 - 2) SP
 - 3) MSFL
 - 4) DLL
 - 5) CNL
 - 6) FDC
 - 7) DSI
 - 8) FMI/FMS
 - 9) MDT (pressures and fluid samples)
 - 10) MSCT (rotary sidewall cores)
 - 11) CSAT (VSP or checkshots up to geophysicist)

15.1.4 Late Cretaceous Interval

The Late Cretaceous Succession has been found to be hydrocarbon bearing in some of the Wiriagar Deep Structure wells, where it is a fractured marl. However, the formation is sandier and water bearing at the Vorwata structure. Also the basal Paleocene, or top-most Cretaceous interval, has an over-pressured water zone on the Vorwata structure, which has flowed uncontrollably into several of the Vorwata structure wellbores (ie. N-1, V-1, and V-9).

The data acquisition program for this chronostratigraphic interval would probably be driven, for the most part, by hydrocarbon exploration perspectives, especially if hydrocarbons are discovered in the overlying Paleocene succession interval. However, from a 'disposal' perspective, water-bearing 'aquifers' in the Cretaceous have a possible potential for the injection and sequestration of various material ranging from CO₂, or produced formation waters, to drill cuttings. Water sampling from aquifers (particularly clastic aquifers) is recommended, and can be obtained at minimal cost via wireline MDT tool pressure sampling, and fluid pump-out followed by multi-sampling in 450 cc chambers. A DST program is possibly recommended for hydrocarbon discoveries, if petrophysical analysis indicates sufficient moveable volumes, but DST testing is not recommended for aquifer water samples alone (needed for injection/disposal options in a saline aquifer). Likewise, conventional core is not necessary for 'water disposal' purposes, but might be advisable for hydrocarbon discoveries. Wireline MSCT rotary sidewall cores in potential seal lithologies (i.e. shale, marl, or dense tight carbonate) would be adequate for MICP 'seal capacity', and XRD analyses; and cost less (especially in terms of rig-time) than obtaining conventional core.

The use of MSFL and DLL and SP are recommended in this hole section if water based mud (WBM) is used. If OBM (oil based mud) is used as the drilling fluid then the ILD/AIT tool can be retained on the wireline logging suite.

Therefore the following data acquisition program recommendations are:

- A) Record drill gas and sample 10' intervals for drill cuttings
- B) Conventional cores or rotary sidewall cores (in sealing cap rock lithologies and in reservoir/aquifer lithologies)
- C) Wireline Log Suite (if WBM used)
 - 1) SGR (spectral gamma ray)
 - 2) SP
 - 3) MSFL

- 4) DLL
- 5) CNL
- 6) FDC
- 7) DSI
- 8) FMI/FMS
- 9) MDT
- 10) MSCT (rotary sidewall cores)
- 11) CSAT (VSP or checkshots up to geophysicist)

D) DST(for possible significant hydrocarbon reservoirs only)

15.1.5 Jurassic Sequences (Aalenian Unit, Bajocian Roabiba Formation, Callovian Roabiba Formation, Pre-Ayot Unit, Ayot Limestone Formation, and Late Jurassic Shale Unit Intervals)

The Jurassic Formation has been found to be a significant hydrocarbon reservoir in the Wiriagar Deep, Ubadari, Roabiba, Ofaweri, Wos, and Vorwata wells, where there is structural closure.

The data acquisition program for this chronostratigraphic interval would likely be driven, for the most-part, by hydrocarbon exploration perspectives. Compaction, with loss of porosity and permeability quality due to excessive burial depth, at the deepest Jurassic level over much of the Arguni and eastern Babo PSC's will possibly result in tight formations and preclude injection/disposal potential and possibly hydrocarbon production potential.

However, at shallower depths (i.e. above -15,000 ft TVDss) where favorable porosity and permeability characteristics have possibly been preserved in the Jurassic there is a potential, from a 'disposal' perspective, for water-bearing 'aquifers' to be sites for injection and sequestration of various material ranging from CO₂ to produced formation waters. Water sampling from aquifers is recommended, and can be obtained at minimal cost via wireline MDT tool pressure sampling, and fluid pump-out followed by multi-sampling in 450 cc chambers. A DST program is recommended for hydrocarbon discoveries if petrophysical analysis indicates sufficient moveable volumes. DST testing is not recommended solely to obtain formation water samples. Conventional core, in reservoir zones, have been demonstrated, by this study, to be invaluable for CO₂ injection and disposal study purposes. The Jurassic sandstones, specifically, have been identified in the Tangguh area as a viable, environmentally-sustainable, and technologically feasible CO₂ sequestration/storage option. Furthermore, conventional core may be important for

hydrocarbon exploration purposes, if significant hydrocarbon shows are encountered on exploratory wells in the Arguni/Babo areas. Wireline MSCT rotary sidewall cores in potential ‘cap rock’ (i.e. shale, marl, or dense tight carbonate) would be adequate for MICP ‘seal capacity’ and XRD analyses, and cost less (especially in terms of rig-time) than obtaining conventional core in seal intervals.

The use of MSFL and DLL and SP are recommended in this hole section if water based mud (WBM) is used. If OBM (oil based mud) is used as the drilling fluid then the ILD/AIT tool can be retained on the wireline logging suite. Therefore the following data acquisition program recommendations are:

- A) Record drill gas and sample 10’ intervals for drill cuttings
- B) Conventional cores or rotary sidewall cores (in sealing cap rock lithologies and in reservoir/aquifer lithologies)
- C) Wireline Log Suite (if WBM used)
 - 1) SGR (spectral gamma ray)
 - 2) SP
 - 3) MSFL
 - 4) DLL
 - 5) CNL
 - 6) FDC
 - 7) DSI
 - 8) FMI/FMS
 - 9) MDT (pressures and fluid samples)
 - 10) MSCT (rotary sidewall cores)
 - 11) CSAT (VSP or checkshots up to geophysicist)
- D) DST (for possible significant hydrocarbon reservoirs)

15.1.6 Triassic and Permian Sequences

The Permian sandstones in the Permo-Triassic succession have hydrocarbon reserves in wells in the Wiriagar Deep, Wasian-Mogoi, and Vorwata structures. The sandstones are generally very tight, and while probably a target for future secondary recovery as ‘tight gas reservoirs’, they are generally not suitable for ‘disposal options’ due to poor injectivity and insufficient storage volume.

The data acquisition program for this chronostratigraphic interval would probably be driven, for the most-part, by hydrocarbon exploration perspectives. From a ‘disposal perspective’ the Permo-Triassic reservoirs have very limited potential. The burial depth of the Permo-Triassic probably makes it generally tight, with poor

injectivity characteristics. Wireline MSCT rotary sidewall would be adequate for MICP ‘seal capacity’, petrographic, and XRD analyses.

The use of MSFL and DLL and SP are recommended in this hole section if water based mud is used. If OBM (oil based mud) is used as the drilling fluid then the ILD/AIT tool should be used. Therefore the following data acquisition program recommendations are:

- A) Record drill gas and sample 10’ intervals for drill cuttings
- A) Rotary sidewall cores (in sealing cap rock lithologies and in reservoir/aquifer lithologies)
- B) Wireline Log Suite (if WBM used)
 - 1) SGR (spectral gamma ray)
 - 2) SP
 - 3) MSFL
 - 4) DLL
 - 5) CNL
 - 6) FDC
 - 7) DSI
 - 8) FMI/FMS
 - 9) MDT (Pressures and fluid samples)
 - 10) MSCT (rotary sidewall cores)
 - 11) CSAT (VSP or check shots)
- D) DST (for possible significant hydrocarbon reservoirs)

15.1.7 Final Remarks on Data Acquisition

It should be noted that an eLOT (i.e. “extended Leak-off Test”) is recommended by the ASP’s Geomechanics Group (chaired by Professor Richard Hillis) after drilling at least 10’ of new hole below a casing shoe or liner shoe. An eLOT is a conventional LOT repeated once or twice more, and pumping an additional 2 bbls of fluid beyond the ‘leak-off pressure/volume’ established during the original, first LOT. There is an excellent article regarding eLOT’s in the 1996 APPEA Journal *“Recent Experience With Extended Leak-Off Tests For In-Situ Stress Measurements in Australia”* (Enever, et al., 1996).

The purpose of the eLOT is to obtain data relating to stress fields and stress orientations at the casing shoe. This data is then incorporated into studies analyzing fault and fracture opening/reactivation induced from fluid pressure. This study concept obviously plays an important, key role in an assessment of CO₂ or water injection into formations for disposal and sequestration, as described in Chapter 12.

15.2 Conclusions

While it is not the intent to recommend a full ‘exploratory hydrocarbon data acquisition’ program for Bird’s Head region wells, it is necessary to touch on it due to potential ‘overlaps’ of techniques, and equipment/tools with injection and sequestration data acquisition programs. There is a synergistic advantage to combining rationales of both data acquisition perspectives, and for that reason the ‘exploratory data acquisition’ perspective has been pointed out.

The use of LWD/MWD for logging data obtained whilst drilling has not been addressed in this paper. The technique is complex, being highly dependant on the *exact* drilling fluid, the *exact* service company contractor used (Schlumberger, Sperry-Sun, Baker-Hughes, etc.), and the *exact* type of tools used (near-bit vs. behind the bit, negative pulse vs. positive pulse., etc.), and the *exact* purpose for the data acquisition. Therefore, recommendations can be formulated in a general way.

Lastly, a few notes regarding drilling fluids used, such as seawater or water based mud (WBM) versus oil based muds (OBM). Seawater is likely to be used in the Kais Limestone/Faumai Formations (NGLG) hole section due to ‘lost circulation’ and ‘blind drilling’.

The use of extremely high-KCL WBM or OBM drilling fluids, and logging of massive carbonate sequences with resistivities far greater than 200 ohmm, precludes the use of the superior MSFL/ DLL tool combination for resistivity measurements and necessitates the use of the ILD/AIT tool (conductivity) to obtain best resistivity data. The use of the OFA (optical fluid analyzer) instruments during MDT runs is also handicapped by the use of OBM fluids in the borehole. These issues need to be coordinated with the geological/geophysical team involved with the wells, in conjunction with the ‘operations geologists’ and drilling department engineers, well in advance of the actual well drilling operations.

16.0 EVALUATION OF SUBSURFACE CO₂ MONITORING

Numerous techniques for the monitoring of subsurface CO₂ injection and migration have been proposed, tested, or carried out either as pilot projects or as large-scale projects (Sherlock, 2002). Some of these techniques have been verified as feasible and valid for monitoring by pilot projects or as large-scale projects, and some have been determined to be experimentally feasible, while still others have been proposed as ‘possible’ but not fully examined and verified as appropriate for CO₂ injection and migration monitoring.

The main purpose of this report is to provide an overview of the various options, their respective limitations and potential applicability to Tangguh if potential subsurface CO₂ disposal programs are implemented, and recommend those options that BP may wish to explore further as the most technically feasible and cost effective at Tangguh.

The various methods potentially available include surface measurements at wellheads; a suite of seismic methods; a suite of electromagnetic methods; gravity surveys; tracers added to injected CO₂ volumes; drilling of monitoring wells; and ‘smart well completions’ to development wells and/or re-entry work-over wells. The purpose of the monitoring will be to:

- 1) Verify subsurface CO₂ disposal volume remains in the subsurface.
- 2) Verify subsurface CO₂ migrates into the targeted sequestration/storage trap as modelled.
- 3) Verify that the CO₂ sweep and storage efficiencies are optimized, and potentially adjust injection rates and/or pressures to ensure maximum optimization of migration and storage performances.
- 4) Identify, at the earliest possible time, any breach of seal or potential escape of the CO₂ disposal volume into non-designated strata.

Many of these techniques and methodologies have limitations that would prevent their applicability to the Tangguh Project, while others have yet to be demonstrated either in the field or laboratory as practical and feasible in this case.

16.1 Surface Measurements

The simplest and most economical method of monitoring injected CO₂ utilizes

surface measurements. Sensors for CO₂ detection can be placed on wellheads at surface, or at fault expressions at surface, to detect the unwanted presence of previously injected CO₂ back at surface. These sensors are quite effective at detecting leakage at surface but fail to provide an early warning of subsurface CO₂ breaching the containment seal.

Other CO₂ monitoring methods including seismic, electromagnetic, and gravity measurements may include a surface component, or be located entirely downhole in an existing wellbore. These other methodologies will be examined in greater detail separately.

16.2 Smart Well Completions

New technology is now making commonplace the practice of ‘smart completions’, where optic fibers connect down-hole sensors into the completion program. This system is an all optic-fiber monitoring system, developed by Weatherford International, that allows multiple downhole sensors, including temperature, pressure, multi-phase fluid flow, acoustic sources, and seismic accelerometer receivers to be permanently and simultaneously operable in the wellbore at the desired strata. For CO₂ injection and sequestration monitoring purposes, the placement of downhole sensor arrays on a single optic-fiber strand for temperature, pressure, multi-phase fluid flow, and CO₂ detection could potentially give early, and relatively economic, monitoring of supercritical CO₂ plume migration rates and directions.

Fiber-optic seismic sensor monitoring systems can also be incorporated into the downhole well completion, as described by Wallace (2003). Many of these various sensors and methods located downhole in wellbores are either monitored at surface, or are run in conjunction with surface surveys such as 3D seismic, and are discussed in further detail below.

Furthermore, on a potential CO₂ injector well, a vertical pilot hole drilled prior to sidetracking for the horizontal injector leg could be ‘smart well completed’ and the borehole used as a monitoring well during the initial production updip. The monitoring well could verify through temperature, pressure and fluid movement sensors the updip production from the production well prior to injecting CO₂, to verify intra-reservoir communication between the potential injector well and the known and proven containment area where the hydrocarbon accumulation is located.

Verification of communication between the monitoring well and the hydrocarbon containment area would increase the degree of confidence for ESSCI CO₂ migration into the proposed long-term sequestration/storage area.

16.3 Seismic

The most highly recommended monitoring systems for CO₂ injection, migration, and sequestration/storage verification are varieties of seismic monitoring (Sherlock, 2002). There are various seismic methods either utilized or proposed for CO₂ monitoring, but the most promising one is time-lapse 3D seismic surveys (also known as '4D seismic'). However, the successful application of any seismic survey at surface (2D, 3D, or 4D) requires that the local subsurface geology is conducive to that particular geophysical methodology. The presence of a thick succession of carbonates near the surface, such as the Kais/Faumai carbonates present at Tangguh, clearly preclude the use of standard surface geophysical techniques.

The other variants of seismic monitoring include 'in-well VSP surveying', 'cross-well seismic tomography', 'single-well sonic' logging, and 'microseismic' surveys. These various seismic methods are summarized below.

16.4 Time-Lapse 3D ('4D') Seismic Surveys

The most favored monitoring technique in large-scale commercial CO₂ sequestration/storage projects is 3D seismic surveys at surface, where 3D surveys are repeatedly done at varying time intervals since commencement of the CO₂ injection (Lewis and Shinn, 2001). This process results in a time-lapse 3D (or 4D) seismic survey set, with individual 3D seismic survey images compared and contrasted against each other to visualize the CO₂ plume migration rate and direction over time. It is also possible to estimate the subsurface CO₂ volume to compare and verify it against the injected volumes from the surface, however this technique has large margin of error without additional monitoring method results, such as cross-well seismic and VSP (Sherlock, 2002).

The 4D seismic methodology is currently employed at in Statoil's North Sea Sleipner West Field, where almost 1 million tonnes per year (tpy) of CO₂ have been injected and sequestered into a saline aquifer at 800m TVD SS. Norway's Statoil also has plans to inject and sequester CO₂ in another shallow saline aquifer at their North

Sea Snøhvit Field in the near future. This project also plans to use 4D seismic surveys for monitoring (Moritis, 2003).

This method of monitoring has serious limitations in that it appears to work reasonably well at relatively shallow depths, and where there is good seismic resolution (Sherlock, 2002). In areas such as Tangguh, where proposed bottom-hole injection sites are located at –14,000 ft TVDss and are overlain by a vuggy, fractured several thousand foot thick carbonate sequence, the potential for 4D is not promising. The 3D seismic survey data currently available over the Vorwata area lacks sufficient resolution to directly interpret the Jurassic's Roabiba Reservoir, therefore, the potential for 4D surveys to identify CO₂ breaching the seal is unlikely.

16.5 Downhole Seismic

Downhole seismic methods are seismic geophysical monitoring techniques that utilize either seismic sources, or seismic receivers, in the subsurface (located down wellbores) for monitoring CO₂. There are several different methods, one of which overlaps with surface measurements at wellheads discussed above in section 16.1 in conjunction with 'smart well completions'. That method utilizes downhole optic fibers relaying data from borehole located sensors to the surface. Other downhole seismic geophysical monitoring techniques include VSP's run on wireline, sonic logging run on wireline, cross-well seismic tomography, and microseismic surveys. These will be addressed separately below.

16.5.1 VSP

VSP stands for Vertical Seismic Profiling, and is a common wireline logging service, provided by all the major wireline service companies. On its own, it is incapable of tracking or verifying subsurface injected CO₂ plume migrations and volumes. However, in cases where surface seismic surveys (3D or 4D) lack the resolution to image CO₂ plume migrations and volumes, the use of 'walk-away' VSP wireline runs integrated with a simultaneous 3D seismic survey at surface can allow detection and assessment of injected subsurface CO₂ saturations in thin porous sequestration strata. The method requires low frequency analyses of the VSP data, integrated with the 3D seismic data set. This technique has been successfully demonstrated in the New Mexico's Vacuum Field, where 'huff and puff' or 'slug' injection of CO₂ began in 1999 for enhanced oil recovery (Bard and Pratner, 1999).

16.5.2 Cross-well Seismic Tomography

Cross-well seismic tomography is a seismic method that combines a downhole acoustic source in one well, with multiple wells each having downhole receivers. This methodology produces a notable increase in seismic resolution over other seismic methods such as surface surveys (i.e., ‘standard’ 3D or 4D seismic surveys), or even downhole acoustic acquisition combined with surface acoustic sources i.e. VSP’s).

This technique is theoretically capable of producing good resolution over large-scale reservoirs with CO₂ volumes being injected and sequestered, assuming that the well locations and spacing have been designed for optimum imaging. The data is usually acquired over a series of time periods providing a time-lapse data set to monitor the CO₂ plume’s migratory direction and speed. Velocity tomography measures travel times from the acoustic source, to calculate velocities within the reservoir between wells containing the source and the receiver(s). Analyses of each of the source and receiver paired wells produces a suite of ray paths, which can then be manipulated to produce a velocity image of the reservoir between the various wells called a tomogram (Washbourne and Bube, 1998).

This technique has been successfully demonstrated for CO₂ monitoring in the West Texas McElroy Field, where CO₂ injection for EOR began in 1994 (Sherlock, 2002). This technique, however, has error bars where the downhole source and receiver wells are horizontal wells. This technique was used in Canada’s Weyburn Field with mixed results, because CO₂ injection into the carbonate reservoir with relatively low velocities ‘sandwiched’ between formations with higher velocity produced different wave modes that arrived at the horizontal well receiver at approximately the same time (Sherlock, 2002).

16.5.3 Single-well Sonic Logging

Single-well sonic logging is a potential subsurface CO₂ monitoring technique that utilizes a wireline logging ‘array-sonic’ tool downhole. Near-wellbore CO₂ volumes can be imaged from the wireline tool dataset, however it is very limited in its application to large field CO₂ injection and sequestration monitoring due to its close-to-well-proximity imaging. It has been tested on a single well by Lawrence Berkeley National Laboratories in the Lost Hills Field, but the dataset also benefited from having dual cross-well surveys performed. This technique basically has some very

specialized applications where it is appropriate for monitoring, such as in fractured reservoirs, and potentially holds greater promise subject to more research and perhaps a new generation of tools. At present, however, it appears to be unfeasible for large-scale reservoir CO₂ monitoring (Sherlock, 2002)

16.5.4 Microseismic Imaging

Microseismic image analysis involves specialized processing and mapping of seismic survey volumes with downhole geophone receivers, an example of which was performed by Robert and Shapiro (2001) using a technique named Seismicity Based Reservoir Characterization (or SBRC). The methodology has been developed by oil/gas service companies such as Schlumberger, to image hydraulic fracturing at wells during well stimulations. This technique has recently been applied to injected water and gas wells, and utilizing either a permanent or temporary array of downhole geophones. The basic principle is that injection of even minor amounts of fluid can cause microseismicity and induce microfracturing, even in the top seal cap rock.

Fault stress and reactivation studies, such as provided for this study by Hillis and Meyer (2003), rely on in-situ stress vector evaluation with a Mohr-Coloumb failure radius used to estimate the risk of fault reactivation to major mappable faults. While this methodology results in generally valid predictions for each individual fault risk of reactivation, it is limited by the available data, which is primarily interpreted fault plane surfaces derived from traditional 3D seismic survey. The inducement of microseismicity and its resultant microfracturing is beyond the resolution of traditional 3D seismic imaging, even with the best of data, and does not provide the high degree of certainty that direct, continuous downhole monitoring can provide (Sminchak, et al, 2001).

Maxwell and Urbancic, in 2001, conducted downhole monitoring of the waterflooding EOR at Norway's Ekofisk Field for 18 days and were apparently able to detect gas migration images that allowed identification of microfault patterns that were below the resolution of the marine 3D seismic survey at surface. Microfaulting and microfracturing were detected up to 2 km away from the well (Maxwell, et al., 2003).

This, and other studies, discussed by Sherlock (2002) support the contention that microseismic imaging and mapping could be of great *potential* value during the injection phase of a CO₂ subsurface disposal project. However, the method requires a

monitoring well at this stage, and there is evidence that the downhole geophones, if placed in the injection wellbore, may have poor data quality from noise associated with fluid flow in the well. This methodology would therefore require sensors in direct contact with the subsurface formation so that true ground motion only is recorded, and this provides considerable well-completion challenges.

16.6 Electromagnetic Methods

Electrical-magnetic measurements are standard downhole measurements in the petroleum industry. Resistivity, conductivity wireline logging tools are today being supplemented by 'magnetic resonance imaging tools (Schlumberger's CMR, and Numar/Atlas MRIL), micro-resistivity formation imaging tools (i.e. Schlumberger's FMS/FMI), and other instrumentation. These are fundamentally different from seismic and acoustic techniques, as described above. Their recent application to detection and imaging of subsurface CO₂ disposal opens new avenues of CO₂ monitoring. Because there is a greater contrast in electrical properties (such as resistivity) with brine and supercritical CO₂, than there is between oil and supercritical CO₂, the use of electromagnetic measurements for monitoring injected supercritical CO₂ holds greater potential in saline aquifer sequestration projects than in EOR projects. In addition, CO₂ injection into oil reservoirs results in a greater miscibility of the CO₂ in oil making them harder to distinguish, whereas supercritical CO₂ results in only a thin film of miscible CO₂ with brine forming on the leading edge of the supercritical plume as it migrates (Ennis-King, et al 2002).

16.7 Surface Electromagnetic Measurements

Surface electromagnetic surveying is in the infancy stage at this time, but holds promise. Application of electromagnetic methodology, such as long-offset transient electromagnetic method (LOTEM), has been suggested by Strack and Vozoff (1996) for use in CO₂ monitoring. A time-lapse variant of this methodology was field tested in St. Illiers, France, by Hördt, et al (2000). They looked for changes in the shape and direction of natural gas injected into a brine, but found that the signal to noise ratio was too high to yield successful results. However, they stated that the results were promising, and that the methodology could be successful if the signal to noise ratio was improved by one order of magnitude and permanent transmitters and receivers were used to monitor CO₂ continuously.

16.8 Cross-well Electromagnetic Methods

Cross-well electromagnetic methods require transmitter and receiver tools to be placed downhole in wellbores, with an experimental set of instruments recently constructed by Lawrence Berkeley National Laboratories, and due to be field tested at the Lost Hills test location in California (Wilt, et al, 2001). The receiver tool is fixed with the transmitter tool being moved slowly up the wellbore. The receiver tool is then relocated and remains stationary again while the transmitter is then moved slowly up the wellbore over the exact same interval at the same speed. This is repeated several times to acquire a 3D electromagnetic data set. The cross-well electromagnetic 3D survey is then re-run several times to acquire a time-lapse data set on the rate of CO₂ migration and its' direction. The electromagnetic time-lapse data results are processed by 2D inversion programs with the images best utilized if run and interpreted in conjunction with simultaneous cross-well seismic discussed previously (Sherlock, 2002).

This technique is quite complex and requires numerical simulations of forward and inverse modelling to assess the viability of the technique and to calibrate the sensitivities to fluid saturation changes caused by the migrating CO₂ plume within the reservoir. The applicability to steel-cased holes is also problematic, with testing being carried out on an experimental basis in fiberglass-cased wells only. Tests with one steel-cased hole and one fiberglass-cased hole have been promising, and it may eventually prove possible to have the instrumentation located exclusively in steel-cased wells, in the manner of standard oil/gas well completions (Wilt, et al, 2001).

16.9 Downhole to Surface Electromagnetic Methods

Downhole to surface electromagnetic surveys involve having a powerful electromagnetic transmitter moved to various locations, while a single receiver located downhole in one well is moved slowly up over the same interval for each surface transmitter location in the survey. The technique is occasionally used in mineral exploration (Dyck, 1991), but its application to monitoring CO₂ injection and migration is only theoretical at this time.

16.10 ERT (Electrical Resistance Tomography)

ERT is an experimental methodology using multiple electrodes vertically arrayed in multiple wellbores. Testing has been limited to several shallow

experimental holes cased with fiberglass and/or plastic but its feasibility for monitoring CO₂ injection and migration is only theoretical at this time. However, the steel casing commonly used in well completions could theoretically be used as giant, long electrodes, which would allow both vertical and horizontal well casings to be used to acquire virtually 3D images of a supercritical plume's electrical contrast with the reservoir's brine (Sherlock, 2002).

Numerical simulations and ERT modelling indicate this may well be a promising avenue to explore for monitoring CO₂ injection and migration (Newmark, et al, 2001), but at this point in time ERT methodology is still highly experimental.

16.11 Gravity

Gravity and gradiometer techniques are being explored for monitoring CO₂ injection and migration, with the basic principles being that fluid displacement of brine by migrating supercritical CO₂ plumes result in a change in overall subsurface density, which could be theoretically monitored as changes in the subsurface gravitational field of gravity gradient. This methodology is highly theoretical at this point in time, and its applicability to monitoring of injected CO₂ injection at any great depth is hypothetical.

16.12 Tracers

Tracers are compounds, either natural or fabricated, that are added to the injected CO₂ volume at surface, in order to track the progress of the CO₂ plume's migration via sensors placed in pre-existing subsurface wellbores away from the injection wells. Isotope tracers have been successfully used both in Texas and in Canada. Halogen compounds, particularly halocarbon-11, halocarbon-12, and hexafluoride were successfully used to monitor produced CO₂ sourcing in Texas during the 1980's. The project was a waterflood project with an unidentified source of CO₂ causing corrosion problems. The use of the tracers led to the successful identification of the source of the CO₂ breakout from the nine injection wells. Sweep efficiency was evaluated as well, and as a result sweep efficiency for the field optimized when the injection rates were modified (Craig III, 1985).

Isotope tracers have also been used in western Canada's Weyburn Field where CO₂ injection has been used for EOR since 2000. Tracer sensors located in monitoring wells detected migration plume tracer signatures, with CO₂ injection

enhancing oil production as modelled (Ian Hutchinson, personal communication, 2002).

Injected CO₂ can itself be a tracer if sensors are located either in monitoring wells or in production wells. This methodology is one of the most conclusive monitoring techniques, be it using isotopic tracers or the CO₂ injection volume itself.

16.13 Limitations and Advantages

Many of the techniques and methodologies for monitoring the migratory direction, depth, and rate of movement of injected subsurface CO₂ plumes, for the purpose of sequestration/storage, discussed above have limitations, and advantages, which were briefly mentioned. The limitations, and advantages, of these various methodologies are summarized in Table 16.1.

16.14 Subsurface CO₂ Monitoring Conclusions and Recommendations

In summary, some of the methods are clearly either not feasible or not applicable to Tangguh (Table 16.1). In order of decreasing applicability, the following methods may be appropriate for CO₂ monitoring in the Tangguh Project.

1. Sensors at surface, both at wellheads and at geological features such as fault lineaments, are recommended to detect any potential escape of CO₂ at surface. The use of tracers is the least costly and most direct method of monitoring injected CO₂ plume migration. CO₂ sensors, or isotope tracer sensors, located at surface on production wells could detect the arrival of the supercritical CO₂ at the production area. CO₂ sensors, or isotope tracer sensors, located at surface on fault lineaments could detect the arrival of the supercritical CO₂ at surface. However, these sensor locations would only detect the worst-case scenario of ‘unplanned migration’ either to surface or to the natural gas production area, and would not produce an early warning of the migratory supercritical CO₂ plume direction and rate of movement. Nor would any vertical breach of seal or vertical migration along faults/fractures be detected early. Therefore, this method is recommended for use in conjunction with other subsurface monitoring techniques.

2. The smart well completion option holds great potential and has already been applied commercially in various parts of the world. As discussed in detail above, not

only could pressure, temperature, and tracers sensors be placed on full optic fiber arrays during completion of production wells, but permanent VSP and seismic sensors can be located in the development wells in conjunction with similar ‘smart well completions’ done in vertical pilot holes of the injection wells. Cement plugs isolating the horizontal injector legs from the vertical pilot holes would place the supercritical injection plume between the injector and production well arrays. This would provide great resolution within the Roabiba Reservoir and the Pre-Ayot top seal. With this method, not only would continuous imaging and monitoring of the supercritical plume be achieved, which would allow maximization of sweep and storage efficiency by modifying injection rates and pressures, but any breach of seal or fault/fracture migration would be detected early on and perhaps mitigated. A smart completion for the vertical pilot-hole phase of the proposed injection wells for the Tangguh area could be used for monitoring initial production updip at the Vorwata natural gas accumulation, and hence verify intra-reservoir communication before committing to drilling the horizontal injector leg of the hole.

3. The use of any 3D seismic survey alone at Tangguh is precluded, due to poor resolution of imaging at the Mesozoic level, unless perhaps it is combined with either VSP or cross-well seismic tomography. This could be accomplished by combining a 3D seismic survey shoot with the continuous VSP or seismic monitoring from the smart well completions discussed above. If CO₂ injection had already commenced, and additional development wells were being drilled on the Vorwata structure, then the running of a downhole VSP survey tool at a single newly-drilled development well, combined with the 3D seismic survey shoot, might yield excellent results. Likewise, cross-well seismic tomography could be run in combination with a surface 3D seismic survey, with the cross-well seismic tomography run between vertical pilot hole completions for the horizontal injector wells and any newly-drilled in-field development wells. The VSP survey or cross-well seismic tomography would be performed prior to the completion of the well for production, but simultaneously with the surface 3D seismic survey.

4. The use of single-well sonic logging or microseismic techniques are fairly experimental, but may be worth testing at Tangguh if CO₂ injection had already

commenced, and was being monitored by other means at reservoir-scale, and there was a particular concern about microfracturing in a small area close to a given well.

5. Other methods and techniques, such as electromagnetic methods, ERT, and gravity are not practical at Tangguh at this time due to their theoretical or experimental state of development, but may warrant further appraisal at a later stage of development.

The highest risk in regard to the seal for the Vorwata structure Roabiba Reservoir appears to be from the well boreholes previously drilled on the structure by ARCO and BG (author, in memo to BP, 2002). As noted previously, the cement commonly used in well-completions is highly reactive with CO₂ in either a purely gaseous or supercritical state. The reactive nature of the cement in Vorwata structure wellbores may pose the greatest risk for breach of seal should the structure be used for CO₂ injection and storage. Reactive cements dissolve with exposure to high concentrations of CO₂, potentially providing a ‘superhighway’ for the CO₂ plume migration to the surface. The rheology of the cements used in completion and abandoning of the Vorwata area wells is not known to the authors and needs to be verified by BP, however, it is highly probable that ‘CO₂ reactive cement’ was used in the casing completions, and abandonment plug operations, for all of the Vorwata wells.

It is recommended that the issue of cement reactivity with CO₂ be investigated and the possibility of having a work-over drilling rig perform borehole re-entry on selected wells for the purpose of remedial ‘non-reactive cement’ squeeze jobs and abandonment plugs explored, (i.e. behind casing and on top of cement retainers and EZSV plugs set within the casing strings), so as to minimize risk of seal breach by CO₂ via existing wellbores. The SE or ‘main’ Vorwata Jurassic reservoir compartment is likely to be the primary compartment for development of the field and is also the compartment being recommended by this study for long-term geologic CO₂ sequestration. Therefore, the seven wellbores potentially posing a high risk for CO₂ leakage at the Vorwata structure include the V-2, V-4, V-5, V-6, V-9, V-10, and the V-11. In addition, the V-8 may possibly be in communication with that particular fault block, and also may need to be considered for potential remedial cementation programs.

As part of both the remedial well ‘work-over’ plans, and the development and/or injection well plans, some of the potential CO₂ monitoring technologies could be included into the well completions. The synergistic economics of combining monitoring techniques for potential CO₂ plume injection and migration verification with planned development wells, and any ‘work-over’ re-entries into pre-existing well bores should result in a major cost savings, as opposed to drilling stand alone ‘monitoring-wells’.

This study recognizes the possibility of unexplored structures, such as the ‘S’ (ie. Saritu) structure, as both a potential hydrocarbon reservoir and a potential CO₂ injection and sequestration/storage site. Although the Saritu structure was ranked as a very high risk due to lack of data, the drilling of any future exploration well on the structure for hydrocarbon exploration could potentially acquire data that would enable a reassessment of that risk. Clearly, a significant commercial hydrocarbon accumulation in the Roabiba Reservoir directly under the proposed LNG plant location at Saritu would probably lead to early development of the newly identified reserves, with further data acquired during the development phase. This would open up very cost effective CO₂ injection and sequestration/storage options at the Saritu structure. The same CO₂ injection and sequestration/storage method proposed by this study for the Vorwata Roabiba Reservoir (i.e. injection into the down-dip, water leg of the reservoir) might be possible at Saritu structure, if the estimated supercritical CO₂ storage capacity is adequate for the estimated 2.4 TCFsc CO₂ disposal volume.

Future wells drilled, including for example the “S” structure (ie. Saritu) exploration wells, and any potential development wells, should incorporate non-CO₂ reactive cement programs into the testing, completion, and abandonment programs. In conjunction with ‘CO₂ completions’ (i.e. non-CO₂ reactive cement) on future exploration or development wells or remedial reentry work-overs, is the possibility of ‘smart completions’. Combining smart completions with the non-CO₂ reactive cement completions would result in maximizing the options for future development at Tangguh while minimizing future potential CO₂ sequestration/storage costs.

Methodology	Limitations	Advantages
Surface Measurements at Wellheads	Relies on sensors located downhole in wells. Faulty sensors and instrumentation may be costly and difficult to repair/replace.	Monitoring wells with downhole sensors can directly measure CO2 or its attribute/signature for location, depth, and rate of movement. Rather than extrapolating or calculating CO2 estimated location, depth, and rate of movement. Possible to directly detect seal breaches by CO2.
Smart Well Completions	Relies on sensors located downhole in wells. Faulty sensors and instrumentation may be costly and difficult to repair/replace.	Drilling of stand alone monitoring wells is not absolutely necessary, if pre-planning incorporates smart well completions into exploration, development, injector, remedial well designs. This should result in lower monitoring costs/economics.
Surface 4D Seismic Surveys	Due to the New Guinea Limestone Group (Kais and Faumai Formations) thickness and proximity to near-surface (Oligocene to Miocene), seismic imaging at depth of interest (Mesozoic) lacks sufficient resolution for CO2 monitoring in the Tangguh area. 3D seismic surveys run at Tangguh area are expensive due to remote location, and need for land, transition, and marine surveys to be run and merged for complete coverage of structures.	If resolution is good, imaging (especially 4D time-lapse evaluations) is very accurate for the CO2 plume's migratory location, depth, and rate of movement. Excellent resolution can even permit detection of seal breaches by CO2.
VSP (combine with 3D/4D seismic)	Relies on wireline logging tools run downhole in pre-existing wellbores. For CO2 monitoring it must be used in conjunction with 3D or 4D seismic surveys at surface. 3D seismic surveys run at Tangguh area are expensive due to remote location.	Possibility that the resolution of 3D or 4D seismic quality at Tangguh might be enhanced, and provide good resolution data. Injection at proposed location sites #1 and #2 (IS-1 and IS-2) in this study would make feasible the running of only marine 3D seismic survey (or 4D) over polygon area bounded by the IS-1, IS-2, and Vorwata-10, Vorwata-11 wells. This potentially can resolve the limitation of surface 3D/4D seismic discussed above.
Crosswell Seismic Tomography	Relies on wireline logging tools run downhole in pre-existing wellbores. Limited applicability in horizontal wells or thinly bedded formations with low velocities between 2 high velocity formations. For CO2 monitoring it must be used in conjunction with 3D or 4D seismic surveys at surface. 3D seismic surveys run at Tangguh area are expensive due to remote location.	Even better resolution than using VSP downhole combined with with 3D or 4D seismic surveys at surface. Thin bedding limitation not present for Mesozoic reservoirs at Vorwata.
Single-well Sonic Logging	Relies on wireline logging tools run downhole in pre-existing wellbores. Limited extent of survey from borehole, not practical for large-scale reservoir monitoring of CO2.	Applicability limited to near-well increased resolution for fractures.
Microseismic	Experimental methodology, requiring a monitoring well with downhole geo-phone receivers, limited applicability to resolving microfractures in potential seal lithologies.	Superior to Mohr-Coloumb circle fault reactivation studies as it directly measures fractures and faulting, even on a micro-scale. Can detect microfracturing of the seal (and hence potential breaches) when they occur due to CO2 injection pressures, or CO2 total column height pressures exceeding seal capacity.
Surface Electromagnetics	Experimental methodology, with significant noise-to-signal ratio problems to be resolved first.	
Crosswell Electromagnetics	Experimental methodology, with complex measurements in a monitoring well, with complex post data-acquisition processing. Currently limited to non-steel cased holes (i.e. fiberglass and plastic). For CO2 monitoring it must be used in conjunction with 3D or 4D seismic surveys at surface. 3D seismic surveys run at Tangguh area are expensive due to remote location.	
Downhole to Surface Electromagnetics	Limited to relatively shallow, mineral exploration. Applicability to CO2 monitoring is theoretical only at this time.	
ERT (Electrical Resistance Tomography)	Experimental methodology, with complex measurements in a monitoring well, with complex post data-acquisition processing. Currently limited to non-steel cased holes (i.e. fiberglass and plastic).	If theoretical applications using steel-casing used as long electrodes are tested and viable, then this methodology could be very promising using all injector and development wells completed for ERT monitoring to be passive, but potentially high resolution monitoring sensors at surface.
Gravity	Theoretical, and hypothetical.	
Tracers	Requires monitoring wells. Although development wells could be utilized as monitoring stations, these may be of limited value for tracking CO2 plumes prior to reaching development wells at Tangguh.	A direct monitoring technique with a proven potential for CO2 monitoring. Relatively low cost compared to other methodologies.

Table 16.1: Limitations and Advantages of Various CO2 Monitoring Techniques and Methodology.

PART VI
CONCLUSIONS, POSTSCRIPT, AND REFERENCES

17.0 CONCLUSIONS

This body of work contains numerous modules in order to conclude the aim of the study. Specifically, the study evaluates concepts to develop an applied practical plan for environmentally-sustainable disposal of CO₂ from the Tangguh LNG Project in Papua, Indonesia. A technically feasible and environmentally suitable plan for this disposal is urgently needed to mitigate anthropogenic emissions from the Tangguh LNG Project contributing to the acceleration of global warming and resultant climatic change.

- **CO₂ Sequestration Options**

The Tangguh LNG Project is expected to produce 24 TCFsc of natural gas, composed of 10% CO₂. This directly translates to 2.4 TCFsc of CO₂, in addition to the additional CO₂ expected to be generated from the LNG power plant and refrigeration emissions.

This CO₂ sequestration research project screened the various non-geologic CO₂ disposal options for the Tangguh LNG Project's greenhouse gas emissions and production by-products. The screening of various types of CO₂ disposal available for the Bird's Head area of Papua, Indonesia included geological subsurface storage, deep-ocean disposal, 'forest and agricultural sinks', and direct commercial usage.

Deep-ocean sequestration was found to be unproven with abundant environmental risks associated with it. 'Forest and agricultural sinks' are an assortment of various proposals to use the natural carbon cycle to 'absorb' CO₂ atmospheric venting, or at least, off-set vented CO₂ by means of 'carbon credits'. 'Biosphere sinks' were regarded as unrealistic given the potentially very large volume of CO₂ to be disposed of at Tangguh (at least 2.4 TCFsc). The 'direct use' of CO₂ in commercial or industrial production was also considered, but the potential for any large-scale commerce or manufacturing in remote and technologically-impooverished Papua, Indonesia was found to be unfeasible.

The evaluation concluded that the geological subsurface sequestration/storage option was the only technically feasible, economically viable, and realistic CO₂ disposal option available for the disposal of CO₂ at the Tangguh LNG Project. A range of subsurface geological options were considered, evaluated, and ranked. The geological subsurface sequestration/storage options included:

1. Saline aquifer sequestration
2. Enhanced oil recovery
3. Enhanced gas recovery
4. Depleted gas/oil fields sequestration
5. Deep unmineable coal-bed sequestration
6. Enhanced coal-bed methane recovery
7. Subsurface cavity or void sequestration

In order of increasing importance, the detailed geological evaluation concluded that the potential sequestration of CO₂ in Tangguh area subsurface **cavities or voids** was limited to the Kais Limestone Formation, Faumai Carbonate Formation, and the Oligocene carbonates collectively comprising the New Guinea Limestone Group (NGLG). This option was found to be high risk due to a significant lack of data, poor seal, and crestal top structure subsurface depth above the shallowest depth required to keep injected CO₂ in a supercritical state.

The two options involving injection into **coal seams**, (the deep unmineable coal-bed sequestration and the enhanced coal-bed methane recovery options) were not feasible due to the lack of significant coal seams in the Tangguh area subsurface. The minor coals encountered in the lower Jurassic and Permian intervals are extremely thin-bedded, deeply buried, and of limited continuity. They would not have sufficient capacity to adsorb any significant volumes of CO₂.

Sequestration of CO₂ in **depleted gas and oil fields** was eliminated as a viable option after detailed evaluation and consideration of the depleted or near-depleted Salawati Basin, Wiriagar Shallow, Wasian, and Mogoi oil fields, located in the Bird's Head. The enhanced gas and oil recovery options of the near-depleted fields of Salawati Basin, Wiriagar Shallow, Wasian, and Mogoi fields were also evaluated in conjunction with the depleted field option. There was minimal potential for 'added-value' from enhanced oil recovery in these fields since the strong water-drive in the fields has resulted in very good recovery efficiencies already. As a result there is no enhanced oil/gas recovery option present in the Tangguh region. All of the aforementioned fields have primary reservoirs in the NGLG carbonates, and this reservoir was found to be high-risk. The evaluation also included a preliminary economic/distance weighting of the Salawati Basin fields, which concluded that the great distance between the proposed Tangguh LNG Plant location and the Salawati Fields (almost 300 km) made Salawati commercially non-viable. Finally, the

remaining fields (Wiriagar Shallow, Wasian, Mogoi) have insufficient storage capacity for the estimated CO₂ volume needed to be disposed of at Tangguh.

The **saline aquifer** sequestration option is identified as the only technically feasible and economically viable option of the various geological subsurface CO₂ disposal methods evaluated for the Tangguh region. The detailed geological subsurface disposal options evaluated included saline aquifer sequestration, deep unmineable coal-bed injection, enhanced coal-bed methane recovery, depleted gas/oil field sequestration, enhanced oil recovery, enhanced gas recovery, and subsurface cavity/void storage.

With the identification of the **saline aquifer** sequestration option as the only viable CO₂ disposal option, a detailed summary of the Tangguh area exploration and production history was documented, as were the types, and sources, of subsurface data available for Bintuni Basin, Papua – Indonesia, where the Tangguh LNG Project is located. Most data is sourced from oil and gas exploration and development drilling in the basin. Well data is clustered around the hydrocarbon fields found to date including Wiriagar Deep, Vorwata, Roabiba, Ofaweri, Vos, and Ubadari. Rarely is well data available away from known hydrocarbon accumulations (such as the East Onin #1).

- **Injectivity**

The study involved a review of existing detailed sedimentology and stratigraphy data, and resulted in the construction of a sequence stratigraphic framework that is subsequently used for the GeoCARD 3D geological model.

The lithostratigraphy of Bintuni Basin was examined and evaluated in order to identify prospective saline reservoir injection strata and probable seal intervals. A review of the sedimentological data and integration into the revised stratigraphic framework resulted in a coherent and comprehensive model of the sequence stratigraphy of the Jurassic interval illustrated by paleo-geographic facies maps over the Tangguh area. The maps represent a series of approximate time slices showing shifting facies belts through the Jurassic including fluvial-deltaic, to shoreline, barrier-lagoon, and offshore environments. The maps predict a continuous high quality seal coverage over the Vorwata anticline and also predict a thick Jurassic ‘Roabiba’ sandstone interval reservoir with favorable porosity and permeability characteristics at the two proposed potential CO₂ injection site locations.

A comprehensive evaluation of the various potential reservoirs was undertaken. The reservoir characterizations integrated both existing well data with new, empirical data of the author's from core plug and core chip analyses. The reservoirs in the Bintuni Basin area examined and evaluated included:

1. Late Permian Fluvio-Deltaic Channel Sandstones
2. Aalenian (Marine) Sandstone Formation
3. Callovian and Bathonian/Bajocian Roabiba Sandstone Formation
4. Ayot Limestone Formation
5. Late Cretaceous Marl Succession
6. Late Paleocene Succession
7. NGLG (Faumai Limestone Formation and Kais Limestone Formation)

The evaluation concluded that the Middle Jurassic reservoirs, which include the Aalenian Sandstone Formation and the Callovian and Bathonian/Bajocian Roabiba Sandstone Formations possess the optimum injectivity characteristics of all the strata in Bintuni Basin, especially regarding porosity and permeability ranges.

Effective porosity ranges from 9% to almost 20% for the Aalenian Sandstone Formation and the Callovian and Bathonian/Bajocian Roabiba Sandstone Formations in Bintuni Basin, with an average effective porosity of 10% or better for the Middle Jurassic reservoirs at the Wiriagar Deep and Vorwata fields. Effective permeability ranges from less than 0.1 mD to almost 2000 mD, with average effective permeability of 100 mD or better found in the major fields (ie. Vorwata and Wiriagar Deep). Porosity and permeability characteristics favorable to CO₂ injection and sequestration are also found at great depths (13,600 ft at Vorwata), and in the saline water-leg of reservoirs down-dip from known GWC (in the V-10 well).

- **Containment**

The study selected and ranked potential CO₂ injection sites locations by evaluating quantitative and qualitative data factoring matrices. This technique is widely used in probabilistic hydrocarbon exploration evaluations by Rose (2000), Nakanishi and Lang (2001), and others, and has been applied by the author to probabilistic quantitative and qualitative data factoring for potential subsurface greenhouse gas injection and disposal.

A series of quantitative and qualitative data factoring matrices was created to evaluate and rank the various potential injection site locations in the Tangguh area.

The quantitative and qualitative data factoring stratum matrix for all the various potential sequestration/storage strata was constructed. The matrix clearly resulted in a high degree of confidence for CO₂ injection into the Middle Jurassic reservoirs (the Aalenian Sandstone Reservoir and the Roabiba Sandstone Reservoir). Other potential CO₂ storage strata were eliminated due to the high risk associated with their respective low degree of confidence.

The evaluation of trapping mechanisms for potential CO₂ injection and sequestration concluded that stratigraphic and hydrodynamic trapping mechanisms are not viable in the Tangguh area. Conversely, structural trapping had a high degree of confidence, particularly in proven traps such as the Vorwata, Wiriagar Deep, Roabiba, Ofaweri, Wos and Ubadari structures. The quantitative and qualitative data factoring structure matrix was therefore created for the Middle Jurassic interval at Tangguh. Vorwata, followed by the Wiriagar Deep structural closure, ranked the highest, with the greatest degree of confidence for long-term injected CO₂ containment. The structures were then subjectively evaluated for injectivity permeability, CO₂ containment capacity, and seal potential. A rating for the Middle Jurassic reservoirs at each structure was then created that was the product of the structure matrix factor, the reservoir matrix factor, the injection permeability, the CO₂ capacity, and the seal potential. The ratings, expressed as fractions indicating the degree of confidence, are ranked in decreasing order as follows:

Middle Jurassic Reservoir at Vorwata:	0.88
Middle Jurassic Reservoir at Wiriagar Deep:	0.53
Middle Jurassic Reservoir at Ubadari:	0.52
Middle Jurassic Reservoir at Roabiba:	0.23
Middle Jurassic Reservoir at Ofaweri:	0.21
Middle Jurassic Reservoir at Wos:	0.05

The Middle Jurassic Reservoir at Vorwata ranked the best with an 88% degree of confidence in the quality and quantity of data showing successful geological ESSCI suitability.

The relative distances from the proposed LNG plant location (the CO₂ emissions point source) to the various structural locations were also weighted probabilistically in a distance and economic product rating, the results of which are as follows:

Middle Jurassic Reservoir at Vorwata:	0.88
Middle Jurassic Reservoir at Wiriagar Deep:	0.24
Middle Jurassic Reservoir at Ubadari:	0.09

Therefore, the best geographic locations for Tangguh CO₂ injection with the best/most data providing a high degree of geologic confidence for ESSCI suitability was found to be the Middle Jurassic Bajocian/Bathonian Roabiba Reservoir at Vorwata.

The study found potential CO₂ injection and sequestration/storage sites in the immediate vicinity of the proposed LNG plant location (Saritu structure) as unsuitable due to the lack of subsurface data at the structure. The study predicts high quality Roabiba Sandstone Reservoir (Bajocian/Bathonian and Callovian) may have been deposited at the Saritu (“S” structure) location, as well as the ‘Pre-Ayot Shale’ sealing lithology. Whilst data is not currently available to confirm this, new subsurface data from future drilling on Saritu structure could be readily integrated into the study and, the geological model updated to include this data.

The research addressed the evaluation of top and regional seal capacity, geometry, integrity, and potential for the Roabiba Reservoir at the Vorwata anticlinal structure. A Core Plug/Chip Atlas presented the new integrated empirical data set for almost 100 whole core plug or chip samples, which had some combination of MICP, SEM, petrography, bulk XRD, Helium porosity, and air permeabilities performed. Of particular significance were the results from whole core plugs or chips taken in the probable sealing unit rocks. Virtually no work had been done previously on seals in the Tangguh area dataset.

The results of the seals integrated data set were evaluated for seal capacity, geometry, and integrity for the ‘Pre-Ayot Shales’ sequence stratigraphy interval, which directly ‘caps’ the Roabiba Reservoir at Vorwata and is, therefore, the top and lateral seal for the proposed injection target reservoir. The seal potential for the ‘Pre-Ayot Shales’ top and lateral seal were evaluated in detail, and concluded that the seal can hold at least a 3000 ft (914 m) CO₂ column height in the underlying Roabiba Reservoir, and more-likely a maximum CO₂ column height of 4666 ft (1422 m). The seal geometry is predicted by paleo-depositional facies mapping to extend beyond the known areal extent supported by well data, to the two previously proposed ESSCI injection site locations. The seal integrity evaluation concluded that the seal currently

holds a 2200 ft (671 m) hydrocarbon column, and the maximum estimated 3000 to 4666 ft (914 to 1422 m) CO₂ column height is unlikely to cause fault/fracture reactivation between the proposed injection site locations and the current hydrocarbon gas accumulation. Paleo-depositional facies studies previously concluded that the marine-flooding shale seal facies would actually be thicker at the proposed injection site locations and over the water-leg of the migration path. Therefore, the seal potential for the proposed CO₂ injection into the Roabiba Reservoir, and the subsequent CO₂ plume sequestration/storage updip in the anticlinal trap is considered very good. The major risk relates to the lack of seismic data to confirm the areal extent and thickness of the Pre-Ayot Shales top seal unit at the proposed CO₂ injection locations.

In addition to the Pre-Ayot Shales top/lateral seal analyses, the seal capacity, geometry, and integrity of various regional sealing units were also analyzed with their respective seal potentials evaluated. These units included the Paleocene shale units, the Late Cretaceous Marls, the Upper Late Jurassic Shales, and the Ayot Limestone, which although a 'top seal' for the Roabiba Reservoir at the Wiriagar Deep anticlinorium, is a 'regional seal' for the Roabiba Reservoir at the Vorwata anticlinal structure. 'Top seal' is regarded as the primary seal immediately capping the reservoir, and 'regional seals' are regarded as potential secondary sealing rocks at much shallower depths to the reservoir pervasive over the region. In the event that any CO₂ breaches the top seal, the secondary seals would act as further containment lithologies preventing the CO₂ from reaching the surface.

The seal capacity of the Ayot Limestone for maximum CO₂ column height is 4705 ft (1434 m), the seal capacity of the Upper Late Jurassic Shales for maximum CO₂ column height is 3230 ft (985 m), and the seal capacity of the Late Cretaceous Marls for average maximum CO₂ column height is 3794 ft (1156 m). In regard to seal geometry, these three regional seals have a widespread areal extent over the entire Wiriagar Deep and Vorwata areas. The thickness of the Ayot Limestone is quite uniform, the Upper Late Jurassic Shales thickness varies considerably, and the Late Cretaceous Marls has slightly varying thickness. Only the top Upper Late Jurassic Shales, and the base of Late Cretaceous marls are imaged on 3D seismic with fair to good resolution, and this surface is found to be prevalent over the entire Tangguh area of interest. However, the seal integrity of all three of these potential sealing units is of high risk due to low ductility, and high degree of brittleness. Confirmation of the

fractured and faulted nature of these seals at the Wiriagar Deep area is documented, where FMI/FMS images and whole core have confirmed open faults/fractures. Furthermore, breaching of the sealing units can be deduced from the presence of significant hydrocarbon accumulations in or above each of these units at the Wiriagar Deep area.

The seal capacity of the Paleocene sealing units range between a minimum of 546 ft (166 m), and a maximum of 3181 ft (970 m), of CO₂ column height. Determination of the potential of the Paleocene sealing units as a regional seal for CO₂ sequestration/storage at Vorwata is hindered by a lack of data. There is a complete lack of whole core in the Vorwata wells, and interpreted seismic over the Vorwata area, for this interval, is not available. This dearth of data results in poor understanding of the Paleocene's potential seal geometry and integrity over the Vorwata anticline. In spite of the Paleocene seal at Wiriagar Deep area holding the greatest column of natural gas in rocks having the highest formation overpressure in the Tangguh area, the seal potential of the Paleocene sealing units as a regional seal is highly uncertain, and thus poses a high degree of risk.

An evaluation for the propensity or risk of fault reactivation induced by CO₂ Injection' was carried out, especially in regard to the proximity and impact on the two proposed injection sites. The fault reactivation risking included interpretation and evaluation of the following: borehole image log analysis, pressure data from well testing, rock integrity from well data (eg. leak-off tests) and geomechanical modelling. The analysis concluded that vertical faults striking ~110° N are at the lowest risk of reactivation, requiring an increase in pore pressure of ~10,000 psi (703 kg/cm²) at the proposed injection depth of -14,000 ft TVDss (-4267 m TVDss). Vertical faults striking ~45° N and ~185° N are at the highest risk of reactivation, requiring a pore pressure increase of ~1,460 psi (103 kg/cm²) over hydrostatic pressure gradient at the proposed injection depth of -14,000 ft TVDss (-4267 m TVDss). The dominant faults orientation in the Tangguh area are steeply deeping and striking roughly north-south or east-west. The east-west striking faults are at a low risk of reactivation, requiring a pore pressure increase of ~6,220 psi (437 kg/cm²) over hydrostatic at -14,000 ft TVDss (-4267 m TVDss). The north-south striking faults are at a relatively high risk of reactivation if CO₂ injection results in a pore pressure increase of ~1,770 psi (124 kg/cm²) over hydrostatic at -14,000 ft TVDss (-4267 m TVDss). The conclusions are that the two proposed injection wells are

located >10 km from the two highest risk of re-activation faults. Furthermore, those two faults require a formation pressure increase of more than 1450 psi (102 kg/cm²) over, and above, the present hydrostatic pressure found in the formation to risk a potential fault re-activation. This is considered unlikely to be caused by injection pressure alone, due to the large distance between either of the injection sites and the faults. The migrating plume is also not anticipated to cause a pressure increase during migration.

- **Site Recommendations**

The study selection process then recommended the following two surface locations in targeting Vorwata's top structure Roabiba Reservoir at depth -14,000 ft TVDss (-4267 m TVDss) for CO₂ injection and sequestration/storage:

Site Location	Latitude	Longitude	X	Y
1	-2.358405	133.3605	651,280	9,739,250
2	-2.389640	133.2716	641,390	9,735,806

Injection Site Location 1) Surface location situated approximately 10 km to the east of the Vorwata-10 well surface location, with proposed injection into the base of the Roabiba Sandstone Reservoir. Structurally, this location is on broad, gently dipping east flank of the Vorwata anticlinal and below the established GWC.

Injection Site Location 2) Surface location situated approximately 6 km to the south of the Vorwata-10 well surface location, with injection into the base of the Roabiba Sandstone Reservoir proposed. This structural location is towards the downdip SE end of the Vorwata anticlinal structure and below the established gas-water contact (GWC).

For the final phase of the study, the author integrated the various results and conclusions from the investigations and new research carried out in sedimentology, reservoir characterization, sequence stratigraphy, seal evaluation, and fault re-activation risk assessment, and incorporated them into the first detailed 3D geocellular model ever constructed for the Mesozoic interval in Bintuni Basin in the Tangguh area. The study details the geologic modelling strategy and documents the methodology, parameters, and the various inputs and limitations for the construction

of the 3D geological model. This study also briefly documents the history of development of the Tangguh 3D geologic model, including data and software problems encountered, the manner in which those problems were resolved, and how the model ultimately evolved into the final version. The Tangguh 3D geologic model was created using GEOCARD software, developed by GeoVisual Systems Pty. Ltd.

The model was completed and the grid and attribute files were then successfully imported into Landmark's VIP reservoir simulator program, by BP Indonesia, who carried out preliminary visualizations through 25 years of simulated LNG production and CO₂ injection.

The reservoir simulation preliminary visualization results are encouraging, and validate the previously studied two 'best-ranked' locations as potential CO₂ injection sites. The reservoir simulation visualization showed the CO₂ Injected Site 1 Location (IS1L), with three projected injection boreholes at the IS1L. The visualization simulated CO₂ injection into the saline aquifer leg of the Bathonian/Bajocian Roabiba Reservoir migrating updip within the Vorwata anticline structural closure toward the NW. The visualization showed the CO₂ plume reaching the original gas-water contact (GWC) after 20 years of continuous LNG production and CO₂ injection. The CO₂ plume did not appear to reach the natural gas accumulation being produced updip from the same reservoir, even after 25 years of natural gas production and CO₂ injection. Although the reservoir simulation preliminary result did not proceed further than 25 years, it appears that the proposed CO₂ injection site locations do not compromise the hydrocarbon reserves or LNG production. Furthermore, the supercritical CO₂ plume appears to migrate at the rate and the direction anticipated.

The reservoir simulation results, based on the Tangguh 3D geologic model, support the selection of the potential CO₂ Injection Site 1 and Injection Site 2 locations. The injected CO₂ plume migrates updip into a known structural closure with proven seal integrity, and does not appear to co-mingle with the proven natural gas reserves, nor interfere with the gas production from development wells updip.

A key limitation with the Tangguh 3D geologic model is the lack of actual dipping fault surfaces. During discussions with BP it was agreed that due to the lack of interpreted seismic fault surfaces only major 'approximated' fault polygons would be incorporated into the model as vertical, strike-slip faults. These major faults were created in the GEOCARD model as a series of fault network polygons linked to a 'transmissibility multiplier' attribute. As a result of this approach, the existing model

could be modified or expanded at a later date to include mapped fault surfaces in the same manner. In addition, new log data from future wells drilled in the area can easily be added within the final model. This is particularly of importance in respect to the “S” (or Saritu) structure. This seismically interpreted structure lies under the proposed LNG plant location, and as such may be suitable for future potential CO₂ sequestration/storage. Although the lack of well data for this structure resulted in it being appraised as ‘high risk’, future drilling may result in re-classification if well data evaluated from a CO₂ perspective suggested it as a potential ESSCI site. The new well data could then be incorporated into the current Tangguh 3D geologic model. This example of additional ongoing uses for this study and the geologic model could, perhaps, lead to the possibility of additional prospective subsurface injection and sequestration/storage site locations for CO₂ in the Tangguh region, as more data becomes available.

- **Implementation**

The study provided some guidelines regarding potential data acquisition for future exploration and injection wells in the Tangguh area based on the detailed subsurface analyses performed during this study. It is emphasized that additional, fresh cores be obtained through key seals when monitoring or development wells are drilled in the area.

The study also provided a detailed, up-to-date summary of subsurface CO₂ monitoring techniques, and evaluates the various methodologies, especially in regard to their respective applicability to potential monitoring of subsurface CO₂ for the Tangguh project. The ability of the operator to monitor and measure the injected CO₂ volume, as well as the CO₂ direction and rate of migration, is necessary to verify the success of any subsurface disposal project. The ability to detect any seal breach by the CO₂ is also essential for long-term environmental safety. Theoretical and experimental monitoring techniques summarized were evaluated with suggestions as to their future applicability in Bintuni Basin. Methodologies that are not viable or feasible in the Tangguh project area, for technical or economic reasons, were discussed in detail. Finally, techniques and methods that are considered technically feasible and economically viable were recommended.

These methodologies include ‘smart well completions’ for gas production wells at Vorwata Field, injection wells (particularly vertical pilot hole sections drilled

prior to horizontal injector leg completions), and even ‘work-overs’ of previously drilled exploration/appraisal wells for possible remedial non-CO₂ reactive cement squeeze jobs. Sensors downhole can include temperature, pressure, CO₂ detection, and 4D seismic tomography sensors. These sensors can monitor subsurface CO₂ plume migrations continuously, detect seal breaches, and provide data to optimize sweep efficiency and reservoir storage by modifying injection pressures, rates, and volumes at surface.

Current 3D seismic resolution is too poor for stand-alone monitoring, and is also too low a resolution to be of use in production geo-engineering models at Tangguh. Some subsurface CO₂ monitoring techniques can be used in conjunction with surface 3D seismic surveys to enhance the resolution of the 3D seismic volume, which could potentially be of use in both subsurface CO₂ monitoring, and in natural gas production from the Vorwata Field.

The best proposal would be for a vertical pilot well to be drilled at the IS #1 location, and the well cored and wireline logged according to recommendations made in this study. This vertical wellbore could then be completed as a smart well completion for monitoring purposes. After production begins at the Vorwata field, downhole monitoring of pressures, temperatures, and fluid migrations at the proposed water-leg injection site location could be used to verify reservoir communication with the known updip gas production. After favorable injection characteristics are confirmed at the vertical monitoring hole, the well could be plugged back and sidetracked for use as a horizontal CO₂ injection well. The vertical leg of the hole could still be used for injection monitoring during the CO₂ injection phase of operations.

- **Contributions to Geoscience**

This thesis presents numerous new evaluations and analyses, with unique results, to arrive at several original and valuable conclusions in the field of geological earth science.

A new screening process is devised for examining all options for the disposal of carbon dioxide from a source in the Bird’s Head area of Papua, Indonesia. This was the first time that the options for disposal of CO₂ are identified, reviewed, and appraised for this region. The screening process, after a detailed review and appraisal

of the various non-geological and geological options for the disposal of CO₂ in the Bird's Head, concluded that subsurface injection of CO₂ was the only viable options for the disposal. The subsurface geological options for the disposal of CO₂ in the Bintuni Basin of the Bird's Head are for the first time examined and evaluated in detail.

The evaluation of the subsurface geological options required the construction of a sequence stratigraphic framework for Bintuni Basin, with a detailed Mesozoic sequence stratigraphy model. This is the first detailed and comprehensive sequence stratigraphic framework and model of the Mesozoic interval in Bintuni Basin ever attempted, supported by the first original set of detailed paleogeographic depositional facies maps in conjunction with detailed paleo-depositional isopach maps.

Evaluation of reservoir characteristics and sedimentology precipitated the new analysis of whole core plug samples for porosity and permeability, original mercury injection capillary and pressure analysis.

Evaluation of seal potential required mercury injection capillary pressure analysis of whole core plug or chips samples for seal capacity, delineation of seal geometry, and evaluation of seal integrity. The results of fault reactivation evaluation in Bintuni Basin by Hillis and Meyer (2002) are summarized and integrated into the seal potential evaluation.

The conclusion is that subsurface injection and sequestration in a saline aquifer is the most technically feasible option for the disposal of CO₂ in the Bintuni Basin.

The geological disposal of CO₂ into saline aquifers then evaluates various trapping mechanisms, reservoirs, structures, and seals in the Bintuni Basin by application of a new and unique geological expression of confidence matrix for data quality and quantity. This technique, modified and adapted from petroleum exploration geological expression of confidence matrix method, has potential applicability worldwide for data and risk analyses in CO₂ disposal.

This new methodology concludes that the Middle Jurassic reservoir at the Vorwata structure, with Pre-Ayot Shales as the seal have the greatest confidence of sustainable, environmentally-safe containment. Two suitable bottom-hole injection coordinates for the disposal of CO₂ into a saline Middle Jurassic aquifer were thereby identified.

This study created a detailed geo-cellular model of the Mesozoic interval at Bintuni Basin, near the Tangguh LNG Project development area. This is the first detailed geo-cellular model stochastically populated with reservoir and seal attributes for the Mesozoic interval in Papua, Indonesia. The stochastically populated geo-cellular model for the Bintuni Basin also uses the novel set of paleo-depositional facies maps for the Mesozoic interval to constrain attribute value ranges.

The geo-cellular model was subsequently imported into a reservoir simulator by BP Indonesia, as part of this study. A 25-year simulation of natural gas production simultaneous with CO₂ injection and migration has been performed. This simulation resulted in a verification of this study's predicted CO₂ migration rate and path, confirming the bottom-hole injection site locations with an increased degree of confidence. These detailed reservoir simulations had not been previously attempted by BP due to the lack detailed geo-cellular model, now available due to this study.

Recommendations regarding the acquisition of further data specific to the disposal of CO₂ in Bintuni Basin during drilling operations are identified. Various methods of monitoring CO₂ injection and migration are also evaluated from a site-specific perspective, allowing recommendations for specific techniques and methods to be presented.

Finally, the new and unique sequence stratigraphic framework for the Bintuni Basin, has allowed the development of a new dataset for paleotectonic reconstructions of the northwest margin of the Australian-New Guinea (ANGP) plate margin. A new and original paleo-tectonic history is presented for the Bird's Head micro-continent (BHMC) detachment from the ANGP during the Late Jurassic or Early Cretaceous due to extensional rifting and thermal sag. The subsequent tectonic collision of three plates first in the Oligocene and then again in the Miocene (ANGP, Eurasian Sundaland plate, and the Pacific Caroline plate) resulted in the re-accretion of the Bird's Head to the ANGP, and the creation of the Banda Arc.

This new paleotectonic history of plate and microplate interaction along the NW Shelf and Papua, Indonesia is sure to refocus attention on an under-investigated and poorly understood geologic region of the world.

18.0 POSTSCRIPT

At the time of this publication, indications from BP are that the preliminary reservoir simulation modeling has confirmed the probable success of the proposed potential CO₂ injection sites, and the proposed ESSCI strata and structure. Specifically, the two highest ranked injection sites, IS #1 and IS #2, have been modeled with simulated injections into the basal Bathonian/Bajocian Roabiba Sandstone Formation, at the eastern flank of the Vorwata structure aquifer leg, and the simulated supercritical CO₂ plume migrates slowly, within the model, updip and into the known containment area of the hydrocarbon reservoir after the hydrocarbons have been produced and the reservoir strata depleted. No unwanted vertical or horizontal migration has been noted, as yet, within any of the simulated runs (Frans Silitonga, BP Reservoir Engineer, personal communication, June 30th, 2004).

A high-resolution palynological study of the Mesozoic cores in Vorwata wells was initiated by BP, on the author's recommendation, in 2002. This high-resolution study was conducted by Christopher Bates, of PT Robertson Utama Research Indonesia, unfortunately, not available in time for inclusion in the study and the 3D geologic model. While the results have not been incorporated directly into this Ph.D. thesis project due to the late date of availability, the recent results of the new study were evaluated (N. Davis, personal communication, 2004).

This research carried out with the re-interpretation of existing palynological/biostratigraphic integrated with other datasets (including ichnological, sedimentological, and stratigraphic) concluded that no Aalenian Sandstone Formation reservoir was present at any of the Vorwata well locations cored, and that the Bathonian/Bajocian sands were deposited in an onlapping manner from the SW initially and eventually from the S-SW. Furthermore, re-interpretation of the original palynological/biostratigraphic data by Waton et al. (1994a through 1998e) possibly indicated that the Roabiba Sandstone Formation reservoir was not entirely Bathonian to Bajocian in age, and confirmed that there is an intra-reservoir unconformity in the upper-most section delineating the lower Bathonian/Bajocian Roabiba sandstone unit from an overlying Callovian Roabiba sandstone unit. The unconformity is surmised to be an MJ-2 erosional unconformity caused by a relative fall in sealevel. Subsequent Callovian (MJ-1/LJ-11) marine transgression deposited on-lapping sedimentary units over the unconformity from the present-day S-SE. The Callovian units deposited were initially shoreface and foreshore sandstone paleofacies,

eventually followed by a sudden drowning event over the Berau/Bintuni Basins area that deposited a deep-marine shale with an MFS clearly defining a sequence boundary on top of the Callovian Roabiba sandstone units (Figure 6.40). This marine shale is the Pre-Ayot Shales sequence stratigraphy succession (PA10 through PA30), and is the top seal for the Bathonian/Bajocian and Callovian Roabiba Sandstone Formation reservoirs.

And finally, this work concluded that the location of the Vorwata #4 well was the site of active structuring and fault movement during the time of paleo-deposition in the Middle Jurassic, based on the fact that the V-4 has only the mid Bathonian/Bajocian Roabiba stratigraphic units present within the Roabiba sandstone reservoir. The V-4 lacked the lower-most Bathonian/Bajocian Roabiba sandstone stratigraphic units due to not receiving the early transgressive on-lapping units, and also lacks the upper-most Bathonian/Bajocian Roabiba *and* Callovian Roabiba sandstone stratigraphic units. Yet, it was 'capped' by the deep-marine Pre-Ayot Shales of the Late Callovian, as all of the other Vorwata wells are. Clearly this supported the contention that active structuring (in terms of fault uplift) must have been penecontemporaneous with the widespread paleo-deposition of shoreface and foreshore facies over the rest of the entire area.

A complete understanding and evaluation of this reservoir and seal couplet is crucial to the success of any potential Mesozoic CO₂ injection and sequestration/storage plan for the Tangguh area.

The recent high-resolution palynological/biostratigraphic study of the Mesozoic whole cores in Vorwata wells, almost completely validates the sequence stratigraphic framework developed in this study. The new study by C. Bates (2003) found:

1. The stratigraphically deepest cores from the V-2 and V-4 wells indicated Bajocian sedimentary rocks overlying the top Late Permian unconformity, with no Aalenian sedimentary rocks.
2. There is an intra-reservoir unconformity present within the Roabiba Sandstone Formation at most Vorwata well locations with whole core.
3. The Roabiba intra-reservoir unconformity is an erosional (not non-depositional) surface.

4. The lower, massive portion of the reservoir is Bathonian/Bajocian.
5. The upper, on-lapping portion of the reservoir is Callovian.
6. The overlying shale is Callovian.
7. The overlying Callovian shales (Pre-Ayot Shales) represent a rapid transgressive event, and a deeper marine paleo-depositional facies.
8. The Vorwata #4 well lacks the Callovian Roabiba sandstone unit, in addition to the upper-most Bathonian/Bajocian Roabiba sandstone units.

In regard to the Vorwata #4 well, it is stated, “*Palynological evidence at 12302’ 9” confirms the penetration of Permian sediments...This contact marks a significant stratigraphic hiatus with sediments of the C. halosi zone (‘lower’ Bathonian to Bajocian) overlying those assigned to the Permian (probably Upper Permian). Sediments relating to the lowermost part of the Middle Jurassic, the entire Lower Jurassic to Triassic and possibly part of the Upper Permian are absent*” (Bates, p.46, 2003). This clearly indicates that no Aalenian sandstones are present in this rare whole core of the Jurassic/Permian contact in the Vorwata area.

Confirmation of the active structuring through fault uplift is apparent as the only mechanism allowing upper-most Bathonian/Bajocian and Callovian Roabiba sandstone units to be present at the Vorwata-4 area. “*Sediments relating to the ...earliest Callovian to latest Bathonian age, respectively, appear to be absent...Vorwata #4 is the only well studied to date where the actual contact of the Roabiba sandstone with the overlying shales has been examined*” (Bates, p.41, 2003). While at the adjacent Vorwata #5 area (~5 km SE from V-4) it was found that the, “*...boundary between the ‘Upper’ and ‘Main’ Roabiba Sandstone units is marked by a stratigraphic hiatus as evidenced by [sandstone] sediments assigned to the Wanaea digitata zone (Callovian) overlying those of the Wanaea verrucosa zone (Bathonian)*” (Bates, p.55, 2003).

The minor difference the results presented in this thesis and the new high-resolution study is the stratigraphic unit ascribed to the Roabiba sandstone at the Vorwata-7 well location. This researcher interpreted the original data by Waton (see PART III.6) based only on drill cuttings as indicating the Roabiba sandstone was very thin-bedded at the V-7 location due to a deep erosional incision during the MJ-2 relative sealevel fall removing the Bathonian/Bajocian Roabiba sandstone units. This incised valley was then subsequently in-filled during the Callovian (MJ-1/LJ-11)

marine transgression with first Callovian Roabiba shoreface sands, and then the deep-marine Pre-Ayot Shales.

The new high-resolution palynological study of the Vorwata cores has analyzed the two rather short interval V-7 whole cores for the first time. Bates (2003) found the MJ-2 erosional event at V-7 to have removed most, but not all of the Bathonian/Bajocian Roabiba sandstone, with the sandstone captured in the two cores dating as Bathonian/Bajocian. The top-most portion of the Roabiba sandstone reservoir was not captured in core at V-7, therefore the Callovian Roabiba sandstone unit may be present at the V-7 location overlying the Bathonian/Bajocian Roabiba unit, albeit thinly –bedded.

The difference in sandstone unit dating between the cuttings samples and whole core has limited impact on this study. The presence of the incised valley that removed the top-most units of the onlapping Bathonian/Bajocian Roabiba sandstone was confirmed by Bates in Figure 18.1 (2003). Since no erosional events and time periods are depicted in the paleogeographical facies maps generated for this study, the change in V-7 whole core Roabiba sandstones from Callovian to Bathonian/Bajocian has no impact. Sandstone is still mapped at V-7 as a paleo-depositional onlapping facies during the Bathonian/Bajocian, the adjacent areas in Vorwata are confirmed as receiving onlapping Callovian Roabiba sandstone units overlying the Bathonian/Bajocian Roabiba, and the entire Vorwata area, including V-7, have confirmed Callovian Pre-Ayot Shale marine flooding units drowning them. The paleo-geographic maps and associated isopachs are not impacted by the minor discrepancy at V-7 in age dating for the thin-bedded Roabiba sandstone.

The aim of this research was to identify, risk, evaluate, and then model the Tangguh area for possible CO₂ injection and sequestration. The reservoir characterization inputted to the 3D geo-cellular model were based on whole core plug quantitative analyses and empirical wireline log attributes recorded at all of the wellbores. Apart from the ‘stratigraphic name’ assigned to the sandstone body at V-7, the geostatistical methodology, the fluid characteristics, and the potential CO₂ migration through the reservoir is unaffected by the name given to the V-7 unit.

The only impact of the new biostratigraphic age dating for the Roabiba sandstone unit at V-7 is in the stratigraphic cross-sections of Figure 6.3 and 6.5, where the V-7 Roabiba sandstone reservoir should correlate to the mid

Bathonian/Bajocian Roabiba units (R40/R50/R60) rather than Callovian Roabiba units (CU10/CU20/CU30).

This different correlation is only valid with the assumption that the whole core sandstone palynological age dating for V-7, based on palynomorph assemblages, is correct and the that the previous one based on cutting samples is the spurious one. In any case, it has negligible impact on this study in regard to CO₂ injection and sequestration.

REFERENCES

19.0 REFERENCES

- Ali, S.T.; Asama, K.; Bando, Y.; Chen, C.; Dickens, J.M.; Ichikawa, K.; Inazumi, A.; Ishii, K.; Kapoor, H.M.; Kristan-Tollman, E.; Liao, Z.; Matsuda, T.; Murata, T.; Nakamura, K.; Nakazawa, K.; Okimura, Y.; Qureshi, K.A.; Ross, C.A.; Rui, L.; Saito, Y.; Sakagami, S.; Sheng, J.; Shimizu, D.; Shuja, T.A.; Tokuoka, T.; Tollman, A., (1985); in Eds. Nakazawa K. and Dickens J.M., *The Tethys: Her Paleogeography, and Paleobiology, From the Paleozoic to Mesozoic*; Tokai University Press, Japan.
- Ali, J.R. and Hall, R. (1995); 'Evolution of the boundary between the Philippine Sea plate: palaeomagnetic evidence from eastern Indonesia'; in *Tectonophysics*, v.251; pp.251-275.
- Allen G. P., and Chambers, J. L., (1998); 'Sedimentation in the modern and Miocene Mahakam delta'; in *Proceedings Twenty-seventh Annual Conference Indonesian Petroleum Association*; Jakarta, Indonesia, 236 p.
- Allen, G.P., Laurier, D., and Thouvenin, J., (1979); 'Etude sédimentologique du delta de la Mahakam'; in *Notes et Mémoires, TOTAL, Compagnie Française des Pétroles No. 15*, 156 pp.
- Allen, G.P., and Mercier, F., (1988); 'Subsurface sedimentology of deltaic systems'; in *Journal of the Petroleum Exploration Society of Australia*, Adelaide, Australia, pp. 30-46.
- Allen, G. P., and Posamentier H. W., (1993), 'Sequence stratigraphy and facies model of an incised valley fill: the Gironde estuary, France'; *Journal of Sedimentary Petrology*, v. 63, pp. 378-392.
- Allen, G. and Posamentier, H.W., (1999); *Siliciclastic Sequence Stratigraphy – Concepts and Application's, SEPM Concepts in Sedimentology and Paleontology #7*; SEPM Publications; Tulsa, Okla., USA.
- Alvarez, L.W., Alvarez, F., Asaro, F., and Michel, H.V., (1980); 'Extraterrestrial cause for the Cretaceous-Tertiary extinction'; in *Science*, v.208, pp1095-1108.
- American Geological Institute, (1990); *Glossary Of Geology*; Thompson-Shore Publishing Inc., Virginia USA.
- American Geophysical Union News Online (AGU), (2001); 'Norwegian Sea Proposed as Storage Site for Carbon Dioxide', AGU Newsletter 2001 No. 01-21, June 18th, 2001.
- ARCO: Bulling, T.P., Versept, T.D., Samsu, D.H., Yusuf, B.E., Meizarwin, Kusumanegara, Y., Suffendy, L.T., Keho, T.H. (1998); *Tangguh Fields: 1998 Final Reserves Certification Report (Confidential Report)*; Atlantic Richfield Berau Inc. & Atlantic Richfield Wiriagar Inc.; Jakarta, Indonesia.

Australian Greenhouse Office (1998); 'Outcomes from Kyoto and the implications for Australia', [website available on 12 December 2001],
http://www.greenhouse.gov.au/puns/factsheet/fs_kyoto.html.

Bachu, S., Gunter, W.D., Perkins, E.H.; (1994); 'Aquifer Disposal of CO₂: hydrodynamic and mineral trapping'; *Energy Conversion and Management*, vol. 35, pp.269-279.

Bachu, S.; (2000); 'Sequestration of CO₂ in Geological Media: criteria and approach for site selection in response to climate change'; *Energy Conversion and Management*, vol. 41; pp. 953-970.

Bachu, S.; (2001); 'The transformation of geological space into the CO₂-phase space: A step toward the identification of CO₂-storage capacity in sedimentary basins'; in Williams, D.J., Durie, R.A., McMullen, P., Paulson, C.A.J., and Smith, A.Y. Eds. *Greenhouse Gas Control Technologies-5 (GHGT-5)*; pp. 284-289; CSIRO Publishing, Sydney Australia, 2001.

Bard, K.C. and Pratner, M.J. (1999); 'Tracking Miscible Processes in the Subsurface Utilizing Time-Lapse Shear Wave Seismic Data'; in *SPE Annual Technical Conference and Exhibition, Society of Petroleum Engineers; SPE Paper 56689*; USA.

BBC NEWS & Kirby, A.; (2001); [Available on website, BBC News Online, Sci-Tech; at 18:03 GMT, 17 May 2001 'Science Academies Back Kyoto Findings',
http://www.news.bbc.co.uk/hi/english/sci/tech/newsid_1562000/1562191.stm.

Becker L., Poreda R.J., Basu A.R., Pope K.O., Harrison T.M., Nicholson C., Iasky R. (2004); 'Bedout: A Possible End-Permian Impact Crater Offshore of Northwestern Australia' in *Science*, 4 June 2004, Vol. 304 Issue 5676, pp.1469-1476.

Beecy, David, U.S. Dept. of Energy; Kuuskraa, Vello; Dipietro, Phil; (2001); 'Economic benefits of Carbon Sequestration R&D to the U.S. Economy and Oil and Gas Industry'; in *Public Presentation at American Association of Petroleum Geologists' National Conference & Exhibition*; Denver, Colorado; June 5th, 2001.

Beer, J.M., Mende, W., Stellmacher R.; (2000); 'The Role of the Sun in Climate Forcing', in *Quaternary Science Review vol.19*; USA, pp.403-415.

Bell, J.S., (1996); 'Petro Geoscience 1. In-situ stresses in sedimentary rocks (part 1): measurement techniques', in *Geoscience Canada*, v.23; Toronto, Canada; pp.85-100.

Berggren, W.A., Kent, D.V., Swisher, C.C., Aubry, M., (1995); 'A revised Cenozoic geochronology and chronostatigraphy'; in Berggren W.A., Kent, D.V., Aubry, M., Hardenbol, J., Eds. "Geochronology, Time-scales, and Global Stratigraphic Correlations: A Unified Temporal Framework for an Historical Geology"; *SEPM Special Publications* vol. 54, pp. 129-212 and appendices.

Bouma, A.H., (1962); 'Sedimentology of some flysch deposits: a graphic approach to facies interpretation', *Elsevier*, Amsterdam, pp.168-199.

Bouma, A.H., and Stone, C.G., 2000; 'Fine-grained turbidite systems', in *American Association of Petroleum Geologists, Memoir 72*, pp.342-388.

Boyd, R., Ruming, K., Davies, S., Payenberg, T., and Lang, S.C., 2004: 'Fraser Island and Hervey Bay: a classic modern sedimentary environment', in Boulton, P.J., Johns, D.R., and Lang, S.C. Eds. *Proceedings PESA Eastern Australian Basins Symposium II*, Adelaide, Australia; September 2004.

BP, 2001; (Confidential and Proprietary Data) provided by BP Indonesia, via Perez. G., on ftp transfers November/December 2001.

BP, 2002; (Confidential and Proprietary Data) provided by BP Indonesia, via Perez. G., on ftp transfers November 2002.

BP, 2004; [Available on website 27 August 2004];
<http://www.bp.com/genericarticle.do?categoryId=120&contentId=2001326>,

Briggs, H., (2001); [Available on website; BBC NEWS, 25 September 2001];
http://www.news.bbc.co.uk/hi/english/sci/tech/newsid_1562000/1562191.stm.

Bradshaw, J., Nicoll, R.S., and Bradshaw, M., (1990); 'The Cambrian to Permo-Triassic Arafura basin, Northern Australia'; *APPEA Journal v.30*, pp.107-127.

Bradshaw, J., Sayers, J., Bradshaw, M., Kneale, R., Ford, C., Spencer, L., Lisk, M., (1994b); 'Palaeogeography and its Impact on the Petroleum Systems of the North West Shelf, Australia'; in Purcell, R.R. and Purcell, P.G. Eds. *The Sedimentary Basins of Western Australia vol. 2*; Daniels Publishing Ltd., Perth, Australia, pp. 96-111.

Bradshaw, J.; Rigg, A.; Lang, S.C.; (2000); 'The Search for Sites For Geological Sequestration of CO₂ in Australia: A Progress Report on APCRC GEODISC'; in *Proceedings American Association of Petroleum Geologist's International Conference & Exhibition 2001*; Bali, Indonesia.

Bradshaw, J. and Rigg, A.J. (2001); 'The GEODISC Program: Research into Geological Sequestration of CO₂ in Australia', *Environmental Geosciences v.8 no3*, 2001, pp.166-176.

Bradshaw, J.; Bradshaw, B.E.; Allison, G.; Rigg, A.J.; Nguyen, V.; and Spencer, L.; (2002); 'The Potential For Geological Sequestration of CO₂ in Australia: Preliminary findings and implications to new gas field development in Australia'; *APPEA Journal v.42, (1)*, 2002, pp.25-46.

Bradshaw, J., Allison, G., Bradshaw, B.E., Nguyen, V., Rigg, A.J., Spencer, L., and Wilson, P. (2003); 'Australia Geological CO₂ Storage Potential and matching of Emissions Sources to Potential Sinks', in Gale, J. and Kaya J. Eds. Y. *Greenhouse Gas Control Technologies GHGT-6, Kyoto, Japan 2003*, Elsevier Science Publishing, pp.633-639.

- Bradshaw, M.T., Yeates, A.N., Beynon, R.M., Brakel, A.T., Langford, R.P., Totterdell, J.M., and Yeung, M., (1988); 'Palaeogeographic evolution of the North West Shelf region', in Purcell, P.G., and Purcell, R.R. Eds. *The North West Shelf Australia, Western Australian Branch of PESA*, Perth, Australia, pp.29-54.
- Bradshaw, M.T., (1993), 'Australian Petroleum Systems', *PESA Journal* v.33, pp.43-53.
- Bradshaw, M.T., Bradshaw, J., Murray, A.P., Needham, D.J., Spencer, L., Summons, R.E., Wilmot, J., and Winn, S., (1994a); 'Australian petroleum systems in west Australian basins', in Purcell, P.G., and Purcell, R.R. Eds. *The Sedimentary Basins of Western Australia, Western Australian Branch of PESA*, Perth, Australia, pp.93-118.
- Bradley, W.B., (1979); 'Failure of inclined boreholes', *Journal of Energy Resource Technology*, v.101; pp.232-239.
- Britannica 2001, *Britannica Encyclopaedia 2001*. Britannica Publishing Co., London U.K.
- Broecker, W.S., (1975); 'Climate Change: Are We on the Brink of a Pronounced Global Warming?' in *Science* vol. 189, p. 460.
- Broecker, W.S., (2001); 'Are we headed for a thermohaline catastrophe?', in *Geological Perspective of Global Climate Change, AAPG Studies in Geology #47*; pp. 53-98; AAPG, Tulsa, Ok., USA.
- Bulling, T.P., Verseput, T.D., Samsu, D.H., Yusuf, B.E., Meizarwin, Kusumanegara, Y., Suffendy, L.T., Keho, T.H. (1998); 'Tanggung Fields: 1998 Final Reserves Certification' (Confidential Report); ARCO (Atlantic Richfield Berau Inc. & Atlantic Richfield Wiriagar Inc.), Jakarta, Indonesia.
- Busch, D. A., and Link, D.A., 1985, 'Exploration Methods for Sandstone Reservoirs', *Oil and Gas Consultants International Inc.*, Tulsa, Oklahoma, USA, p.327.
- Bush, G.W. (2001); interview by *Financial Times of London*, 12 November 2001, UK.
- Byrer, C.W. and Guthrie, H.D., (2001), 'Unminable Coals in Eastern U.S. Basins: Potential Reservoirs for Sequestering Carbon Dioxide', in Williams, D.J., Durie, R.A., McMullan, P., Paulson, C.A.J., and Smith, A.Y. Eds. *Greenhouse Gas Control Technologies-5 (GHGT-5)*; CSIRO Publishing, Australia.
- Capen, E. (1992); 'Dealing with Exploration Uncertainties'; in Steinmetz, R. Eds. *The Business of Petroleum Exploration*, AAPG Publications; Tulsa, Oklahoma U.S.A.; pp. 29-62.
- Celia, M.A. and Bachu, S., (2003); ' Geological Sequestration of CO₂: Is Leakage Unavoidable and Acceptable?'; in Gale, J. and Kaya, Y. Eds. *Greenhouse Gas Control Technologies-6 (GHGT-6)*, Kyoto, Japan, Elsevier Science Publishing, pp.477-484.

- Chadwick, R.A., Zweigel, P., Gregersen, U., Kirby, G.A., Holloway, S., and Johannessen, P.N., (2003); 'Geological Characterization of CO₂ Storage Sites: Lessons From Sleipner, Northern North Sea', in Gale, J. and Kaya, Y. Eds. *Greenhouse Gas Control Technologies-6 (GHGT-6)*, Kyoto, Japan, Elsevier Science Publishing, pp.321-327.
- Charlton, T. R.; (2000a); 'Permo-Mesozoic Rifting in Gondwanan Eastern Indonesia'; in *AAPG Abstracts, American Association of Petroleum Geologists International Conference and Exhibition 2000*; Bali, Indonesia, October 2000.
- Charlton, T. R.; (2000b); 'Late Cretaceous evolution of the Bird's Head, Irian Jaya; a failed rift', in *AAPG Abstracts; American Association of Petroleum Geologists International Conference and Exhibition 2000*; Bali - Indonesia, October 2000.
- Chemicalogic (2004); [chemical database website available 10 August 2004], <http://www.chemicalogic.com/co2tab/downloads.htm>
- Chevallier, B., and Bordenave, M. L., (1986); 'Contribution of Geochemistry to the Exploration in Bintuni Basin, Irian Jaya'; in *Proceeding Fifteenth Annual Convention Indonesian Petroleum Association*, pp. 439-460.
- Collins English Dictionary*, (1990); Collins Publishing, Sydney Australia.
- Cook, P.J., Rigg, A., Bradshaw, J., (2000); 'Putting it back where it came from: Is geological disposal of carbon dioxide an option for Australia?', *APPEA Journal*, Vol.40, (1) pp. 654-666; Australia, 2000
- Copin, P.A., Ayotte, K.W., Steggel, N., Hurley, P.J., Azzi, M., (2001); 'Recent Advances in Wind Energy Resource Assessment', in Williams, D.J., Durie, R.A., McMullen, P., Paulson, C.A.J., and Smith, A.Y. Eds. *Greenhouse Gas Control Technologies (GHGT-5)*; pp. 839-844; CSIRO Publishing, Sydney Australia.
- Core Labs (1996); unpublished celluloid core photographs; Core Laboratories, Jakarta, Indonesia; 1996.
- Craig III, F.F. (1985); 'Field Use of Halogen Compounds to Trace Injected CO₂'; in *SPE 60th Annual Technical Conference and Exhibition; Society for Petroleum Engineers; SPE paper 14309*, USA.
- Czernichowski-Lauriol, I., Rochelle, Brosse, E., Springer, N., Bateman, K., Kervevan, C., Pearce, J.M., Sanju, B., and Serra, H., (2003); 'Reactivity of Injected CO₂ with the Utsira Sand Reservoir at Sleipner, Northern North Sea'; in Gale, J. and Kaya, Y. Eds. *Greenhouse Gas Control Technologies-6 (GHGT-6)*, Kyoto, Japan, Elsevier Science Publishing, pp.1617-1623.
- DeBoer, J. D., 2004; [website active 30 August 2004], <http://members.lycos.nl/FotoRik/nngpm.htm>

- Denison, R.E. and Koepnick, R.B.; (1995); 'Variation in ⁸⁷Sr/⁸⁶Sr of Permian Seawater'; in Scholle, P.A.; Peryt, T.M.; Ulmer-Scholle, D.S. Eds. *The Permian of Northern Pangea, Paleogeography, Paleoclimates, Stratigraphy - vol. 1*; 1995; Springer-Verlag Publishers Ltd.; Berlin Germany.
- Dewhurst, D.N., Jones, M.J., Raven, M.D. (2001); 'Seal Capacity, Microstructure, and Composition of the Muderong Shale'; in *GEODISC Project 4: Mechanics and Petrophysics Report*(Confidential Report); APCRC; October 2001.
- DOE (US Department of Energy) (2004); [available website with reports, 25 August 2004];
http://www.energy.gov/engine/content.do?BT_CODE=ENERGYEFFICIENCY
- Dolan, P. J., and Hermany, (1988); 'The Geology of the Wiriagar Field', in *Proceedings Seventeenth Annual Convention, Indonesian Petroleum Association*, v.1, pp. 53-87.
- Dott, R.H., and Batten, R.L.; (1976); 'Evolution of the Earth'; McGraw-Hill Publishing; NY; 1976.
- Downey, M. W.; 'Evaluating Seals for Hydrocarbon Accumulations'; *AAPG Bulletin*, vol. 68, no. 11; *American Association of Petroleum Geologists*; Tulsa, Oklahoma; USA; November 1984.
- Drange, H.; Alendal, G.; Johannessen, O. M.; (2001); 'Ocean Release of Fossil Fuel CO₂: A Case Study'; *Geophysical Research Letters Journal*, Vol. 28, no. 13, July 2001.
- Dunkel, C, (2001); 'Significance of the Monterey Formation, California OCS' [available on September 2004, U.S. Department of Interior website],
<http://www.westcoastpttc.org/presentations/00-01/062001/Dunkel.pdf>
- Dunstan, R., (2002); 'Benefits and Risks of Nuclear Power in California', (*Scientific report produced by the California Research Bureau (CRB) for the California State Legislature as requested by Assembly Member Helen Thomson, CRB-02-008*); 2002.
- Dyck, A.V. (1991); 'Drill-hole Electromagnetic Methods: Electromagnetic Methods In Applied Geophysics'; *SEG vol. 2, Society of Exploration Geophysicists*; pp 881 – 930; USA.
- Edmonds, J.A., Reilly J., Trabalka, J.R., Reichle, D.E., Rind, D., Lebedeff, S., Palutikof J.P., Wigley, T.M.L., Lough, J.M., Blasing, T.J., Solomon, A.M., Seidel, S., Keyes, D., Steinberg, M.; (1986); *Future Atmospheric Carbon Dioxide Scenarios and Limitation Strategies*, Noyes Publications, New Jersey USA.
- EEA (2004); 'EEA Report No.2/2004: Impacts of Europe's Changing Climate'; European Environment Agency [Eds. Voight, T. and van Minnen J.]; 2004.

Embleton, B.J.J. (1986), 'Continental Paleomagnetism'; Phanerozoic Earth History of Australia', in Veevers, J.J. Eds. *Phanerozoic Earth History of Australia*; Oxford University Press, N.Y. U.S.A. pp. 3-27.

Enever, R.J., Yassir, N., Willoughby, D.R., and Addis, M.A., (1996); 'Recent experiences with extended leak-off tests for in-situ stress measurements in Australia', in *The APPEA Journal 1996 vol 36*, Part I; Darwin, N.T. pp.528-535.

Ennis-King, J. and Paterson, L., (2001); 'Reservoir Engineering Issues in the Geological Disposal of Carbon Dioxide', in Williams, D.J., Durie, R.A., McMullen, P., Paulson, C.A.J., and Smith, A.Y. Eds. *Greenhouse Gas Control Technologies-5 (GHGT-5)*; pp. 290-295; CSIRO Publishing, Sydney Australia, 2001.

Ennis-King, J., Gibson-Poole, C., Lang, S.C., Paterson, L. (2002);: 'Long-term Numerical Simulation of Geological Storage for CO₂ in the Petrel Sub-Basin, North West Australia'; in *Petrel Basin – GEODISC ESSCI Report*; (GEODISC Project; APCRC); October 2002 (Confidential Report).

Ennis-King, J. (2003); [GEODISC website available on 22 November 2003]; <http://www.dpr.csiro.au/people/jonathan/internal/calculator/properties3.html>

Enos, P., (1974); 'Surface sediment facies of the Florida-Bahamas Plateau', in *Geological Society of America, Series MC-5*, p.4.

Enos, P., (1983); 'Shelfs', in Scholle, P.A., Bebout, D.G., Moore, C.H., Eds. *Carbonate Depositional Environments, AAPG Memoir #33; American Association of Petroleum Geologists*, Tulsa, Okla., USA, pp. 267-297.

EO NASA (2004), Earth Observatory (EO) – National Aeronautical and Space Administration (NASA) library website [available on 12 August 2004]; <http://earthobservatory.nasa.gov/Library/CarbonCycle/>

ESR(2004); Earth and Space Research website by NASA, NSF, and NOAA [available on 10 August 2004]; http://www.esr.org/outreach/climate_change/climate_index.html

Erickson, D. and Jensen, J.R. H.D., (2001), 'CO₂ Sequestration in an Unminable Coalbed – San Juan Basin, Colorado, USA'; in Williams, D.J., Durie, R.A., McMullen, P., Paulson, C.A.J., and Smith, A.Y. Eds. *Greenhouse Gas Control Technologies-5 (GHGT-5)*; pp. 689-695; CSIRO Publishing, Australia, 2001.

Esteban, M. and Klappa, C.F., (1998); 'Subaerial Exposure'; in Scholle, P.A., Bebout, D.G., and Moore, C.H. Eds. *Carbonate Depositional Environments, AAPG Memoir #33; American Association of Petroleum Geologists*; Tulsa, Oklahoma, USA; pp.1-54; and also 'Paleokarst Development' pp.93-97.

Evans, W.C., Kling, G.W., Tuttle, M.L., Tanyileke, G., and White, L.D., (1993); 'Gas buildup in Lake Nyos, Cameroon: The recharge process and its consequences', in *Applied Geochemistry, vol. 8*, pp. 207-221.

Evans, W.C., White, L.D., Tuttle, M.L., Kling, G.W., Tanyileke, G. and Michel, R.L., (1994); 'Six years of change at Lake Nyos, Cameroon, yield clues to the past and cautions for the future', in *Geochemistry*, vol. 28, pp. 139-162.

Financial Times of London; 12 November 2001; FT.com website; <http://globalarchive.ft.com/globalarchive/article.html?id=011109002264&query>; 2001.

Folk, R.L., and Asserto, R., (1976); 'Comparative fabrics of length-slow and length-fast calcite and calcitized aragonite in a Holocene spelethem, Carlsbad Caverns, New Mexico'; in *Journal of Sedimentary Petrology*, v.46; pp.486-496.

Forbes, D.F.S., (1998); *Vorwata-10 Final Well Report*, British Gas; Jakarta, Indonesia; June 1998.

Forest, C, Webster M., Reilly, J.; (2004); 'Narrowing Uncertainty in Global Climate Change', *The Industrial Physicist Magazine*; pp. 22-25; Issue July 23, 2004.

Fourmilab (2002); [map from website active 22 February 2002], <http://www.fourmilab.ch/cgibin/uncgi/earth>.

Frame, P., Wantoro, Sukarno, (1997a); '*Well Wiriagar Deep-1, Wiriagar Block, Irian Jaya: High Resolution Biostratigraphy of the Paleocene 5400' – 7310'*'; Atlantic Richfield Wiriagar Inc., Core Labs File #GSI-97033, May 1997, Jakarta – Indonesia.

Frame, P., Wantoro, Sukarno, (1997b); '*Well Wiriagar Deep-2, Wiriagar Block, Irian Jaya: High Resolution Biostratigraphy of the Paleocene 6180' – 7990'*'; Atlantic Richfield Wiriagar Inc., Core Labs File #GSI-97032, May 1997, Jakarta – Indonesia.

Frame, P., Wantoro, Sukarno, (1997c); '*Well Wiriagar Deep-3, Wiriagar Block, Irian Jaya: High Resolution Biostratigraphy of the Paleocene 7500' – 8940'*'; Atlantic Richfield Wiriagar Inc., Core Labs File #GSI-97032, May 1997, Jakarta – Indonesia.

Frame, P., Wantoro, Sukarno, (1997d); '*Well Wiriagar Deep-4, Wiriagar Block, Irian Jaya: High Resolution Biostratigraphy of the Paleocene 7260' - 8530'*'; Atlantic Richfield Wiriagar Inc., Core Labs File #GSI-97032, June 1997, Jakarta – Indonesia.

Frame, P., Wantoro, Sukarno, (1997e); '*Well Wiriagar Deep-5, Wiriagar Block, Irian Jaya: High Resolution Biostratigraphy of Paleocene 7230' - 8990'*'; Atlantic Richfield Wiriagar Inc., Core Labs File #GSI-97032, June 1997, Jakarta – Indonesia.

Frame, P., Wantoro, Sukarno, (1997f); '*Well Wiriagar Deep-6, Wiriagar Block, Irian Jaya: High Resolution Biostratigraphy of the Paleocene 6292' - 7711.4'*'; Atlantic Richfield Wiriagar Inc., Core Labs File #GSI-97032, December 1997, Jakarta – Indonesia.

Frame, P., Wantoro, Sukarno, (1997g); '*Well Wiriagar Deep-7, Wiriagar Block, Irian Jaya: High Resolution Biostratigraphy of the Paleocene 6130' - 7971.2'*'; Atlantic Richfield Wiriagar Inc., Core Labs File #GSI-97032, September 1997, Jakarta – Indonesia.

Frame, P., Wantoro, Sukarno, (1997h); 'Well Wiriagar Deep-8, Wiriagar Block, Irian Jaya: High Resolution Biostratigraphy of the Paleocene 6130' - 7971.2'; Atlantic Richfield Wiriagar Inc., Core Labs File #GSI-97032, September 1997, Jakarta – Indonesia.

Frame, P., Wantoro, Sukarno, (1997i); 'Well Wiriagar Deep-8, Wiriagar Block, Irian Jaya: High Resolution Biostratigraphy of the Paleocene 5700' - 7580'; Atlantic Richfield Wiriagar Inc., Core Labs File #GSI-97032, October 1997, Jakarta – Indonesia

Fraser, T.H., Bon, J., and Samuel, L., (1993); 'A New Dynamic Mesozoic Stratigraphy For The West Irian Micro-Continent Indonesia and Its' Implications', in Proceedings Twenty-Second Annual Convention 1993, *Indonesian Petroleum Association*, v.1, IPA93-1.1-024, pp. 707-761.

Fuller, K. and Dahlini, D., 1998; 'Vorwata-7/ST-1 Well – Geological Final Well Report'; Jakarta, Indonesia, May 1998.

Galloway, W.E.; (1989); 'Genetic stratigraphic sequences in Basin Analysis Part I: architecture and genesis of flooding-surface bounded depositional units'; *AAPG Bulletin vol.73*; Tulsa, Okla. USA.

Gantner, U., Jakob, M., and Hirschberg, S., (2001); 'Total greenhouse gas emissions and costs of alternative Swiss energy supply strategies', in Williams, D.J., Durie, R.A., McMullen, P., Paulson, C.A.J., and Smith, A.Y. Eds. *Greenhouse Gas Control Technologies-5 (GHGT-5)*; pp. 991-996; CSIRO Publishing, Sydney Australia, 2001.

Geographix (1997); MAGELLAN Map of Indonesia [website available 16 December 2001] www.geographix.com/GeoGraphix/products/exploration+and+developmentgeology/gesexplorer, Geographix Corp., Santa Barbara, Ca., USA.

Gani, M.R., 2003; 'Crises for a general term referring to all types of sediment gravity flow deposits: gravite'; *Geological Society of America Abstracts with Programs*, v.43; No.7; pp. 171-181.

Gani, M.R., 2004; 'From Turbid to Lucid: A straightforward approach to sediment gravity flows and their deposits'; *The Sedimentary Record*, v.2; No.3; pp. 4-8.

Giddings, J.W., Santana, W., and Pigram, C., (1993); 'Interpretation of palaeomagnetic results from the Bird's Head, Irian Jaya: new constraints on the drift history of the Kemum Terrane'; *Exploration Geophysics*, v.24, pp.283-290.

Gifford, J., Hooper, G., Hall, P., Senelwa, K., Robertson, K., McGimpsey, N., Davison, J., (2001); 'Large Scale Power Generation and Greenhouse Gas Mitigation Using Forestry By-Products', in Williams, D.J., Durie, R.A., McMullen, P., Paulson, C.A.J., and Smith, A.Y. Eds. *Greenhouse Gas Control Technologies-5 (GHGT-5)*; pp. 891-896; CSIRO Publishing, Sydney Australia.

- Grady, M.M.; Hutchinson, R.; McCall, G.J.H.; Rothery, D.A. (Editors) (1998); *'Meteorites: Flux with Time and Impact Effects'*, Geological Society Special Publication No. 140; The Geological Publishing Society House; Bath, U.K.
- Grunau, H.R. (1981); "Worldwide Review of Seals for Major Accumulations of Natural Gas"; *AAPG Bulletin*, vol. 65, no. 9; American Association of Petroleum Geologists; Tulsa, Oklahoma; USA; 1981.
- Hall, R., (1996); 'Reconstructing Cenozoic S.E. Asia', in Hall, R. and Blundell, D.J. Eds. *Tectonic Evolution of Southeast Asia*; Geological Society Special Publication No. 106; The Geological Publishing Society House; Bath, U.K.
- Hall, R.; (2000); [website available 12 July 2002]; <http://www.gl.rhbnc.ac.uk/seasia/html/landseamaps.html>
- Hall, Robert; (2001); 'No Fault of its own, Buffer Plate Turns'; *AUSGEO NEWS*, Issue No. 60; March/April 2001; AGSO National Capital Printing; Canberra, Australia; pp. 16-17.
- Hallam, A., (1998); 'Mass extinctions in Phanerozoic time', in Grady, M.M., Hutchinson, R., McCall, G.J.H., and Rothery, D.A. Eds. *Meteorites: flux with time and impact effects*; Geological Society Special Publication No. 140; Cambridge University Press, Bath, UK, 1998, pp. 259-274.
- Harrington, J. (1997); 'Source Rock Study of Permian Coals/ Coaly Shales and Claystones/ Shales (Including one Middle Jurassic Coal) From Wiriaragar Wells # WD1, WD2, WD3, & WD6ST, Bintuni Basin; Atlantic Richfield Inc.'; Core Labs; July 1997, Jakarta, Indonesia, Confidential Report.
- Harrington, H.J., Brakel, A.T., Hunt, J.W., Wells, A.T., Middleton, M.F., O'Brien, P.E., Hamilton, D.S., Beckett, J., Weber, C.R., Radke, S., Totterdell, J.M., Swaine, D.J., Schmidt, P.W., (1989); *Permian Coals of Eastern Australia, 1989 Bureau of Mineral Resources Bulletin 231*; Australian Government Publishing Services; Canberra, Australia.
- Haq, B.U., Hardenbol, J., Vail, P.R., (1987); 'Chronology of fluctuating sea levels since the Triassic', in *Science* v.235, pp.1157-1167.
- Haq, B.U. (1993); 'Deep-sea response to eustatic change and significance of gas hydrates for continental margin stratigraphy', in Posamentier, H.W., Summerhayes, C.P., Haq, B.U., and Allen, G.P. Eds. *Sequence Stratigraphy and Facies Associations: International Association of Sedimentologists Special Publication No.18*; Blackwell Publications, pp. 93-108.
- Herzog, H., Eliasson, B., Kaarstad, O., (2000); 'Capturing greenhouse gases'; *Scientific American*, February 2000; pp. 54-61.

- Herzog, H., Adams, E., Akai, G., Alendal, L., Golmen, P., Haugen, P., Masuda, S., Matear, R., Masutani, S., Ohsumi, T., Wong, C.S., (2001), 'Update on the International Experimentation on CO₂ Ocean Sequestration', in Williams, D.J., Durie, R.A., McMullen, P., Paulson, C.A.J., and Smith, A.Y. Eds. *Greenhouse Gas Control Technologies-5 (GHGT-5)*; pp. 399-404; CSIRO Publishing, Sydney Australia.
- Hetherington, J. and Thambimuthu, K., (2003); "In-Situ Gasification, Enhanced Methane Recovery, and CO₂ Storage in Deep Coal Seams", in Gale, J. and Kaya, Y. Eds. *Greenhouse Gas Control Technologies GHGT-6, Kyoto, Japan 2003*, Elsevier Science Publishing, pp.709-717.
- Hillis, R.R. (1998); 'Mechanisms of dynamic seal failure in the Timor Sea and Central North Sea', in *The Sedimentary Basins of Western Australia*, v.2; Australia 313-324.
- Hillis, R. R. and Meyer, J. J. (2003); "Appendix B: Geomechanical Modelling of the Propensity for Fault Reactivation Induced by CO₂ Injection, Tangguh Project, Papua – Indonesia", in Salo, J. Eds. *Tangguh CO₂ Capture and Sequestration/Storage Study – Phase II Report*; National Centre for Petroleum Geology & Geophysics, University of Adelaide; Australia; February 2003 (Confidential Report).
- Hirai, S., Takamatsu, R., Tabe, Y., Suzuki, K., Okazaki, K., (2001); Formation of liquid CO₂ droplets and ject with deformation and growth of hydrate films', in Williams, D.J., Durie, R.A., McMullen, P., Paulson, C.A.J., and Smith, A.Y. Eds. *Greenhouse Gas Control Technologies-5 (GHGT-5)*; pp. 481-486; CSIRO Publishing, Sydney Australia, 2001.
- Holloway, S.; van der Straaten, R.; (1995); 'The Joule II Project: The underground disposal of carbon dioxide'; *Energy Conversion and Management*, vol. 36, 1995.
- Holloway, S. (1996), 'An Overview of the Underground Disposal of Carbon Dioxide', in *British Geological Survey Proceedings from 3rd International Conference on CO₂ Removal*, Cambridge, Ma. USA, Pergamon, 9-11 September 1996, pp.193-196.
- Holloway, S., Heederik, J.P., van der Meer, L.G.H., Czernichowski-Lauriol, I., Harrison, R., Lindeberg, E., Summerfield, I.R., Rochelle, C., Schwartzkopf, T., Kaarstad, O., Berger, B., (1996); 'The Underground Disposal of Carbon Dioxide: Joule II Project No.CT92-0031, Final Report'; *British Geological Survey*, Nottingham, UK, 1996.
- Holtz, M.H., Carr, D.L., Nance, P.K., (2000); "Reduction of 'greenhouse gas' emissions through underground CO₂ sequestration in Texas oil and gas reservoirs", in the *American Association of Petroleum Geologists International Conference 2000*; Bali, Indonesia, 2000.
- Hördt, A., Andrieux, P., Neubauer, F.M., Ruter, H., Vozoff, K. (2000); 'A 1st Attempt at monitoring Underground Gas Storage by Means of Time-Lapse Multi-Channel Transient Electromagnetics'; in *Geophysical Prospecting*, no. 48, pp 489-509; 2000.

Houghton, J., (1997, 2nd Edition); *Global Warming – The Complete Briefing* (IPCC), Cambridge University Press, Cambridge; U.K.

House, M.R.; (1995); ‘Orbital Forcing Timescales: an introduction’, in House, M.R. and Gale, A.S. Eds. *Orbital Forcing Timescales and Cyclostratigraphy*, Geological Society Special Publication No.85; Geological Society Publishing, London, 1995.

Howe, W., and Henderson-Sellers A., (1997); *Assessing Climate Change*, Gordon and Breach Science Publishers, Amsterdam Netherlands.

Hubbert, M.K. and Rubey, W.W. (1959); ‘Role of Fluid Pressure in Mechanics of Overthrust Faulting: 1. Mechanics of fluid-filled porous solids and its application to overthrust faulting’, in *Geological Society of America Bulletin*, v.70; 1959, USA; pp. 115-166.

Hubbert, M.K. and Willis D.G., (1957); ‘Mechanics of hydraulic fracturing’, in *AIME Petroleum Transactions*, v.210; pp.153-166.

Huizinga, B.J. (2000); *Gas Compartmentalization and Gas Origin in the Vorwata Field, Irian Jaya (East Indonesia)*; Confidential AEPT/ARCO Report; Plano – Texas; 2000

Indro, S., Dachlan, D., Shackleton, T., (1997); *Wiriagar Deep-7 Final Well Report*; (Confidential ARCO Report); Jakarta – Indonesia, June 1997.

IPCC (1997), *Climate Change 1997*; [Houghton, J. Eds.], Cambridge University Press, Cambridge; U.K., 2001.

IPCC (2001), *Climate Change 2001: The scientific basis*; [Watson, R.T. Eds.], Cambridge University Press, Cambridge; U.K., 2001.

Isworo, H. (2002); ‘Kais and Faumai Water Salinity Study’; *Powerpoint Presentation, BP Indonesia*; Jakarta, Indonesia, 2002.

Jean-Baptiste, P., and Ducroux, R., (2001); ‘Which role for nuclear power in the battle against global warming?’, in Williams, D.J., Durie, R.A., McMullen, P., Paulson, C.A.J., and Smith, A.Y. Eds. *Greenhouse Gas Control Technologies-5 (GHGT-5)*; pp. 1180-1185; CSIRO Publishing, Sydney Australia, 2001.

Kaldi, J.G. (2003); ‘Evaluation of Reservoir and Seals’; *Course Notes; University of Adelaide - NCPGG*; Adelaide, S.A., Australia; 2003

Kaldi, J.G. and Atkinson, C.D. (1993); ‘Seal Potential of the Talang Akar Formation, BZZ Area, Offshore NW Java, Indonesia’; in *The Proceedings Twenty Second Annual Convention Indonesian Petroleum Association*, October 1993; IPA Press; Jakarta, Indonesia; October 1993.

Kasim, A. T., Titus, I., Roberts, J. W., and Bulling, T. P., (2000); ‘The Tangguh LNG Gas Fields: Conceptual Development Overview’, in *Proceedings Society of Petroleum Engineers International Oil and Gas Conference 2000, SPE 64706*, Beijing, China.

Keho, T. and Samsu, D., 2002. 'Depth Conversion of Tangguh Gas Fields', *Society of Exploration Geophysicists Journal, The Leading Edge*, October 2002, pp. 966-971.

Knutson, T. (2004); "Climate Impact of Quadrupling Atmospheric CO₂: An Overview of GFDL Climate Model Results", on the U.S. Government's National Oceanic and Atmospheric Administration (NOAA) [available on website 30 August 2004] http://www.gfdl.noaa.gov/~tk/climate_dynamics/climate_impact_webpage.html

Krauskopf, K.B. (1967); *An Introduction to Geochemistry*; McGraw-Hill Publishing; USA; 1967.

Kurushima, M., (2001); 'Methods for technology transfer on climate control', in Williams, D.J., Durie, R.A., McMullen, P., Paulson, C.A.J., and Smith, A.Y. Eds. *Greenhouse Gas Control Technologies-5 (GHGT-5)*; pp. 1177-1179; CSIRO Publishing, Sydney Australia, 2001.

Kuustaa, V.A. and Pekot, L.J., (2003); 'Defining Optimum CO₂ Sequestration Sites for Power and Industrial Plants', in Gale, J. and Kaya, Y. Eds. *Greenhouse Gas Control Technologies GHGT-6, Kyoto, Japan 2003*, Elsevier Science Publishing, pp.633-639.

Lang, S.C., Jell, J.S., and Draper, J.J., (1990); 'Depositional evolution of the Devonian-Carboniferous intracratonic Burdekin Basin, north Queensland'; *Proceedings, Pacific Rim Congress 90, The Australasian Institute of Mining and Metallurgy*, Melbourne, Australia, v.3, 791 - 800.

Lang, S.C., Kassan, J., Benson, J.M., Grasso, C.A. and Avenell, L.C., (2000). 'Applications of modern and ancient geological analogues in characterisation of fluvial and fluvial-lacustrine deltaic reservoirs in the Cooper Basin', *APPEA Journal*, 40 (1), 393-415.

Lang, S.C. (2001); 'Concepts and Applications of Sequence Stratigraphy'; *NCPGG Course Notes Publication, National Centre for Petroleum Geology & Geophysics*, University of Adelaide, May 2001.

Levine, J.S. (2004); 'Ozone, Climate and Global Atmospheric Change', on National Aeronautical and Space Administration (NASA) [website available 1 August 2004]; http://asd-www.larc.nasa.gov/biomass_burn/ozone.html.

Lewis, C.A., and Shinn, J. H., (2001); 'Global Warming: an oil and gas company perspective; prospects for geological sequestration?', in Eds. Bradshaw J., and Cook, P., *CO₂ Sequestration, AAPG Environmental Geosciences vol. 8*, pp.177-186.

Livsey, A. R., Duxbury, N., and Richards, F., (1992); 'The Geochemistry of Tertiary and Pre-Tertiary Source Rocks and Associated Oils in Eastern Indonesia'; in *Proceedings Twenty First Annual Convention, Indonesian Petroleum Association, v.1*, pp. 500-520.

Livsey, A. R. and Charlton, T. R.; (2000); 'Palaeogeographic Controls on Pre-Tertiary Source Rock Distribution on the Northern Australian Continental Margin'; *AAPG*

Abstract – Public; American Association of Petroleum Geologists International Conference and Exhibition; Bali - Indonesia, October 2000.

Longley, I.M., Buessenschuett, C., Clydesdale, L., Cubitt, C.J., Davis, R.C., Johnson, M.K., Marshall, N.M., Murray, A.P., Sumerville, R., Spry, T.B., Thompson, N.B., (2002); ‘The North West Shelf of Australia: a Woodside perspective’; *Proceedings of Western Australia Basin Symposium 2002; PESA Publication; Australia; pp. 27-88.*

Lord Browne, J. (2003); Transcript of address to British Parliament [website available 20 August 2004],
http://www.pewclimate.org/companies_leading_the_way_belc/company_profiles/bp_amoco/browne.cfm.

Loucks, R.G., (1977); ‘Porosity development and distribution in shoal-water carbonate complexes-subsurface Pearsall Formation (Lower Cretaceous) South Texas’, in Bebout and Loucks, R.G., Eds. *Cretaceous Carbonates of Texas and Mexico, Bureau of Economic Geology, Austin University Texas, Report no.89*, pp. 97-126.

Lowe, D.R., (1998); ‘*Supplementary Report: Sedimentology, Petrography, and Depositional Patterns of Paleocene Deep-water Sedimentary Rocks, Wiriagar/Bintuni Bay Area*’; (Confidential ARCO Report) March 1998, Stanford University, California.

Lowe, D.R., and Guy, M., (2000) ‘Slurry-flow deposits in the Britannia Formation (Lower Cretaceous), North Se: A new perspective on the turbidity current and debris flow problem’; *Sedimentology*, v.47, pp.31-70.

MacKenzie, F.T., Lerman, A., Ver, L.M.B., (2001); ‘Recent past and future of the global carbon cycle’, in *Geological Perspective of Global Climate Change, AAPG Studies in Geology #47*; pp. 51-82; AAPG, Tulsa, Okla., USA.

Maguire, P.K.H.; Mackenzie, G.D.; Denton, P.; Trejo, A.; Kind, R.; (1998); ‘Mapping the Chicxulub Crater Structure with Gravity and Seismic Reflection Data’; *Meteorites: Flux with Time and Impact Effects; Geological Society Special Publication no. 140*; Geological Publishing Society House; Bath, U.K.; pp 177-195.

Mann, M.E., Bradley, R.S., Hughes, M.K. (1999); ‘Northern hemisphere temperatures during the past millennium: inferences, uncertainties, and limitations’; *Geophysical Research Letters No.26*; 1999.

Masuda, S., (2001); ‘CO₂ Ocean Sequestration Project in RITE’, in Williams, D.J., Durie, R.A., McMullen, P., Paulson, C.A.J., and Smith, A.Y. Greenhouse Eds. *Gas Control Technologies-5 (GHGT-5)*; pp. 487-491; CSIRO Publishing, Sydney Australia.

Mathews, S.; (1976); ‘What’s Happening To Our Climate?’; *National Geographic Magazine*; November 1976 Issue, pp. 576-615.

- Maxwell, S., Urbancic, T., McLellan, P., (2003); 'Assessing the Feasibility of Reservoir Monitoring Using Induced Seismicity', Presented at the EAGE 65th Conference and Exhibition, Stavanger, Norway, June 2-5, 2003.
- McCaffery, R.; (1988); 'Active tectonics of the eastern Sunda and Banda arcs'; *Journal of Geophysical Research*, v.93, pp.15163-15182.
- McCaffery, R.; (1989); 'Seismological constraints and speculations on Banda Arc tectonics', in *Proceedings of the Snellius II Symposium, Theme: Geology and Geophysics of the Banda Arc and Adjacent Areas; Part I, Netherlands Journal of Sea Research*, v.24, pp. 141-152.
- McCaffery, R.; (1996); 'Slip Partitioning at Convergent Plate Boundaries'; in Hall, R. and Blundell, D.J. Eds. *Tectonic Evolution of Southeast Asia; Geological Society Special Publication No. 106*; Geological Society Publishing House; Bath U.K.; pp. 3-18.
- McConachie, Bruce; King, Howie; Keyang, Ma; (2001); 'Old Fault Controlled Foldbelt Structures and the Petroleum Systems of Warim in West Papua'; *AAPG Abstract - Public; American Association of Petroleum Geologists National Conference; June 2001*; Denver, Colorado.
- Metcalf, I., (1996); 'Pre-Cretaceous Evolution of SE Asian Terranes', in Hall, R. and Blundell, D. Eds. *Tectonic Evolution of SE Asia; Geological Society of London, Special Pub. 106*, pp.97-122.
- Messent, B.E.J., Goody, A.K., Collins, E., Tobias, S. (1994); in Purcell, R.R. and Purcell, P.G. Eds., 'Sequence Stratigraphy of the Flamingo Group, Southern Bonaparte Basin'; *The Sedimentary Basins of Western Australia* vol. 1; Frank Daniels Publishing Ltd., Perth Australia, pp. 243-257.
- Miall, A.D. (1991); 'Stratigraphic sequences and their chronostratigraphic correlations'; *Journal of Sedimentological Petrol. Vol.61*; 1991.
- Milam, K. (2004); 'Wind Power Fuss Blows Hard', *AAPG Explorer* vol. 25, No.7; July 2004 Issue; *American Association of Petroleum Geologists*; Tulsa, Okla., USA, pp. 16-17.
- Milankovitch, M.; (1920); 'Theorie Mathematique des Phenom enes Thermiques Pproduits par la Radiation Solaire'; *Academie Yugoslave des Sciences et des Arts de Zagreb*; Gauthiers-Villiers Publishing; Paris, France; 1920.
- Milner, A.C., (1998); 'Timing and Causes of Vertebrate Extinction at the K/T Boundary', in Grady, M.M., Hutchison, R., McCall, G.J.H., and Rothery, D.A. Eds. *Meteorites: Flux With Time and Impact Effects, Geological Society Special Publication No.140*; *The Geological Society*, Cambridge University Press, Bristol, UK, 1998, pp. 247-259

- Mitchum, R.M. (1977); 'Seismic stratigraphy and global changes of sea level Part I'; in Payton, C.E. Eds. *Seismic Stratigraphy – Applications to Hydrocarbon Exploration*; AAPG Memoir #26; American Association of Petroleum Geologists, Tulsa, Okla., USA.
- Moritis, G. (2003); 'Sequestration Adds New Dimension to Oil, Gas Production'; *Oil & Gas Journal*, vol. 101.9; Pennwell Publishing; Tulsa, Oklahoma; March 3, 2003.
- Nakanishi, T., and Lang, S.C. (2001); 'The Search for Stratigraphic Traps Goes On – Visualisations of Fluvial-Lacustrine Successions in the Moorari 3D Survey, Cooper-Eromanga Basin'; *APPEA Journal 2001*; Australia; pp. 115-137.
- Nakanishi, T. and Lang, S.C, 2002; 'Towards an efficient exploration frontier: constructing a portfolio of stratigraphic traps in fluvio-lacustrine successions, Cooper-Eromanga Basin', in *APPEA Journal*, v.42, 2002, pp.131-150.
- NASA/EROS (1979); Photographic negative from LANDSAT satellite was purchased by J. Salo from the National Aeronautics and Space Administration (NASA) / EROS Center in 1995. Photograph was taken on January 22nd, 1979 with an estimated 40% cloud cover.
- National Aeronautics and Space Administration (NASA), (1986); *Atmospheric Ozone 1985*; World Meteorological Organization, Report No. 16, UN Publications.
- Netherwood, R., 2000: 'The Petroleum Geology of Indonesia', *Schlumberger 2000 Reservoir Optimization Conference Publication, Chapter 4*, pp.174-227.
- Newmark, R.L., Ramirez, A.L., Daily, W.D. (2001); 'Monitoring CO₂ Sequestration Using Electrical Resistance Tomography (ERT) – Sensitivity Studies'; in *First National Conference on Carbon Sequestration; National Energy Technology Laboratory paper 7a1*; USA, 2001.
- NIST (2003); National Institute of Standards and Technology (US Gov. Bureau of Standards) NIST Standard Chemistry Reference: [website available 1 August 2004], <http://webbook.nist.gov/cgi/cbook.cgi?ID=C124389&Units=SI>
- NOAA (2004); Geophysical Fluid Dynamics Laboratory-National Oceanic and Atmospheric Administration (gfdl_NOAA) [website available 1 August 2004], http://www.gfdl.noaa.gov/~tk/climate_dynamics/climate_impact_webpage.html
- NTFA (2004); National Tidal Facility of Australia; Flinders University [website available 1 August 2004], http://www.ntf.flinders.edu.au/TEXT/NEWS/PacificCountryReport_fj_2003.pdf
- Nummedal, D., Riley, G.W., and Templet, P.L. (1993); 'High resolution sequence architecture: a chronostratigraphic model based on equilibrium profile studies', in Posamentier, H.W., Summerhayes, B.U., Haq, B.U., Allen, G.P. Eds. *Sequence Stratigraphy and Facies Associations; Special Publications Series #18, International Association of Sedimentologists*; Blackwell Publishing; pp. 55-68.

- Nurzaman, Z.Z., and Pujiyanto, A., (1994); 'Geology and Reservoir Characterization of Wiriagar Field as a Diagenetic Facies for Reservoir Simulation'; in *Proceedings for Indonesian Petroleum Association Twenty-Third Annual Convention 1994*, IPA94-2.1-044, V.2, pp. 29-49.
- Obdam, A., van der Meer, L.G.H., May, F., Kerveyen, C., Bech, N., Wildenborg, A., (2003); 'Effective CO₂ Storage Capacity in Aquifers, Gas Fields, Oil Fields, and Coal Fields', in Gale, J. and Kaya, Y. Eds. *Greenhouse Gas Control Technologies-6 (GHGT-6)*, Kyoto, Japan 2003, [Elsevier Science Publishing, pp.339-345.
- Ohga, K., Sasaki, K., Deguchi, G., and Fujioka, M., (2003), 'Fundamental Tests on Carbon Dioxide Sequestration into Coal Seams', in Gale, J. and Kaya, Y. Eds. *Greenhouse Gas Control Technologies-6 (GHGT-6)*, Kyoto, Japan 2003, [Elsevier Science Publishing, pp.531-535.
- O'Leary, H.E., Akhurst, M.A., Rutter, P.R., (2001); 'Greenhouse Gas Reduction Inventories what then?', in *Greenhouse Gas Control Technologies (GHGT-5)* [Eds: Williams, D.J., Durie, R.A., McMullen, P., Paulson, C.A.J., and Smith, A.Y.]; pp. 1139-1144; CSIRO Publishing, Sydney Australia, 2001.
- Ori, G. G., Roveri, M., and Vannoni, F., (1986); 'Plio-Pleistocene sedimentation in the Apenninic-Adriatic foredeep (Central Adriatic Sea Italy)', in Allen, P. A., and Homewood P. Eds. *Foreland Basins, International Association of Sedimentologists Special Publication No.8*.
- Packham, G.; (1996); 'Cenozoic SE Asia: Reconstructing Its Aggregation and Reorganization'; in Hall R. and Blundell D. Eds. *Tectonic Evolution of Southeast Asia; Geological Society Special Publications No. 106*; The Geological Society Publishing House; Bath U.K.; pp. 142-143.
- Pemberton, S.G. (1997a); Ichnological Dynamics of the Permian Interval of the Wiriagar Deep Cores, Offshore Irian Jaya, Indonesia (ARCO in-house report); University of Alberta, February 1997.
- Pemberton, S.G. (1997b); Ichnological Dynamics of the Jurassic Interval of the Wiriagar Deep Cores, Offshore Irian Jaya: Part Two (ARCO in-house report); University of Alberta, February 1997.
- Pemberton, S.G. (1997c); Ichnological Dynamics of the Cretaceous and Paleocene Interval of the Wiriagar Deep Cores, Offshore Irian Jaya; Part One' (ARCO in-house report); University of Alberta, March 1997.
- Pemberton, S.G. (1997d); Ichnological Dynamics of the Cretaceous and Paleocene Interval of the Wiriagar Deep Cores, Offshore Irian Jaya; Part Two (ARCO in-house report); University of Alberta, March 1997.
- Pemberton, S.G. (1997e); Ichnological Dynamics of the Wiriagar Deep Cores, Offshore Irian Jaya (ARCO in-house report); University of Alberta, March 1997.

Pemberton, S.G. (1997f); Ichnological Dynamics of the Wiriagar Deep, Vorwata, and East Onin Cores, Offshore Irian Jaya (ARCO in-house report); University of Alberta, 1997.

Perkins, T. W. and Livsey, A. R., (1993); 'Geology of the Jurassic Gas Discoveries in Bintuni Bay, Western Irian Jaya', in *Proceedings Twenty Second Annual, Indonesian Petroleum Association, v.1, IPA93-1.1-023*, pp. 793-830.

Perry, K., (1997); Vorwata-1 Geological Final Well Report; Confidential ARCO Report); Jakarta – Indonesia, June 1997.

Perry, K., Indro., S., Dahlini D., (1997); Vorwata-2 Geological Final Well Report; Confidential ARCO Report); Jakarta – Indonesia, June 1997.

Petit, J.R., Jouzel, J., Raynaud, D., Barkov, N.I., Barnola, J.M., Basile, I., Benders, M., Chappellaz, J., Davis, M., Delayque, G., Delmotte, M., Kotlyakov V.M., Legrand, M., Lipenkov, Y.V., Lorius, C., Pepin, L., Ritz, C., Saltzman, E., Stievenard, M.; (1999); 'Climate and atmospheric history of the past 400,000 years from the Vostok ice core, Antarctica', in *Nature vol. 399*; pp. 429-436.

Pieters, P.E., Pigram, C.J., Trail, D.S., Dow, D.B., Ratman, N., Sukanto, R., 1983; 'The Stratigraphy of western Irian Jaya', in *Indonesian Geological Research and Development Centre (GRDC) Bulletin #8*, 1983; pp.14-48.

Pigram, C.J. and Panggabean, H., (1981); 'Pre-Tertiary geology of western Irian Jaya and Misool Island: Implications for the tectonic development of eastern Indonesia', in *Proceedings Indonesian Petroleum Association Tenth Annual Convention 1981, v.1*, pp.385-398.

Pigram, C.J. and Panggabean, H., (1984); 'Rifting of the northern margin of the Australian continent and the origin of some microcontinents in eastern Indonesia', *Tectonophysics, v.107*, pp.331-353.

Pigram, C.J. and Sukanta, U., (1989); 'Geology of the Taminabuan Sheet Area, Irian Jaya'; in *GRDC Bulletin 1989* (with map enclosure), *Indonesian Geological Research and Development Centre*; Bandung, Indonesia; pp.1-51.

Pigram, C. J., and Davies, H. L., (1987); 'Terranes and the accretion of the New Guinea orogen'; *BMR Journal Australian Geology and Geophysics. v.10, no.3*, pp. 193-211.

Plumb, R.A. and Hickman, S.H., (1985); 'Stress-induced borehole elongation: A comparison between Four-Arm Dipmeter and the Borehole Televiewer in the Auburn Geothermal Well'; *Journal of Geophysical Research, v.90*; pp.5513-5521.

PMEL NOAA (2004); Pacific Marine Environmental Library (PMEL) at National Oceanic and Atmospheric Administration (NOAA) US Government Library [website available 1 August 2004], <http://www.pmel.noaa.gov/co2/co2-home.html>

Posamentier, H.W., Allen, G.P., James, D.P., and Tesson, M.; (1992); 'Forces Regressions in a Sequence Stratigraphic Framework'; *AAPG Bulletin vol. 76*; Tulsa, Ok. USA.

Posamentier, H. and Chamberlain, C.J. (1993); 'Sequence Stratigraphic analysis of lowstand beach deposits at Joarcam Field, Alberta Canada'; in Posamentier, H. Eds. *Sequence Stratigraphy and facies Associations: International Association of Sedimentologists Special Publication No. 18*; Blackwell Publications, pp.253-277.

Posamentier, H. and James, D.P. (1993); 'An Overview of sequence-stratigraphic concepts: uses and abuses'; in Posamentier, H.W., Summerhayes, C.P., Haq, B.U., and Allen, G.P. Eds. *Sequence Stratigraphy and Facies Associations: International Association of Sedimentologists Special Publication No. 18*; Blackwell Publications, pp. 3-18.

Posamentier, H. & Allen, G. (1999); "*Siliciclastic Sequence Stratigraphy – Concepts and Applications*": *SEPM Concepts in Sedimentology and Paleontology No. 7*; SEPM Publications; Tulsa, Okla. USA.

Post W.M., Chavez F., Mulholland P.J., Pastor J., Peng T.H., Prentice K., and Webb III, T. (1992); 'Climatic Feedbacks in the Global Carbon Cycle,' in Dunnette D.A. and O'Brien R.J. Eds. *The Science of Global Change: The Impact of Human Activities on the Environment, American Chemical Society Symposium Series 483*, ACS Publications, USA.

Purcell, W.R., (1949); 'Capillary Pressures – Their Measurement Using Mercury and the Calculation of Permeability Therefrom'; in *Petroleum Transactions, AIME*, v.186, pp. 39-48.

Quinlan, J.F., (1972); 'Karst-related mineral deposits and possible criteria for the recognition of paleo-karsts; a review of preservable characteristics of Holocene and older karst terranes'; in *24th International Geological Congress, Montreal, Canada, Section 6*; pp.156-168.

Reinecker, J., O. Heidbach, M. Tingay, P. Connolly, and B. Müller, (2002); World Stress Map, Heidelberg Academy of Science and Humanities, University of Karlsruhe, [website available 30 August 2004], <http://www.world-stress-map.org>.

Reinson, G. E., (1984); 'Barrier-island and associated strand plain systems', in Walker, R. G., Ed. *Facies Models: Geological Association of Canada, Geoscience Canada Reprint Series 1*, p. 119-140.

Reinson, G. E., (1992); 'Transgressive barrier island and estuarine systems', in Walker, R. G. and James N. P. Eds. *Facies Models, response to Sea Level Change, Geological Association of Canada*, p.179-195.

Retallack, G.J. (1990), *Soils of the Past: An Introduction to Paleopedology*; Unwin Hyman, Boston, Mass., U.S.A., pp. 520.

Retallack, G.J. (1995), 'Permian-Triassic life crisis on land', *Science* vol. 267, pp. 77-80.

Retallack, G.J., J.J. Veevers, and R. Morante, (1996), 'Global early Triassic coal gap between Late Permian extinction and Middle Triassic recovery of peat-forming plants'; *Bulletin of the Geological Society of America* vol.108: pp. 195-207.

Riding, J.B., Czernichowski-Lauriol, I., Lombardi, S., Quattrocchi, F., Rochelle, C.A., Savage, D., Springer, N., (2003); 'The IEA Weyburn CO₂ Monitoring and Storage Project – The European Dimension'; in Gale, J. and Kaya, Y. Eds. *Greenhouse Gas Control Technologies-6 (GHGT-6)*, Kyoto, Japan 2003, Elsevier Science Publishing, pp.1629-1634.

Rigg, A. and Bradshaw, J., (2001); 'The GEODISC Program: research into geological sequestration of CO₂ in Australia', in Williams, D.J., Durie, R.A., McMullan, P., Paulson, C.A.J., and Smith, A.Y. Eds. *Greenhouse Gas Control Technologies-5 (GHGT-5)*; CSIRO Publishing, Australia; pp. 254-259.

Rigg, A.J., Allison, G., Bradshaw, J., Ennis-King, J., Gibson-Poole, C.M., Hillis, R.R., Lang, S.C., Streit, J.E. (2001); 'The search for sites for geological sequestration of CO₂ in Australia: A progress report on GEODISC', *APPEA Journal*, v.41, (1), 2001; pp. 711-725.

Robert, E. and Shapiro, S.A. (2001); 'Microseismic Reservoir Characterization: Numerical experiments and case studies'; *SEG 71st Annual Meeting and International Exposition; Society of Exploration Geophysicists Paper RC 2.4*, pp. 1584-1587; 2001.

Robertson, J. D. and Downey, M. W., (2000); 'Analysis, Guts Trump Paralysis'; in *AAPG Explorer; American Association of Petroleum Geologists*, November 2000 Issue, Tulsa, Okla., USA.

Robertson, J. D., (2004); 'Tangguh: The First Major Pre-Tertiary Discovery In Indonesia', at the *Houston Geological Society International Meeting*, Westchase Hilton Hotel, [website available on 16 March 2004],
http://www.hgs.org/attachments/calendarevents/90/Abstract_Tangguh.pdf

Robinson, P.H., Stead, H.S., O'Reilly, J.B., Guppy, N.K., (1994); 'Meanders to Fan: A Sequence Stratigraphic Approach to Upper Jurassic – Lower Cretaceous Sedimentation in the Sahul Syncline, North Bonaparte Basin'; in Purcell, R.R. and Purcell, P.G. Eds. *The Sedimentary Basins of Western Australia* vol. 1; Frank Daniels Publishing Ltd., Perth Australia, pp. 223-242.

Rose, P.R. (2001); Risk Analysis and Management of Petroleum Exploration Ventures; *AAPG Exploration series vol. 12, American Association of Petroleum Geologists*, Tulsa, Okla., USA; pp. 5-13.

Royal Society (press release 17 August 2004); 'Royal Society launches investigation into rising acidity of oceans'; [website available 20 August 2004],
<http://www.royalsoc.ac.uk/templates/press/releasedetails.cfm?file=549.txt>

Salo, J.P., (1994); Geological Final Well Report - Wiriagar Deep No. 1; (Confidential ARCO Report); Jakarta – Indonesia, December 1994.

Salo, J.P., (1996a); Geological Final Well Report – East Onin No. 1 vol.1; (Confidential ARCO Report); Jakarta – Indonesia, July 1996.

Salo, J.P., (1996b); Geological Final Well Report – East Onin No. 1 vol.2; (Confidential ARCO Report); Jakarta – Indonesia, July 1996.

Salo, J.P., (1996c); Geological Final Well Report – Wiriagar Deep No. 2; (Confidential ARCO Report); Jakarta – Indonesia, October 1996.

Salo, J.P., (1997a); Geological Final Well Report – Wiriagar Deep No. 4; (Confidential ARCO Report); Jakarta – Indonesia, January 1997.

Salo, J.P., (1997b); Geological Final Well Report – Wiriagar Deep No. 3 vol. 1; (Confidential ARCO Report); Jakarta – Indonesia, April 1997.

Salo, J.P., (1997c); Geological Final Well Report – Wiriagar Deep No. 3 vol. 2; (Confidential ARCO Report); Jakarta - Indonesia, April 1997.

Salo, J.P., (1997d); Geological Final Well Report – Wiriagar Deep No. 5 vol.1; (Confidential ARCO Report); Jakarta - Indonesia, June 1997.

Salo, J.P., (1997e); Geological Final Well Report – Wiriagar Deep No. 5 vol. 2; (Confidential ARCO Report); Jakarta - Indonesia, June 1997.

Salo, J.P., Indro S., Dahlini D., (1997f); Geological Final Well Report – Wiriagar Deep No. 8; (Confidential ARCO Report); Jakarta - Indonesia, August 1997.

Salo, J.P., (1997g); Geological Final Well Report – Vorwata No. 4; (Confidential ARCO Report); Jakarta – Indonesia, December 1997.

Salo, J.P., (1998a); Geological Final Well Report – Vorwata Deep No. 9 vol. 1; (Confidential ARCO Report); Jakarta – Indonesia, June 1998.

Salo, J.P., (1998b); Geological Final Well Report – Vorwata No. 9 vol. 2; (Confidential ARCO Report); Jakarta – Indonesia, July 1998.

Salo, J. P., Casarta, L. J., Tisnawidjaja, S., Sampurno, S. (2004); ‘Wiriagar Deep: The discovery that triggered Tangguh’, in “*Proceedings Deepwater and Frontier Exploration in Asia and Australia International Conference 2004*”, Indonesian Petroleum Association and the American Association of Petroleum Geologists.

Schapp, H., and McMullan, P., (2001); ‘Reducing Greenhouse Gas Emissions from Electricity Supply in Australia’, in Williams, D.J., Durie, R.A., McMullen, P., Paulson, C.A.J., and Smith, A.Y. Eds. *Greenhouse Gas Control Technologies-5 (GHGT-5)*; CSIRO Publishing, Sydney Australia, pp. 795-802.

Schmidt, P.W. and Clark, D.A., (2000); 'Paleomagnetism, Apparent Pole-Wander Path, & Paleolatitude'; in Veevers, J.J. Eds. *Billion-year Earth History of Australia and Neighbors in Gondwanaland*; GEMOC Press; Sydney, Australia.

Schowalter, T.T. (1979); 'Mechanics of Secondary Hydrocarbon Migration and Entrapment'; *AAPG Bulletin*, vol. 63, no. 5; American Association of Petroleum Geologists; Tulsa, Oklahoma; USA; May 1979.

Schumm, S.A. (1993); 'River response to base level change: implications for sequence stratigraphy'; *Journal of Geology* vol.101; 1993.

Scotese, C. and McKerrow, W.S. (1990); 'Revised World Maps', in McKerrow, W.S. and Scotese, C. Eds. *Palaeozoic palaeogeography and biogeography*; Geological Society of London Memoir 12, pp.1-21.

Scotese, C., (2000); "Palaeomap Project"; [website available 18 February 2002], <http://www.scotese.com/earth.htm>

Shaviv, N.J., Veizer, J.; (2003); 'Celestial driver of Phanerozoic climate?'; *GSA Today*, Issue July 2003; Geological Society of America, USA.

Shackleton, N.J.; (2000); 'The 100,000-Year Ice-Age Cycle Identified and Found to Lag Temperature, Carbon Dioxide, and Orbital Eccentricity'; in *Science*, vol. 289 Issue 5486, 15 September 2000, pp 1897-1905.

Shanmugan, G., (1996); 'High-density turbidity currents: are they only sandy-debris flows'; *Journal of Sedimentary Research*, v.66, pp.2-10.

Shanmugan, G., (2000); '50 Years of Turbidite Paradigm (1950's-1990's): deepwater processes and facies models – a critical perspective'; *Marine and Petroleum Geology*, v.17, pp.285-342.

Sherlock, D. (2002); 'Geophysical Monitoring of Subsurface CO₂'; *CSIRO Petroleum Report No. 02-006*; (Confidential Report) CSIRO Publishing; Kensington, Australia; January 2002.

Shinn, J., Kheshgi, H., Grant, J., Bernstein, L.; 'Technology Assessment in Climate Change Mitigation', in Williams, D.J., Durie, R.A., McMullen, P., Paulson, C.A.J., and Smith, A.Y. Eds. *Greenhouse Gas Control Technologies-5 (GHGT-5)*; CSIRO Publishing, Sydney Australia; pp. 1171-1176.

Sloss, L.L. (1991); 'The tectonic factor in sea level change: a countervailing view'; *Journal of Geophysical Research* vol. 96; 1991.

Sminchak, J., Gupta, N., Bryer, C., Bergman, P. (2001); 'Issues Related to Seismic Activity Induced by the Injection of CO₂ in Deep Saline Aquifers'; *First National Conference on Carbon Sequestration Science, National Energy Technology Laboratory; Technical Poster #37*; 2001.

- SMSUSt.A (2004); School of Mathematics and Statistics University of St. Andrews, Scotland; [website available 22 August 2004], <http://www-gap.dcs.st-and.ac.uk/~history/Mathematicians/Fourier.html>
- Sneider, R.M. (1987); 'Practical Petrophysics for Exploration and Development'; *AAPG Education Dept., Short Course Notes; American Association of Petroleum Geologists* 1987.
- Stocker, T.F., and Schmitter, A., (1997), 'Influence of CO₂ emission rates on the stability of the thermohaline circulation', in *Nature vol. 388*, pp.862-865; UK.
- Strack, K.M. and Vozoff, K. (1996); 'Integrating Long-offset Transient Electromagnetics (LOTEL) with Seismics in an Exploration Environment'; in *Geophysical Prospecting, no. 44*, April 1996 Issue, pp.997-1017.
- Struckmeyer, H. I. M., Yueng, M., and Pigram, J., (1995); 'Mesozoic to Cainozoic plate tectonic and palaeogeographic evolution of the New Guinea region', in Carman C.J. and Carman Z. Eds. *Petroleum Exploration and Development In Papua New Guinea*, Proceedings of Second PNG Petroleum Convention 1995, Port Moresby, PNG, pp. 261-290.
- Surdam, R.C., Boese, S.W., Crossey, L.J. (1984); 'The Chemistry of Secondary Porosity'; in McDonald, D.A. and Surdam, R.C. Eds. *Clastic Diagenesis*, UK.
- Tollman, A. and Krystan-Tollman, E.; (1985); 'Paleogeography of the Tethys from the Paleozoic to the Mesozoic', in Nakazawa, K. and Dickens, J.M. Eds. *The Tethys: Her Paleogeography, and Paleobiology, From the Paleozoic to Mesozoic*, Tokai University Press; Japan; pp. 20-199.
- Trenberth, Kevin; National Center for Atmospheric Research staff; (2001); 'Global Warming Is Happening'; *Public Presentation at American Association of Petroleum Geologist's National Conference & Exhibition 2001*; Denver, Colorado; June 5th, 2001.
- Tye, R.S., Hickey, J.J.; (1999); 'Reservoir Architecture of the Roabiba Sandstone, Tangguh Gas Fields, Irian Jaya, Indonesia'; ARCO Exploration and Technology Operations; (Confidential Report) TSR 99-0031; September 1999, Plano Texas, USA.
- Uchida, T., Takeya, S., Ebinuma, T., Narita, H., (2001); 'Replacing Methane with CO₂ in Clathrate Hydrate: Observations Using Raman Spectroscopy', in Williams, D.J., Durie, R.A., McMullen, P., Paulson, C.A.J., and Smith, A.Y. Eds. *Greenhouse Gas Control Technologies-5 (GHGT-5)*; CSIRO Publishing, Sydney, Australia, pp. 399-404.
- UNFCCC (United Nations Framework Convention on Climate Change) [website available 20 August 2004], <http://unfccc.int/resource/convkp.html>
- UND, 2004; University of North Dakota, Earth Science Department [website available 20 August 2004], http://volcano.und.nodak.edu/vwdocs/volc_images/africa/nyos.html.

Vail P. R., Hardenbol, J., and Todd, R. G., 1984, 'Jurassic unconformities, chronostratigraphy, and sea-level changes from seismic stratigraphy and biostratigraphy', in J. S. Schlee Eds. *Interregional unconformities and hydrocarbon accumulation, American Association of Petroleum Geologists Memoir 36*, Tulsa, Okla., USA, pp. 129 – 144.

van der Meer, L.G.H., (1995); 'The Storage Efficiency of Aquifers', in *Energy Conservation and Management, No.6-9, Vol. 36*, pp.513-518, Netherlands, 1995.

van Bergen, F., Pagnier, H.J.M., van der Meer, L.G.H., van den Belt, F.J.G., Winthagen, P.L.A., and Westerhoff, R.A., (2003); 'Development of a Field Experiment of CO₂ Storage in Coal Seams in the Upper Silesian Basin of Poland (RECOPOL)', in Gale, J. and Kaya, Y. Eds. *Greenhouse Gas Control Technologies-6 GHGT-6, Kyoto, Japan 2003*, Elsevier Science Publishing, pp.569-578.

Van Wagoner, J.C., Mitchum, R.M., Campion, K.M., and Rahmanian V.D. (1990); 'Siliciclastic sequence stratigraphy in well logs, cores and outcrops: concepts for high-resolution correlation of time and facies'; *AAPG Methods in Exploration Series #7, American Association of Petroleum Geologists*; Tulsa, Okla., USA.

Vavra, C.L., Kaldi, J.G., Sneider, R.M. (1992); 'Geological Applications of Capillary Pressure: A Review'; *AAPG Bulletin, vol. 76, no. 6; American Association of Petroleum Geologists*; Tulsa, Oklahoma; USA.

Veevers, J.J.; Embleton, B.J.J.; Conaghan, P.J.; Flood, R.H.; Johnson, B.D.; Jones, J.G.; Jones, J.G.; McDonnell, K.L.; Powell, C.M.; Shaw, S.E.; Talent, J.A.; Wass, S.Y.; Williams, M.A.J.; Quilty, P.G. (1986); *Phanerozoic Earth History of Australia*; Oxford University Press, N.Y. U.S.A.

Veevers, J.J.; Morgan, P., O'Reilly, S.Y., Walter, M.R., Scheibner, E., Clark, D.A., Schmidt, P.W., Clark, S., Gaina, C., Muller, R.D., Kennett, B.L.N., Williams, M.A.J. (2000); '*Billion-year Earth History of Australia and Neighbors in Gondwanaland*'; GEMOC Press; Sydney, Australia.

Vendetti, Jan; (2001); '*Geo-engineering Norwegian CO₂*', News Notes, [http:// Geotimes Magazine Website](http://Geotimes Magazine Website), [website available on 21 July 2001], <http://www.geotimes.org/current/>

Visser, W. A., and Hermes, J. J., 1962. Geological Results of the Exploration for Oil in the Netherlands, New Guinea, (*Verhandelingen van het Koninklijk Nederlands Geologisch Mijnbouw Kundig Genootschap, Serie V.20*). pp. 1- 256.

Wall, D., Baky, A., Bates, C.D., Clowser, D., Ong, G.B., Ludi, P.H., 1990; 'Roabiba-1 well, Berau Block, Offshore Irian Jaya, Occidental Berau of Indonesia, Inc., Biostratigraphy and Paleoenvironments', P.T. Robertson Utama, Jakarta Indonesia, November 1990; (Confidential Report).

Wallace, R. (2003); '*Permanent Fiber-Optic In-Well 4D Seismic Sensor Successfully Deployed*'; *Journal of Petroleum Technology* v.80, Society of Petroleum Engineers, June 2003 Issue, pp.5-6, Tulsa, Oklahoma; USA.

Watson, P.V., Hulsbos, R.E., Sukarno, Wantoro, (1994); 'The Biostratigraphy of the Well Wiriagar Deep-1, (Interval 1100' – 8500' TD), Wiriagar PSC, Irian Jaya'; Atlantic Richfield Wiriagar Inc., Core Labs File #GSI-94023; October 1994, Jakarta – Indonesia.

Watson, P.V., Hulsbos, R.E., Sukarno, Wantoro, (1996a); 'Well Wiriagar Deep-2, Offshore Berau Block, Irian Jaya, Biostratigraphy and Paleoenvironments of the interval 2050'(SWC) - 9755' TD'; Atlantic Richfield Wiriagar Inc., Core Labs; April 1996, Jakarta – Indonesia.

Watson, P.V., Hulsbos, R.E., Sukarno, Wantoro, (1996b); 'Well Wiriagar Deep-3, Offshore Berau Block, Irian Jaya, Biostratigraphy and Paleoenvironments of the interval 2200' - 9964' TD'; Atlantic Richfield Wiriagar Inc., Core Labs; October 1996, Jakarta – Indonesia.

Watson, P.V., Hulsbos, R.E., Sukarno, Wantoro, (1996c); 'Well Wiriagar Deep-4, Offshore Berau Block, Irian Jaya, Biostratigraphy and Paleoenvironments of the interval 3100' - 9622' TD'; Atlantic Richfield Wiriagar Inc., Core Labs; April 1996, Jakarta – Indonesia.

Watson, P.V., Hulsbos, R.E., Sukarno, Wantoro, (1996d); 'Well Wiriagar Deep-5, Offshore Berau Block, Irian Jaya, Biostratigraphy and Paleoenvironments of the interval 3400' - 10000' TD'; Atlantic Richfield Wiriagar Inc., Core Labs; November 1996, Jakarta – Indonesia.

Watson, P.V., Hulsbos, R.E., Sukarno, Wantoro, (1996e); '*Well East Onin-1, Onshore Babo Block, Irian Jaya, Biostratigraphy and Paleoenvironments of the interval 40' - 7710' TD*'; Atlantic Richfield Bomberai Inc., Core Labs; January 1996, Jakarta – Indonesia.

Watson, P.V., Hulsbos, R.E., Sukarno, Wantoro, (1997a); 'Well Wiriagar Deep-6, Offshore Berau Block, Irian Jaya, Biostratigraphy and Paleoenvironments of the interval 6090' - 9158' TD'; Atlantic Richfield Wiriagar Inc., Core Labs; February 1997, Jakarta – Indonesia.

Watson, P.V., Hulsbos, R.E., Sukarno, Wantoro, (1997b); 'Well Vorwata-1, Offshore Berau Block, Irian Jaya, Biostratigraphy and Paleoenvironments of the interval 5310' – 12,665' TD'; Atlantic Richfield Wiriagar Inc., Core Labs; 1997, Jakarta – Indonesia.

Watson, P.V., Hulsbos, R.E., Sukarno, Wantoro, (1997c); 'Well Vorwata-2, Offshore Berau Block, Irian Jaya, Biostratigraphy and Paleoenvironments of the interval 10,610' – 13,365' TD'; Atlantic Richfield Wiriagar Inc., Core Labs; 1997, Jakarta – Indonesia.

Watson, P.V., Hulsbos, R.E., Sukarno, Wantoro, (1997d); 'Well Vorwata-3, Offshore Berau Block, Irian Jaya, Biostratigraphy and Paleoenvironments of the interval 5520' – 12,782' TD'; Atlantic Richfield Wiriagar Inc., Core Labs; 1997, Jakarta – Indonesia.

Watson, P.V., Hulsbos, R.E., Sukarno, Wantoro, (1997e); 'Well Vorwata-4, Offshore Berau Block, Irian Jaya, Biostratigraphy and Paleoenvironments of the interval 10,610' – 12,970' TD'; Atlantic Richfield Wiriagar Inc., Core Labs; 1997, Jakarta – Indonesia.

Watson, P.V., Hulsbos, R.E., Sukarno, Wantoro, (1997f); 'Well Vorwata-5, Offshore Berau Block, Irian Jaya, Biostratigraphy and Paleoenvironments of the interval 11,830' – 13,110' TD'; Atlantic Richfield Wiriagar Inc., Core Labs; 1997, Jakarta – Indonesia.

Watson, P.V., Hulsbos, R.E., Sukarno, Wantoro, (1997g); 'Well Vorwata-6, Offshore Berau Block, Irian Jaya, Biostratigraphy and Paleoenvironments of the interval 10,610' – 12,970' TD'; Atlantic Richfield Wiriagar Inc., Core Labs; 1997, Jakarta – Indonesia.

Watson, P.V., Hulsbos, R.E., Sukarno, Wantoro, (1997h); 'Well Vorwata-7, Offshore Muturi Block, Irian Jaya, Palynostratigraphy and Paleoenvironments of the interval 13060' - 13420'; Atlantic Richfield Wiriagar Inc., Core Labs; 1997, Jakarta – Indonesia.

Watson, P.V., Hulsbos, R.E., Sukarno, Wantoro, (1997i); 'Well Ubadari-1, Offshore Berau Block, Irian Jaya, Palynostratigraphy and Paleoenvironments of the interval 4330' - 8640'(SWC); Atlantic Richfield Wiriagar Inc., Core Labs; November 1997, Jakarta – Indonesia.

Watson, P.V., Hulsbos, R.E., Sukarno, Wantoro, (1998a); 'Well Vorwata-8, Offshore Muturi Block, Irian Jaya, Palynostratigraphy and Paleoenvironments of the interval 3790m - 3925m TD'; British Gas Ltd., Core Labs; August 1998, Jakarta – Indonesia.

Watson, P.V., Hulsbos, R.E., Sukarno, Wantoro, (1998b); 'Well Vorwata-9, Offshore Berau Block, Irian Jaya, Biostratigraphy and Paleoenvironments of the interval 11340' - 13565' TD; Atlantic Richfield Wiriagar Inc., Core Labs; August 1998, Jakarta – Indonesia.

Watson, P.V., Hulsbos, R.E., Sukarno, Wantoro, (1998c); 'Well Vorwata-10, Offshore Muturi Block, Irian Jaya, Palynostratigraphy and Paleoenvironments of the interval 3820m - 4152m TD'; British Gas Ltd., Core Labs; August 1998, Jakarta – Indonesia.

Watson, P.V., Hulsbos, R.E., Sukarno, Wantoro, (1998d); 'Well Vorwata-11, Offshore Muturi Block, Irian Jaya, Palynostratigraphy and Paleoenvironments of the interval 3701m - 4155m TD; British Gas Ltd., Core Labs; August 1998, Jakarta – Indonesia.

Watson, P.V., Hulsbos, R.E., Sukarno, Wantoro, (1998e); 'Well Ubadari-2, Offshore Berau Block, Irian Jaya, Palynostratigraphy and Paleoenvironments of the interval 400' - 9200' TD; Atlantic Richfield Wiriagar Inc., Core Labs; August 1998, Jakarta – Indonesia.

Waton, P.V., Hulsbos, R.E., Sukarno, Wantoro, (1998f); 'Well Nambumbi-1, Offshore Berau Block, Irian Jaya, Biostratigraphy and Paleoenvironments of the interval 3250m - 4092m TD; British Gas Ltd., Core Labs; 1998, Jakarta – Indonesia.

Waton, P.V., Hulsbos, R.E., Sukarno, Wantoro, (1998g); 'Well Wos-1, Offshore Berau Block, Irian Jaya, Palynostratigraphy of the interval 9130' - 9700' TD; Core Labs (Commissioned by ARCO); August 1998, Jakarta – Indonesia.

Watson, R.T. (2001); 'Climate Change 2001', on Intergovernmental Panel on Climate Change (IPCC), [website available on 20 December 2001], <http://www.ipcc.ch/press/sp-cop6.htm>

Watson, M.N., Zwingmann, N., Lemon, N.M. (2003a); 'The Ladbroke Grove-Katnook Carbon Dioxide Natural Laboratory: A Recent CO₂ Accumulation in a Lithic Sandstone Reservoir', in Gale, J. and Kaya, Y. Eds. *Greenhouse Gas Control Technologies GHGT-6, Kyoto, Japan 2003*, Elsevier Science Publishing, pp.435-439.

Watson, M.N., Zwingmann, N., Lemon, N.M., Tingate, P.R. (2003b); 'Onshore Otway Basin Carbon Dioxide Accumulations: CO₂-Induced Diagenesis in Natural Analogues for Underground Storage of Greenhouse Gas'; *APPEA Journal 2003*, Australia.

Webster, M, Forest C.; (2003); 'Uncertainty analysis of climate change and policy response', in *Climatic Change vol. 61 (3) March 2003 Issue*; pp. 295-320.

Whibley, M. and Jacobson, T. (1990); 'Exploration in the Northern Bonaparte Basin, Timor Sea – WA-199-P'; *The APPEA Journal 1990 vol.30 Part 1*; Keating Printing Ltd.; Australia; pp. 7-25.

Whitehouse, (2002); US Government website posting, [website available 29 November 2002], <http://www.whitehouse.gov/news/releases/2002/02/climatechange.html>

Whittam, D.B., Norvick, M.S., McIntyre, C.L., (1996); 'Mesozoic and Cainozoic tectonostratigraphy of western ZOCA and adjacent areas'; *APPEA Journal 1996 vol. 36 part I*; Beck Books; Queensland Australia; pp. 209-231.

WHOI, (2004); Woods Hole Oceanographic Institute's 'Abrupt Climate Change' study [website available October 2004]; http://www.whoi.edu/institutes/occi/currenttopics/climatechange_wef_en1.html

Wilgus, C.K., Hastings, B.S., Kendall, G St. C, Posamentier, H.W., Ross, C.A., and Van Wagoner, J.C. (1988); 'Sea-Level Changes: An intergrated approach'; *SEPM Special Publications #42*; Tulsa, Ok. USA; 1988.

Wilt, M., Zhang, P., Morea, M., Julander, D., Mock, P. (2001); 'Using Cross-well Electromagnetics to Map Water saturations and Formation Structures at Lost Hills'; *SPE Western Regional Meeting; Society of Petroleum Engineers paper 37532*; 2001.

- Wollast, R. and Mackenzie, F.T., (1989); 'Global Biogeochemical Cycles and Climate,' *Climate and Geoscience*, D. Reidel Publishing Co.
- World Meteorological Organization, (1989); [website available in December 2002]; <http://www.wmo.int/index-en.html>
- World Meteorological Organization, (2001); [website available in December 2002]; <http://www.wmo.int/index-en.html>
- Wright, V.P. (1986); *Paleosols: their Recognition and Interpretation*, Blackwell Scientific Publications, Oxford, U.K., pp.315.
- Yeates, A.N., Bradshaw, M.T., Dickens, J.M., Brakel, J.M., Exon, N.F., Langford, R.P., Mulholland, S.M., Totterdell, J.M., and Yeung, M., (1987); 'The Westralian Superbasin: an Australian link with Tethys', in McKenzie, K.G. Eds. *Shallow Tethys 2 Symposium* at Wagga Wagga, NSW 1987; Balkema Publications, Rotterdam, pp.199-213.
- Yoshino, H., Tanaka, T., Yamaguchi, H., (2003); 'Petroleum Geology in Bintuni Basin in East Indonesia – A case study of exploration and evaluation of giant gas fields', *Journal of the Japanese Association for Petroleum Technology*, v. 68, no.2-3, May 2003 Issue, Tokyo, Japan.
- Zaitlin, B.A., Dalrymple, R.W., Boyd, R. (1994); 'The Stratigraphic Organization of Incised-Valley Systems Associated with Relative Sea-Level Changes', in *Incised-Valley Systems: Origin and Sedimentary Sequences; SEPM Special Publication No. 51*; SEPM Publications; Tulsa, Ok. USA.